A provenance study of Upper Jurassic hydrocarbon source rocks of the Flemish Pass Basin and Central Ridge, offshore Newfoundland, Canada

By
Matthew William Scott

A thesis submitted to the School of Graduate Studies in partial fulfillment of the requirements for the degree of Master of Science

Department of Earth Sciences

Memorial University of Newfoundland

May 2018

St. John's   Newfoundland and Labrador

Abstract

This project is a provenance study of Upper Jurassic source and reservoir rocks from the Flemish Pass Basin and Central Ridge, offshore Newfoundland, Canada. It is aimed at adding a new dataset to contribute to our understanding of the geology of this area, where a number of recent hydrocarbon discoveries have been made, but limited geological information is available. A primary goal of the project is to determine the provenance and paleodrainage patterns of the Upper and Lower Kimmeridgian Source Rock and Upper and Lower Tempest Sandstone of the Flemish Pass Basin and the Central Ridge. It is likely that the source rock and reservoir units increase in thickness toward their source terranes and this provenance study would thus help define where thicker sequences of hydrocarbon source rocks and reservoir units are located in the region. In total, sixty samples of both mudstones and sandstones were acquired, processed and analyzed from four wells (Baccalieu I-78, Panther P-52, South Tempest G-88 and Lancaster G-70) to determine provenance. A combination of detrital zircon geochronology, whole rock geochemistry, and heavy mineral proxies were used to decipher provenance. In addition, core logging and thin section descriptions were completed to gain an understanding of the depositional environment. This analysis indicates a basinal setting with sediment being delivered by turbidity currents. The Upper Kimmeridgian Source Rock, Lower Kimmeridgian Source Rock and the Rankin Formation are interpreted to be composed of detritus from the Avalon Zone, Central Mobile Belt, and underlying basement. Detritus would have been derived from the northeast, and thicker sequences of these units would be expected in the northeastern portions of the Flemish Pass Basin and Central Ridge. The Upper Tempest and Lower Tempest Sandstone are also characterized by material from the Avalon Zone. However, some of the detritus from these units is also interpreted to be derived from Iberia to the east. In addition, the Upper

Tempest Sandstone contains Mesozoic zircons, which helped constrain the depositional age of this unit. Mesozoic zircons were not found in samples from the other units. The Tempest Sandstone units are interpreted to be derived from the east, which means thicker sequences of this unit would be expected towards the eastern edges of the Central Ridge and Flemish Pass Basin. Knowledge of where the thickest packages of these units exist may be an important consideration for petroleum exploration in the region.

In addition to these provenance findings, another important conclusion is that although provenance analysis methods such as detrital zircon geochronology are more common in sandstones, it is evident that using these techniques to analyze fine-grained sedimentary rocks is indeed feasible and useful. Additionally, the detrital zircon distributions in interbedded sandstone and mudstone beds were compared. These distributions suggested provenance of these pairs is very similar, an important implication for future use of this method in mudstones.

Acknowledgements

First of all, I would like to thank my two thesis supervisors, Dr. Paul Sylvester and Dr. Derek Wilton. Working on this project was a great opportunity for me and I benefited greatly from your expertise. I appreciate having your guidance when necessary but also the freedom to work independently. I would also like to thank Dr. Richard Hiscott for his insightful and thorough input.

Financial support for this project was provided by the Research and Development Corporation of Newfoundland and Labrador in the form of an Ocean Industries Student Research Award and is gratefully acknowledged. The MITACS Accelerate program also contributed to this project financially and is certainly appreciated.

There are many others who have helped and contributed to the completion of this project in some way. Although I can't name them all, those working at the CREAIT Network at Memorial University such as Dylan Goudie, David Grant, Sarah Jantzi and Pam King were extremely helpful to me with guidance and timely analyses for the various methods undertaken. My officemates Michelle English, Marie-Eve Lajoie and Nico Kastek were a great sounding board and were always there for support if needed. Additional support from geoscientists at Suncor Energy in St. John's including Michael Livingstone, Jody Hodder, and Eric Albrechtsons was certainly appreciated. I would also like to thank the C-NLOPB, particularly David Mills and Jason Newell, for access to the core and sample materials. Kate Souders and Angela Norman helped significantly by teaching me sample preparation methods as well as helping with analytical techniques. I am very grateful for all your help.

Finally, I would like to express my gratitude to my family. To my parents and brother, I thank you for the constant support, guidance, and belief in my abilities. To my fiancé, Emily-Ann, I thank you for the support, patience and understanding you have shown me. I am exceptionally grateful to you all.

Table of Contents

List of Tables

List of Figures

List of Appendices

Chapter 1 – Introduction and Geological Setting

1.1 - Introduction and Purpose

The prolific Kimmeridgian source rocks of the Grand Banks of Newfoundland (Figure 1.1) have received considerable attention as they are the primary oil source rock for this significant petroleum district. The Egret Member, the Kimmeridgian source rock of the Jeanne d'Arc Basin has been studied in detail there, where there are three producing fields and a fourth is scheduled to commence production in 2017. Nearby basins such as the Flemish Pass Basin and Orphan Basin (Figure 1.1) contain similar geology and structures, and are thought to hold significant potential for hydrocarbon discoveries. These nearby basins, however, have been studied in a more limited fashion.

The Flemish Pass Basin, in particular, has had significant hydrocarbon discoveries at the Mizzen area in 2009, and the Harpoon and Bay du Nord areas in 2013, spurring industry exploration (Enachescu, 2014). The region has been the focus for academic research as well (Lowe et al., 2011). The Flemish Pass Basin is separated from the Jeanne d'Arc Basin by a topographic high called the Central Ridge (Figure 1.1), where hydrocarbon discoveries have also been made. Tithonian-aged sandstone, consisting of four siliciclastic intervals interbedded with shale, is the primary oil reservoir at Mizzen (Cody et al., 2012). The primary source for the oil is considered to be a Kimmeridgian organic-rich shale, likely equivalent to the Egret Member in the Jeanne d'Arc Basin (Fowler et al., 2007). The Egret Member (Figure 1.3) consists of brown to grey shale of marine origin, with interbedded marlstone/limestone, and fine-grained sandstone and siltstone (Bateman, 1995).

Previous work on the Upper and Lower Kimmeridgian Source Rocks in the Flemish Pass has focused on the organic geochemistry and hydrocarbon source potential of the units

(McCracken et al., 2000; Creaney & Allison, 1987). This study will present new mineral data that contribute to the understanding of this important interval within the basin. As very little information is available on this unit in the area of interest, detailed core and thin section descriptions have been completed to help define the mineralogy and interpret the depositional environment of the source rocks.

The goal of this study is to determine the provenance and paleodrainage patterns that supplied detritus to the Kimmeridgian source rocks as well as interbedded Tempest Sandstones within the Flemish Pass Basin and Central Ridge. Lowe et al. (2011) determined provenance patterns within the coarse-grained reservoir intervals within the basin using detrital zircon geochronology as well as geochemistry of detrital tourmaline. For this project, detrital zircon geochronology, major and trace element geochemistry, and heavy mineral analyses will be applied to help predict where the thickest accumulations of fine-grained, organic-rich source rocks are located. All of the information gathered will enable a more accurate prediction of prospective areas for hydrocarbon exploration.

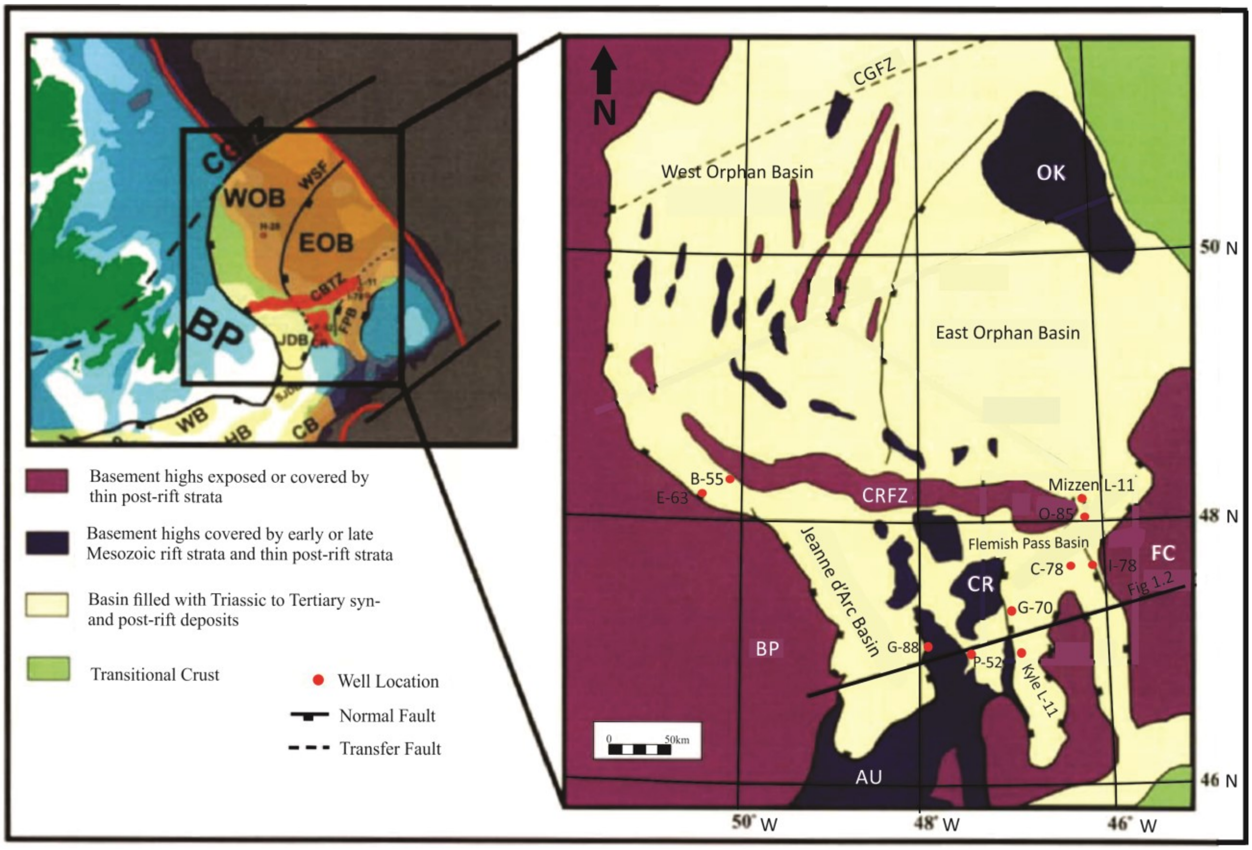

Figure 1.1: Regional location and geology of the Newfoundland Grand Banks. Line shows location of cross-section in later figures. BP=Bonavista Platform; CGFZ=Charlie-Gibbs Fracture Zone; CR=Central Ridge; CRFZ=Cumberland Ridge Fault Zone; FC=Flemish Cap; OK=Orphan Knoll; WOB=West Orphan Basin; EOB=East Orphan Basin; JDB=Jeanne d'Arc Basin; CB=Carson Basin; WB=Whale Basin; FPB=Flemish Pass Basin; AU=Avalon Uplift. Wells: P-52=Panther P-52; I-78=Baccalieu I-78; G-70=Lancaster G-70; G-88=South Tempest G-88; Mizzen L-11, Kyle L-11; O-85=Harpoon O-85; C-78=Bay du Nord C-78; B-55=Cumberland B-55; E-63=Linnet E-63. Modified from Lowe (2009) and Enachescu (1987).

1.2 - Regional Mesozoic Geological and Tectonic Setting

Mesozoic rocks of offshore Newfoundland are restricted to a series of interconnected northeast-trending rift basins. These basins are typically half-graben structures separated by Precambrian and Paleozoic basement highs and include the Jeanne d'Arc, Flemish Pass, East Orphan, and West Orphan basins (Figure 1.1). A cross section across the Jeanne d'Arc Basin, Central Ridge, and Flemish Pass Basin (Figure 1.2) highlights the deep crustal relationship between the two basins. These Mesozoic basins were formed by rifting associated with the break-up of Pangea, spanning from the Permo-Triassic to the mid-Cretaceous (Enachescu, 1987

& 1988; Tankard & Welsink, 1987). Rifting progressed from south to north during the Late Triassic to the Early Cretaceous, which provided the conditions necessary for basin formation on the continental margin of Newfoundland. From the mid-Cretaceous to the present day, the evolution of the basins has been controlled by North Atlantic seafloor spreading and passive margin sedimentation (Enachescu, 1987 & 1988; Tankard & Welsink, 1987). Of these basins, the Jeanne d'Arc Basin is the most prolific hydrocarbon province, with three producing fields and a fourth scheduled to begin production in 2017. The basin is adjacent to the main listric detachment, and it therefore possesses the thickest succession of sediment (22 km) and most complete syn-rift succession (14 km) (Keen et al., 1987; Enachescu, 1987; Tankard & Welsink, 1987; Tankard et al. 1989; Driscoll & Hogg, 1995). Although this thesis will focus on the Flemish Pass Basin and Central Ridge, the adjacent Jeanne d'Arc Basin has widespread well control, and has been studied by other workers in great detail. This makes it an excellent analogue for studies of Mesozoic basins elsewhere in offshore Newfoundland, and it is therefore reviewed in detail.

Three rifting stages, interpreted to have affected sedimentation in many of the North Atlantic Basins (Enachescu, 1987; Sinclair, 1988), are clearly important in both the Flemish Pass and Jeanne d'Arc basins. The three rifting phases, according to Sinclair (1988), include: 1) Triassic to Early Jurassic rifting during a period of NW-SE oriented extension, resulting in the break-up of Africa and North America; 2) Tithonian to early Valanginian rifting, during a period of E-W oriented extension, resulting in the break-up of Iberia and the Grand Banks; 3) Aptian-Albian rifting, during a period of NE-SW oriented extension, resulting in the break-up of Europe and North America. From the Late Cretaceous onwards, thermal subsidence was the dominant mechanism affecting the newly created continental margins. At this point, the Atlantic margin became a passive margin and hence associated passive margin sediments were deposited which continues to the present day.

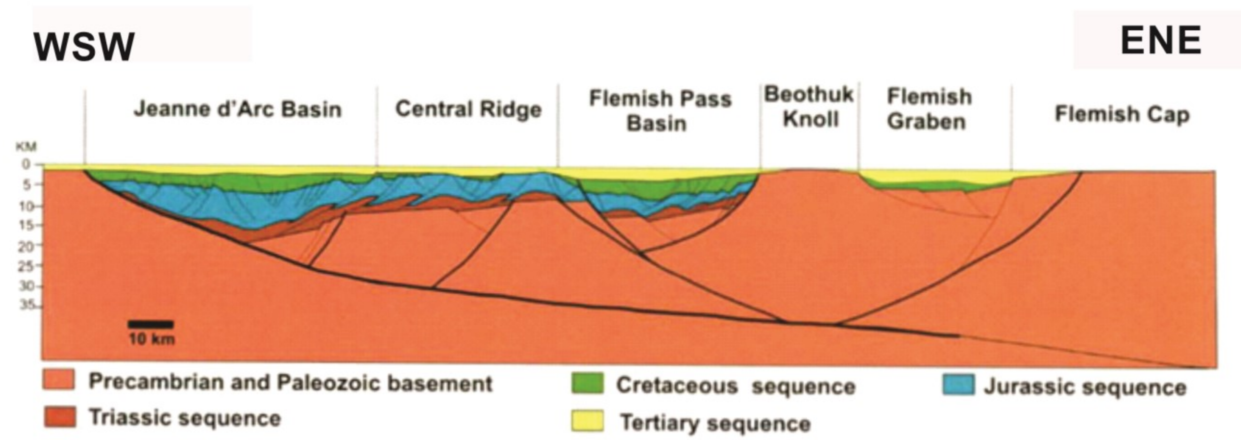

Figure 1.2: Cross-section from west to east across the Jeanne d'Arc Basin, Central Ridge, Flemish Pass Basin, Beothuk Knoll, Flemish Graben, and Flemish Cap.; from Enachescu (1988); modified by Lowe (2009).

A generalized stratigraphy of the Jeanne d'Arc Basin is presented in Figure 1.3. This stratigraphic chart is also considered applicable to the Flemish Pass Basin, as both possess a common stratigraphy and evolutionary history (Enachescu, 2012). All ages presented in this section follow the absolute timescale of Cohen et al. (2013). Precambrian metamorphic and Paleozoic metasedimentary and igneous rocks comprise the pre-Mesozoic basement (Enachescu, 1987). These rocks are considered to be an offshore extension of the Avalon terrane of the Appalachian Orogenic Belt (Williams & Hatcher, 1983; Haworth & Lefort, 1979; King et al., 1985; 1986). Upper Triassic sediments unconformably overlie the pre-rift basement and are associated with NW-SE oriented extension and the first rifting stage that affected the Grand Banks. These sediments comprise continental red beds of the Eurydice Formation and evaporites of the Argo Formation, the latter a result of recurrent influxes of salt water from the Tethys Sea

(Tucholke et al., 1989; McAlpine, 1990). This syn-rift fill was followed by regional thermal subsidence, and marine transgression, depositing thick accumulations of shale and limestone. The marine transgression is well represented by the Iroqouis Formation, where anhydritic dolomite is overlain by limestone (Sinclair, 1988). Overlying the limestone, the Downing Formation is a continuous shale sequence deposited in low energy conditions from the Pliensbachian (190.8 to 182.7 Ma) to the Bathonian (168.3 to 166.1 Ma) (Sinclair, 1988). From the Bathonian to Callovian (166.1 to 163.5 Ma), Voyager Formation was deposited over the Downing Formation (Sinclair, 1988). The Voyager Formation consists of an interbedded succession of shale, sandstone and limestone (Sinclair, 1988). The Rankin Formation, which is Oxfordian (163.5 to 157.3 Ma) to Kimmeridgian (157.3 to 152.1 Ma) in age, was deposited near the end of the thermal subsidence phase. Organic-rich shales were deposited in the Kimmeridgian, which represent the regional oil and gas source rock, and are the focus of this thesis.

A second rifting phase occurred during the Tithonian (152.1 to 145.0 Ma) to Valanginian (139.8 to 132.9 Ma) which reactivated movement along major faults. The onset of this rifting caused broad regional warping, uplift of the Avalon Uplift to the South, and the appearance of the Central Ridge structure (Sinclair, 1988). The appearance of the Central Ridge, in particular, marks the first point in time when the Jeanne d’Arc Basin and the northern Flemish Pass Basin could be considered two separate basins (Sinclair, 1988). During the Tithonian, the primary reservoir target in the Terra Nova Field, the Jeanne d'Arc Formation, was deposited. The Jeanne d’Arc Formation is interpreted as being derived from north-south oriented fluvial systems which eroded limestone, metaquartzite, chert cobbles and silica sand from the underlying Rankin Formation and deposited them near the Jeanne d’Arc Basin’s ancient shoreline (Sinclair, 1998).

The Terra Nova Formation is composed of sandstones, conglomerates, and shales (Sinclair, 1988). The boundary between the Rankin Formation and Jeanne d'Arc Formation represents an unconformity, with a significant time gap (Sinclair, 1988). At the end of the Tithonian, transgression resulted in marine silts and muds of the Fortune Bay Formation covering the Jeanne d'Arc Formation fluvial sands. During the Berriasian (145.0 to 139.8 Ma), the continuation of the second rifting phase caused continued uplift of sediment source regions, resulting in northward progradation of fluvio-deltaic sands of the Hibernia Formation into the Jeanne d'Arc Basin (Sinclair, 1988; Brown et al., 1989). The Hibernia Formation is the primary reservoir target for the Hibernia Field with the main reservoirs being medium- to very coarse-grained channel deposits and very-fine to medium-grained delta front sandstones. (Brown et al., 1989). Above the Hibernia Formation, the "B" marker Member oolitic, bioclastic limestone of the Whiterose Formation was deposited in the late Valanginian during the thermal sag phase of the second rifting episode and indicates a period of basin stability (Dearin, 2006; Sinclair, 1988). Overlying the "B" marker Member, the Catalina Member, composed of thinly interbedded shales and calcareous sandstones, was deposited (Sinclair, 1988). The thick, Hauterivian (132.9 to 129.4 Ma) shale sequence of the Whiterose Formation was deposited above the Catalina Member (Sinclair, 1988). In the Barremian (129.4 to 125.0 Ma), the "A" marker limestone, similar in composition to the "B" marker (Dearin, 2006), was deposited, as seen at both the Hibernia and White Rose fields.

In the Barremian, a coarsening upward succession of shales and sandstones known as the Avalon Formation prograded over the "A" marker limestone (Sinclair, 1988). This northward progradation is likely a result of rejuvenated uplift in the south (Avalon Uplift), which resulted in the development of the Aptian-Albian (~ 113.0 Ma) unconformity (Sinclair, 1988). The deposition of the Avalon Formation represents a period of basin-wide regression (Sinclair, 1988).

Deposition of the Ben Nevis Formation was significantly affected by the third and final rifting episode to affect the Grand Banks Basins, which occurred during Aptian-Albian time (Sinclair, 1993). As with the older Hibernia and Jeanne d'Arc Formations, coarse sediments of the Ben Nevis Formation were deposited in fluvial systems draining from north-south (Sinclair, 1988). These coarse sediments possess a transgressive character, hence a fining upward sequence which is recognizable throughout the Jeanne d'Arc Basin (Sinclair, 1988). They are composed of predominantly back-barrier to shoreface sediments (Sinclair, 1993). Stratigraphic stacking patterns were significantly affected by faulting during deposition of the Ben Nevis Formation (Dearin, 2006). Additionally, faulting during this time created structures such as tilted fault blocks where the majority of hydrocarbons are found in the basin (Sinclair, 1988). In addition to fault activity, salt diapirism was also important during Aptian-Albian time, resulting in localized salt ridges and pillars (Enachescu et al., 2000). As the Ben Nevis Formation is a regressive succession, eventually the laterally equivalent Nautilus Formation, composed of offshore shales, transgressed over the Ben Nevis Formation (Sinclair, 1988).

In the Cenomanian (100.5 to 93.9 Ma), the lower Dawson Canyon Formation and Petrel Member lime mudstones were deposited during a period of subsidence and low clastic input (Dearin, 2006). The deposition of these units represents the initiation of the final thermal sag within the basin (Dearin, 2006). Coarse-grained sandstones of the Otter Bay and Fox Harbour members were deposited during the late Cretaceous (Sinclair, 1988). These sandstones mark an important change in sediment provenance within the basin as they are interpreted as being derived from easterly prograding deltaic systems with a westerly source (Sinclair, 1988).

However, previous reservoir units (Jeanne d'Arc, Hibernia, Ben Nevis Formations) are interpreted as being derived from the south (Sinclair, 1988). The rapid progradation of these sandstones corresponds with the rift moving into the drift phase of the Falvey (1974) rift model where exponentially slowing thermal subsidence and expanding of the continental shelf and slope take place (Sinclair, 1988).

The Base Tertiary unconformity marks the top of the Upper Cretaceous succession, and is marked in the western Jeanne d'Arc Basin by a thin, highly radioactive bed, equivalent to the iridium-rich bed, which occurs worldwide at the Cretaceous-Tertiary boundary (Alvarez et al. 1980; Sinclair, 1988). This unconformity represents a large regional drop in relative sea level, perhaps caused by a regional rebound of the Atlantic margin (Enachescu & Hogg, 2005). Throughout the Tertiary, a marine succession with little deformation was deposited as low sediment input and long term subsidence dominated (McAlpine, 1990). This is indicative of a passive margin setting bordering the spreading Atlantic Ocean (Deptuck et al., 2003).

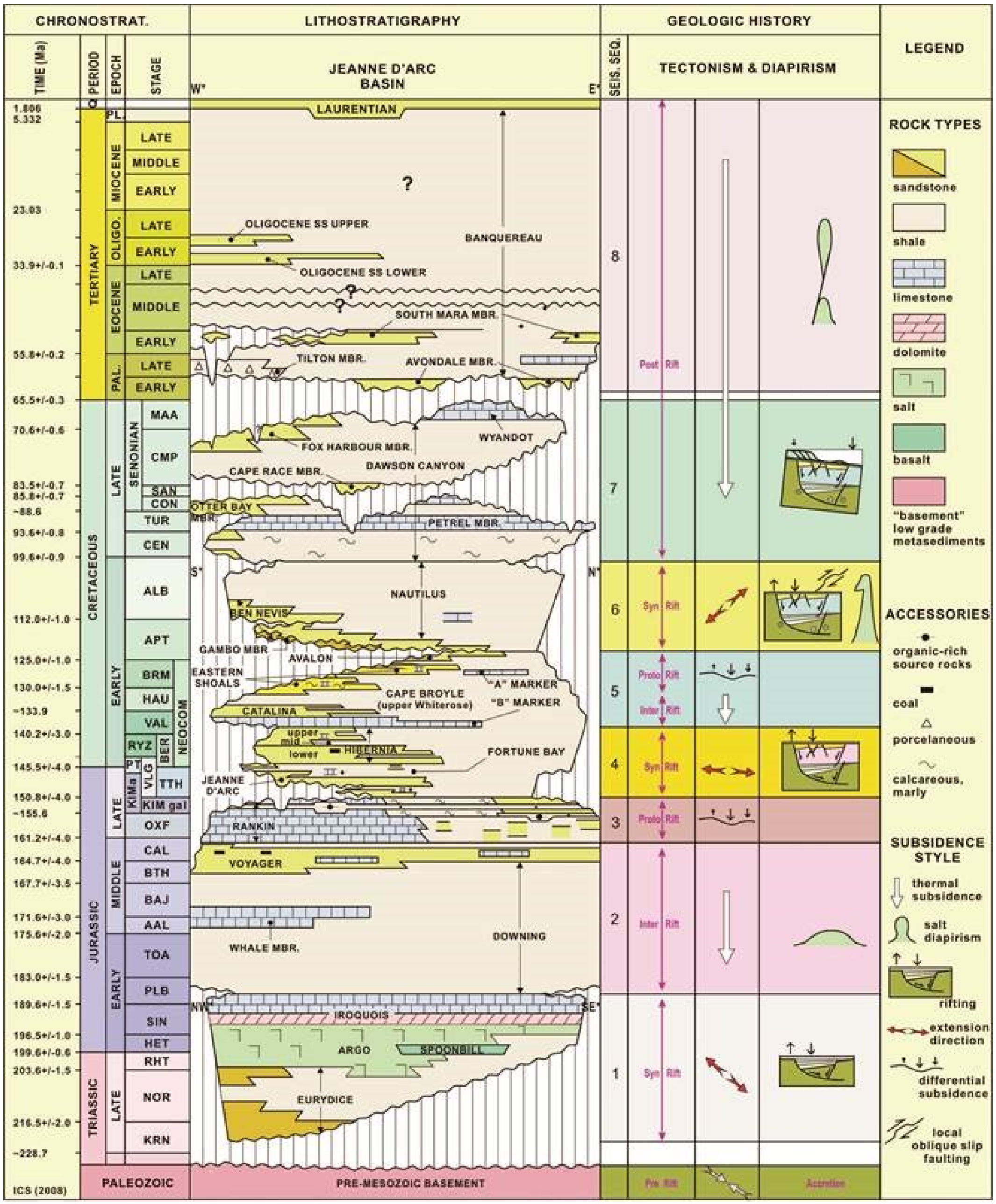

Figure 1.3: General stratigraphy of the Jeanne d'Arc Basin (broadly applicable to the Flemish Pass Basin). Primary reservoir units are the Jeanne d'Arc, Hibernia, and Ben Nevis/Avalon formations; from Enachescu (2012); originally modified from Sinclair (1993). The primary regional source rock is the Egret Member of the Rankin Formation. It is noted in this chart as a thin shale unit near the top of the Rankin Formation.

1.3 - Flemish Pass Basin Geological Overview

The Flemish Pass Basin is located on the continental shelf of the Grand Banks approximately 400 km east of St. John's, Newfoundland. It covers an area of approximately 30,000 km^2 with water depths between 400 and 1100 m (Foster & Robinson, 1993; DeSilva, 2000). The basin is separated from the Jeanne d'Arc Basin to the southwest by the Central Ridge, bounded to the east by Beothuk Knoll and Flemish Cap basement high, to the north by the Cumberland High, and to the South by the Avalon Uplift (Enachescu, 1987; Foster & Robinson, 1993; DeSilva, 2000) (Figure 1.1).

The Flemish Pass Basin shares a similar stratigraphy and common evolutionary history with the Jeanne d'Arc Basin (Enachescu, 2012). The geological history and a seismic-stratigraphic interpretation of the Flemish Pass Basin were reviewed by Foster & Robinson (1993), the latter based on seismic profiles and data from seven wells that had been drilled in the basin at that time. The basin was divided into megasequences, which are defined by Hubbard (1988) as genetically-related sets of sequences bounded by regional unconformities. Kimmeridgian source rocks fall within the MS1 megasequence (Figure 1.4). Because of the burial depth of the MS1 megasequence and the lack of well control, the authors struggled to map and interpret this megasequence across the whole basin. However, it was subdivided into smaller sequences and the MS1-50 sequence, which contains Kimmeridgian source rocks, was mapped and interpreted across the whole basin.

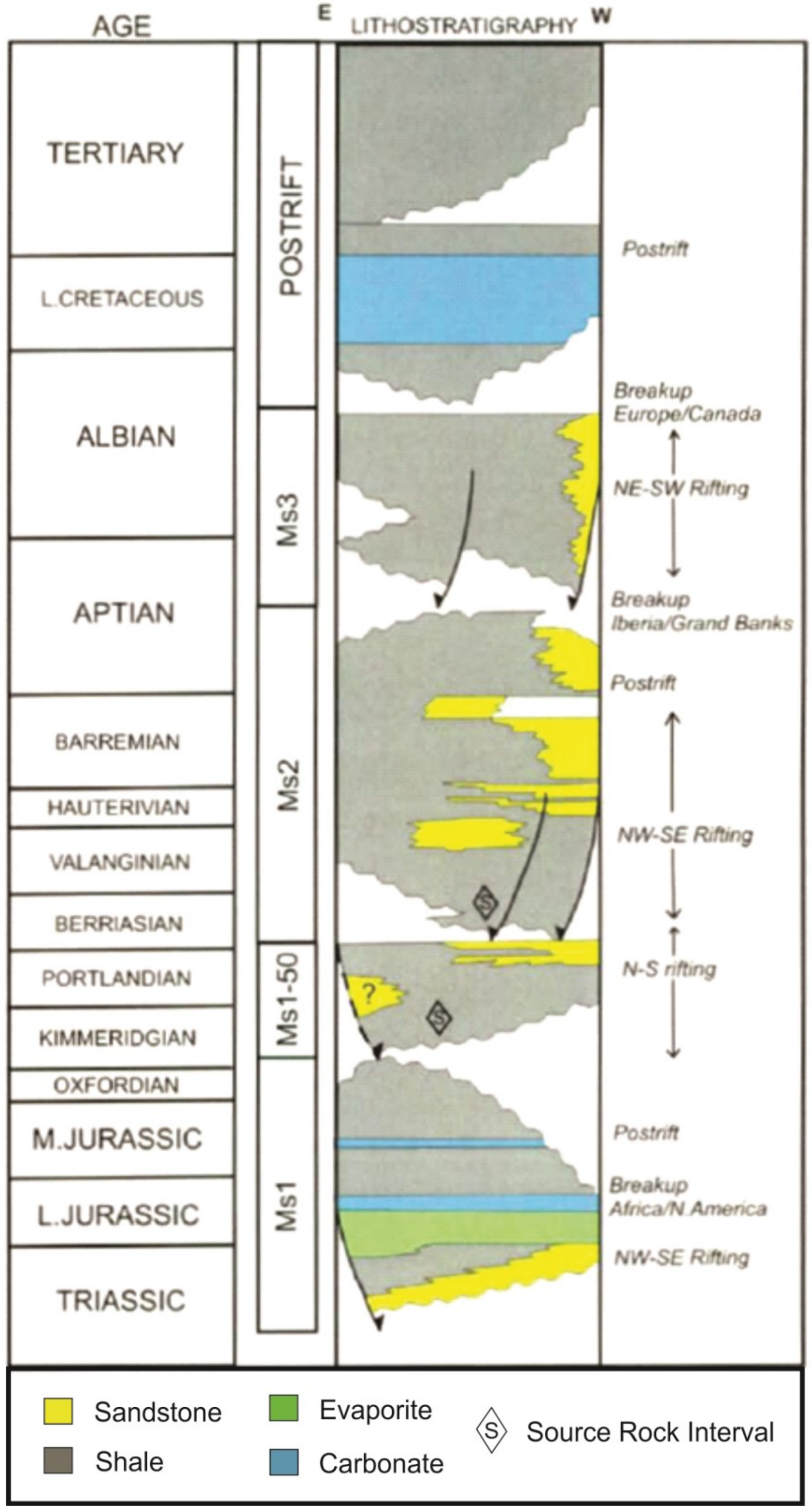

Figure 1.4: Generalized stratigraphy of the Flemish Pass Basin. Kimmeridgian source rocks fall within the MS1-50 sequence; modified from Foster & Robinson (1993).

Sediments of the MS1-50 sequence are found in two separate subbasins oriented in an approximately east-west orientation and divided by an intervening high found northeast of the Gabriel C-60 well (Figure 1.5) (Foster & Robinson, 1993). The majority of the northern subbasin lies to the west of the Baccalieu I-78 well (Foster & Robinson, 1993). Sediments in this northern subbasin onlap the subbasin margins to the south and east while in the southern subbasin, sediments onlap the previously mentioned intervening high (Figure 1.5) (Foster & Robinson, 1993). Foster & Robinson (1993) concluded that the MS1-50 unit thins to the south. They postulated that there is likely a facies change to limestone overlain by thick sandstone as seen in the Kyle L-11 well. The source rock facies are thought to be restricted to the central parts of the subbasins (Foster & Robinson, 1993). Foster & Robinson (1993) indicated that the source-rock facies itself is marine mudstone restricted to the lower part of the MS1-50 sequence. These mudstones grade upwards into marine or shoreline sandstones. These authors also suggested that the source rock facies is likely widespread in both subbasins as the seismic character of the unit is extremely uniform.

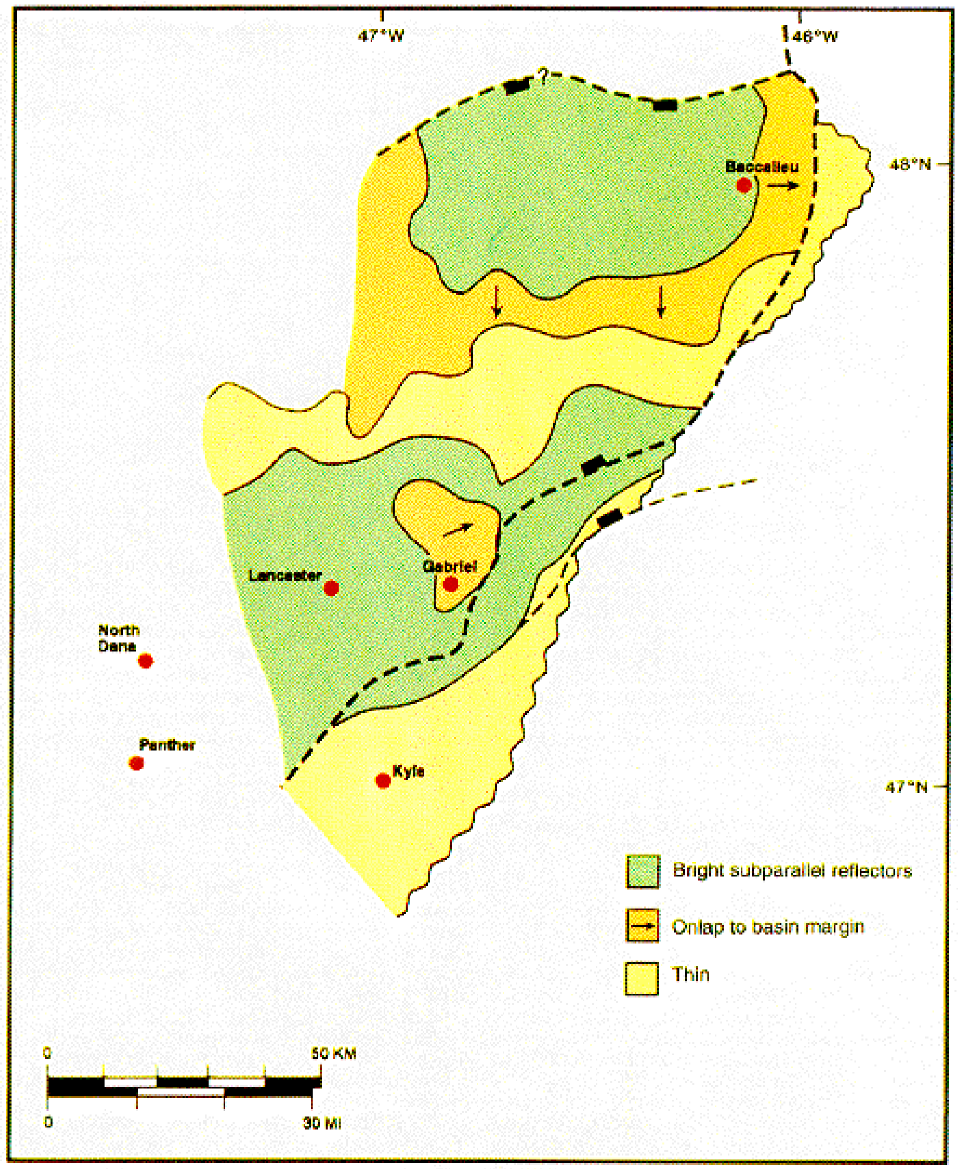

Figure 1.5: Seismic character map for the MS1-50 Sequence from Foster & Robinson (1993).

The overlying MS2 megasequence comprises sediments from the lower Berriasian to Aptian (Foster & Robinson, 1993). MS2 sediments were deposited in northeast-southwest trending subbasins: the southern Gabriel subbasin, and the Baccalieu subbasin to the North, between an intervening high (Foster & Robinson, 1993). The base of MS2 represents a major unconformity, and the onset of major faulting in the early Berriasian (Foster & Robinson, 1993).

Deposition of deep water mudstones began at the base of MS2, as this boundary also corresponds to significant regional subsidence (Foster & Robinson, 1993). The top of MS2 is likely Aptian, although it is difficult to determine as most of the wells are drilled in areas where much of the MS2 sequence is absent due to erosion during MS3 deposition (Foster & Robinson, 1993). The major Aptian unconformity found in the Jeanne d'Arc Basin is also present in the Flemish Pass Basin (Jansa & Wade, 1975; Tankard & Balkwill, 1989).

Sediments of the MS3 megasequence are Aptian to Albian in age and were deposited in basins oriented northwest–southeast (Foster & Robinson, 1993). However, deposition during the MS2 megasequence was in basins oriented northeast–southwest, indicating a significant change in basin orientation at MS3 time (Foster & Robinson, 1993). Some areas that were depocenters during MS2 deposition formed highs during the Aptian-Albian, and vice-versa (Foster & Robinson, 1993). Renewed extension in the Aptian likely contributed to rejuvenated dextral strike-slip motion along major northeast-southwest-trending faults (Sinclair, 1988). This movement resulted in the rearrangement of subbasins within the Flemish Pass Basin with the base of MS3 as a major unconformity (Foster & Robinson, 1993). Due to the lack of well control, depositional environment interpretations are limited to seismic facies analysis, which indicate the presence of muddy sediments containing sand-grade turbidites deposited in a deep marine environment (Foster & Robinson, 1993). The top of the MS3 megasequence is synchronous with the end of active tectonism and faulting within the basin and represents an important unconformity (Foster & Robinson, 1993).

The final megasequence as described by Foster & Robinson (1993) was deposited from the Albian to the present day. The base of this sequence coincides with the conclusion of active faulting and units deposited in this megasequence are equivalent to those deposited in the Jeanne d'Arc Basin at the same time such as the Petrel limestone (Foster & Robinson, 1993). The base of this sequence onlaps MS3 and older highs and fills in adjacent lows, while the upper portion of the sequence is primarily a regressive Cenozoic shelf system with sediment being derived from the northwest (Foster & Robinson, 1993). Deposition of this shelf system continues to the present day (Foster & Robinson, 1993).

The oil and gas potential of the Flemish Pass Basin has been of great interest, particularly in recent years, as several large discoveries have been made and the existence of mature Upper Jurassic source rocks (the focus of this thesis), as well as the presence of potential reservoir units of Late Jurassic and Early Cretaceous age, has been confirmed. Additionally, industry 3-D seismic mapping has identified numerous significant structural traps, particularly some large faulted extensional anticlines (DeSilva, 2000; Enachescu & Hogg, 2005). In 2004, the Canada-Newfoundland and Labrador Offshore Petroleum Board and the Geological Survey of Canada estimated that the Flemish Pass Basin contains 1.7 billion barrels of undiscovered petroleum resources (50% probability), with a range of field sizes from 528 to 44 million barrels (Enachescu, 2014).

The Kimmeridgian source rocks are the primary focus of this thesis and will be discussed in detail in the next section, but a brief overview of the source rock potential will be presented here. Mature Kimmeridgian source rocks were intersected in the Baccalieu I-78 well in the northern Flemish Pass. RockEval analysis of samples from this well from McCracken (2000) defined total organic carbon (TOC) values from 0.92 – 4.83% (average 2.1%), and hydrogen indeces (HI) ranging from 109 – 510 mg HC/g TOC (average 355 mg HC/g TOC), indicating type II, marine source rocks. Analyses of oil samples from sandstone reservoir intervals in Mizzen L-11 (Fowler, 2007) and Gabriel C-60 (Creaney & Alsion, 1987) indicated the source rock possessed characteristics similar to the Egret Member of the Jeanne d'Arc Basin, with a likely more terrestrial component to the organic matter. Excellent reservoir quality sandstones were intersected in the Mizzen L-11 well into Upper Jurassic sandstones as well as 5 m of non-commercial oil pay in Cretaceous sandstone (Enachescu, 2006). In 2009, StatoilHydro drilled the Mizzen O-16 well, and discovered 26 m of oil pay. They successfully tested the discovery and were able to secure a Significant Discovery License from the Canada-Newfoundland and Labrador Offshore Petroleum Board (Cody et al., 2012). Oil was found in the uppermost sand of the Tithonian, in a unit laterally equivalent to the Jeanne d'Arc sandstone of the Jeanne d'Arc Basin (Cody et al., 2012). This discovery in the North Flemish Pass Basin has demonstrated the existence of a proven petroleum system, and Statoil has continued their evaluation of this system with a series of regional projects (Cody et al., 2012). In addition to the O-16 well, Statoil made significant discoveries in both the Harpoon O-85 and Bay du Nord C-78 wells in 2013. In these wells, light, sweet oil was discovered in Tithonian fluvial sandstones (McDonough, 2014). The Bay du Nord prospect is estimated to contain over 300 million barrels of recoverable oil (McDonough, 2014). The data from these wells, however, remains classified at this time.

1.4 - Central Ridge Geological Overview

In addition to wells in the Flemish Pass Basin, samples for this thesis were also collected from two wells, Panther P-52, and South Tempest G-88, located in the adjacent Central Ridge (Figure 1.1 & Figure 1.2). The Central Ridge is a faulted intrabasinal high that separates the Jeanne d'Arc and Flemish Pass basins. The geological evolution of the Central Ridge is similar to that of the Flemish Pass Basin. Some of the wells drilled in the Central Ridge are mentioned by Foster & Robinson (1993) and included in their interpretation of the Flemish Pass Basin. Enachescu (1987, 1988) stated that the Central Ridge was a relatively high area during the initial Late Triassic rifting episode. It was likely in a relatively elevated position until the late Jurassic

(Enachescu, 1988). Sinclair (1988) demonstrated that the major appearance and uplift of the Central Ridge structure was predominantly Tithonian, and that this marks the initial isolation of the Jeanne d'Arc Basin from the northern Flemish Pass Basin. By the Early Cretaceous, the ridge reached its maximum elevation, and was exposed as an island chain or peninsula (Enachescu, 1988). Since the island chain or peninsula was subaerially exposed, some of the Upper Jurassic and Lower Cretaceous sediments were eroded and are missing (Enachescu, 1988). However, approximately 5 km of Upper Triassic to Upper Jurassic sediments remain a part of the succession at the Central Ridge (Enachescu, 1988).

There have been both oil and gas discoveries in the Central Ridge despite sparse drilling. Oil has been found in the South Tempest G-88 well, and gas at both North Dana I-43 and Trave E-87. High quality Kimmeridgian source rocks have been intersected in North Dana I-43, South Tempest G-88, and Panther P-52 and the ridge possesses a variety of structural trapping configurations (Enachescu, 2014; DeSilva, 1994). These include tilted fault blocks, and inversion structures, in addition to a number of stratigraphic trapping possibilities (DeSilva, 1994). Kimmeridgian Upper and Lower Tempest sandstone units are interbedded with shales and siltstones of the Upper and Lower Kimmeridgian Source Rock units. The Tempest sandstones are described as fine- to medium-grained sandstones interbedded with shales. They are interpreted as turbidite deposits (Sinclair 1988; McAlpine, 1990; DeSilva, 1994) and flowed oil and gas at rates up to 1250 bbl per day and 4.9 mmcf per day, respectively, in the South Tempest G-88 well (Canada-Newfoundland and Labrador Offshore Petroleum Board (CNLOPB), 1990). The North Dana I-43 well flowed 12 mmcf and 292 bbl per day of gas and condensate, respectively, from the equivalent Tempest sandstones (CNLOPB, 1990). The Tempest sandstones are interpreted as having been deposited from turbidity currents flowing to the north as structurally high areas exist to the South (DeSilva, 1994). In addition to addressing the provenance of Kimmeridgian source rocks, this thesis will also investigate the provenance of interbedded Tempest sandstones, and determine whether heavy mineral data support the interpretation of a southerly provenance.

1.5 – Grand Banks Kimmeridgian Source Rock

This study is focused predominantly on Kimmeridgian source rocks of the Flemish Pass Basin and Central Ridge and numerous studies have investigated their source rock potential. These Kimmeridgian source rocks are divided into specific members of the Rankin Formation. The members are called the Upper Kimmeridgian Source Rock and Lower Kimmeridgian Source Rock although McCracken (2000) showed that the Rankin Formation itself also possesses great source rock potential. In the Jeanne d'Arc Basin, these studies have been focused on the Egret Member, the laterally equivalent Kimmeridgian source rock. Although not directly related to provenance, previous studies on the source rock geochemistry provide important information about the depositional environment of these units as well as the amount of clastic input in the area at this time. These factors are important to this study. Creaney & Allison (1987) studied the Egret Member in the Jeanne d'Arc Basin and Central Ridge and attempted to correlate the unit with rocks of the Flemish Pass Basin. Their aim was to quantitatively characterize the organic geochemistry of the source interval using oil chromatograms, high H indices, and H/C ratios. Their results indicated that oil from the Egret Member was derived from type II, marine, algal-dominated organic matter. Creaney & Allison (1987) concluded that the source rock appears to be present in the centre of the basin as a thick, organic-rich mudstone where sedimentation was not affected by eustatic changes. However, at the basin margins, the Egret Member is thinner, and interbedded with reservoir sands and carbonates. They postulated that as sea level varied, the oxic/anoxic boundary in the water column probably fluctuated accordingly. This led to interbedded source and non-source intervals in these areas.

Creaney & Alison (1987) examined one well (Gabriel C-60) in the Flemish Pass Basin. The well did not penetrate Kimmeridgian source rocks, but an oil sample was obtained from a reservoir interval at 3995 m depth. This Gabriel oil had a higher pristine/phytane ratio than the samples from the Jeanne d'Arc Basin indicating that the source rock in the Gabriel well was likely deposited in a somewhat more oxidizing environment (Creaney & Alison, 1987). Creaney & Alison (1987) suggested that the source rock at Gabriel was deposited in a more proximal environment in the Flemish Pass. This is consistent with Foster & Robinson's (1993) interpretations that the source rock at this location onlaps the basin margins to the east.

McCracken et al. (2000) were the first to analyze the organic geochemistry of samples from the Kimmeridgian source rocks in the Flemish Pass Basin. Samples for their study were collected from the Baccalieu I-78 well in the northern Baccalieu subbasin. McCracken et al. (2000) confirmed, from geochemical and geophysical evidence, the existence of Upper Jurassic organic-rich source rocks that extend northeastward from the Jeanne d'Arc Basin into the northern Flemish Pass.

RockEval analysis results demonstrate TOC values from 0.92 – 4.83% (average 2.1%), and HI ranging from 109 – 510 mg HC (hydrocarbons)/g TOC with an average of 355 mg HC/g TOC (McCracken et al., 2000). HI is an abbreviation for the Hydrogen Index; which is derived from the ratio of Hydrogen to TOC (McCarthy et al., 2011). It is often used as a maturation indicator for source rocks. McCracken et al. (2000) classified most of the samples as Type II, marine source rocks, similar to those in the Jeanne d'Arc Basin. Additionally, biomarker analyses indicate that the samples are genetically similar to oils in the Jeanne d'Arc Basin (McCracken et al., 2000).

McCracken et al. (2000) noted a distinct gravity and magnetic anomaly near the Baccalieu well that continued into the Jeanne d'Arc Basin. McCracken et al. (2000) theorized that this anomaly corresponds to the regions in which the Upper Jurassic source-rock facies was deposited and remains preserved today.

Fowler et al. (2007) analyzed a small sample of oil from Upper Jurassic sandstone in the Mizzen L-11 well. For the most part, the sample possesses characteristics similar to oils from the Egret Member in the Jeanne d'Arc Basin (Fowler et al., 2007). Similarities include the saturate hydrocarbon and gasoline range characteristics, and terpane distributions (Fowler et al., 2007). However, pristane/phytane ratios of the Mizzen oil are elevated in comparison with those analyzed from Jeanne d'Arc Basin oils (Fowler et al., 2007). This indicates a potential terrestrial component to the organic matter (Fowler et al., 2007). This terrestrial component indicates potential changes in the depositional environment of the Upper Jurassic source rock in the Flemish Pass Basin (Fowler et al., 2007). Alternatively, it may reflect the mingling of hydrocarbons from multiple sources (Fowler et al., 2007); an interpretation supported by the presence of multiple source rock intervals in other nearby wells such as Panther P-52 (Enachescu, 2012).

Bateman (1995) completed a study on numerous wells intersecting the Egret Member in the Jeanne d'Arc Basin in which he analyzed the mineralogical and geochemical (organic and inorganic) compositions of the source rock unit. Several analytical techniques were used including X-ray diffraction, whole rock geochemistry, and Rock-Eval analysis. XRD analysis revealed samples from the eastern side of the basin had elevated quartz contents whereas samples from the southern edge of the basin possessed high calcite contents (Bateman, 1995). The elevated quartz contents on the eastern side of the basin were attributed to the presence of a Late Jurassic delta complex which resulted in an influx of terrestrial-derived sediments in this area (Fowler & McAlpine, 1994; Bateman, 1995). The high calcite contents in the southern portion of the basin were attributed to being in close proximity to a nearby carbonate bank or shelf (McAlpine, 1990; Bateman, 1995). With respect to the clay mineralogy, Bateman (1995) suggested that the prevalence of illite and illite/smectite indicated that detritus in these source rock samples was likely delivered from source terranes composed of mica-rich granites and metamorphic rocks (Weaver, 1989). In addition, Bateman (1995) found that Egret Member shales possessed abundant quantities of kaolinite relative to other Mesozoic shales. Weaver (1960) stated that kaolinite is uncommon in marine offshore sediments. Bateman (1995) interpreted the increased abundances of kaolinite in Egret Member samples to indicate a detrital influx from weathered kaolinite-rich rocks. A similar interpretation was suggested by Hurst (1981) for North Sea Jurassic shales. Gradstein et al. (1990) reported that deposition of kaolinite-rich sediments in the Jurassic was common due to the humid, subtropical climate of that time. Bateman (1995) suggests that chlorite in the samples is derived from mica-rich granites and chlorite-bearing metamorphic rocks (Weaver, 1989).

Bateman's (1995) whole rock geochemistry of the Egret Member shales is consistent with the XRD data of varying quartz and calcite contents within the basin. In addition to these observations, a lower than expected P_2O_5 concentration was noted in the Egret shales by Bateman (1995). This was attributed to samples containing minor amounts of apatite (Bateman, 1995). Apatite precipitation is uncommon under anoxic conditions (Ingall et al., 1993; Riediger

& Bloch, 1995). Bateman (1995) suggests that the low apatite content is indicative of anoxic bottom waters during Egret deposition. Bateman (1995) also evaluated the whole rock geochemistry of the Egret samples which allows for an evaluation of the C-Fe-S systematics of the depositional system. Results reveal elevated sulfur values, suggesting deposition in a euxinic environment (Leventhal, 1983).

Bateman (1995) compared Egret Member samples to PAAS (post Archean average shale from Taylor & McLennan (1985)) and BPS (Average British Paleozoic shale from Jones & Plant (1989)). Egret Member samples were found to contain less alkalis than the PAAS & BPS. Bateman (1995) attributed this to a lack of feldspars and chlorite in the Egret Member. Citing Norry et al. (1994), Bateman (1995) concluded that the Egret is likely a very mature sediment and that feldspar and chlorite have been lost through several sedimentary cycles.

Bateman (1995) described four main lithological facies within the Egret Member: 1) a dark brown laminated shale; 2) a grey to grey-brown shale; 3) a light brown marlstone/limestone; 4) a fine-grained sandstone and siltstone, and provided a depositional model to explain the origin of these units. According to the model, dark brown laminated shales were deposited during highstands via pelagic sedimentation of clays and marine organisms (Bateman, 1995). The grey to grey-brown unlaminated shales are interpreted to have been deposited in a shallower environment during periods of lower sea level (Bateman, 1995). The marlstones and claystones were likely deposited under oxic conditions during periods of low sea level (Bateman, 1995). Meanwhile, Bateman (1995) links sandstone deposition to turbidity currents that deposited sediments from more proximal environments into more distal, basinal environments.

1.6 - Pre-Mesozoic Basement Geology

Introduction – 1.6.1

Source areas supplying detritus to the Flemish Pass Basin and Central Ridge during the Kimmeridgian include pre-Mesozoic basement rocks from possibly both sides of the North Atlantic, including the North American Conjugate Margin as well as the Irish and Iberian conjugate margins. The geology of each potential source region will be reviewed here. To accompany the description of each individual region, isotopic age constraints are provided for the major rock units. This provides the foundation for correlations to detrital zircon U-Pb geochronology presented in this study in later chapters that will address the provenance of Kimmeridgian rocks using U-Pb detrital zircon geochronology. In addition, a summary chart is presented in Figure 1.6 with the major ages of each potential source terrane.

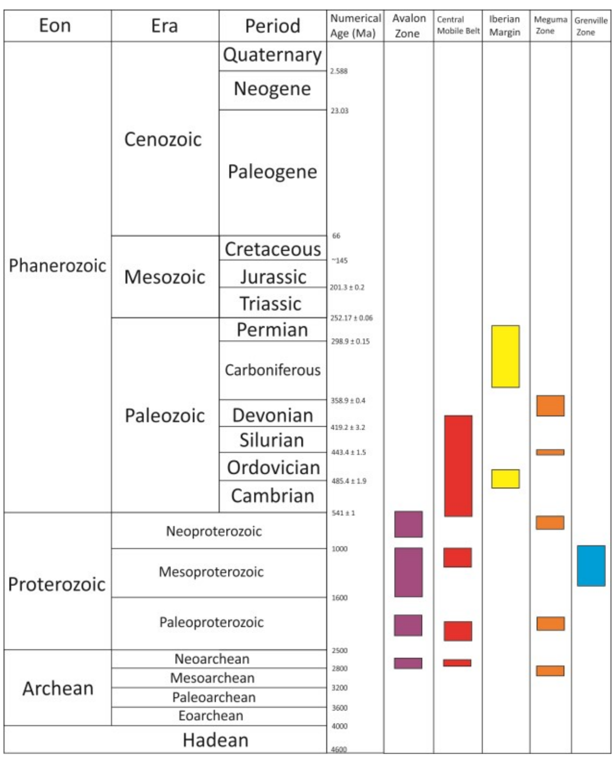

Figure 1.6 - Summary chart of major ages of potential source terranes. Ages of time periods from Cohen et al. (2013).

1.6.2 - Avalon Zone

The pre-Mesozoic basement underlying the Grand Banks is composed of rocks of the Avalon Zone of the Appalachian Orogen (Haworth & Lefort, 1979; King et al., 1985, 1986; Williams et al., 1999) (Figure 1.7). The Avalon Zone in Newfoundland is a Late Precambrian succession of volcanic rocks with associated intrusive rocks. This volcanic succession is overlain by deep-marine, deltaic, and terrestrial sedimentation (King, 1988). Similar rocks can be found in the southern part of the British Caledonides, the Hercynides of France and Iberia, and on the northern and eastern margins of the West African shield (Rast et al., 1976; Rast, 1980; O'Brien et al., 1983). The entire Late Precambrian succession is relatively unmetamorphosed (King, 1990) and ranges in age from 760 – 540 Ma (Pollock et al., 2009). The rocks have been subject to two major deformation events: the late Precambrian Avalonian Orogeny and the mid-Paleozoic Acadian Orogeny (King, 1990).

The base of the Late Precambrian successions of the Avalon Zone on the island of Newfoundland comprise arc phase magmatic and volcanic igneous rocks such as the Marystown and Harbour Main groups and Holyrood Granite, with U-Pb zircon ages from 586 to 632 Ma (Krogh et al., 1987). Older units, such as the Wandsworth Gabbro of the Burin Group, Burin Peninsula, the Tickle Point Formation calc-alkaline rhyolite flows, and granites of the Furby's Cove Intrusive Suite were radiometrically dated at 767 ± 2.2 Ma, 682.8 ± 1.6 Ma, and 673 ± 3 Ma, respectively (Krogh et al., 1987; Swinden & Hunt, 1991; O'Brien et al., 1996). Overlying the Neoproterozoic magmatic and volcanic rocks is a succession of clastic sequences including the Conception, Connecting Point, St. John's, Musgravetown and Long Harbour groups. Detrital zircons in the Conception Group and St. John's Group are predominantly 570 – 650 Ma with minor Mesoproterozoic and Paleoproterozoic input (Pollock et al., 2009). In parts of the onshore Newfoundland Avalon Zone, Cambrian – Ordovician marine-shelf sedimentary rocks unconformably overlie the Neoproterozoic clastic sequences (King, 1990). Detrital zircons from the Cambrian – Ordovician cover sequences are dominantly 500 – 680 Ma, but unlike Neoproterozoic rocks on the Avalon Peninsula, have larger quantities of Mesoproterozoic (1.0 – 1.6 Ga) and Paleoproterozoic (1.9 – 2.3 Ga), and also some Late Archean zircons (2.7 – 2.8 Ga) (Pollock et al. 2009).

Information about the offshore Avalon Zone is limited as, typically, exploration or petroleum wells rarely reach basement. However, magnetic anomalies indicate that the Avalon Zone extends as far east as the edge of the Grand Banks (Haworth & Lefort, 1979). Magnetic anomalies that can be traced from onshore also suggest that some of the basement is composed of arc-phase igneous rocks; however, Precambrian igneous basement has not been encountered offshore besides at the Flemish Cap (Haworth & Lefort, 1979; King et al., 1985). Samples of granodiorite from the Flemish Cap, a submarine knoll east of the Flemish Pass Basin, gave discordant U-Pb zircon ages with upper intercepts of 751 and 833 Ma (King et al., 1985). This suggests an age of intrusion sometime between ca. 750 and 830 Ma (King et al., 1985). The Flemish Cap granodiorite is thus interpreted to be part of the Avalon Zone, although it likely represents a much older part of the Avalon Terrane than what is seen further west on the island of Newfoundland (King et al., 1985).

The offshore subcrop extensions of the Neoproterozoic clastic sequences onshore are poorly constrained (Lowe, 2009). However, in the Virgin Rocks – Eastern Shoals area on the Bonavista Platform and on the Flemish Cap, Precambrian cover sequences have been drilled (Lilly, 1966; King et al., 1985). It is thought that these cover sequences extend over the eastern margin of the Bonavista Platform, the Central Ridge area, and beneath the shallow cover sequences of the Flemish Cap (King et al., 1985; Bell & Howie, 1990). Lower Paleozoic clastic cover sequences found offshore are considered equivalent to those of the Avalon Peninsula's Bell Island Group, and are thought to occur in the Avalon Uplift and Bonavista Platform areas, as well as on the shelf and slope area beneath the West Orphan Basin, the Northern Jeanne d'Arc Basin, and Flemish Pass Basin (King et al., 1986; Bell & Howie, 1990). These Lower Paleozoic clastic rocks have been drilled at both the Cumberland B-55 well and the Linnet E-63 well (Figure 1.1), where 400 m of Ordovician shales and siltstones, and 320 m of Lower Paleozoic shales and siltstones were encountered (CNLOPB, 2007). The Kyle L-11 (Figure 1.1) well in the Flemish Pass Basin drilled a significant section (700 m) of metasedimentary basement rocks (CNLOPB, 2013). However, the age of this sequence is not reported.

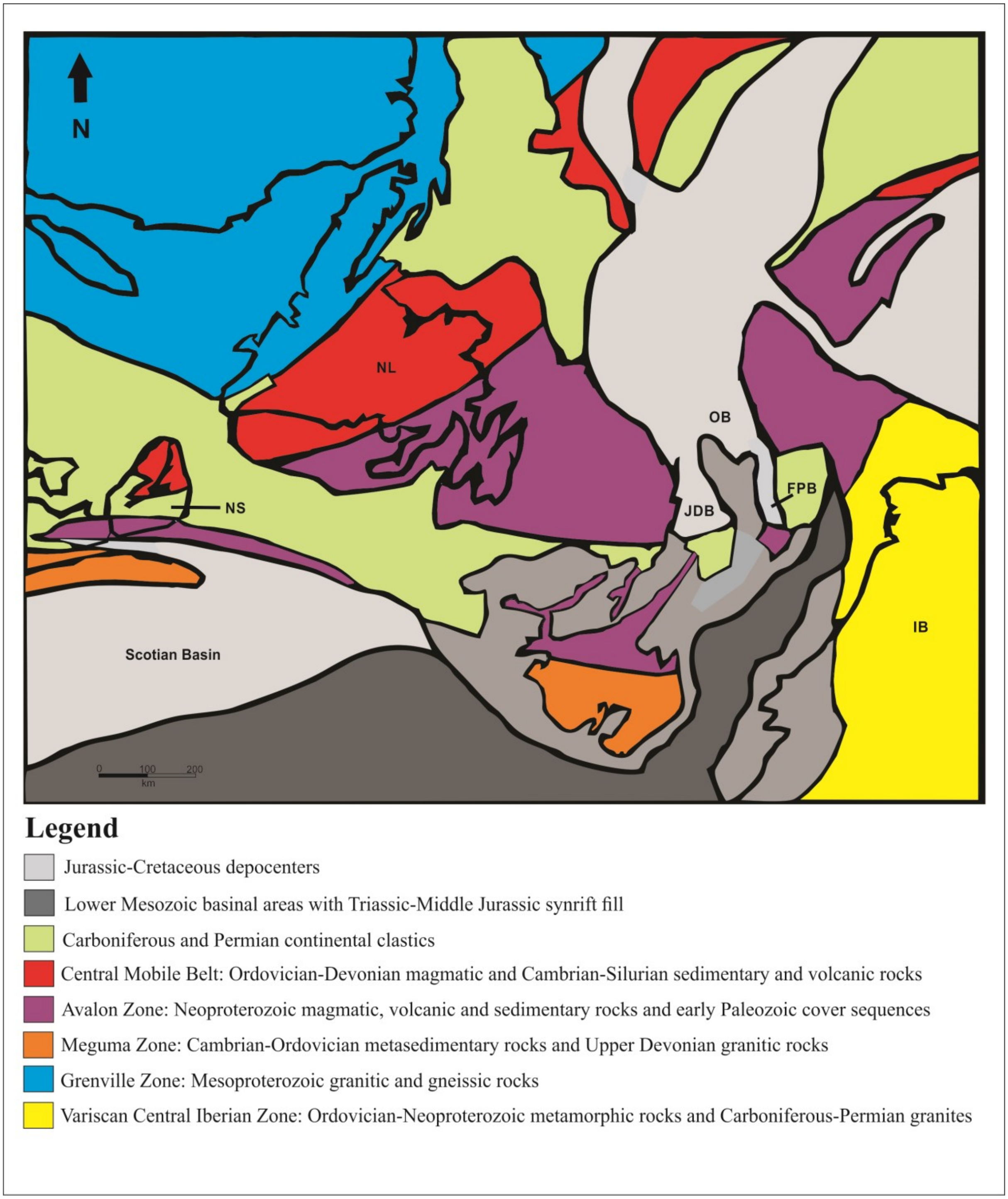

Figure 1.7 - Pre-Mesozoic basement geology of the Grand Banks and surrounding regions; modified from Lowe et al. (2011). Basement geology compiled from Haworth & Lefort (1979), Barrs et al. (1979), Priem & den Tex (1984), King et al. (1986), Capdevila & Mougenot (1988), Bell & Howie (1990), and Johnson et al. (2001). Black lines represent boundaries between terranes as well as modern day coastline. Study area is the Grand Banks of Newfoundland, eastern Canada. NL – Newfoundland; NS – Nova Scotia; OB – Orphan Basin; JDB – Jeanne d'Arc Basin; FPB – Flemish Pass Basin; IB – Iberian Peninsula.

1.6.3 - Meguma Zone

The furthest outboard Appalachian terrane, the Meguma Zone, may have also been an important source for detritus to the Grand Banks during the Late Jurassic (Figure 1.7). The Meguma Zone is exposed onland in southern Nova Scotia, but extends over a much larger area off shore (Hutchinson et al., 1988; Keen et al., 1991; Pe-Piper & Jansa, 1999). The Cambrian – Ordovician Goldenville Group was deposited on a Gondwanan passive margin and is composed of the oldest exposed rocks of the Meguma Zone (van Staal, 2007). The Goldenville Formation was deposited on the slope to outer shelf (van Staal, 2007) and is overlain by the Halifax Group, a Lower Ordovician shallowing-upward succession (Schenk, 1997). The Annapolis Supergroup, composed of Upper Ordovician to Lower Devonian shallow marine siliciclastic rocks as well as Upper Ordovician – Lower Silurian (~442-438 Ma) rift-related bimodal volcanic rocks, disconformably overlies the Halifax Group (van Staal, 2007; Schenk, 1997; Keppie & Krogh, 2000; MacDonald et al., 2002). Unconformably overlying the Annapolis Supergroup are continental and shallow-marine, Upper Devonian – Lower Carboniferous sedimentary rocks (Martel et al., 1993). These are overlain by Upper Carboniferous continental sedimentary rocks. During the Acadian Orogeny (Middle to Late Devonian; 380 – 365 Ma), numerous metaluminous to peraluminous granites were emplaced in the Meguma Zone (Clarke et al., 1997; Kontak et al., 2004).

Krogh & Keppie (1990) analyzed detrital zircons from the Goldenville Formation of the Meguma Zone. They found major populations of late Neoproterozoic (550 – 750 Ma), Middle Paleoproterozoic (2.0 – 2.2 Ga), and Archean (2.8 – 3.0 Ga) zircon grains. White et al. (2008) analyzed detrital zircons from younger sequences of the Meguma Zone. Similar detrital zircon ages to the Goldenville Formation were found, except that Archean aged grains are absent and a small population of Mesoproterozoic (1.0-1.2 Ga) grains is present (White et al., 2008).

Magnetic anomalies in the basement rocks indicate offshore extensions of the Meguma Zone reach as far as the southern Grand Banks, and comprise the basement to the Avalon Uplift (Haworth & Lefort, 1979). The Collector Magnetic Anomaly represents the boundary between the Meguma and Avalon zones (Haworth & Lefort, 1979). Furthermore, rocks of the Meguma Zone have been encountered as basement in a number of offshore wells. In particular, the Jaeger A-49 well in the southern Grand Banks encountered granitic basement, which yielded a K-Ar whole-rock isotopic age of 376 ± 17 Ma (Amoco Canada, 1973). This is indicative of the Meguma Zone as this zone is intruded by abundant Late Devonian granites (Kreuger Enterprises, 1972; Clarke et al., 1997; Kontak et al., 2004). Although Late Devonian intrusions also exist in Newfoundland, the Meguma Zone is characterized by abundant intrusions of this age, and represents a more likely correlative for this offshore extension. Pe-Piper & Jansa (1999) dated a number of plutonic rocks encountered in wells drilled offshore Nova Scotia and found predominantly Devonian intrusions.

1.6.4 - Central Mobile Belt

Rocks of the Gander and Dunnage zones of the Newfoundland Central Mobile Belt are also potential important sources for detritus to the Grand Banks during the Kimmeridgian (Figure 1.7). Rocks in these zones are composed of the vestiges of the Iapetus Ocean, and are also present in the offshore as basement (Lowe, 2009). The Dunnage Zone consists of arc-related rocks and terranes that existed within the Iapetus Ocean (Stern & Bloomer, 1992) that have peri-Laurentian (further west) or peri-Gondwanan origins (further east) separated by a major suture. Rock types within the Dunnage Zone include arc-associated volcanic rocks and related sedimentary successions. The Gander Zone, however, represents a fragment of a Gondwanan passive margin (van Staal, 1994). Sedimentary rocks are important in the Gander Zone, but Silurian to Devonian granites are also common, as well as some metamorphic rocks. For the most part, magmatic rocks of the Gander and Dunnage zones range in age from Late Cambrian to Early Devonian, with some rare Late Devonian granites (Dallmeyer et al., 1981; Chorlton & Dallmeyer, 1986; Dickson, 1990; O'Neill, 1991; Currie, 1995; Dube et al., 1996; Valverde-Vaquero et al., 2003; Valverde-Vaquero et al., 2006). O'Neill (1991) analyzed detrital zircons from the Gander Zone's Jonathans Pond Formation and found zircons of Mesoproterozoic (1.0 – 1.3 Ga), Paleoproterozoic (2.0 – 2.2 Ga), and Archean (~2.7 Ga) ages, as well as an individual Early Cambrian (~540 Ma) grain. Pollock et al. (2007) analyzed the detrital zircons from Late Ordovician to Silurian sedimentary successions in the Dunnage Zone and revealed populations with abundant Ordovician to Late Neoproterozoic (450 – 550 Ma), Mesoproterozoic (1.0 – 1.5 Ga), and Late Paleoproterozoic (1.6 – 1.8 Ga) grains, and minor Late Archean (2.7 – 2.5 Ga) grains.

1.6.5 - Carboniferous Sedimentary Basins

Numerous Carboniferous sedimentary basins were developed atop the Appalachian Orogen in Newfoundland, the Northeast Newfoundland Shelf, and elsewhere in the Maritimes and may represent significant potential sources for Late Jurassic detritus to the Grand Banks (Figure 1.7). These Carboniferous Basins include the Deer Lake and Bay St. George basins on the island of Newfoundland, as well as offshore extensions of these Carboniferous basins in the St. Anthony, Magdalen, and Sydney basins. The Carboniferous rocks are predominantly continental clastic sedimentary rocks, and have been intersected by several offshore wells. For instance, a thick (1500 m) succession of Carboniferous red-brown sandstones and siltstones were drilled in the Hare Bay E-21 well, West Orphan Basin. Other Carboniferous clastic sequences were intersected in the southern Grand Banks area in wells Hermine E-94, Gannet O-54, and Sandpiper J-77 (Bell & Howie, 1990). Each of the drilled sequences have been considered equivalent to adjacent Horton, Windsor, Canso, Riversdale, or Pictou Groups onshore in Nova

Scotia (BP Canada, 1979; Bell & Howie, 1990). The Avalon Uplift, south of the Flemish Pass Basin, is also thought to be covered by equivalent Upper Paleozoic (Devonian – Pennsylvanian) sequences (Barrs et al., 1979, Bell & Howie, 1990). Detrital zircons from the Horton Group, mainland Nova Scotia, were analyzed by Murphy & Hamilton (2000) and exhibit major populations of Neoproterozoic (550 – 700 Ma), and Paleoproterozoic (2.0 – 2.2 Ga) grains with less significant Devonian (370 – 380 Ma) and Silurian (411 Ma) grains. On the island of Newfoundland, detrital zircons from sandstones of the Carboniferous Deer Lake and Bay St. George basins are predominantly Ordovician – Silurian in age and are thought to have been derived from volcanics of the Newfoundland Dunnage Zone (Sylvester, 2012). Some Mesoproterozoic grains are also present, likely derived from Grenvillian basement to the north and west (Sylvester, 2012).

1.6.6 - Mesozoic Igneous Rocks

In addition to pre-Mesozoic basement, contemporaneous rift-related igneous rocks may also have been an important source for detritus to the Grand Banks in the Late Jurassic. Syn-rift igneous rocks have been identified onland in Newfoundland, as well as in offshore wells. In Central Newfoundland, a small ultramafic pluton called the Budgell Harbour Stock was dated and yielded a K-Ar biotite age of 139 ± 9 Ma (Helwig et al., 1974). On the Avalon Peninsula of Newfoundland, diabase dikes along the trans-Avalon aeromagnetic lineament gave a Late Triassic age of 201.1 ± 2.6 Ma (Hodych & Hayatsu, 1980). Offshore, in the West Orphan Basin, granite from the Bonavista C-99 well was dated at 146 ± 6 Ma using the K-Ar whole-rock method (BP Canada, 1975). Yet to be dated Triassic-Jurassic basalts were drilled in both the Spoonbill C-30 & Cormorant N-83 wells (Amoco et al., 1973; Jansa & Pe-Piper, 1986). On the Southern Grand Banks, Upper Jurassic volcanic rocks were intersected at Brant P-87 and Twillick G-49. At Brant P-87, K-Ar dating revealed an age of 135 ± 6 Ma for 55 m of basalt and pyroclastics and 123 m of diabase sills, while at Twillick G-49, K-Ar dating revealed an age of 177 ± 5 Ma on a 15 m thick porphyritic diabase (Jansa & Pe-Piper, 1988).

1.6.7 - Irish Conjugate Margin

During deposition of the Kimmeridgian source rocks, the Irish and Iberian conjugate margins were relatively close to the study area, and thus might be potential source areas (Lowe, 2009) (Figure 1.7). It is therefore necessary to review the major crustal ages of these margins that could help distinguish European sources from the east and North American sources from the west.

The Paleozoic basement geology of the Irish Conjugate Margin is similar to that of the Newfoundland Margin as the major crustal blocks resulted from the development and subsequent closure of the Iapetus Ocean . In particular, the Irish Margin is largely comprised of Lower to Middle Paleozoic sequences overlain by Carboniferous clastic rocks and carbonates. One of the dated basement exposures on the Irish mainland is the Annagh Gneiss which has a U-Pb zircon age of 963 ± 8 Ma (Daly & Flowerdew, 2005). In addition, Lower Ordovician magmatic rocks have been dated from Northwestern Ireland, with ages ranging from 467 ± 6 Ma to 474 ± 5 Ma (Flowerdew et al., 2005). Upper Silurian to Lower Devonian plutons and batholiths have also been found. One of these is the Galway Granite, with U-Pb zircon ages between 395 and 405 Ma (Feely et al., 2004).

Less information is available about the Paleozoic basement offshore Ireland, although in the Porcupine Basin and Porcupine Ridge, it is likely a continuation of the crustal blocks of the Appalachian-Caledonian orogeny. Johnson et al. (2001) interpreted the Clare Lineament, a major feature that divides the Porcupine Basin from the Porcupine Seabight Basin, as the boundary between the Avalon and Central Mobile Belt crustal blocks, and as an extension of the Charlie-

Gibbs Fracture Zone found offshore Newfoundland. It is likely that Carboniferous sedimentary rocks are present offshore Ireland as well as those found onshore. In the Porcupine Basin, reworked Carboniferous palynomorphs have been found in younger Mesozoic clastic rocks (Smith & Higgs, 2001). The Porcupine Median high is an igneous feature thought to be Early Cretaceous in age (Tate & Dobson, 1988). This feature represents a potential source of Mesozoic detrital zircons from offshore Ireland. However, it has not been sampled, making its proposed age speculative.

1.6.8 - Iberian Conjugate Margin

The Iberian Margin is the direct conjugate margin to the Grand Banks (Figure 1.7), and extension from the Tithonian to Valanginian resulted in seafloor spreading between the two margins (Sinclair, 1988). The majority of basement rocks present on the Iberian Peninsula are Paleozoic granitoids and were produced in the Mississippian (330 – 320 Ma), Pennsylvanian (310 – 300 Ma), and Early Permian (290 – 280 Ma) (Priem & Tex, 1984). The rest of the basement of the Iberian Peninsula is composed of Lower Ordovician gneisses with U-Pb ages ranging from 460 Ma to 490 Ma (Priem & Tex, 1984; Valverde-Vaquero & Dunning, 2000).

The Paleozoic basement of offshore northern and central Iberia is likely represented by a continuation of the onshore Central Iberian Zone with Carboniferous–Permian granitoids (Priem & Tex, 1984; Capdevila & Mougenot, 1988) as well as equivalent lithologies to the onshore Ossa Morena Zone (Capdevila & Mougenot, 1988). The Ossa Morena Zone is composed of Neoproterozoic metasedimentary and volcanic and intrusive rocks, in addition to volcanic and intrusive igneous rocks which formed during the Cambrian to Early Ordovician, and Mississippian (Romeo et al., 2006; Sola et al., 2008).

Additional Iberian-related sources may include Hercynian foreland basin sedimentary rocks. This scenario was described in detail in Hiscott et al. (2008). By analyzing a combination of paleocurrent data, ages of detrital micas, and sediment composition, Hiscott et al. (2008) determined that post-rift sediments from the Grand Banks were likely derived from Hercynian foreland basin sediments. It is likely that the Hercynian orogenic belt was in close proximity to the Grand Banks during the Carboniferous/Permian. Therefore, the deformation front for this orogen was near the eventual dividing line between Iberia and the Grand Banks. The associated Hercynian foreland basin would have existed 200-300 km to the west of this orogenic front (Allen & Homewood, 1986; Hiscott et al., 2008). Given this information, it is likely that sediments of this foreland basin would have blanketed at least some of the Grand Banks, particularly in the region of the Avalon Uplift (Hiscott et al., 2008). These foreland basin sediments would have been deposited in the Late Carboniferous or Permian, and would have likely contained substantial quantities of Permo-Carboniferous zircons from the Iberian granitoids which would have subsequently been available for erosion and deposition into Mesozoic basins.

Chapter 2 – Methods, Wells Studied & Sampled Intervals

2.1 - Introduction

This chapter describes the mudstone intervals sampled for analysis, and provides an overview of the wells in the study area. Additionally, sample preparation and analytical methods are reviewed.

Conventional cores and cuttings samples of Kimmeridgian source rocks were collected from four wells within the Flemish Pass and Central Ridge area. The wells chosen were Baccalieu I-78 (Figure 2.2), Lancaster G-70 (Figure 2.3), South Tempest G-88 (Figure 2.4), and Panther P-52 (Figure 2.5) because they all intersected Kimmeridgian source rocks, and because of their distribution in the basin. Baccalieu I-78 is within the northern Baccalieu subbasin, while Lancaster G-70 is located in the southern Gabriel subbasin. Panther P-52 and South Tempest G-88 are both within the Central Ridge. Collecting samples from these separate areas permits a more thorough interpretation of the provenance and paleodrainage patterns during this time. To ensure consistent sampling from different wells, biostratigraphic reports and lithostratigraphic picks were used. Although there are several distinct interpretations, there is a consensus on where Kimmeridgian source rocks (or Egret Member equivalent source rocks) occur. There are distinct interpretations because different microfossil assemblages were used by different authors as well as different terminologies. For example, in the biostratigraphic reports, several of the available publications have older terminology, no longer used by the International Commission on Stratigraphy (ICS). The older terminology creates confusion with respect to the length of the Kimmeridgian Stage. In 1990, the International Subcommission on Jurassic Stratigraphy voted to discontinue the use of the Kimmeridgian *'sensu Anglico'* in favour of the Kimmeridgian *'sensu Gallico,'* both with different zonal content and boundaries (Zeiss, 1991; 2003). Thus, reports using the current *'sensu Gallico'* terminology are used in this thesis. Reports found using the older terminology were avoided as a late Kimmeridgian age using the '*sensu Anglico'* terminology would actually correspond in part to a Tithonian age using the '*sensu Gallico'* terminology.

2.2 – Sample Collection

The available cores and cuttings were logged and sampled at the CNLOPB Core Storage and Research Centre in St. John's, Newfoundland. Although samples from conventional cores are preferred for this study, the entire Kimmeridgian source rock interval was not cored. Thus, cuttings were sampled where cores were unavailable. With cores, samples were collected from a mudstone unit as well as within interbedded siltstones of the same section. This permits a comparison between heavy-mineral distributions of the finer and coarser grained intervals within the same section with likely the same source region, to ensure there is no sample bias from a specific size fraction.

2.3 – Analytical Methods

2.3.1 - Introduction

Several different analytical methods were employed in this study. Polished thin sections were observed first using an optical microscope and then analyzed on a scanning electron microscope using mineral liberation analysis techniques (hereafter referred to as MLA-SEM) to identify minerals and determine mineral modes. For detrital zircon geochronology, MLA-SEM imaging was the first step, followed by laser-ablation microprobe (LAM) ICP-MS analysis. Techniques employed for whole rock geochemical analysis include X-Ray Fluorescence, and inductively coupled plasma mass spectroscopy (ICP-MS). An assessment of heavy mineral suites and provenance-sensitive heavy mineral ratios was also undertaken using the MLA-SEM.

2.3.2 - Optical Petrography of Thin Sections

Thin sections from the sampled intervals were examined by transmitted light microscopy and MLA, to provide a better understanding of the petrology and provenance characteristics of the source rocks. The composition of the constituent detrital grains, as well as the mineralogical and textural maturity were assessed in order to determine provenance. Dickinson & Suczek (1979) demonstrated that the framework mineralogy of sandstone is a good proxy for provenance. Diagenetic overprints were also evaluated. For example, features such as grain dissolution that could affect the composition of the rock or the diversity of heavy mineral assemblage were analyzed. The source rock petrology was described and interpreted. The MLA was used to determine modal mineral abundances. The MLA-SEM is described in detail in Section 2.3.4. It is useful for the determination of exact mineral abundances and as well as mineral associations. In addition, it is useful for identifying rare and small heavy mineral grains. The descriptions and interpretations supplemented other assessments of source area composition, sedimentary recycling, and transport distances.

2.3.3 – Sample Preparation for Detrital Zircon Geochronology

Different methods were used to prepare samples for detrital zircon geochronology depending on whether the material in question was from a core or from cuttings. Where cores were available, it was only possible to obtain a small (5 x 3 x 3cm) sample because the detrital zircon analysis is destructive. With such a small sample, crushing and heavy liquid separation are not feasible as material would likely be lost through the sample preparation process. Therefore, numerous thin sections were made from each small sample. Even if heavy minerals are not abundant in the sample, there should be enough grains to evaluate if several thin sections are cut from the same interval. An initial assumption made with fine-grained sediments is that there are likely not any heavy minerals large enough (>20 µm for LA-ICP-MS at Memorial University) to separate and analyze. However, studies by Totten & Hanan (1998, 2007) indicate that heavy minerals can be just as abundant, if not more abundant, in shales than sandstones with some possessing sizes large enough to analyze.

For work on cuttings, approximately 50 g samples are available from the CNLOPB. The cuttings were taken from 5 m intervals and were unwashed. For the thesis work, the cuttings were gently disaggregated, cleaned, and wet sieved through a 15 µm mesh to remove the drilling mud and fine clays. Tap water was used for this process. This mesh size is considered appropriate because the ability of the LAM-ICP-MS to analyze zircons smaller than 15 µm is limited by the spot size of the laser. After the samples are cleaned, they were left to dry overnight and then sieved through a 180 µm mesh. This split the sample into two fractions: one 15 - 180 µm and the other > 180 µm. The 15 – 180 µm fractions were used for analysis. For heavy mineral analysis, studies such as Lowe et al. (2011) analyzed the 63 – 180 µm fraction, following procedures outlined in Morton & Hallsworth (1994). For heavy mineral analysis, this size fraction was chosen because all heavy minerals were thought by those authors to exist within this size fraction. Thus, bias based on the grain size distribution from the parent rocks and subsequent hydrodynamic sorting is likely diminished when comparing ratios of different heavy minerals (Morton & Hallsworth, 1994). Lowe et al. (2011) also considered this size fraction appropriate for detrital zircon geochronology. However, Totten & Hanan (2007) stated that the median grain size of heavy minerals within shales is approximately 25 µm less than in sandstones. Because this study analyzed fine-grained hydrocarbon source rocks, a lower limit on the particle size to be considered was set at 15 µm rather than 63 µm. Further details on the rationale for the grain size bracket used are presented in Section 5.2.

2.3.4 - MLA-SEM Imaging for Detrital Zircon Geochronology

Once the cuttings had been cleaned and sieved, samples were prepared for imaging on the MLA-SEM. In the SEM lab, Bruneau Innovation Centre, Memorial University, the samples were mounted in epoxy, left to cure overnight, and polished the next day. Polishing cuts into the embedded sedimentary particles and removes scratches and bumps or ridges on the epoxy surface, which permits proper imaging by the SEM. Polishing exposes the cores of grains in order to remove the outer surfaces of grains, which are typically enriched in adsorbed uranium (Krogh, 1982). Care must be taken to ensure that none of the zircons are polished away or plucked out of the mounts. After polishing, the samples are ready for imaging on the SEM.

Unlike a traditional optical microscope, which collects light, the SEM collects emitted electrons and can image small specimens at 100 to 100,000x their actual size. The images produced possess an extreme and realistic depth of focus. The SEM is equipped with an energy dispersive X-ray (EDX) detector, an electron backscatter diffraction (EBSD) system and a cathode-luminescence (CL) detector. In addition, the SEM is equipped with MLA® (Mineral Liberation Analysis) software, which is capable of X-ray aided image analysis. The technique relies primarily on backscattered electron imaging (BEI), and energy-dispersive X-ray (EDX) analysis, which classify the grains as known minerals. The MLA software has the ability to spatially quantify mineral abundances, define associations of areas, and indicate sizes and shapes of minerals in a systematic fashion. The instrument used for this study is the FEI MLA 650F. In addition, the high throughput EDS (energy-dispersive X-ray spectroscopy) detector was advantageous in reducing run times where samples contained abundant (>100,000) grains. Further details on the MLA-SEM are available in Sylvester (2012).

During MLA runs, typical instrument settings included voltage set at 25 KeV, a beam current of 10 nA, a working distance of 13.5 mm, and a spot size of about 5.5 µm. Between 10,000 and 300,000 particles were identified and analyzed in each individual sample. Unknown mineral phases were identified based on matching their spectra to that of Mineral EDX spectra standards. This is completed using the MLA Image Processing Tool software. Minerals of interest from the sample (i.e., zircon) were then imaged manually using the MLA Viewer Software. This permits the user to image and choose only the zircons that are optimal for age dating (i.e., free of inclusions, cracks, or other imperfections that could influence the analysis). The MLA then outputs coordinates for the location of the imaged zircons within the thin section or grain mount.

It is worth noting that the abundances of several heavy mineral phases, such as garnet, allanite, and ilmenite were erroneous, as the MLA method was ineffective at distinguishing these minerals from finely disseminated clays, micas, pyrite, and carbonate material, which are common components in samples for this study. Due to the method in which mineral spectra are obtained through spot analysis, the EDX elemental peaks for both these finely disseminated grains as well as the mentioned heavy minerals appeared very similar, which led to some misclassifications. This problem was also encountered by Lowe (2009) in sandstones of the Flemish Pass Basin. The abundances of the affected heavy mineral grains, therefore, were not included in the analysis of heavy mineral assemblages in Chapter 5. This problem is also apparent in the identification of clay minerals. Due to the nature of the spot analysis, differentiation between this finely disseminated material is difficult and the acquired spectra often represented a mixture of a number of different minerals. It was therefore necessary to group these minerals into new categories that represent a combination of the mineral spectra.

These include blends of fine-grained quartz and clay, as well as a mixture of fine-grained silicate and carbonate. However, it was still possible to identify minor quantities of individual clay minerals.

Another complication encountered was the abundance of the mineral Barite ($BaSO_4$). Barite was abundant in all heavy mineral fractions from cuttings samples, as it is used as an additive in drilling mud. The sample preparation process removes significant amounts of the barite, but it was not always possible to completely eliminate this contaminant. However, the naturally occurring abundances of other heavy minerals are not expected to be affected by the occurrence of barite since the barite in these samples is industrial, and is derived from evaporite deposits. The barite may be associated with minerals such as gypsum and anhydrite, but those minerals are unrelated to the clastic sediments analyzed in this study.

2.3.5 - LAM-ICP-MS for Detrital Zircon Geochronology

LA-ICPMS U-Pb zircon geochronology was carried out at Memorial University of Newfoundland using a Thermo-Scientific ELEMENT XR magnetic sector, single-collector ICPMS coupled to a Lambda Physik ComPex Pro 110 ArF excimer GeoLas laser ablation system operating at a wavelength of 193nm and a pulse width of 20 ns. The laser was operated at an energy density of 5-7 J/cm^2 and a repetition rate of 4-5 Hz, with a spot diameter of 20 micrometers. The sample aerosol is transported from the sample cell to the ICP using a He-carrier gas to reduce sample redeposition within the ablation cell, improving sample transport efficiency and resulting in more stable time-resolved signals.

Data acquisition for each analysis is about two minutes, with the first ~30 seconds used to measure the gas background followed by ~40 sec of laser ablation, and ~50 sec of wash out. Measurements are carried out in peak-jumping mode with one point measured per peak. Isotopes measured are ^{200}Hg, ^{202}Hg, ^{204}Hg+Pb, ^{206}Pb, ^{207}Pb, ^{208}Pb, ^{232}Th, ^{235}U and ^{238}U from both the zircon and gas background. Intensities for ^{235}U were calculated from ^{238}U assuming a natural, present-day ^{238}U/^{235}U ratio (137.88), as the measured ^{235}U intensities for many analyses were low and thus had large uncertainties.

Raw data are dead-time corrected and reduced off-line using the Iolite 2.5 software (Paton et al. 2011) with the VizualAge DRS (Petrus and Kamber 2012), which carries out background and signal interval selections, gas background subtraction, signal drift corrections, external calibration, and age and uncertainty calculations. The external calibration provides corrections for instrumental mass bias and laser-induced U/Pb fractionation. In this study, signal intensities of zircon of unknown age were calibrated against standard reference material 91500 zircon (1065 ± 3 Ma; Wiedenback et al. 1995). Ages and 2-sigma uncertainties were calculated from the corrected ^{207}Pb/^{206}Pb, ^{207}Pb/^{235}U and ^{206}Pb/^{238}U ratios. Age determinations were calculated using the decay constants of Jaffey et al. (1971). Final concordia diagrams, U-Pb age histograms and probability density plots were produced using the Isoplot/Ex3.75macro (Ludwig 2012).

Common Pb corrections were made where ^{204}Pb was detected above gas background using the the method of Andersen (2002) in the Iolite/VizualAge software. The Andersen method was preferred to the ^{204}Pb common Pb correction method because ^{204}Hg made up a majority of the total measured 204-peak in many analyses and thus uncertainties on the ^{204}Pb intensities were large.

In order to monitor the efficiency of the instrumental mass bias and laser-induced fractionation corrections, standard reference materials, 02123 zircon (295 ± 1 Ma; Ketchum et al. 2001), Plesovice zircon (337.13 ± 0.37 Ma; Slama et al. 2008) and OG-1 zircon (3465.4 ± 0.6

Ma; Stern et al. 2009) were analyzed between every 8 unknown zircons during each analytical session. These standard measurements also monitor the accuracy and reproducibility of U-Pb analyses. The weighted mean $^{206}Pb/^{238}U$ age for all analyses of 02123 is 294.63 ± 0.8 Ma (2σ, MSWD = 1.7; n = 203), for Plesovice is 342.4 ± 1.6 Ma (2σ, MSWD = 2.4; n = 85), and for 91500 is 1062.0 ± 1.6 Ma (2σ, MSWD = 0.78; n = 368) over the course of all the U-Pb analytical sessions. The weighted mean $^{207}Pb/^{206}Pb$ age for all analyses of OG-1 is 3475.5 ± 2.5 Ma (2σ, MSWD = 1.7; n = 79) over the course of all the U-Pb analytical sessions. All data for reference standards is available in Appendix B.

For detrital zircon geochronology, the aim is to analyze as many zircons as possible to reduce the probability of missing an age population. Fedo et al. (2003) stated that the analysis of 59 randomly selected zircon grains from a sedimentary rock that has a normal abundance of zircon grains reduces the possibility of missing an age population to 5%. Similarly, Dodson et al. (1988) indicate at least 60 grains must be analyzed to reduce the possibility of missing an age population greater than 0.05 to 95%. However, Vermeesch (2004) states that to be 95% confident that no age population greater than 0.05 has been missed, 117 grains must be dated. However, this assumes that the sample has a perfectly uniform distribution where each age group has the same amount of grains (Vermeesch, 2004). This type of distribution is uncommon in naturally occurring populations. Therefore, Vermeesch (2004) states that if there is prior knowledge indicating the populations are not uniformly distributed, it is sufficient to date 95 grains to be 95% confident no age population greater than 0.05 has been missed. Vermeesch (2004) suggests that if fewer than 117 grains are dated per sample, the probability of missing at least one age fraction should be reported.

In this study, as many grains as possible were analyzed in each sample. However, as discussed in Section 2.3.3, since these samples are derived from core and cuttings from offshore wells, a limited amount of sample material is available. Where cuttings were used, only 50 g samples over 5 m intervals were available (Figure 2.1). Samples could have been combined to cover 10 m or greater intervals, but this would result in lower resolution for the provenance analysis and was therefore avoided. In samples where fewer grains were analyzed, it is important to note that it is possible that only the major age peaks were detected. However, given that this is the first study of this nature on the Kimmeridgian rocks offshore Newfoundland, the major age peaks will still provide unique datasets and important provenance information. For each sample, the probability that an age peak has been missed will be noted as suggested by Vermeesch (2004).

Figure 2.1 - Image of approximately 50 g cuttings sample from the Baccalieu I-78 well (5000 m).

2.3.6 – Sample Preparation and MLA/SEM for Evaluation of Heavy Mineral Ratios

Heavy mineral ratios are assessed to determine the provenance fingerprint of the studied units. Provenance sensitive heavy mineral ratios using zircon, monazite, titanite, chromite, and rutile are considered useful for provenance discrimination and assessing sedimentary recycling. Cuttings are used for this portion of the project and the procedure for processing the samples and heavy mineral separation are similar to the methods used for detrital zircon geochronology discussed previously. These samples are mounted in epoxy and analyzed on the MLA-SEM. The ability of the MLA software to identify heavy minerals and demonstrate the sizes and shapes of grains permits for a meaningful comparison of the provenance fingerprints of different stratigraphic units of this study.

2.3.7 - X-Ray Fluorescence for Whole Rock Lithogeochemistry

Samples for X-ray fluorescence were taken from conventional cores, and prepared in the crushing room in the Department of Earth Sciences at Memorial University. Sample preparation involves pulverizing the rock into a fine powder using the Siebtechnik grinding mill. Strict laboratory protocols were followed to prevent contamination throughout this process.

The X-ray fluorescence analysis was completed at the TERRA lab facilities, Memorial University. The XRF facility uses a Fisons/Applied Research Laboratories model 8420+ sequential wavelength-dispersive x-ray spectrometer which has the capability for qualitative and quantitative determination of elements. The detection system utilizes an argon/methane flow proportional counter and also a scintillation counter. A combination of fused glass beads and pressed pellets is used to obtain a full analysis of all, major, minor and trace elements. For the preparation of the pressed pellets, approximately 9 g of rock powder is weighed and mixed with 2.7 g of wax binder. This mixed powder is then put in a Herzog Pellet Press and pressed at 276 MPa for 10 seconds. The final preparation step is baking the pellet at 90°C for 15 minutes. The pressed pellet analysis for trace elements, Fe_2O_3 and MnO is completed on a Bruker S8 Tiger

WDXRF using the Geo-Quant T package. Two geological reference standards (SGR-1B-1 and SDO-1-1) were analyzed with each group of 13 samples to confirm accuracy and precision for the results. These reference standards are of the Green River Shale and the Devonian Ohio Shale, respectively. The accepted values for the geological reference materials analyzed are also given with the results sheets. The reference materials are combined with a reagent blank to measure the reagent contribution to the values. XRF is considered an excellent and robust method for the determination of the major and more abundant trace elements in rock samples. It will provide additional information on the provenance of the Kimmeridgian mudstones.

2.3.8 - ICP-MS for Whole Rock Lithogeochemistry

The concentrations of certain elements, particularly Th, in the samples are below the limit of detection of the XRF instrument. To obtain a complete analysis, ICP-MS (inductively coupled plasma mass spectrometer) is used because of its precise nature and sensitivity in trace element analysis. ICP-MS analyses were carried out at the TERRA lab facilities at Memorial University. The data obtained were combined with the XRF data to produce a more complete geochemical analysis of the samples. For introduction of rocks into the ICP-MS as solutions, samples must be digested in acid before analysis. All results are given in ppm. The analytical procedure is as follows: 1) Initial digestion of a 0.1 g sample aliquot using HF/HNO_3 (also boric and oxalic acids); and 2) the resultant solution is analyzed using inductively coupled plasma mass spectrometry correcting for matrix effects using the method of standard addition. Full details of the procedure are given in Jenner et al. (1990). If any sample material is not dissolved fully in HF/HNO_3, it is treated with HCl/HNO_3. In some samples, some resistant phases, most notably zircon, may not always dissolve completely. In these cases, Zr, Hf, and HREE values should be considered minimum concentrations. For samples in this study, it was noted that Zr values from ICP-MS were significantly lower than those from the XRF analyses. Therefore, it is concluded that the lower Zr values from ICP-MS are a result of zircon not completely dissolving. Zr values used in graphs and geochemical analysis in this study were consequently taken from the XRF analyses. For quality control, two geological reference standards (SGR-1B-1, and SDO-1-1) were prepared and analyzed with the other samples as outlined in Section 2.3.7.

In ICP-MS analysis, there are a number of inter-element interferences present. The instrument used has been optimized so that the interferences are at a low enough level that they can be corrected for most rock types. The most noteworthy of these interferences is a Ba molecular ion interference on Eu. A correction is applied, but the error in this correction can be significant, especially at very high Ba/Eu ratios. This Ba-Eu interference is not considered an issue for samples in this study as these elements were not used in provenance graphs or analysis.

2.4 - Wells Studied

2.4.1 - Baccalieu I-78

Baccalieu I-78, drilled in 1985 in 1092.8 m water depth by an Esso Parex-led consortium, is an abandoned exploratory well located in the Northern Flemish Pass Basin (47° 57' 41.49" N, 46° 10' 46.76" W). The total depth of the well is 5134.5 m and it intersected approximately 600 m of Tertiary, 1500 m of Lower Cretaceous, and 1500 m of Upper Jurassic strata (Figure 2.2). Potential reservoirs were encountered in the Cretaceous section, where texturally mature sandstone was penetrated between 3195 and 3275 m. This reservoir is considered equivalent to the Hibernia Formation of the Jeanne d'Arc Basin. A more poor reservoir, thought to be equivalent to the Avalon Formation, was penetrated between 2030 and 2220 m. The Upper Jurassic Jeanne d'Arc Formation equivalent sandstone is encountered between 3715 and 3780 m (McAlpine, 1989; CNLOPB, 2011). Kimmeridgian source rocks were encountered between 4398 and 4804 m, and also from 4975 to 5135 m, designated as the Upper and Lower Kimmeridgian

Source Rock units, respectively (CNLOPB, 2011). Samples were collected for provenance analysis from both Kimmeridgian Source Rock units, as well as samples from the Rankin Formation, which is interbedded with the source rock units (Table 2.1). In combination with the lithostratigraphic picks, biostratigraphic interpretations were also used to ensure sampling was focused on the intended Kimmeridgian interval. Biostratigraphic reports from both Esso Resources (1986) and Robertson Research (2002) place the majority of the sampled units with the Kimmeridgian Stage. A limited amount of conventional drill core is available from this well; therefore the majority of sampled units are drill cuttings. However, conventional core was available between 4135 and 4153 m, and several samples were acquired from this interval.

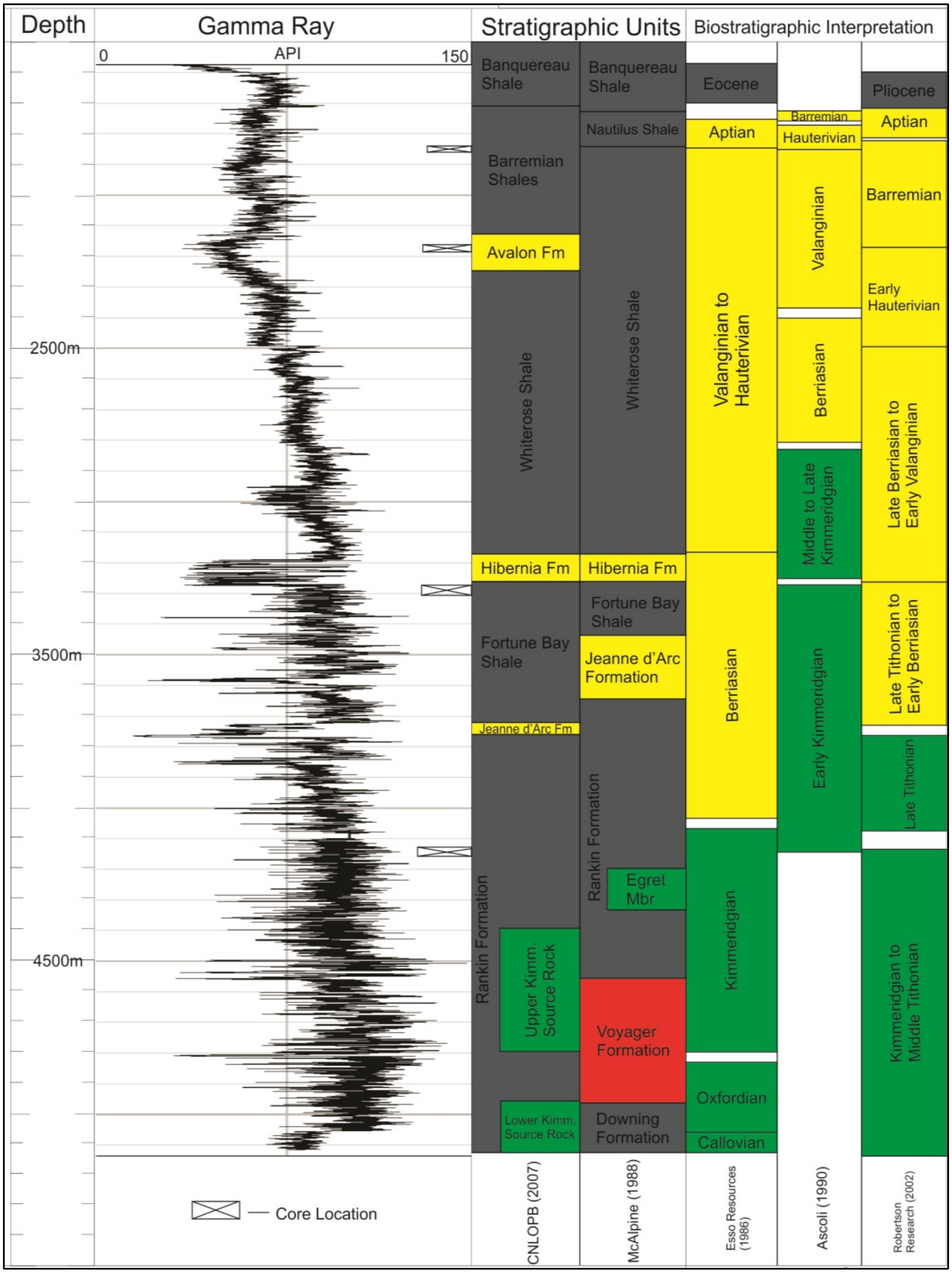

Figure 2.2 - Combined gamma ray, stratigraphic, and biostratigraphic log for the Baccalieu I-78 well.

Well	Depth below KB (m)	Formation*					Lithology**		Sample Type		Type of Analysis***		
		UTS	UKSR	RF	LTS	LKSR	SS	MS	Core	Cuttings	GC	DZG	HMA
South Tempest G-88	3500-3505	X					X			X			X
	3600-3605	X						X		X			X
	3700-3705	X						X		X			X
	3830.1		X				X		X		X		
	3832.0		X				X		X		X		
	3832.0 (B)		X				X		X		X		
	3837.3		X				X		X			X	
	3838.4		X				X		X		X		
	3838.4 (B)		X				X		X		X		
	3843.4		X					X	X		X		
	3843.4 (B)		X					X	X		X		
	4000 - 4005			X						X			X
	4183.9				X			X	X		X		
	4183.9 (B)				X			X	X		X		
	4185.1				X			X	X		X		
	4185.4				X			X	X		X		
	4188.1				X		X		X		X		
	4188.1 (B)				X		X		X		X		
	4195.8				X		X		X			X	
	4198.0				X			X	X		X		
	4325.4					X		X	X		X		
	4327.3					X		X	X		X		
	4327.6					X		X	X		X		
	4329.6					X		X	X		X		
	4330.0					X	X		X		X		
	4331.3					X		X	X		X		
	4495-4500					X		X		X			X
	4600-4605			X				X		X			X
Panther P-52	3210.0	X					X			X		X	X
	3400.0		X					X		X			X
	3500.0		X					X		X			X
	3600.0				X			X		X			X
	3754.0				X			X	X		X		
	3756.7				X			X	X		X		
	3757.0				X			X	X		X		
	3757.0 (B)				X			X	X		X		
	3950.0					X		X		X			X
Baccalieu I-78	4135.3			X			X		X			X	
	4135.8			X				X	X		X		
	4138.5			X				X	X		X		
	4140.9			X				X	X		X		
	4142.2			X				X	X			X	
	4145.9			X				X	X		X		
	4146.0			X				X	X		X		
	4147.6			X				X	X		X		
	4148.3			X				X	X		X		
	4148.3 (B)			X				X	X		X		
	4151.8			X				X	X		X		
	4500-4505		X					X		X		X	X
	4705-4710		X					X		X			X
	4900-4905			X				X		X			X
	5000-5005					X		X		X			X
	5075-5080					X		X		X			X
Lancaster G-70	3305-3310		X					X		X			X
	3500-3505		X				X			X			X
	3715-3720		X					X		X			X
	4200-4205			X				X		X			X
	4405-4410			X			X			X		X	X
	4740-4745					X		X		X			X
	4820-4825					X		X		X			X

*UTS=Upper Tempest Sandstone, UKSR=Upper Kimmeridgian Source Rock, RF=Rankin Formation, LTS=Lower Tempest Sandstone, LKSR=Lower Kimmeridgian Source Rock

**SS=sandstone, MS=mudstone

***GC=Whole rock major and trace element geochemistry, DZG=detrital zircon geochronology, HMA=heavy mineral analysis

Table 2.1 – List of samples and types of analyses performed.

2.4.2 - Lancaster G-70

Lancaster G-70 is also an abandoned exploratory well drilled in 1986 in the Southern Flemish Pass Basin (47° 19' 22.34" N, 47° 09' 40.77" W). The well was drilled by Petro-Canada in a water depth of 726 m and to a total depth of 5701 m. The well encountered 2500 m of Tertiary, and 2500 m of Jurassic strata (Figure 2.3). The well was drilled on a Jurassic high, and therefore the Cretaceous section is missing. Reservoir sections encountered in this well were thin, as the more prospective Cretaceous section is missing; however, some thin to moderately thick sandstones were encountered in the Upper Jurassic section which had limited reservoir quality due to cementation (NL Dept. of Mines and Energy, 2003). Lower Tempest sandstones were penetrated from 3764 to 3789 m. Kimmeridgian source rocks were encountered between 3207 and 3761 m, and also from 4736 to 4856 m, designated as the Upper and Lower Kimmeridgian Source Rock units, respectively (CNLOPB, 2007). Samples from this well were taken from the Upper and Lower Kimmeridgian Source Rock units, as well as the interbedded Kimmeridgian Rankin Formation, and Lower Tempest sandstone (Table 2.1). The biostratigraphic reports available for this well are somewhat contradictory, but were used nonetheless to ensure sampling was concentrated on the Kimmeridgian section. Conventional core for this well is limited to the Middle Jurassic section; consequently all of the samples obtained consist of drill cuttings.

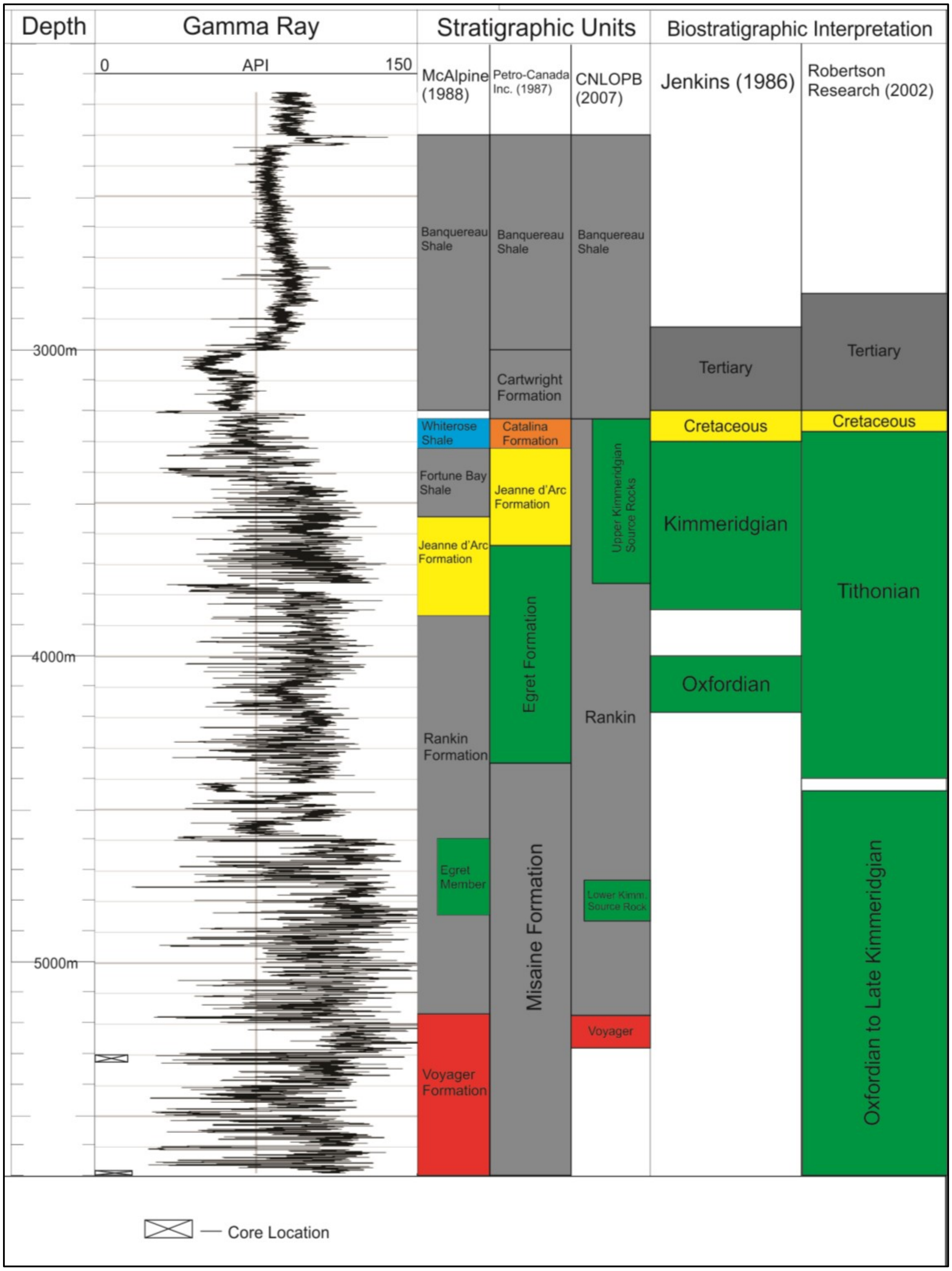

Figure 2.3 - Combined gamma ray, lithostratigraphic, and biostratigraphic log for the Lancaster G-70 well.

2.4.3 - South Tempest G-88

The South Tempest G-88 well was drilled in 1980 by Mobil and Petro-Canada and is located in the Central Ridge area of the Grand Banks (47° 07' 19.57" N, 47° 57' 26.49" W). It is considered an abandoned oil well and was drilled to a depth of 4675 m in a water depth of 158 m. The well penetrated approximately 2500 m of Tertiary, 500 m of Cretaceous, and 1500 m of Upper Jurassic strata (Figure 2.4). Good reservoir quality sandstones as well as light oil (41° API) are present within the Kimmeridgian Tempest sandstone. This reservoir flowed at 1250 bopd, but was later abandoned. The Tempest sandstones are interbedded with the Upper and Lower Kimmeridgian Source Rock units. These are found between 3730 and 3977 m and 4324 and 4585 m, respectively. Samples from this well were collected from both source rock units, as well as the Tempest sandstones and Rankin Formation (Table 2.1). Similar to the Lancaster G-70 well, biostratigraphic reports were somewhat conflicting with respect to the boundaries of Kimmeridgian and Tithonian stages within the Late Jurassic. Three separate conventional cores are available for this well, from 3828 to 3846 m, 4181 to 4199 m, and 4322 to 4332 m. This allowed for direct sampling of the Upper and Lower Kimmeridgian Source Rock, as well as the Lower Tempest sandstone. Additional samples from this well came from drill cuttings.

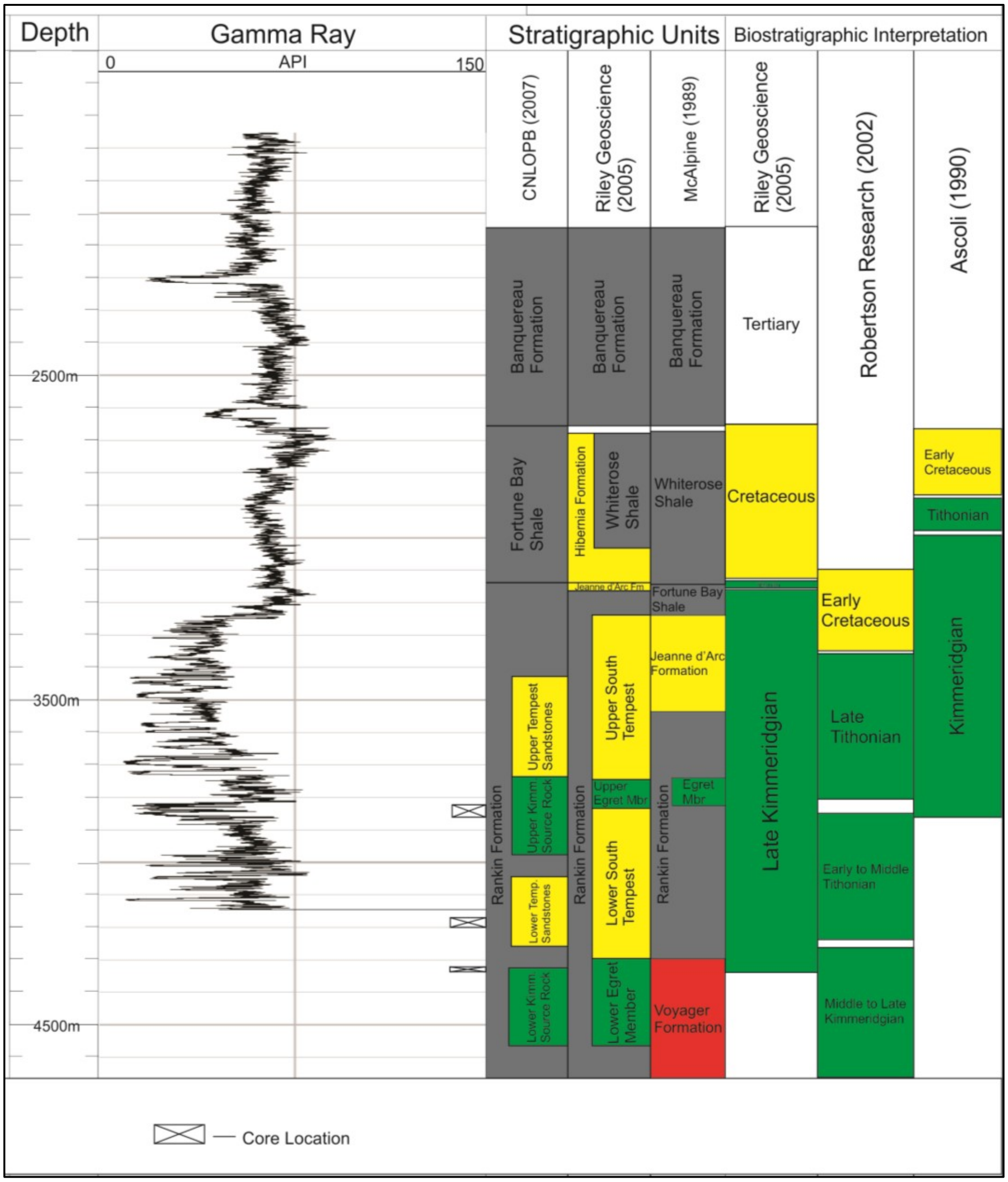

Figure 2.4 - Combined gamma ray, lithostratigraphic, and biostratigraphic log for the South Tempest G-88 well.

2.4.4 - Panther P-52

Panther P-52 is an abandoned exploration well drilled in 1985 by a Husky-led consortium. It is located at 47° 01' 53.01" N, 47° 37' 39.81" W with 191 m of water depth and a total depth of 4203 m. Intersected were approximately 2500 m of Tertiary, 200 m of Cretaceous, and 1400 m of Upper Jurassic strata (Figure 2.5). Potential reservoirs were not encountered in the Cretaceous section, however two potential reservoirs were penetrated in the Jurassic section including the Upper Tempest Sandstone (2969 – 3256 m) and the Lower Tempest Sandstone (3576 – 3758 m). The Upper and Lower Kimmeridgian Source Rock units were encountered from 3256 to 3566 m, and 3794 to 4003 m, respectively. Samples from this well were collected from both source rock units as well as interbedded Tempest sandstones and Rankin Formation shales (Table 2.1). The majority of these samples were from drill cuttings; however, one section of conventional core was available from 3752 to 3758 m, and a number of samples were taken from this interval as well. Once again, biostratigraphic reports were contradictory regarding the boundaries of the Kimmeridgian and Tithonian stages. However, when combined with lithostratigraphic picks, it was possible to focus sampling on the Kimmeridgian section.

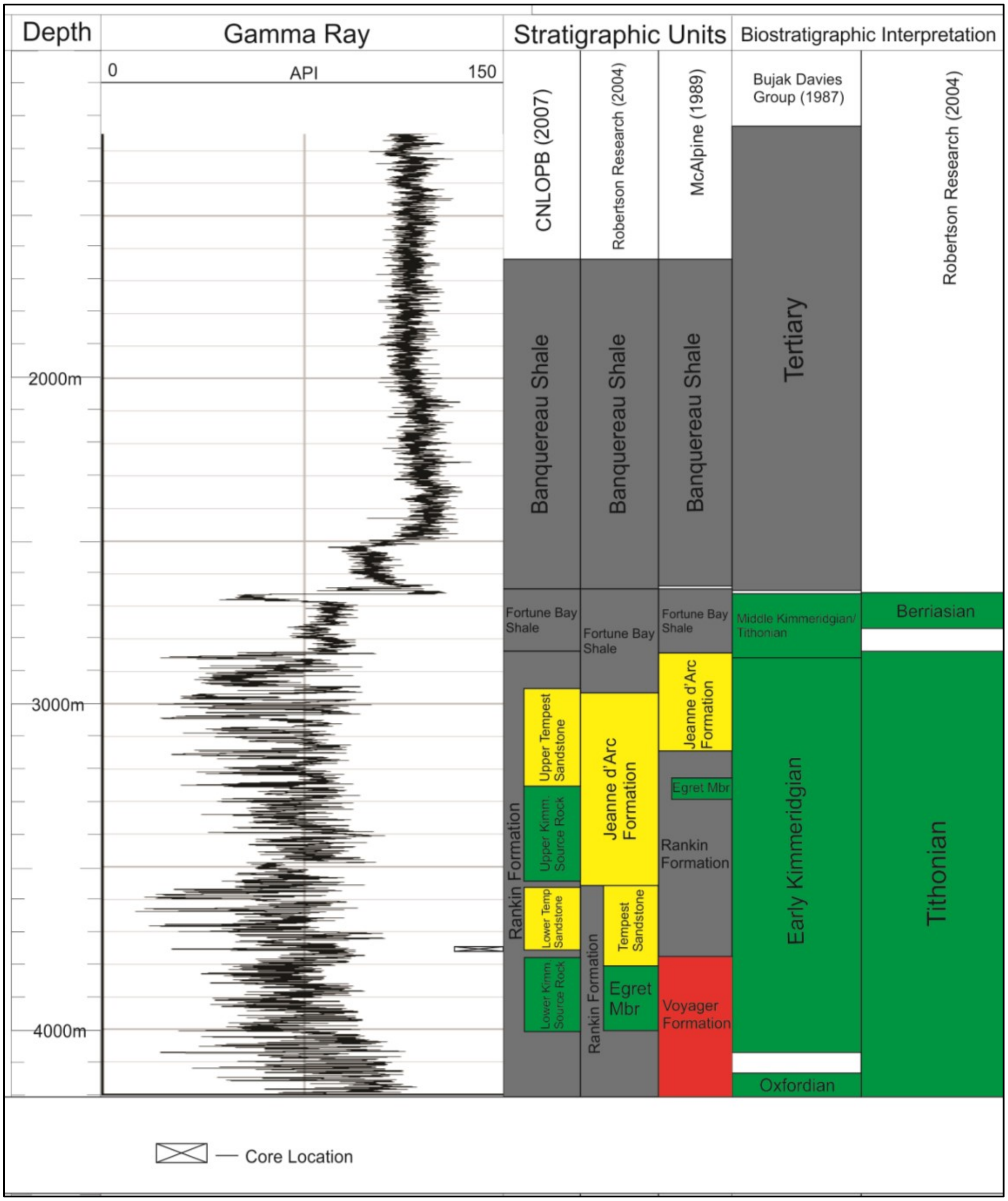

Figure 2.5 - Combined gamma ray, lithostratigraphic, and biostratigraphic log for the Panther P-52 well.

Chapter 3 – Core Logging and Sedimentary Petrology

3.1 - Introduction

Prior to sampling, cores from the Upper Jurassic source rock intervals within the studied wells were logged and described. Very little information is available describing the source rocks in the Flemish Pass / Central Ridge area. Therefore, the core logging was completed to understand lithologic and facies variations within the source rocks, and to note any important sedimentary structures or trace and body fossils. Detailed interpretations of the depositional environment of the source rocks throughout the basin, however, were not made, in part due to the scarcity of cores and well coverage in the area, but also because interpretations of this nature are outside the scope of this study. However, the level of marine versus non-marine influence and interpretations of the depositional environment of individual cores will be made and may be useful for the development of provenance and depositional models.

3.2 - Baccalieu I-78 – Kimmeridgian Rankin Formation

A conventional core between 4135 and 4153 m was described (Figure 3.1). The basal five metres of the section (4153 – 4148.53 m) are composed predominantly of dark grey mudstones with fine siltstone interbeds. The interbedded siltstones range from about 0.5 to 3 cm thick and they compose about 30% of this basal section. Soft sediment deformation features are typical and scour marks (Figure 3.6A) and load casts are common at the base of the coarser-grained beds. Coarser intervals have abundant mud clasts and minor carbonaceous organic debris. The next two metres of the core (4148.53 - 4146.14 m) are similar to the basal section; however, this section contains two 3–10 cm thick ungraded beds that are dominated by very coarse detritus (Figure 3.6B). Numerous brown concretionary layers ranging from 2–4 cm thick are present here as well. The upper 11 m of the core (4146.14 – 4135 m) possess similar characteristics to the basal section; however, there is a higher proportion (60%) of silt and very fine sand layers. The thickness of these layers is typically around 0.5 cm. The majority of the layers can therefore be considered laminae. The thickest layers are around 6 cm and are thus considered beds. The muddy interbeds also average about 0.5 cm thick with a maximum thickness of only 2 cm. This interval also contains beds of very coarse detritus as well as a number of concretionary layers. Trace fossils are absent in this core; only a couple of examples of potential burrows were found. Body fossils are also absent.

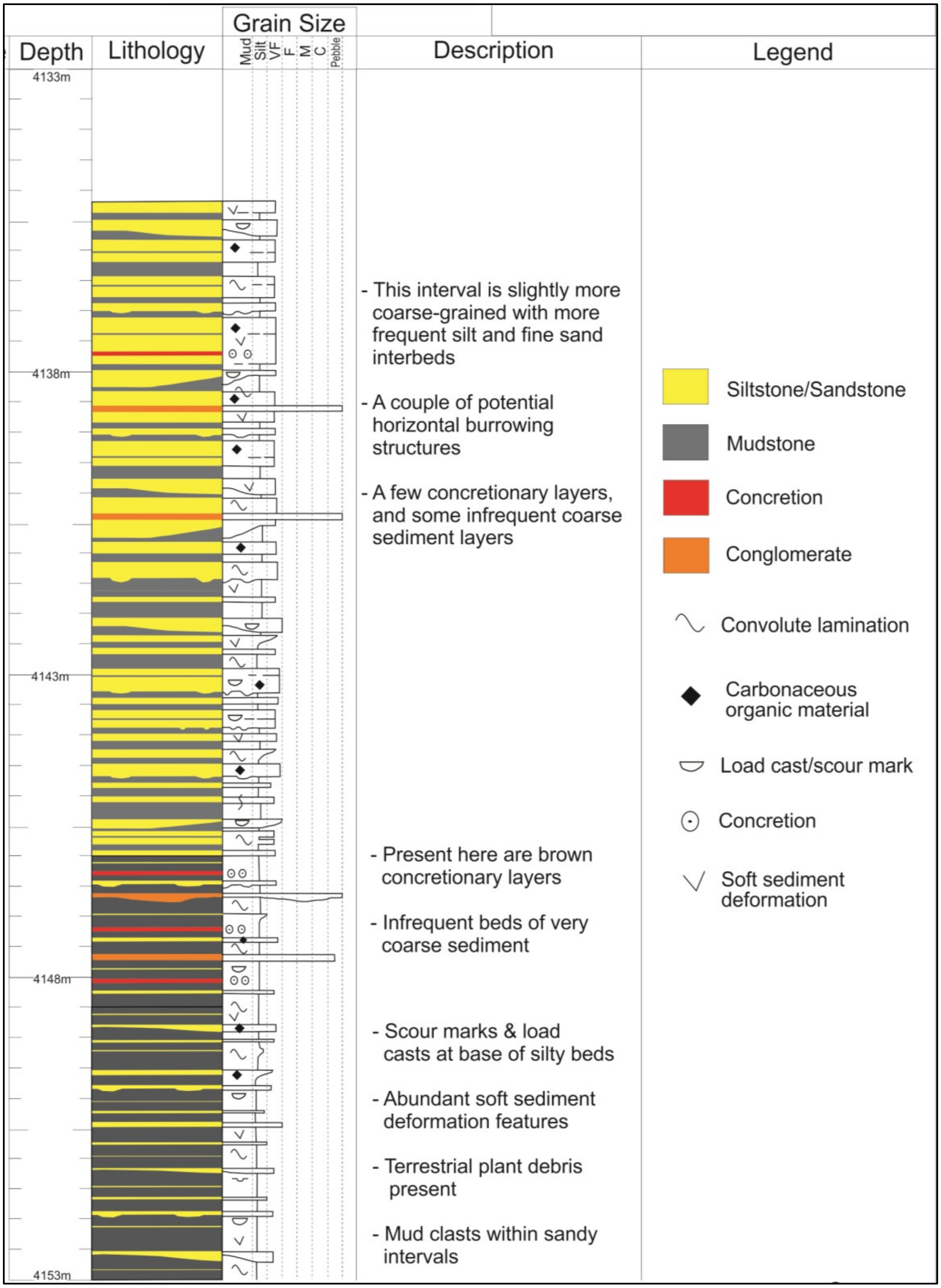

Figure 3.1: Core Log for the Kimmeridgian Rankin Formation from the Baccalieu I-78 well.

3.3 - Panther P-52 – Kimmeridgian Lower Tempest Sandstone

The only conventional core obtained from this well (3757.9 – 3752.4 m) was described (Figure 3.2). This core displays similar characteristics to that of Baccalieu I-78, although this core is slightly coarser grained overall. The basal section (3757.9 – 3756.25 m) is composed of interbedded mudstones and siltstones with about 60% of the beds being mudstones. All the laminae average about 0.5 cm thick, with the maximum bed thickness being about 5 cm. As seen in the Baccalieu I-78 core, abundant soft sediment deformation features were seen here as well as particles of terrestrial plant debris in coarse-grained sections. The overlying section from 3756.25 – 3753.9 m is composed of fine-grained sandstone. Overall, this interval has about 90% sandstone and 10% interbedded mudstone. The mudstone beds are typically less than a centimeter thick, while the sand beds are on average 10 – 15 cm thick. Numerous mud clasts were found within the sandstone intervals. From 3753.9 to 3753.55 m, there is an abrupt change to fine-grained sediments as seen in the basal section. The main difference is that in this interval there are a number of tensional features such as veins, and fractures and slickensides visible on some bedding planes in the shale. The overlying section from 3753.70 to 3752.7 m is composed of thickly bedded, featureless, medium-grained sandstone. A number of minor (~1 mm) veins run vertically through the sandstone. The top of this core (3752.7 – 3752.4 m) consists of interbedded mudstones and siltstones as seen in the basal section. Similarly to the Baccalieu I-78 core, trace and body fossils are not present.

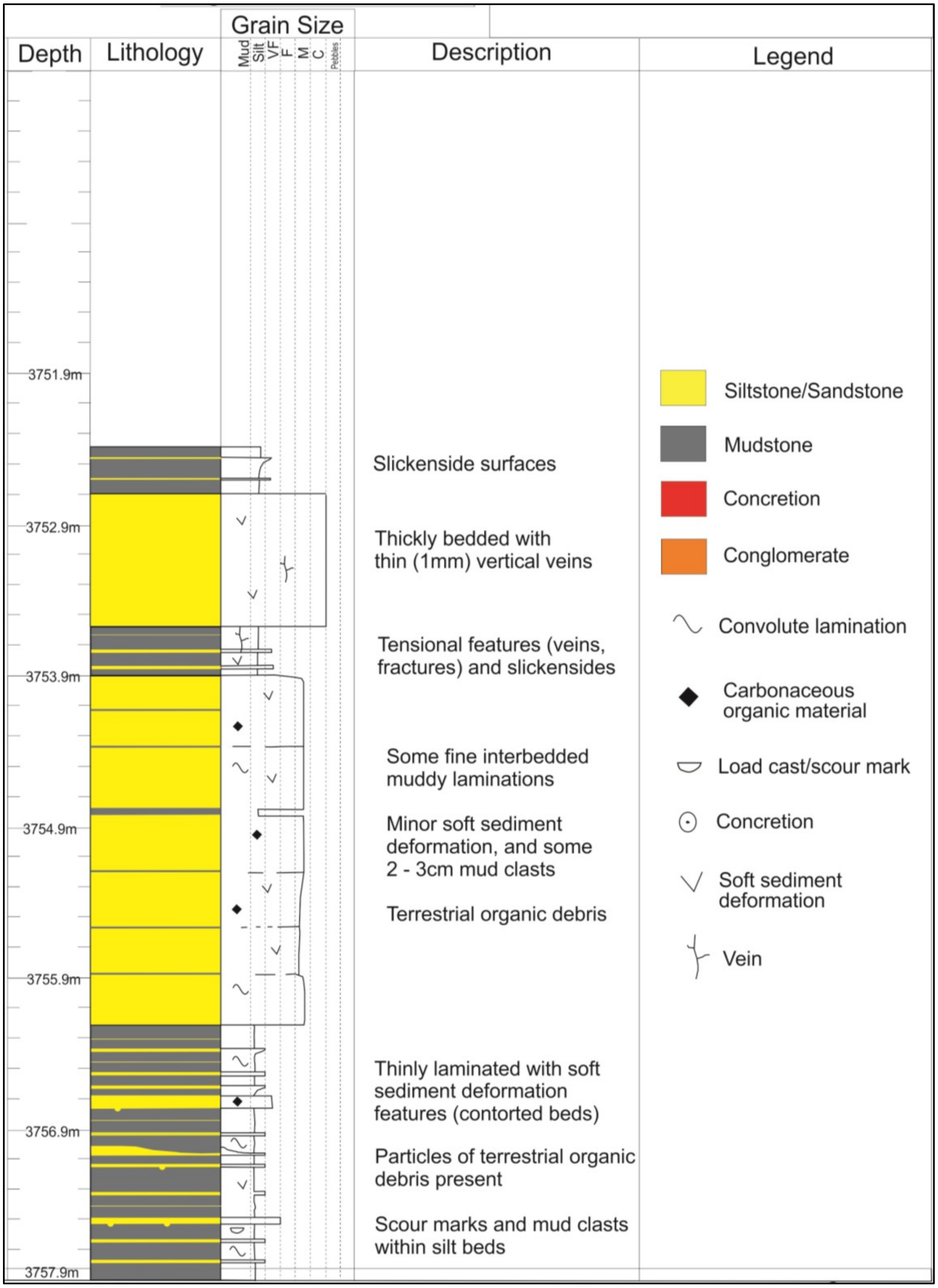

Figure 3.2: Core log for the Lower Tempest Sandstone from the Panther P-52 well.

3.4 - South Tempest G-88 Lower Kimmeridgian Source Rock

Three conventional core samples were retrieved from the South Tempest G-88 well, the first being from 4332.0 to 4322.1 m (Figure 3.3). These cores are described by DeSilva (1994). This core is located in the Lower Kimmeridgian Source Rock stratigraphic unit. The basal section (4332.0– 4328.9 m) consists of interbedded black mudstone, and grey siltstone to fine-grained sandstone. The mudstone beds are typically about 1 cm thick, with a maximum of about 5 cm, and make up 80% of this section (Figure 3.6C). The siltstone and fine-grained sandstone laminae are on average 1-2 mm thick with a maximum of 1 cm. These beds made up about 20% of the interval. Soft sediment deformation is common here, as well as load casts. Near the top of the interval is a 2 cm thick concretionary layer. The overlying section from 4328.9 to 4326.6 m is similar to the basal section; however, the ratio of mudstone beds to siltstone and fine-grained sandstone beds is about 50/50. The average lamina thickness in this section is about 3 mm, with a maximum of 3 cm. From 4326.6 to 4323.9 m, the rock returns to a facies similar to the basal section with about 80% mudstone beds and 20% interbedded siltstone and fine-grained sandstone. The top of the core, from 4323.9 to 4322.1 m is similar to the middle section with a mudstone to siltstone and fine-grained sandstone ratio of 50/50. Trace and body fossils are not present in this core.

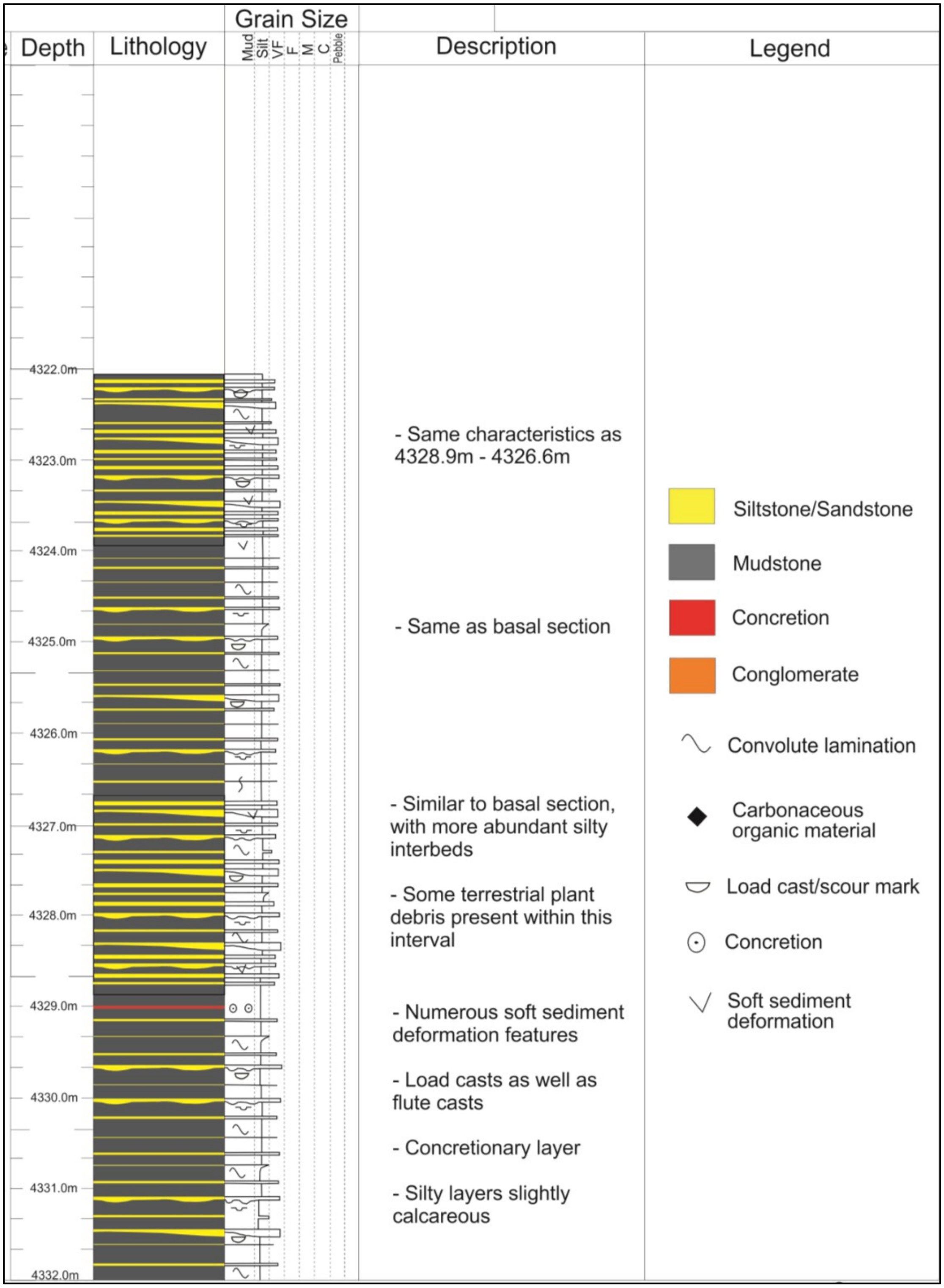

Figure 3.3: Core log for the Lower Kimmeridgian Source Rock from the South Tempest G-88 well.

3.5 - South Tempest G-88 Lower Tempest Sandstone

The Lower Tempest Sandstone was cored from 4199.0 to 4180.6 m (Figure 3.4). Despite being formally termed a sandstone unit, this particular section was similar to the previously described fine-grained lithologies. The basal section of this core from 4199.0 to 4197.03 m is composed of interbedded mudstone (50%) and siltstone and fine-grained sandstone (50%). Soft sediment deformation is prevalent throughout the core, and load casts are common, as well as beds with erosive bases. In the siltstone and fine-grained sand beds, some carbonaceous debris is present. Several brown, 1 cm thick concretions are present in this section. At 4197.03 m, there is an abrupt change to fine- to medium-grained sandstone. The sandstone is slightly less than 5 m thick and continues until 4192.77 m. It has sub-rounded to rounded grains and is moderately well sorted with abundant visible quartz grains. Scattered muddy lenses ranging from 1 mm to 10 mm thick cut the sandstone. The overlying section from 4192.77 to 4186.87 m consists of interbedded siltstone (65%) and mudstone (35%). Fine-grained sandstone beds are uncommon in this section. The average thickness of silt beds is about 4 cm with the maximum thickness being 10 cm whereas mudstone beds are typically 1 cm thick but may reach 3 cm in thickness. Soft sediment deformation is very prevalent in this section with a 10 cm vertical clastic dike present (Figure 3.6D). The upper portion of the core (4186.87 to 4180.6 m) is more of a mud-dominated succession and has about 80% mudstone to 20% interbedded siltstone. The thickest mudstone beds are around 12 cm thick but average 5 cm thick, and the average silt laminae are 2–3 mm thick with a maximum thickness of about 1 cm. This upper interval possesses 2–3 cm-thick, brown concretionary layers and similar soft sediment deformation features to the previous sections. Trace and body fossils are absent from this whole core.

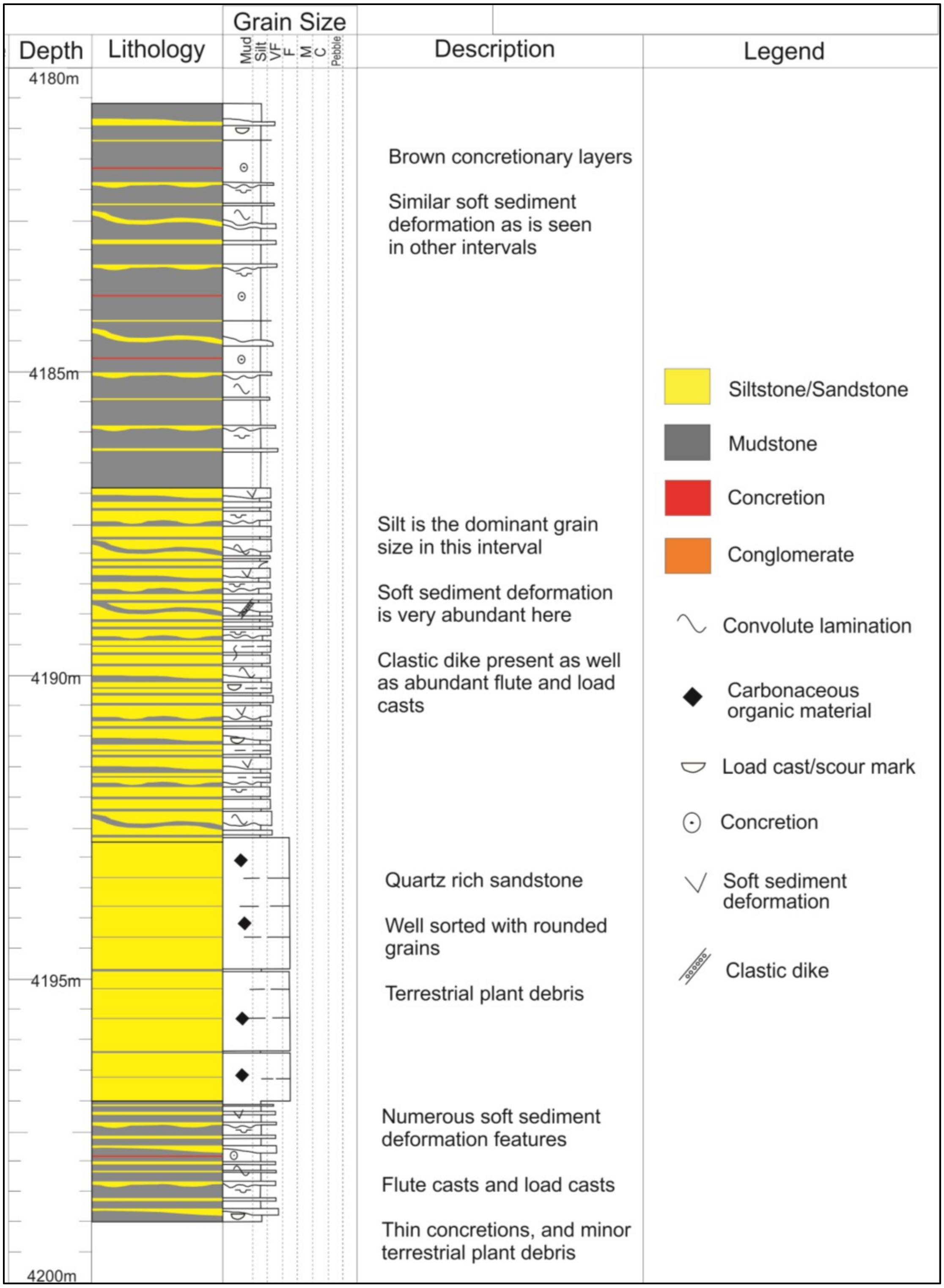

Figure 3.4: Core log for the Lower Tempest Sandstone from the South Tempest G-88 well.

3.6 - South Tempest G-88 – Upper Kimmeridgian Source Rock

A portion of the Upper Kimmeridgian Source Rock unit was cored from 3845.7 to 3827.7 m (Figure 3.5). Despite being designated as the source rock unit, this core was actually the most coarse-grained of any cores examined. The base of the section from 3845.7 to 3844.38 m is composed of brown to grey fine- to medium-grained sandstone interbedded with thin (1 mm) muddy lenses. Abundant carbonaceous debris is present, as is some soft sediment deformation. The sandstone appears quartz-rich, with sub-rounded grains that are moderately sorted. The overlying interval from 3844.38 to 3842.75 m is defined by slightly finer-grained sediments. Siltstone (60%) is interbedded with abundant mudstone layers (40%). The majority of the beds average 1 cm in thickness but may reach 2–3 cm. Soft sediment deformation is prevalent here and creates confusion when trying to define bed thicknesses and original depositional features (Figure 3.6E). Some load casts are present, however, and a single, 5 mm-thick concretionary bed occurs near the middle of the section. Features from 3842.75 to 3837.1 m are similar to the basal section; however, there is about 40% siltstone, 40% sandstone, and 20% mudstone here, with abundant carbonaceous debris. The top section of the core is composed of fine- to medium-grained sandstone interbedded with scattered, 1 mm muddy lenses. Carbonaceous debris is very abundant here (Figure 3.6F) and even forms a couple of 1–2 cm-thick coal layers. The sandstone is moderately sorted, with sub-rounded grains, and abundant quartz. Some less significant soft sediment deformation is present here as well. Trace and body fossils are once again absent.

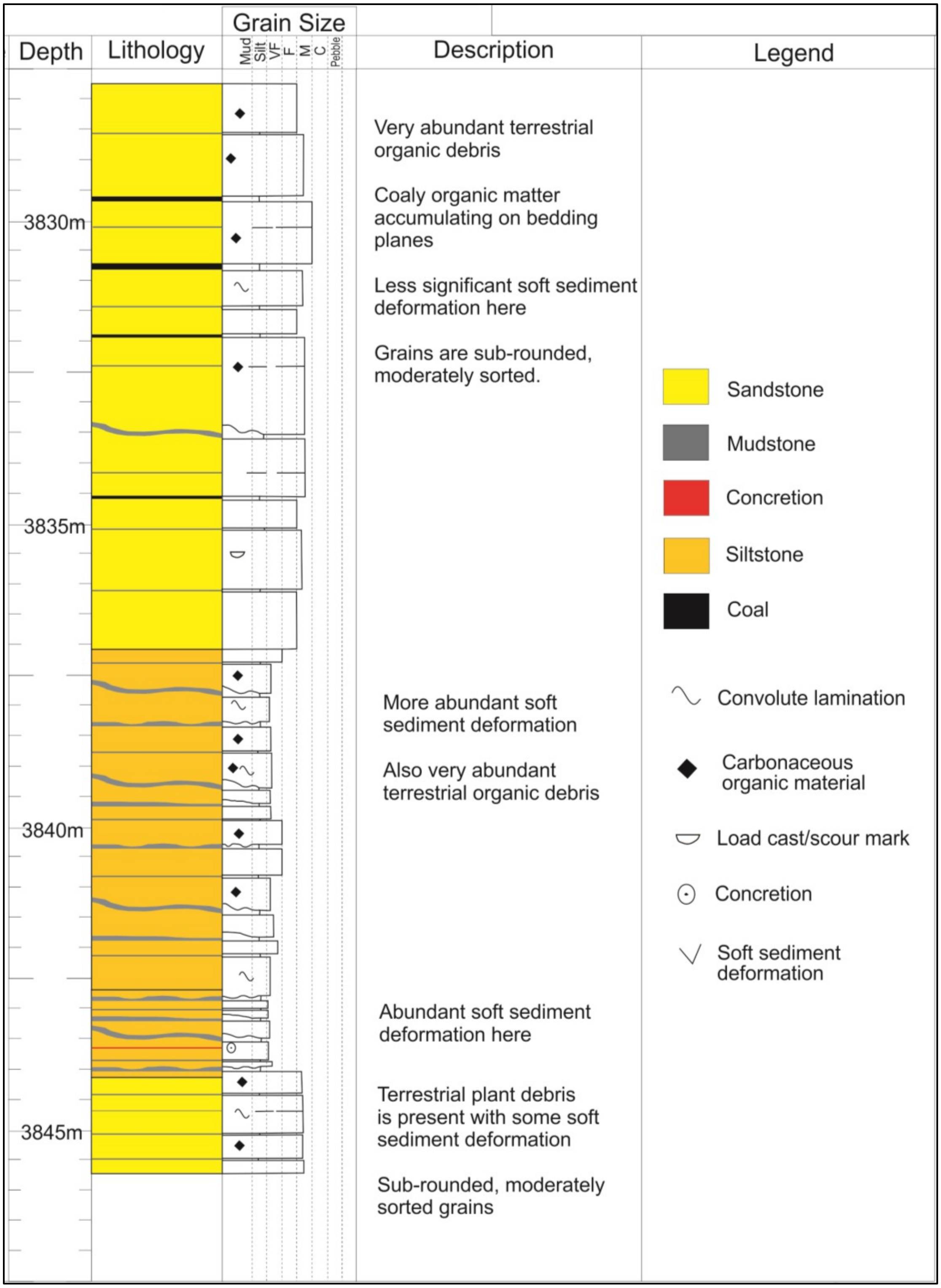

Figure 3.5: Core log for the Upper Kimmeridgian Source Rock from the South Tempest G-88 well.

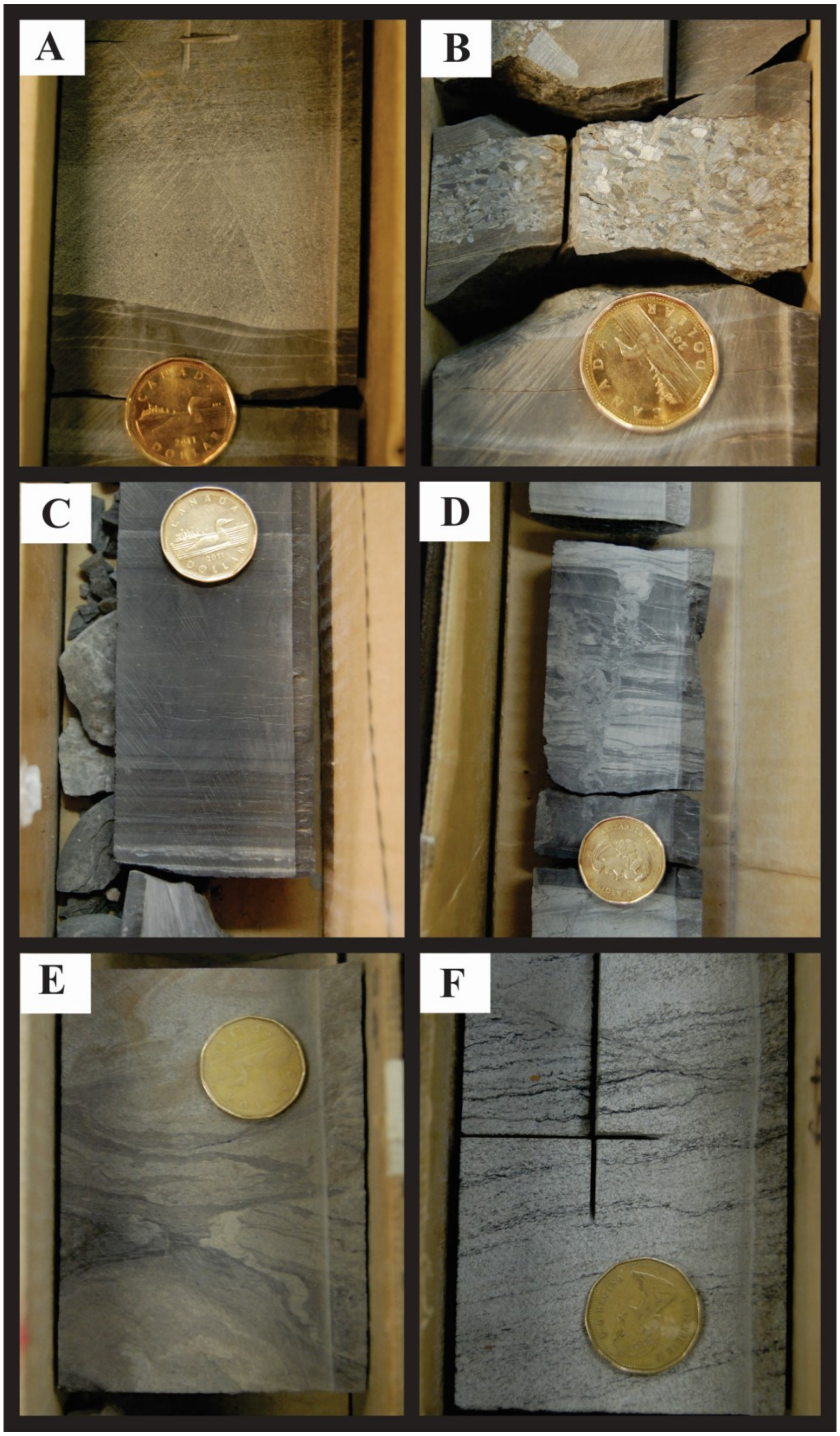

Figure 3.6: Photographs of various Kimmeridgian cores. Canadian one-dollar coin for scale (diameter = 2.5 cm) (A) Scour marks in the Baccalieu I-78 Rankin Formation core. (B) Granules and small pebbles in a sandstone matrix in Baccalieu I-78 Rankin Formation core. (C) Dark grey laminated mudstone in the South Tempest G-88 Lower Kimmeridgian Source Rock core. (D) Clastic dike in the South Tempest G-88 Lower Tempest Sandstone. (E) Soft sediment deformation in the South Tempest G-88 Upper Kimmeridgian Source Rock. (F) Carbonaceous debris in the Upper Kimmeridgian Source Rock of the South Tempest G-88 well.

3.7 - Core Interpretation

A number of features are ubiquitous throughout the Kimmeridgian core samples from the Baccalieu I-78, Panther P-52, and South Tempest G-88 wells. Before interpreting these features, an understanding of the regional depositional setting is essential. McAlpine (1990) described the depositional setting of the proto-Atlantic Ocean in the Late Jurassic as a restricted, silled basin that was relatively shallow (<200 m).

Bateman (1995) created a depositional model for the laterally equivalent Egret Member in the Jeanne d'Arc Basin which related deposition of dark-brown, laminated, organic-rich shales of the Kimmeridgian Egret Member to high sea level, bottom water anoxia, and pelagic sedimentation of marine organisms. Other facies encountered within the Egret Member include unlaminated, grey-brown shales with lower organic contents, as well as some marlstones, claystones, and sandstones (Bateman, 1995). The unlaminated shales were interpreted to have been deposited during a lowering of sea level, in a more proximal environment (Bateman, 1995). The marlstones and claystones were interpreted to be deposited during lowstands, in an oxidizing environment, and the sandstones via turbidity currents which transported slope and shelf sediments into more basinal environments (Bateman, 1995). During periods of high sea level, while deposition of organic-rich shales took place in the basin centre, the other facies (such as the grey-brown shales or sandstones) may have been deposited near the basin margins (Bateman, 1995). When considering the interpretations of Bateman (1995), it is important to note that pelagic sedimentation of marine organisms cannot be the sole process responsible for the deposition of the organic-rich source rock facies. Since there are a significant proportion of detrital clay minerals within this facies, it would be more appropriate to call them hemipelagic deposits.

Kimmeridgian cores from the Flemish Pass Basin and Central Ridge seem to be slightly different than the facies described in the Jeanne d'Arc Basin by Bateman (1995). In all of the described cores, fine-grained mudstones are interbedded with siltstones and sandstones as well as rare coarser beds containing granules and fine pebbles. The presence of these coarse beds, locally interbedded with mudstones, indicates variable energy conditions. Other important features are the abundant scours, erosive bases, flute casts and load casts. In addition, soft sediment deformation is very common and bioturbation is absent. All of these features indicate these sediments were deposited by turbidity currents in a poorly oxygenated environment. The turbidite interpretation was also preferred by Sinclair (1988), McAlpine (1990) & DeSilva (1994) for the Kimmeridgian Tempest Sandstone. Furthermore, a basinal depositional setting is suggested based on the regional depositional setting (McAlpine, 1990; Bateman, 1995), the lack of bioturbation in described cores, as well as black, laminated shales in the described cores which likely represent background sedimentation between turbidity currents (Figure 3.6). A turbidity current model can account for the presence of sands and gravels in this more basinal environment. Boggs (2006) stated that "the single most important mechanism for transporting sands and gravels to deeper water are high-velocity turbidity currents generated on the shelf or upper slope." In addition, the base of turbidite sequences commonly possess sole markings such as flute and load casts and the turbidites themselves generally lack bioturbation (Boggs, 2006). These are characteristics that all of the described cores share, and therefore the turbidite interpretation is preferred. Soft sediment deformation and convolute lamination are abundant in the described cores and are most commonly found in turbidite successions (Boggs, 2006). These features are typical of high depositional rates (Allen, 1982) which would be expected in submarine fans and other turbidite systems.

Evidently, the depositional environment of these individual cores in the Central Ridge and Flemish Pass Basin is different from that of Kimmeridgian source beds in the Jeanne d'Arc Basin. The presence of turbidites was mentioned by Bateman (1995); however, the main source rock facies was interpreted to be deposited by pelagic sedimentation. It appears the source rock of the Flemish Pass Basin and Central Ridge has a different depositional environment than in the Jeanne d'Arc Basin, while still possessing excellent source rock potential (McCracken, 2000). The different depositional environment; however, appears to be reflected in the type of oil expelled by the source beds. Organic geochemistry (Creaney & Alison, 1987; Fowler et al. 2007) indicates that oils from within Flemish Pass Basin sandstones were derived from a source rock with a greater terrestrial component. This matches well with the abundant terrestrial carbonaceous debris observed in the cores, and the input of terrigenous detritus from turbidity currents originating on the shelf or upper slope. This terrigenous detritus would have diluted the marine component of the source rock, which was more important in the Jeanne d'Arc Basin. If the source rock in the Flemish Pass and Central Ridge is in fact more terrigenous in nature, this is an important consideration for interpreting potential provenance of the unit as well as the basin entry points. Presumably, being in closer proximity to the source terrane would supply more abundant, and more terrigenous, detritus to the basin. The depositional environment of the source rock is another important consideration for provenance, as is the influence of marine vs. non-marine conditions, as well as the transport distances of the interpreted system that would be incorporated into a paleodrainage and depositional model.

3.8 - Thin Section Petrography (Introduction and Methodology)

Polished thin sections of mudstones and interbedded sandstones and siltstones were viewed in transmitted light using a petrographic microscope. Mudstones were classified using a classification diagram from Macquaker & Adams (2003). Sandstones and siltstones were classified using a classification diagram from Pettijohn (1975) (Figure 3.7). The mudstone classification of Macquaker & Adams (2003) aims to first identify whether the sample is dominated by allochthonous (detrital), autochthonous (productivity-derived), or components with indeterminate origins. If components are predominantly clastic in origin, as are the samples from this study, the relative abundances of sand, silt, and clay are used for classification. According to Macquaker & Adams (2003), this nomenclature is thought to more accurately define the constituents of fine-grained sediments and can describe the variability found within fine-grained sedimentary successions with more precision than previous schemes. Provenance characteristics of mudstones may be difficult to detect due to the fine grain size, and abundant mineralogical changes from weathering, transport and diagenesis. Previous work linking modal composition of sediments to specific tectonic settings and source terranes has been focused on sand-sized sediments (Dickinson & Suczek, 1979; Dickinson & Valloni, 1980). This highlights the necessity when working with fine-grained rocks to evaluate in-situ geochronology as in this thesis as provenance characteristics may be more difficult to detect, and implementing techniques used in sand-sized sediments may not be feasible (i.e., point counting). Framework minerals, however, may give insight into source terranes, and textures or dissolution features may indicate the effect of diagenesis on the sediment composition.

The sandstone classification scheme of Pettijohn (1975) uses the relative percentages of quartz, feldspars, and lithics (QFL) as well as the amount of matrix present to classify sandstones. The QFL proportions are all normalized to 100% before plotting on a ternary classification diagram; proportions of authigenic minerals, pore space, heavy minerals, detrital carbonate grains, micas and matrix are not included. If the sand and mud fractions have similar sources, provenance characteristics may be more easily identifiable in the interbedded sandstone units. First of all, textural and mineralogical maturity can provide information about degree of sedimentary recycling and transport distances. Additionally, the mineralogy of sandstones has been linked to the tectonic affinities of source areas (Dickinson & Suczek, 1979). In quartz-rich sands, however, discriminating between continental block and recycled orogeny affinities may be difficult because of variable inputs of sedimentary lithic grains (Dickinson et al., 1983; Cox and Lowe, 1995b). Furthermore, processes such as weathering, transport, and diagenesis may alter the composition of the sandstone significantly from that of its parent rock, and these factors might not be considered sufficiently in interpretations of tectonic affinity based on modal mineralogy (Cox & Lowe, 1995a; Weltje & Eynatten, 2004). Evidently, this method has its limitations, but may be useful to supplement provenance interpretations from U-Pb detrital zircon geochronology and whole rock geochemistry.

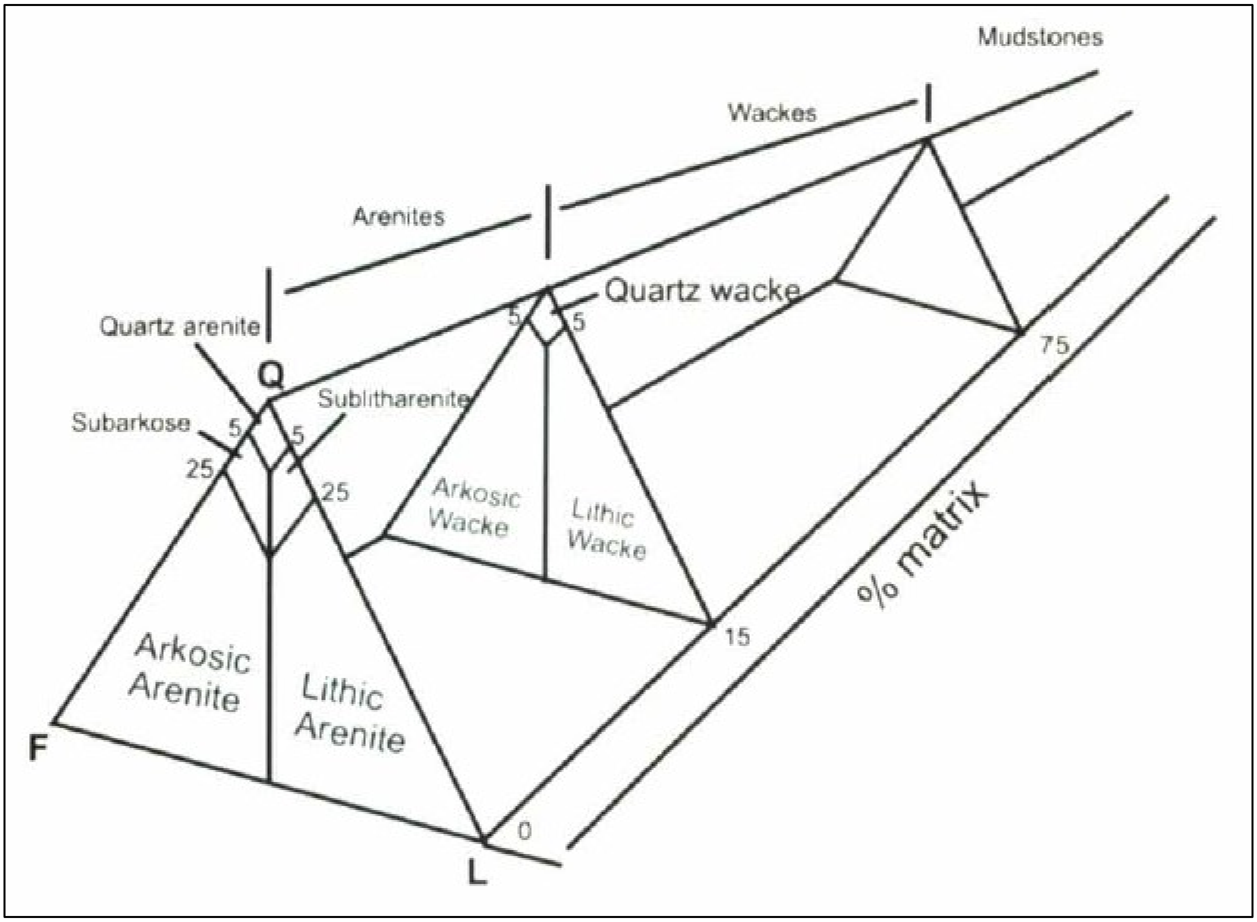

Figure 3.7: Sandstone classification diagram from Pettijohn (1975). Classification is based on modal abundances of quartz grains (Q), feldspar grains (F), and lithic grains (L), as well as the amount of detrital matrix present.

In addition to work with the petrographic microscope, all thin sections were viewed and analyzed on the MLA-SEM. Mineralogical data acquired from this method are also presented with the petrographic results for each sample. The MLA-SEM method is described in Section 2.3.4.

3.9 – Mudstone Petrographic Interpretations

3.9.1 - Introduction

Thin sections from Kimmeridgian mudstones and interbedded sandstones were analyzed from all available conventional cores. Unfortunately, conventional core is unavailable for a number of the important stratigraphic units. For example, the Baccalieu I-78 well has a conventional core within the Rankin Formation, but none within the Upper or Lower Kimmeridgian Source Rock stratigraphic units. Although this is unfortunate for petrographic work, in the following chapters, cuttings samples were used to provide additional heavy mineral data. Abundant sampling for the purpose of petrographic work was not undertaken since the purpose of this study is focused on heavy mineral and geochemical provenance, and also because of a scarcity of core material. However, the samples obtained are interpreted to be representative of the mudstones or sandstones within that individual core.

3.9.2 - Baccalieu I-78 – Rankin Formation

A single thin section from a mudstone unit was examined from the Baccalieu I-78 well (4142.2 m depth) which is stratigraphically within the Rankin Formation (CNLOPB, 2011). Core samples from this well did not penetrate the Kimmeridgian Source Rock units. Although just a single mudstone sample is described, this sample is superficially similar to other mudstone beds within this core. As previously mentioned in Section 3.2, this core is composed of interbedded mudstones, siltstones, and fine-grained sandstones. The mudstone beds are dark grey, and laminated and possess similar features throughout the full section.

Although some minor carbonate cement is present (<5%), this thin section is classified as a sand- and clay-bearing, silt-rich mudstone (Macquaker & Adams, 2003; Figure 3.8). The sample is organized into 2 mm-thick silt and very fine sand laminae interlaminated with 2–7 mm-thick clay-rich layers (Figure 3.9A). There is approximately 15% very fine sand, 45% silt, and 40% clay sized material in the thin section. The 2 mm-thick silt and very-fine sand laminae are abundant in quartz and carbonate cement, as well as minor clay minerals and muscovite, minor organic matter, and trace amounts of opaque heavy minerals. Grains are typically subrounded to subangular with an average size of 0.1 mm with the largest grains around 0.2 mm.

Muddy layers have abundant clay minerals and organic matter, with minor quartz grains and framboidal pyrite. Body fossils are absent in this thin section and there is no evidence of trace fossils or bioturbation.

MLA-SEM analysis indicates a mineralogy similar to that seen in the petrographic work with abundant quartz and muscovite, and common clay minerals, pyrite, calcite, and organic material (Figure 3.10A). The MLA identified illite and chlorite as two individual clay mineral groups present. As mentioned in Section 2.3.4, some complications exist in identifying finely disseminated grains due to the nature of the MLA spot analysis. However, it is possible to group these minerals into broader groups such as 'fine-grained qtz-clay', 'quartz-felds-mix', and 'fine-grained-silicate-carbonate'. A false-colored image generated by the MLA is presented in Figure 3.11A. The false-colored image does not reveal much more than was previously recognized using petrographic techniques; however, the alternating clay-rich and quartz-rich laminae are quite distinct and the compositional differences in these layers are noticeable.

3.9.3 - South Tempest G-88 – Upper & Lower Kimmeridgian Source Rock

Mudstone samples from the South Tempest G-88 well were analyzed from two depths (3843.5 & 4322.75 m). These samples are from the Upper Kimmeridgian, and Lower Kimmeridgian Source Rock stratigraphic units, respectively, and are interpreted to be representative of the mudstones within these cores (i.e., mudstones show similar characteristics throughout both core sections). They are classified as silt-bearing, clay-rich mudstones and are similar to the mudstone described from Baccalieu I-78, with a lack of very-fine sand sized grains (Figure 3.8). The sample from 3843.5 m contained 60% clay sized grains and 40% silt sized grains. The sample was divided into 5–10 mm-thick clay-rich laminations and 2–3 mm-thick silty laminations (Figure 3.9B). The silty laminations are rich in quartz grains, muscovite, and microcrystalline carbonate cement. These grains range from angular to subrounded. The muddy laminations are composed of abundant clay minerals and microcrystalline calcite cement with some organic matter and muscovite and infrequent opaque heavy minerals and quartz grains. The sample from 4322.75 m is very similar, with a mixture of muddy laminae (70%) interbedded with more silty laminae (30%). The sample is finely laminated into alternating ~5 mm-thick clay-rich and silt-rich laminae and possesses a similar mineralogy to the previous sample. The average grain size of the sample is in the clay size range, with the largest grains being about 0.01 – 0.02 mm.

SEM-MLA analysis of these two samples revealed a similar mineralogy to that interpreted from petrographic work (Figure 3.10B, 3.10C). However, although the mineralogy of both samples appeared similar petrographically, the MLA revealed a slight difference in the mineralogy of the finely agglomerated material. The fine-grained material of the Upper Kimmeridgian Source Rock sample is predominantly composed of a mixture of fine-grained quartz and clay, while the finely agglomerated material of the Lower Kimmeridgian Source Rock sample is composed of clay with a mixed silicate-carbonate second component. Illite and chlorite were identified as the most abundant clay minerals in both samples. The false colored images (Figure 3.11B, 3.11C) once again highlight the alternating clay-rich and silt-rich laminae and their compositional differences.

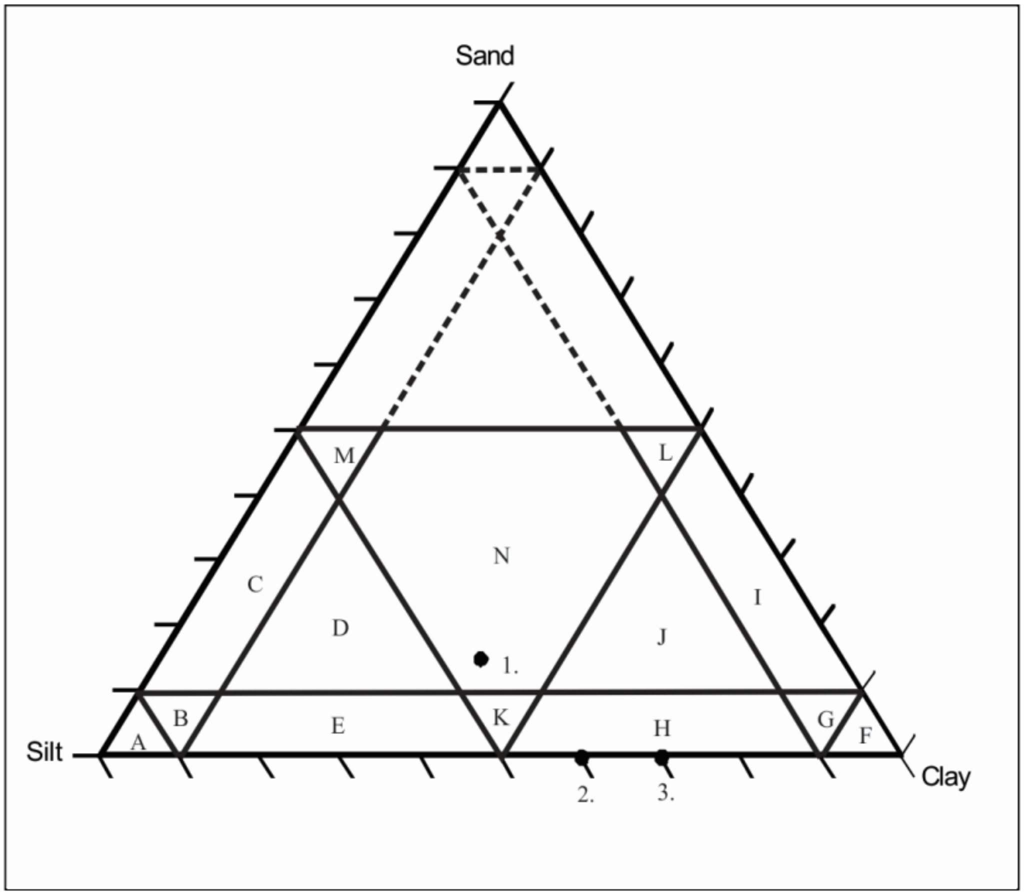

Figure 3.8: Mudstone Classification diagram from Macquaker & Adams (2003). (A) Silt-dominated mudstone; (B) Silt-rich mudstone; (C) Sand-bearing, silt-rich mudstone; (D) Sand and clay-bearing, silt-rich mudstone; (E) Clay-bearing, silt-rich mudstone; (F) Clay-dominated mudstone; (G) Clay-rich mudstone; (H) Silt-bearing, clay-rich mudstone; (I) Sand-bearing, clay-rich mudstone; (J) Sand and silt-bearing clay-rich mudstone; (K) Silt and clay-bearing mudstone; (L) Sand and clay-bearing mudstone; (M) Sand and silt-bearing mudstone; (N) Sand, silt and clay-bearing mudstone. (1) Baccalieu I-78 Rankin Formation sample; (2) South Tempest G-88 Upper Kimmeridgian Source Rock sample; (3) South Tempest G-88 Lower Kimmeridgian Source Rock sample.

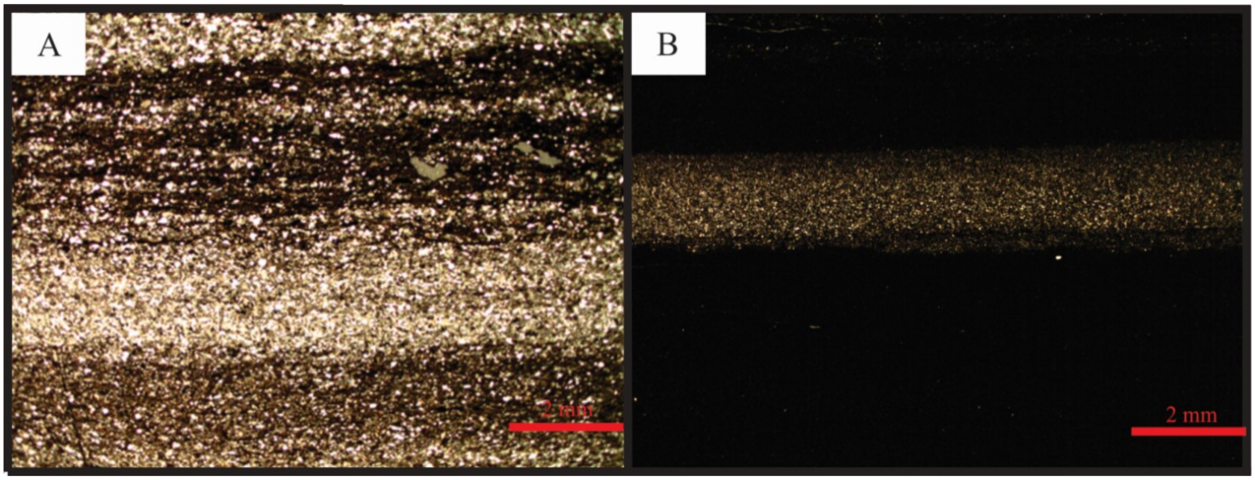

Figure 3.9: Photomicrographs of mudstone samples under crossed polars. (A) Baccalieu I-78 Rankin Formation; (B) South Tempest G-88 Upper Kimmeridgian Source Rock.

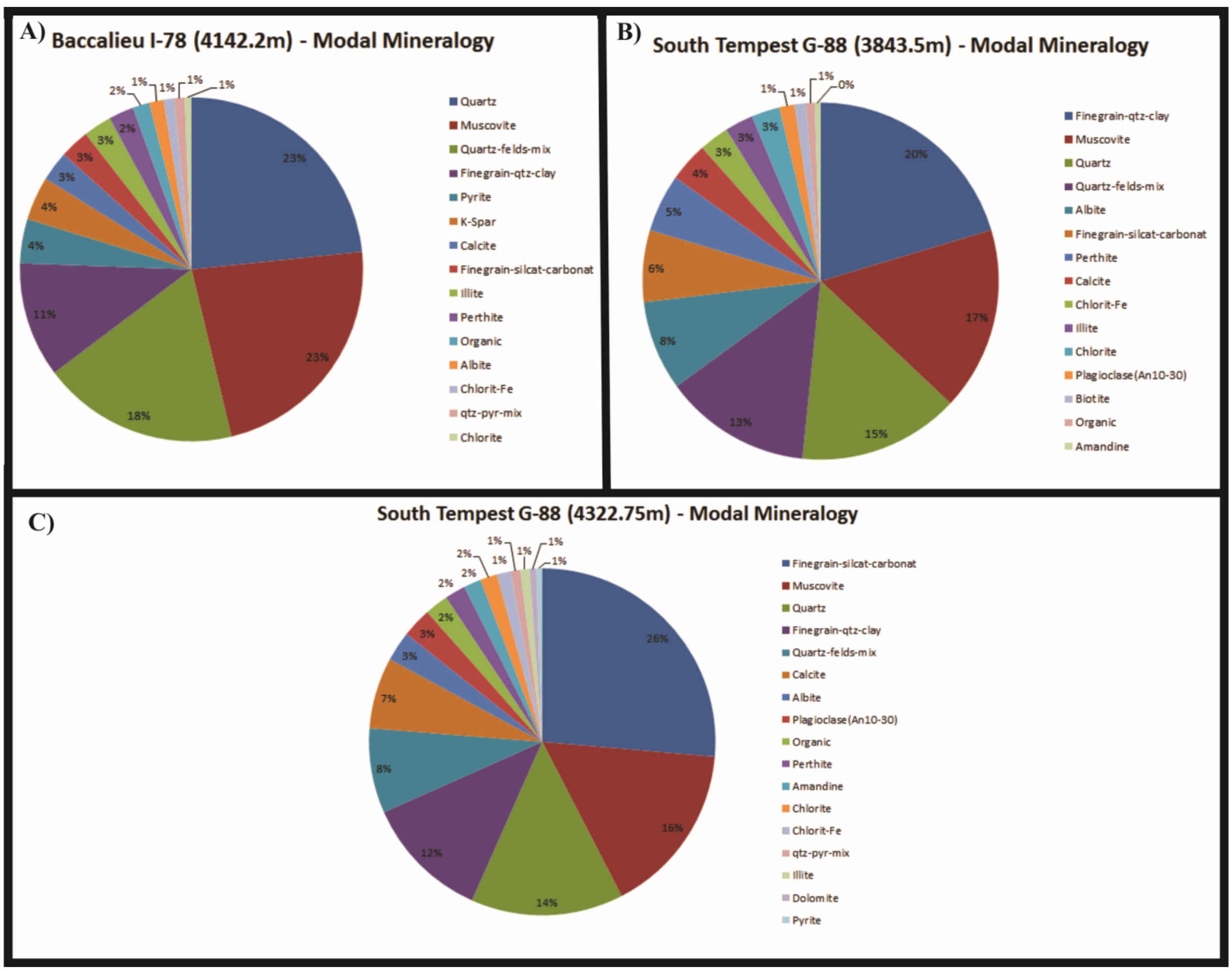

Figure 3.10: Modal Mineralogy (weight %) of three mudstone samples from MLA-SEM analysis. Minerals with less than 0.5 wt. % are not included.

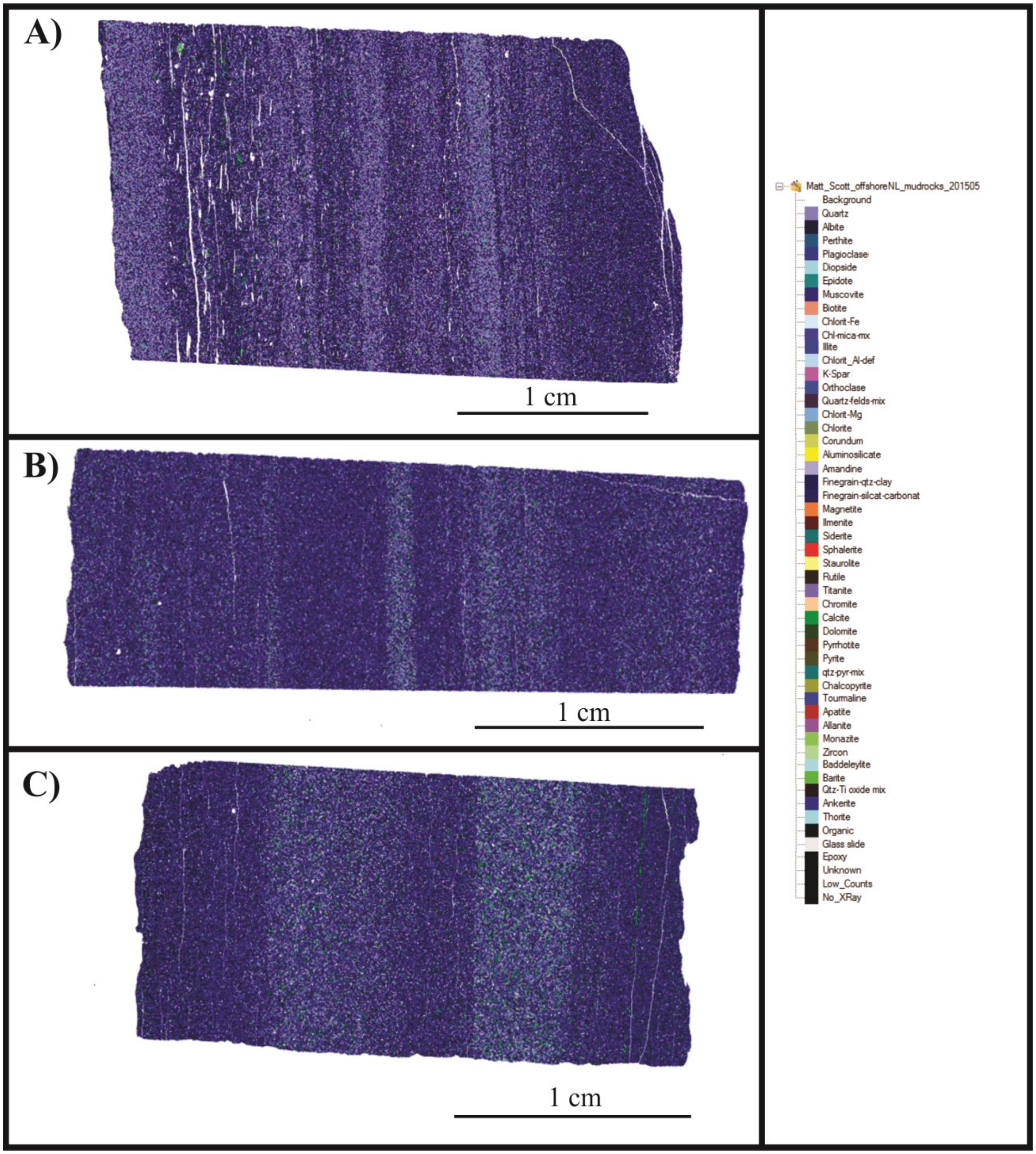

Figure 3.11: False-color images of mudstone samples. Identification of individual minerals here is difficult, but the images demonstrate how the MLA software fully classifies minerals in these fine-grained rocks. (A) Baccalieu I-78 (4142.2m). Most abundant minerals in this sample are quartz, muscovite, a quartz-feldspar mix, and a fine-grained quartz-clay mix. (B) South Tempest G-88 (3843.5m). Most abundant minerals in this sample are a fine-grained quartz-clay mix, muscovite, quartz and a quartz-feldspar mix. (C) South Tempest G-88 (4322.75m). Most abundant minerals in this sample are a fine-grained silicate-carbonate mix, muscovite, quartz, and a fine-grained quartz-clay mix.

3.10 – Petrographic Interpretations of Siltstones and Sandstones

3.10.1 - South Tempest G-88 – Upper Kimmeridgian Source Rock

A single sample from the South Tempest G-88 well (3837.3 m) is an arkosic wacke based on the classification scheme of Pettijohn (1975) (Figure 3.7). Although just one sample was analyzed, it is macroscopically representative of the interbedded sandstones within this section of core. The sample is composed predominantly of quartz, carbonate cement, and a fine clay matrix (Figure 3.12A, Figure 3.12B). Also present are feldspars, lithic fragments, muscovite and minor pyrite and opaque minerals. Albite is the most abundant feldspar present, although some K-feldspar is present as well. It must be noted, however, that no stain was applied to the thin sections. Therefore, only twin laws were used to distinguish K-feldspar from plagioclase. The grains are subangular to subrounded and moderately well sorted. The carbonate cement is fairly abundant (15 %), and appears to have formed early, as there is a significant amount of intergranular volume, as well as few indications of compaction before cementation such as sutured quartz grain contacts or deformed clay-rich lithic grains. The porosity of the sandstone appears very low (3-5%) due to the abundant cementation. Bioturbation from this sample is absent.

SEM-MLA analysis of this sample reveals a similar mineralogy to that described from petrographic observations (Figure 3.13A). In particular, the MLA revealed that the relative feldspar proportions (albite more abundant than K-feldspar) previously identified by petrography were indeed correct, despite no staining in the thin sections. Minerals identified by the MLA which were not observed petrographically include illite and chlorite. The false-colored image (Figure 3.14A) highlights the lack of laminations or bedding in this sample.

3.10.2 - Baccalieu I-78 – Rankin Formation

A representative sample of interbedded sandstone from the Baccalieu I-78 well (4135.29 m) was analyzed and also plots as an arkosic wacke using the classification scheme of Pettijohn (1975) (Figure 3.7). The sample is composed of quartz, carbonate cement, feldspars, and lithic fragments (chert and sedimentary rock fragments), with minor shell fragments, and a fine clay matrix (Figure 3.12C). Also present are opaque iron oxides and framboidal pyrite. Feldspars present include albite and K-feldspar, with albite being the dominant feldspar. The grains are subrounded to subangular and moderately sorted. Average grain size is 0.25 mm, but ranges from 0.1 – 0.5 mm. Similar to the G-88 sample, carbonate cement is fairly abundant (20%), occludes porosity, and appears to have formed early due to the lack of sutured grain contacts and preservation of significant intergranular minus-cement porosity. Shell fragments present here are likely remnants of bivalve shells with one example of a crinoid stem. Many are fractured, disaggregated or broken. Bioturbation is absent from this sample.

SEM-MLA analysis of this sample supports the mineralogical observations from petrography (Figure 3.13B). Quartz, carbonate cement (identified by the MLA as calcite), and feldspars are most important. Of the feldsaprs, albite is more abundant than K-feldspar. Illite and chlorite were two clay mineral types identified. The false colored image (Figure 3.14B) shows the lack of laminations or bedding in the sample.

3.10.3 - Panther P-52 – Lower Tempest Sandstone

At 3754.95 m of the Panther P-52 core, a representative sandstone sample was analyzed and plots as a subarkose (Pettijohn, 1975) (Figure 3.7). The sample is the most coarse-grained of all those sampled. It is composed of quartz, carbonate cement, feldspars, lithic fragments (chert and sedimentary rock fragments), muscovite, and a minor clay mineral matrix (Figure 3.12D).

As with the previous samples, albite is more abundant than K-feldspar, although both are present. Grains are subrounded to subangular and poorly sorted. In contrast to previous samples, many of the quartz grains in the sample are fractured. The grain size averages 0.4 mm but ranges from 0.1 - 0.8 mm. Carbonate cement is present at about 10%, although not as abundant as in the previous samples. The cement likely formed before significant compaction; however, minus-cement porosity is lower than in previous samples, and long grain contacts indicate some compaction has taken place. Bioturbation is not present in this sample; however, a few minor shell fragments were noted as detritus.

An additional sandstone sample from 3757.5 m was analyzed and possesses a similar composition to the sandstone from 3754.95 m. This sample contains abundant quartz, feldspars (predominantly albite), muscovite, lithic fragments (mostly sedimentary rock fragments), calcite cement, and a clay mineral matrix. The matrix of this sample is greater than 15%, so it is therefore classified as an arkosic wacke (Pettijohn, 1975) (Figure 3.7). Grains present are angular to sub-rounded and range from 0.01 – 0.1 mm with an average of about 0.05 mm. This sample also possesses more abundant calcite cement than previous samples (20%), which is microcrystalline in nature. The cement appears to have preceded compaction and significantly occludes any porosity. No bioturbation is observed in this sample. A 2 cm-long, 0.5 mm-thick shell fragment is present.

Analysis of these two samples by MLA-SEM indicates a similar mineralogy to that observed petrographically, with abundant quartz, albite, carbonate cement (identified by the MLA as calcite), and muscovite (Figure 3.13C, 3.13D). The MLA identified chlorite as the most important clay mineral as well as the presence of some Fe-carbonate minerals such as ankerite and siderite that were less important in previous samples. The false-colored images (Figure

3.14C, 3.14D) help to emphasize the grain size contrast between the coarse-grained sample from 3754.95 m and the finer-grained sample from 3757.5 m. The absence of laminations or bedding is also observed.

3.10.4 - South Tempest G-88 – Lower Kimmeridgian Source Rock

The one sample, G-88 (4322.2 m), from the Lower Kimmeridgian Source Rock stratigraphic unit plots as a subarkose (Figure 3.7; Pettijohn, 1975). This sample contains abundant quartz, feldspars (mostly albite), muscovite, and lithic fragments. The lithic fragments are predominantly chert and minor sedimentary rock fragments. The grains are on average 0.05 mm with a maximum of 0.1 mm and are subangular to subrounded. Also present is a minor clay mineral matrix, and abundant microcrystalline calcite cement that makes up about 30% of the sample. The cement occludes any porosity, and appears to pre-date compaction. No bioturbation is present in this sample.

MLA-SEM analysis of this sample supported the mineralogy results from petrographic analysis as quartz, calcite cement, albite, and muscovite are important framework minerals (Figure 3.13E). The MLA identified the presence of ankerite as well as dolomite, and found chlorite to be the most abundant clay mineral. The false colored image (Figure 3.14E) does not reveal any previously unidentified features, although the fine-grained nature of the sample is evident from the image.

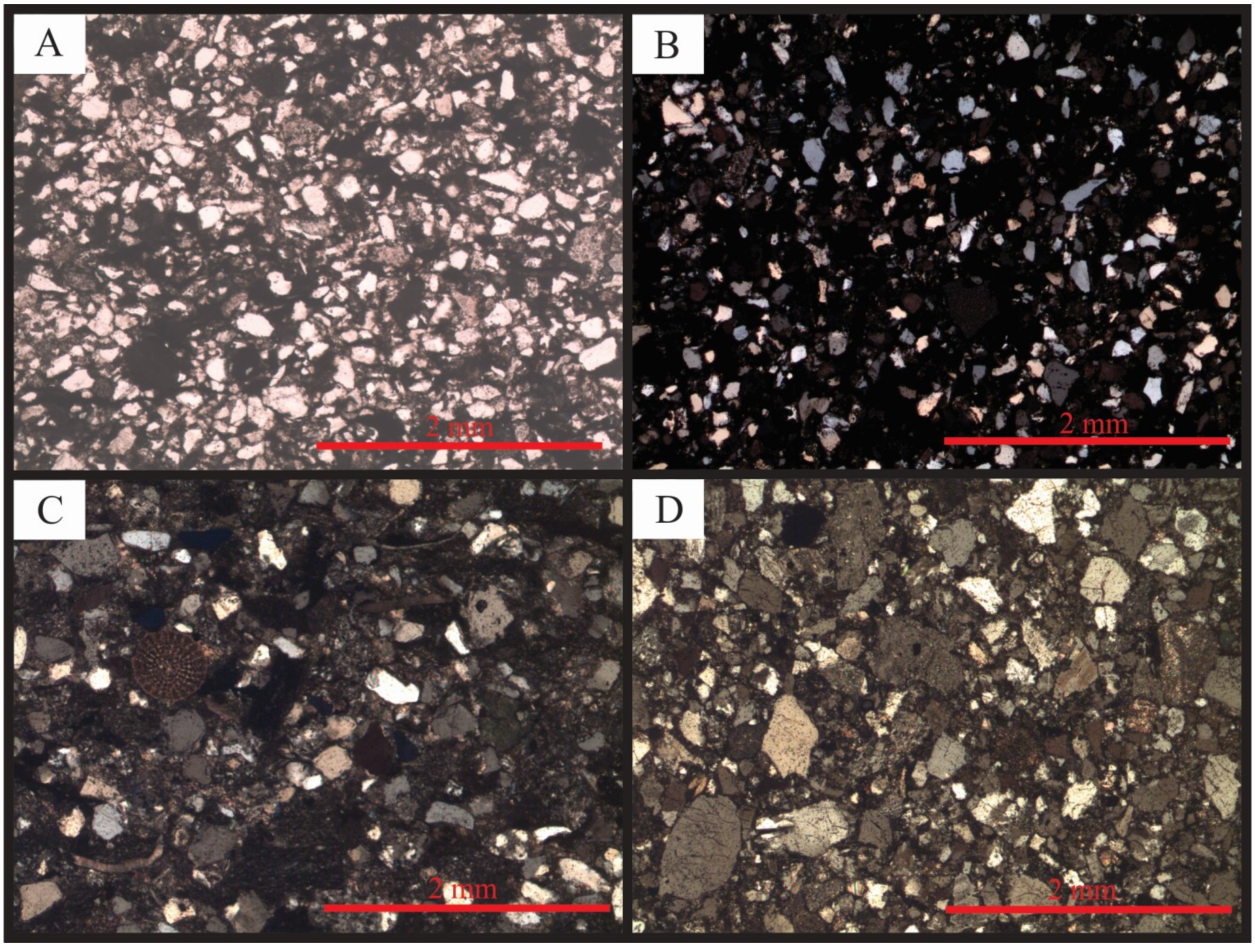

Figure 3.12: Photomicrographs of sandstone samples. (A) Sandstone from the South Tempest G-88 Upper Kimmeridgian Source Rock under plane polarized light; (B) Sandstone from the Upper Kimmeridgian Source Rock from South Tempest G-88 under crossed polars; (C) Sandstone from the Rankin Formation of Baccalieu I-78 under crossed polars; (D) Sandstone from Panther P-52 in the Lower Tempest Sandstone under crossed polars.

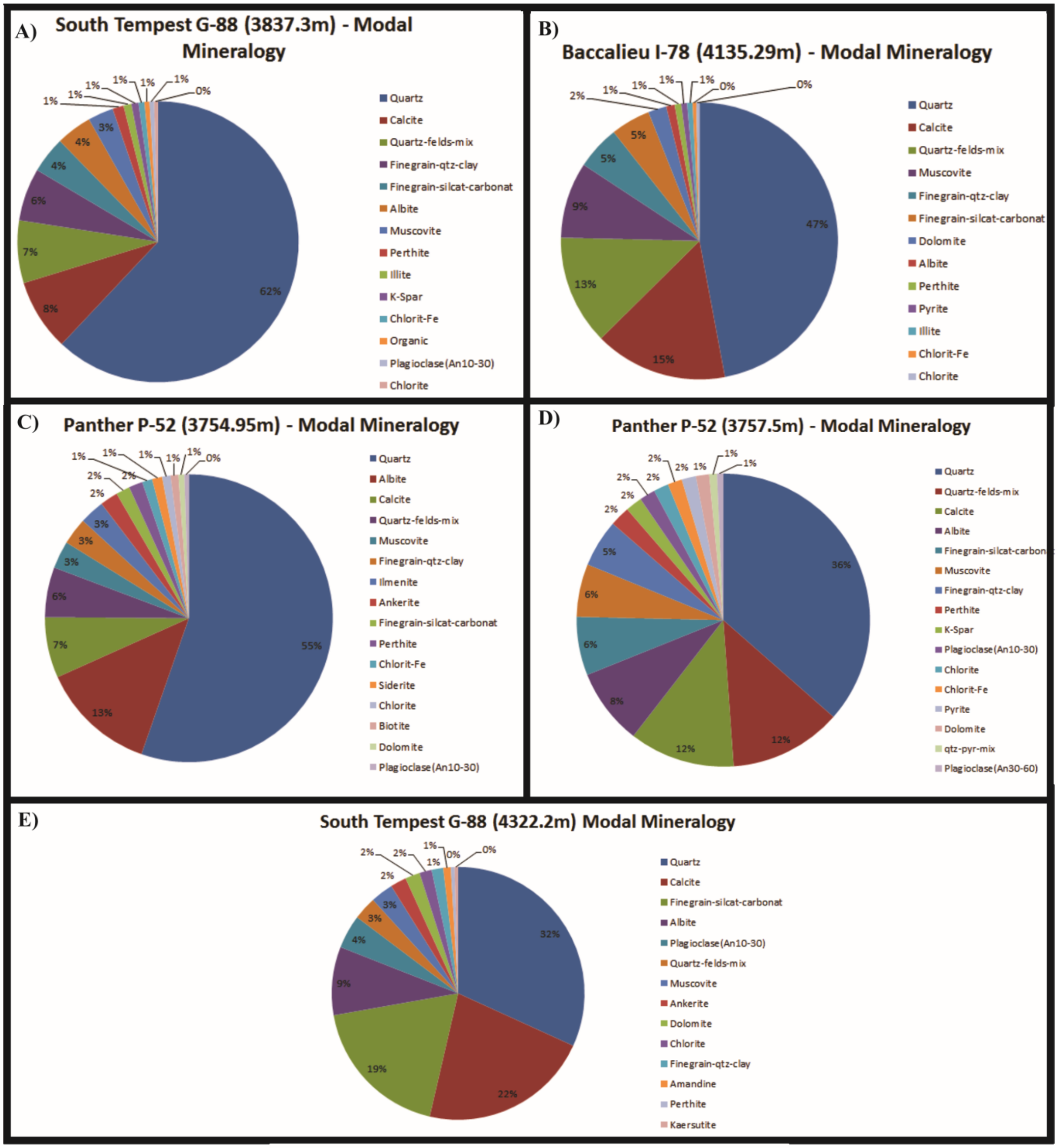

Figure 3.13: Modal mineralogy (weight %) of five sandstone samples from MLA-SEM analysis. Minerals with less than 0.5 weight % are not included.

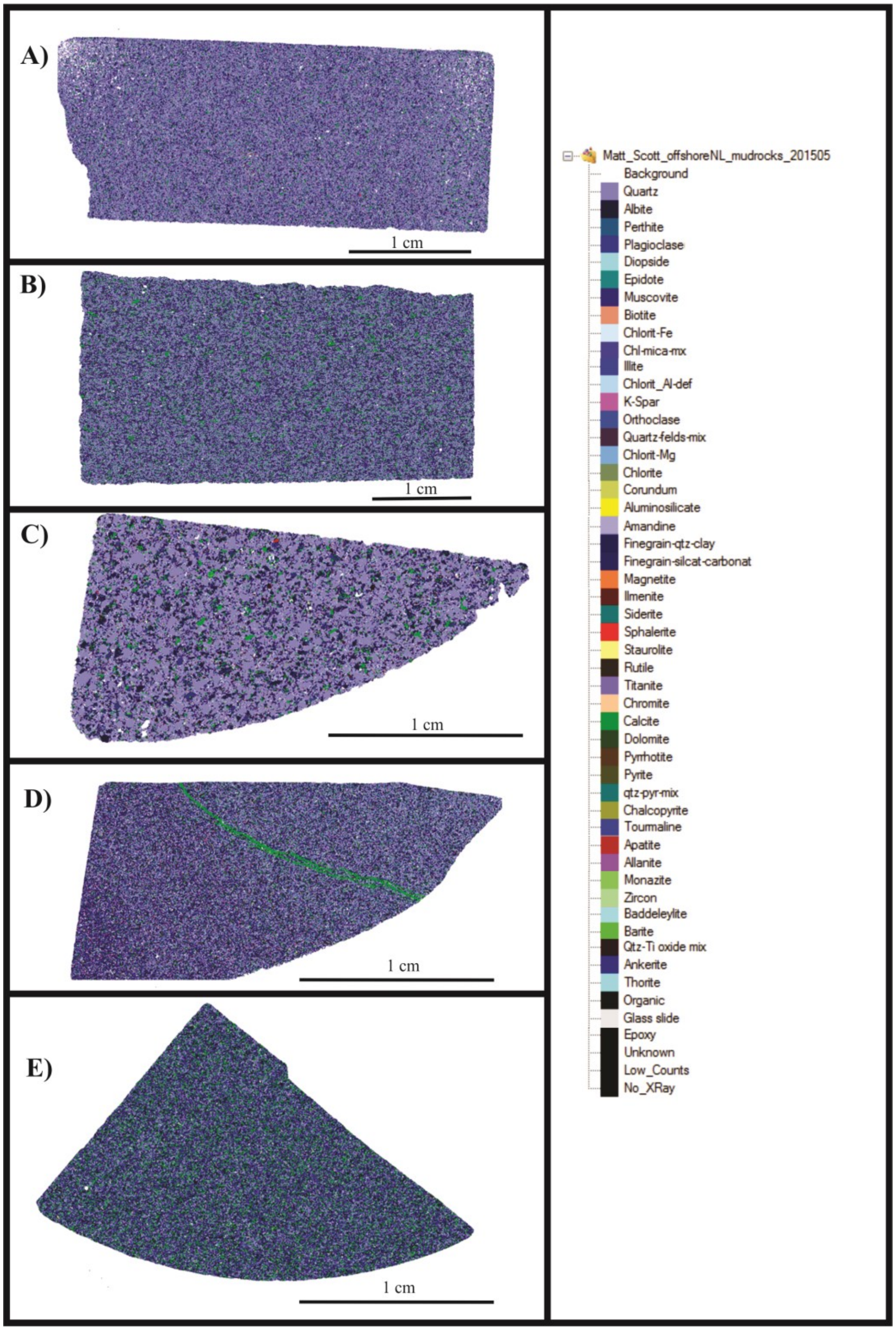

Figure 3.14: False-colored images of sandstone samples. (A) South Tempest G-88 (3837.3m). Most abundant minerals in this sample are quartz, calcite, a quartz-feldspar mixture and a fine-grained quartz-clay mixture. (B) Baccalieu I-78 (4135.29m). Most abundant minerals in this sample are quartz, calcite, a quartz-feldspar mixture, and muscovite. (C) Panther P-52 (3754.95m). Most abundant minerals in this sample are quartz, albite, calcite, and a quartz-feldspar mixture. (D) Panther P-52 (3757.7m). Most abundant minerals in this sample are quartz, a quartz-feldspar mixture, calcite, and albite. (E) South Tempest G-88 (4322.2m). Most abundant minerals in this sample are quartz, calcite, a fine-grained silicate-carbonate mixture, and albite.

3.11 - Petrographic Interpretations and Implications for Provenance

3.11.1 - Mudstones

Interpreting provenance characteristics from mudstone petrography is challenging due to the fine grain size, and abundant diagenetic mineralogical changes. However, several features in the samples studied were found to provide information about potential source terranes and provenance. Despite the abundant clay minerals, and organic matter in the mudstone samples, there are also silty layers with some detrital grains present. The detrital grains are predominantly quartz and muscovite, which are characteristic of an upper crustal or granitic source. The morphologies of grains, however, are highly variable. Many grains are rounded, but there were also subrounded, subangular, and angular grains as well. This indicates varying provenance and transport histories of the grains. It is difficult to determine whether the mudstone units were derived from previous sedimentary rocks, or are first-cycle crystalline detritus. Likely, these mudstones result from a combination of both recycled sedimentary and first-cycle sources, as the surrounding terranes described in Chapter 1 are composed of a mixture of sedimentary as well as intrusive and extrusive volcanic rocks. It is difficult to determine the level of sedimentary recycling undergone by the grains from these mudstones, as previous studies linking mineralogical maturity (ie. the predominance of quartz grains) to sedimentary recycling (Dickinson & Suczek, 1979; Critelli et al., 2003; Arribas & Tortosa, 2003) all deal with sandstones, and are not necessarily comparable to mudstones. It may also be difficult to link the quartz grain morphology to the level of sedimentary recycling. In sandstones, angular grains indicate a lack of prolonged abrasion, and potential input from first-cycle sources (Blatt & Christie, 1963; Suttner et al., 1981; Cox & Lowe, 1995a). However, in addition to transport distance and level of abrasion, the rate of rounding of quartz is also a function of the particle size (R. Hiscott, personal communication). Silt-sized quartz will always be more angular than sand-sized quartz from the same source and with the same transport history (R. Hiscott, personal communication). Therefore, it is difficult to determine if the angularity of the quartz grains is a function of the level of sedimentary recycling, or if it is just a function of the fine-grain size of these samples. Evidently, it is difficult to quantify the proportion of recycled to first-cycle material in these mudstones; however, the following chapters focused on heavy mineral analyses and geochemistry will address the degree of sedimentary recycling.

In mudstones, the type of clay minerals present may also be indicative of source terrains (Weaver, 1989; Potter et al., 2005). Although XRD analyses were not undertaken for these samples, the MLA-SEM modal mineralogy of all samples indicates that illite and chlorite are the most common clay minerals. These clay minerals may be indicative of their original sources; however, due to the burial depth of these samples, it is possible that they are in part diagenetic products. Nonetheless, Potter et al. (2005) state that illite may be derived from igneous, sedimentary, or metamorphic rocks with various weathering intensities and chlorite may be derived from sedimentary or metamorphic rocks that have undergone various degrees of weathering. This, combined with the presence of abundant muscovite grains, indicates a detrital supply from a combination of igneous, metamorphic and recycled sedimentary sources. The presence of abundant muscovite in most samples suggests mica-rich granites were an important supplier of detritus. Rocks of this composition are ubiquitous in the basement terranes that surround the continental margin of Newfoundland such as the Avalon Zone, and Central Mobile Belt. However, rocks of the Meguma Terrane of Nova Scotia and those of the Iberian Peninsula are also characterized by abundant granitic rocks. Generally, these mudstone units appear to be composed of a mixture of recycled and first-cycle material that was sourced from an upper crustal source that undoubtedly includes granites. This terrane could correlate with a number of surrounding basement blocks known in the Grand Banks area. Detrital zircon geochronology and heavy mineral data in the following chapters will address the question of which terrane these Kimmeridgian rocks were most likely derived from.

3.11.2 - Sandstones

The sandstone samples provide a significant amount of provenance information. Two of the samples are subarkoses, while the other three are arkosic wackes. In general, they possess similar mineralogies with quartz, feldspars, lithic fragments, muscovite, calcite cement, and a clay mineral matrix. Mineralogically, the samples can be considered submature, as feldspars and lithic fragments make up >10% of these samples. This mineralogy indicates erosion of first-cycle rocks (plagioclase and potassium feldspars) and also recycled sedimentary rocks (sedimentary lithic fragments). Texturally, these sandstones are submature as well. The samples generally have a significant portion of clay matrix and grains tend to be moderately sorted and range from angular to subrounded. This suggests a lack of significant abrasion of grains and a mixture of first-cycle and recycled sedimentary detritus. Shell fragments (bivalves and crinoid stem) are found in the sandstone samples. These fragments have features indicative of transport as they are often fragmented or fractured. Overall, similar to the mudstone units, the sandstones appear to result from the erosion of both first cycle and recycled sedimentary material. Potential source areas, such as the Avalon Zone and Central Mobile Belt of Newfoundland are characterized by a mixture of plutonic and volcanic igneous rocks, as well as abundant sedimentary cover sequences. It is therefore plausible to expect a mixture of recycled and first-cycle grains in the Kimmeridgian rocks of the Flemish Pass and Central Ridge. This would account for the presence of both plagioclase and potassium feldspar grains from first-cycle sources as well as the sedimentary lithic fragments from sedimentary rocks.

In terms of reservoir quality, the Kimmeridgian sandstones described here would be low quality reservoir rocks. Porosity is generally very low, and abundant clay material as well as carbonate cement occludes pore spaces. Preserving significant porosity is likely reliant on grain dissolution of feldspars or unstable minerals as the grain shape and sorting of the majority of grains in these samples is inconsistent with abundant primary or intergranular porosity.

3.11.3 - Summary

Both mudstone and sandstone units sampled from the various wells display similar provenance characteristics. They were likely derived from a mixture of first-cycle igneous rocks (especially granites), metamorphic rocks, as well as recycled sedimentary rocks. This type of source rock is reasonable given the proximity to the Avalon Zone and Central Mobile Belt of Newfoundland, and to Iberia, where these types of igneous rocks and sedimentary cover sequences are common. It is difficult to determine potential transport distances of the detrital material using the texture and composition as seen in thin sections, because weathering and diagenesis have a large effect on these features. Detrital zircon geochronology and heavy mineral data in subsequent chapters will address this issue more thoroughly.

Chapter 4 – Whole Rock Geochemistry

4.1 - Introduction

Whole rock geochemical analyses were completed on samples of Upper Jurassic source rocks from the Central Ridge and Flemish Pass Basin. Since a significant amount of core was available over the Late Jurassic interval, all samples were of conventional core. This is preferable as cuttings samples may possess unknown levels of contaminants from drill bit shavings or drilling mud.

Major and trace element geochemical analyses were undertaken to supplement the provenance interpretations as deduced from detrital zircon geochronology (next chapter). Changes in sediment provenance for mudstones can be reflected in their chemical compositions (Hurst and Morton, 2001). Although McLennan et al. (2002) state that a dominant control on the composition of a sedimentary rock is the composition of the source rock from which it was derived, there are additional factors that control the chemistry of a sedimentary rock such as the amount and type of weathering, hydraulic sorting, and diagenesis. These factors will all be addressed in this section.

A combination of both major element and trace element analyses was undertaken to interpret provenance of the Upper Jurassic source rocks studied in this project. Datasets are presented in Appendix B. Sampling and analytical methods are reviewed in Section 2.3.7 as well as 2.3.8. In total, 20 samples were analyzed from the South Tempest G-88 well, 9 from Baccalieu I-78, and four from the Panther P-52 well. The South Tempest G-88 samples were from the Lower Kimmeridgian Source Rock, Lower Tempest Sandstone, and Upper Kimmeridgian Source Rock stratigraphic units. The Baccalieu I-78 samples were all from the Rankin Formation, and the Panther P-52 samples are from the Lower Tempest Sandstone.

4.2 - Major Elements

4.2.1 - Introduction

Major elements are not as useful as trace elements for identifying provenance signatures because they are much more susceptible to post-depositional alteration. Major element suites are most useful in determining how much weathering, and the type(s) of weathering, that a particular sample has undergone (Potter & Maynard, 2005). Several indices, such as the CIA (chemical index of alteration), can be used to quantify the weathering effects.

The CIA is a quantitative measure and is most useful for determining the degree of chemical weathering (Nesbitt & Young, 1982; Fedo et al. 1995). During chemical weathering, labile cations such as Ca^{2+}, Na^{+}, and K^{+} are more easily removed relative to more stable elements such as Al^{3+}, and Ti^{4+} (Nesbitt & Young, 1982). Elevated CIA values suggest the formation of fine-grained clay minerals such as illite and kaolinite. Conversely, low CIA values indicate an absence of chemical weathering with physical weathering dominant. Physical weathering is most common in cool or arid conditions where source rock degrades into finer-grained material, but in contrast to chemical weathering, the resulting sediment retains the mineralogical and geochemical signature of the source rock (Nesbitt & Young, 1982; 1996). CIA values of around 50 represent fresh, unweathered rock, whereas values between 50 and 100, represent variably chemically weathered rocks. Samples with abundant clay minerals will possess CIA values of 75 or higher (Nesbitt, 2003). Fedo et al. (1995) define the procedures for calculating the CIA. It should be noted that the contributions of CaO from calcite, dolomite, and apatite must be removed from the calculations. For samples in this study, the amount of CaO from silicate rocks became negligible, and therefore a value of 0 weight % was used for CaO.

A useful feature of the CIA ratio is the capability to plot it on a ternary plot and identify weathering trends; i.e., it may be possible to identify a trend from the least weathered to the most weathered samples in the data. Furthermore, by extrapolating such a trend, it may be possible to identify the original composition of the source rock. It may be possible to use this method to supplement provenance interpretations from detrital zircon geochronology for the Upper Jurassic source rocks.

4.2.2 - CIA Results

CIA values were calculated for all 33 samples, of which 25 were fine-grained enough to be considered mudstones. The mudstone samples are from four different stratigraphic units: the Lower Tempest Sandstone, Lower Kimmeridgian Source Rock, Rankin Formation and Upper Kimmeridgian Source Rock. The other eight samples are of the more uncommon, coarser-grained, sandstone beds from the Upper Kimmeridgian Source Rock and Lower Tempest Sandstone stratigraphic units. Results are illustrated on Figures 4.1 and 4.2. The minimum CIA value observed is 73, whereas the maximum is 80; the average is 77. The mudstone samples possess an average CIA value of 77, and the sandstone samples exhibit an average CIA value of 76. Samples from different wells display similar CIA values, and samples from different stratigraphic units also display little variation. There is a slight difference in CIA values within different lithologies, and the mudstones tend to have slightly higher values than the sandstones. Evidently, all these samples underwent weathering in an environment dominated by chemical weathering, converting feldspars to clay minerals. Unfortunately, due to the lack of variation in CIA values, it is difficult to define any weathering trends. In the adjacent Jeanne d'Arc Basin, Dearin (2006) analyzed rocks from the Ben Nevis Formation and was able to identify the original source rock for these sandstones as having been granodioritic in composition using the weathering trends of the CIA diagram (Figure 4.3).Trace element diagrams in the next section proved to be more helpful for the identification of source rock composition(s) for the Upper Jurassic units in this study.

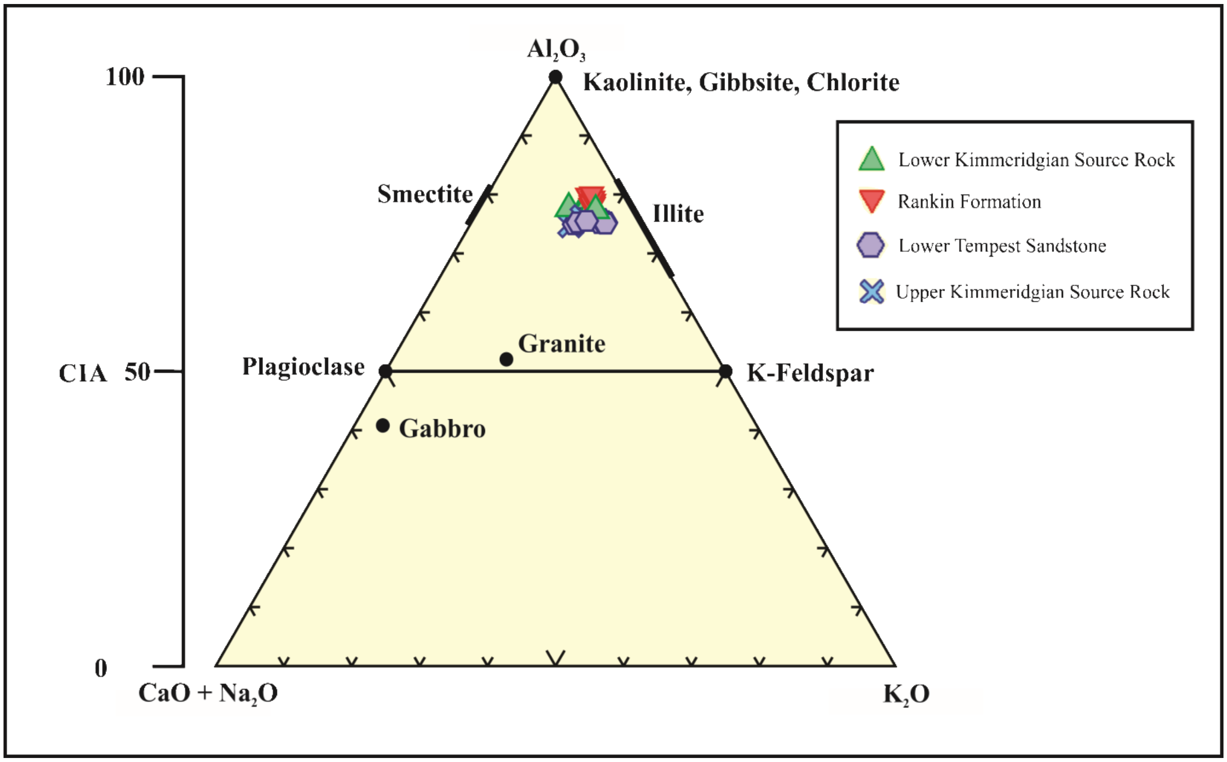

Figure 4.1 - CIA Diagram for Upper Jurassic mudstone samples.

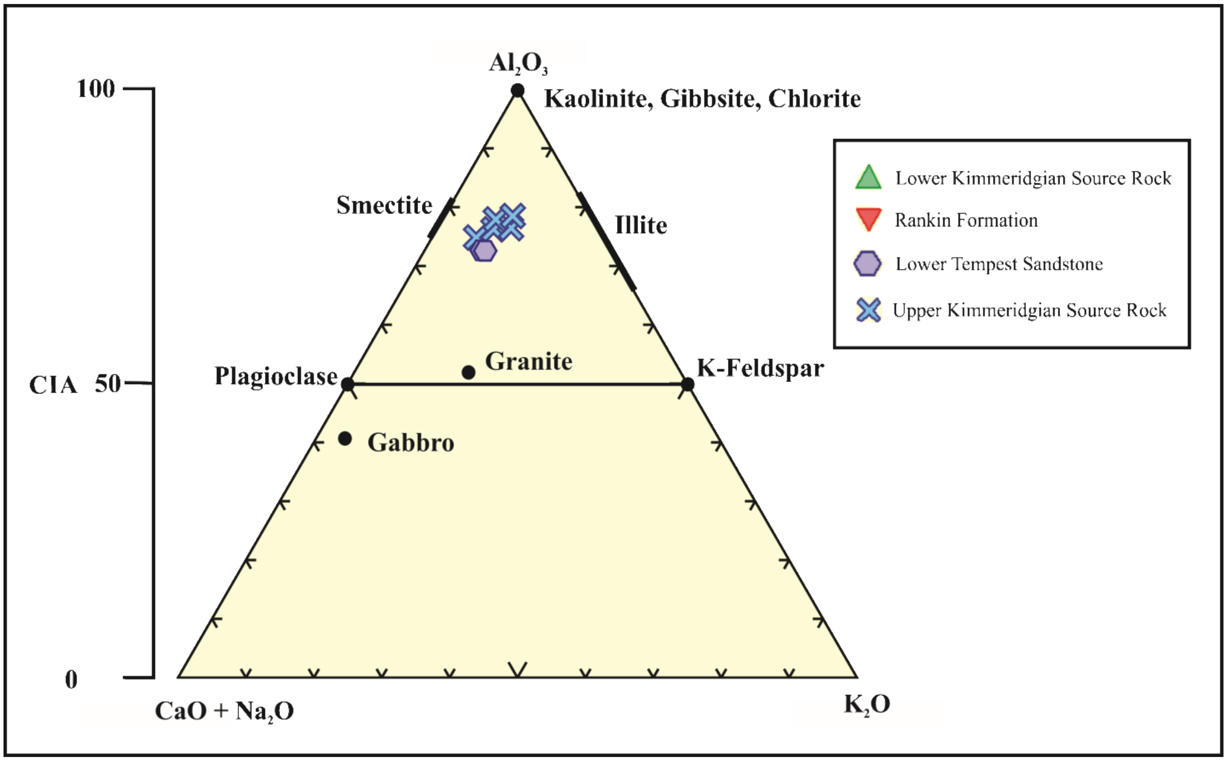

Figure 4.2 - CIA Diagram for Upper Jurassic sandstone samples.

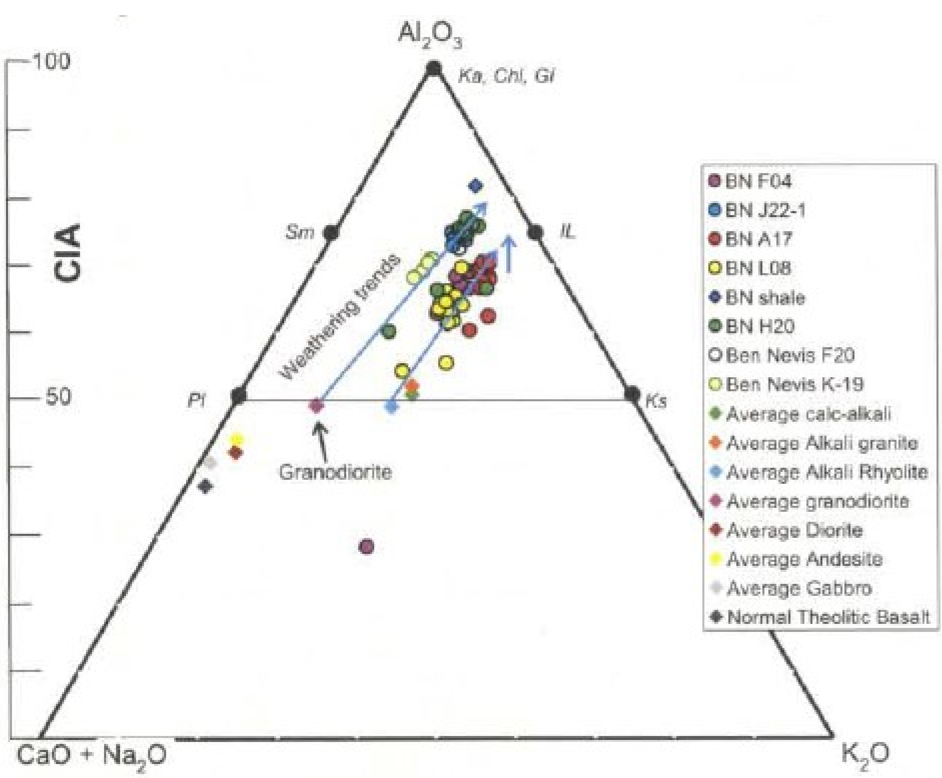

Figure 4.3 - CIA diagram from Dearin (2006).

4.3 - Trace Element Data

4.3.1 - Introduction

To help ascertain the composition of the source region(s) and determine provenance, a number of trace element plots were examined. Typically, the distribution of trace elements such as Ti, Mn, Zr, Hf, Nb, Sn, Cr, Ni, V, Co, La-Lu, Y, and Sc are sensitive to the nature of their source region (McLennan et al. 2003). These elements have less residence time in seawater and are less susceptible to mobilization during sedimentary processes (McLennan et al. 2003). The next section presents an analysis of the mobility for a number of trace elements, followed by a number of plots that are used to determine the nature of the source region.

4.3.2 - Element Mobility

A major issue in sediment provenance geochemistry is determining which elements are least mobile (Fralick, 2003). The composition of the source area can only be accurately estimated if elements present within the resulting sediment have not been significantly mobilized. The elements mentioned in the previous section are considered less susceptible to mobilization and are used where possible in the trace element analysis in this study. Other elements that can be mobilized in certain redox conditions, especially in organic-rich shales include U, Th, V, Mo, Ni and Cr (Quinby-Hunt & Wilde, 1994). MacLean (1990) developed a technique to help determine element mobility during alteration of volcanic rocks and suggests that the method can be used for sedimentary rocks as well. This technique may be useful to define the behavior of elements within the Upper Jurassic samples from the Flemish Pass Basin and Central Ridge. The method is based on the premise that as mobile elements are gained, or lost from the rock, immobile elements will exhibit apparent increases or decreases in concentration (Fralick, 2003). Therefore, when two immobile elements are plotted against one another, a linear trend will be defined with samples plotting progressively closer to, or further away from the origin, as the detritus is depleted in, or enriched in mobile elements (Fralick, 2003). Essentially, if both elements are immobile, the points will define an isochemical line with the origin because the mass loss or gain from the rocks should affect both elements identically (Fralick, 2003).

When this technique was applied to the samples from this study, the majority of trace elements appear to have been immobile to chemical weathering. For instance when Th is plotted vs. Sc, La, TiO_2, Cr, Ni, and Nb linear trends are defined towards the origin (Figure 4.4A, 4.4B, 4.4C, 4.4D, 4.4E, 4.4F). These elements can therefore be considered to have been immobile, and their signatures within the detritus are likely the same as in their original source rock. The scatter on the plots may be associated with minor differences in provenance. It is also possible that the scatter is due to slight mobilization of these elements in certain samples. However, the degree of this mobilization is clearly not significant, as the general trend with the origin is maintained.

In Figure 4.4G, Th is plotted vs. Co, and a negative trend is defined which is to be expected when a mobile element on the y-axis is plotted vs. an immobile element on the x-axis (Fralick, 2003). Essentially, the mass loss or gain affects Th and Co in different ways. Since Th appears to be immobile based on previous plots, it is interpreted that Co behaved as a mobile element and it should therefore not be used to interpret provenance.

In Figure 4.4H, Th is plotted vs. Zr. There is considerable scatter in the data points, and the sandstone samples define a different trend from that of the mudstone samples. At first glance, this may appear to indicate mobile behavior of Zr. However, when the sandstone and mudstone populations are plotted separately (Figure 4.5A, 4.5B), they both define linear trends. The scatter of points (and the variation in trends between sandstone and mudstone) is interpreted to be a result of hydraulic sorting. This is because hydraulic sorting causes heavy minerals such as zircon to be enriched in sands and sandstones (Pettijohn et al., 1973). The enrichment of zircon within the sandstone beds results in an enrichment of the element, Zr. Therefore, it is concluded that Zr was immobile, but may exist in higher concentrations in the sandstone beds due to sorting of the mineral zircon. These findings are of particular interest for provenance deductions, as Zr may be either enriched or depleted in interbedded sandstone and mudstone units due to sorting.

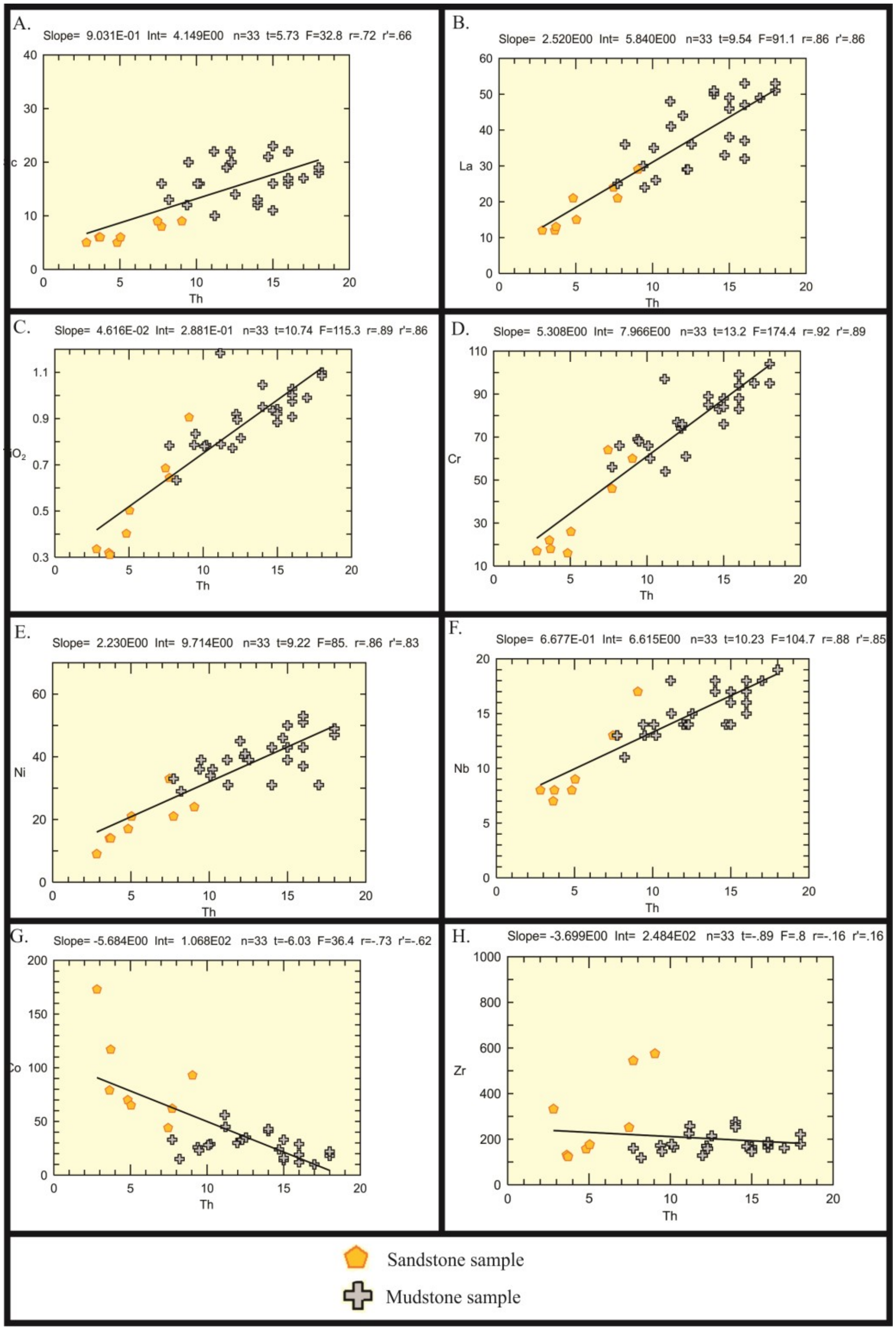

Figure 4.4 - Mobility diagrams for trace elements of Upper Jurassic sandstones and mudstones. Samples are from the Upper Kimmeridgian Source Rock, Lower Kimmeridgian Source Rock, Rankin Formation, and Lower Tempest Sandstone stratigraphic units from wells Baccalieu I-78, Panther P-52, and South Tempest G-88.

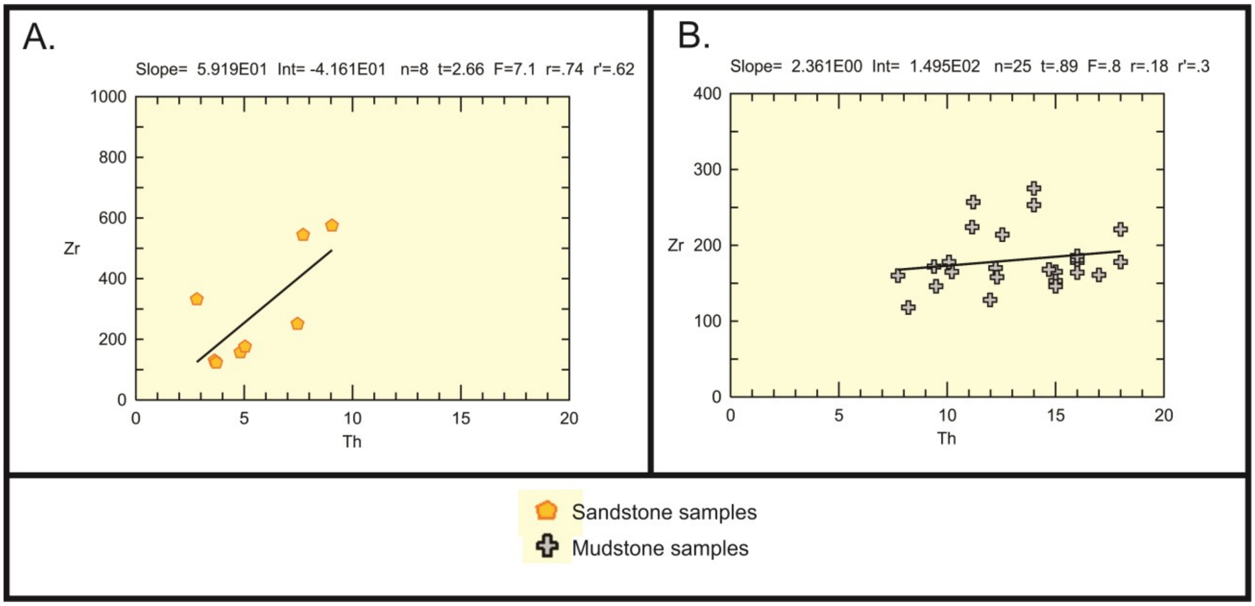

Figure 4.5 – Mobility diagrams for trace elements Th and Zr for sandstones (A) and mudstones (B). Samples are from the Upper Kimmeridgian Source Rock, Lower Kimmeridgian Source Rock, Rankin Formation, and Lower Tempest Sandstone stratigraphic units from wells Baccalieu I-78, Panther P-52, and South Tempest G-88.

4.3.3 – Introduction to Trace Element Provenance Plots

Following documentation that most trace elements in the Upper Jurassic samples were immobile to chemical weathering, the samples are plotted on trace element plots to ascertain the composition of the principal source region(s). The mudstone (Figure 4.6) and sandstone samples (Figure 4.7) were plotted on separate diagrams due to the previously documented sorting differences.

4.3.4 - Zr/Sc vs. Th/Sc Plot

Figures 4.6A and 4.7A are adapted from McLennan et al. (1990) and further described by McLennan et al. (2003). The Zr/Sc vs. Th/Sc plot is used because it allows the distinction of felsic from more mafic detritus, as well as defining amounts of sedimentary recycling. The graph plots Zr/Sc on the x-axis and Th/Sc on the y-axis. A simple relationship exists between the two ratios in detritus from active margins; the more felsic the detritus, the higher those ratios will be. This is because Th and Zr are both incompatible and thus both ratios will increase with igneous differentiation (McLennan et al. 2003). The plotted location of a sample is therefore a good indication of the type of source material (felsic or mafic). In passive margin settings, however, sedimentary recycling processes are much more important. These processes lead to an increase in the Zr/Sc ratio almost independently from the Th/Sc ratio as the heavy mineral zircon tends to be preferentially concentrated during sorting and sedimentary recycling (McLennan et al. 2003). If samples plot in this region of the diagram, it is likely they were deposited in a passive margin environment where sedimentary recycling processes were dominant. However, this feature may only be noticeable in sandstones, as sedimentary recycling and hydraulic sorting processes are much more important in sandstones than mudstones (Section 4.3.2).

The mudstone samples in Figure 4.6A plot in the upper region of the diagram with elevated Zr/Sc and Th/Sc ratios, an area that matches an upper crustal composition. There is no significant variation between the plotted locations for samples from the different formations, although the Rankin Formation and Lower Kimmeridgian Source Rock samples exhibit a slightly enhanced upper crustal signature compared to the Lower Tempest Sandstone and Upper Kimmeridgian Source Rock samples, which possess a more mixed signature.

The sandstone samples in Figure 4.7A also plot in the upper region of the diagram with elevated Th/Sc ratios but even higher Zr/Sc ratios than the mudstone samples. Unlike the mudstone samples, these sandstones plot in the area associated with passive margin sedimentary rocks. This includes samples from the Upper Kimmeridgian Source Rock, Lower Kimmeridgian Source Rock, and Lower Tempest Sandstone.

4.3.5 - Sc – Th – Zr Ternary Plot

A ternary plot of Sc, Th, and Zr from Bhatia & Crook (1986) is also used to decipher provenance (Figure 4.6B, 4.7B). Although the plot is designed for sandstones, it may still be valuable in mudstone samples for detecting quantities of mafic or felsic detritus. However, as shown in the previous sample, significant hydraulic sorting is possible within sandstone samples. This may cause the sandstone and mudstones to plot in different regions of the plot.

In general, samples deposited in oceanic arc environments will typically plot in the field represented by "A" as these samples should contain more Sc than other tectonic environments (Figure 4.6B, 4.7B). Samples deposited in continental island arcs, or active continental margins, will typically plot in the "B" and "C" fields, respectively, as sediments derived from these environments generally contain more Th and Zr than oceanic arc environments. Finally, sediments deposited in passive margins typically exhibit higher Zr/Th ratios (Bhatia & Crook, 1986), plotting towards Zr represented by "D". This plot is based on the premise that the geochemical nature of sedimentary rocks reflects that of their source region and that their source regions contain rock types that are diagnostic of a particular tectonic environment.

The mudstone samples (Figure 4.6B) plot in the middle region of the diagram, mostly in the continental island arc field. The different formations do not display much variation; however, the Lower Kimmeridgian Source Rock and Rankin Formation samples plot further to the right (more Zr-rich) than the Lower Tempest Sandstone and Upper Kimmeridgian Source Rock samples.

The sandstone samples (Figure 4.7B) define a considerably different signature than the mudstone samples, plotting much further towards Zr on the ternary plot. Some of the samples plot in the continental island arc field, whereas a couple of others lie just outside the passive margin field. There is minimal discrepancy in the plotted location of the different formations, although three samples from the Upper Kimmeridgian Source Rock plot much closer to Zr than any other samples.

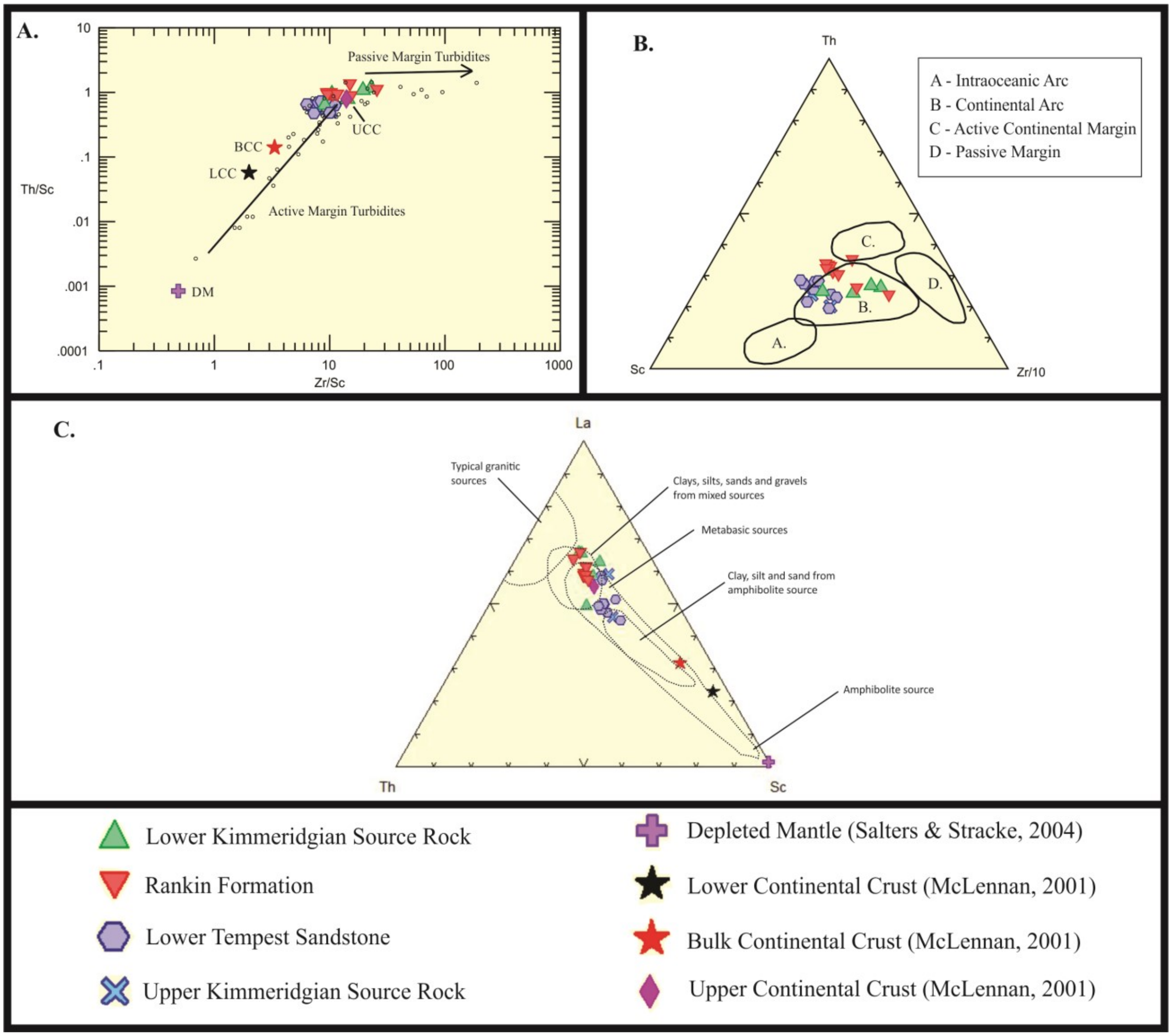

Figure 4.6 - Trace element provenance diagrams for Upper Jurassic mudstone samples. Samples from this study include four samples from the Lower Kimmeridgian Source Rock unit; one sample from the Upper Kimmeridgian Source Rock unit; nine samples from the Rankin Formation; nine samples from the Lower Tempest Sandstone unit.

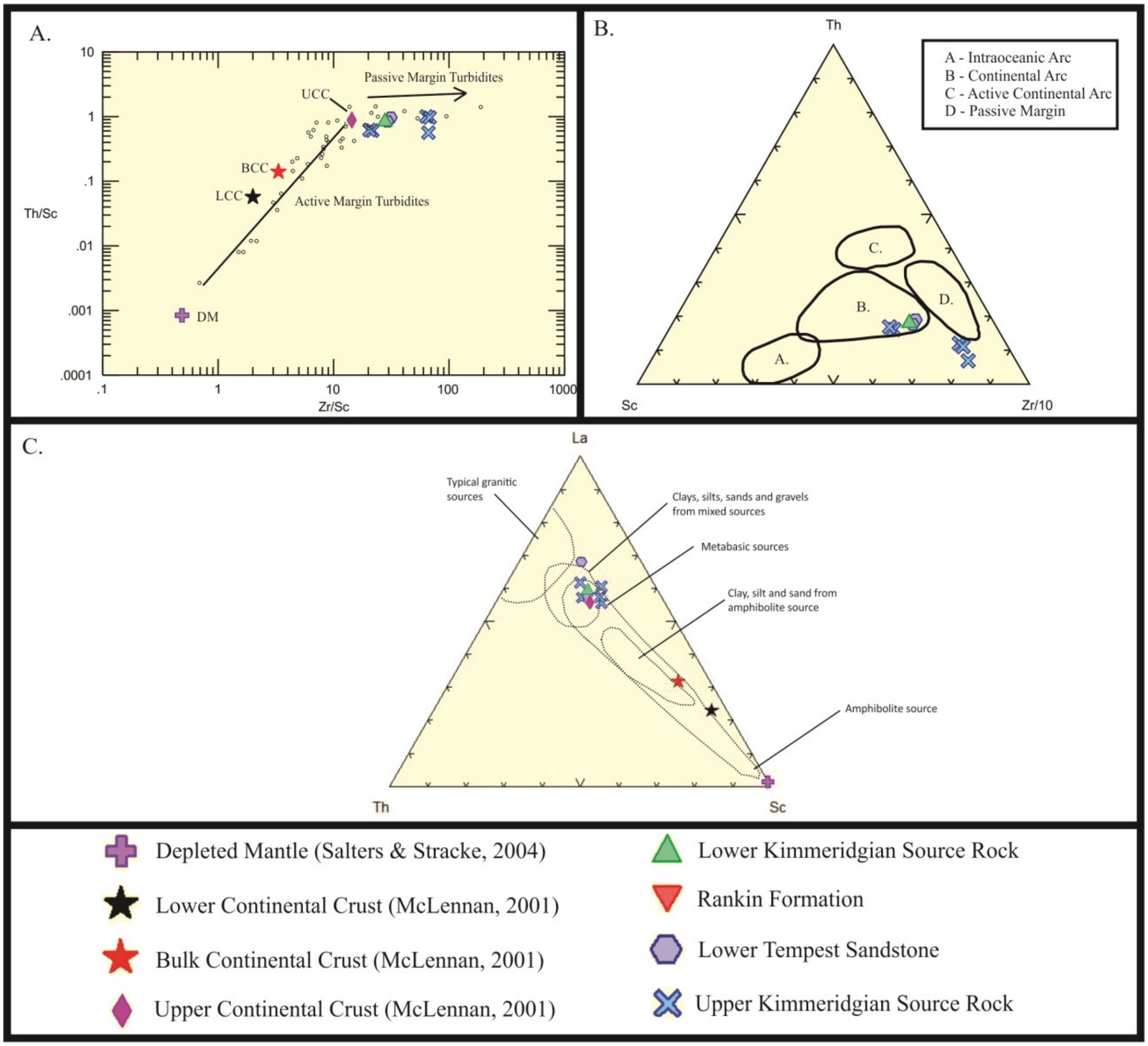

Figure 4.7 - Trace element provenance diagrams for Upper Jurassic sandstones samples. Samples from this study include five samples from the Upper Kimmeridgian Source Rock unit; two samples from the Lower Tempest Sandstone unit; one sample from the Lower Kimmeridgian Source Rock unit.

4.3.6 – Th-La-Sc Ternary Plot

The provenance plot presented as Figure 4.6C, 4.7C is from Bhatia & Crook (1986) and uses the fields defined by Cullers (1994). This plot is useful for distinguishing between upper crustal and more mafic detritus. Samples from mafic or amphibolite sources will plot towards the Sc pole. Samples from mixed sources will plot in the middle region of the diagram and samples with felsic sources will plot in the upper left region. Unlike the Sc-Th-Zr/10 ternary plot, this ternary diagram is not able to distinguish passive margin sediments.

The mudstone samples show a fair amount of scatter, with some samples plotting in the field suggesting mixed sources, while others plot in the region indicating metabasic or amphibolite sources (Figure 4.6C). The Upper Kimmeridgian Source Rock samples are scattered, but the Rankin Formation and Lower Kimmeridgian Source Rock samples consistently plot in the field suggesting mixed sources, close to the average composition of the upper continental crust. However, the Lower Tempest Sandstone samples almost all plot further towards the Sc pole, suggesting more mafic sources for this unit.

The sandstone samples almost all cluster in the area of the plot that indicates a mixed source for the detritus (Figure 4.7C). All the samples plot close to the area where the average composition of the upper continental crust plots. All the samples from the four different formations plot in the same area of the diagram.

Chapter 5 – Heavy Mineral Concentrate Data

5.1 – Introduction

This chapter provides an overview of detrital heavy mineral data for drill cuttings of the fine-grained, Upper Jurassic samples analyzed in this study. Provenance-sensitive heavy mineral ratios are the main focus, although for each sample, the entirety of the heavy mineral suite as well as their associated textures are also described. Data were collected using the Mineral Liberation Analyser – Scanning Electron Microscope (MLA-SEM) at Memorial University; sample preparation techniques and analytical methods are described in Chapter 2. Provenance-sensitive heavy mineral ratios of zircon, monazite, titanite, chromite, and rutile are considered useful for provenance discrimination and assessing sedimentary recycling.

5.2 – Heavy Mineral Analysis Methods

Methods for analyzing heavy minerals in this study follow the process outlined by Morton & Hallsworth (1994, 1999). This approach has been applied by numerous authors to sandstones (Hallsworth et al. 2000; Morton et al. 2002; Morton et al. 2005; Lowe et al. 2011) as it employs detrital heavy mineral ratios to "fingerprint" the provenance of a given sample. This "fingerprint" is useful for correlation with provenance signatures from other units and to detect changes in provenance over time. For the method to be effective, it must be shown that the minerals used in the ratios are indeed detrital and not authigenic. This will be demonstrated for the samples presented in this study, primarily based on textures of the heavy minerals. It is also necessary to use heavy minerals that are not significantly differentiated by hydraulic sorting during transport, and are not susceptible to dissolution during diagenesis. Minerals chosen for the ratios therefore have similar densities and are considered stable during burial diagenesis.

The types of ratios used in this study include the monazite-zircon index (MZi: 100 x monazite count/(total monazite + zircon)), the rutile-zircon index (RZi: 100 x rutile count/(total rutile + zircon)), and the chromite-zircon index (CZi: 100 x chromite count/(total chromite + zircon)). One of the common indexes used (the apatite-tourmaline index) was not used in this study as tourmaline was too uncommon in the studied samples; 15 of the 23 analyzed samples possessed no tourmaline. It was therefore decided to omit this index as the sample size is too small to draw conclusions from, and other indexes could be used.

Another widely used ratio is the ZTR (zircon-tourmaline-rutile) index (Hubert, 1962). This index measures the percentage of zircon, tourmaline and rutile grains among all non-opaque and non-micaceous heavy minerals such as zircon, tourmaline, rutile, apatite, monazite, chromite, and titanite (ZTR= (Z+T+R)/(Z+T+R+A+Mz+Cr+Ti)*100). The minerals in the denominator of the ZTR ratio are more susceptible to breakdown and dissolution during weathering and transport processes (Morton & Hallsworth, 1999). As the detritus is subject to progressively greater weathering and transport, it will become enriched in the more stable heavy minerals (chemically and mechanically) such as zircon, tourmaline and rutile compared to the unstable heavy minerals (Hubert, 1962). Therefore, this index is considered a great measure of sedimentary recycling (Hubert, 1962). This is the same principle as some of the plots from the bulk rock trace element geochemical data of Chapter 4, particularly the Zr/Sc vs. Th/Sc plot. The heavy mineral data dovetails well with the bulk rock geochemical data, and therefore will be useful in obtaining a thorough understanding of the nature of the detritus and source regions.

One consideration for this study with respect to the ZTR index is that the minerals used in the denominator do not include all of the possible non-opaque, non-micaceous heavy minerals as in the standard definition of the ZTR index. The excluded minerals (such as epidote and olivine) are more unstable under diagenesis and were not included in the denominator of the ZTR index in this study. Since the dissolution of unstable phases and the variable nature of the effects of intrastratial solution are not well understood between these samples from different wells, it was important that only the diagenetically stable minerals listed in the previous paragraph were used for this study. These minerals have been shown to be diagenetically stable up to depths of 4 km (Morton, 1979; Smale & Morton, 1987; Milliken, 1988; Morton & Hallsworth, 1999). This allows for a reasonable comparison of maturity levels and contribution of first-cycle or recycled sources between samples. To ensure diagenetic processes had not significantly affected the heavy mineral suites, textures of the heavy mineral grains were also assessed to identify authigenic features.

Typically, heavy mineral counts for conventional ratios are completed using a fine sand size bracket (63-177 μm) (Lowe et al. 2011; Morton & Hallsworth, 1994). This grain size is typically chosen because within this range, all of the heavy minerals are considered to exist inherently (Morton & Hallsworth, 1994). A 63-177 μm size range is unsuitable for this study of fine-grained mudstones. Totten & Hanan (2007) stated that the median size of heavy minerals in shales is approximately 25 μm less than those found in sandstones. Therefore, placing the low end of the size bracket at 63 μm would eliminate a significant portion of the heavy minerals in the samples studied. In Macquaker & Adams (2003) mudstone classification chart, they indicate a mudstone is any rock with >50% of the grains that are <63 μm. Understanding hydraulic equivalency (Rubey, 1933), it is reasonable to expect heavy minerals within the mudstones and siltstones of this study to be significantly smaller than 63 μm. Therefore, the lower end of the size range used for these samples was 10 μm. Many of these samples were also analyzed for detrital zircon geochronology as well as heavy mineral ratios. Using the LA-ICP-MS method, larger zircons typically result in more accurate analyses as it is easier to avoid any cracks, inclusions or other imperfections in a particular grain. Therefore, to ensure no large zircon grains were eliminated in these samples, the maximum size range was set at 180 µm. To determine whether this size bracket is appropriate, and if size sorting was important in the studied samples, the average sizes for each heavy mineral phase from each sample were calculated using MLA data. The average sizes are then expressed in a ratio corresponding to the heavy mineral ratio pairs. For example, the average monazite size is divided by the average zircon size (M/Z_{size}) corresponding to the MZi ratio. If the ratios have values near 1, this means that there is little size difference between the two different mineral phases, and implies that overprints of size sorting are insignificant and that the size fraction used for analysis is appropriate. Ratios are presented in Table 5.1. For all samples, the average M/Z_{size} is 0.79 ± 0.55, which indicates monazite grains are generally smaller than zircon grains. However, this is not a significant size difference, and likely means overprints of size sorting are negligible. The same can be said for the R/Z_{size} (rutile/zircon size) as well as C/Z_{size} (chromite/zircon size) ratios, which averaged 0.97 ± 0.23 and 1.16 ± 0.42 respectively. The R/Z_{size} and C/Z_{size} ratios, however, do not include values from one sample G-70 (4740m) which is considered anomalous with ratios of 10.7 and 3.7, respectively. This sample was therefore excluded from the analysis. It is concluded that the size fraction used (10 – 180µm) can be considered appropriate. In addition to the table below, grain size distributions for heavy minerals from each sample are presented in Appendix B.

Sample	Formation	Average Msize (um)	Average Zsize (um)	Average Rsize (um)	Average Csize (um)	Sorting Effects (M/Zsize)	R/Z size	C/Zsize
G-70 (3305)	Upper Kimmeridgian Source Rock	26.00	15.50	22.00	15.00	1.68	1.42	0.97
G-70 (3500)	Upper Kimmeridgian Source Rock	26.00	28.00	25.00	29.00	0.93	0.89	1.04
G-70 (4740)	Lower Kimmeridgian Source Rock	-	10.00	107.00	37.00	-	10.70	3.70
G-70 (4820)	Lower Kimmeridgian Source Rock	14.00	17.00	21.00	20.00	0.82	1.24	1.18
G-70 (4200)	Rankin Formation	6.00	32.00	22.00	25.00	0.19	0.69	0.78
G-70 (3715)	Upper Kimmeridgian Source Rock	9.00	30.00	25.00	41.00	0.30	0.83	1.37
G-70 (4405)	Rankin Formation	9.00	37.00	30.00	30.00	0.24	0.81	0.81
P-52 (3600)	Lower Tempest Sandstone	14.00	40.00	40.00	33.00	0.35	1.00	0.83
P-52 (3950)	Lower Kimmeridgian Source Rock	6.00	33.00	22.00	23.00	0.18	0.67	0.70
P-52 (3210)	Upper Tempest Sandstone	21.00	37.00	29.00	30.00	0.57	0.78	0.81
P-52 (3400)	Upper Kimmeridgian Source Rock	37.00	41.00	52.00	45.00	0.90	1.27	1.10
P-52 (3500)	Upper Kimmeridgian Source Rock	54.00	29.00	27.00	38.00	1.86	0.93	1.31
G-88 (3600)	Upper Tempest Sandstone	15.00	25.00	18.00	25.00	0.60	0.72	1.00
G-88 (3700)	Upper Tempest Sandstone	7.00	21.00	20.00	26.00	0.33	0.95	1.24
G-88 (4000)	Rankin Formation	22.00	13.00	13.00	20.00	1.69	1.00	1.54
G-88 (3500)	Upper Tempest Sandstone	28.00	34.00	30.00	31.00	0.82	0.88	0.91
G-88 (4495)	Lower Kimmeridgian Source Rock	-	24.00	23.00	21.00	-	0.96	0.88
G-88 (4600)	Rankin Formation	28.00	24.00	31.00	37.00	1.17	1.29	1.54
I-78 (5000)	Lower Kimmeridgian Source Rock	20.00	12.00	10.00	22.00	1.67	0.83	1.83
I-78 (4500)	Upper Kimmeridgian Source Rock	7.00	26.00	26.00	23.00	0.27	1.00	0.88
I-78 (4705)	Upper Kimmeridgian Source Rock	6.00	7.00	10.00	17.00	0.86	1.43	2.43
I-78 (4900)	Rankin Formation	12.00	27.00	27.00	43.00	0.44	1.00	1.59
I-78 (5075)	Lower Kimmeridgian Source Rock	-	13.00	9.00	10.00	-	0.69	0.77
Average						**0.79**	**0.97**	**1.16**
Standard Deviation						**0.55**	**0.23**	**0.42**

Table 5.1 – Average grain sizes of monazite, zircon, rutile and chromite as computed by MLA. Monazite/zircon size (M/Z size), rutile/zircon size (R/Z size), and chromite/zircon size (C/Z size also listed.

A potential drawback of the heavy mineral ratio approach in this study is the inability of the analytical equipment to differentiate between rutile and other TiO_2 minerals such as anatase and brookite. Morton & Hallsworth (1994) proposed that for heavy mineral ratios, only rutile grains be counted, excluding anatase and brookite grains. As the MLA method relies on chemistry for the identification of different mineral phases, it cannot differentiate between detrital rutile and other TiO_2 phases. Therefore, MLA counts of rutile may also include some anatase and brookite. Another potential drawback with this method is that rutile, brookite and anatase can all be found as authigenic phases and are common in sedimentary rocks (Morad, 1986; Pe-Piper et al., 2011). Minerals such as ilmenite or biotite break down and provide Ti ions in solution which contribute to the formation of authigenic TiO_2 minerals (Morad, 1986). The detrital TiO_2 minerals may be difficult to distinguish from diagenetic phases as the detrital grains often have secondary porosity or inclusions. In addition, the authigenic grains may sometimes be fairly homogenous (eg. Morad, 1986; Pe-Piper et al., 2011), particularly when dealing with fine grain sizes such as in this study. Textures of several rutile grains were analyzed in each sample with the aim of identifying the presence of authigenic grains. However, given the caveats mentioned, it is possible that authigenic TiO_2 grains may not have been identified. This is a consideration for the analysis of provenance based on heavy mineral ratios.

Another potential drawback of this approach involves the use of detrital apatite for provenance. The abundance of apatite is affected by chemical weathering as well as provenance. It has been shown that a significant reduction of the proportions of detrital apatite takes place due to weathering during erosion, transport, and alluvial storage (Morton & Hallsworth, 1994). Therefore, ZTR values may be different for two different samples with the same provenance as a result of chemical weathering of apatite. Morton & Hallsworth (1999) suggest that environments with hot, humid climates, and low relief drainage are the most effective in the weathering and removal apatite. However, in arid or semi-arid climates, as well as marine environments, apatite weathering is considered to be less extensive. Samples from this study are interpreted to have been deposited in a marine environment. However, it is possible that apatite may have been depleted on land before being deposited in the marine environment. It is therefore a consideration that ZTR values may be affected by weathering of apatite. An additional issue with apatite is that it can form authigenically as noted by Pe-Piper & Weir-Murphy (2008) and Lowe et al. (2011). Authigenic apatite forms as nodular, porous cements or overgrowths and if present, could affect ratios in which it is included. The authigenic grains can be identified based on texture, and some representative grains from each sample will be noted in this study to ensure grains included in heavy mineral ratios are indeed detrital.

Some additional considerations include the amount of grains necessary for robust heavy mineral ratios as well as the size fraction analyzed. Morton & Hallsworth (1994) discussed the necessary amount of grains to produce accurate data for provenance interpretations and state that a minimum of 100 grains per mineral pair are necessary; although ideally 200 grains should be counted. As shown in Appendix B, significantly more than 200 grains were counted from each rutile-zircon pair for each sample of this study. However, less than 100 grains were counted in several samples from the chromite-zircon and monazite-zircon pairs. This will be taken into consideration when interpreting these ratios. Previous heavy mineral provenance studies (Lowe et al., 2011; Piper et al., 2012; Morton & Hurst, 1995) were focused on the 63-177 μm size fraction of sandstones. As seen in the diagrams in Appendix B, the grain size of heavy minerals from mudstones in this study typically range from 10 to a maximum of 100 μm. An interesting question for consideration in this section is whether the results yielded from mudstone samples are as effective for provenance discrimination as they are in sandstones. The feasibility of using provenance-sensitive heavy mineral ratios in mudstones will be assessed in this study.

5.3 - Results

5.3.1 - Upper Kimmeridgian Source Rock

Counts of zircon, tourmaline, rutile, apatite, monazite, chromite, titanite, staurolite and epidote were obtained from seven 5 m thick cuttings intervals from the Upper Kimmeridgian Source Rock. Heavy mineral counts for all samples are shown in Appendix B. Three samples were from the Lancaster G-70 well, from depths of 3305m, 3500m, and 3715m, respectively. In addition, two samples were from the Panther P-52 well (3400 and 3500 m), and two samples from the Baccalieu I-78 well (4500 and 4705 m). A pie chart of proportions of heavy minerals in these samples is presented in Figure 5.1. Evidently, apatite is an important mineral, comprising 7-45% of the total heavy minerals in a given sample. However, in the samples from 3305m and

3715m from the Lancaster G-70 well, the apatite grains have features that indicate many of the grains are authigenic (Figure 5.2). The grains exhibit crude concentric layering (Figure 5.2A), nodular forms, and secondary pores (Figure 5.2B), which are distinctive features of authigenic apatite (Pe-Piper & Weir-Murphy, 2008; Lowe et al. 2011). This is an important consideration for the heavy mineral ratios. The proportion of authigenic to detrital apatite grains is unknown, as both varieties were not systematically counted. Both authigenic and detrital varieties must be present in these two samples, and thus the actual proportion of detrital apatite grains must be lower than the number of grains mapped by the MLA. The presence of authigenic grains may explain the greater proportion of apatite in the sample from 3715 m (Figure 5.1). Detailed investigations into diagenetic changes of these samples are outside the scope of this study, but Pe-Piper & Weir-Murphy (2008) noted that authigenic phosphorite is common in environments with abundant marine organic matter. Abundant P from marine organic matter can then be incorporated into diagenetic phosphorite or apatite. It is not surprising that some of the samples from the Upper Kimmeridgian Source Rock would possess authigenic apatite, as this unit is also rich in marine organic matter (Creaney & Alison, 1987; McCracken, 2000).

Rutile is generally the most abundant heavy mineral in these samples by far, at 40-74%. Based on the observed textures, all of the rutile grains appear detrital in nature; similar to the homogenous rutile grains in Figure 5.3 without any inclusions, secondary pores or crude zoning. However, given the caveats mentioned in Section 5.2, it is possible that authigenic rutile may share these features and may not have been identified here.

In addition to apatite and rutile, the heavy mineral fractions also contain zircon (3-17%), minor monazite (0-1%), minor chromite (0-6%), and minor titanite (1-9%). Tourmaline is absent from all the Upper Kimmeridgian Source Rock samples except two samples from the Lancaster

G-70 well (3305m and 3500m), which contained 33% and 10% tourmaline, respectively. Apart from the apatite grains discussed above, all heavy mineral grains in these samples lack the features of authigenic grains such as inclusions, secondary porosity and concentric layering patterns and are thus considered detrital (i.e. Figure 5.3).

The G-70 (3305m) sample possesses an RZi of 93.65, an MZi of 30.91, and a CZi of 11.63. The sample from G-70 (3500m) possesses a similar RZi of 91.71, with slightly different MZi and CZi ratios of 12.94 and 2.63, respectively. The ZTR ratio from this sample is 81.45. The sample from G-70 (3715m) possesses an RZi of 89.70, an MZi of 13.89, and a CZi of 18.42. The ZTR ratios for both the G-70 (3305m) and G-70 (3715m) sample are not included because of the potential influence authigenic apatite may have had on these samples.

The P-52 (3400m) and P-52 (3500m) samples possess similar heavy mineral ratios. RZi ratios are 85.01 and 86.50, MZi ratios 10.53 and 7.34 and CZi ratios 14.53 and 36.48. The ZTR ratios of these samples are 63.18 and 74.73, respectively.

Both the I-78 (4500m) and I-78 (4705m) samples possess very similar heavy mineral ratios. The sample from 4500 m has an RZi of 82.75, an MZi of 6.90, a CZi of 5.26 and a ZTR of 89.94 whereas the 4705m sample has an RZi of 80.11, an MZi of 2.70, a CZi of 2.70 and a ZTR of 87.65.

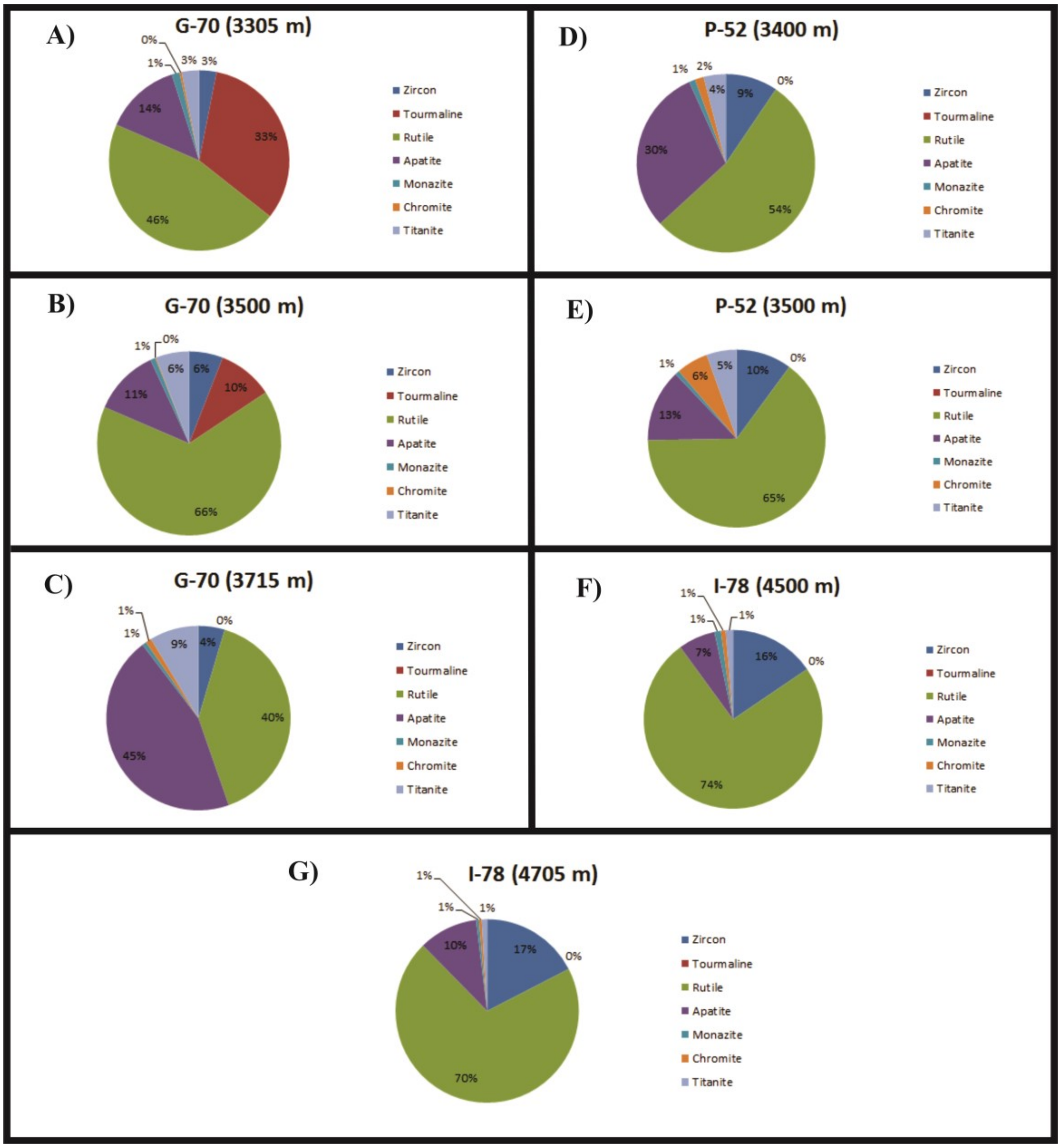

Figure 5.1 - Pie charts of detrital heavy mineral proportions of samples from the Upper Kimmeridgian Source Rock of the Lancaster G-70, Panther P-52 and Baccalieu I-78 well.

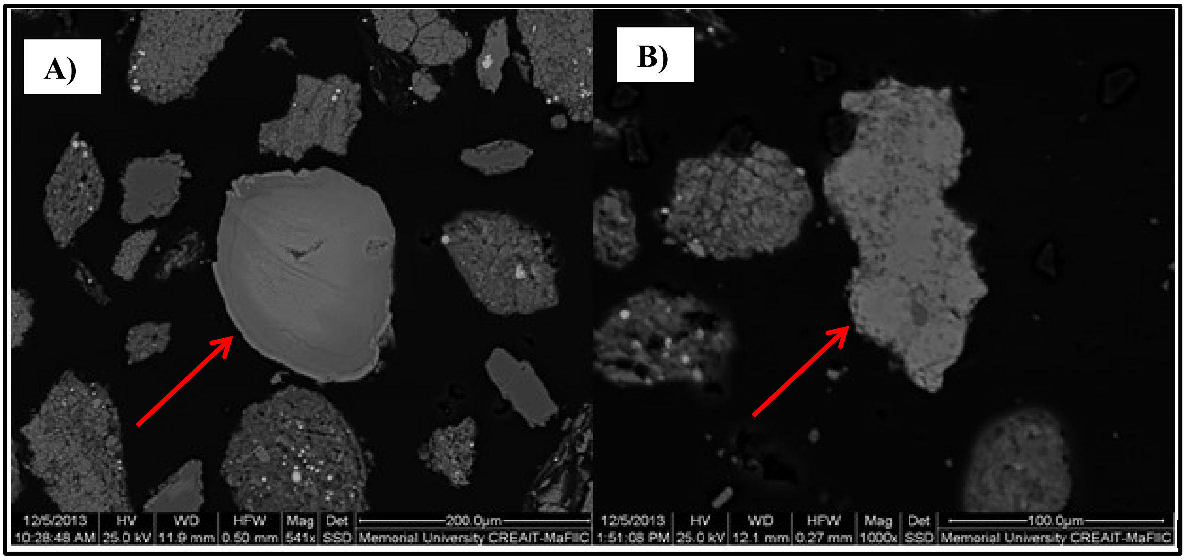

Figure 5.2 - Authigenic apatite grains from samples of the Lancaster G-70 well. Arrows point to interpreted authigenic apatite grains. The image on the left shows an apatite grain with crude concentric layering. The image on the right shows an apatite grain with secondary porosity and nodular forms.

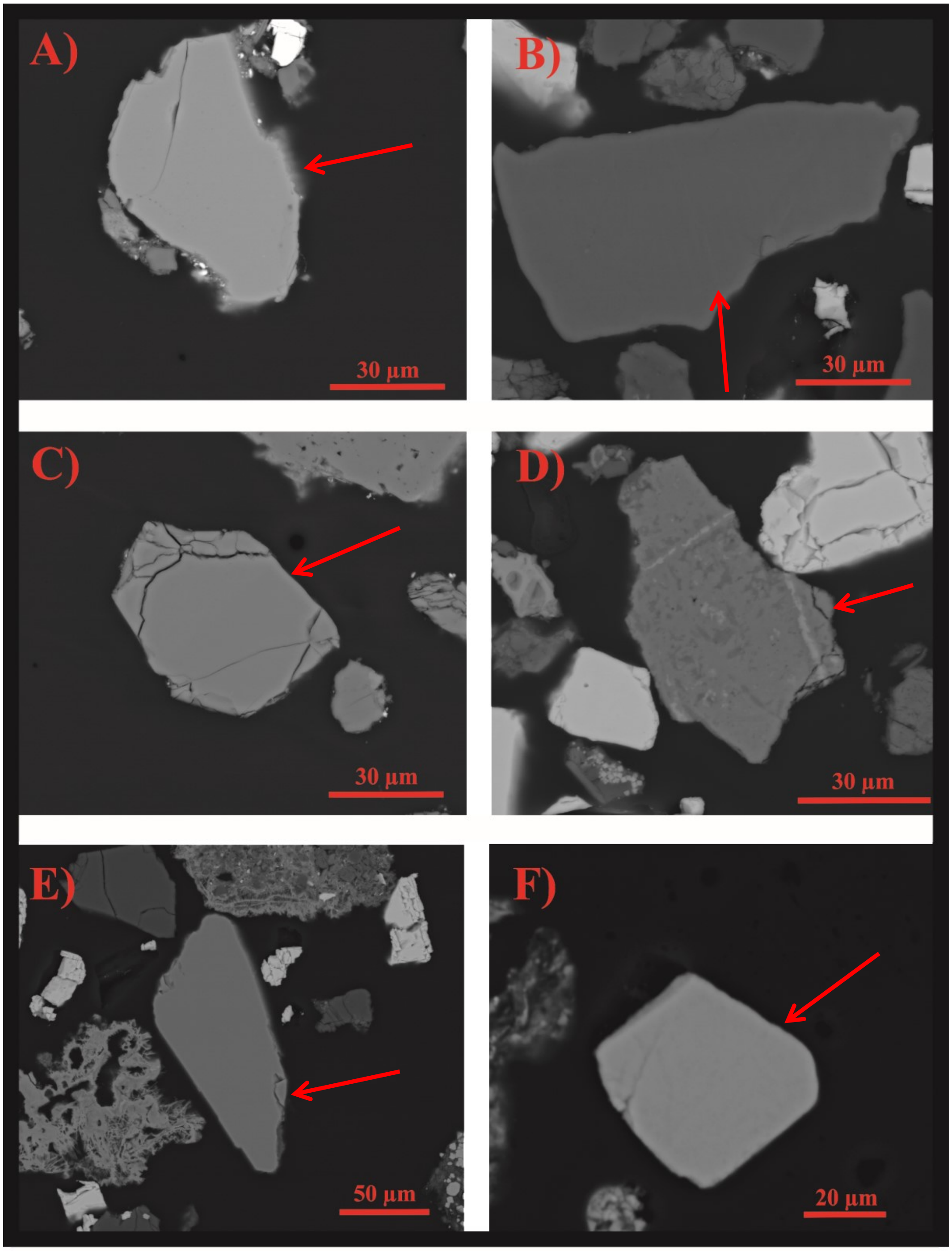

Figure 5.3 - Examples of rutile grains imaged in this study that possess characteristics suggesting a detrital origin. This is based on their overall homogeneity, lack of secondary pores, inclusions and crude zoning. Arrows point to the rutile grains.

5.3.2 - Lower Kimmeridgian Source Rock

Several 5 m interval cuttings samples were collected of the Lower Kimmeridgian Source Rock including one sample from the Lancaster G-70 well (4820m), one sample from the Panther P-52 well (3950m), one sample from the South Tempest G-88 well (4495m) and two samples from the Baccalieu I-78 well (5000m and 5075m). Pie charts of the heavy mineral proportions for these samples are presented in Figure 5.4. Rutile is generally the most abundant heavy mineral, comprising 30-71%. However, in the sample from the P-52 well (3950 m), apatite is the most abundant heavy mineral (34%). In the other samples, apatite is common (7-23%). Titante comprises 2-20% of these samples, while zircon makes up 2-17%. Chromite and monazite are uncommon at 1-2% and 0-1%, respectively. Tourmaline is only present in two samples (G-70 (4820m) and P-52 (3950m)), but it is fairly common at 11% and 27%, respectively. All heavy mineral phases discussed are interpreted to be detrital in nature and exhibit features similar to those in Figure 5.3. However, as discussed in Section 5.2, it is possible authigenic rutile grains are present.

The sample from G-70 (4820m) has an RZi of 93.01, an MZi of 20.00, a CZi of 8.57 and a ZTR of 86.75. The sample from P-52 (3950m) possesses an RZi of 92.83, an MZi of 6.82, a CZi of 18. The ZTR for this sample is fairly low at 59.48. Additionally, the sample from G-88 (4495m) possesses an RZi index of 87.84, an MZi of 0.00, a CZi of 9.26 and a fairly low ZTR of 55.82. The samples from the Baccalieu I-78 well possess fairly similar heavy mineral ratios. The sample from 5000 m has an RZi of 80.41, an MZi of 2.53, a CZi of 5.52, and a ZTR of 87.63. The sample from 5075 m possesses an RZi of 80.61, an MZi of 0.65, a CZi of 7.88 and a ZTR of 88.49.

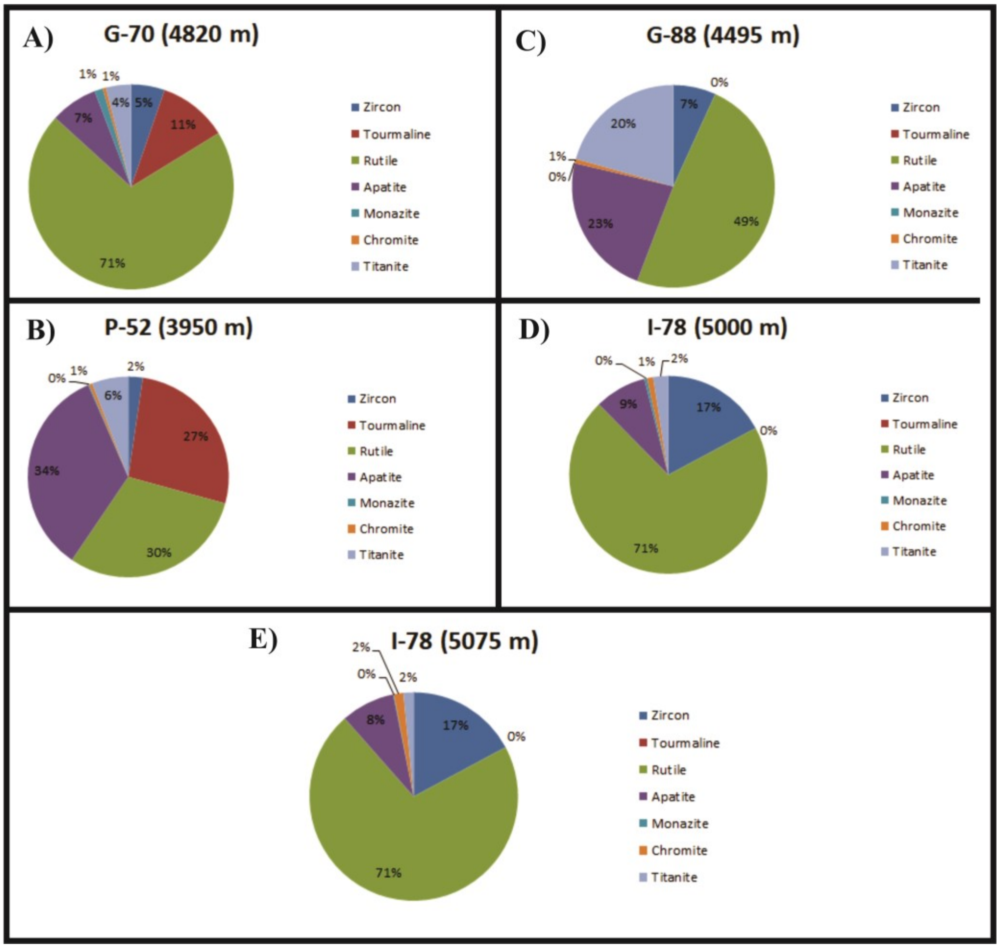

Figure 5.4 - Pie charts of detrital heavy mineral proportions of sample of the Lower Kimmeridgian Source Rock from Lancaster G-70, Panther P-52, South Tempest G-88 and Baccalieu I-78.

5.3.3 - Rankin Formation

Several 5 m interval cuttings samples were collected for analysis from the Rankin Formation. Two samples are from the Lancaster G-70 well from a depth of 4200 and 4405 m. An additional two samples are from the South Tempest G-88 well (4000m and 4600m) and one sample is from the Baccalieu I-78 well (4900m). The heavy mineral proportions in these samples are presented in Figure 5.5. All heavy minerals assessed possess features similar to those displayed in Figure 5.3, suggesting a detrital origin for all heavy mineral phases. There is some potential for the presence of authigenic rutile grains, as discussed in Section 5.2. For the most part, all of these samples show very similar heavy mineral proportions. Rutile is the most abundant mineral in all of the samples (61-68%), followed by apatite (10-17%). Other common heavy minerals include zircon (8-13%), and titanite (4-11%). Chromite comprises just 1% of the total heavy minerals in samples G-70 (4200m), G-88 (4000m) and G-70 (4405m). However, in samples G-88 (4600m) and I-78 (4900m), chromite comprises 10% and 5% of the total heavy minerals, respectively. Monazite comprises just 0-1% in all samples and tourmaline is absent in all of these samples.

The sample from G-70 (4200m) possesses an RZi of 86.93, an MZi of 6.12, a CZi of 9.80 and a ZTR of 77.19. The sample from G-70 (4405) m has an RZi of 88.28, an MZi of 14.77, a CZi of 7.41 and a ZTR of 75.50. The samples from the South Tempest G-88 well The G-88 (4000m) sample possesses an RZi of 83.42, an MZi of 5.95, a CZi of 4.24 and a ZTR of 81.73. The RZi for the G-88 (4600m) sample is 88.85, the MZi is 3.39, the CZi is 53.28 and the ZTR is 75.84. The I-78 (4900m) sample has an RZi of 88.87, an MZi of 10.94, and a CZi of 41.24. The ZTR for this sample is 68.67.

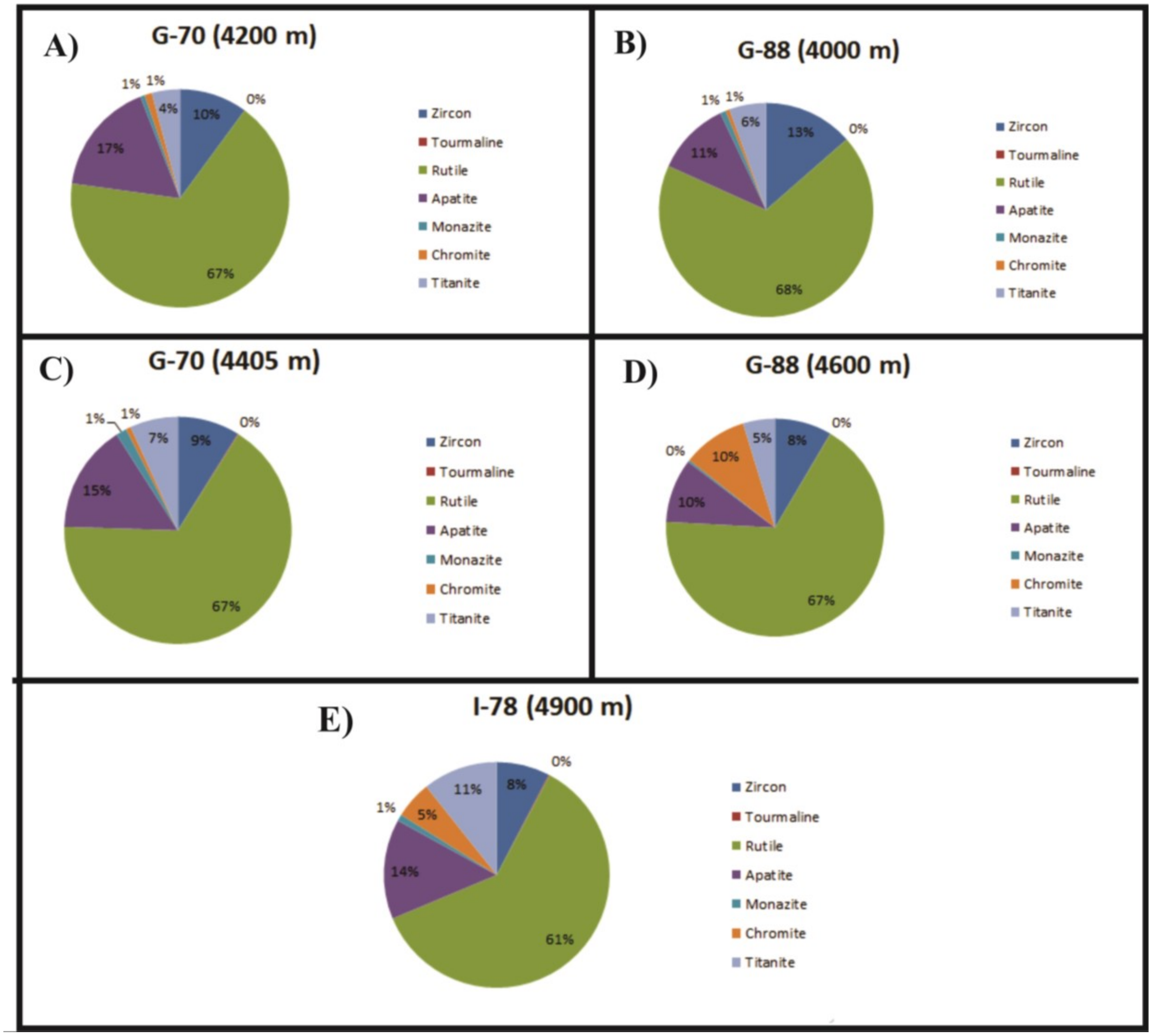

Figure 5.5 - Pie charts of detrital heavy mineral proportions of samples of the Rankin Formation from Lancaster G-70, South Tempest G-88 and Baccalieu I-78.

5.3.4 - Upper Tempest Sandstone (Panther P-52)

Heavy mineral counts were obtained from 5 m cuttings intervals of the Upper Tempest Sandstone from the Panther P-52 well (3210m) and the South Tempest G-88 well (3500m, 3600m, and 3700m). A pie chart of the heavy mineral proportions for these samples is available in Figure 5.6. Rutile is the most abundant heavy mineral in all samples except the Panther P-52 (3210m) sample. It comprises 65-75% of the South Tempest samples but only 34% of the

Panther P-52 (3210m) sample. Zircon is the most abundant mineral in the P-52 (3210m) sample at 61%. It comprises 9-12% of the South Tempest G-88 samples. Other heavy minerals in all samples include apatite (3-15%), chromite (1-4%), monazite (0-1%) and titanite (<1-4%). Once again, all grains assessed possess features similar to those in Figure 5.3, suggesting the contribution of authigenic heavy minerals to these counts is negligible. However, the contribution of authigenic grains to rutile counts is possible as discussed in Section 5.2.

The heavy mineral ratios of the P-52 (3210m) sample include an RZi of 35.74, a MZi of 2.20, a CZi of 2.20, and a ZTR of 94.18. For the South Tempest G-88 well, the sample from 3500 m has an RZi of 86.12, an MZi of 2.53, a CZi of 6.76 and a ZTR of 86.71. The sample from 3600 m possesses an RZi of 88.89, an MZi of 10.71, a CZi of 21.88 and a ZTR of 83.03 while the sample from 3700 m possesses an RZi of 85.88, an MZi of 3.92, a CZi of 27.94 and a ZTR of 76.10.

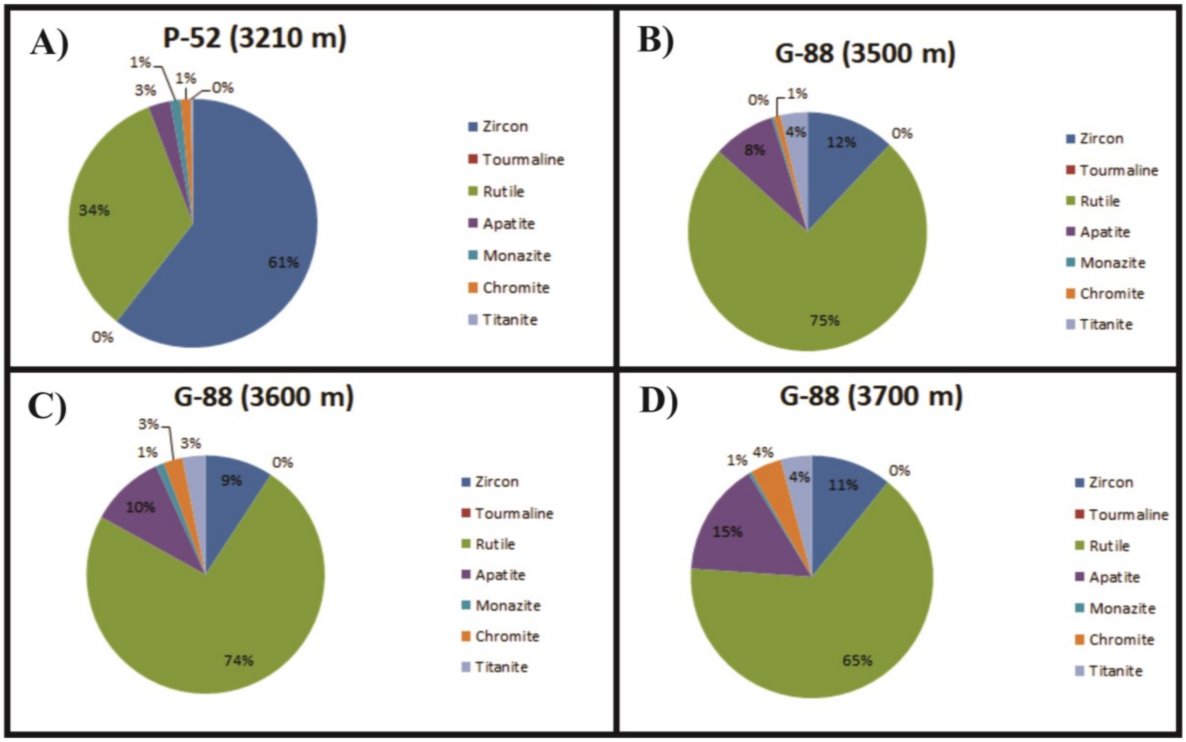

Figure 5.6 - Pie charts of detrital heavy mineral proportions of samples from the Upper Tempest Sandstone from Panther P-52 and South Tempest G-88.

5.3.5 - Lower Tempest Sandstone (Panther P-52)

One 5 m interval cuttings sample was collected from the Lower Tempest Sandstone of the Panther P-52 well from a depth of 3600 m. A pie chart of the heavy mineral proportions is presented in Figure 5.7. All heavy minerals of this sample possess features similar to those shown in Figure 5.3, suggesting that detrital rutile is most important in this sample. As with other samples, there is a chance some authigenic rutile grains were not identified as discussed in Section 5.2. Rutile is the most abundant heavy mineral, representing 32% of the total heavy mineral counts. This is followed by apatite (23%), tourmaline (15%), titanite (4%), zircon (3%), chromite (2%), and monazite (<1%).

Heavy mineral ratios for this sample include an RZi of 93.01, an MZi of 12.20, a CZi of 46.27 and a ZTR of 63.14.

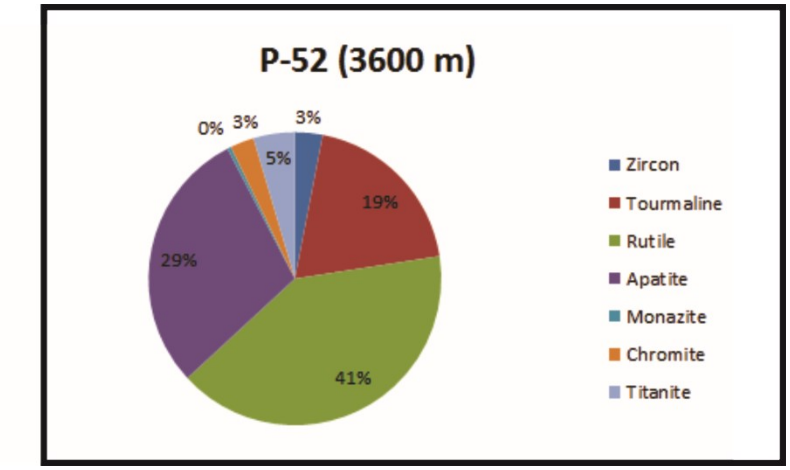

Figure 5.7 - Pie charts of detrital heavy mineral proportions of sample from the Lower Tempest Sandstone of the Panther P-52 well.

5.4 - Heavy Mineral Ratio Diagrams

Plots of heavy mineral ratios are presented in Figure 5.8. Figure's 5.8A, 5.8B, and 5.8C are scatter plots containing all combinations of RZi, MZi and CZi values, and Figure 5.8D is a plot of the ZTR index values for each sample arranged horizontally by formation. Figure 5.9 shows the same plots as Figure 5.8, but with averaged heavy mineral indexes from each formation with standard error bars. These plots are not intended to pinpoint precise source terranes, but are considered useful for provenance discrimination and providing a provenance "fingerprint" for a particular formation.

5.4.1 - Observations

The first plot (Figure 5.8A) has the MZi (monazite-zircon index) on the x-axis and the RZi (rutile-zircon index) on the y-axis. Samples from all formations possess a fairly high RZi with most samples >80. MZi values tend to be more variable ranging from near zero up to about

30. Using standard errors (Figure 5.9A), none of the formations are really discriminated from one another as most of the standard errors overlap with one of the other formations. The one unit that possesses a slightly different signature is the Upper Tempest Sandstone, which has a much lower average RZi, and lower MZi values in general. However, this feature is the result of a single outlier sample with a very low RZi and MZi value which may not be representative of the formation as a whole. In addition, the standard error for the Upper Tempest Sandstone samples is fairly large, and does overlap with the other formations. It is difficult to draw any meaningful conclusions from the Lower Tempest Sandstone as only one sample was available from this unit. However, this one sample plots in a similar region to points for most other formations.

The next plot (Figure 5.8B) shows the CZi (chromite-zircon index) plotted vs. the RZi (rutile-zircon index). Similar to the MZi, CZi values are fairly variable, ranging from near zero to almost 60. Using the standard error plot (Figure 5.9B), all the formations have a broadly similar provenance signature as most of the standard errors overlap with one of the other formations. Once again, the Upper Tempest Sandstone appears to possess a slightly different signature, although this may be attributed to the influence of an outlier sample, and the standard errors for this formation overlap with the other units. The Lower Tempest Sandstone sample plots with a high CZi value, although it is difficult to draw meaningful conclusions as just one sample was available from this unit.

The MZi vs. CZi plot (Figure 5.8C) shows a large scatter. The standard error plot (Figure 5.9C) shows that most formations have similar values, and any individual formation has a standard error that overlaps with that of another. The Lower Tempest Sandstone is fairly anomalous here as the CZi value is much higher than that of any other formation. However, it is once again difficult to say if this is part of a larger trend or if it is anomalous as just one sample was available from the Lower Tempest Sandstone.

The final plot (Figure 5.8D) shows the ZTR values of the various formations. Substantial scatter is present for the Upper and Lower Kimmeridgian Source Rock units, while the Upper Tempest Sandstone and Rankin Formation samples are better constrained. Once again, having only a single sample from the Lower Tempest Sandstone limits the significance of an interpretation of this interval. Overall, looking at the standard error plot (Figure 5.9D), it appears that most of the formations possess a similar average ZTR value in the range of 70-80. However, the average ZTR of the Upper Tempest Sandstone is slightly higher, at 85.

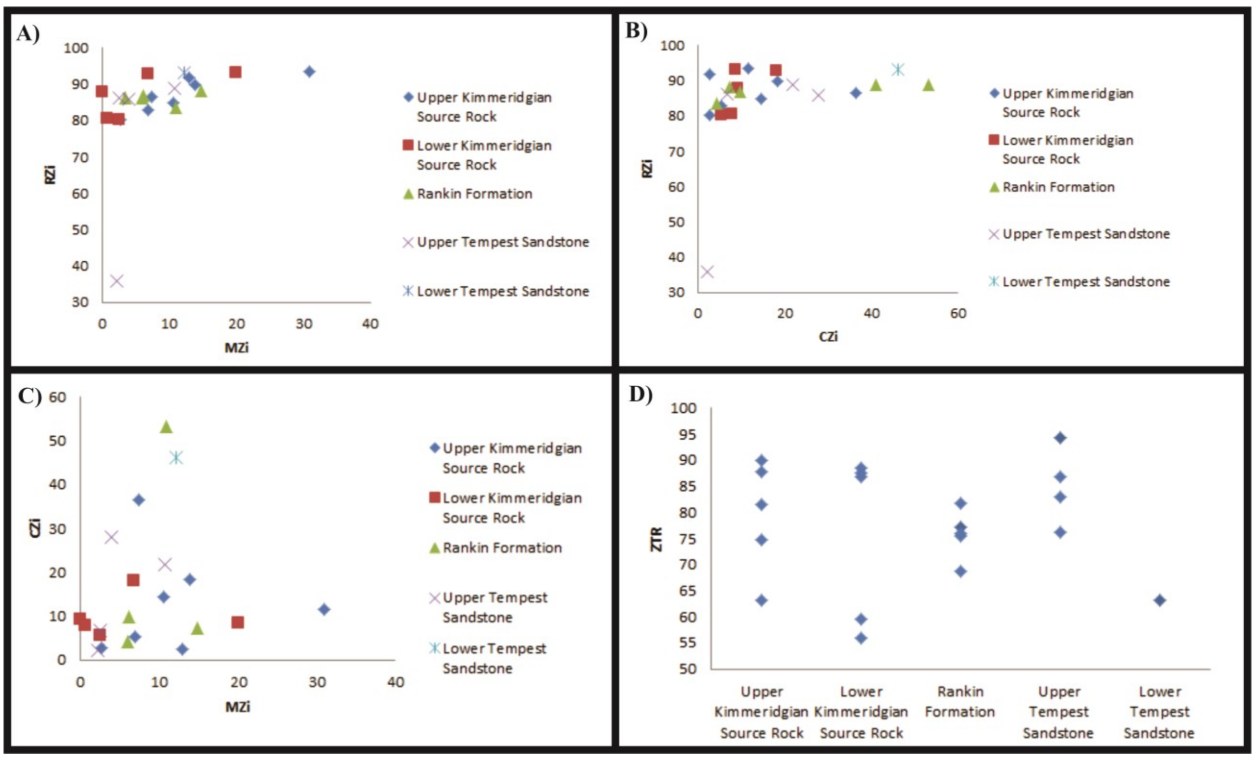

Figure 5.8 - Plots of heavy mineral ratios. (A) MZi vs. RZi, (B) CZi vs. RZi, (C) MZi vs. CZi, (D) ZTR. Samples with authigenic apatite removed from ZTR ratio diagram.

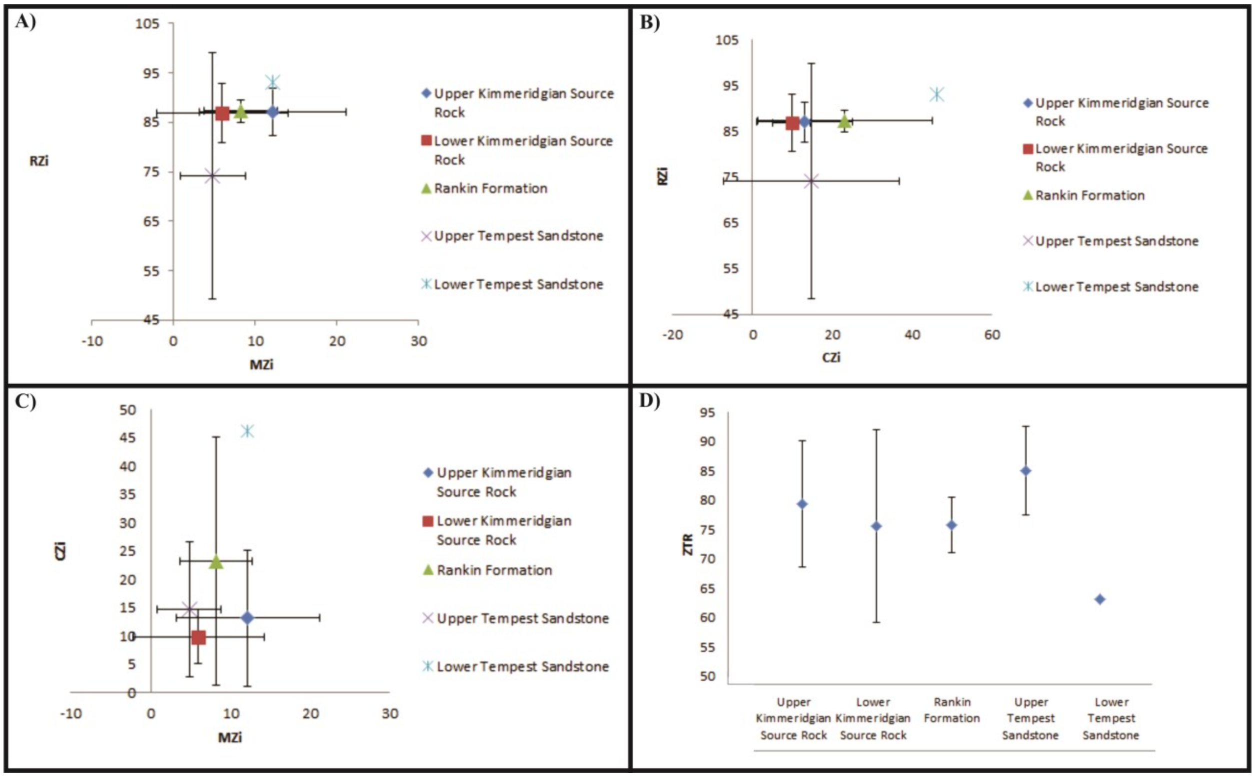

Figure 5.9 - Plots of heavy mineral ratios with standard error bars (1 SE) for the average heavy mineral index value from each formation. (A) MZi vs. RZi, (B) CZi vs. RZi, (C) MZi vs. CZi, (D) ZTR. Samples with authigenic apatite removed from ZTR ratio diagram.

Chapter 6 – Detrital Zircon Geochronology

6.1 – Introduction

The geochronological analyses for this study were undertaken to define detrital zircon ages for mudstone and interbedded sandstone beds from the Kimmeridgian units of the Central Ridge and Flemish Pass Basin, offshore Newfoundland. Many of the samples consisted of grain mounts of cuttings, whereas others were thin sections taken from conventional core samples. The data will provide direct indications of the age(s) and nature(s) of the source region(s) and may elucidate provenance questions that petrographic techniques are not able to address. Seven samples were analyzed from the Kimmeridgian rocks with approximately 30 to 80 detrital zircons analyzed per sample. The location of the wells sampled from is shown on Figure 1.1. In addition to ages of detrital zircon grains, features such as Th/U, grain sizes, and morphologies will also be described. Taken together these data will be useful for grouping zircon grain populations and interpreting source regions. Although important, zoning patterns were not used as a means of classification. Back scattered electron (BSE) images were taken using the SEM and the majority of grains imaged did not exhibit any zoning since many of the grains were actually just grain fragments or very fine-grained (Figure 6.1). The few grains that did exhibit zoning only possessed two or three different growth zones, which made it difficult to distinguish between types of zoning. Since these grains are detrital, the majority were likely broken in transport. A misinterpretation here would potentially lead to a misclassification of the grain origin. It was therefore decided to eliminate zoning as a means of grain classification. This study employs methods similar to Lowe et al. (2011), and the methods are described in detail in Chapter 2. Geochronological data are presented in Appendix A.

6.2 – Quantitative/Qualitative Approaches

U-Pb ages obtained from laser ablation inductively coupled plasma mass spectrometry (LA-ICP-MS) analysis alone can be very diagnostic of provenance, and are particularly useful for constraining paleogeography, and tectonic reconstructions (Fedo et al., 2003). Lowe et al. (2011) demonstrated that source terranes for Upper Jurassic and Cretaceous reservoir sandstones in the Flemish Pass Basin could be pinpointed using this method. This study will expand this previous work into the fine-grained, organic-rich, Kimmeridgian source rocks and Tempest sandstones.

The morphology of zircon grains can indicate the amount of sedimentary recycling that a grain has been subjected to (eg. Lowe et al, 2011; Piper et al, 2012). Grains in this study were classified as first-cycle, or polycyclic based on morphology. First-cycle zircons typically show euhedral to subhedral morphologies. Therefore, grains with angular, or euhedral crystal faces were interpreted as being first-cycle. Grains with rounded, subrounded, or subangular shapes, however, are interpreted to have been derived from older sedimentary rocks and thus are considered polycyclic. There are recognized uncertainties using this technique as rounded grains may also be of metamorphic origin (Hoskin & Schaltegger, 2003) and first-cycle zircons that have been transported long distances may present as rounded grains. In addition, it is possible that polycyclic grains that have not been subject to significant attrition or long distances of transportation may not appear rounded. This method does provide a preliminary means of classifying and distinguishing different zircon populations and, given evidence about the robustness of zircon (although there are exceptions), rounded grains are likely polycyclic.

Other features, such as Th/U, grain surface area, and grain aspect ratios are also important in distinguishing the parent rock type of detrital zircons. For example, igneous zircons typically have Th/U greater than 0.5, whereas metamorphic zircon grains are characteristically more rounded with lower Th/U, and irregular zoning (Lowe et al., 2011). Features such as subhedral morphologies, and high aspect ratios are diagnostic of volcanic zircons (Hoskin & Schaltegger, 2003). These features were recorded for each zircon grain dated to provide a thorough interpretation of the parent rocks and drainage patterns for the Kimmeridgian rocks of the Flemish Pass Basin and Central Ridge.

Grain surface area as well as aspect ratio are two features recorded by the MLA. As many of the samples in this study are polished grain mounts, the surface area recorded for a particular grain may be affected by how far the polishing process cut into the grain. However, to ensure grains were not significantly polished away or even removed, great care was taken in the sample preparation process and some of the aggressive polishing steps were scaled back. Therefore, the number of grains significantly affected by this is likely minimal. In addition, the aspect ratio recorded by the MLA will be affected by the orientation of the grain in the epoxy mount. However, the vast majority of grains would naturally lie along their long axis as opposed to standing on end. It is therefore unlikely that a significant number of grains were affected by this. Despite these caveats, surface area and aspect ratio may provide a useful means of distinguishing groups of zircons when combined with other grain features discussed.

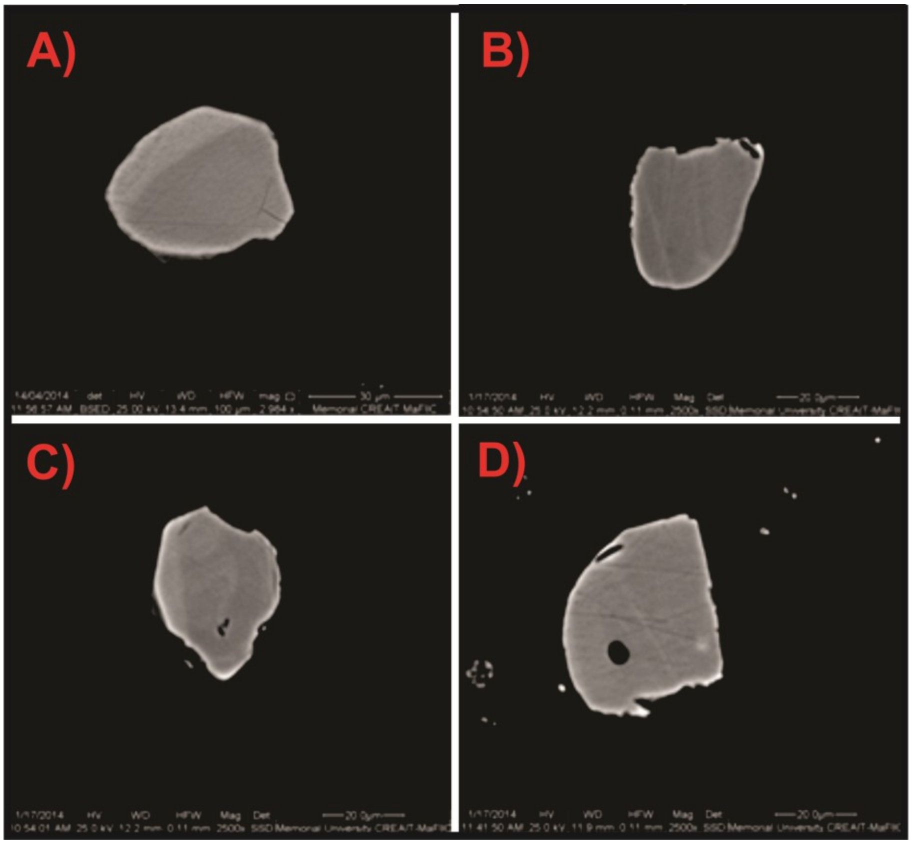

Figure 6.1 - SEM images of zircons demonstrating potential sources of error in classifying zoning types. Grains shown are small and do not display zoning or display insufficient zoning to assess zoning type.

6.3 – Data Presentation

U-Pb zircon ages are presented on conventional Concordia plots, as well as, age vs. frequency cumulative probability histograms using the ISOPLOT/Ex program (version 4.15) of Ludwig (2012). Concordia plots, age vs. frequency histograms, Th/U plots, zircon grain surface area plots, and aspect ratio plots are presented with every individual sample. On the Concordia plots, only concordant results are shown, but in Appendix C, Concordia plots are presented that show all the data. Grains that are up to 10% discordant are considered acceptable for detrital studies. Therefore, any grains that were less than 10% discordant are considered concordant in the following text. These plots use $^{206}Pb/^{238}U$ and $^{207}Pb/^{235}U$ ages which are plotted with 2σ error ellipses. For the age vs. frequency cumulative probability histograms, if grains are younger than

1.2 Ga, the $^{206}Pb/^{238}U$ age is plotted against the number of zircons for all concordant grains. If grains are older than 1.2 Ga, the $^{207}Pb/^{206}Pb$ age is plotted against the number of zircons for all concordant grains. In addition, a cumulative probability curve is presented which helps define age peaks in the samples.

6.4 – Baccalieu I-78: Upper Kimmeridgian Source Rock

6.4.1 – Results

A cuttings sample from 4500 – 4505m yielded sufficient detrital zircons for analysis. Based on observations of the cuttings, this interval was dominated by fine-grained mudstones with some interbedded siltstone. The sample processing involved separating the sample into three grain size fractions for heavy mineral separation using the hydroseparator. The 48-100µm size fraction was used for the isotope analysis as the smaller size fraction contained very few zircon grains. Of the 37 zircon grains imaged, 33 were ablated and 27 yielded concordant U-Pb ages (Figure 6.2A, Figure 6.2B). Four grains were skipped as they were smaller than the laser spot size of 20 µm. With 27 dated grains, using the method of Vermeesch (2004), there is a 95% confidence that no fraction >0.16 was missed. The analyses are characterized by three primary age groups of zircon grains (Figure 6.2B). The first is a peak of eight Cambrian- to Devonian-aged grains (507 – 363 Ma) that comprise 30% of the sample. The peak defined by the cumulative probability plot is at *ca.* 365 Ma (Figure 6.2B) but the mean of the $^{206}Pb/^{238}U$ ages of this group is 408 ± 46 Ma. The second is a major peak of 10 Neoproterozoic-aged grains (552 – 635 Ma) that comprise 37% of the sample. The peak as defined by the cumulative probability plot is *ca.* 625 Ma (Figure 6.1B), but the mean of the $^{206}Pb/^{238}U$ ages of this group of grains is 598 ± 29 Ma. The final major cluster of grains is a group of five zircon grains older than 1 Ga consisting of grains at 1024 ± 25 Ma, 1222 ± 36 Ma, 1257 ± 42 Ma, 1464 ± 44 Ma, and 1749 ±

30 Ma which comprise 19% of the total sample. Four of the grains are Mesoproterozoic, with one older Paleoproterozoic grain (Figure 6.2B).

In addition, outlier grains of 529 ± 17 Ma, 661 ± 18 Ma, 822 ± 20 Ma, and 949 ± 21 Ma were also present.

Another notable aspect of the dated grains are the Th-U ratios, which range from 0.10 to 1.05 (Figure 6.2C). The Cambrian – Devonian group of grains possess Th/U ranging from 0.18 – 1.05 with an average of 0.47. Grains from the prominent late Neoproterozoic peak have Th/U values from 0.41 to 0.95 with an average of 0.62, while grains from the > 1 Ga group have much lower Th/U with values ranging from 0.10 – 0.50 with an average of 0.29.

The morphology of all dated grains was also documented and may be the most important feature for determining the level of sedimentary recycling and/or the transportation distance (Figure 6.2D). Subangular grains are the most abundant type of grain making up 41% of all those dated. The Cambrian – Devonian group of grains is composed of mostly subangular grains with minor angular, subrounded, and rounded grains present as well. The late Neoproterozoic group of grains are also mostly subangular, however, subrounded and rounded grains are more important here than in the younger Cambrian – Devonian group. In the >1 Ga group of grains, the majority of grains are subrounded and rounded, with only one subangular grain. Evidently, older grains appear to have more rounded morphologies than the younger, euhedral or angular grains. This is evidence that the older grains have been subject to potentially numerous cycles of sedimentation and have been therefore more mechanically abraded.

Surface area of dated grains range from 854 – 6152 μm^2 (Figure 6.2E). Grains from the Cambrian – Devonian group possess surface areas ranging from 854 – 3178 μm^2 with an average surface area of 2191 μm^2. The late Neoproterozoic grains have surface areas ranging from 1283 – 6152 μm^2, averaging 2939 μm^2. The >1 Ga group of grains is composed of mostly smaller grains, with surface areas ranging from 1719 – 2840 μm^2, and averaging 2273 μm^2.

Aspect ratios of dated grains were also documented and range from 1.04 – 2.91 (Figure 6.2F). The Cambrian – Devonian grains have aspect ratios from 1.11 – 2.91 with an average aspect ratio of 1.62. The grains for the late Neoproterozoic group possess aspect ratios with an average of 1.34 and ranging from 1.04 – 2.04. Values for the > 1 Ga group of grains were similar to the late Neoproterozoic group, and ranged from 1.17 – 1.70 with an average of 1.37.

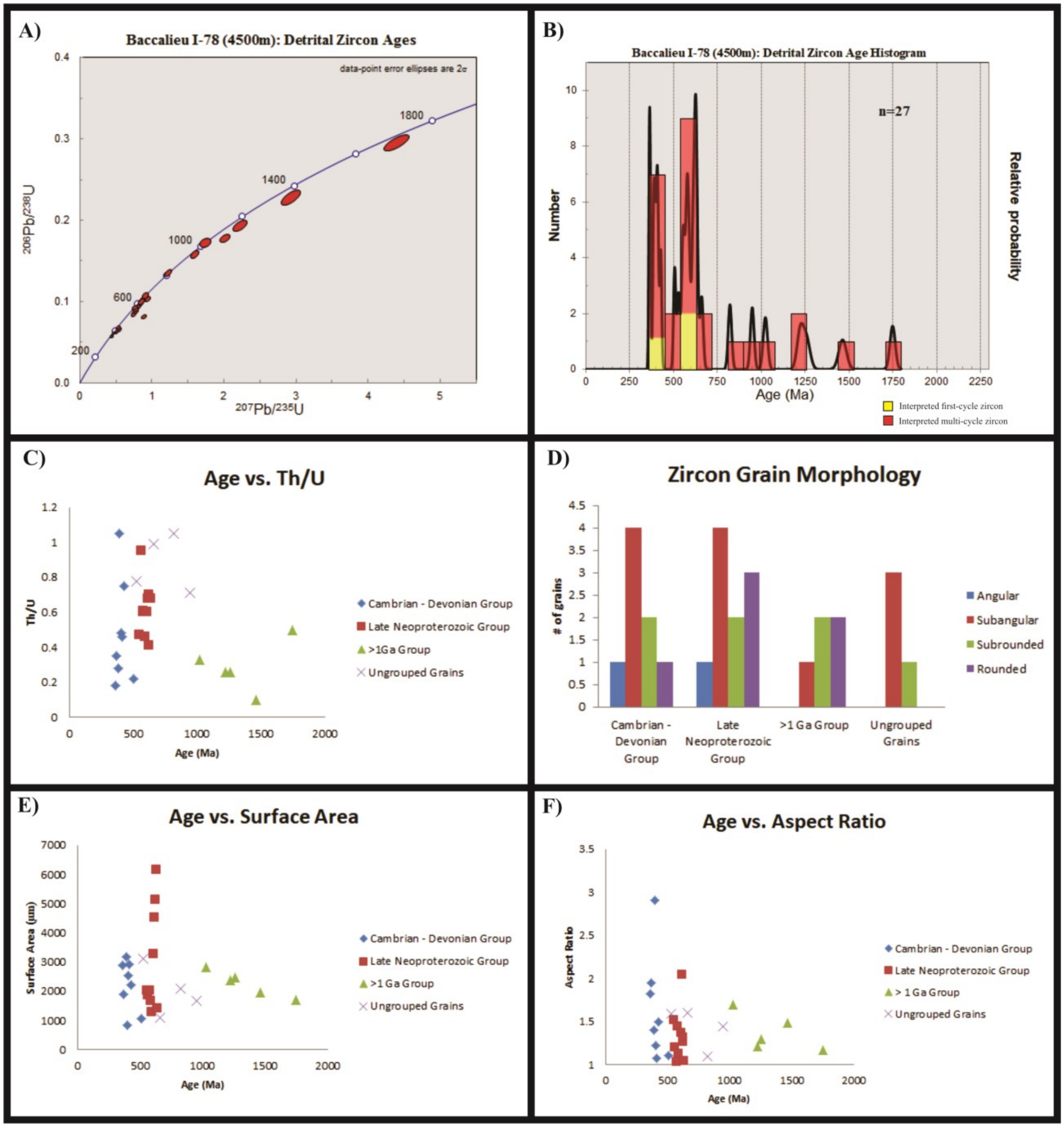

Figure 6.2 - Graphs for detrital zircons of the Baccalieu I-78 (4500 m) sample. (A) Concordia diagram with detrital zircon ages. (B) Detrital zircon age histogram. (C) Age vs. Th/U. (D) Zircon grain morphology. (E) Age vs. Surface Area. (F) Age vs. Aspect Ratio.

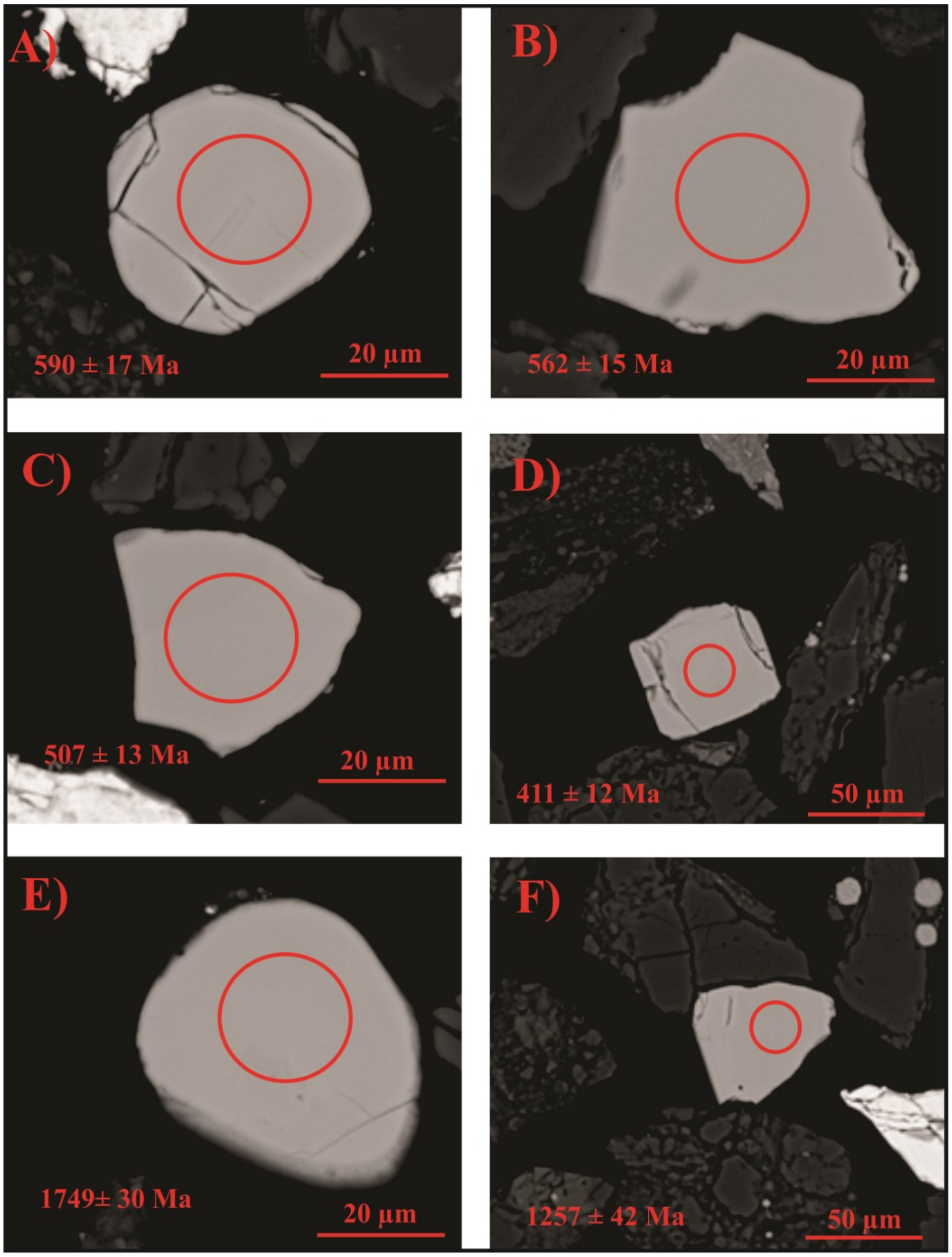

Figure 6.3 - SEM images of detrital zircon grains from each identified age group in the Baccallieu I-78 (4500 m) sample. The 20 µm red circle represents location the grain was ablated.

6.4.2 – Interpretations

Three major clusters of zircon grains populate the cumulative probability histogram for this sample. The most abundant group of grains is late Neoproterozoic. These grains have morphologies that are angular to rounded, indicating a mixture of grains that are possibly both first-cycle and polycyclic. Variable Th/U, as well as a range of grain sizes also support a mixture of first-cycle and polycyclic sources for the late Neoproterozoic grains. The large grain size of a number of zircons from this group may indicate the importance of plutonic igneous rocks as a source.

The second largest cluster of zircons is the Cambrian – Devonian group. This group is characterized by a mixture of morphologies, with a higher proportion of angular grains than the late Neoproterozoic group. Therefore, polycyclic grains are interpreted to be less important in this group than in the late Neoproterozoic group. However, variable Th/U, and aspect ratios, suggest that there is a mixture of volcanic and plutonic igneous rocks, as well as recycled sedimentary rocks that comprise the source region for this group.

The final group (> 1 Ga grains) is characterized by more rounded morphologies, low Th/U, and smaller grain surface areas and aspect ratios. These characteristics are indicative of polycyclic grains, potentially with some grain input from metamorphic rocks. This is anticipated of older grains such as these, as they have likely been subject to significant reworking.

6.5 – South Tempest G-88: Upper Kimmeridgian Source Rock

6.5.1 – Results

Several thin sections were prepared from a core sample from the South Tempest G-88 well at 3837.3 m depth. This interval is considered to be within the Upper Kimmeridgian Source Rock (CNLOPB, 2007). This sample is defined as an arkosic wacke, as described in Chapter 3.

Zircons from three thin sections were imaged and dated. Of the 71 zircons imaged, 68 were ablated (three were rejected due to their small size), yielding 56 concordant U-Pb ages (Figure 6.4A, 6.4B). With 56 dated grains, using the method of Vermeesch (2004), there is a 95% confidence that no fraction >0.10 was missed. The zircon populations from this sample are similar to those in the previous sample from the Baccalieu I-78 well. Three major populations of zircons were present. The first was a peak of 11 Cambrian – Devonian aged grains (533 – 405 Ma) that comprises 20% of all dated grains. The cumulative probability plot categorizes a couple of probability peaks, with the larger at *ca.* 404 Ma and *ca.* 526 Ma (Figure 6.4B). The average of the $^{206}Pb/^{238}U$ ages from this group is 476 ± 52 Ma. The second group is a major peak of 20 late Neoproterozoic-aged grains (626 – 544 Ma) which comprises 36% of all grains analyzed. The cumulative probability plot defines a peak at *ca.* 582 Ma (Figure 6.4B), and the mean of the $^{206}Pb/^{238}U$ ages is 594 ± 29 Ma. The third group is composed of 19 grains > 1 Ga (2740 – 970 Ma) that make up 34% of the sample. One grain was actually dated as early Neoproterozoic (970 ± 21 Ma), and although this is not >1Ga, it was included in this group due to its proximity to a group of grains that were dated near 1 Ga. There are six Mesoproterzoic grains in this group, as well as ten Paleoproterozoic grains, and two grains from the Neoarchean (Figure 6.4B). In addition to these main clusters, a couple of minor other groups were noted as well. Two grains were dated at 281 ± 8 Ma and 341 ± 8 Ma, respectively, forming a minor Carboniferous – Permian population. Three grains were dated at 788 ± 16, 789 ± 18 Ma, and 841 ± 19 Ma, respectively, defining a minor population of Middle Neoproterozoic grains. A single outlier grain of 941 ± 26 Ma was also dated.

The Th-U ratios vary from 0.11 – 1.24 (Figure 6.4C). The Cambrian – Devonian-aged grains have Th-U ratios ranging from 0.11 – 0.99, averaging 0.49. Grains from the prominent late Neoproterozoic peak have Th-U ratios ranging from 0.21 – 1.24 with an average of 0.62, and grains from the older, > 1 Ga group have Th-U ratios ranging from 0.21 – 1.01 with an average of 0.61. It is noteworthy that the average of 0.61 for the >1 Ga group is significantly higher than the average for the previous sample from the Baccalieu I-78 well, where the average Th/U for the >1 Ga group was 0.29. The minor group of Carboniferous – Permian grains have Th-U ratios of 0.35 and 1.05, and the group of Middle Neoproterozoic grains has Th-U ratios of 0.24, 0.33, and 0.50.

The key feature of grain morphology is also assessed for the dated grains from this sample (Figure 6.4D). Of all the grains, a subangular morphology was most common as 39% of all dated grains were subangular in shape. Five Cambrian – Devonian grains are subrounded, with four subangular, and two angular grains as well. Late Neoproterozoic grains are predominantly subangular (11 grains), with four angular grains, two subrounded grains, and three rounded grains. The group of > 1 Ga grains are composed primarily of subrounded grains (10 grains), with five rounded and four subangular grains present as well. The two youngest grains dated (Permian – Carboniferous) were both angular and in the three Middle Neoproterozoic grains, two were subangular, and one angular in shape. The most notable feature observed is that grain morphologies are similar to those in the Kimmeridgian Source Rock sample from the Baccalieu I-78 well. The > 1 Ga grains appear to possess much more rounded shapes than the younger grains, indicating more abrasion than the younger grains, probably a reflection of recycling through a number of sedimentary cycles.

Surface areas of dated grains range from 610 – 3604 μm^2 (Figure 6.4E). Grains from the Cambrian – Devonian group have surface areas ranging from 610 – 2909 μm^2 with an average of 1651 μm^2. Grains from the prominent late Neoproterozoic group have surface areas ranging from

866 – 3210 μm^2 with a mean surface area of 1770 μm^2. The group of >1 Ga grains have surface areas ranging from 1046 – 3604 μm^2 with an average of 1989 μm^2. The two Carboniferous – Permian grains have surface areas of 1331 and 1762 μm^2 and the three Middle Neoproterozoic grains have surface areas of 954, 1015, and 1341 μm^2.

Aspect ratios of all dated grains range from 1.04 – 2.73 (Figure 6.4F). The Cambrian – Devonian grains have variable aspect ratios ranging from 1.04 – 2.71 with an average of 1.51. Aspect ratios of grains of the late Neoproterzoic peak are very similar, and range from 1.08 – 2.73 with an average of 1.51. Grains from the > 1 Ga group had slightly smaller aspect ratios in general, with an average of 1.42. In addition, values were much less variable than the younger grains, as the values for the >1 Ga grains range from just 1.15 – 1.88. The two Carboniferous – Permian grains possess aspect ratios of 1.09 and 1.76, while the three Middle Neoproterozoic grains have aspect ratios of 1.42, 1.44 and 1.95.

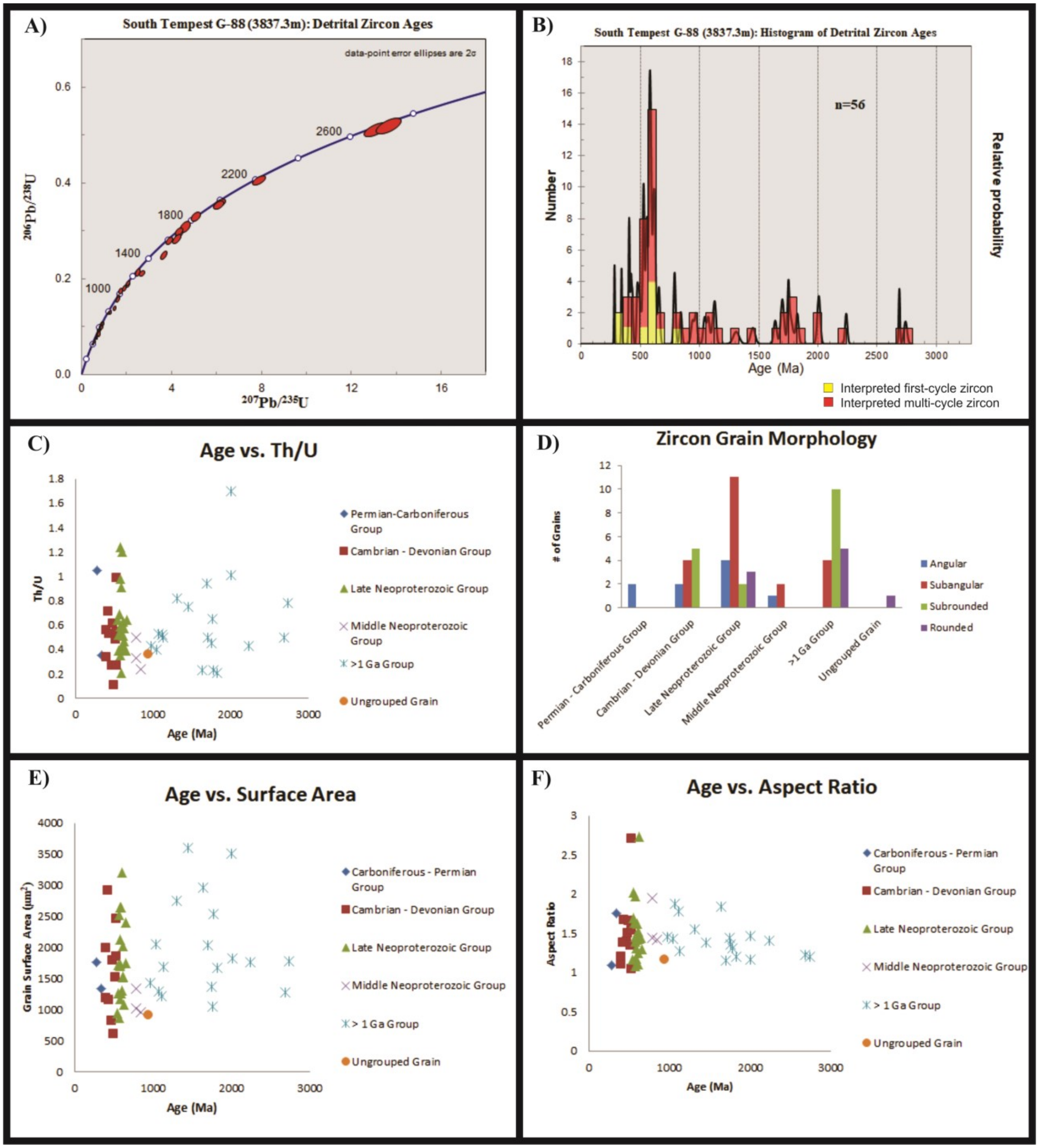

Figure 6.4 - Graphs for detrital zircons of the South Tempest G-88 (3837.3 m) sample. (A) Concordia diagram with detrital zircon ages. (B) Detrital zircon age histogram. (C) Age vs. Th/U. (D) Zircon grain morphology. (E) Age vs. Surface Area. (F) Age vs. Aspect Ratio.

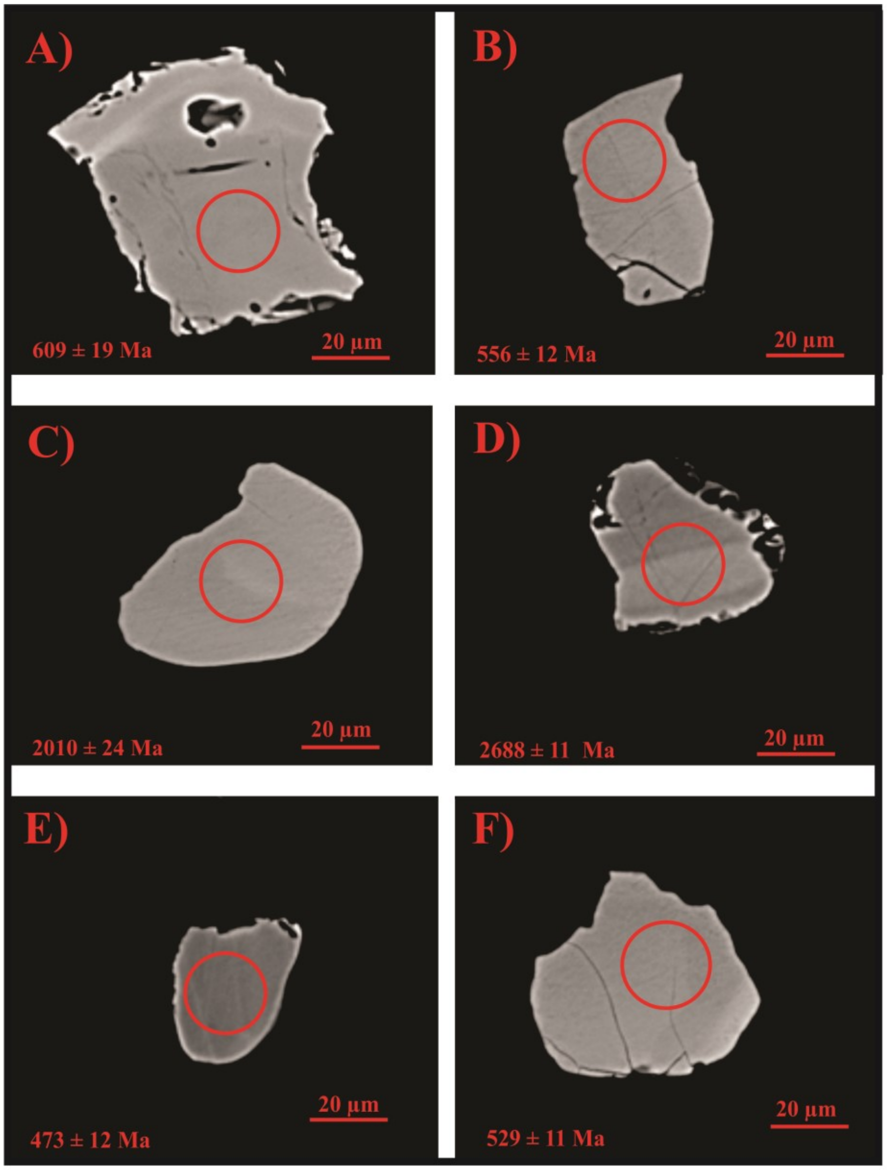

Figure 6.5 - SEM images of detrital zircon grains from each identified age group in the South Tempest G-88 (3837.3 m) sample. The 20 µm circle represents location grain was ablated.

6.5.2 – Interpretations

Similar to the Kimmeridgian Source Rock sample from the Baccalieu I-78 well, this sample contains three main groups of detrital zircons. The most abundant grains, the late Neoproterozoic group, are characterized by predominantly subangular grains, variable Th/U, and variable aspect ratios and surface areas. These features probably indicate a mixture of types of source rocks. These likely include some plutonic and volcanic igneous rocks (based on some high Th/U, and variable surface areas), as well as recycled sedimentary rocks (some rounded grains).

The second most abundant group of grains in this sample is the > 1 Ga grains. These grains have mostly subrounded and rounded shapes, variable Th/U, and surface areas, with small, well constrained aspect ratios. These characteristics indicate that recycled sedimentary rocks was probably an important source for the > 1 Ga group (rounded grain shapes, small aspect ratios). Metamorphic rocks may also have been source rocks, as there are some low Th-U ratios, and metamorphic zircons are known to be rounded as well. However, the Th-U ratios in this sample are considerably larger than those in the Baccalieu I-78 Kimmeridgian Source Rock sample, indicating more of an igneous component in the > 1 Ga grains analyzed in this sample.

The Cambrian – Devonian group of grains possess mostly subrounded and subangular morphologies. As with most other groups, the Th-U ratios are fairly variable, as well as the aspect ratios and overall grain surface areas. It is interpreted that these grains are likely derived from a mixture of igneous rocks (high Th/U, high surface area grains) and recycled sedimentary rocks (subrounded grains, low aspect ratio grains).

The two Carboniferous – Permian grains are both angular in shape, one with a high Th/U and aspect ratio, the other with a low Th/U and aspect ratio. Both grains are near the overall average in surface area. These grains are likely derived from igneous rocks based on their morphology, but not enough information is available on the group to draw conclusions about the Th/U, aspect ratio, or surface area.

Of the three Middle Neoproterozoic grains, two are subangular, and the other is angular in morphology. All of the grains possess Th/U values of 0.5 or below, aspect ratios below 2 and relatively small surface areas. As with the Carboniferous – Permian grains, it is difficult to draw conclusions from features such as the Th/U, aspect ratio, and surface area from relatively few grains, but the angular and subangular morphologies indicate a derivation from igneous rocks.

6.6 – Lancaster G-70 – Rankin Formation

6.6.1 – Results

A cuttings sample from the Rankin Formation at 4405 – 4410m contained sufficient detrital zircons to be analyzed. Observations from the cuttings indicated this interval was predominantly fine-grained, consisting of mudstones interbedded with minor siltstones and fine-grained sandstones. This sample was separated into three grain size fractions for heavy mineral separation using the hydroseparator. The 20 – 48 and 48 – 100 µm fractions were the size fractions analyzed as very few zircons were found in the other size fractions. Of the 70 zircon grains imaged, 62 were ablated (eight were rejected as they were less than 20 µm in size). Unfortunately, many of the grains contained abundant ^{204}Pb, and yielded discordant results. ^{204}Pb, also known as common lead, is a problem because its' presence in a zircon means that the calculated U-Th-Pb ratios, and hence calculated ages, no longer represent that of the crystallization age (Andersen, 2002). In this sample, of the 62 grains ablated, only 20 were less than 10% discordant. However, a common lead correction was applied to the grains, and many of the previously discordant grains plotted as concordant. The correction was completed using the VizualAge software within the Iolite program (Petrus & Kamber, 2012). Additional details of the correction itself are available in Andersen (2002). Essentially, the Andersen (2002) correction uses an algorithm that assumes that the time of lead loss (if any) can be determined, and that the U/Th ratio of the grain is undisturbed. This method is particularly useful when the measured abundances of ^{204}Pb are not recorded or unreliable (Petrus & Kamber, 2012). This is often the case in LA-ICP-MS analyses due to the low natural abundance of ^{204}Pb and interference from ^{204}Hg (Petrus & Kamber, 2012). ^{204}Pb was measured in this study, but as mentioned above, may not provide the most reliable results in LA-ICP-MS analyses. This is likely why the Andersen (2002) correction was so effective in these samples, as this correction does not use the ^{204}Pb data. After applying the correction, 57 of the 62 ablated grains plotted concordantly. Of these 57 concordant grains, however, only 56 are included in the detrital zircon analysis (Figure 6.6A, 6.6B) as calculated date of the rejected grain was 112 ± 5 Ma, inconsistent with the established Late Jurassic biostratigraphic age of this interval as defined by Robertson Research (2002), a discrepancy of around 40 Ma. Other biostratigraphic reports from Jenkins (1986) and BP Exploration (1991) also date this interval as latest Callovian to earliest Oxfordian (~160 Ma) and Early Kimmeridgian (~157 Ma), respectively. Although a divergence between the biostratigraphic and detrital zircon ages is possible, it is unlikely to be this large. Therefore, the result for this 112 ± 5 Ma detrital zircon grain is discarded. Since this sample is from drill cuttings, it is likely that this zircon grain was derived from higher in the stratigraphic section, from cavings of Cretaceous or younger strata. This interpretation is preferred given that the age of the unit is well established and that only a single grain of 112 ± 5 Ma was found. With 56 dated grains, using the method of Vermeesch (2004), there is a 95% confidence that no fraction >0.10 was missed.

The grains define five prominent clusters: The youngest group is composed of seven Late Devonian – Permian-aged grains (361 – 248 Ma) that make up 13% of all dated grains. These zircons comprise 13% of all dated grains and define two cumulative probability peaks at *ca.* 267 Ma and *ca.* 360 Ma, respectively (Figure 6.6B). The average of the $^{206}Pb/^{238}U$ ages of grains in this group is 300 ± 42 Ma. Another group consists of 13 Cambrian to Silurian-aged zircons (532 – 431 Ma) which comprises 23% of the sample. This group forms a cumulative probability peak at *ca.* 456 Ma, although there is an additional peak at *ca.* 538 Ma (Figure 6.6B). The average $^{206}Pb/^{238}U$ ages of grains in this group is 488 ± 35 Ma. A group of 11 late Neoproterozoic grains (664 – 548 Ma) comprises 20% of all dated grains. The cumulative probability peak formed by this group is *ca.* 612 Ma (Figure 6.6B) and the average of the $^{206}Pb/^{238}U$ ages of grains in this group is 620 ± 30 Ma. A smaller group of three Middle Neoproterozoic grains (837 – 817 Ma) makes up 5% of the total sample. They form a cumulative probability peak at *ca.* 833 Ma (Figure 6.6B) and have an average $^{206}Pb/^{238}U$ age of 830 ± 9 Ma. The largest group is composed of 19 grains with ages > 1 Ga (2636 – 1017 Ma) and comprises 34% of all grains analyzed. In this group, there are 8 Mesoproterozoic grains, 8 Paleoproterozoic grains and 3 Neoarchean grains. (Figure 6.6B). Two other grains were dated with ages of 545 ± 22 Ma and 539 ± 27. Additionally, one Upper Jurassic grain was dated at 175 ± 9 Ma (Figure 6.6A, 6.6B).

The Th/U of grains from this sample range from 0.06 – 1.6 (Figure 6.6C). The Jurassic grain has a Th/U of 1.27. The Late Devonian to Permian grains have Th-U ratios ranging from 0.3 – 1.31, with an average of 0.75. The Cambrian to Silurian group has Th-U values ranging from 0.06 – 1.15 with an average of 0.64. The late Neoproterozoic grains have Th-U values ranging from 0.3 – 1.19 with an average of 0.64. The Middle Neoproterozoic grains have Th-U values ranging from 0.29 – 1.12 with an average of 0.58. The > 1 Ga grains have much more variable Th-U values ranging from 0.15 – 1.60 with an average of 0.65.

The most common grain shape here is subangular, with 46% of the grains possessing this morphology (Figure 6.6D). The Jurassic grain is subangular, wheras the Late Devonian to Permian grains are characterized by three angular and four subangular grains. The Cambrian –

Silurian grains possess a wide range of morphologies, with three angular, six subangular, three subrounded and one rounded grain. The Late Neoproterozoic grains are characterized by one angular, five subangular, three subrounded, and two rounded grains. The Middle Neoproterozoic group is composed of one subangular and two subrounded grains. The group of >1 Ga grains is predominantly subrounded (nine grains), with two rounded grains, seven subangular grains, and one angular grain. This group, as was noted with previous samples, was probably subject to numerous sedimentary cycles to produce mostly subrounded and rounded grains. The two ungrouped grains are both subangular.

The surface area of all grains dated ranges from 650 – 3930 μm^2 (Figure 6.6E). The Jurassic grain possesses a surface are of 752 μm^2. The Late Devonian to Permian grains have surface areas ranging from 650 – 3863 μm^2 with an average of 1448 μm^2. The Cambrian to Silurian grains possess surface areas ranging from 673 – 1571 μm^2 with an average of 999 μm^2. Late Neoproterozoic grains are characterized by surface areas ranging from 886 – 2629 μm^2 with an average of 1496 μm^2. The Middle Neoproterozoic grains all range from 1079 – 1107 μm^2 with an average of 1094 μm^2 while the > 1 Ga grains had variable surface areas ranging from 725 – 3930 μm^2 with an average of 1618 μm^2. The two ungrouped grains possess surface areas of 1315 μm^2 and 1656 μm^2, respectively.

Aspect ratios of dated grains vary from 1.07 – 2.21 (Figure 6.6F). The Jurassic grain possesses an aspect ratio of 1.38. The Late Devonian – Permian grains are characterized by aspect ratios between 1.14 – 1.89 with an average of 1.55. The Cambrian – Silurian grains possess aspect ratios between 1.08 – 1.77 with an average of 1.31. The Late Neoproterozoic grains are characterized by aspect ratios between 1.1 and 1.77 with an average of 1.37 while the Middle Neoproterozoic grains possess aspect ratios ranging from 1.15 – 1.93 with an average of

1.47. The older, >1 Ga grains are characterized by aspect ratios ranging from 1.07 – 2.21 with an average of 1.46. The two ungrouped grains possess aspect ratios of 1.63 and 1.83, respectively.

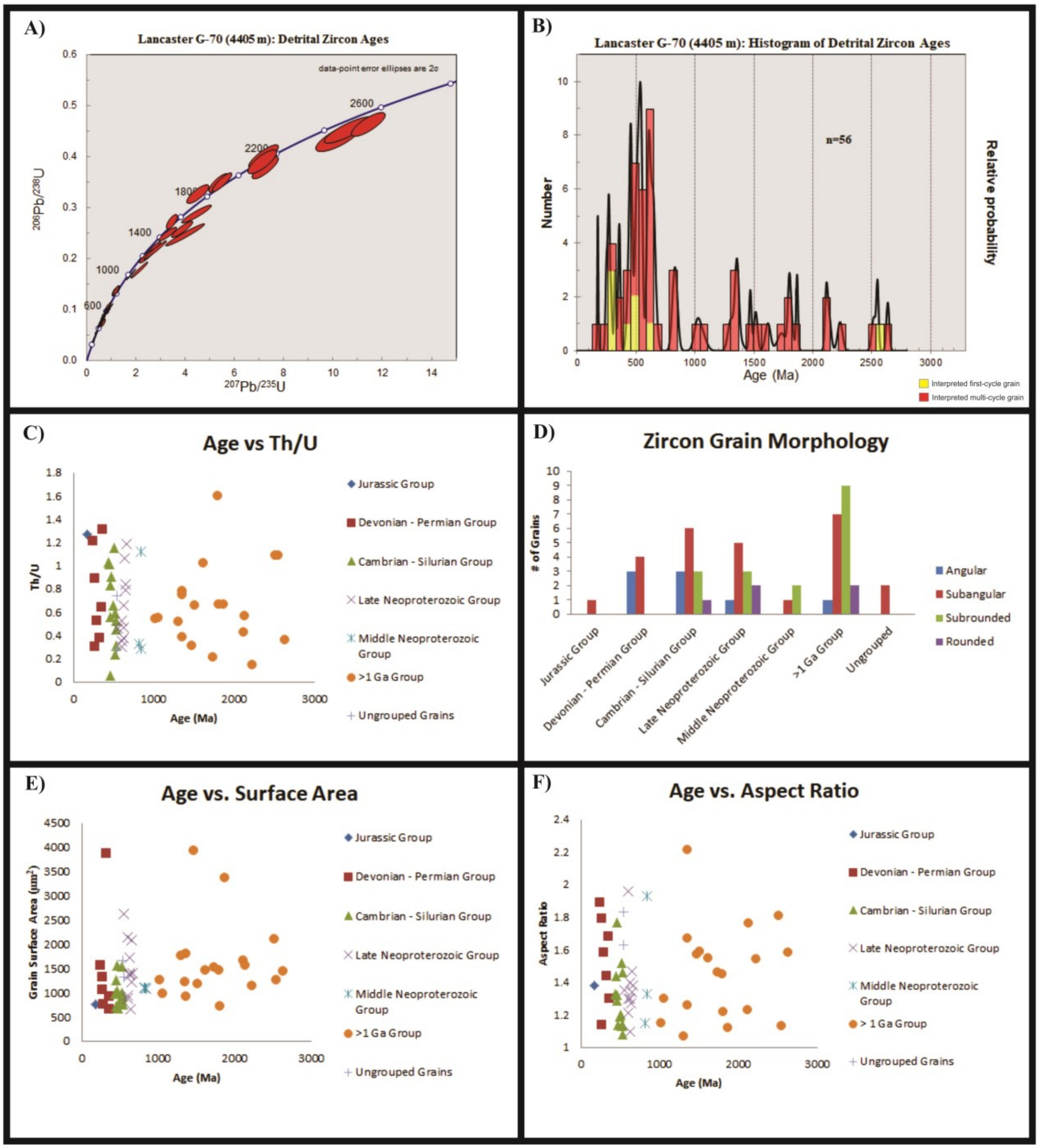

Figure 6.6 - Graphs for detrital zircons of the Lancaster G-70 (4405 m) sample. (A) Concordia diagram with detrital zircon ages. (B) Detrital zircon age histogram. (C) Age vs. Th/U. (D) Zircon grain morphology. (E) Age vs. Surface Area. (F) Age vs. Aspect Ratio.

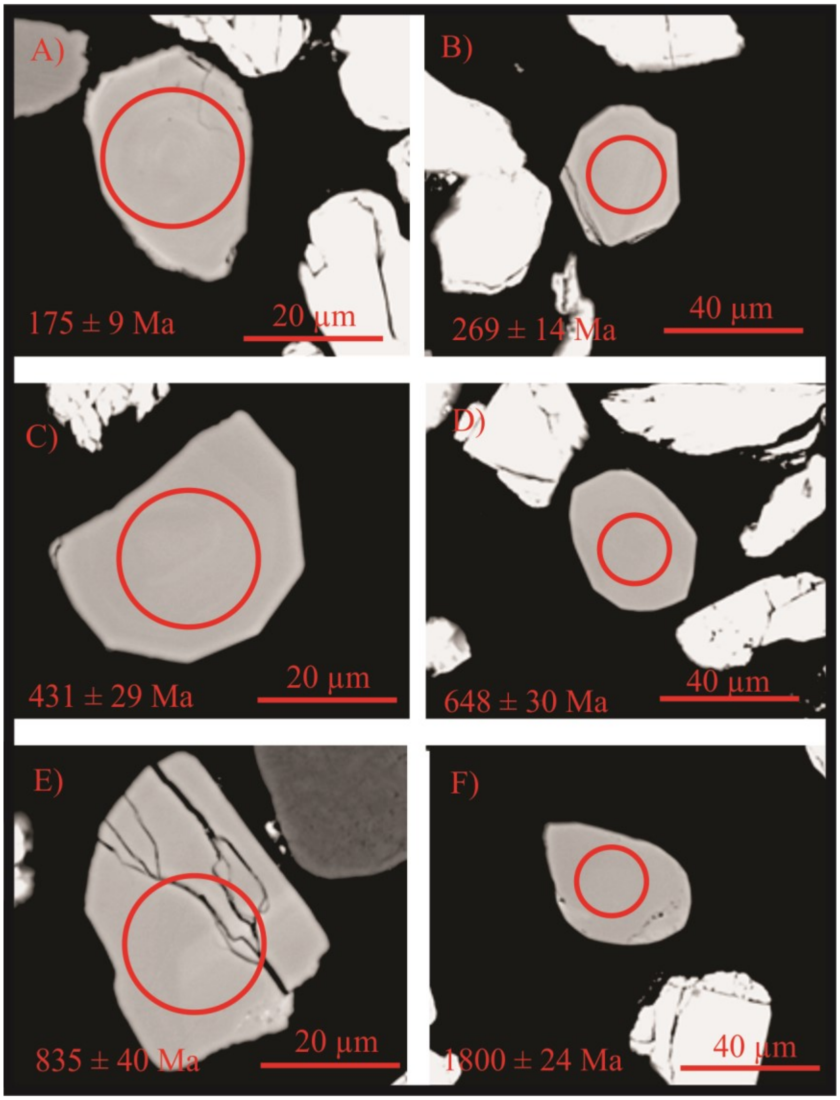

Figure 6.7 - SEM images of detrital zircon grains from each identified age group in the Lancaster G-70 (4405 m) sample. 20 µm circle represents location grain was ablated.

6.6.2 – Interpretations

This sample is composed of five major zircon grain populations. The Late Devonian – Permian grains are characterized by angular and subangular morphologies, Th/U averaging greater than 0.75 and variable surface areas and aspect ratios. Based predominantly on the subangular and angular grain morphologies as well as fairly high Th/U, it is likely that these grains are derived from igneous rocks as first or second cycle sediments.

The Cambrian – Silurian grains are characterized by very variable Th/U and grain morphologies, but generally low aspect ratios and surface areas. Grains with more rounded morphologies, aspect ratios and surface areas are likely polycyclic, but other grains with high Th/U and more angular morphologies are likely first-cycle, and derived from igneous rocks.

Grains of the late Neoproterozoic group possess similar Th/U values to the Cambrian – Silurian grains, and variable grain morphologies, surface areas, and aspect ratios. This suggests a mixed origin for the late Neoproterozoic grains. Many of the grains with more rounded morphologies, low surface areas and aspect ratios are likely derived from sedimentary rocks. The grains with high Th/U and more angular morphologies are likely derived from igneous rocks.

The Middle Neoproterozoic grains are characterized by variable Th/U, two subrounded and one subangular grain, surface areas near 1100 μm^2 and variable aspect ratios. It is difficult to pinpoint the type of source rock based on only three grains; however the relatively small surface areas and subrounded grain morphologies indicate recycled sedimentary rocks are likely important sources of these Middle Neoproterozoic grains. One of the grains possesses a very high Th/U and is likely derived from igneous sources.

The abundant, >1 Ga grains are characterized by mostly subrounded grain morphologies, highly variable Th/U, as well as a wide range of aspect ratios and surface areas. Due to the abundance of rounded and subrounded grain morphologies, it is likely that many of these grains are polycyclic and derived from recycled sedimentary rocks. However, metamorphic rocks may also be important as a source because metamorphic zircon grains may also be rounded with low Th/U ratios.

6.7 – Baccalieu I-78 – Rankin Formation (Mudstone Interval)

6.7.1 – Results

A sample from conventional core at 4142.2m was used to make several thin sections, which contained sufficient detrital zircons for analysis. This sample was described in Chapter 3 as a sand- and clay-bearing, silt-rich mudstone. 23 zircons from this sample were imaged and ablated, and yielded 20 concordant analyses (Figure 6.8A, 6.8B). With 20 dated grains, using the method of Vermeesch (2004), there is a 95% confidence that no fraction >0.21 was missed. The 20 concordant analyses are defined by similar age abundance peaks as the G-70(4405m) sample. A group of 11 late Neoproterozoic grains are present (553 – 675 Ma) (Figure 6.8B) which comprise 55% of the total sample. This group forms a cumulative probability peak at *ca*. 570 Ma (Figure 6.8B), although the average $^{206}Pb/^{238}U$ age of all grains in this group is 603 ± 41 Ma. There is also a group of seven >1 Ga grains (1155 – 2060 Ma), which comprise 35% of all grains analyzed. Three of the >1 Ga grains are Mesoproterozoic, and the other four are Paleoproterozoic (Figure 6.8B). One Devonian grain (415 ± 17 Ma), and one Middle Neoproterozoic grain (814 ± 30 Ma) are also present (Figure 6.8B).

Th/U of all grains range from 0.13 – 1.24 (Figure 6.8C). The late Neoproterozoic grains have Th/U values ranging from 0.32 – 1.24 with an average of 0.67. The > 1 Ga grains have markedly lower Th/U which range from 0.13 – 0.66 with an average of 0.37. The Devonian grain has a Th/U of 0.43, and the Middle Neoproterozoic grain possess a Th/U of 0.58.

The most common grain morphology of the dated grains is subangular, as 45% of all the grains have this shape (Figure 6.8D). The late Neoproterozoic grains are predominantly subangular (four grains), however three angular grains, three subrounded grains, and one rounded grain is also present. The > 1 Ga grains are characterized by three subangular grains, two subrounded grains and two rounded grains. It appears these grains have been subject to more attrition than the Neoproterozoic grains, although probably not as significant as the >1 Ga grains in previous samples, as subangular grains are most abundant in this particular sample. The Devonian grain as well as the Middle Neoproterozoic grain both possess subangular morphologies.

Surface areas of all dated grains range from 589 – 2072 μm^2 (Figure 6.8E). The late Neoproterozoic grains have surface areas ranging from 589 – 1892 μm^2 with an average of 1207 μm^2. The > 1 Ga grains have slightly larger surface areas ranging from 931 – 2072 μm^2 with an average of 1438 μm^2. The Devonian grain has a surface area of 826 μm^2 while the Middle Neoproterozoic grain possess a surface area of 1397 μm^2.

Aspect ratios of all grains range from 1.04 – 2.17 (Figure 6.8F). The late Neoproterozoic grains are defined by variable aspect ratios ranging from 1.04 – 2.17 with an average of 1.67. Grains >1 Ga possess aspect ratios ranging from 1.15 – 2.11 with an average of 1.46. The Devonian grain has an aspect ratio of 1.31 and the Middle Neoproterozoic grain has an aspect ratio of 1.42.

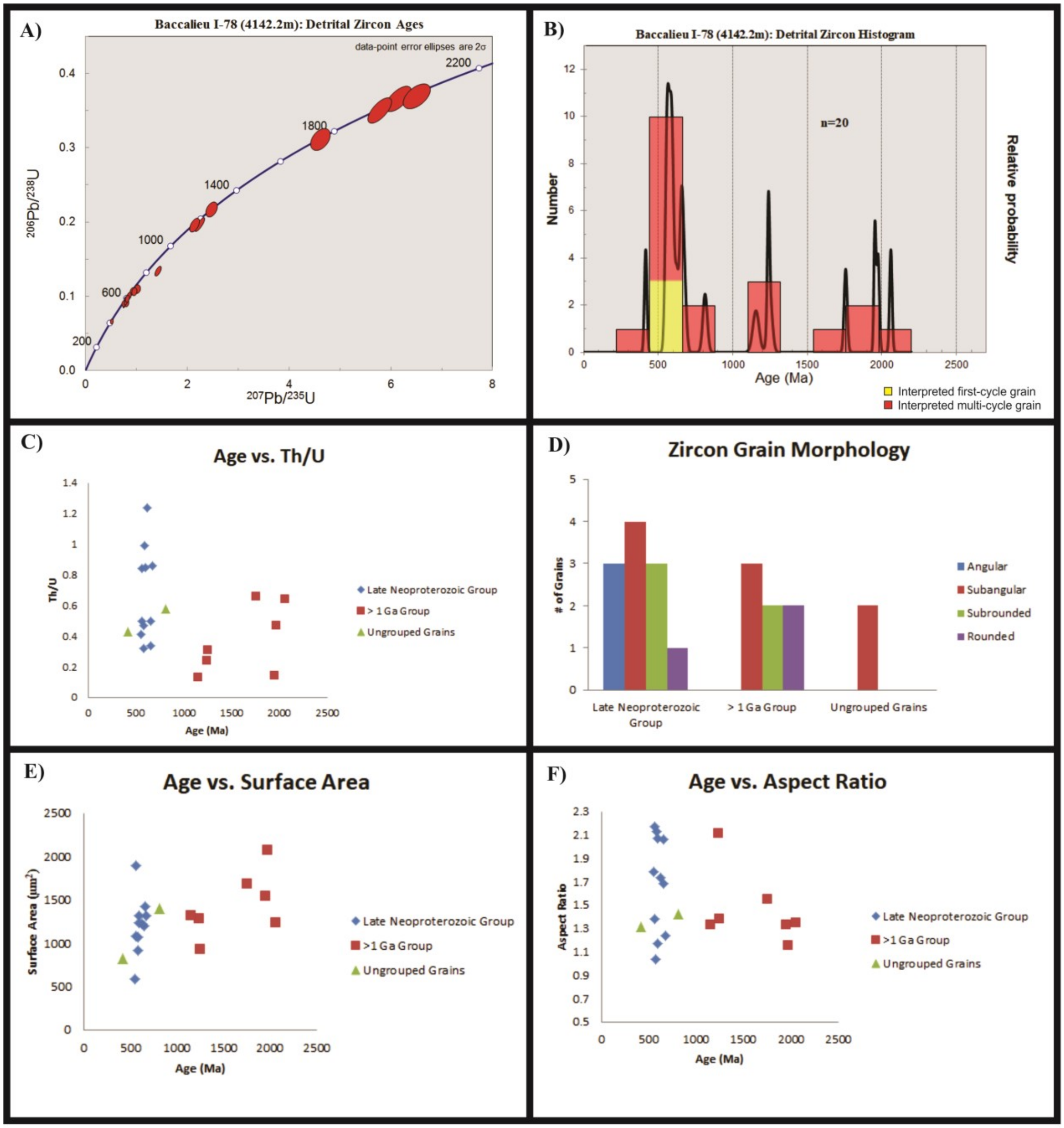

Figure 6.8 - Graphs for detrital zircons of the Baccalieu I-78 (4142.2 m) sample. (A) Concordia diagram with detrital zircon ages. (B) Detrital zircon age histogram. (C) Age vs. Th/U. (D) Zircon grain morphology. (E) Age vs. Surface Area. (F) Age vs. Aspect Ratio.

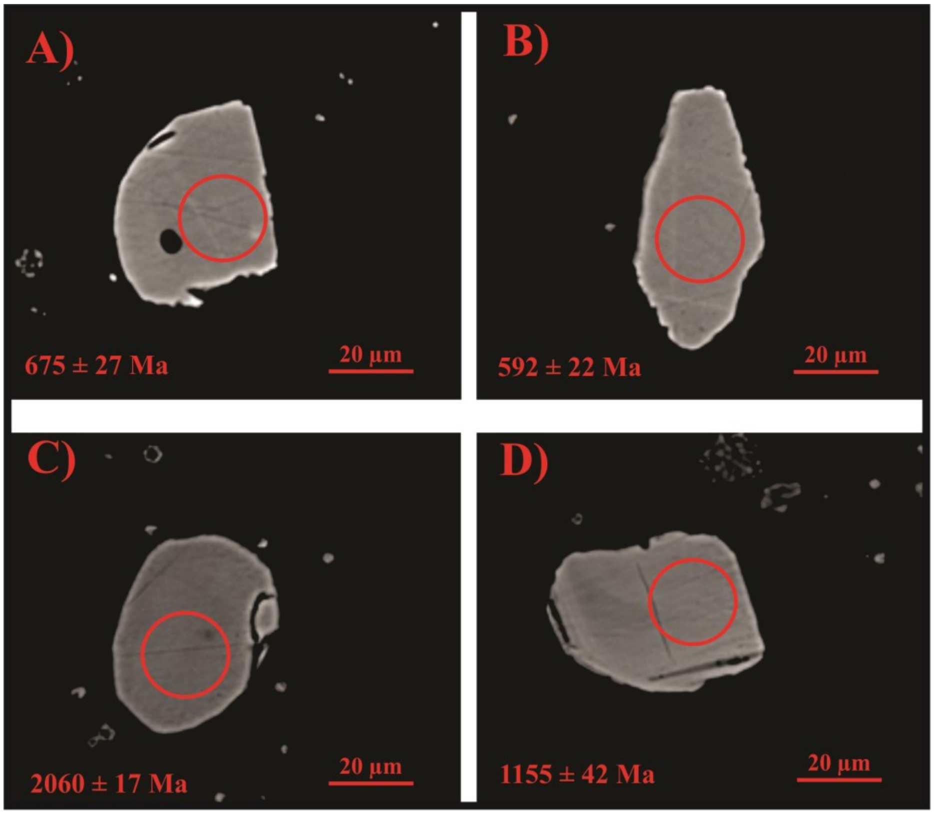

Figure 6.9 - SEM images of detrital zircon grains from each identified age group in the Baccalieu I-78 (4142.2 m) sample. 20 µm circle represents location grain was ablated.

6.7.2 – Interpretations

The most abundant group of zircons in this sample is this late Neoproterozoic group. These grains are characterized by variable Th/U, subangular grain morphologies, variable surface areas as well as a wide range of aspect ratios. As with the late Neoproterozoic grains from previous samples, there is likely a range of parent rock types for these zircons. Plutonic and volcanic rocks are likely important (high Th/U, angular grains) but recycled sedimentary rocks are likely also an important source based on the presence of some subrounded and rounded grains.

The >1 Ga grains are characterized by subangular to rounded grain morphologies, with low Th/U and variable surface areas and aspect ratios. These features are indicative of a derivation from recycled sedimentary rocks (rounded grain morphologies) as well as metamorphic rocks (low Th/U).

The two outlier grains (Devonian & Middle Neoproterozoic) both possess subangular morphologies. The Middle Neoproterozoic grain has a Th/U of 0.58, and was likely derived from an igneous source, while the Devonian grain has a Th/U of 0.43 and may be derived from a metamorphic source, or potentially a recycled sedimentary rock.

6.8 – Baccalieu I-78 – Rankin Formation (Sandstone Interval)

6.8.1 – Results

A sample was obtained from conventional core at 4135.29m, and several thin sections were made from this sample. The sample is described in Chapter 3, and is termed an arkosic wacke. This sample was analyzed, in addition to the mudstone sample at 4142.2m, because it is of interest to determine if detrital zircon populations are the same in both the fine-grained mudstone beds, as well as the coarser sandstone beds. An important topic in the study on mudstone provenance is the issue of whether interbedded mudstones and sandstones were both derived from the same source (Potter & Maynard, 2005; McLennan et al., 2003). Potter & Maynard (2005) ponder whether muds may be derived from a more distant source whereas sands and silts from a source much closer? McLennan (2003) suggested that this question has received inadequate study and that in deep sea turbidites, many sand-mud pairs within individual Bouma cycles show systematic differences in their trace element compositions which indicates different provenance. Hence, it was of interest for this study to determine if detrital zircons indicate a similar or different provenance for interbedded mud-sand pairs in the Kimmeridgian rocks from offshore Newfoundland. Both the mudstone (from I-78 (4142.2m)) as well as this sandstone sample from I-78 (4135.29m) were examined to determine whether the detrital zircons indicate a common provenance. 47 zircons from this sample were imaged, and 37 were ablated. Ten were skipped because of their small size (<20 µm). Of these grains, 34 yielded concordant analyses (Figure 6.10A, 6.10B). With 34 dated grains, using the method of Vermeesch (2004), there is a 95% confidence that no fraction >0.14 was missed. The zircon groups are similar to that of the mudstone sample from 4142.2m. The most abundant group of grains is late Neoproterozoic, and 15 grains of this age are present (546 – 674 Ma) comprising 44% of the sample (Figure 6.10B). They form a cumulative probability peak at *ca.* 598 Ma (Figure 6.10B), and the average of the $^{206}Pb/^{238}U$ age of all grains in this group is 611 ± 33 Ma. The second most abundant group is the > 1 Ga grains, which is made up of 12 grains (1084 – 2130 Ma) comprising 35% of all dated grains (Figure 6.10B). The >1 Ga grains include 5 Mesoproterozoic, as well as 7 Paleoproterozoic grains. A small group of 4 Silurian – Devonian grains were also present (370 – 404 Ma) (Figure 6.10B) comprising 12% of the sample. The Silurian – Devonian grains comprise 12% of all concordant grains and form a cumulative probability peak at *ca.* 372 Ma (Figure 6.10B), with an average of the $^{206}Pb/^{238}U$ age of all grains in this group of 395 ± 27 Ma. Three outlier grains of 683 ± 42 Ma, 862 ± 37 Ma, and 938 ± 52 Ma were also dated (Figure 6.10B).

Th/U of all dated grains range from 0.02 – 1.61 (Figure 6.10C). The late Neoproterozoic grains possess values ranging from 0.1 – 1.61 with an average of 0.83. The > 1 Ga grains have values ranging from 0.03 – 0.83 with an average of 0.35. The Silurian – Devonian grains have values ranging from 0.2 – 0.65 with an average of 0.44. The outlier grains of 683, 862, and 938 Ma possess Th/U values of 0.02, 0.37, and 0.36 respectively.

The most common grain morphology of all dated grains is subangular, as 50% of the grains possess this shape (Figure 6.10D). The late Neoproterozoic grains are mostly subangular (eight grains), although four angular grains and three subrounded grains are also present. The >1 Ga grains are predominantly subangular as well (six grains), although two subrounded and four rounded grains were also present in this group. The Silurian – Devonian grains are characterized by three subangular grains and one angular grain. The outlier grains of 683 and 938 Ma are both subrounded while the grain of 862 Ma is angular. Evidently, the grains which have faced the most attrition are the >1 Ga grains, although most here are subangular, which is not consistent with >1 Ga grains from most other samples.

Surface areas of all dated grains range from 803 – 5555 μm^2 (Figure 6.10E). The late Neoproterozoic grains have values that range from 1082 – 5251 μm^2 with an average surface area of 1978 μm^2. The group of >1 Ga grains possess much smaller surface areas ranging from 803 – 2034 μm^2 with an average of 1252 μm^2. The Silurian – Devonian grains have surface areas ranging from 857 – 5555 μm^2 with an average of 2810 μm^2. The outlier grains of 683, 862, and 938 Ma possess surface areas of 1894, 1093, and 1471 μm^2, respectively.

Aspect ratios of all grains vary from a minimum of 1.0 to a maximum of 2.7 (Figure 6.10F). The late Neoproterozoic grains possess aspect ratios ranging from 1.21 – 2.19 with an average of 1.56. The >1 Ga grains have aspect ratios ranging from 1.10 – 2.5 with an average of 1.45. The Silurian – Devonian grains possess aspect ratios between 1.07 – 2.43 with an average of 1.68. The outlier grains of 683, 862, and 938 Ma possess aspect ratios of 2.7, 1.0, and 1.46 respectively.

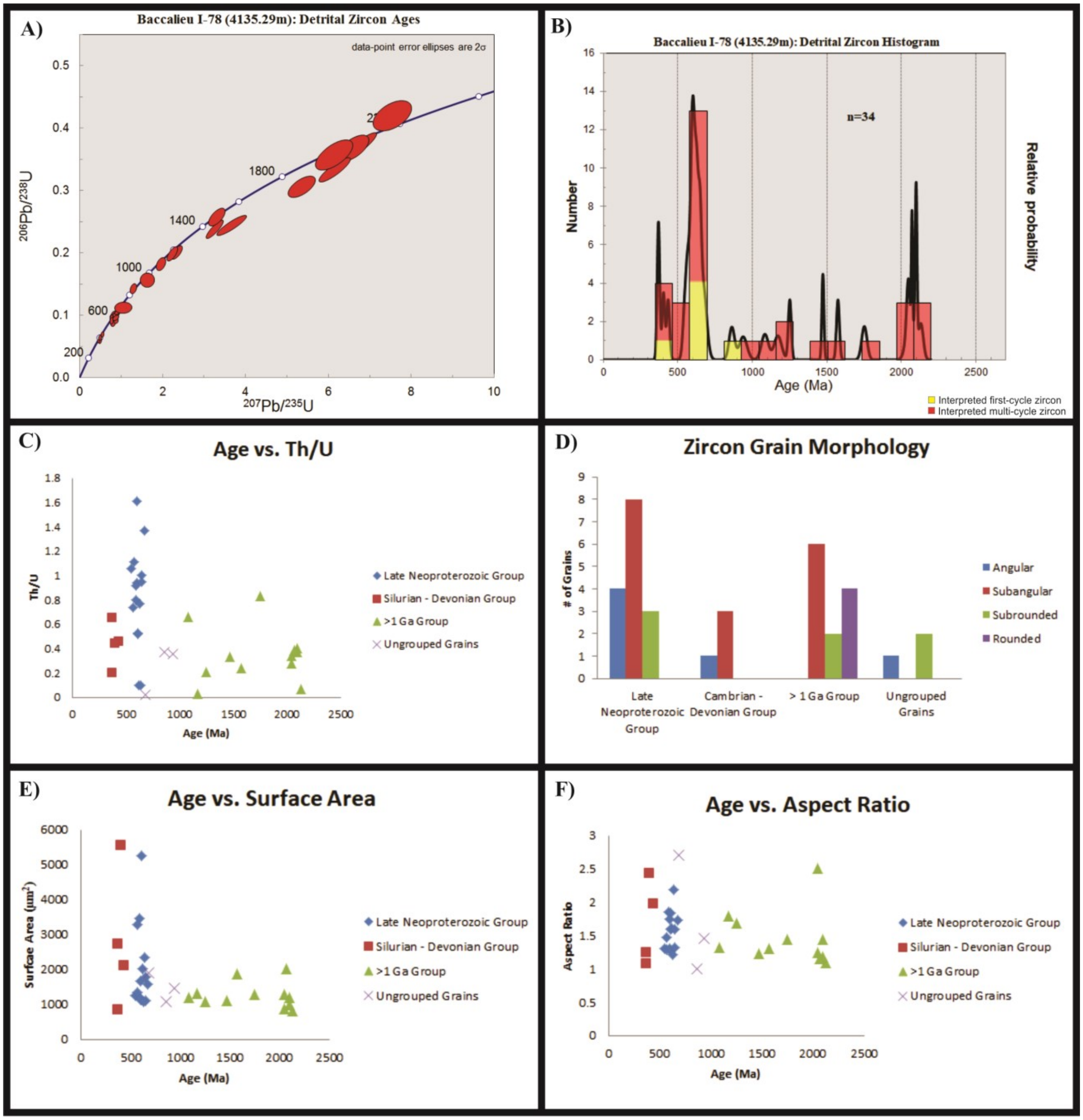

Figure 6.10 - Graphs for detrital zircons of the Baccalieu I-78 (4135.29 m) sample. (A) Concordia diagram with detrital zircon ages. (B) Detrital zircon age histogram. (C) Age vs. Th/U. (D) Zircon grain morphology. (E) Age vs. Surface Area. (F) Age vs. Aspect Ratio

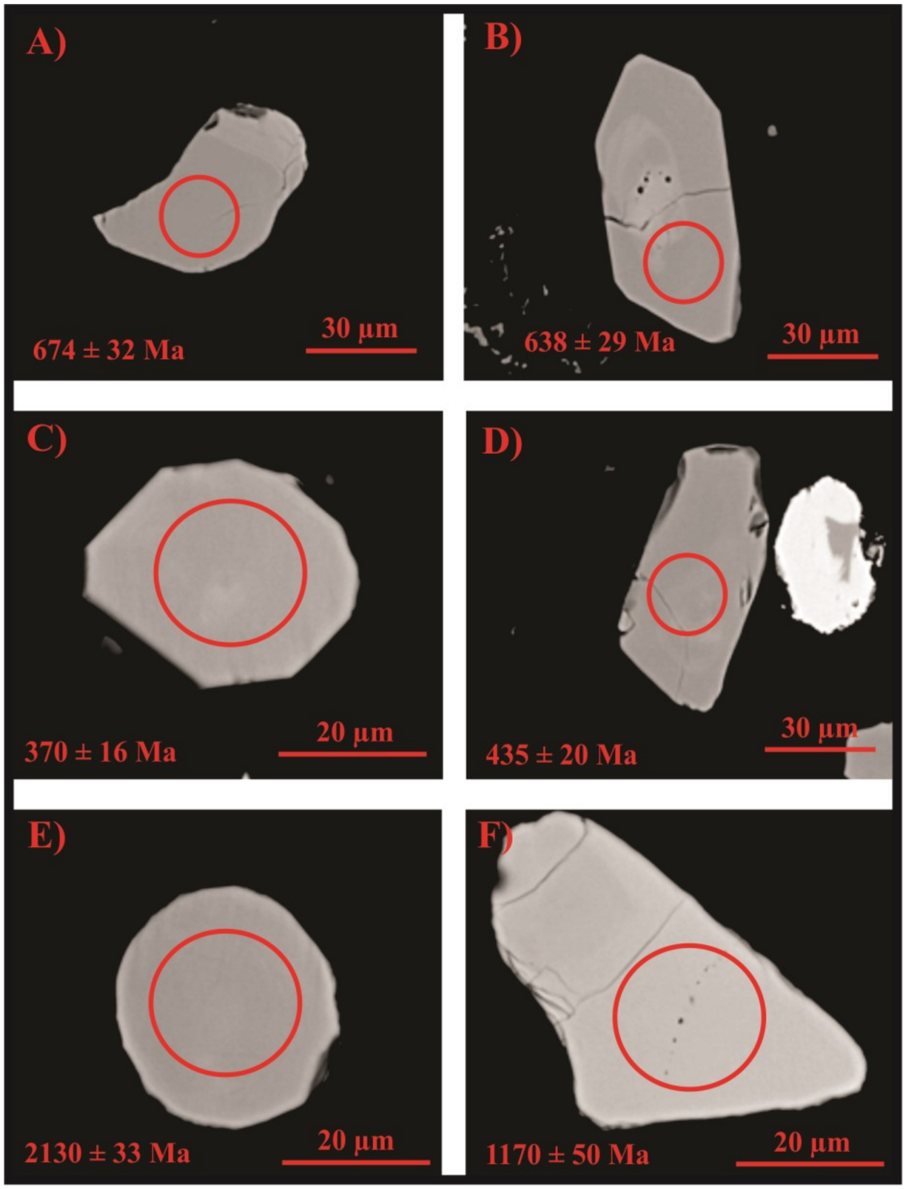

Figure 6.11 - SEM images of detrital zircon grains from each identified age group in the Baccalieu I-78 (4135.29 m) sample. 20 µm circle represents location grain was ablated.

6.8.2 – Interpretations

The most abundant group of grains in this sample is the late Neoproterozoic group. These grains are characterized by variable, but generally high Th/U, subangular grain morphologies, and variable surface areas and aspect ratios. These features indicate, as seen in previous samples, a range of parent rock types for these grains. High Th/U and angular grains indicate plutonic and volcanic igneous rocks were likely an important source, while the presence of more rounded grains indicates recycled sedimentary rocks may have also been important sediment sources.

The >1 Ga grains are characterized by low Th/U, low surface areas, variable aspect ratios, and a mixture of grain morphologies from subangular to rounded. Likely, these grains have been subject to more attrition than the late Neoproterozoic grains and are derived from recycled sedimentary rocks (rounded morphologies) as well as metamorphic rocks (low Th/U).

The Silurian – Devonian grains possess low Th/U, angular to subangular grains and variable surface areas and aspect ratios. These features indicate a derivation from metamorphic rocks (low Th/U) as well as plutonic and volcanic igneous rocks (angular grains and variable surface areas).

The outlier grains of 683 and 938 Ma are both likely derived from recycled sedimentary rocks (rounded morphologies), and the grain of 862 Ma may be derived from a volcanic igneous rock due to its angular morphology and small surface area.

6.9 – Panther P-52 – Upper Tempest Sandstone

6.9.1 – Results

A 5 m thick cuttings sample interval from the Upper Tempest Sandstone at 3210 – 3215m contained sufficient detrital zircons for analysis. Observations of the cuttings indicated that the interval was predominantly composed of fine-grained sandstone with some minor interbedded siltstones and mudstones. 66 zircon grains were imaged. Of those, 52 were ablated, and 29 yielded concordant analyses (Figure 6.12A, 6.12B). With 29 dated grains, using the method of Vermeesch (2004), there is a 95% confidence that no fraction >0.15 was missed. The grain populations are significantly different than previous samples from the Rankin Formation and Upper Kimmeridgian Source Rock. Five major groups of zircons are present. The most abundant group of grains is the late Neoproterozoic group, and 8 grains of this age are present (545 – 649 Ma) (Figure 6.12B) comprising 28% of all concordant grains. A cumulative probability peak is formed at *ca*. 621 Ma (Figure 6.12B) and the average of the $^{206}Pb/^{238}U$ age of all grains in this group is 603 ± 30 Ma. The next most abundant group consists of 7 Permian – Carboniferous grains (275 – 345 Ma) (Figure 6.12B) comprising 24% of the sample. They form a cumulative probability peak at *ca*. 294 Ma (Figure 6.12B), and the average of the $^{206}Pb/^{238}U$ age of all grains in this group is 299 ± 23 Ma. 6 older grains form a cluster of >1 Ga grains which range from 1026 – 2752 Ma (Figure 6.12B) comprising 21% of all dated grains. The group of > 1 Ga grains is composed of 3 Mesoproterozoic grains, 2 Paleoproterozoic grains, and one Neoarchean grain. Another cluster is composed of 3 grains that are Late Jurassic in age (145 – 150 Ma) (Figure 6.12B) and comprise 10% of all grains. These grains form a cumulative probability peak at *ca*. 147 Ma (Figure 6.12B), and the average of the $^{206}Pb/^{238}U$ age of all grains in this group is 148 ± 3 Ma. The final group is composed of two grains that are Ordovician and Devonian, respectively (Figure 6.12B) and comprises 7% of all dated grains. The grains do not form a major peak, but the average of their $^{206}Pb/^{238}U$ ages is 425 Ma with a standard deviation of 53 Ma. Other outlier grains present include grains of 691 ± 19, 714 ± 29, and 743 ± 21 Ma.

Th/U of all concordant grains range from 0.17 – 1.04 (Figure 6.12C). The late Neoproterozoic grains possess values from 0.33 – 1.03 with an average of 0.63. The Permian – Carboniferous grains have values ranging from 0.23 – 0.55 with an average of 0.38. The > 1 Ga grains have Th/U values ranging from 0.17 – 0.64 with an average of 0.31. The Jurassic grains possess higher Th/U values ranging from 0.64 – 0.91 with an average of 0.75. The final group consists of two grains of Ordovician and Devonian age which possess high Th/U of 0.78 and

0.88 with an average of 0.83. The outlier grains of 691 ± 19, 714 ± 29, and 743 ± 21 Ma possess Th-U ratios of 0.55, 0.37, and 1.04 respectively.

Of all concordant grains, the most common morphology is angular, as 38% of all grains possess this shape (Figure 6.12D). The late Neoproterozoic grains, however are predominantly subangular (4 grains), with 3 subrounded and 1 angular grain. The Permian – Carboniferous grains, which are a new population not detected in previous samples, are predominantly angular (5 grains) with one subangular and one subrounded grain. These grains are a younger population, and the angular shape of the majority of these grains is evidence they have been subject to less attrition that some of the older populations. This can also be said for the Upper Jurassic grains, which are predominantly angular (2 grains), with one subangular grain. The >1 Ga grains are markedly different, as 4 of these grains are rounded, with 1 subrounded grain, and one angular grain. These grains have clearly been subject to more weathering and erosion than the other grains, as is evidenced by their predominantly rounded shapes. The Ordovician grain is subangular, while the Devonian grain is angular in shape. The ungrouped grains of 691 ± 19, 714 ± 29, and 743 ± 21 Ma possess subangular, subrounded, and angular morphologies, respectively.

Surface areas of all dated grains range from 781 – 14985 μm^2 (Figure 6.12E). The late Neoproterozoic grains possess values ranging from 1330 – 14985 μm^2 with an average of 4105 μm^2. The Permian – Carboniferous grains have surface areas ranging from 1127 – 6406 μm^2 with an average of 2349 μm^2. The > 1 Ga grains possess smaller surface areas ranging from 781 – 2789 μm^2 with an average of 1860 μm^2. The upper Jurassic grains have variable surface areas of 1197, 3625, and 8759 μm^2 with an average of 4527 μm^2. The Ordovician and Devonian grains have surface areas of 913 and 3317 μm^2 respectively. Other ungrouped grains of 691 ± 19, 714 ± 29, and 743 ± 21 Ma possess surface areas of 2025, 1345, and 1211 μm^2, respectively.

Aspect ratios of all concordant grains vary from 1.01 – 2.03 (Figure 6.12F). The group of late Neoproterozoic grains has aspect ratios ranging from 1.18 – 1.82 with an average of 1.37. The group of Permian – Carboniferous grains possess aspect ratios varying from 1.01 – 2.03 with an average of 1.58. The > 1 Ga grains have lower aspect ratios ranging from 1.07 – 1.39 with an average of 1.22. Upper Jurassic grains possess aspect ratios ranging from 1.17 – 1.65 with an average value of 1.36. The final group consisting of just two grains (Ordovician and Devonian) has aspect ratios of 1.33 and 1.29, respectively. The ungrouped grains of 691 ± 19, 714 ± 29, and 743 ± 21 Ma possess aspect ratios of 1.11, 1.3, and 2.02, respectively.

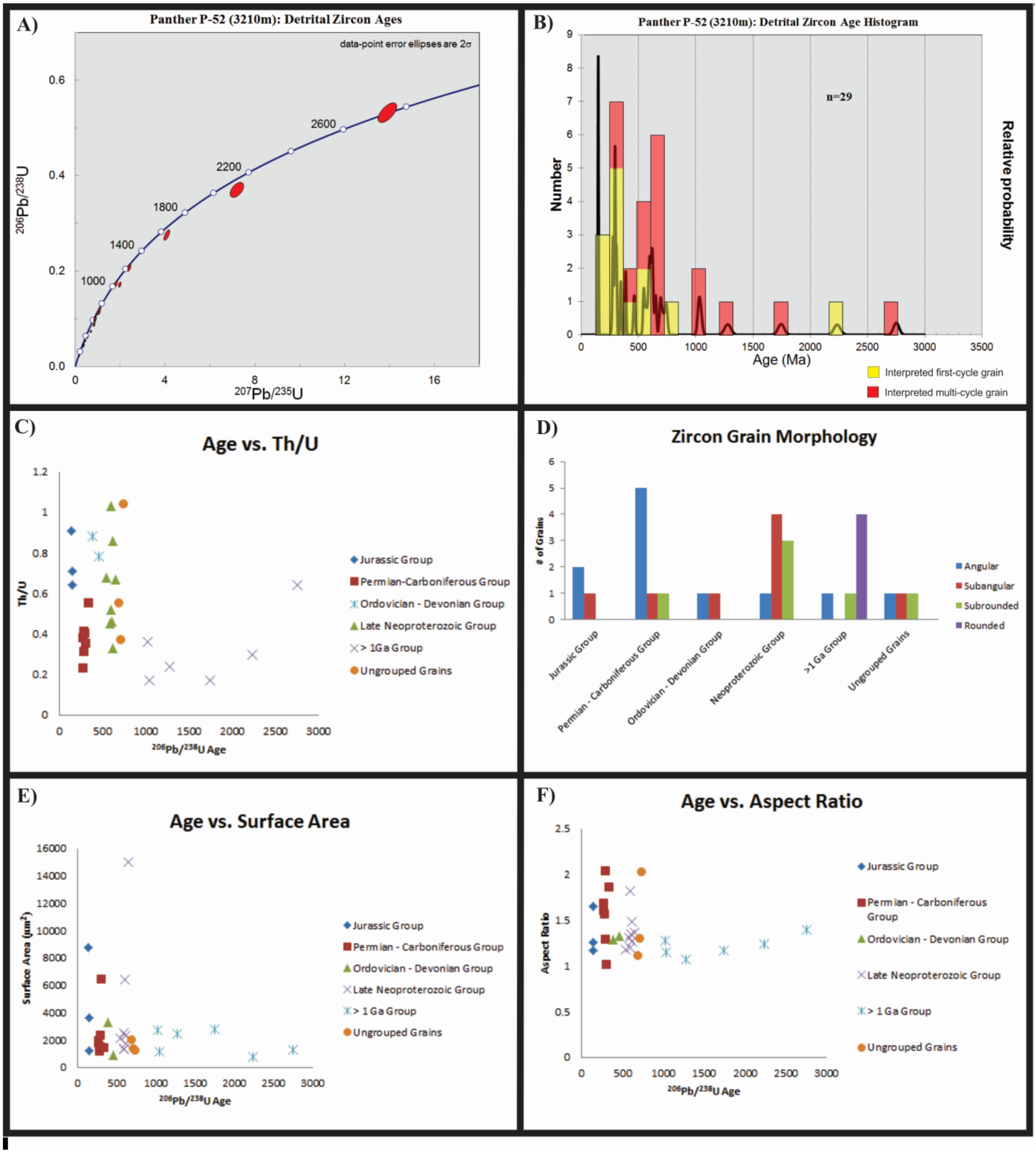

Figure 6.12 - Graphs for detrital zircons of the Panther P-52 (3210 m) sample. (A) Concordia diagram with detrital zircon ages. (B) Detrital zircon age histogram. (C) Age vs. Th/U. (D) Zircon grain morphology. (E) Age vs. Surface Area. (F) Age vs. Aspect Ratio.

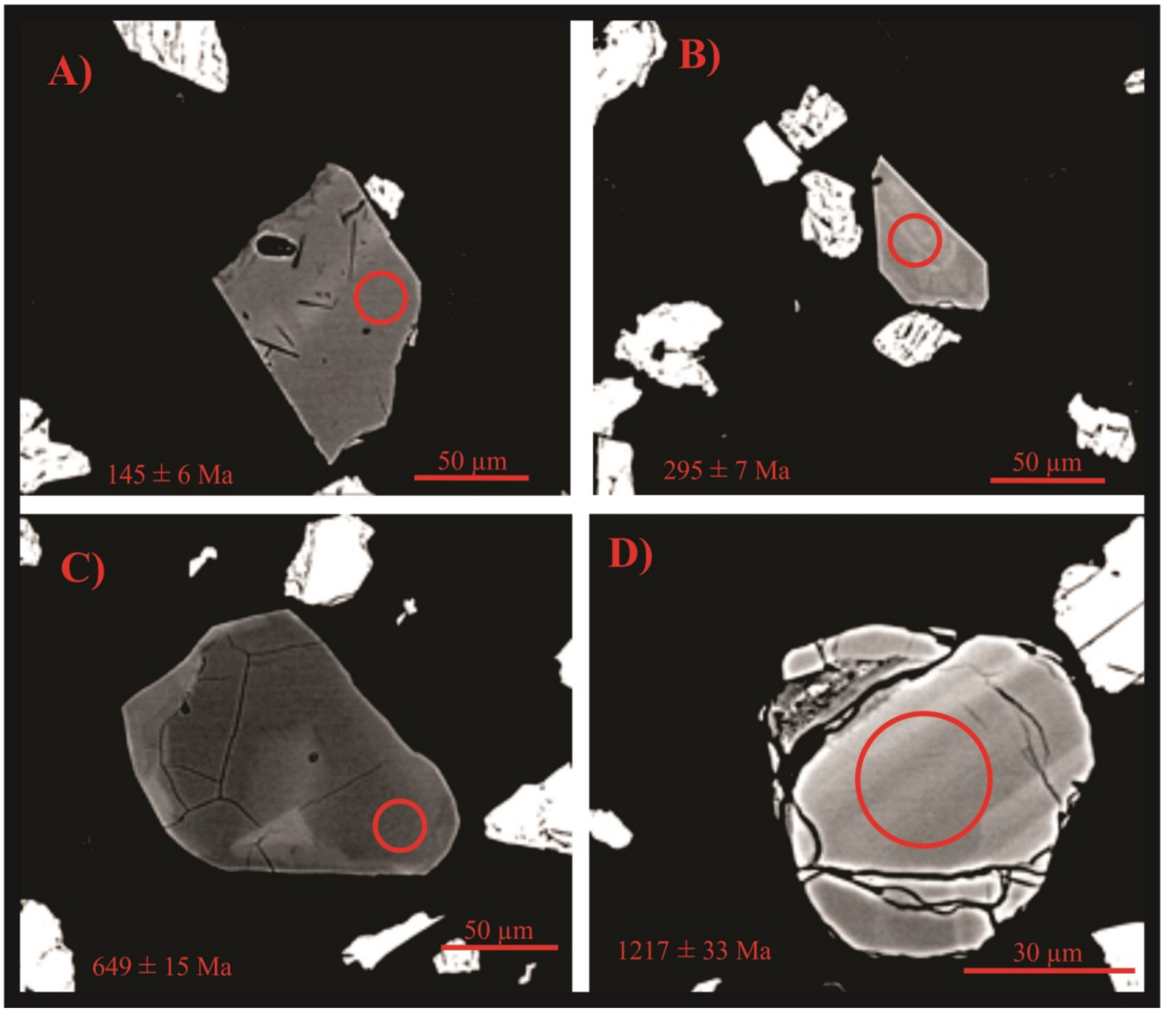

Figure 6.13 - SEM images of detrital zircon grains from each identified age group in the Panther P-52 (3210 m) sample. 20 µm circle represents location grain was ablated.

6.9.2 – Interpretations

The late Neoproterozoic grains are the most abundant in this sample. They are characterized by variable Th/U, subangular and subrounded grain morphologies, variable surface areas, and low aspect ratios. These features indicate a mixture of parent rock types, which is consistent with findings from previous samples. Igneous rocks were likely an important source (high Th/U). Variable grain surface areas indicate plutonic and volcanic igneous sources were important. Grain morphologies suggest recycled sedimentary rocks are also a potentially important source.

The Permian – Carboniferous grains are characterized by low Th/U values, variable surface areas and aspect ratios, and predominantly angular grain morphologies. These features are somewhat contradictory as they indicate derivation from different types of source terrains. Most of the grains are angular and exhibit euhedral crystal faces. This suggests the grains are first-cycle and derived from igneous rocks, or potentially second cycle sedimentary grains which have not suffered excessive weathering and erosion. However, the Th-U ratios are almost all below 0.5, which is characteristic of metamorphic rocks. This makes an interpretation difficult, but due to the euhedral nature of the grains, the preferred interpretation is that they are derived from igneous rocks (first-cycle) or from sedimentary rocks that have not undergone significant attrition (second-cycle). As seen in previous samples, it is possible for grains from igneous rocks to possess Th-U ratios below 0.5.

The >1 Ga grains possess low Th/U, rounded grain morphologies, low aspect ratios and low surface areas. These features are comparable to those observed in previous samples, and the interpreted grain origins are also similar. These grains are likely derived from recycled, polycyclic sedimentary rocks (rounded grain morphologies, low aspect ratio & surface areas), as well as metamorphic rocks (low Th/U).

The Upper Jurassic grains are characterized by high Th/U, variable aspect ratios, variable surface areas, and angular grain morphologies. The likely source for these grains is from first-cycle plutonic or volcanic igneous rocks. This is shown specifically in the high Th/U characteristic of igneous zircons as well as the angular grains shapes which often display euhedral crystal faces.

The Ordovician and Devonian grains both possess high Th/U, subangular to angular morphologies, average surface areas and typical aspect ratios. Therefore, these grains appear to be derived from first cycle igneous rocks (angular morphologies and high Th/U).

The other ungrouped grains appear to have different origins. The 691 ± 19 and 743 ± 21 Ma grains likely have an igneous origin due to their angular to subangular morphology and high Th/U. However, the 714 ± 29 Ma grain is subrounded with a low Th/U. It is therefore interpreted as being derived from recycled sedimentary rocks or potentially metamorphic rocks.

6.10 – South Tempest G-88 – Lower Tempest Sandstone

6.10.1 – Results

A sample was obtained from a conventional core at 4195.8m. The sample is described as a fine-grained sandstone and contains abundant detrital zircons for analysis. Unlike the other conventional core samples which were made into thin sections, this sample was crushed and separated into three different grain size fractions (20-48µm, 48-100µm, & 100-180µm). It was then taken to the hydroseparator for heavy mineral separation, and heavy mineral fractions were mounted in epoxy for analysis by the MLA/SEM. Zircons were imaged from the three grain size fractions. However, the 48-100µm fraction was chosen for further analysis on the LA-ICP-MS as this fraction contained the most zircon grains that were suitable for analysis. From this grain mount, 102 zircons were imaged, 87 were then ablated, and all 87 yielded concordant results (Figure 6.14A, 6.14B). With 87 dated grains, using the method of Vermeesch (2004), there is a 95% confidence that no fraction >0.07 was missed. These grains fall into four major groups. The first is a group of 57 late Neoproterozoic grains (570 – 682 Ma) which comprise 66% of the total sample. The grains form a cumulative probability peak at *ca*. 613 Ma (Figure 6.14B), while the average of all $^{206}Pb/^{238}U$ ages of this group is 621 Ma with a standard deviation of 27 Ma. The second group is composed of 16 grains >1 Ga (986 – 2838 Ma) which make up 18% of all dated grains. This group consists of 5 Mesoproterozoic, 8 Paleoproterozoic, 1 Neoarchean and 1 Mesoarchean grain, as well as one grain from the early Neoproterozoic (986 ± 34 Ma) that was close in age to a cluster of Mesoproterozoic grains, and was therefore included within this group. 3) A cluster of 6 Carboniferous – Permian grains (286 – 298 Ma) make up 7% of all concordant grains and form a cumulative probability peak at *ca.* 288 Ma (Figure 6.14B). The average of the $^{206}Pb/^{238}U$ ages of all grains in this group is 294 Ma with a standard deviation of 5 Ma. A group of 5 Cambrian – Devonian grains (416 – 503 Ma) comprises 6% of all concordant grains. The grains do not form a major cumulative probability peak but the average $^{206}Pb/^{238}U$ age of all grains is 444 Ma with a standard deviation of 31 Ma. Three additional ungrouped grains were present with $^{206}Pb/^{238}U$ ages of 541 ± 18, 696 ± 33, and 707 ± 34 Ma.

Th-U ratios of all concordant grains range from 0.08 – 2.03 (Figure 6.14C). The late Neoproterozoic grains possess Th/U values between 0.08 – 1.35 with an average of 0.61. The >1 Ga grains possess Th-U ratios ranging from 0.15 – 2.03 with an average of 0.53. The Permian – Carboniferous grains have Th-U ratios between 0.34 – 0.81 with an average of 0.60 and the Cambrian – Devonian grains possess Th-U ratios ranging from 0.09 – 0.61 with an average of 0.40. The ungrouped grains with $^{206}Pb/^{238}U$ ages of 541 ± 18, 696 ± 33, and 707 ± 34 Ma have Th-U ratios of 0.40, 0.93, and 0.12 respectively.

The most common grain morphology of all concordant grains is subangular, as 56% of the grains possess this shape (Figure 6.14D). The late Neoproterozoic grains are mostly subangular (34 grains), although 13 angular grains and 10 subrounded grains are also present.

The >1 Ga grains are composed of six subangular, six subrounded and four rounded grains. As observed in previous samples, these grains tend to have more mature morphologies, indicating more attrition than the younger zircon groups. Of the six Permian – Carboniferous grains, four are subangular, while the other two are angular. The Cambrian – Devonian grains are composed of two subangular grains, two subrounded grains, and one angular grain. The ungrouped grains are all subangular in shape.

The surface areas of all concordant grains range from 2102 – 8447 μm^2, which is generally larger than grains of previous samples (Figure 6.14E). The late Neoproterozoic grains possess surface areas ranging from 2130 – 8447 μm^2 with an average of 3291 μm^2. The >1 Ga grains are the smallest of all groups and have surface areas that range between 2102 – 3635 μm^2 with an average of 2656 μm^2. Permian – Carboniferous grains have surface areas ranging from 2204 – 4285 μm^2 with an average of 2924 μm^2. The final group of Cambrian – Devonian grains possesses surface areas that range from 2510 – 3744 μm^2 with an average of 3187 μm^2. The ungrouped grains with $^{206}Pb/^{238}U$ ages of 541 ± 18, 696 ± 33, and 707 ± 34 Ma have surface areas of 3392, 2204, and 3023 μm^2 respectively.

Aspect ratios of all concordant grains vary from a minimum of 1.03 to a maximum of 2.52 (Figure 6.14F). The late Neoproterozoic grains possess aspect ratios ranging from 1.04 – 2.52 with an average of 1.46. The >1 Ga grains have aspect ratios ranging from 1.04 – 1.82 with an average of 1.36. Permian – Carboniferous grains have aspect ratios that range between 1.26 – 1.97 with an average of 1.68. The final group of Cambrian – Devonian grains possesses much smaller aspect ratios between 1.03 and 1.45 with an average of 1.29. The ungrouped grains with $^{206}Pb/^{238}U$ ages of 541 ± 18, 696 ± 33, and 707 ± 34 Ma have aspect ratios of 1.40, 1.66 and 1.34 respectively.

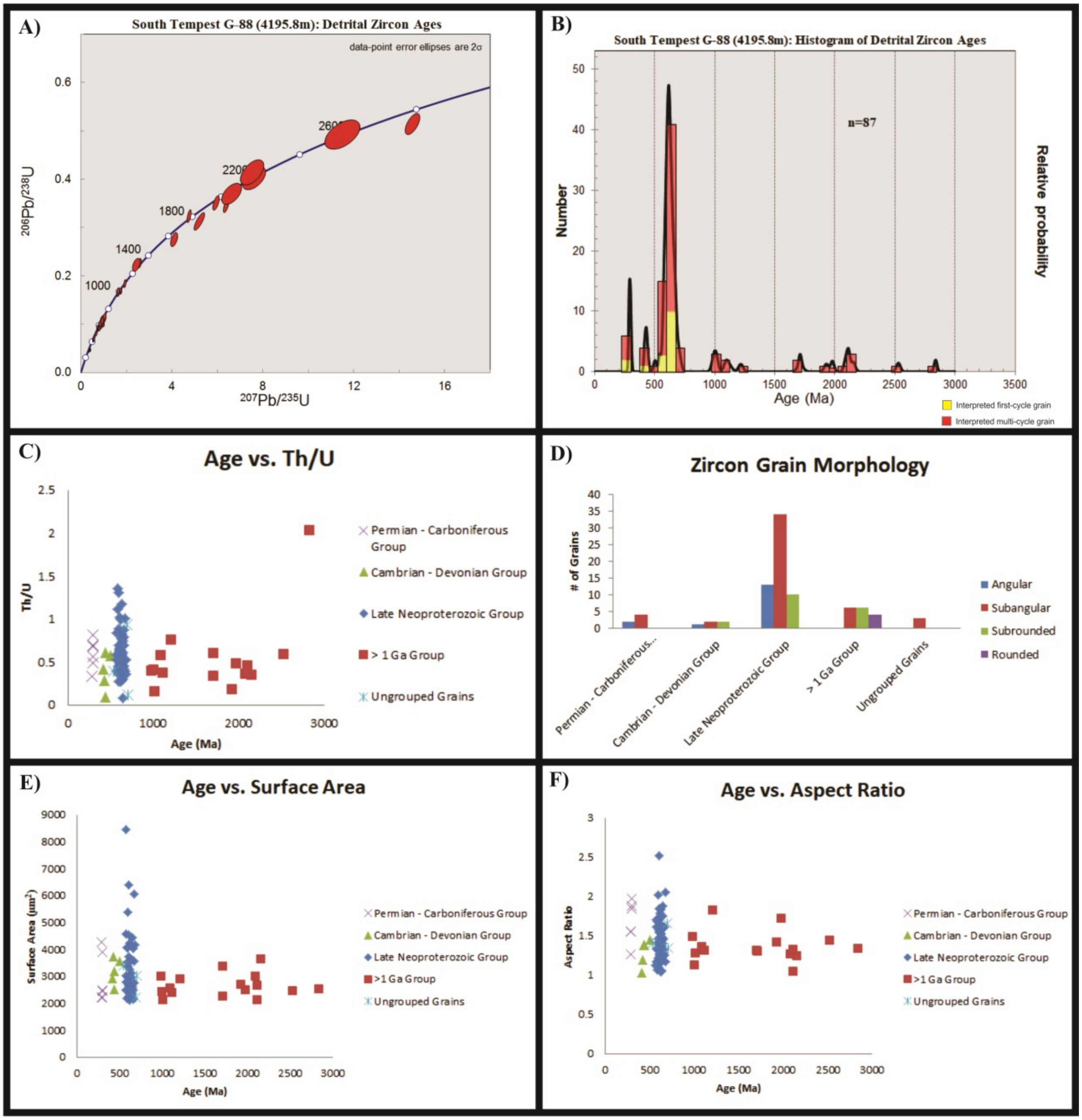

Figure 6.14 - Graphs for detrital zircons of the South Tempest G-88 (4195.8 m) sample. (A) Concordia diagram with detrital zircon ages. (B) Detrital zircon age histogram. (C) Age vs. Th/U. (D) Zircon grain morphology. (E) Age vs. Surface Area. (F) Age vs. Aspect Ratio.

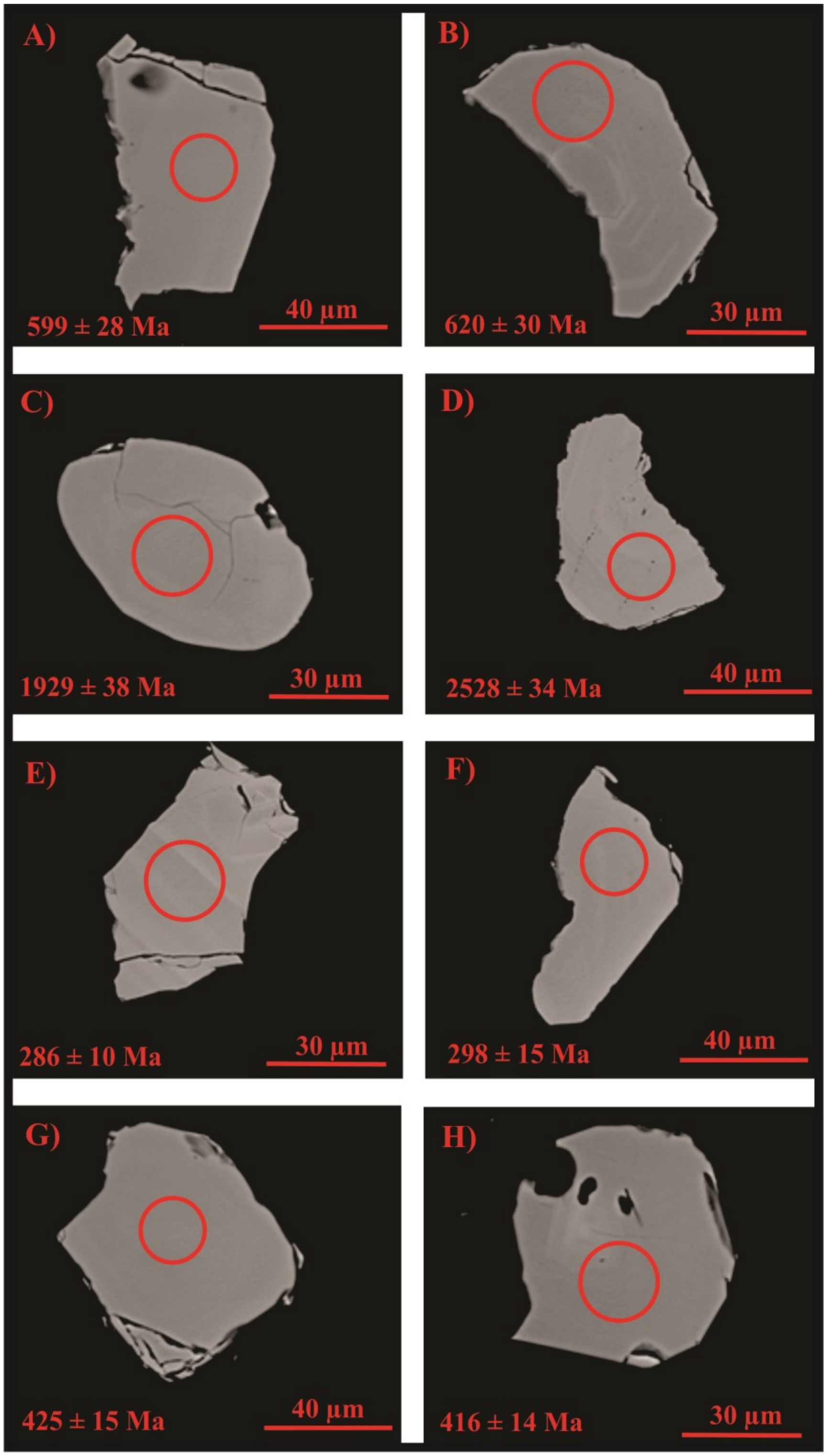

Figure 6.15 - SEM images of detrital zircon grains from each identified age group in the South Tempest G-88 (4195.8 m) sample. 20 µm circle represents location grain was ablated.

6.10.2 – Interpretations

In this sample, the late Neoproterozoic grains are by far the most abundant and are characterized by variable but generally high Th/U, mostly subangular grain morphologies, variable aspect ratios and variable surface areas. These features were also noted in previous samples, and indicate a mixture of different parent rock types. Igneous parent rocks are indicated by the high Th/U and some angular grain shapes. High surface areas of some of these grains suggest an importance of plutonic igneous rocks. Recycled sedimentary rocks are a probable source of the more rounded grains and metamorphic rocks are also a potential source of grains with low Th/U.

The >1 Ga grains possess low Th/U, a mixture of subangular – rounded grains, low surface areas, and low aspect ratios. As interpreted in previous samples, based on the low surface areas, low aspect ratios and more rounded grains, these grains are interpreted to be derived from recycled sedimentary rocks. However, based on the low Th/U of many grains, many of these grains may also be derived from metamorphic parent rocks.

The Permian – Carboniferous grains are characterized by variable but generally high Th/U, angular to subangular grain morphologies, high aspect ratios, and variable surface areas. These features suggest these grains are likely derived from igneous source rocks (high Th/U, angular grains high aspect ratios), or potentially second-cycle sedimentary rocks (subangular grains).

The Cambrian – Devonian grains possess low Th/U, grains that are angular – subrounded, low aspect ratios and low surface areas. It is likely these grains are derived from a variety of different parent rock types. Low Th-U ratios are indicative of a derivation from metamorphic rocks, however angular grains suggest derivation from igneous sources and subrounded grains indicate derivation from sedimentary rocks.

The ungrouped grains also likely have different origins. The grain dated at 696 ± 33 Ma is likely derived from an igneous source based on its' high Th/U and subangular morphology. The two other ungrouped grains (541 ± 18, 707 ± 34 Ma) are both subangular but have low Th/U, indicating derivation from recycled sedimentary rocks or potentially metamorphic sources.

Chapter 7 - Provenance Interpretations

7.1 - Interpretations of Geochemical Plots – Weathering Diagrams

An important observation from the CIA diagrams (Figure 4.1; Figure 4.2) is that the mudstone and sandstone samples plot in different regions. Although they have similar CIA values, the mudstone samples plot further to the right of the diagrams, due to greater amounts of K_2O. This is interpreted to result from increased clay mineral content (particularly illite) within the mudstone samples. Illite is a clay mineral that results from diagenetic reactions at depth. It can be derived from the breakdown of smectite and K-feldspar, or alternatively from the breakdown of kaolinite with the addition of K^+ from outside the system (Sutton & Maynard, 1996). Since illite and clay minerals are more abundant in the mudstone beds, it is expected that these samples would plot closer to the Al_2O_3 – K_2O line. The grouping of sands and muds into distinct populations is also described by McLennan et al. (2003).

Using the CIA diagram to identify major element trends is useful to indicate the degree of weathering within the Upper Jurassic source rocks for the Flemish Pass and Central Ridge. Evidently, these samples possess high weathering indices (average of 77) indicating chemical weathering was most important for these samples. This is consistent with interpretations of Bateman (1995) for the laterally equivalent Egret Member of the Jeanne d'Arc Basin. Bateman (1995) suggested the climate during deposition of the Egret Member was humid, and subtropical based on clay minerals present identified using XRD. A humid, subtropical climate is supported by the high weathering indices seen in these samples.

It is difficult to identify a source rock for either the sandstone or the mudstone samples, as weathering trends are absent. However, trace element data in the next section will provide more details on the source rock.

7.2 – Interpretations of Trace Element Diagrams

7.2.1 - Zr/Sc vs. Th/Sc Plots

Analysis of mudstone samples using a Zr/Sc vs. Th/Sc plot (Figure 4.6A) revealed some noteworthy provenance characteristics. This plot indicates detritus for these Upper Jurassic units was predominantly from an upper crustal or felsic terrane. Interestingly enough, despite deposition on a rifted margin, the mudstone samples do not plot in the field where passive margin sediments typically lie (McLennan et al. 1990). This suggests that sedimentary recycling processes were not too important in these mudstones, and that the majority of the detritus was likely first-cycle in nature. However, examination of the Zr/Sc vs. Th/Sc plot for the Upper Jurassic sandstone samples (Figure 4.7A) revealed some notably different results from the mudstone samples. The sandstones show a distinctly different signature than the mudstones as they plot in the region of the diagram associated with passive margin sediments. Despite plotting in different areas of the diagram than the mudstones, these sandstones are not interpreted to have a different provenance. The sandstone samples are locally interbedded with the mudstone samples and are not separated by any unconformity, or fault. In addition, both sandstones and mudstones possess relatively high Th/Sc as well as Zr/Sc ratios indicating upper crustal signatures. It is therefore probable that their provenance is not significantly different. The reason the sandstones plot in a different region of the diagram is linked to hydraulic sorting of the heavy mineral zircon. As described in Section 4.3.2, Zr is often more abundant in sandstone beds than mudstones, likely due to the enrichment of the heavy mineral zircon in sands. McLennan (2003) describes how Zr is strongly associated with heavy minerals, and is therefore subject to heavy mineral fractionation during sorting and sedimentary recycling processes. Therefore, it is interpreted that sorting and sedimentary recycling processes acted to enrich Zr in the sandstone samples.

Mudstone samples (Figure 4.6A) from different stratigraphic units appear to have a similar provenance based on this plot, however, the Lower Tempest Sandstone samples plot slightly closer to the average composition of the Bulk Continental Crust, indicating a slightly more mafic component and potentially different provenance for the Lower Tempest Sandstone detritus. Within the sandstone samples (Figure 4.7A), there is no major difference in Th/Sc between the different formations but the Zr/Sc does vary somewhat. This can be directly tied to the amount of sedimentary recycling or hydraulic sorting that the detritus has undergone. Knowing this, it appears that three samples from the Upper Kimmeridgian Source Rock of the South Tempest G-88 well have experienced the most sedimentary recycling.

In the previous section, it was mentioned that it did not appear sedimentary recycling processes were important in the mudstone beds and that the detritus was likely first-cycle in nature. The data from the sandstones, however, contradicts this statement. Based on the abundances of Zr in the sandstone beds, it appears that hydraulic sorting and sedimentary recycling processes were very important, and therefore that recycled sedimentary rocks were likely a major source of detritus. It is an interesting question to determine which lithology more accurately estimates the provenance. It is clear that both sands and muds possess an upper crustal signature, but how important are recycled sedimentary rocks to the detritus?

McLennan et al. (1990) analyzed both muds and sands from a wide range of tectonic environments and found that in active tectonic settings, sands and muds possessed no systematic differences. This led them to conclude that in these environments, heavy mineral fractionation is not an important process (McLennan et al. 1990). However, in passive margins, the sands were considerably enriched in Zr compared to the associated mud due to sedimentary recycling and hydraulic sorting of heavy minerals (McLennan et al. 1990). Therefore, it can be concluded that if sedimentary recycling and hydraulic sorting are important, these features will only be noticeable in the sand-sized grain size fraction. These observations from McLennan et al. (1990) are comparable to what is observed in the Upper Jurassic samples from this study. Since the signatures seen in both the sandstones and mudstones from the Central Ridge/Flemish Pass Basin are typical of signatures of passive margin sands and muds from McLennan et al. (1990), it is interpreted that recycled sediments are an important source of detritus for both sandstone and mudstone beds. However, considering the abundance of igneous and metamorphic sources in adjacent terranes, first-cycle sources cannot be considered insignificant.

7.2.2 - Sc-Th-Zr Plot

The Sc-Th-Zr ternary plot (Figure 4.6B) gave similar results to the previous plot, as all mudstones samples did not plot within the passive margin field. Most samples plotted within the continental arc field, once again suggesting an upper crustal type of source material. This is expected based on the results of the previous plot, and the fact that passive margin mudstones will not exhibit comparable Zr enrichment that is seen in passive margin sandstones (McLennan et al. 1990). Most formations appear to demonstrate a similar provenance on this plot, although once again, the Lower Tempest Sandstones show higher Sc abundances, indicating slightly more mafic detritus.

Examination of the Sc-Th-Zr ternary plot for the sandstones (Figure 4.7B) once again revealed different results for the sandstones than the mudstones. The sandstones plot much closer to the passive margin field, towards the Zr axis, than the mudstone samples. As was interpreted in the previous diagram, this is likely related to hydraulic sorting of zircon in the sandstone beds. It is therefore interpreted that recycled sediment is an important component to the detritus, although once again, first cycle sources cannot be ruled out based on the abundance of igneous and metamorphic sources in adjacent terranes.

Three samples from the Upper Kimmeridgian Source Rock plot further towards the Zr end-member than the other samples, indicating sedimentary recycling was more important in those particular samples. Other than these three, the other samples plot in much the same area, suggesting a similar provenance.

7.2.3 – Th-La-Sc Ternary Plot

The final provenance plot for mudstones (Figure 4.6C) is a Th-La-Sc ternary plot. Based on the fields of Cullers (1994), most of these samples appear to be derived from mixed felsic and mafic sources. Although they plot in this field, most samples plot close to the average composition of the upper continental crust, meaning that upper crustal sources are likely most important for these samples which is a similar interpretation to the other trace element geochemical plots. Most formations appear to demonstrate a similar provenance on this plot, although once again, the Lower Tempest Sandstones plot closer to the Sc pole, indicating slightly more mafic sources.

Examination of the Th-La-Sc ternary plot for the sandstone samples (Figure 4.7C) reveals a similar signature to that observed in the mudstone samples. All of the sandstone samples possess an upper crustal affinity, and plot in the same area as the mudstones. Little variability is noted here between the samples from different formations. This diagram does not have the capability of identifying sedimentary recycling, but nonetheless it does reinforce the importance of upper crustal detritus in these Upper Jurassic samples.

7.3 – Geochemical Provenance Interpretations

7.3.1 - Introduction

Provenance interpretations based on geochemical analysis are presented here. In later sections, the geochemical interpretations are combined with the U-Pb geochronology data to obtain a more complete interpretation of the provenance of the Upper Jurassic units of the Central Ridge and Flemish Pass Basin. This section will address the correlations to potential source terranes based on the geochemical signatures discussed in the previous section.

7.3.2 - Rankin Formation, Upper Kimmeridgian Source Rock, Lower Kimmeridgian Source Rock

Samples from the Rankin Formation, Upper Kimmeridgian Source Rock and Lower Kimmeridgian Source Rock all possess similar geochemical signatures. All plots (Figure 4.6; 4.7) suggest that the detritus was derived from felsic rocks as their compositions are similar to that of the average composition of upper continental crust. Sedimentary recycling also appears to be important because the sandstone samples plot in the field associated with passive margin sediments. Based on this information, potential source areas must be predominantly continental in nature, with abundant sedimentary rocks. The terranes in close proximity to the Grand Banks, such as the Avalon Zone, the Central Mobile Belt, and the Meguma Zone definitely fit this description. Other potential sources include the rocks of Iberia, where abundant felsic intrusions are present, and the rocks of Ireland, which are composed of Early to Middle Paleozoic sequences similar to those seen in Central Newfoundland.

A source region that can likely be ruled out based on the presented geochemical data is the Humber Zone of western Newfoundland. Significant ophiolitic sequences are present in the Humber Zone, and if this region was a significant source, it is likely that the resulting detritus would possess a chemistry that reflects the presence of these ophiolitic sequences.

7.3.3 - Lower Tempest Sandstone

Samples from the Lower Tempest Sandstone possess slightly different geochemical signatures than those of the Rankin Formation, Upper Kimmeridgian Source Rock, and Lower Kimmeridgian Source Rock. Although interpreted to be derived from predominantly upper crustal material, the Lower Tempest Sandstones possess a more mafic signature than the units discussed in the previous section. The same source rocks are still likely important for the Lower Tempest Sandstone samples, as they possess an overall upper crustal signature, and are surrounded by the same potential source terranes. However, a couple of possibilities exist to explain the more mafic signature noted in these samples. Dearin (2006) studied the provenance of the Ben Nevis Formation sandstones of the Jeanne d'Arc Basin and noted that samples analyzed from earlier in the rifting stage possessed a more mafic component. Dearin (2006) attributed this to more mafic basement rocks being exposed during earlier stages of rifting. However, the basement offshore is thought to be composed of Avalon Zone rocks (Haworth & Lefort, 1978; King et al., 1985, 1986; Williams et al., 1999), which are not known to have a significant mafic component. Therefore, it is not likely this more mafic signature can be associated with the Avalon Zone basement rocks.

Another potential source of the mafic detritus is, as previously discussed, the ophiolites of western Newfoundland. Although the Central Mobile Belt is predominantly felsic in nature, some ophiolites and mafic rocks are present as well. These may represent a potential mafic source. Rift-related Mesozoic rocks discussed in Section 1.6.6 may also represent a mafic source. The majority of known Mesozoic igneous rocks from the island of Newfoundland or offshore Newfoundland have been mafic in composition such as the ultramafic Budgell Harbor Stock in Central Newfoundland, diabase dikes on the Avalon Peninsula, and basalt from the Spoonbill C-30, Cormorant N-83, and Brant P-87 wells from the South Grand Banks (Helwig et al., 1974;

Hodych & Hayatsu, 1980; Amoco et al., 1973; Jansa & Pe-Piper, 1986; Jansa & Pe-Piper, 1988). Mesozoic igneous rocks from the Lusitanian Basin on the Iberian margin are also all mafic in composition (Pinheiro et al., 1996). If these Mesozoic sources were important, their input would likely result in a mafic signature in the detritus. Another potential source of the mafic detritus is from rocks from the Iberian margin. Although the Iberian margin is dominated by Carboniferous – Permian granitoids, mafic rocks are also fairly common. The Ossa Morena Zone, in particular, contains noteworthy mafic igneous rocks, such as gabbroic sequences of the Beja Igneous Complex (Jesus et al., 2006) and the Beja-Acebuches Amphibolite unit (Azor et al., 2008).

Using just whole rock geochemistry, it is difficult to determine which of these options are most likely to explain the slightly different signature of the Lower Tempest Sandstones. However, the next chapter will include an interpretation of the detrital zircon analyses, which will help elucidate the provenance of the Lower Tempest Sandstone samples further.

7.4 – Provenance Interpretations of Heavy Mineral Data

7.4.1 - Introduction

Provenance correlations based on heavy mineral analysis are presented here. In later sections, these interpretations are combined with the U-Pb geochronology and whole rock geochemical data to obtain a more complete interpretation of the provenance of the Upper Jurassic units of the Central Ridge and Flemish Pass Basin. This section will address the heavy mineral "fingerprints" of each formation analyzed and determine which formations possess different or similar source terranes.

7.4.2 – Upper Kimmeridgian Source Rock, Lower Kimmeridgian Source Rock, Rankin Formation

All heavy mineral ratios are interpreted to show a similar provenance for all of the Upper Jurassic units examined. This is particularly true for the Upper Kimmeridgian Source Rock, Lower Kimmeridgian Source Rock and Rankin Formation samples, which all possess similar RZi, MZi, CZi and ZTR values. Each of these units has a similar heavy mineral signature, suggesting the source terranes were similar in nature. However, the Upper and Lower Tempest Sandstone units possess slightly different heavy mineral ratios and are interpreted to have a slightly different provenance.

Overall, ZTR ratios for the Upper Kimmeridgian Source Rock, Lower Kimmeridgian Source Rock, and Rankin Formation are high, with averages of 79 ± 11, 76 ± 16, and 76 ± 5 respectively. Considering that these formations are mudstone units, and that stable heavy minerals are inherently less abundant in mudstones than sandstones (McLennan et al. 1990), a ZTR of ~75 indicates that sedimentary recycling was a potentially important process for deposition of the mudstone beds.

7.4.3 – Upper Tempest Sandstone and Lower Tempest Sandstone

The RZi ratios of the Upper Tempest Sandstone possess are unique compared to that of the Upper and Lower Kimmeridgian Source Rock, and Rankin Formation samples previously discussed. Yet, as discussed in Section 5.4.1, this heavy mineral signature (RZi) has been largely affected by a single outlier sample (Figure 5.8), and the other three Upper Tempest samples plot in similar regions to the other formations. From Figures 5.8C and 5.9C, it is evident that the MZi and CZi ratios of the Upper Tempest Sandstone are similar to those of the other formations. If the outlier is disregarded, then it is interpreted that the Upper Tempest Sandstone possesses a similar provenance to the previous formations.

The Upper Tempest Sandstone possesses a higher average ZTR index value than the Upper and Lower Kimmeridgian Source Rock, and the Rankin Formation. This is despite being interpreted to have a similar provenance based on MZi and CZi ratios. The principal reason for the higher ZTR in the Upper Tempest Sandstone is associated with the amount of sedimentary recycling. One potential explanation of this is that sedimentary rocks are more important as a source for this Upper Tempest Sandstone unit. However, the preferred interpretation is that the source terrane is likely similar to that of the previously discussed formations, but that the detritus has simply undergone more sedimentary recycling. This is a more likely explanation given that the Upper Tempest Sandstone samples are more coarse-grained and composed of a greater abundance of sandstone material than the 5 m cuttings intervals from the mudstone units (Kimmeridgian Source Rocks, Rankin Formation). The greater abundance of coarse-grained material would likely be more enriched in stable heavy minerals such as zircon and rutile due to hydraulic sorting. This feature was also discovered in the geochemical plot of Zr/Sc vs. Th/Sc (Figure 4.6A, 4.7A) and discussed in Section 7.2.1. Therefore, it is concluded that the higher ZTR index values of the Upper Tempest Sandstone are related to sedimentary sorting and enrichment of stable heavy minerals within sandstone beds, and not a major shift in provenance.

It is difficult to draw meaningful conclusions for the Lower Tempest Sandstone unit, as only a single sample from this unit was analyzed. However, the CZi for this sample is much higher (46) than other units and plots at a greater value than the error bars for the other samples (Figure 5.9). This potentially indicates a unique provenance for this unit, but this is uncertain due to the absence of other samples.

7.4.4 - Summary

Overall, the provenance of all units based on heavy mineral ratios appears broadly similar. This is particularly true for the Upper Kimmeridgian Source Rock, Lower Kimmeridgian Source Rock and Rankin Formation as RZi, MZi, CZi and ZTR values for these formations are all comparable. The Upper Tempest Sandstone is also thought to have a similar provenance, as

MZi and CZi ratios are very similar to those of other formations, and when a single outlier is excluded, the RZi is also comparable. The Upper Tempest Sandstone also possesses a higher ZTR index value than the other formations analyzed. This is interpreted to be related to a greater amount of sedimentary recycling in this unit, which is much more coarse-grained than the mudstones of the Kimmeridgian Source Rock or Rankin Formation.

7.5 - Provenance Interpretations of Geochronological Data – Upper Kimmeridgian Source Rock

7.5.1 - Introduction

Accurate dating of zircons from fine-grained Upper Jurassic sediments has been instrumental in pinpointing their source regions and parental rocks. Geochemical data have also contributed important information for this objective. This section presents interpretations of the provenance and drainage patterns of the Upper Jurassic units based on detrital zircon geochronology.

7.5.2 - Late Neoproterozoic Grains

Analysis of the detrital zircons of the Upper Kimmeridgian Source Rock from both the South Tempest G-88 and Baccalieu I-78 wells revealed similar results. The most abundant grains in these samples are late Neoproterozoic (~600 Ma). Ages of these grains closely match and hence the grains are interpreted to have been derived from Avalon Zone rocks (see Section 1.6.2). The Avalon Zone represents basement to the Grand Banks and is present west, south, and east of the Flemish Pass Basin (Haworth & Lefort, 1979; King et al., 1985, 1986; Krogh et al., 1987) (Figure 1.7). The presence of these grains is therefore expected, but not overly indicative of drainage orientations. As discussed in Section 6.4.2 and 6.5.2, these grains are likely derived from a mixture of recycled sedimentary rocks as well as plutonic and volcanic igneous rocks.

This is consistent with a derivation from the Avalon Zone, as this terrane is characterized by volcanic and intrusive igneous rocks and associated sedimentary successions. Below (Figure 7.1) is a figure demonstrating the similarity in detrital zircon age peaks between grains previously dated from the Avalon Zone (Pollock et al., 2009) and from the late Neoproterozoic detrital zircon ages from this study. It is evident that the main detrital zircon peak seen in the data of Pollock et al. (2009) matches nearly identically with the main late Neoproterozoic peak seen in grains from this study. In addition, data from other offshore Newfoundland samples from Lowe et al. (2011) are plotted. These are also interpreted to be derived from Avalon Zone rocks, and also share the late Neoproterozoic age peak.

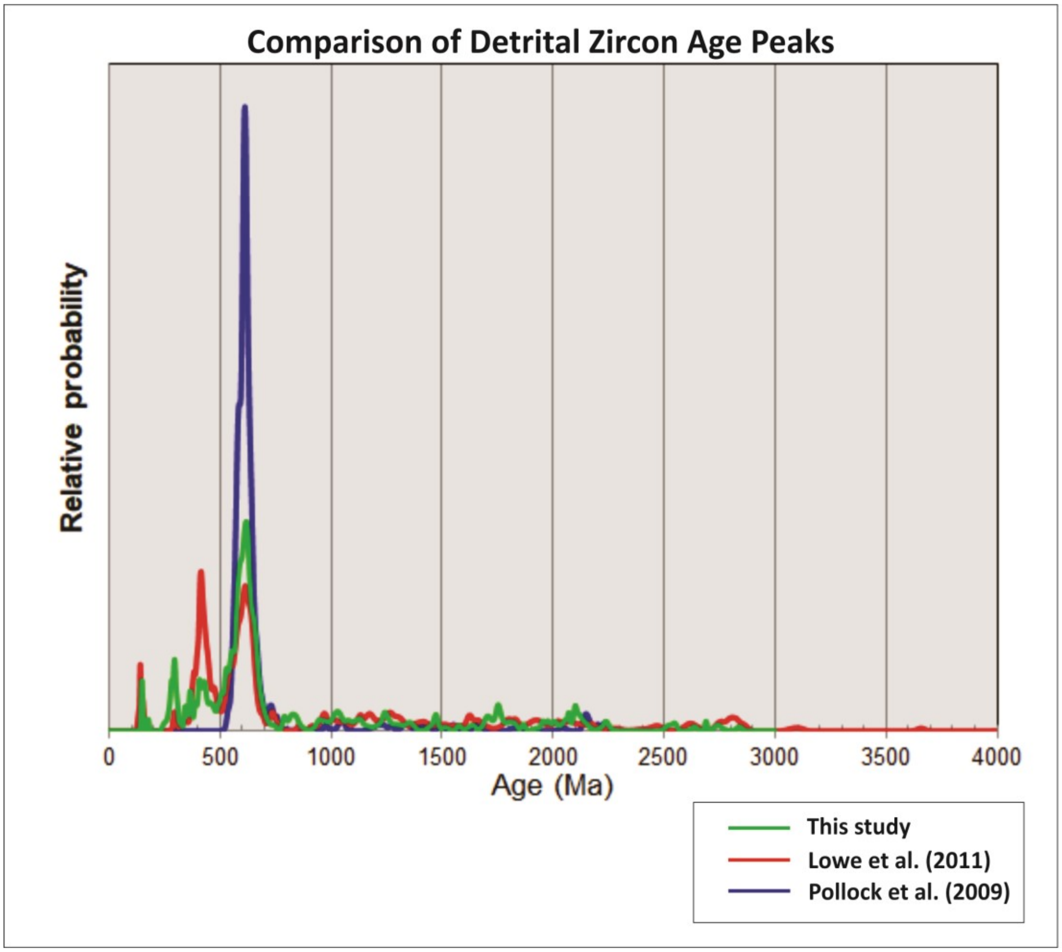

Figure 7.1 – Comparison of detrital zircon age peaks from this study, Lowe et al. (2011) and Pollock et al. (2009). For this study, all grains were plotted (n=310). All grains from Lowe et al. (2011) (n=335) and Pollock et al. (2009) (n=278) were also plotted. Data from Lowe et al. (2011) are from Mesozoic sedimentary rocks offshore Newfoundland while samples from Pollock et al. (2009) are from Neoproterozoic to Cambrian sedimentary rocks of the Avalon Zone onshore Newfoundland.

7.5.3 - > 1 Ga Grains

It is likely that the Avalon Zone was also an important source for the group of grains of >1 Ga. Grains ranging from the Mesoproterozoic to the Late Archean are thought to be related to the basement of Avalonia. It has been proposed that the Avalon terrane is built upon a dominantly *c.* 1.0 – 1.2 Ga basement with a smaller component of *c.* 1.6 Ga crust (Kerr et al. 1995; Murphy et al. 1996). Furthermore, rare *c.* 2.0 and 2.4 Ga xenocrystic zircons have been detected by Bevier & Barr (1990) in the Mira terrane and Zartman & Hermes (1987) in New

England in Avalonian plutonic rocks. Therefore, it is possible the >1 Ga grains are derived directly from Avalon basement. However, these grains are also common in Avalon Zone cover sequences, especially within the Cambrian – Ordovician cover sequences, as discussed in Section 1.6.2. These Lower Paleozoic cover sequences are thought to occur in the Avalon Uplift and Bonavista Platform areas, in addition to beneath the West Orphan, Northern Jeanne d'Arc and Flemish Pass Basins (King et al., 1986; Bell & Howie, 1990). If the >1 Ga grains are derived from Cambrian – Ordovician cover sequences, a source from the east, south, or north is possible, which is also not overly diagnostic. The characteristics of these grains, such as their low Th/U as well as their predominantly rounded to subrounded nature, were much more helpful in determining the parent rock type. It is probable that they were derived from a mixture of sedimentary and metamorphic sources as discussed in Section 6.4.2 and 6.5.2. This is reasonable because grains of this age would likely have experienced either significant sedimentary recycling or metamorphism. The rounded characteristic of these grains supports derivation from cover sequences of the Avalon Zone. >1 Ga grains from the Early Paleozoic cover sequences would have been subject to numerous sedimentary cycles, and would have many of the same features seen in the >1 Ga grains analyzed in the Upper Kimmeridgian Source Rock sample.

Another potential source of the >1 Ga grains is the Grenville basement of western Newfoundland and Labrador. The Grenville basement of this area has been shown to be composed of gneisses and granites with ages of approximately 1000 Ma and 1500 Ma (Heaman et al. 2002). Although this could explain the presence of some of the > 1 Ga grains in the samples from the Upper Kimmeridgian Source Rock, it cannot account for the grains that are aged > 1.5 Ga. Many of the samples of the Upper Kimmeridgian Source Rock have several grains > 1.5 Ga. If these are compared to those dated by Pollock et al. (2009) from sedimentary rocks of the Avalon Zone of eastern Newfoundland (Figure 7.1), a much better match is observed. There are numerous zircons from these samples dated at >1.5 Ga, and these would represent a good match for the >1.5 Ga grains from the Upper Kimmeridgian Source Rock. Evidently, many of the other grains dated between 1.0 and 1.5 Ga are likely to be derived from the Avalon Zone as well, since grains of this age are important in the study of Pollock et al (2009). It is possible that a small number of the grains aged between 1.0 and 1.5 Ga are sourced from the Grenville basement, but these would represent a small proportion of all the grains in general, meaning that this source region likely represents an insignificant source of detritus at this time. In addition, grain characteristics listed in the previous paragraph suggested Avalon Zone sources for this group are most probable.

7.5.4 - Cambrian – Devonian Grains

The youngest significant cluster of grains from the Upper Kimmeridgian Source Rock material is a Cambrian – Devonian group of grains. The ages of these grains closely match those of rocks found in the Gander and Dunnage zones of the Central Mobile Belt. As shown in Figure 7.1, the Cambrian – Devonian age peak from grains of this study closely matches that of Lowe et al. (2011), suggesting the grains have a similar origin. Lowe et al. (2011) also interpreted these grains to be derived from the Central Mobile Belt. This terrane is described in detail in Section 1.6.4 and is located about 400 – 500 km to the west and northwest of the sample locations in Newfoundland, but also to the north and northeast in the offshore extensions of the Porcupine Bank and Basin (Lowe et al. 2011). This implies sediment supply from either a significant distance to the west or from the northeast. To explain the presence of Ordovician – Devonian aged grains in Tithonian sandstones of the Flemish Pass Basin, Lowe et al. (2011) interpreted these grains to be derived from the west. This interpretation would appear feasible for the Upper Kimmeridgian Source Rock as well, although it is also possible that sediment was derived from the northeast from offshore extensions of the Porcupine Bank and Basin, which possesses a similar geology to that of the Central Mobile Belt. This interpretation is further supported by Cody et al. (2012), who analyzed 2D and 3D seismic data combined with well data and facies interpretations of Upper Jurassic reservoir intervals in the Mizzen area of the northern Flemish Pass. Cody et al. (2012) interpreted major river systems to be entering the basin from the northeast at this time. Since the detrital zircon ages would be similar if derived from the northeast or the west, the interpretation here is that both options are feasible.

An additional consideration for the source of the Cambrian - Devonian grains is that they may have been derived from Carboniferous sedimentary rocks. Abundant Carboniferous sedimentary rocks are present both in the Maritimes basins as well as onshore and offshore Ireland. The St. Anthony Basin as well as the Sydney Basin both extend from northwestern and southwestern Newfoundland towards the east to the Northeast Newfoundland Shelf and the southern Grand Banks, respectively (Figure 1.7). As mentioned in Section 1.6.5, a number of wells on the southern Grand Banks intersected Carboniferous clastic sequences (Howie & Bell, 1990). These Carboniferous sediments would probably be filled with Cambrian – Devonian-aged zircons as they most likely formed from the erosion of the Central Mobile Belt. This is the case for the Carboniferous clastic rocks of the Deer Lake and Bay St. George Basins of western Newfoundland which are dominated by zircons of Ordovician and Silurian age (Sylvester, 2012). This would likely be the same case for Carboniferous clastics deposited both onshore and offshore Ireland, as they would have been eroding rocks analogous to those of the Central Mobile Belt. Carboniferous clastic rocks, therefore, may be a significant source of Cambrian – Devonian grains as well. If Carboniferous sedimentary rocks are an important supply of clastic material, it similarly does not help distinguish drainage orientations, as input from the west as well as northeast are both possible.

The characteristics of the Cambrian – Devonian grains are reviewed in Section 6.4.1 and 6.5.1 and show a mixture of morphologies as well as variable Th/U and aspect ratios. This indicates a mixture of parent rock types for these grains including both igneous and sedimentary sources. Therefore, it is likely that rocks found within the Central Mobile Belt (Cambrian to Silurian sedimentary rocks, volcanic rocks, and Silurian to Devonian granites) are more important as a source than the Carboniferous clastic rocks. If Carboniferous clastics were the predominant source, there would likely be more rounded grains than what is observed for the Cambrian – Devonian grains, which were often angular to subrounded. Although some of these are probably polycyclic, this can be explained from a derivation from sediments of the Central Mobile Belt. It is therefore concluded that the Cambrian – Devonian grains may be derived from the west from rocks of the Central Mobile Belt of Newfoundland, or alternatively from the northeast from analogous rocks from the Irish conjugate margin.

7.5.5 - Middle Neoproterozoic Grains

Three Middle Neoproterozoic grains were dated in the Upper Kimmeridgian Source Rock of the South Tempest G-88 well. These grains are interesting as although they are likely derived from the Avalon terrane, there are fewer known correlative sources for grains of this age. Some of the oldest rocks of the Avalon Zone such as the Burin Group are dated at *ca.* 763 ± 2 Ma (Krogh et al. 1987) and represent a potential source. A more likely source, however, is the more proximal Flemish Cap granodiorite. With an age in the 750 – 830 Ma range (King et al. 1985), it is located to the east and northeast of the Flemish Pass Basin. This would indicate an easterly or northerly derived provenance. The angular to subangular morphology of these grains indicates they were likely derived from igneous rocks, which also supports a derivation from the Flemish Cap granodiorite or equivalent rocks.

Other grains present within the Upper Kimmeridgian Source Rock samples that did not fall within a specific group are scarce, and should be considered minor sources. This includes the two Permian – Carboniferous grains in the South Tempest G-88 sample. Although these are interesting grains, they are not abundant and cannot be considered a significant group. The presence of these Carboniferous-Permian aged grains and their origins will be addressed in subsequent samples, where they are more abundant, and are considered a major group.

7.6 – Provenance Interpretations of Geochronological Data - Upper Tempest Sandstone

7.6.1 - Introduction

One sample was analyzed from the Upper Tempest Sandstone from a depth of 3210m from the Panther P-52 well. The results from this sample are markedly different than those from the Upper Kimmeridgian Source Rock samples.

7.6.2 – Constraints on depositional ages

The first point of interest is the presence of detrital zircon grains that provide constraints on the maximum depositional age of this unit. Lowe (2009) was able to constrain maximum depositional ages for reservoir units within the Flemish Pass Basin and help refine interpretations where biostratigraphic results were conflicting. Dickinson & Gehrels (2009) propose several ways to calculate the maximum depositional age of strata. The more statistically robust method is to calculate the weighted average of the youngest three or more grains that overlap at 2σ (Dickinson & Gehrels, 2009). This method is possible in this sample since three Jurassic grains were dated whose ages overlap at an uncertainty of 2σ. The weighted average of these three grains is 147.5 ± 2.8 Ma (MSWD = 0.85). However, this method is a conservative method, and can sometimes result in an age that is older than the depositional age (Dickinson & Gehrels, 2009). Another method is to accept the age of the youngest single grain. This technique can be potentially misleading as results from a single grain may not be reproducible. However, in the dataset of Dickinson & Gehrels (2009) it more often results in ages closer to the actual depositional age. In the Upper Tempest Sandstone sample, the youngest grain was dated at 144.9 ± 5.6 Ma. Both of these methods result in a Late Tithonian age for the Upper Tempest Sandstone as the Tithonian Stage ranges from 152.1±0.9 to ~145 Ma (ICS, 2015). An Earliest Cretaceous age is possible, as the youngest grain is dated at the Tithonian/Berriasian boundary, but the uncertainty on the measurement is 5.6 Ma, and as discussed, using the average of the three ages is likely a more statistically robust technique. When compared to biostratigraphic interpretations for this interval, a Late Tithonian age is consistent with findings from Robertson Research (2004), but conflicts with interpretations from the Bujak Davies Group (1987) who interpreted this interval to be Early Kimmeridgian in age (Figure 2.5). Based on the detrital zircon age results, and the Robertson Research (2004) report, the Upper Tempest Sandstone from the Panther P-52 well is considered to have a Late Tithonian age. Because cuttings were used for this sample, there is a possibility that caving occurred (material from previously penetrated beds uphole) and potentially contaminated this sample with younger detrital zircons from above. However, given the abundance of Upper Jurassic grains in this sample and the absence of any Cretaceous or younger grains, it is improbable they originated from cavings.

7.6.3 - Identified Grains

Unlike previous samples, the Upper Tempest Sandstone has a distinctly different population of detrital zircons. In addition to previously described zircon groups (Late Neoproterozoic group, >1 Ga group, Cambrian – Devonian Group), two new groups were observed. These include a group of Permian – Carboniferous grains, as well as a group of Upper

Jurassic grains discussed in the previous section. The late Neoproterozoic and >1 Ga grains likely represent detritus from Avalonia, and are not overly indicative of drainage orientations. The Cambrian – Devonian grains are uncommon, but likely represent minor detritus from either the Central Mobile Belt from the west or from the northeast. Since they are such a small population, however, the Central Mobile Belt was likely only a minor source of detritus at this time.

7.6.4 - Carboniferous – Permian Grains

Seven Permian – Carboniferous grains were dated from the Upper Tempest Sandstone unit of the Panther P-52 well at 3210 m. These grains are noteworthy as there are few known correlative sources from Newfoundland or the Newfoundland offshore. As shown in Figure 7.1, grains of this age were not detected by Lowe et al. (2011) in other rocks from offshore Newfoundland. There are some late Devonian intrusions on the island of Newfoundland such as the St. Lawrence Granite and Francois Granite, dated at 374 ± 2 and 378 ± 4 Ma, respectively (Kerr et al. 1993). In addition, there are a number of shear zones on the island of Newfoundland that are thought to be related to the Hercynian deformation event in the Carboniferous (B. O'Brien, personal communication). Shear zones can be accompanied by magmatism, such as the Dover Fault in eastern Newfoundland (D'Lemos et al. 1997), and it may therefore be possible that Carboniferous igneous rocks once existed in Newfoundland, although none have been observed. If they did exist, they were either eroded, or are just very uncommon. However, even if Carboniferous igneous rocks were present in Newfoundland, it is unlikely that they would make statistically significant detrital zircon populations in offshore sediments, as Avalon, Gander, and Dunnage Zone related grains would be much more abundant. Additionally, if Carboniferous igneous rocks existed in Newfoundland, it is likely that the Carboniferous sedimentary rocks on the island would have a population of Carboniferous zircon grains.

Sylvester et al. (2012) found no Carboniferous detrital zircon grains in the sedimentary rocks of the Deer Lake or Bay St. George Basins. Therefore, the presence of seven Carboniferous – Permian grains, making up 24% of this sample implies a source external to Newfoundland.

A couple scenarios may explain the presence of Carboniferous zircons in this Upper Tempest Sandstone sample. The first option is that these grains are derived directly from Iberia. As explained in Section 1.6.8, Permian-Carboniferous granitic intrusions are abundant on the Iberian Peninsula, and therefore, detritus of this age would be abundant if the Iberian Peninsula represented a significant source. However, the Tithonian represents the initiation of a rifting phase that separated the Grand Banks from Iberia (Sinclair, 1988). Despite the initiation of the rift, as the Tempest Sandstones are interpreted to be deposited by turbidity currents, it is possible that if sediment from Iberia gained access to the rift, it may have been able to reach the Grand Banks region.

The second option is that the Permian-Carboniferous grains are derived from recycled sediments from the Hercynian foreland basin. This option is more complicated, but could still explain the presence of Permian – Carboniferous grains in the Upper Tempest Sandstone sample. Hiscott et al. (2008) preferred this interpretation to explain the presence of Permian – Carboniferous aged detrital micas within post-rift sediments in the Newfoundland Basin, east of the Grand Banks. This model is based on the fact that the Hercynian orogenic belt was in close proximity to the Grand Banks during the Carboniferous/Permian. Therefore, the deformation front for this orogen was near the eventual dividing line between Iberia and the Grand Banks (Hiscott et al. 2008). The associated Hercynian foreland basin would have existed 200-300 km to the west of this orogenic front (Allen & Homewood, 1986; Hiscott et al., 2008). Given this information, it is likely that sediments of this foreland basin would have blanketed at least some of the Grand Banks, particularly in the region of the Avalon Uplift (Hiscott et al., 2008). These foreland basin sediments would have been deposited in the Late Carboniferous or Permian, and would have likely contained substantial quantities of Permo-Carboniferous zircons from the Iberian granitoids which would have subsequently been available for erosion and deposition into Mesozoic basins.

It is difficult to say which option is more likely based on the detrital zircon ages alone. However, the characteristics of the Permian-Carboniferous grains are noteworthy. As described in Section 6.9.2, the preferred interpretation is that the grains are derived from first-cycle igneous rocks based on the predominantly euhedral to subangular grain shapes. This would appear to support a derivation directly from igneous rocks from Iberia. It is less likely that sediments from the Hercynian foreland basin would possess this morphology, as they would have been through at least two sedimentary cycles by the time of their deposition in the late Jurassic. It is therefore interpreted that these are first-cycle grains from Iberian intrusions.

7.6.5 - Jurassic Grains

Three Jurassic grains (145 ± 5 Ma, 148 ± 4 Ma, 150 ± 6 Ma) were dated in the Upper Tempest Sandstone sample (Panther P-52 (3210 m)) and were used in Section 7.6.2 to help refine the depositional age of this unit. The provenance of these grains is difficult to identify as there are few known correlatives to these grains. Some potential Mesozoic sources are outlined in Section 1.6.6. These sources range from areas in the South Grand Banks, to the Orphan Basin, to potential sources on the island of Newfoundland. The ages of the Upper Jurassic grains most closely match that of the granite encountered in the Bonavista C-99 well in the Orphan Basin which was dated at 146 ± 46 Ma (BP Canada, 1975). However, the large uncertainty in this date makes this correlation less reliable. Basalt encountered in the Spoonbill C-30 and Cormorant N-

83 wells from the South Grand Banks has not been dated, and may represent a potential source (Amoco et al. 1973; Jansa & Pe-Piper, 1986). However, as these rocks are basaltic, they are unlikely to contain zircon. Therefore, it is unlikely these rocks are the source of the Mesozoic zircon grains. Other volcanics from the South Grand Banks have ages that do not correspond to the Tithonian ages from this sample. It is therefore possible that these grains are derived from the west from correlative igneous rocks to those intercepted in the Bonavista C-99 well. However, it is also a possibility that they are from a currently unknown source that represents contemporaneous magmatism within the basin. The high Th/U as well as angular shapes of these grains indicate they are likely derived from igneous sources, and are first-cycle in nature. This leaves the Bonavista C-99 granite, as well as other local magmatic rocks as plausible sources.

7.7 – Provenance Interpretations of Geochronological Data - Lower Tempest Sandstone

7.7.1 - Overview

One sample was analyzed from the Lower Tempest Sandstone unit from the South Tempest G-88 well from 4195.8 m. This sample contains very abundant late Neoproterozoic grains, significant >1 Ga grains, and minor Permian – Carboniferous and Cambrian – Devonian grains. As interpreted in previous samples, the late Neoproterozoic and >1 Ga grains are attributed to detritus from the Avalon Zone, while the Cambrian – Devonian grains are linked to grains derived from the Central Mobile Belt. Permian – Carboniferous grains are likely from Iberia or possibly from recycled Hercynian foreland basin sediments. Based on their angular to subangular morphologies, it is likely these grains are first-cycle and derived from Iberia. An important observation for this sample is the abundance of Avalonian-related grains compared to other groups. The late Neoproterozoic and >1 Ga groups comprise 84% of all grains dated in this sample.

7.8 – Provenance Interpretations of Geochronological Data - Rankin Formation

7.8.1 - Overview

Three samples from the Rankin Formation stratigraphic unit were analyzed. Two of these samples were from the Baccalieu I-78 well at depths of 4142.2m and 4135.29m, respectively. The other sample was the only analyzed from the Lancaster G-70 well, from a depth of 4405m. The two samples from the Baccalieu I-78 well possess detrital zircon signatures similar to those of the Upper Kimmeridgian Source Rock samples where major zircon groups included abundant late Neoproterozoic grains and common > 1 Ga grains (both related to Avalonia), as well as some Cambrian – Devonian aged grains (from the Central Mobile Belt).

7.8.2 – Lancaster G-70 Sample

The Rankin Formation sample from the Lancaster G-70 well (4405 m) possesses a different detrital zircon signature than those analyzed from the Baccalieu I-78 well. They do possess similar zircon groups such as the late Neoproterozoic group, the >1 Ga group, and the Cambrian – Devonian grains. As previously discussed, these grains are likely linked to local Avalonian sources as well as sources related to the Central Mobile Belt. However, in this sample, the >1 Ga group of grains is much more significant than in other Rankin Formation samples. Additionally, the presence of a significant population of Upper Devonian to Permian-aged zircon grains is indicative of a different provenance. This population of grains, with similar ages and characteristics, is also found in the previously discussed Tempest Sandstone samples. In those samples, the Upper Devonian – Permian-aged grains are interpreted as being derived from Iberia or alternatively from Hercynian foreland basin sediments that likely once covered areas on the Southern Grand Banks. Both of these possibilities exist for the Upper Devonian – Permian-aged grains in the Lancaster G-70 sample as well. However, based on the angular to subangular morphologies of these grains they are likely first-cycle and derived from Iberia.

The single Jurassic-aged grain found in this sample is also fairly interesting. It is not overly indicative of provenance directions since only a single grain was found; however the $^{206}Pb/^{238}U$ age of 175 ± 9 Ma may be correlated to a diabase dike dated from the Twillick G-49 well on the Southern Grand Banks at 177 ± 5 Ma (Jansa & Pe-Piper, 1988). This grain may not be directly derived from this intrusion, but is likely related to a contemporaneous event within the basin. It suggests the diabase from the Twillick G-49 well may not be just a localized body, and that magmatism at this time may have been more widespread throughout the basin.

7.9 - Late Jurassic Provenance Model

7.9.1 - Upper Kimmeridgian Source Rock

The major detrital zircon groups within the Upper Kimmeridgian Source Rock (Figure 6.2; Figure 6.4) suggest a provenance from rocks of the Avalon Zone and Central Mobile Belt from a mixture of first-cycle igneous rocks, recycled sedimentary rocks, and minor metamorphic rocks. It is difficult to conclusively say whether these grains were derived from the west or the east, as rocks from both the Avalon Zone and Central Mobile Belt exist both west and east of the study area. Geochemical analysis also supports sediment derivation from the Avalon Zone or equivalent rocks, with potential input from the Central Mobile Belt. Geochemical plots (Figure 4.6; Figure 4.7) also suggest recycled sedimentary rocks were an important contributor of detritus. Both geochronological and geochemical datasets rule out a source from the Humber Zone of western Newfoundland.

Although determining whether sediment was derived from the west or east is difficult, the presence of detritus interpreted to be from the Flemish Cap granodiorite or correlative sequences suggests that sediment input was likely from the northeast, although minor input from the west is also possible. It is likely that basin entry points did exist to the north, as was interpreted by Cody et al. (2012) for Upper Jurassic reservoir units of the Flemish Pass Basin. Figure 7.2 shows the interpreted large-scale drainage routes and Figure 7.3 shows the interpreted basin-scale entry points, and areas of either abundant and restricted sediment supply. The provenance interpretation introduced here for the Flemish Pass Basin and Central Ridge appears to concur with previous published data of the Jeanne d'Arc Basin for the Kimmeridgian. Information from the Jeanne d'Arc Basin indicates that during deposition of the equivalent Kimmeridgian Egret Member of the Jeanne d'Arc Basin, the source rock possessed more terrigenous qualities based on the pristine-phytane ratios near the Central Ridge (Fowler & McAlpine, 1994) towards the northeast, as well as increased sedimentation rates towards the same area (Huang et al., 1996). In addition, the southern part of the basin was very restricted, and deposition of limestone and marls was common (Bateman, 1995; Magoon et al., 2005). Finally, Magoon et al. (2005) also noted that the thickness of the Kimmeridgian source rock increased greatly towards the east to over 500 m thick in some wells on the Central Ridge. Magoon et al. (2005) also noted facies change towards the east as the Egret Member source rock becomes split by the Tempest Sandstone into an Upper and Lower Kimmeridgian Source rock (Figure 7.4). This information indicates that during the Kimmeridgian, areas towards the northeast experienced high sedimentation rates and more proximal depositional environments. This indicates that sediment sources were likely in the northeast, which matches the detrital zircon interpretation in this study that indicated derivation from the northeast.

If sediment was derived from the north, this implies sediment supply would have been much more abundant in the northern regions of the basin, with a likely thicker source rock sequence. This is an important consideration for the petroleum potential of the source rock. If the source rock is indeed more proximal to sediment supply in the north, then it is likely that the source rock has a more terrestrial component in this region and would likely generate different types of oil. A terrestrial component to the Flemish Pass source rock was proposed by both Creaney & Alison (1987) as well as Fowler (2007) based on the pristane/phytane ratios of Flemish Pass oils. This information supports the interpretation that the Flemish Pass Basin and Central Ridge were closer to the major sources of detritus at this time in comparison to the Jeanne d'Arc Basin, where the source rock is much more marine in nature (Magoon et al. 2005). Another important consideration is the effect of abundant sediment supply on the preservation of organic matter. Bohacs et al. (2005) outline the importance of clastic input in source rock systems in order to preserve the organic matter. However, for high quality hydrocarbon source rocks, it is also important that the clastic input is not too high, and does not dilute the organic content of the source beds. Evidently, if clastic input into the Flemish Pass Basin and Central Ridge was from the north, it means that the balance between clastic input and accumulation of organic material may be different here than elsewhere on the Grand Banks (such as the Jeanne d'Arc Basin) during this time period.

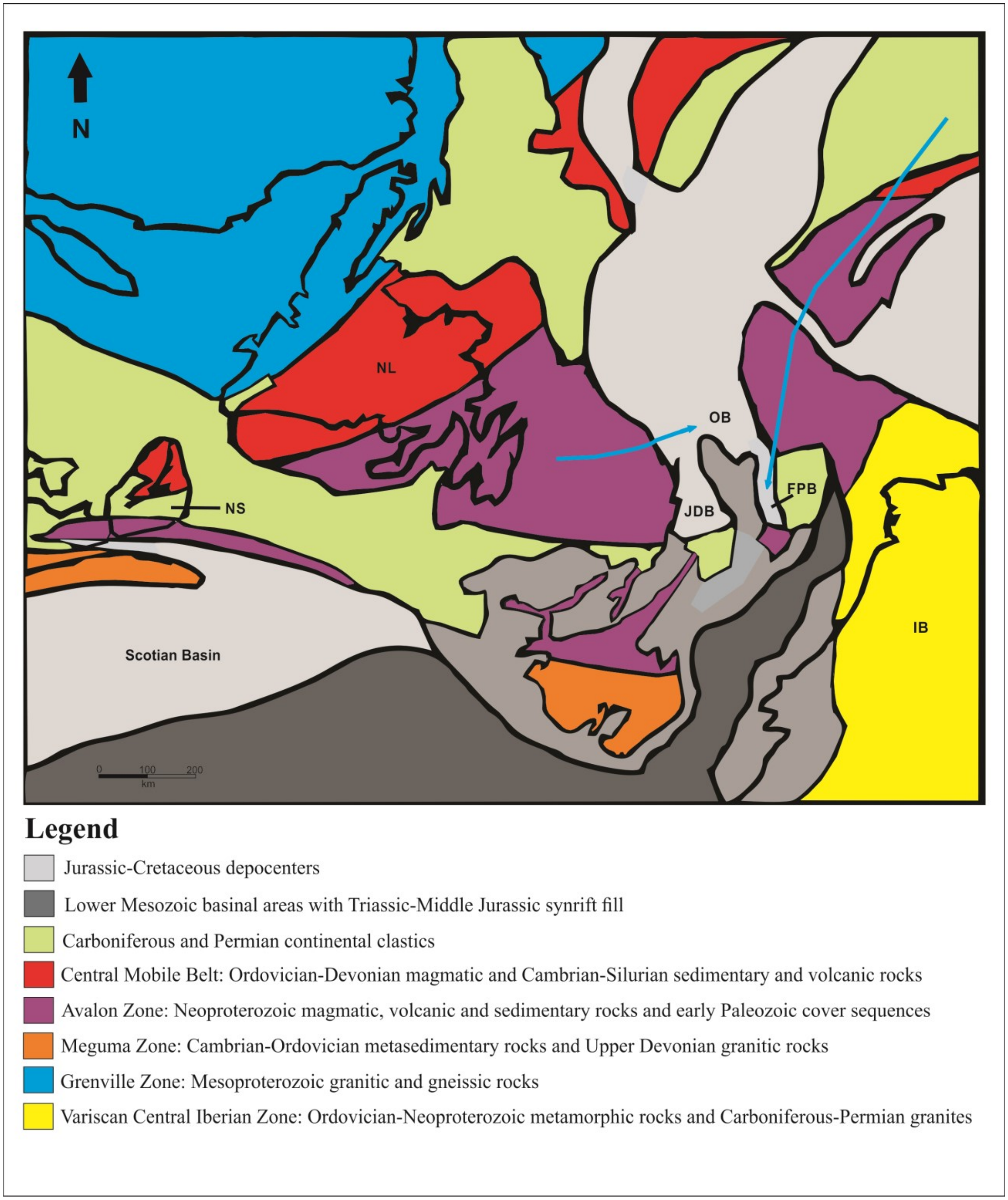

Figure 7.2 - Interpreted large scale drainage routes during deposition of the Upper & Lower Kimmeridgian Source Rock, and the Rankin Formation. Based on results from detrital zircon geochronology, whole rock geochemistry and heavy mineral ratios. Black lines trace terrane boundaries as well as modern day landmasses (NL- Newfoundland; NS- Nova Scotia; IB- Iberian Peninsula; JDB- Jeanne d'Arc Basin; OB- Orphan Basin; FPB- Flemish Pass Basin). Arrows show interpreted drainage routes. Figure modified from Lowe et al. (2011).

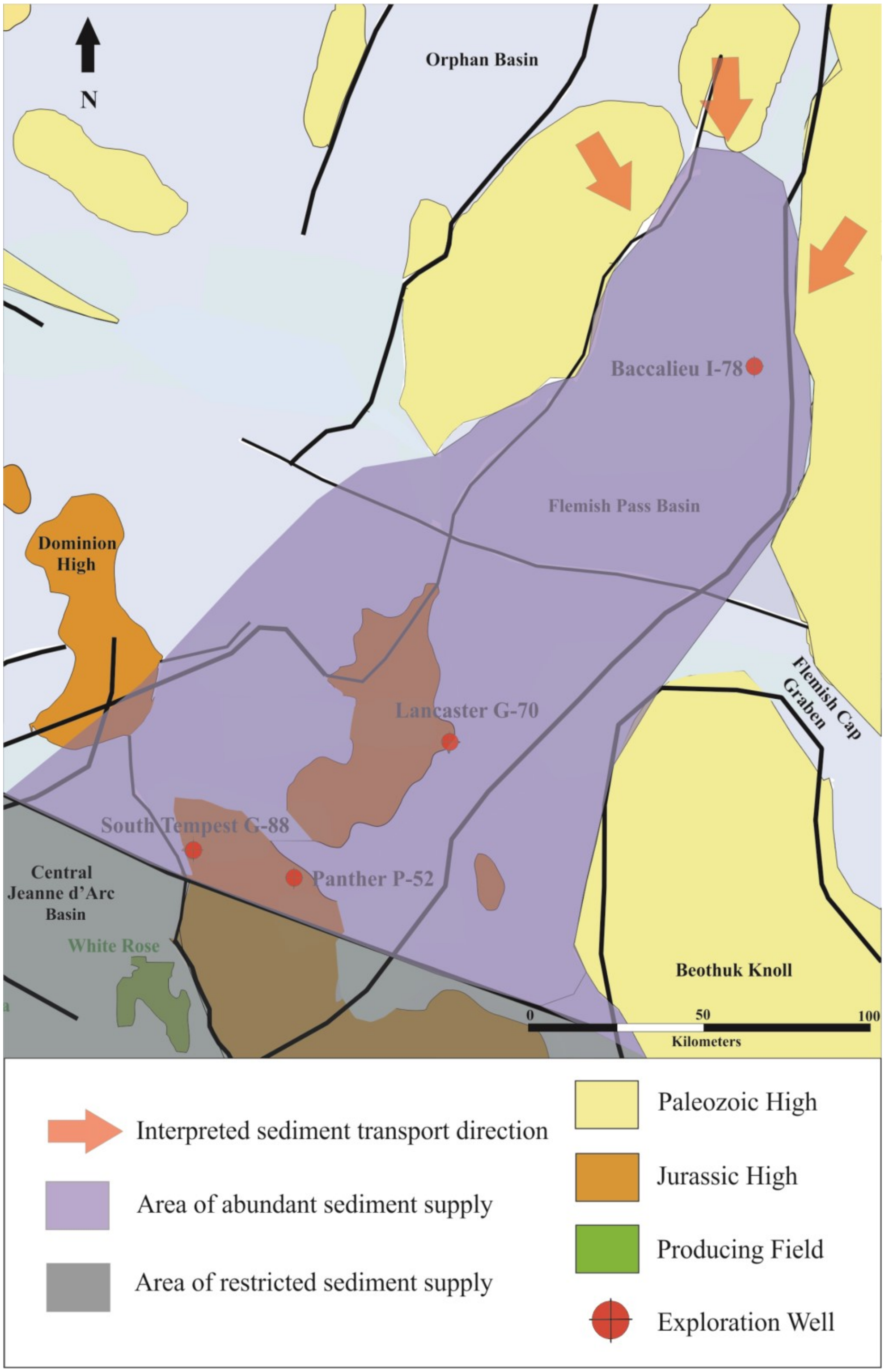

Figure 7.3 - Interpreted basin entry points and areas of abundant and restricted sediment supply during deposition of the Upper & Lower Kimmeridgian Source Rock, and the Rankin Formation. Black lines represent major faults. Figure modified from Cody et al. (2011).

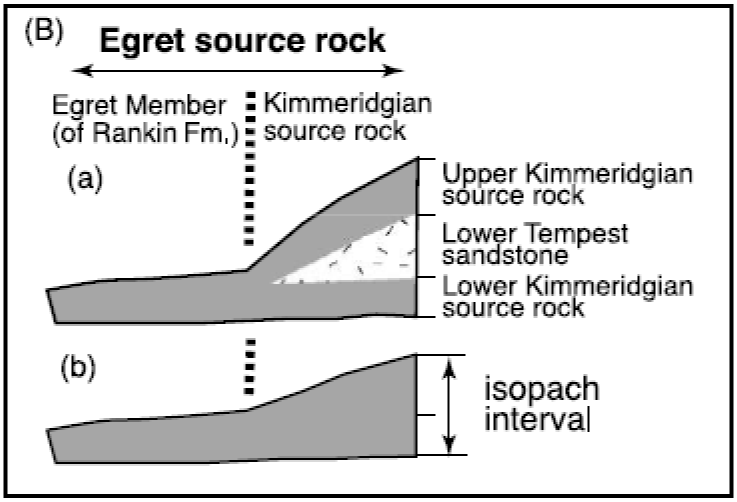

Figure 7.4 - Spatial variation in the Kimmeridgian Source Rock on the Grand Banks. From Magoon et al. (2005).

7.9.2 - Rankin Formation and Lower Kimmeridgian Source Rock

The detrital zircon populations of the Rankin Formation samples and their associated characteristics are very similar to those from the Upper Kimmeridgian Source Rock samples (Figure 6.8; Figure 6.10). Detrital zircon analysis was unsuccessful for the Lower Kimmeridgian Source Rock as insufficient zircons were obtained from the samples from these intervals. However, the geochemical signatures and heavy mineral ratios of both the Rankin Formation and Lower Kimmeridgian Source Rock are similar to what was observed in the Upper Kimmeridgian Source Rock samples. Therefore, the provenance interpretation is also similar. A provenance from the northeast supplying detritus from the Avalon Zone as well as from the Central Mobile Belt is considered probable. Therefore, drainage routes in Figures 7.2 and 7.3 are applicable for the Rankin Formation and Lower Kimmeridgian Source Rock as well. The geochemical data and the ZTR heavy mineral index indicate recycled sedimentary rocks are an important source of detritus for both these units. This is confirmed in the Rankin Formation by the morphologies of zircon grains as many are likely recycled, although some grains from first-cycle igneous and metamorphic sources are noted as well.

7.9.3 - Rankin Formation Exception – Lancaster G-70 Sample

The sample analyzed from the Lancaster G-70 well (4405m) displays a slightly different provenance than the other Rankin Formation and Upper Kimmeridgian source rock samples. This was a cuttings sample, and was not analyzed geochemically for reasons discussed in Chapter 4. Heavy mineral ratios do not suggest a major difference in provenance, as ratios for this sample all fall within the range of the error bars of the Upper Kimmeridgian Source Rock, and Lower Kimmeridgian Source Rock as well as other Rankin Formation samples (Figure 5.8; Figure 5.9). However, the detrital zircon analysis has detected a slightly different provenance not suggested by heavy mineral ratios. In this sample, most of the same zircon populations are present; however these populations are in different proportions. In this sample, the most abundant grains are actually the >1 Ga grains. As mentioned previously, these grains are associated with the Avalon Zone, and are common within Ordovician cover sequences (Pollock et al. 2009). The abundance of these grains within the Lancaster G-70 sample indicates that the source for the detritus at this time may have included the aforementioned Ordovician cover sequences. These cover sequences were abundant in late Neoproterozoic grains but also the >1 Ga grains. However, another potential option is that these >1 Ga grains are more directly sourced from the Avalonian basement. Since the >1 Ga grains comprise 34% of all those analyzed from the Lancaster G-70 sample, it is possible that they are sourced directly from an uplifted Avalonian basement source, rather than just from Paleozoic cover sequences.

In addition to the abundance of >1 Ga grains, a prominent group of Upper Devonian – Permian grains were detected in this sample which were not common in previous Rankin

Formation samples. As described in Section 7.6.4, it is difficult to say definitively where these grains are from, although they are likely derived from Iberia based on their ages and grain morphologies. This information suggests some input from the east for this unit. This can explain the presence of Upper Devonian – Permian grains, and can also account for the late Neoproterozoic, and >1 Ga grains, which are thought to be found in Avalon Zone rocks which surround and underlie the Grand Banks (Haworth & Lefort, 1979; King et al., 1985). However, an eastern provenance does not explain the presence of a major population of Cambrian – Silurian grains. The Cambrian – Silurian grains are found in the majority of samples that are interpreted as being derived from the northeast in other Upper Kimmeridgian Source Rock and Rankin Formation samples. However, the Tempest sandstone samples, which are interpreted as being derived from the east, possess only minor populations of these grains. It is therefore contradictory to see both populations in this sample.

The preferred interpretation to explain the presence of both Upper Devonian – Permian grains as well as Cambrian – Silurian grains is that the grains are predominantly derived from the northeast, similar to other Rankin Formation and Upper Kimmeridgian Source Rock samples. Because of the abundance of >1 Ga grains in this sample, a major portion of this area was likely covered by Ordovician cover sequences or in close proximity to Avalonian basement. However, in addition to input from the northeast, it is likely that some input existed from the south or east at this time as well, and this would have been the source of the Upper Devonian – Permian grains. Figures 7.2 and 7.3 are interpreted to apply to this sample; however an important consideration is that there may have also been periodic input of detritus from more of an easterly direction at this time.

7.9.4 - Upper Tempest Sandstone

Samples of the Upper Tempest Sandstone were only available from cuttings, as this interval was not cored in any of the wells studied. For this reason, no geochemical analyses are available for this unit. Major zircon groups present in the Upper Tempest Sandstone sample (Figure 6.12) indicate an easterly provenance. An easterly provenance is suggested by the presence of a significant number of Permian – Carboniferous grains. The grains, as well as their relatively angular morphologies, indicate derivation from intrusions of Iberia. A provenance from the east can also account for the late Neoproterozoic and >1 Ga grains that are linked to the Avalon terrane as Avalonian basement is present to the east of the Grand Banks. Some minor Cambrian – Devonian grains, as well as Jurassic grains may indicate minor input from the west, however. Although an overall easterly provenance is favoured in this study for this unit, observations of Sinclair (1988) and Jansa & Wade (1975) suggest the uplift of the area of the Avalon Uplift began in the late Jurassic. If this is the case, the area to the South would have become a major region of sediment supply and would suggest sediment derivation from the south. This southerly derived provenance was also suggested by DeSilva (1994) for the Tempest sandstones, and also by Enachescu (1994) for the Jeanne d'Arc Formation sandstones in the Terra Nova Field of the Jeanne d'Arc Basin. Since the Jeanne d'Arc Formation is Tithonian in age, it is laterally equivalent to the Upper Tempest Sandstone in question here, whose age was refined to late Tithonian based on ages of detrital zircons present. However, the ages and morphologies of the Permian – Carboniferous zircon grains indicate an easterly provenance for the Upper Tempest Sandstone (Figure 7.5). This is the preferred interpretation based on the detrital zircon data.

The heavy mineral data for this interval are somewhat inconsistent with the detrital zircon results. The detrital zircon data indicates a distinct provenance for this unit, but as discussed in

Section 7.4.3, the heavy mineral ratios of the Upper Tempest Sandstone indicate similar sources as seen in the other analyzed formations.

There are a couple of potential reasons why heavy mineral ratios do not detect the provenance shift indicated by detrital zircon data. One explanation is that since Avalonian detritus is so important in all analyzed samples, including the Upper Tempest Sandstone, that the heavy mineral signature is mostly reflective of this terrane. So, in a sense, it is possible that the Permian – Carboniferous aged grains detected by detrital zircon geochronology are not sufficient to suppress the heavy mineral "fingerprint" of Avalonia. Another possibility is that the heavy mineral "fingerprint" of both Avalonian and other source terranes are very similar. Therefore, if a new provenance region appears, it may not be detected due to the similar nature of both terranes. This interpretation is preferred, because a new source terrane was undoubtedly detected by detrital zircon analysis. An easterly provenance as indicated previously is still the favored interpretation despite the lack of detection from heavy mineral ratios.

As the Tempest Sandstone units are important reservoir intervals on the Grand Banks (flowed 1250 bopd in the South Tempest G-88 well), the drainage orientations and basin entry points have important implications for reservoir quality during this time. Presumably, accumulations of coarse-grained, high quality reservoir rocks are more likely to occur in close proximity to sediment supply and basin entry points whereas finer-grained shales would be deposited basinward. If this is applied to the current interpretation for the Tempest sandstone, it is likely that thicker, higher reservoir quality rocks would be deposited in the east, with decreasing reservoir grade to the west (Figure 7.6). This may be an important consideration for further exploration and drilling in this area.

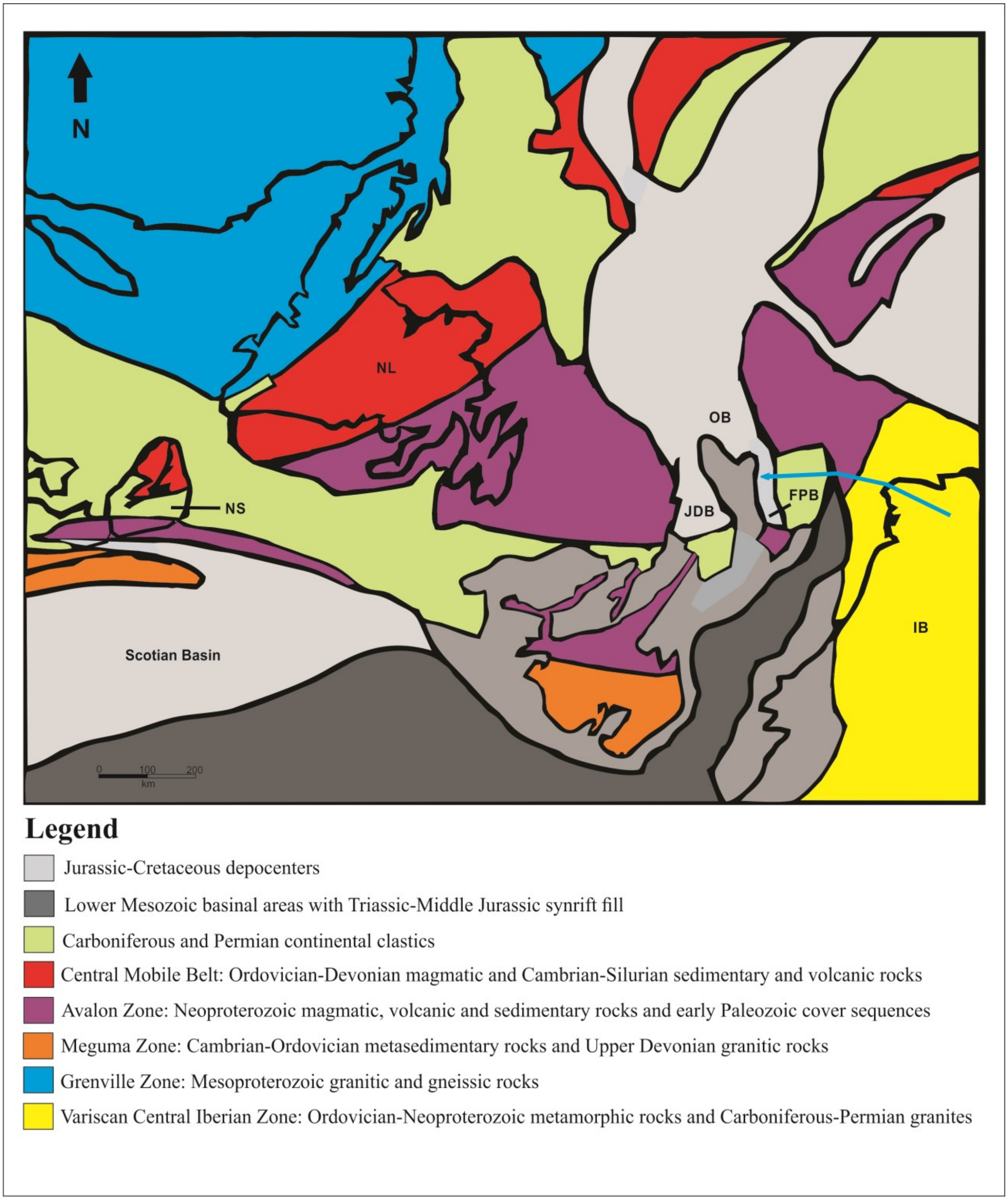

Figure 7.5 - Interpreted large scale drainage routes during deposition of the Upper & Lower Tempest Sandstone. Based on results from detrital zircon geochronology, whole rock geochemistry and heavy mineral ratios. Black lines trace terrane boundaries as well as modern day landmasses (NL- Newfoundland; NS- Nova Scotia; IB- Iberian Peninsula; JDB- Jeanne d'Arc Basin; OB- Orphan Basin; FPB- Flemish Pass Basin). Arrows show interpreted drainage routes. Figure modified from Lowe et al. (2011).

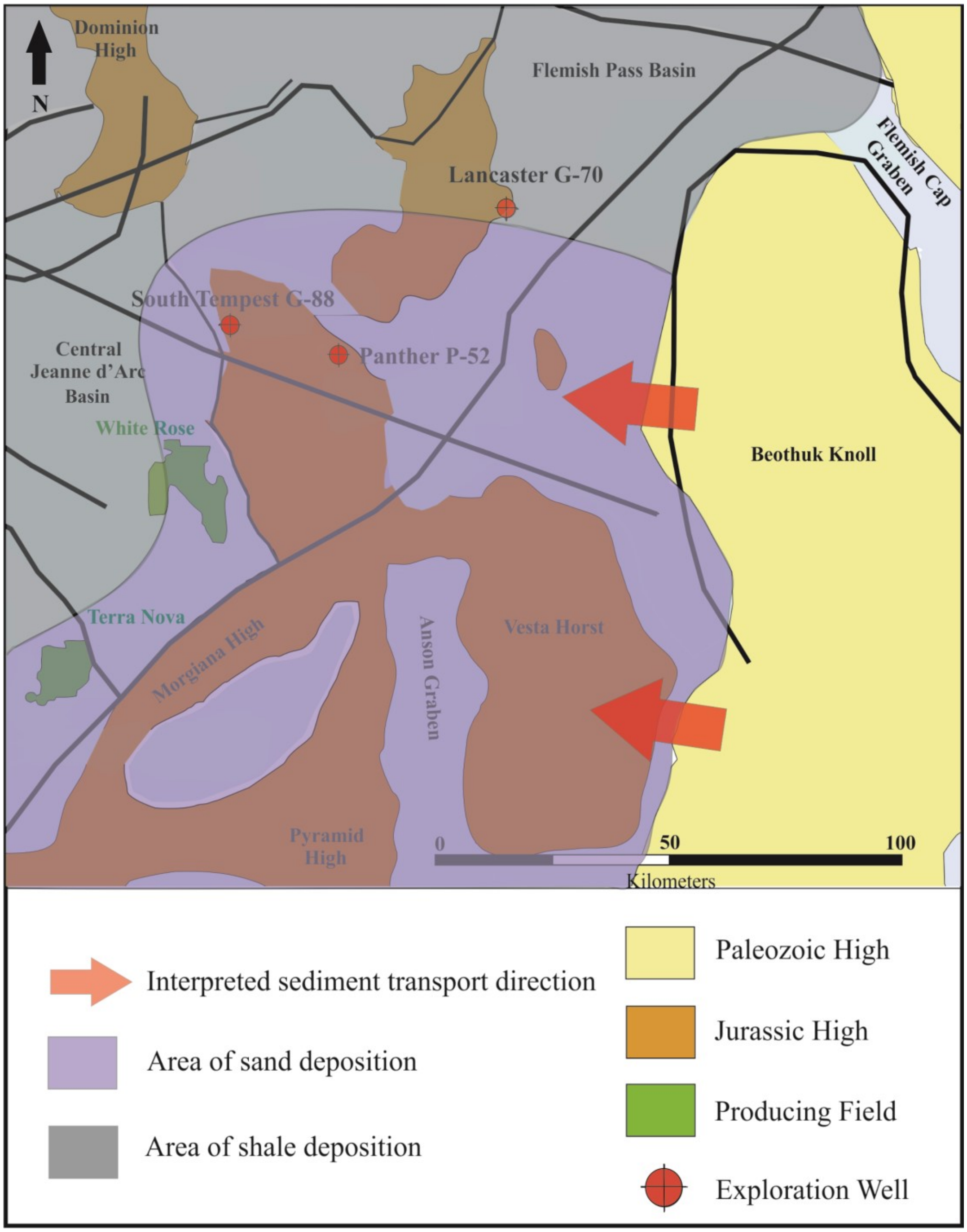

Figure 7.6 - Interpreted basin entry points and areas of abundant and restricted sediment supply during deposition of the Upper and Lower Tempest Sandstone. Figure modified from Cody et al. (2011).

7.9.5 - Lower Tempest Sandstone

Detrital zircon analysis revealed an abundance of late Neoproterozoic and >1 Ga grains (Figure 6.14), suggesting that local, Avalonian detritus is most important in the Lower Tempest Sandstone. Large, westerly- or northeasterly-derived drainage systems are not the preferred interpretation, as they would likely result in more abundant Cambrian – Devonian grains. However, the presence of some of these grains indicates minor input from the west or northeast, or reworking of older Mesozoic rocks with Cambrian – Devonian grains. The Permian-Carboniferous grains composed just 7% of all grains in this sample. A larger proportion of these grains would be expected if major drainage systems were entering the basin from the east (as seen in the Upper Tempest Sandstone sample). However, the presence of a minor population of Permian – Carboniferous grains suggests there was some minor input from the east at this time.

As described in Section 7.3.3, geochemical analysis supports a different provenance for the Lower Tempest Sandstone than the other analyzed units. Although sources from upper crustal rocks such as the Avalon Zone are still likely important, the geochemistry indicated a slightly more mafic source for these samples. Some possibilities for the mafic source include the ophiolites of western Newfoundland and the Central Mobile Belt, Mesozoic igneous rocks as well as mafic rocks of Iberia. When the detrital zircon populations are considered, it is likely that both the ophiolites of western Newfoundland and the Central Mobile Belt can be ruled out. Very few detrital zircons were noted from either the Grenville Zone or the Central Mobile Belt, which would be expected if sources from western or central Newfoundland were important. The potential Mesozoic sources discussed in Section 7.3.3 are almost all basaltic, which contain scarce zircons. It is difficult to say whether these sources were important as they would likely not be easily detected in the detrital zircon analysis. However, a number of Permian – Carboniferous grains in the detrital zircon populations indicate that some detritus was derived from Iberia. This may also explain the mafic source noted in the geochemistry, as the Ossa Morena Zone of Iberia also contains noteworthy mafic igneous rocks. Therefore, it appears both geochronological and geochemical datasets correspond and suggest a provenance of local Avalonian detritus as well as input from Iberia.

Heavy mineral data presented in this study (Figure 5.8; Figure 5.9) are insufficient to draw meaningful provenance conclusions from. But, the one sample from the Lower Tempest Sandstone (Panther P-52 (3600 m)) did possess a fairly unique heavy mineral signature, which, when combined with the geochronological and geochemical datasets helps to support the notion of a different provenance for this unit than the Upper Kimmeridgian Source Rock, Lower Kimmeridgian Source Rock and Rankin Formation units.

Overall, it appears the Lower Tempest Sandstone was sourced from predominantly local sources, making it difficult to define a paleodrainage direction. However a provenance from the east would explain the presence of Permian-Carboniferous, the local Avalonian grains, as well as the geochemical signatures. This option is therefore preferred and the provenance shown in Figure 7.5 is applicable for this unit as well. There may also be some minor drainage from the west or northeast, which would explain the presence of the Cambrian – Devonian grains. However, the small population of these grains indicates they are more likely derived from reworking of older Mesozoic clastic sequences, which would indicate very local detritus, and could have been picked up in westerly flowing paleodrainage systems.

The provenance and basin entry points for the Lower Tempest Sandstone are important considerations for reservoir quality within this unit. As mentioned for the Upper Tempest Sandstone, accumulations of coarse-grained, high quality reservoir rocks are more likely to occur in close proximity to sediment supply and basin entry points. Therefore, for the Lower Tempest Sandstone, it is reasonable to expect higher quality reservoir sandstones to be deposited in the east with decreasing reservoir quality towards the west (Figure 7.6). This may be important for future exploration and development of the Tempest Sandstones.

7.9.6 - Provenance of Interbedded Sandstone and Mudstone

As discussed in Section 6.8.1, it is of interest to study whether the detrital zircon populations and provenance of interbedded mudstones and sandstones is the same. The samples from Baccalieu I-78 from 4142.2m and 4135.29m are locally interbedded mudstone and sandstone samples, respectively. Detrital zircons were analyzed from both of these samples. It is evident that these two units have similar detrital zircon populations with a predominance of late Neoproterozoic and >1 Ga grains. In addition to having similar ages, the zircon grains found in both samples possess similar characteristics in terms of their morphology, Th-U ratio, and aspect ratios. The only difference in grain characteristics is the surface area, as zircons found in the sandstone sample tended to be larger than those found in the mudstone sample. This is expected, however, and does not appear to have affected the relative proportions of the age groups of grains.

Evidently, detrital zircons of interbedded mudstone and sandstone pairs from Kimmeridgian rocks offshore Newfoundland indicate similar provenances. This doesn't necessarily mean that the provenance of both sands and muds are the same, but it is evidence that the zircon populations within these interbedded units are alike. This may impact future provenance studies of fine-grained rocks. Working with mudstones is challenging as the sample preparation, heavy mineral separation, and age-dating process are more time consuming and sometimes less effective than in coarse-grained rocks predominantly due to the fine-grain size of the heavy minerals. Where a mudstone succession is interbedded with siltstones and sandstones, it may be possible to focus the sampling on the interbedded siltstones and sandstones, as their detrital zircon populations will likely be similar. This will eliminate the complications involved in working with the finer-grained rocks and may encourage workers to expand their interpretations beyond the coarse-grained reservoir intervals into less studied fine-grained source rocks, and other important shales.

From a geochemical standpoint, the samples from this study possess different signatures in both the major elements and trace elements in mudstones and their associated sandstone pairs. This is shown in Chapter 4 as many of the samples from this study show contrasting signatures. In this study, the reason for the majority of the geochemical variances appear to be predominantly associated with hydraulic sorting within the sandstone beds that does not affect the interbedded mudstones to the same degree. So, it appears that their provenance is mostly the same, but sorting affects the proportions of different minerals, and hence elements, within different lithologies. The analysis of heavy mineral suites and ratios shows a similar result. The provenance of two units may be the same, but because one unit is a sandstone and the other is a mudstone, they may show different results because of hydraulic sorting.

Although the analysis of mudstones and sandstones for this study show a similar provenance, it is important to consider that samples from different tectonic environments and different geological eras may not provide the same results and it remains an important question whether sands and muds have the same ultimate provenance.

7.10 - Conclusions

Detailed analysis from this study of the Upper Jurassic rocks of the Flemish Pass Basin and Central Ridge through a combination of core logging, thin section descriptions, detrital zircon geochronology, whole rock geochemistry, and heavy mineral analysis highlights important provenance characteristics of these units. In addition, this thesis shows that the analysis of fine-grained sedimentary rocks using techniques more common in sandstones, such as detrital zircon geochronology, is feasible and useful for understanding provenance of fine-grained sedimentary rocks. Another important finding includes comparing detrital zircon distributions of interbedded sandstone and mudstone pairs. The detrital zircon signatures in both samples are very similar, indicating that the zircons for these samples are derived from the same source.

The depositional environment is defined by core logging, and observing the sedimentary sturctures of the Upper Jurassic rocks. Based on analysis of cores from the Baccalieu I-78, Panther P-52, and South Tempest G-88 wells, the depositional environment can likely be described as a basinal setting with low oxygen levels, where sediment was derived by turbidity currents. This interpretation is supported by a number of features described in Chapter 3. This turbidite interpretation implies a somewhat different depositional environment for the Kimmeridgian Source Rock unit in the Flemish Pass Basin and Central Ridge, than what is noted in the Jeanne d'Arc Basin in the equivalent Upper Jurassic Egret Member. This may explain some differences noted in the type of oil expelled from the source beds in the Flemish Pass Basin (Creaney & Alison, 1987; Fowler et al. 2007). Information from thin section descriptions was helpful in identifying initial provenance characteristics of the sandstone and siltstone beds such as grain angularity and composition. This information indicated a mixture of both first cycle and recycled grains as a sediment source for the sand- and siltstones. Determining this information from the mudstone beds was much more difficult. Nonetheless, the mineralogy of the mudstone beds identified by the MLA-SEM, particularly the presence of illite, chlorite and muscovite, as well as petrographic observations indicated that a mixture of sources was also likely for these fine-grained rocks.

Whole rock geochemistry was employed on both Upper Jurassic sandstones and mudstones as it is a useful tool for identifying sediment provenance. Both major and trace elements were analyzed; however the trace element diagrams created were most useful in revealing provenance characteristics of the rocks. The samples are interpreted to be derived from a source with an upper crustal signature, commonly seen in passive margins. Sedimentary recycling is interpreted as an important process in these Upper Jurassic samples. Samples from the Upper Kimmeridgian Source Rock, the Lower Kimmeridgian Source Rock as well as the Rankin Formation possess similar characteristics, and thus likely similar source regions. The Lower Tempest Sandstone, however, appears to have a more mafic signature, suggesting a slightly different provenance for this unit.

To supplement interpretations from whole rock geochemistry, heavy mineral ratios were also analyzed in the Upper Jurassic samples from the Flemish Pass Basin and Central Ridge. Heavy mineral ratios are not intended to be used to determine the composition of the source terrane. However, they are useful in identifying a fingerprint for a particular unit or formation. Analyzing heavy mineral ratios from these samples indicates that most of the formations possess a similar provenance fingerprint. This is particularly true for the Upper Kimmeridgian Source Rock, the Lower Kimmeridgian Source Rock, and the Rankin Formation as all heavy mineral ratios within these formations were very comparable. Ratios from the Upper Tempest Sandstone are also similar, with some minor variations likely due to an outlier sample.

In addition to the whole rock geochemistry and heavy mineral ratios, detrital zircon geochronology revealed significant provenance information and were the most important for generating a provenance and paleodrainage model. Samples from the Upper Kimmeridgian Source Rock, Lower Kimmeridgian Source Rock, Rankin Formation, Upper Tempest Sandstone, and Lower Tempest Sandstone were analyzed. Zircon populations from within the Upper Kimmeridgian Source Rock, Lower Kimmeridgian Source Rock, and the Rankin Formation were all similar, with grains likely derived from the Avalon Zone, Central Mobile Belt, and underlying basement. Samples from the Upper Tempest Sandstone and Lower Tempest Sandstone had overall similar detrital zircon populations. However, a significant population of Permian – Carboniferous grains are present in these Tempest Sandstone samples. This suggests derivation from intrusive rocks of Iberia. This change in provenance within the Tempest Sandstones was also noted in the whole rock geochemical analysis in the Lower Tempest Sandstone samples.

In addition to important provenance information, Upper Jurassic detrital zircons helped to constrain the age of the Upper Tempest Sandstone to within the Tithonian. This is particularly useful as conflicting ages exist in the published biostratigraphic interpretations.

By examining the zircon morphologies, Th-U ratios, sizes and aspect ratios, it appears that both first cycle as well as recycled sediments were important in forming all of these Upper Jurassic samples. This is consistent with the whole rock geochemical data.

After examining all datasets, a provenance model for the Late Jurassic of the Central Ridge and Flemish Pass Basin was developed. The Upper Kimmeridgian Source Rock, Lower Kimmeridgian Source Rock and Rankin Formation are all interpreted as being derived from the northeast. Drainage systems at this time may have reached as far northeast as what is currently

Ireland. This type of drainage system implies the thickest package of these units would likely be present in the northeastern regions of the basin.

A considerably different model is proposed for the Tempest Sandstone units. These units are interpreted as being derived from the east. Therefore, the thickest packages of Tempest Sandstones are likely to be found in the eastern regions of the Central Ridge and Flemish Pass Basin.

References Cited

Abbey, S. (1983). Studies in "standard samples" of silicate rocks and minerals 1969-1982. *Canadian Geological Survey Paper 83-15*, 1-114.

Allen, J.R.L. (1982). Structures and sequences related to gravity-current surges. *In* Sedimentary Structures. Their Character and Physical Basis. Elsevier, Amsterdam. 395-431.

Allen, P.A. & Homewood, P. (1986). Foreland basins: an introduction. *In* Foreland Basins. *Edited by* P.A. Allen & P. Homewood. *International Association of Sedimentologists, Special Publication 8*, 3-14.

Alvarez, L.W., Alvarez, W., Asaro, F., Michel, H.V. (1980). Extraterrestrial cause for the Cretaceous-Tertiary Extinction. *Science,* **208**, 1095-1108.

Amoco Canada Petroleum Company Ltd. (1973). Spoonbill C-30 Well History Report.

Andersen, T. (2002). Correction in common lead in U-Pb analyses that do not report ^{204}Pb. *Chemical Geology*, **192**, 59-79.

Arribas, J. & Tortosa, A. (2003). Detrital modes in sedimenticlastic sands from low-order streams in the Iberian Range, Spain; the potential for sand generation by different sedimentary rocks. *Sedimentary Geology*, **159**, 275-303.

Azor, A., Rubatto, D., Simancas, J.F., Gonzalez Lodeiro, F., Martinez Poyatos, D., Martin Parra, L.M. & Matas, J. (2008). Rheic Ocean ophiolitic remnants in southern Iberia questioned by SHRIMP U-Pb zircon ages on the Beja-Acebuches amphibolites. *Tectonics,* **27**, 11 pgs.

Barrs, M.S., Bujak, J.P. & Williams, G.L. (1979). Palynological zonation and correlation of sixty-seven wells, Eastern Canada. *Geological Survey of Canada, Paper No. 78-24*.

Bateman, J.A., (1995). Mineralogical and geochemical traits of the Egret Member oil source rock Kimmeridgian, Jeanne d'Arc Basin, offshore Newfoundland, Canada. MSc. Thesis. Dalhousie University.

Bell, J.S. & Howie, R.D. (1990). Paleozoic Geology. *In* Geology of the Continental Margin of Eastern Canada. *Edited by* M.J. Keen & G.L. Williams, 141-165.

Bevier, M.L. & Barr, S.M. (1990). U-Pb age constraints on the stratigraphy and tectonic history of the Avalon terrane, New Brunswick, Canada. *Journal of Geology,* **58**, 53-63.

Bhatia, M.R. & Crook, K.A.W. (1986). Trace element characteristics of graywackes and tectonic setting discrimination of sedimentary basins. *Contributions to Mineralogy and Petrology,* **92**, 181-193.

Blatt, H. & Christie, J.M. (1963). Undulatory extinction in quartz of igneous and metamorphic rocks and its significance in provenance studies of sedimentary rocks. *Journal of Sedimentary Petrology,* **33**, 559-579.

Boggs, S. (2006) Principles of Sedimentology and Stratigraphy, 4th Edition. 662 pgs.

Bohacs, K.M., Grabowski, G.J., Carroll, A.R., Mankiewicz, P.J., Miskell-Gerhardt, K., Schwalbach, J.R., Wegner, M.B. & Simo, J.A. (2005). Production, destruction and dilution - the many paths to source rock development. *In* The Deposition of Organic-Carbon-Rich sediments: Models, Mechanisms, and Consequences. *Edited by* N. Harris. *SEPM Special Publication*, **82**, 61-101.

BP Exploration Canada Ltd. (1975). Bonavista C-99 Well History Report and Logs.

BP Exploration Canada Ltd. (1979). Hare Bay E-21 Well History Report and Logs.

BP Exploration Canada Ltd. (1991). Biostratigraphic Study of Flemish Pass Wells.

Brown, D.M., McAlpine, K.D., & Yole, R.W. (1989). Sedimentology and sandstone diagenesis of Hibernia Formation in the Hibernia oil field, Grand Banks of Newfoundland. *AAPG Bulletin,* **73,** 5, 557-575.

Bujak Davies Group (1987). Palynological biostratigraphy of the interval 395 – 4203 m, Panther P-52, Grand Banks. GSC Open File Report 1876, 16 pgs.

Capdevila, R. & Mougenot, D. (1988). Pre-Mesozoic basement of the western Iberian continental margin and its place in the Variscan Belt. *Proceedings of the Ocean Drilling Program, Scientific Results*, **103**, 3-12.

Chorlton, L.B. & Dallmeyer, R.D. (1986). Geochronology of early to middle Paleozoic tectonic development in the Southwest Newfoundland Gander Zone. *Journal of Geology*, **94**, 67-89.

Clarke, D.B., MacDonald, M.A., & Tate, M.C. (1997). Late Devonian mafic-felsic magmatism in the Meguma Zone, Nova Scotia. *Memoir – Geological Society of America*, **191**, 107-127.

C-NLOPB (2011). Schedule of Wells – Newfoundland and Labrador offshore area. Baccalieu I-78.

C-NLOPB (2013). Schedule of Wells – Newfoundland and Labrador offshore area. Kyle L-11.

C-NLOPB (2007). Schedule of Wells – Newfoundland and Labrador offshore area. Lancaster G-70, Panther P-52, & South Tempest G-88.

Cody, J., Hunter, D., Schwartz, S., Marshall, J., Haynes, S., Gruschwitz, K., & McDonough, M. (2012). A Late Jurassic play fairway beyond the Jeanne d'Arc Basin: new insights for a petroleum system in the Northern Flemish Pass Basin. *In* 2012 Proceedings: New understanding of the petroleum systems of continental margins of the world, *Edited by* Norman C. Rosen, Paul Weimer, Sylvia Maria Coutes dos Anjos, Sverre Henrickson, Edmundo Marques, Mike Mayall, Richard Fillon, Tony D'Agostino, Art Saller, Kurt Campion, Tim Huang, Rick Sarg, and Fred Schroeder. 32nd Annual Conference, 599-608

Cohen, K.M., Finney, S.C., Gibbard, P.L., & Fan, J.-X. (2013). The ICS International Chronostratigraphic Chart. Episodes 36, 199-204.

Cox, R. & Lowe, D.R. (1995a). A conceptual review of regional-scale controls on the composition of clastic sediment and the co-evolution of continental blocks and their sedimentary cover. *Journal of Sedimentary Research, Section A: Sedimentary Petrology and Processes*, **65**, 1-12.

Cox, R., & Lowe, D.R. (1995b). Compositional evolution of coarse clastic sediments in the Southwestern United States from 1.8 to 0.2 Ga and implications for relationships between the development of crustal blocks and their sedimentary cover. *Journal of Sedimentary Research, Section A: Sedimentary Petrology and Processes,* **65,** 477-494.

Creaney, S., & Allison, B.H. (1987). An organic geochemical model of oil generation in the Avalon/Flemish Pass Sub-basins, East Coast Canada. *Bulletin of Canadian Petroleum Geology,* **35**, 12-23.

Critelli, S., Arribas, J., Le Pera, E., Tortosa, A., Marmaglia, K.M., Marsaglia, K.H. & Latter, K.K. (2003). The recycled orogenic sand provenance from an uplifted thrust belt, Beltic Cordillera, southern Spain. *Journal of Sedimentary Research,* **73**, 72-81.

Cullers, R.L. (1994). The chemical signature of source rocks in size fractions of Holocene stream sediment derived from metamorphic rocks in the wet mountains region, Colorado, USA. *Chem. Geol.,* **113**, 327-343.

Currie, K.L. (1995). Plutonic rocks. *In* Geology of the Appalachian-Caledonian Orogen in Canada and Greenland. *Edited by* H. Williams. 629-680.

Dallmeyer, R.D., Blackwood, R.F. & Odom, A.L. (1981). Age and origin of the Dover Fault; tectonic boundary between the Gander and Avalon zones of the northeastern Newfoundland Appalachians. *Canadian Journal of Earth Sciences*, **18**, 1431-1442.

Daly, J.S., & Flowerdew, M.J. (2005). Grampian and late Grenville events recorded by mineral geochronology near a basement-cover contact in north Mayo, Ireland. *Journal of the Geological Society of London*, **162**, 163-174.

Dearin, A. (2006). Provenance of the Ben Nevis Formation sandstones, White Rose Field, Jeanne d'Arc Basin, Newfoundland, Canada. MSc. Thesis, Memorial University.

Deptuck, M.E., MacRae, R.A., Schimeld, J.W., Williams, G.L., & Fensome, R.A. (2003). Revised Upper Cretaceous and Lower Palaeogene lithostratigraphy and depositional history of the Jeanne d'Arc Basin, offshore Newfoundland, Canada. *AAPG Bulletin,* **87**, 1459-1483.

DeSilva, N. (2000). Flemish Pass Basin: hydrocarbon prospectivity and potential deep water development. *Journal of Canadian Petroleum Technology,* **39**, 22-25

DeSilva, N. (1994). Submarine fans on the northeastern Grand Banks, offshore Newfoundland. GCSSEPM Foundation 15th Annual Research Conference – Submarine Fans and Turbidite Systems, Dec. 4-7, 1994. 95-104.

Dickinson, W.R., Beard, L.S., Brakenridge, G.R., Erjavec, J.L., Ferguson, R.C., Inman, K.F., Knepp, R.A., Lindberg, F.A. & Ryberg, P.T. (1983). Provenance of North American Phanerozoic sandstones in relation to tectonic setting. *GSA Bulletin*, **94**, 222-235.

Dickinson, W.R. & Gehrels, G.E. (2009). Use of U-Pb ages of detrital zircons to infer maximum depositional ages of strata: A test against a Colorado Plateau Mesozoic database. *Earth and Planetary Science Letters,* **288**, 115-125.

Dickinson, W.R. & Suczek, C.A. (1979). Plate tectonics and sandstone compositions. *AAPG Bulletin*, **63**, 2164-2182.

Dickinson, W.R. & Valloni, R. (1980). Plate settings and provenance of sands in modern ocean basins. *Geology*, **8**, 82-86.

Dickson, W.L. (1990). Geology of the North Bay Granite Suite and metasedimentary rocks in southern Newfoundland (NTS 11P/15E, 11P/16 and 12A/2E). Report – Government of Newfoundland and Labrador Dept. of Mines and Energy, Geological Survey.

D’Lemos, R.S., Schofield, D.I., Holdsworth, R.E., & King, T.R. (1997). Deep crustal and local rheological controls on the siting and reactivation of fault and shear zones, northeastern Newfoundland. *Journal of the Geological Society,* **154,** 117-121.

Dodson, M.H., Compston, W., Williams, I.S., Wilson, J.F. (1988). A search for ancient detrital zircons in Zimbabwean sediments. *J. Geol. Soc. (London),* **145**, 977-983.

Driscoll, N.W., & Hogg, J.R. (1995). Stratigraphic response to basin formation: Jeanne d'Arc Basin, offshore Newfoundland. *In* Hydrocarbon Habitat in Rift Basins. *Edited by* J.J Lambiase. *Geological Society of London Special Publication 80,* 145-163.

Dube, B., Dunning, G.R., Lauziere, K. & Roddick, J.C. (1996). New insights into the Appalachian Orogen from geology and geochronology along the Cape Ray fault zone, southwest Newfoundland. *GSA Bulletin*, **108**, 101-116.

Enachescu, M.E., Harding, S.C. & Emery, D.J. (1994). Three-dimensional seismic imaging of a Jurassic paleodrainage system. *26th Annual Offshore Technology Conference*, 179-191.

Enachescu, M.E. (2012). Call for Bids NL12-02, Parcel 1, Petroleum Exploration Opportunities in the Flemish Pass Basin, Government of Newfoundland and Labrador Department of Natural Resources.

Enachescu, M.E. (1988). Extended basement beneath the intracratonic rifted basins of the grand banks of Newfoundland. *Canadian Journal of Exploration Geophysics*, **24**, 48-65

Enachescu, M.E. (2006). Newfoundland and Labrador Call for Bids NL06-01, Jeanne d'Arc Basin.

Enachescu, M.E. & Hogg, J.R. (2005). Exploring for Atlantic Canada's next giant petroleum discovery, *CSEG Recorder,* **30**, 5, 19-30.

Enachescu, M.E. (2014). Petroleum exploration opportunities in the Flemish Pass Basin, Newfoundland and Labrador offshore area; Call for Bids NL13-01, Area "C" – Flemish Pass Basin, Parcel 1. Government of Newfoundland Department of Natural Resources.

Enachescu, M.E., Smee, G.W., Meehan, P.J., Hodder, J., Deutsch, K., Emery, D. (2000). White Rose oil field, offshore Newfoundland; from teaser to trophy. *In* American Association of Petroleum Geologists 2000 annual meeting. Annual Meeting Expanded Abstracts. American Association of Petroleum Geologists 2000. P. 138

Enachescu, M.E. (1987). Tectonic and structural framework of the northeast Newfoundland continental margin. *In* Sedimentary Basins and Basin Forming Mechanisms. *Edited by* C. Beaumont and A.J. Tankard. *Canadian Society of Petroleum Geologists*, 117-146.

Esso Resources Canada Ltd. (1986). Esso Parex et al. Baccalieu I-78 well history reports and logs.

Falvey, D.A. (1974). The Development of continental margins in plate tectonic theory. *Journal of Australian Petroleum Exploration Association,* **14**, 95-106.

Fedo, C.M., Nesbitt, W.H. & Young, G.M. (1995). Unraveling the effects of potassium metasomatism in sedimentary rocks and paleosols, with implications for paleoweathering conditions and provenance. *Geology*, **23**, 10, 921-924.

Fedo, C.M. Sircombe, K.N. & Rainbird, R.H. (2003). Detrital zircon analysis of the sedimentary record. *In* Zircon: Experiments, Isotopes, and Trace Element Investigations. *Edited by* J.M. Hanchar & P.Hoskin. *Mineralogical Society of America, Reviews in Mineralogy,* **53**, 277-303.

Feely, M., Coleman, D., Baxter, S. & Miller, B. (2004). U-Pb zircon geochronology of the Galway Granite, Connemara, Ireland: implications for the timing of late Caledonian tectonic and magmatic events and for correlations with Acadian plutonism in New England. *Atlantic Geology,* **39**, 175-184.

Flowerdew, M.J., Daly, J.S. & Whitehouse, M.J. (2005). 470 Ma granitoid magmatism associated with the Grampian Orogeny in the Slishwood Division, NW Ireland. *Journal of the Geological Society of London*, **162**, 563-575.

Fowler, M.G. & McAlpine, K.D. (1994). The Egret Member, a prolific Kimmeridgian source rock from offshore Eastern Canada. *In* Petroleum Source Rocks. *Edited by* B.J. Katz. 111-130.

Fowler, M.G., Obermajer, M., Achal, S., Milovic, M. (2007). Results of geochemical analyses of an oil sample from Mizzen L-11 well, Flemish Pass, offshore Eastern Canada. *Geological Survey of Canada,* Open File 5342*,* 3 p.

Foster, D.G. & Robinson, A.G. (1993). Geological history of the Flemish Pass Basin, offshore Newfoundland. *AAPG Bulletin*, **77**, 588-609.

Fralick, P.W. (2003). Geochemistry of clastic sedimentary rocks: ratio techniques. *In* Geochemistry of Sediments and Sedimentary Rocks: Evolutionary Considerations to Mineral Deposit-Forming Environments. *Edited by* D.R. Lentz. Geological Association of Canada, GeoText 4, 85-103.

Gladney, E.S. & Roelandts, I. (1988). 1987 Compilation of elemental concentration data for USGS BHVO-1, MAG-1, QLO-1, RGM-1, SCo-1, SDC-1, SGR-1, and STM-1. *Geostandards Newsletter,* **12**, 253-362.

Govindaraju, K. (1994). 1994 compilation of working values and descriptions for 383 geostandards. *Geostandards Newsletter,* **18**, 1-158.

Gradstein, F.M., Jansa, L.F., Srivastava, S.P., Williamson, M.A., Bonham-Carter, G. & Stam, B. (1990). Aspects of North Atlantic paleo-oceanography, Chapter 8. *In* Geology of the Continental Margin of Eastern Canada. *Edited by* M.J. Keen & G.L. Williams. Geological Survey of Canada, Geology of Canada, no. 2, 353-389.

Hallsworth, C.R., Morton, A.C., Claoue-Long, J. & Fanning, C.M. (2000). Carboniferous sand provenance in the Pennine Basin, UK; constraints from heavy mineral and detrital zircon age data. *Sedimentary Geology*, **137**, 147-185.

Haworth, R.T. & Lefort, J.P. (1979). Geophysical evidence for the extent of the Avalon zone in Atlantic Canada. *Canadian Journal of Earth Sciences,* **16**, 552-567.

Heaman, L.M., Erdmer, P. & Owen, J.V. (2002). U-Pb geochronological constraints on the crustal evolution of the Long Range Inlier, Newfoundland. *Canadian Journal of Earth Sciences,* **39**, 845-865.

Helwig, J., Aronson, J. & Day, D.S. (1974). A late Jurassic mafic pluton in Newfoundland. *Canadian Journal of Earth Sciences,* **11**, 1314-1319.

Hiscott, R.N., Marsaglia, K.M., Wilson, R.C.L., Robertson, A.H.F., Karner, G.D., Tucholke, B.E., Pletsch, T. & Petschick, R. (2008). Detrital sources and sediment delivery to the early post-rift (Albian-Cenomanian) Newfoundland Basin east of the Grand Banks: results from ODP Leg 210. *Bulletin of Canadian Petroleum Geology*, **56**, 69-92.

Hodych, J.P. & Hayatsu, A. (1980). K-Ar isochron age and paleomagnetism of diabase along the trans-Avalon aeromagnetic lineament – evidence of late Triassic rifting in Newfoundland. *Canadian Journal of Earth Sciences*, **17**, 491-499.

Hoskin, P.W.O. & Schaltegger, U. (2003). The composition of zircon and igneous and metamorphic petrogenesis. *Reviews in Mineralogy and Geochemistry,* **53**, 27-62.

Huang, Z., Williamson, M.A., Bateman, J., McAlpine, K.D. & Fowler, M.G. (2007). Cyclicity in the Egret Member (Kimmeridgian) oil source rock, Jeanne d'Arc Basin, offshore eastern Canada. *Marine and Petroleum Geology,* **13**, 91-105.

Hubbard, R.J. (1988). Age and significance of sequence boundaries on Jurassic and early Cretaceous rifted continental margins. *AAPG Bulletin,* **72**, 49-72.

Hubert, J.F. (1962). A zircon-tourmaline-rutile maturity index and the interdependence of the composition of heavy mineral assemblages with the gross composition and texture of sandstones. *Journal of Sedimentary Petrology*, **32**, 440-450.

Hurst, A. & Morton, A.C. (2001). Generic relationships in the mineral-chemical stratigraphy of turbidite sandstones. *Journal of the Geological Society of London.* **158**, 401-404.

Hurst, A. (1981). Mid Jurassic stratigraphy and facies at Brora, Sutherland. *Scot. J. Geol.,* **17**, 169-177.

Hutchinson, D.R., Klitgord, K.D., Lee, M.W. & Trehu, A.M. (1988). U.S. Geological Survey deep seismic reflection profile across the Gulf of Maine. *Geological Society of America Bulletin,* **100**, 172-184.

Ingall, E.D., Bustin, R.M., Van Cappellen, P. (1993). Influence of water column anoxia on the burial and preservation of carbon and phosphorous in marine shales. *Geochimica et Cosmochimica Acta*, **57**, 2, 303-316.

Jansa, L.F. & Pe-Piper, G. (1986). Geology and geochemistry of Middle Jurassic and Early Cretaceous igneous rocks on the eastern North American continental shelf. Open File Report 1351 – Geological Survey of Canada.

Jansa, L.F. & Pe-Piper, G. (1988). Middle Jurassic to Early Cretaceous igneous rocks along eastern North American continental margin. *AAPG Bulletin*, **72**, 347-366.

Jansa, L.F. & Wade, J.A. (1975). Geology of the continental margin off Nova Scotia and Newfoundland. *In* Offshore Geology of Eastern Canada. *Edited by* W.J.M. van der Linden & J.A. Wade. Geological Survey of Canada. Paper 74-30, 51-106.

Jenkins, W.A.M. (1986). Palynology of the Lancaster F-70 (G-70) well. Flemish Pass, offshore Newfoundland. Associated Biostratigraphic Consultants, Calgary. December, 1986.

Jenner, G.A., Longerich, H.P., Jackson, S.E. & Freyer, B.J. (1990). ICP-MS – a powerful tool for high precision trace element analyses in earth sciences: evidence from analyses of selected U.S.G.S. reference samples. *Chemical Geology*, **83**, 105-118.

Jesus, A.P., Munha, J., Mateus, A., Tassinari, C. & Nutman, A.P. (2007). The Beja Layered Gabbroic Sequence (Ossa-Morena Zone, southern Portugal): geochronology and geodynamic implications. *Geodinamica Acta,* **20**, 139-157.

Johnson, H., Ritchie, J.D., Gatliff, R.W., Williamson, J.P., Cavill, J. & Bulat, J. (2001). Aspects of the structure of the Porcupine and Porcupine Seabight basins as revealed from gravity modeling of regional seismic transects. *In* Mesozoic successions of the Porcupine and North Porcupine basins, offshore Ireland. The petroleum exploration of Ireland's offshore basins. *Edited by* P.M. Shannon, P.D.W. Haughton & D.V. Corcoran. *Geological Society Special Publications*, **188**, 265-274.

Jones, D.G., & Plant, J.A. (1989). Geochemistry of shales. *In* Mettalogenic models and exploration criteria for buried carbonate-hosted ore deposits – a multidisciplinary study in Eastern England. *Edited by* J.A. Plant & D.G. Jones. British Geological Survey, Keyworth, Nottingham and Institution of Mining and Mettalurgy, London, 65-94.

Kane, J.S., Arbogast, B. & Leventhal, J. (1990). Characterization of Devonian Ohio Shale SDO-1 as a USGS Geochemical Reference Sample. *Geostandards Newsletter,* **14**, 169-196.

Keen, C.E., Boutilier, R., de Voogd, B., Mudford, B., & Enachescu, M.E. (1987). Crustal geometry and extensional models for the Grand Banks of eastern Canada: constraints from deep seismic reflection data. *In* Sedimentary Basins and Basin Forming Mechanisms. *Edited by* C. Beaumont and A.J. Tankard. *Canadian Society of Petroleum Geologists*, 101-115.

Keen, C.E., Kay, W.A., Keppie, D., Marillier, F., Pe-Piper, G. & Waldron, J.W.F. (1991). Deep seismic reflection data from the Bay of Fundy and Gulf of Maine: Tectonic implications for the northern Appalachians. *Canadian Journal of Earth Sciences*, **28**, 1096-1111.

Keppie, J.D., & Krogh, T.E. (2000). 440 Ma igneous activity in the Meguma terrane, Nova Scotia, Canada: part of the Appalachian over-step sequence? *American Journal of Science,* **300**, 528-538.

Kerr, A., Dunning, G.R. & Tucker, R.D. (1993). The youngest Paleozoic plutonism in the Newfoundland Appalachians: U-Pb ages from the St. Lawrence and Francois granites. *Canadian Journal of Earth Sciences,* **30**, 2328-2333.

Kerr, A., Jenner, G.A. & Fryer, B.J. (1995). Sm-Nd isotopic geochemistry of Precambrian to Paleozoic granitoid suites and the deep-crustal structure of the southeast margin of the Newfoundland Appalachians. *Canadian Journal of Earth Sciences*, **32**, 224-245.

Ketchum, J. W., Jackson, S. E., Culshaw, N. G., & Barr, S. M. (2001). Depositional and tectonic setting of the Paleoproterozoic Lower Aillik Group, Makkovik Province, Canada: evolution of a passive margin-foredeep sequence based on petrochemistry and U–Pb (TIMS and LAM-ICP-MS) geochronology. *Precambrian Research*, **105**(2), 331-356.

King, A.F. (1990) Geology of the St. John's Area. *Newfoundland Department of Mines, Mineral Development Division,* Report 90-2, 88pp.

King, A.F. (1988) Late Precambrian sedimentation and related orogenesis of the Avalon Peninsula, Eastern Avalon Zone. *GAC, 1988 St. John's, Field Trip Guidebook,* A4, 1-84.

King, L.H., Fader, G.B., Jenkins, W.A.M., & King, E.L. (1986). Occurrence and regional geological setting of Paleozoic rocks on the Grand Banks of Newfoundland. *Canadian Journal of Earth Sciences,* **23**, 504-526

King, L.H., Fader, G.B., Poole, W.H., & Wanless, R.K. (1985). Geological setting and age of the Flemish Cap granodiorite, east of the grand banks of Newfoundland. *Canadian Journal of Earth Sciences,* **22**, 1286-1298.

Kontak, D.J., Ham, L.J., & Dunning, G. (2004). U-Pb dating of the Musquodoboit Batholith, southern Nova Scotia; evidence for a protracted magmatic-hydrothermal event in a Devonian intrusion. *Atlantic Geology*, **40**, 207-216.

Kosler, J. & Sylvester, P.J. (2003). Present trends and the future of zircon in geochronology; laser ablation ICPMS. *In* Zircon. *Edited by* J.M. Hanchar & P.W.O. Hoskin. *Reviews in Mineralogy and Geochemistry*, **53**, 243-275.

Kreuger Enterprises, Inc. (1972). Amoco-Imperial Jaeger A-49, K-Ar age determination of granite at 3040 feet.

Krogh, T.E. (1982). Improved accuracy of U-Pb zircon dating by selection of more concordant fractions using a high gradient magnetic separation technique. *Geochemica et Cosmochimica Acta*, **46**, 631-635.

Krogh, T.E. & Keppie, J.D. (1990). Age of detrital zircon and titanite in the Meguma Group, southern Nova Scotia, Canada; clues to the origin of the Meguma Terrane, *Tectonophysics,* **177**, 307-323.

Krogh, T.E., Strong, D.F., O'Brien, S.J. & Papezik, V.S. (1987). Precise U-Pb zircon dates from the Avalon Terrane in Newfoundland. *Canadian Journal of Earth Sciences*, **25**, 442-453.

Leventhal, J.S. (1983). An interpretation of carbon and sulfur relationships in Black Sea sediments as indicators of environments of deposition. *Geochimica et Cosmochimica Acta*, **47**, 133-137.

Lilly, H.D. (1966). Submarine surveys on the Great Bank of Newfoundland and in the Gulf of Saint Lawrence. *Maritime Sediments*, **2**, 12-14.

Lowe, D.G. (2009). Provenance and paleodrainage of Late Jurassic and Early Cretaceous reservoir sandstones in the Flemish Pass and Orphan Basins. MSc. Thesis, Memorial University.

Lowe, D.G., Sylvester, P.J., Enachescu, M.E. (2011). Provenance and paleodrainage patterns of Upper Jurassic and Lower Cretaceous synrift sandstones in the Flemish Pass Basin, offshore Newfoundland, east coast of Canada. *AAPG Bulletin,* **95**, 1295-1320.

Ludwig K.R. (2012) User's manual for Isoplot 3.75: A geochronological toolkit for Microsoft Excel. Berkeley Geochronology Center Special Publication No. 5. http://www.bgc.org/isoplot_etc/isoplot/Isoplot3_75-4_15manual.pdf.

MacDonald, L.A., Barr, S.M., White, C.E., & Ketchum, J.W.F. (2002). Petrology, age, and tectonic setting of the White Rock Formation, Meguma terrane, Nova Scotia: Evidence for Silurian continental rifting. *Canadian Journal of Earth Sciences,* **39**, 259-277.

Maclean, W.H. (1990). Mass change calculations in altered rock series. *Mineralium Deposita*, **25**, 44-49.

Macquaker, J.H.S. & Adams, A.E. (2003). Maximizing information from fine-grained sedimentary rocks: an inclusive nomenclature for mudstones. *Journal of Sedimentary Research*, **73**, 5, 735-744.

Magoon, L.B., Hudson, T.L., Peters, K.E. (2005). Egret-Hibernia(!), a significant petroleum system, northern Grand Banks area, offshore eastern Canada. *AAPG Bulletin,* **89**, 9, 1203-1237.

Martel, A.T., McGregor, D.C., & Utting, J. (1993). Stratigraphic significance of Upper Devonian and Lower Carboniferous miospores from the type area of the Horton Group, Nova Scotia. *Canadian Journal of Earth Sciences*, **30**, 1091-1098.

McAlpine, K.D. (1989). Lithostratigraphy of fifty-nine wells, Jeanne d'Arc Basin. Open File Report – Geological Survey of Canada.

McAlpine, K.D. (1990). Mesozoic stratigraphy, sedimentary evolution, and petroleum potential of the Jeanne d'Arc basin, Grand Banks of Newfoundland. Geological Survey of Canada Paper 89-17, 50 p.

McCarthy, K., Rojas, K., Niemann, M., Palmowski, D., Peters, K., Stankiewicz, A. (2011). Basic Petroleum Geochemistry for Source Rock Evaluation. *Oilfield Review,* **23**, 2, 32-43.

McDonough, M. (2014). Paradigm Shift in East Coast Canada: The Lightening of Flemish Pass Oil. Abstract from Playmaker Forum, Calgary, Alberta, May 2014.

McCracken, J.N., Haager, A., Saunders, K.I., Veilleux, B.W. (2000). Late Jurassic source rocks in the northern Flemish Pass Basin, Grand Banks of Newfoundland. (2000). Proceedings of GeoCanada 2000; the millennium geoscience summit. Abstract Volum, Geoscience Association of Canada, Vol. 25.

McLennan, S.M., Bock, B., Hemming, S.R., Hurowitz, J.A., Lev, S.M. & McDaniel, D.K. (2003). The roles of provenance and sedimentary processes in the geochemistry of sedimentary rocks. *In* Geochemistry of Sediments and Sedimentary Rocks: Evolutionary Considerations to Mineral Deposit-Forming Environments. *Edited by* D.R. Lentz. Geological Association of Canada, GeoText 4, 7-38.

McLennan, S.M., Taylor, S.R., McCulloch, M.T. & Maynard, J.B. (1990). Geochemical and Nd-Sr isotopic composition of deep-sea turbidites: crustal evolution of and plate tectonic associations. *Geochemica et Cosmochimica Acta*, **59**, 1153-1177.

Milliken, K.L. (1988). Loss of provenance information through subsurface diagenesis in Plio-Pleistocene sandstones, northern Gulf of Mexico, *Journal of Sedimentary Petrology*, **58**, 992-1002.

Morad, S. (1986). SEM study of authigenic rutile, anatase and brookite in Proterozoic sandstones from Sweden. *Sedimentary Geology,* **46**, 77-89.

Morton, A.C. (1979). Depth control of intrastratal solution of heavy minerals from the Palaeocene of the North Sea. *Journal of Sedimentary Petrology*, **49**, 281-286.

Morton, A.C. & Hallsworth, C.R. (1994). Identifying provenance-specific features of detrital heavy mineral assemblages in sandstones. *Sedimentary Geology*, **90**, 241-256.

Morton, A.C. & Hallsworth, C.R. (1999). Processes controlling the composition of heavy mineral assemblages in sandstones. *Sedimentary Geology,* **124**, 3-29.

Morton, A.C. & Hurst, A. (1995). Correlation of sandstones using heavy minerals: an example from the Statfjord Formation of the Snorre Field, northern North Sea. *In* Dating and Correlating Biostratigraphically-barren strata. *Edited by* R.E. Dunay & E. Hailwood. *Geological Society of London, Special Publication,* **89**, 3-22.

Morton, A.C., Knox, W.R. & Hallsworth, C. (2002). Correlation of reservoir sandstones using quantitative heavy mineral analysis. *Petroleum Geoscience,* **8**, 251-262.

Morton, A.C., Whitham, A.G. & Fanning, C.M. (2005). Provenance of Late Cretaceous to Paleocene submarine fan sandstones in the Norweigan Sea; integration of heavy mineral, mineral chemical and zircon age data. *Sedimentary Geology,* **182**, 3-28.

Murphy, J.B. & Hamilton, M.A. (2000). Orogenesis and basin development; U-Pb detrital zircon age constraints on evolution of the late Paleozoic St. Mary's Basin, central mainland Nova Scotia. *Journal of Geology*, **108**, 53-71.

Murphy, J.B., Keppie, J.D., Dostal, J. & Cousins, B.L. (1996). Repeated late Neoproterozoic-Silurian lower crustal melting beneath the Antigonish Highlands, Nova Scotia: Nd isotopic evidence and tectonic interpretations. *In* Avalonian and Related Peri-Gondwanan Terranes of the Circum-North Atlantic. *Edited by* R.D. Nance & M.D. Thompson. *Geological Society of America, Special Papers,* **304**, 109-120.

Nesbitt, H.W. & Young, G.M. (1982). Early Proterozoic climates and plate motions inferred from major element chemistry of lutites. *Nature,* **299**, 715-717.

Nesbitt, H.W., Young, G.M., McLennan, S.M. & Keayes, R.R. (1996). Effects of chemical weathering and sorting on the petrogenesis of siliciclastic sediments with implications for provenance studies. *Journal of Geology*, **104**, 525-542.

Nesbitt, H.W. (2003). Petrogenesis of siliciclastic sediments and sedimentary rocks. *In* Geochemistry of Sediments and Sedimentary Rocks: Evolutionary Considerations to Mineral Deposit-Forming Environments. *Edited by* D.R. Lentz. Geological Association of Canada, GeoText 4, 39-51.

Newfoundland and Labrador Department of Mines and Energy (2003). C-NOPB request for bids NF-03-01 Parcels 13-14 Flemish Pass Basin.

Norry, M.J., Dunham, A.C., & Hudson, J.D. (1994). Mineralogy and geochemistry of the Peterborough Member, Oxford Clay Formation, Jurassic, UK: element fractionation during mudrock sedimentation. *Journal of the Geological Society, London,* **151**, 195-207.

O'Brien, S.J., O'Brien, B.H., Dunning, G.R. & Tucker, R.D. (1996). Late Neoproterozoic Avalonian and related peri-Gondwanan rocks of the Newfoundland Appalachians. *In* Avalonian and Related peri-Gondwanan Terranes of the Circum-North Atlantic. *Edited by* Nance, R.D. & Thompson, M.D. *Geological Society of America, Special Papers*, **304**, 9-28.

O'Brien, S.J., Wardle, R.J., & King, A.F. (1983). The Avalon Zone: A Pan-African terrane in the Appalachian Orogen in Canada. *Geological Journal*, **18,** 195-222.

O'Neill, P.P. (1991). Geology of Weir's Pond Area, Newfoundland (NTS 2E/1). Report 91-3 Government of Newfoundland and Labrador Dept. of Mines and Energy, Geological Survey.

Oszczypko, N. & Salata, D. (2005). Provenance analyses of the Late Cretaceous-Paleocene deposits of the Magura Basin (Polish Western Carpathians) – evidence from a study of the heavy minerals. *Acta Geologica Polonica*, **55**, 237-267.

Paton, C., Hellstrom, J., Paul, B., Woodhead, J and Hergt, J (2011) Iolite: Freeware for the visualisation and processing of mass spectrometer data. *Journal of Analytical Atomic Spectrometry*, **26**, 2508-2518.

Pe-Piper, G. & Jansa, L.F. (1999). Pre-mesozoic basement rocks offshore Nova Scotia, Canada: New constraints on the accretion history of the Meguma terrane. *Geological Society of America Bulletin,* **111**, 1773-1791.

Pe-Piper, G. & Weir-Murphy, S. (2008). Early diagenesis of inner-shelf phosphorite and iron-silicate minerals, Lower Cretaceous of the Orpheus Graben, southeastern Canada; implications for the origin of chlorite rims. *AAPG Bulletin*, **92**, 1153-1168.

Pe-Piper, G., Karim, A. & Piper, D.J.W. (2011). Authigenesis of titania minerals and the mobility of Ti: new evidence from pro-deltaic sandstones, Cretaceous Scotian Basin, Canada. *Journal of Sedimentary Research,* **81**, 762-773.

Petrus, J.A. & Kamber, B.S. (2012). VizualAge: A novel approach to laser ablation ICP-MS U-Pb geochronology data reduction. *Geostandards and Geoanalytical Research,* **36**, 247-270.

Pettijohn, F.J. (1975). Sedimentary rocks. Harper & Row, Publ., New York, N.Y., United States, 628 p.

Pinheiro, L., Wilson, R., Reis, R.P., Whitmarsh, R., Ribeiro, A. (1996). The western Iberia margin: a geophysical and geological overview. *Proc.Ocean Drill Program Sci. Res.,***149**, 3-23.

Piper, D.J.W., Pe-Piper, G., Tubrett, M., Triantafyllidis, S. & Strathdee, G. (2012). Detrital zircon geochronology and polycyclic sediment sources, Upper Jurassic – Lower Cretaceous of the Scotian Basin, southeastern Canada. *Canadian Journal of Earth Sciences,* **49**, 1540-1557.

Pollock, J.C., Wilton, D.H.C., van Staal, C.R. & Morrissey, K.D. (2007). U-Pb detrital zircon geochronological constraints on the Early Silurian collision of Ganderia and Laurentia along the Dog Bay Line; the terminal Iapetan suture in the Newfoundland Appalachians. *American Journal of Science*, **307**, 399-433.

Pollock, J.C., Hibbard, J.P., Sylvester, P.J. (2009). Early Ordovician rifting of Avalonia and birth of the Rheic Ocean: U-Pb detrital zircon constraints from Newfoundland. *Journal of the Geological Society,* London, **166,** pp. 501-515.

Potter, P.E., Maynard, J.B. & Depetris, P.J. (2005). Mud and Mudstones: Introduction and Overview. *Springer-Verlag Berlin Heidelberg New York.* 304 pgs.

Priem, H.N.A. & den Tex, E. (1984). Tracing crustal evolution in the NW Iberian Peninsula through the Rb-Sr and U-Pb systematics of Paleozoic granitoids; a review. *Physics of the Earth and Planetary Interiors*, **35**, 121-130.

Rast, N., Kennedy, M.J., & Blackwood, R.F. (1976). Comparison of some tectonostratigraphic zones in the Appalachians of Newfoundland and New Brunswick. *Can. J. Earth Sci.,* **13,** 868-875.

Rast, N. (1980). The Avalonian plate in the Northern Appalachians and Caledonides. *In* The Caledonides in the U.S.A. *Edited by* D.R. Wones. International Geologic Correlation Program Project 27 – Caledonide Orogen, 1979 Meeting, Blacksburg, Virginia: Virginia Polytechnic Institute and State University Memoir 2, p. 63-66.

Riediger, C, & Bloch, J. (1995). Depositional and diagenetic controls on source rock characteristics of the Lower Jurassic Nordegg Member, western Canada. *Journal of Sedimentary Research,* **65**, 1, 112-126.

Robertson Research International Ltd. (2004). Palynology (2650-4205 m) and micropaleontology (2635–4210 m), Panther P-52 biostratigraphy report.

Robertson Research International Ltd. (2002). Stratigraphic correlation of Baccalieu I-78, Gabriel C-60, Lancaster G-70, and South Tempest G-88 wells. Robertson Research International Limited Report Number 6268.

Romeo, I., Capote, R., Tejero, R., Lunar, R. & Quesada, C. (2006). Magma emplacement in transpression; the Santa Olalla igneous complex (Ossa-Morena Zone, SW Iberia). *Journal of Structural Geology*, **28**, 1821-1834.

Rubey, W.W. (1933). The size distribution of heavy minerals within a water-laid sandstone. *Journal of Sedimentary Petrology,* **3**, 3-29.

Schenk, P.E. (1997). Sequence stratigraphy and provenance on Gondwana's margin: The Meguma zone (Cambrian to Devonian) of Nova Scotia, Canada. *Geological Society America Bulletin,* **109**, 395-409.

Sinclair, I.K. (1988). Evolution of Mesozoic-Cenozoic sedimentary basins in the Grand Banks area of Newfoundland and comparison with Flavy's (1974) rift model. *Bulletin of Canadian Petroleum Geology,* **34**, 3, 255-273.

Sinclair, I.K. (1993). Tectonism: the dominant factor in mid-Cretaceous deposition in the Jeanne d'Arc Basin, Grand Banks. *Marine and Petroleum Geology*, **10**, 530-549.

Sláma, J., Košler, J., Condon, D.J., Crowley, J.L., Gerdes, A., Hanchar, J.M., Horstwood, M.S., Morris, G.A., Nasdala, L., Norberg, N. and Schaltegger, U. (2008). Plešovice zircon—a new natural reference material for U–Pb and Hf isotopic microanalysis. *Chemical Geology*, **249**(1), 1-35.

Smale, D. & Morton, A.C. (1987). Heavy mineral suites of core samples from the McKee Formation (Eocene-lower Oligocene), Taranaki; implications for provenance and diagenesis. *New Zealand Journal of Geology and Geophysics,* **30**, 299-306.

Smith, J. & Higgs, K.T. (2001). Provenance implications of reworked palynomorphs in Mesozoic successions of the Porcupine and North Porcupine basins, offshore Ireland. *In* Mesozoic successions of the Porcupine and North Porcupine basins, offshore Ireland. The petroleum exploration of Ireland's offshore basins. *Edited by* P.M. Shannon, P.D.W. Haughton & D.V. Corcoran. *Geological Society Special Publications*, **188**, 291-300.

Sola, A.R., Pereira, M.F., Williams, I.S., Ribeiro, M.L., Neiva, A.M.R., Montero, P., Bea, F. & Zinger, T. (2008). New insights from U-Pb zircon dating of Early Ordovician magmatism on the northern Gondwana margin; the Urra Formation (SW Iberian Massif, Portugal). *Tectonophysics*, **461**, 114-129.

Stern, R.J. & Bloomer, B.S.H. (1992). Subduction zone infancy: examples from the Eocene Izu-Bonin-Mariana and Jurassic California arcs: *Geological Society of America Bulletin*, **104**, 1621-1636.

Stern, R. A., Bodorkos, S., Kamo, S. L., Hickman, A. H., & Corfu, F. (2009). Measurement of SIMS instrumental mass fractionation of Pb isotopes during zircon dating. *Geostandards and Geoanalytical Research*, **33**(2), 145-168.

Suttner, L.J., Basu, A. & Mack, G.H. (1981). Climate and origin of quartz arenites. *Journal of Sedimentary Petrology*, **51**, 1235-1246.

Sutton, S.J. & Maynard, J.B. (1996). Basement unconformity control on alteration, St. Francois Mountains, SE Missouri. *J. Geol.*, **104**, 55-70.

Swinden, H.S., & Hunt, P.A. (1991). A U-Pb zircon age from the Connaigre Bay Group, southwestern Avalon Zone, Newfoundland: Implications for regional correlations and metallogenesis. *In: Radiometric Age and Isotopic Studies, Report 4.* Geological Survey of Canada, **90-2**, 3-10.

Sylvester, P.J. (2012). Mineralogy and provenance of Carboniferous sandstone and shale units in the Deer Lake and Bay St. George Basins, western Newfoundland. Government of Newfoundland and Labrador, PEEP (Petroleum Exploration Enhancement Project) Workshop Presentation 2012.

Sylvester, P.J. (2012). Use of the Mineral Liberation Analyzer (MLA) for mineralogical studies of sediments and sedimentary rocks. *Mineralogical Association of Canada Short Course 42*, St. John's, NL, May 2012, 1-16.

Tankard, A.J. & Balkwill, H.R. (1989). Extensional tectonics and stratigraphy of the North Atlantic margins: introduction. *In* Extensional tectonics and stratigraphy of the North Atlantic margins. *Edited by* A.J. Tankard & H.R. Balkwill. *AAPG Memoir 46*, 7-22.

Tankard, A.J. & Welsink, H.J. (1987). Extensional tectonics and stratigraphy of the Hibernia oil field, Grand Banks, Newfoundland. *AAPG Bulletin*, **71**, 1210-1232

Tankard, A.J., Welsink, H.J., & Jenkins, W.A.M. (1989). Structural styles and stratigraphy of the Jeanne d'Arc Basin, Grand Banks of Newfoundland. *In* Extensional Tectonics and Stratigraphy of the North Atlantic Margins. *Edited by* Tankard, A.J. and Balkwill, H.R. *AAPG Bulletin,* Memoir 46, 265-282.

Tate, M.P. & Dobson, M.R. (1988). Syn- and post-rift igneous activity in the Porcupine Seabight Basin and adjacent continental margin W of Ireland. Geological Society Special Publications, **39**, 309-334.

Taylor, S.R. & McLennan, S.M. (1985). The continental crust: its composition and evolution. *Blackwell Scientific Publication, Carlton,* 312 pgs.

Totten, M.W. & Hanan, M.A. (2007). Heavy minerals in shales. *In* Heavy Minerals in Use, Developments in Sedimentology. *Edited by* M.A. Mange & D. Wright. **58**, 323-341.

Totten, M.W. & Hanan, M.A. (1998). The accessory mineral fraction of mudrocks and its significance for whole-rock trace-element geochemistry. *In* Shales and Mudstones. Petrography, Petrophysics, Geochemistry and Economic Geology. *Edited by* J. Schieber & W. Zimmerle. Vol. 2, Schweizerbart, Stuttgart, 35-53.

Tucholke, B.E., Austin, J.A. Jr., & Uchupi, E. (1989). Crustal structure and rift-drift evolution of the Newfoundland basin. *In* Extensional Tectonics and Stratigraphy of the North Atlantic Margins. *Edited by* Tankard, A.J. and Balkwill, H.R. *AAPG Bulletin,* Memoir 46, 265-282.

Valverde-Vaquero, P. & Dunning, G.R. (2000). New U-Pb ages for Early Ordovician magmatism in Central Spain. *Journal of the Geological Society of London,* **157**, 15-26.

Valverde-Vaquero, P., van Staal, C.R., van der Velden, A. & Dunning, G.R. (2003). Acadian orogenesis and high grade metamorphism in the Central Mobile Belt of central Newfoundland. *Abstracts with Programs – Geological Society of America,* **35**, 23.

Valverde-Vaquero, P., van Staal, C.R., McNicoll, V. & Dunning, G.R. (2006). Mid-Late Ordovician magmatism and metamorphism along the Gander margin in central Newfoundland. *Journal of the Geological Society of London,* **163**, 347-362.

van Staal, C.R. (2007). Pre-Carboniferous Tectonic Evolution and Metallogeny of the Canadian Appalachians. *In* Mineral Deposits of Canada: A Synthesis of Major Deposit-Types, District Metallogeny, the Evolution of Geological Provinces, and Exploration Methods.

Edited by W.D. Goodfellow. *Geological Association of Canada, Mineral Deposits Division, Special Publication No. 5*, 793-818.

van Staal, C.R. (1994). The Brunswick subduction complex in the Canadian Appalachians: record of the Late Ordovician to Late Silurian collision between Laurentia and the Gander margin of Avalon. *Tectonics*, **13**, 946-962.

Vermeesch, P. (2004). How many grains are needed for a provenance study? *Earth and Planetary Science Letters,* **224,** 441-451.

Weaver, C.E. (1989). Clays, Muds and Shales. Elseiver, New York, 819 p.

Weaver, C.E. (1960). Possible uses of clay minerals in the search for oil. *Bull. Am. Assoc. Pet. Geol.,* **44**, 1505-1518.

Weltje, G.J. & von Eynatten, H. (2004). Quantitative provenance analysis of sediments; review and outlook. *Sedimentary Geology,* **171**, 1-11.

White, C.E., Waldron, J.W.F., Barr, S.M., Simonetti, A., & Heamon, L.M. (2008). Provenance of the Meguma Terrane, Nova Scotia. *Abstracts with Programs – Geological Society of America,* **40**, 14-15.

Wiedenbeck, M., Alle, P., Corfu, F., Griffin, W.L., Meier, M., Oberli, F., von Quadt, A., Roddick, J.C. & Spiegel, W. (1995). Three natural zircon standards for U-Th-Pb, Lu-Hf, trace element and REE analyses. *Geostandards Newsletter*, **19**, 1-23.

Williams, H., Dehler, S.A., Grant, A.C., & Oakley, G.N. (1999). Tectonics of Atlantic Canada. *Geoscience Canada*, **26**, 51-70.

Williams, H., & Hatcher, R.D. (1983). Appalachian suspect terranes. *In* Contributions to the tectonics and geophysics of mountain chains. *Edited by* Hatcher, R.D. Jr., Williams, H.J., and Zietz, I. *Geological Society of America*, Memoir 159, 33-53.

Zartman, O. & Hermes, D. (1987). Archean inheritance in zircon from late Paleozoic granites from the Avalon zone of southeastern New England: an African connection. *Earth and Planetary Science Letters*, **82**, 305-315.

Zeiss, A. (1991). Report on the voting about the future usage of the Kimmeridgian and Tithonian stage names. *International Subcommission on Jurassic Stratigraphy Newsletter 20.*

Zeiss, A. (2003). The Upper Jurassic of Europe: its subdivision and correlation. *Geological Survey of Denmark and Greenland Bulletin 1*, 75-114.

Appendix A – Geochemical Data

XRF – Major Elements

Lab #	Sample #	Stratigraphic Unit	Na2O	Mgo	Al2O3	SiO2	P2O5	K2O	CaO	TiO2	MnO	Fe2O3	TOTAL
M41868Z	G-88(4185.1m)	LTS	0.71	2.76	16.06	41.74	0.07	3.65	11.27	0.98	0.10	6.37	83.71
M41869Q	G-88(4331.3m)	LKSR	0.88	2.35	15.05	49.85	0.06	2.79	9.18	0.93	0.04	5.91	87.04
M41870B	G-88(4329.6m)	LKSR	0.92	2.72	16.85	64.05	0.07	3.05	2.87	1.12	0.03	3.74	95.42
M41871T	G-88(4327.3m)	LKSR	0.92	2.65	16.28	58.08	0.09	3.04	5.13	1.06	0.04	5.30	92.59
M41872M	G-88(3830.1m)	UKSR	0.53	0.29	3.49	72.43	0.07	0.28	7.02	0.35		0.68	85.14
M41873E	G-88(3832.0m)	UKSR	0.80	0.76	6.51	70.92	0.13	0.66	10.04	0.39	0.03	1.68	91.92
M41874W	G-88(3834.4m)	UKSR	0.95	1.54	9.38	69.96	0.11	1.23	6.66	0.99	0.05	4.64	95.51
M41875P	G-88(3843.4m)	UKSR	1.47	2.63	17.48	52.84	0.11	3.20	5.01	1.03	0.60	5.64	90.01
M41876H	G-88(4183.9m)	LTS	1.17	2.87	14.74	55.36	0.07	2.78	8.52	0.90	0.12	6.23	92.76
M41877Z	G-88(4198.0m)	LTS	0.91	2.44	14.04	50.03	0.09	2.72	10.99	0.93	0.11	5.75	88.01
M41878R	G-88(4327.6m)	LKSR	0.90	2.80	17.00	49.09	0.08	3.36	6.51	1.04	0.05	7.14	87.97
M41879K	I-78(4148.3m)	RF	0.82	1.54	20.07	50.36	0.08	3.44	0.57	1.19	0.39	3.43	81.89
M41880P	I-78(4146.0m)	RF	0.78	1.59	18.87	47.72	0.06	3.66	5.52	1.12	0.12	4.64	84.08
M41881I	I-78(4138.5m)	RF	0.86	1.83	19.26	49.29	0.06	3.68	2.77	1.16	0.13	7.99	87.03
M41882B	I-78(4145.9m)	RF	0.82	1.67	19.72	49.60	0.06	3.80	5.64	1.14	0.08	4.34	86.86
M41883U	I-78(4140.9m)	RF	0.79	1.80	17.81	48.18	0.09	3.44	7.24	1.03	0.23	6.48	87.09
M41884N	I-78(4147.6m)	RF	0.80	1.61	18.77	45.87	0.06	3.53	7.87	1.11	0.14	4.37	84.13
M41885G	I-78(4148.3m)(B)	RF	0.75	1.42	19.51	52.50	0.10	3.71	0.36	1.17	0.07	3.69	83.28
M41886Z	P-52(3757.0m)	LTS	0.88	3.43	18.69	50.63	0.09	4.38	3.82	0.99	0.09	8.95	91.95
M41887R	P-52(3756.7m)	LTS	0.81	2.91	19.11	51.81	0.06	4.52	2.89	1.05	0.07	6.88	90.11
M41888K	P-52(3757.0m)(B)	LTS	0.75	3.38	18.63	46.40	0.09	4.52	3.37	1.01	0.09	10.70	88.94
M41889D	P-52(3754.0m)	LTS	0.86	2.90	20.71	50.77	0.09	5.06	1.69	1.12	0.14	7.92	91.26
M43028	G88(3832.0m)B	UKSR	0.74	0.87	6.66	74.59	0.12	0.62	9.36	0.37	0.02	1.47	94.82
M43029	G88(3838.4m)B	UKSR	0.72	1.27	8.10	58.75	0.09	0.96	12.88	0.76	0.05	3.65	87.23
M43030	G88(4188.1m)	LTS	1.14	1.47	7.19	44.59	0.07	0.77	23.63	0.53	0.23	3.97	83.60
M43031	G88(4188.1m)B	LTS	1.22	1.49	7.88	46.93	0.07	0.90	21.76	0.65	0.21	3.77	84.87
M43032	G88(4330.0m)	LKSR	0.87	2.19	11.99	57.96	0.06	1.88	9.47	0.79	0.09	4.75	90.05
M43033	I78(4151.75m)	RF	0.60	1.51	16.21	54.97	0.08	2.99	4.91	0.91	0.10	5.94	88.21
M43034	I78(4135.4m)B	RF	0.53	1.33	14.97	56.03	0.09	2.64	5.94	0.89	0.09	4.67	87.18
M43035	G88(3843.4m)B	UKSR	1.13	2.60	17.84	51.12	0.11	3.47	3.77	1.28	0.06	6.80	88.17
M43036	G88(4325.4m)	LKSR	0.56	2.57	13.04	35.40	0.13	2.70	18.32	0.81	0.08	6.14	79.76
M43037	G88(4183.9m)B	LTS	1.06	2.68	14.44	53.10	0.06	2.78	7.88	0.88	0.11	6.09	89.09
M43038	G88(4185.4m)	LTS	1.04	3.00	16.81	52.81	0.05	3.46	5.40	0.92	0.09	6.90	90.49
Reference Standards													
SDO-1			0.33	1.58	14.24	46.54	0.11	3.59	1.06	0.70	0.04	9.30	77.49
SDO-1			0.36	1.57	14.25	46.81	0.10	3.61	1.05	0.70	0.04	9.36	77.85
SDO-1			0.35	1.57	14.09	46.96	0.11	3.57	1.05	0.71	0.04	9.29	77.74
SGR-1			2.70	3.52	6.07	26.39	0.34	2.09	11.49	0.35	0.04	3.98	56.97
SGR-1			2.64	3.56	5.95	26.24	0.33	2.08	11.48	0.35	0.05	3.95	56.63
SDO-1			0.29	2.03	13.56	50.15	0.10	3.78	1.35	0.85	0.03	10.88	83.03
SGR-1			2.42	4.18	7.58	26.28	0.31	2.22	12.61	0.44	0.04	4.22	60.30
Reference Standards Accepted Values													
SDO-1			0.38	1.54	12.27	49.28	0.11	3.35	1.05	0.71	0.04	9.34	78.07
SGR-1			2.99	4.44	6.52	28.20	0.33	1.66	8.38	0.25	0.34	3.03	56.15

All values for major elements presented in wt. %. Sample numbers with (B) are duplicate preparations. Stratigraphic units include the Lower Tempest Sandstone (LTS), Lower Kimmeridgian Source Rock (LKSR), Upper Kimmeridgian Source Rock (UKSR), and the Rankin Formation (RF). Reference standards include the SDO-1 (Devonian Ohio Shale) and the SGR-1 (Green River Shale). Accepted values are available from the United States Geological Survey and were established by Kane et al. (1990) for SDO-1 and by Abbey (1983), Gladney and Roelandts (1988) and Govindaraju (1994) for SGR-1.

XRF – Trace Elements

Lab #	Sample #	Stratigraphic Unit	Sc	TiO2	V	Cr	MnO	Fe2O3	Co	Ni	Cu	Zn	Ga	As	Rb	Sr	Y	Zr	Nb	Mo	Sn	Sb	Cs	Ba	La	Ce	Pb	Th	U
Limit of Detection			1.600		1.400	3.300			2.200	1.500	4.700	3.800	0.700	2.900	0.900	0.900	6.500	4.900	0.600	1.000	3.100	1.700	4.700	5.000	5.200	4.000	1.500	12.600	1.500
M41868Z	G-88(4185.1m)	LTS	19.000	0.772	99.000	77.000	0.065	5.139	30.000	45.000	24.000	63.000	20.000	19.000	149.000	324.000	27.000	128.000	14.000	6.000	<LD	5.000	24.000	484.000	44.000	80.000	21.000	<LD	6.000
M41869Q	G-88(4331.3m)	LKSR	12.000	0.786	87.000	69.000	0.038	4.902	26.000	36.000	22.000	55.000	16.000	8.000	122.000	303.000	20.000	172.000	14.000	6.000	<LD	3.000	16.000	398.000	30.000	59.000	17.000	<LD	6.000
M41870B	G-88(4329.6m)	LKSR	12.000	1.046	94.000	89.000	0.037	3.206	41.000	31.000	17.000	52.000	19.000	10.000	133.000	191.000	30.000	275.000	18.000	6.000	<LD	5.000	17.000	283.000	50.000	94.000	14.000	14.000	5.000
M41871T	G-88(4327.3m)	LKSR	13.000	0.950	101.000	85.000	0.041	4.524	43.000	43.000	24.000	60.000	18.000	12.000	134.000	269.000	30.000	253.000	17.000	6.000	4.000	7.000	17.000	680.000	51.000	96.000	24.000	14.000	6.000
M41872M	G-88(3830.1m)	UKSR	5.000	0.335	23.000	17.000	0.018	0.890	173.000	9.000	6.000	16.000	4.000	8.000	12.000	99.000	14.000	332.000	8.000	6.000	<LD	5.000	<LD	182.000	12.000	33.000	<LD	<LD	5.000
M41873E	G-88(3832.0m)	UKSR	6.000	0.319	30.000	22.000	0.023	1.482	79.000	14.000	8.000	21.000	5.000	6.000	23.000	147.000	14.000	130.000	7.000	6.000	<LD	3.000	<LD	103.000	12.000	42.000	9.000	<LD	6.000
M41874W	G-88(3834.4m)	UKSR	9.000	0.905	64.000	60.000	0.045	3.844	93.000	24.000	14.000	26.000	8.000	8.000	52.000	182.000	30.000	575.000	17.000	6.000	<LD	4.000	13.000	132.000	29.000	76.000	8.000	<LD	6.000
M41875P	G-88(3843.4m)	UKSR	22.000	0.920	110.000	74.000	0.060	4.775	33.000	40.000	31.000	63.000	21.000	5.000	118.000	243.000	22.000	170.000	14.000	6.000	<LD	4.000	17.000	494.000	29.000	53.000	18.000	<LD	6.000
M41876H	G-88(4183.9m)	LTS	16.000	0.786	87.000	60.000	0.085	5.196	29.000	36.000	27.000	66.000	16.000	9.000	100.000	224.000	28.000	165.000	13.000	6.000	<LD	5.000	15.000	435.000	26.000	57.000	19.000	<LD	6.000
M41877Z	G-88(4198.0m)	LTS	16.000	0.780	82.000	66.000	0.068	4.702	28.000	34.000	20.000	51.000	15.000	6.000	100.000	288.000	27.000	178.000	14.000	6.000	<LD	<LD	19.000	293.000	35.000	69.000	17.000	<LD	6.000
M41878R	G-88(4327.6m)	LKSR	17.000	0.907	115.000	83.000	0.049	5.999	19.000	43.000	31.000	64.000	20.000	12.000	141.000	661.000	25.000	178.000	15.000	6.000	<LD	3.000	19.000	590.000	32.000	60.000	29.000	16.000	10.000
M41879K	I-78(4148.3m)	RF	18.000	1.100	137.000	104.000	0.353	3.169	18.000	47.000	34.000	75.000	27.000	5.000	211.000	191.000	29.000	178.000	19.000	6.000	<LD	<LD	28.000	466.000	51.000	97.000	29.000	18.000	5.000
M41880P	I-78(4146.0m)	RF	16.000	0.974	127.000	99.000	0.100	4.035	12.000	37.000	24.000	53.000	25.000	9.000	185.000	233.000	25.000	164.000	17.000	6.000	4.000	5.000	23.000	431.000	47.000	83.000	26.000	16.000	5.000
M41881I	I-78(4138.5m)	RF	17.000	1.029	129.000	94.000	0.114	6.867	19.000	51.000	29.000	54.000	24.000	14.000	193.000	180.000	29.000	181.000	18.000	6.000	<LD	3.000	22.000	374.000	53.000	100.000	29.000	16.000	5.000
M41882B	I-78(4145.9m)	RF	17.000	0.990	131.000	95.000	0.071	3.687	10.000	31.000	19.000	51.000	26.000	9.000	195.000	236.000	25.000	161.000	18.000	6.000	<LD	3.000	22.000	519.000	49.000	79.000	25.000	17.000	5.000
M41883U	I-78(4140.9m)	RF	11.000	0.884	111.000	76.000	0.158	5.475	14.000	39.000	23.000	59.000	21.000	14.000	162.000	259.000	25.000	165.000	16.000	6.000	<LD	3.000	15.000	377.000	46.000	78.000	25.000	15.000	6.000
M41884N	I-78(4147.6m)	RF	16.000	0.941	114.000	88.000	0.104	3.752	16.000	43.000	19.000	47.000	25.000	7.000	191.000	260.000	25.000	153.000	17.000	6.000	<LD	3.000	24.000	409.000	49.000	81.000	25.000	15.000	6.000
M41885G	I-78(4148.3m)(B)	RF	19.000	1.085	130.000	95.000	0.076	3.188	22.000	49.000	33.000	84.000	25.000	5.000	193.000	263.000	32.000	221.000	19.000	6.000	4.000	3.000	26.000	480.000	53.000	100.000	27.000	18.000	6.000
M41886Z	P-52(3757.0m)	LTS	20.000	0.895	119.000	76.000	0.083	7.649	33.000	41.000	36.000	67.000	22.000	8.000	151.000	194.000	28.000	158.000	14.000	6.000	<LD	<LD	19.000	623.000	29.000	66.000	26.000	<LD	5.000
M41887R	P-52(3756.7m)	LTS	21.000	0.935	118.000	83.000	0.066	6.009	24.000	46.000	43.000	69.000	24.000	12.000	162.000	183.000	28.000	168.000	14.000	6.000	<LD	3.000	20.000	618.000	33.000	61.000	31.000	<LD	5.000
M41888K	P-52(3757.0m)(B)	LTS	23.000	0.921	124.000	84.000	0.084	9.036	33.000	50.000	37.000	64.000	22.000	9.000	157.000	189.000	28.000	146.000	14.000	6.000	<LD	3.000	13.000	617.000	38.000	73.000	27.000	15.000	5.000
M41889D	P-52(3754.0m)	LTS	22.000	1.001	130.000	88.000	0.128	6.915	29.000	53.000	45.000	60.000	25.000	18.000	177.000	179.000	30.000	186.000	16.000	6.000	<LD	4.000	21.000	610.000	37.000	78.000	46.000	16.000	5.000
M43028	G88(3832.0m)B	UKSR	6.000	0.310	30.000	18.000	0.023	1.507	117.000	14.000	9.000	18.000	6.000	7.000	22.000	150.000	14.000	123.000	8.000	6.000	<LD	4.000	<LD	121.000	13.000	46.000	6.000	<LD	6.000
M43029	G88(3838.4m)B	UKSR	8.000	0.644	48.000	46.000	0.038	3.109	62.000	21.000	12.000	25.000	7.000	5.000	37.000	245.000	26.000	544.000	13.000	6.000	<LD	4.000	10.000	107.000	21.000	60.000	7.000	<LD	6.000
M43030	G88(4188.1m)	LTS	5.000	0.402	34.000	16.000	0.067	3.285	70.000	17.000	11.000	37.000	6.000	5.000	24.000	394.000	21.000	157.000	8.000	6.000	<LD	3.000	8.000	225.000	21.000	45.000	8.000	<LD	8.000
M43031	G88(4188.1m)B	LTS	6.000	0.502	41.000	26.000	0.070	3.173	65.000	21.000	11.000	32.000	6.000	6.000	29.000	391.000	21.000	176.000	9.000	6.000	<LD	4.000	16.000	126.000	15.000	51.000	8.000	<LD	8.000
M43032	G88(4330.0m)	LKSR	9.000	0.685	64.000	64.000	0.067	4.141	44.000	33.000	19.000	50.000	11.000	7.000	77.000	516.000	25.000	251.000	13.000	6.000	<LD	4.000	10.000	333.000	24.000	55.000	13.000	12.000	9.000
M43033	I78(4151.75m)	RF	14.000	0.815	95.000	61.000	0.083	5.135	35.000	39.000	21.000	128.000	16.000	10.000	120.000	204.000	29.000	214.000	15.000	6.000	<LD	5.000	11.000	408.000	36.000	83.000	18.000	13.000	6.000
M43034	I78(4135.4m)B	RF	10.000	0.789	80.000	54.000	0.073	4.070	45.000	31.000	18.000	100.000	14.000	13.000	98.000	216.000	27.000	257.000	15.000	6.000	<LD	3.000	14.000	465.000	41.000	103.000	15.000	13.000	6.000
M43035	G88(3843.4m)B	UKSR	22.000	1.183	130.000	97.000	0.064	5.862	56.000	39.000	33.000	59.000	23.000	8.000	149.000	255.000	29.000	224.000	18.000	6.000	6.000	6.000	13.000	433.000	48.000	96.000	16.000	15.000	6.000
M43036	G88(4325.4m)	LKSR	13.000	0.633	79.000	66.000	0.042	4.903	15.000	29.000	21.000	90.000	16.000	7.000	115.000	439.000	25.000	118.000	11.000	6.000	<LD	2.000	24.000	311.000	36.000	70.000	16.000	11.000	8.000
M43037	G88(4183.9m)B	LTS	16.000	0.783	89.000	56.000	0.082	5.144	33.000	33.000	25.000	67.000	16.000	9.000	101.000	214.000	26.000	160.000	13.000	6.000	<LD	5.000	11.000	441.000	25.000	56.000	18.000	11.000	6.000
M43038	G88(4185.4m)	LTS	20.000	0.834	107.000	68.000	0.082	5.891	23.000	39.000	39.000	89.000	19.000	<LD	129.000	188.000	24.000	146.000	13.000	6.000	<LD	3.000	9.000	588.000	24.000	51.000	25.000	12.000	5.000
Reference Standards																													
	SDO-1		11.000	0.750	140.000	53.000	0.042	8.559	33.000	81.000	49.000	54.000	14.000	58.000	119.000	72.000	39.000	156.000	13.000	150.000	3.000	7.000	7.000	407.000	33.000	68.000	31.000	12.000	38.000
	SDO-1		8.000	0.751	142.000	53.000	0.043	8.640	31.000	80.000	49.000	54.000	15.000	56.000	120.000	71.000	39.000	156.000	13.000	151.000	1.000	5.000	15.000	403.000	34.000	73.000	31.000	14.000	38.000
	SDO-1		10.000	0.760	143.000	51.000	0.042	8.671	34.000	84.000	50.000	54.000	14.000	59.000	121.000	72.000	39.000	157.000	13.000	152.000	3.000	6.000	12.000	408.000	31.000	70.000	30.000	14.000	39.000
	SGR-1		6.000	0.327	127.000	35.000	0.031	2.686	5.000	24.000	52.000	65.000	9.000	51.000	71.000	337.000	9.000	34.000	7.000	32.000	2.000	5.000	12.000	302.000	26.000	36.000	40.000	6.000	7.000
	SGR-1		4.000	0.328	127.000	35.000	0.031	2.691	5.000	26.000	52.000	66.000	8.000	52.000	71.000	339.000	9.000	34.000	7.000	32.000	2.000	4.000	15.000	305.000	28.000	34.000	40.000	6.000	7.000
	SGR-1		3.000	0.330	128.000	34.000	0.032	2.690	5.000	27.000	52.000	66.000	8.000	52.000	72.000	340.000	9.000	34.000	7.000	33.000	3.000	4.000	17.000	309.000	23.000	31.000	41.000	7.000	7.000
	SDO-1		10.000	0.758	142.000	54.000	0.042	8.790	32.000	79.000	52.000	54.000	15.000	58.000	122.000	73.000	40.000	160.000	13.000	153.000	<LD	6.000	10.000	407.000	33.000	77.000	31.000	13.000	38.000
	SGR-1		6.000	0.337	130.000	35.000	0.032	2.745	6.000	27.000	53.000	67.000	9.000	52.000	73.000	346.000	10.000	35.000	7.000	34.000	<LD	6.000	14.000	310.000	23.000	46.000	42.000	<LD	7.000
Accepted Values																													
	SDO-1		13.200	0.710	160.000	66.400	0.042	9.340	46.800	99.500	60.200	64.100	16.800	68.500	126.000	75.100	40.600	165.000	11.400	134.000	3.700		6.900	397.000	38.500	79.300	27.900	10.500	48.800
	SGR-1		4.600	0.253	130.000	30.000	0.034	3.030	12.000	29.000	66.000	74.000	12.000	67.000		420.000	13.000	53.000	5.200	35.000	1.900	3.400	5.200	290.000	20.000	36.000	38.000	4.800	5.400

All values for trace elements presented in ppm. Sample numbers with (B) are duplicate preparations. Stratigraphic units include the Lower Tempest Sandstone (LTS), Lower Kimmeridgian Source Rock (LKSR), Upper Kimmeridgian Source Rock (UKSR), and the Rankin Formation (RF). Reference standards include the SDO-1 (Devonian Ohio Shale) and the SGR-1 (Green River Shale). Accepted values are available from the United States Geological Survey and were established by Kane et al. (1990) for SDO-1 and by Abbey (1983), Gladney and Roelandts (1988) and Govindaraju (1994) for SGR-1.

ICP-MS (Trace Elements)

Lab#	Sample#	Stratigraphic Unit	Ca	Ti	V	Cr	Fe	Mn	Co	Ni	Cu	Zn	As	Se	Br	Mo	Ag	Cd	Sn	Sb	Te	I	La	Ce	Pr	Nd	Er	Tm	Lu	W	Hg	Pb	Bi	Th
Limit of Detection			1747.7053	5.7207	1.6048	3.8882	737.3290	1.2783	0.1430	0.8788	0.9718	2.8634	0.3859	5.9397	21.6858	0.1710	0.2148	0.2282	0.0441	0.1342	0.5970	21.8412	0.0839	0.1699	0.0550	0.2429	0.0149	0.0513	0.0509	0.0091	0.0510	0.1558	0.0477	0.3331
M41868	G-88(4185.1m)	LTS	76321.3481	4053.5324	111.3934	87.2014	32672.1150	664.9561	39.7714	44.4888	27.9987	75.8553	19.4439	2.5979	109.9749	3.8976	0.2234	-0.0189	6.0967	1.3454	0.4212	0.5607	36.7706	76.7130	8.8791	33.1417	1.7304	0.2095	0.1947	196.3680	-0.0099	20.4434	0.2721	11.9790
M41869	G-88(4331.3m)	LKSR	64133.3625	3604.8225	85.3387	68.9334	30272.7839	344.2441	35.4046	35.1898	31.2205	105.2596	7.8195	-0.0444	107.1868	3.1603	0.1305	-0.0669	5.5480	0.7564	-0.0290	-0.3445	26.1553	53.1755	6.1013	22.0133	1.1848	0.1780	0.1491	263.0593	0.0496	16.3627	0.2325	9.3935
M41872	G-88(3830.1m)	UKSR	41427.2890	1166.1110	14.5959	12.2023	3545.4532	95.7724	218.5519	5.4909	8.0841	22.6444	1.8778	0.6883	97.4819	0.8299	0.0853	-0.0467	3.6574	0.2401	0.4452	-0.5185	10.7314	23.1114	2.7618	11.0152	0.5152	0.0682	0.0375	2137.9127	0.1122	3.9867	0.0633	2.8166
M41873	G-88(3832.0m)	UKSR	57787.6680	1197.7001	22.8481	18.9776	7793.9835	158.3420	110.9896	12.3606	8.8762	23.9752	3.1196	1.4742	132.4479	0.9384	-0.0176	0.1974	4.2193	0.2686	0.4626	-1.0486	14.8161	31.3914	3.6456	14.8026	0.7787	0.0818	0.0532	522.3136	-0.0020	7.5718	0.1018	3.6383
M41874	G-88(3834.4m)	UKSR	39489.5078	3346.2428	50.9125	46.5390	23274.9161	343.0521	121.9321	20.0094	17.2300	31.8730	4.3773	1.9285	122.7793	1.3028	0.1876	-0.0895	4.6056	0.4940	0.4677	1.3230	26.2457	52.8180	6.1457	22.9357	1.1649	0.1380	0.1149	402.9238	0.0092	9.9211	0.1735	9.0532
M41875	G-88(3843.4m)	UKSR	35517.3240	4736.4006	122.5347	90.8839	30962.4086	490.5806	46.0212	44.4094	35.5219	79.7531	5.1957	0.0486	117.6629	2.1581	0.1694	0.0336	5.8242	0.5758	0.3276	-0.6803	30.1543	61.1097	7.3911	28.9653	1.5808	0.2140	0.1964	291.7161	-0.0208	16.4406	0.3478	12.2329
M41876	G-88(4183.9m)	LTS	63014.6282	4272.4834	103.6757	72.9160	36099.3968	877.9512	43.5126	40.9441	39.0359	109.0914	7.7193	-0.0541	122.0535	0.5274	0.1584	-0.1392	5.9986	0.6211	0.7315	-0.1218	31.2546	65.8311	7.7784	30.8431	1.9932	0.3069	0.2132	235.7822	-0.0266	21.1594	0.3007	10.2124
M41877	G-88(4198.0m)	LTS	70417.8623	3752.3378	84.1977	68.5445	29623.8462	705.4938	37.3308	36.4677	25.0719	71.4453	6.5030	-1.0605	115.8805	0.8106	0.1674	-0.0209	5.3024	0.8565	0.1355	-0.9728	31.2545	65.4995	7.6377	30.0577	1.6337	0.2396	0.2119	204.9531	-0.0443	18.0559	0.2795	10.0813
M41886	P-52(3757.0m)	LTS	27234.4510	4076.5378	126.1697	89.8372	45250.0435	650.5981	40.1890	45.0983	38.4180	79.4481	9.7334	0.3174	104.4655	1.2359	0.2177	-0.0189	5.2433	1.0372	0.8316	-0.4383	32.5621	66.2784	7.5506	29.6491	1.7606	0.2602	0.2352	244.6481	0.0291	24.7743	0.3001	12.2960
M41887	P-52(3756.7m)	LTS	23692.0367	4765.3485	141.7306	104.4252	39416.4142	544.6854	32.7767	61.1359	51.5524	86.9343	13.7872	4.1136	117.0277	1.3310	0.1725	0.1131	6.3601	1.3703	0.5199	-2.4606	37.5576	77.0172	8.8485	32.9732	1.9414	0.2998	0.2792	117.2463	-0.0562	32.4955	0.3697	14.6966
M41887 DUP		LTS	22244.0392	4297.8560	131.5716	97.7252	36950.4330	509.4749	31.2595	55.4497	50.0860	84.4183	12.4019	2.5529	98.3072	1.4101	0.2071	0.0030	5.3690	1.1473	-0.1611	-2.1184	33.5178	68.2143	8.1727	29.5978	1.7641	0.4357	0.2176	103.4838	-0.0039	29.5028	0.5078	12.5099
M43028	G88(3832.0m)B	UKSR	55970.1957	1255.3480	23.2240	20.2815	8317.7532	167.9966	167.6977	12.5602	9.3033	22.4064	3.7559	1.0555	120.3904	0.6378	-0.0146	-0.1226	4.0030	0.3277	0.3529	0.5274	15.8632	32.9779	4.0656	16.1209	0.8776	0.0981	0.0667	557.6419	0.0881	7.9794	0.0757	3.7117
M43029	G88(3838.4m)B	UKSR	76577.9462	2481.4001	37.9772	32.8260	21000.4373	365.8743	82.8719	15.0032	11.8671	34.1501	3.5506	5.4524	119.7153	1.1589	0.0981	-0.1008	4.1312	0.4141	-0.1716	0.0290	23.2552	48.1312	5.6108	21.0162	1.1202	0.1221	0.1217	329.3631	0.0029	6.8719	0.1612	7.7228
M43030	G88(4188.1m)	LTS	134660.0669	1265.5161	25.7018	21.0884	20980.2307	1186.2619	91.3262	14.0852	10.8092	40.6641	4.9556	0.9210	102.1710	0.6394	0.0133	-0.0065	4.0308	0.4951	0.9935	-0.3971	19.7519	40.4737	5.0902	20.3891	1.1160	0.1191	0.0853	643.5925	0.0055	9.7813	0.1138	4.8287
M43031	G88(4188.1m)B	LTS	135349.9997	1651.7685	32.1609	26.5734	21609.7204	1188.2205	90.8254	16.2273	10.1964	37.6923	3.7915	2.2370	94.4909	0.4221	0.0740	-0.1239	3.8071	0.5529	0.1680	-0.5458	21.9449	43.6053	5.2543	21.1981	1.0843	0.1256	0.1056	638.9081	0.0057	8.0630	0.1117	5.0398
M43032	G88(4330.0m)	LKSR	61318.7638	2774.7183	57.6836	47.9123	27672.6364	646.9697	57.7125	29.9602	18.3306	53.7510	6.6377	4.9931	106.0646	0.9506	0.1046	-0.0130	4.6026	0.6504	0.6138	-1.8329	20.0066	41.0680	4.9044	18.7318	0.9992	0.1255	0.0989	376.8149	0.0151	12.4389	0.1929	7.4639
M43033	I78(4151.75m)	RF	34916.3665	2880.8376	95.7639	68.9372	35897.3643	708.5585	46.5355	41.2225	24.7516	159.1569	5.8543	2.9997	160.3153	1.7313	0.2387	0.0066	5.4442	1.0250	0.0000	-1.7053	37.6224	81.1677	9.4056	36.4234	1.4854	0.1923	0.1814	337.4253	-0.0228	17.5180	0.1869	12.5429
M43034	I78(4135.4m)B	RF	39077.9222	2600.5073	74.7514	55.5855	28100.1553	627.9814	58.4020	36.1564	21.8322	127.4262	8.2872	2.7860	121.9682	2.0855	0.1171	0.2065	5.2667	0.9580	0.4654	-1.7256	40.1901	88.3382	10.1832	38.4895	1.2172	0.1449	0.1409	334.7736	-0.0106	13.7424	0.1853	11.1998
M43035	G88(3843.4m)B	UKSR	26186.7533	4591.2631	123.2114	93.9560	36286.7084	434.6736	63.1037	39.7973	30.5829	62.1080	5.1069	2.3992	121.8653	2.1920	0.1384	0.0390	5.7703	0.4684	0.0149	-2.1642	34.7090	68.4160	7.5884	27.4910	1.2223	0.1518	0.1251	312.9747	0.0052	13.8235	0.2954	11.1538
M43036	G88(4325.4m)	LKSR	115523.3311	2667.0933	81.4400	63.6015	32313.8819	528.9803	22.0735	30.0735	19.7809	98.9788	5.2525	0.1354	112.9752	1.0484	0.0835	0.0274	5.1097	0.5073	0.4230	-1.5999	23.1206	49.0754	5.7583	23.2782	1.3525	0.1823	0.1237	135.4601	0.0143	14.7373	0.2192	8.2059
M43037	G88(4183.9m)B	LTS	55977.4098	2903.8531	96.1156	69.4550	34011.2696	789.3778	46.3851	38.7771	33.9497	87.5237	8.5392	3.7020	119.6886	0.4520	0.0874	-0.0856	4.7406	0.5731	-0.0337	1.8108	22.0724	44.8855	5.4948	21.7855	1.4900	0.1483	0.1498	234.1570	-0.0203	18.2993	0.2449	7.7271
M43038	G88(4185.4m)	LTS	43867.3431	3765.0117	130.7639	90.4819	41532.1043	761.3352	34.0810	48.8958	48.0704	118.7748	3.2942	3.7006	128.7502	0.4777	0.1243	0.1652	6.5514	0.5040	0.1161	1.9134	24.1924	46.7665	5.5306	21.3646	1.2863	0.1764	0.1272	194.3772	-0.0420	25.7546	0.3534	9.4782
M43038 DUP		LTS	40774.2493	3397.8282	120.3071	83.3905	38301.7104	702.4458	30.9467	45.2663	44.8807	115.6501	2.8444	3.7760	114.9475	0.5184	0.0107	0.0355	5.9648	0.5175	0.5580	1.1185	21.8802	42.2977	5.0715	19.9730	1.3108	0.1765	0.1159	184.8222	-0.0102	24.2051	0.2654	8.5198
Reference Standards/Blank																																		
BLANK-33			2245.1401	0.4687	1.5234	0.8954	13.5387	1.6448	-0.1332	0.6624	9.0276	2.2703	0.2103	1.1409	122.3663	0.1318	0.0236	-0.1556	4.7009	0.0044	0.0360	4.1384	-0.0163	-0.0380	-0.0343	0.0738	-0.0097	-0.0075	-0.0332	-0.4945	0.0763	0.2143	0.0798	0.6624
SGR-1B-1			60435.6145	1150.0311	105.2917	29.6629	16623.8665	221.8573	10.3811	28.2328	62.8305	78.6568	12.4956	5.7405	137.7599	47.9042	0.0385	0.9964	5.3083	2.9137	0.5103	1.4111	16.8865	31.6588	3.6202	13.1067	0.8019	0.1107	0.0892	5.4575	0.0532	39.0051	0.9108	5.5605
SDO-1-1			10649.1631	2648.9507	139.5989	53.6287	50972.9563	269.1468	38.7529	84.1739	52.3431	65.1717	31.6208	1.4566	139.5309	210.2283	0.3805	0.3124	4.7019	4.1496	0.1660	0.9846	31.4102	63.9438	7.8442	31.3960	2.6735	0.3444	0.3719	2.4868	0.0365	31.0333	0.3365	11.0374

All values for trace elements presented in ppm. Sample numbers with (B) are duplicate preparations. Stratigraphic units include the Lower Tempest Sandstone (LTS), Lower Kimmeridgian Source Rock (LKSR), Upper Kimmeridgian Source Rock (UKSR), and the Rankin Formation (RF). Reference standards include the SDO-1 (Devonian Ohio Shale) and the SGR-1 (Green River Shale). Accepted values are available from the United States Geological Survey and were established by Kane et al. (1990) for SDO-1 and by Abbey (1983), Gladney and Roelandts (1988) and Govindaraju (1994) for SGR-1.

Lab#	Sample#	Stratigraphic Unit	Li	Rb	Sr	Y	Zr	Nb	Mo	Cs	Ba	La	Ce	Pr	Nd	Sm	Eu	Gd	Tb	Dy	Ho	Er	Tm	Yb	Lu	Hf	Ta	Tl	Pb	Bi	Th	U
Limit of Detection			0.3595	0.1559	0.2125	0.0196	0.0712	0.0197	0.2402	0.0227	0.2638	0.0120	0.0198	0.0088	0.1128	0.0458	0.0259	0.0407	0.0080	0.0201	0.0076	0.0299	0.0081	0.0399	0.0092	0.0559	0.0113	0.0375	0.1378	0.0192	0.0644	0.0194
M41868	G-88(4185.1m)	LTS	87.0641	158.8411	337.0253	16.2572	74.9470	13.8872	0.8675	10.2189	582.4148	37.8238	81.2596	9.3511	35.0315	6.7496	1.3344	4.7331	0.6734	3.6551	0.6642	1.8106	0.2976	1.7568	0.2455	3.9881	1.9665	0.8928	21.6557	0.3171	13.8334	1.9522
M41869	G-88(4331.3m)	LKSR	66.2608	139.6306	342.6913	11.2834	61.5852	13.3908	1.8264	8.3826	464.3940	28.7042	59.2426	6.6463	25.2698	4.1708	0.8145	2.9119	0.4277	2.3931	0.4756	1.3734	0.2402	1.3822	0.1975	3.0109	1.9007	0.7730	17.0595	0.2818	11.4800	1.7945
M41872	G-88(3830.1m)	UKSR	8.9095	10.7158	99.3124	7.1739	32.1541	5.2951	0.4008	0.5141	184.5765	11.7400	25.1719	3.1240	12.8029	2.5119	0.5584	2.2185	0.3100	1.5115	0.2524	0.6183	0.0963	0.5278	0.0778	4.1393	8.5502	0.0287	4.2739	0.0668	3.1857	0.6444
M41873	G-88(3832.0m)	UKSR	13.9008	21.9315	148.4675	8.0579	21.8503	3.9617	0.5379	1.1939	104.5234	15.1036	30.8901	3.8415	15.3996	3.0813	0.6491	2.5520	0.3314	1.7386	0.3247	0.8384	0.1153	0.6284	0.0881	1.7534	3.2859	0.1481	7.8341	0.1103	3.9190	0.7905
M41874	G-88(3834.4m)	UKSR	33.7237	53.4674	183.7520	10.9427	72.7043	11.2412	0.7133	3.0236	138.1922	25.5510	53.6777	6.3491	24.2167	4.7586	0.8712	3.3730	0.4402	2.4965	0.6662	1.3480	0.1922	1.0618	0.1389	3.1815	4.1045	0.3263	10.2237	0.1845	9.2184	1.3761
M41875	G-88(3843.4m)	UKSR	61.7512	115.9620	232.9357	12.4516	67.6618	13.3951	1.2402	5.8879	453.9320	25.3775	53.3336	6.3542	24.6859	4.6771	0.9691	3.7126	0.5114	2.7760	0.5027	1.3999	0.1982	1.3700	0.1749	5.8527	1.7525	0.5868	14.8495	0.2608	11.0675	1.7255
M41876	G-88(4183.9m)	LTS	59.2754	100.5663	221.5499	15.5983	63.1241	11.7442	0.3050	5.9989	441.0536	25.9373	55.2188	6.7568	26.1774	5.4102	1.0830	4.1457	0.6010	3.4462	0.6576	1.6318	0.2713	1.4434	0.2240	3.0487	1.4151	0.5661	18.6668	0.2468	8.9887	1.6233
M41877	G-88(4198.0m)	LTS	61.7224	101.7581	289.6110	14.4484	59.0843	11.8394	0.4027	5.9299	288.2229	28.8459	60.4289	7.1656	27.7497	5.7322	1.1568	4.5074	0.5829	3.1526	0.5665	1.5646	0.2430	1.4389	0.1847	2.7927	1.4728	0.5562	16.8679	0.2296	9.8131	1.6502
M41886	P-52(3757.0m)	LTS	81.1052	153.5303	187.2067	15.6963	85.5469	13.1313	0.7197	9.7341	612.0164	30.5816	63.6238	7.3979	29.2890	5.6879	1.1338	4.2965	0.5726	3.3870	0.6711	1.7674	0.2667	1.9865	0.2524	7.0139	1.5988	0.8929	24.9681	0.2920	12.7202	1.8917
M41887	P-52(3756.7m)	LTS	100.7369	178.1429	197.3869	15.8829	96.3702	14.8643	0.8153	11.4789	721.6906	35.1731	72.4390	8.5388	32.2915	6.1779	1.1899	4.1354	0.6286	3.7174	0.6988	1.9839	0.3399	1.9547	0.3080	4.8383	1.5259	1.0526	31.1597	0.3693	14.1296	2.1893
M41887 DUP		LTS	82.2127	147.8157	162.0034	12.1993	65.0066	11.4756	0.6944	9.6197	531.0332	28.3882	57.9294	6.9439	25.4732	4.8827	0.9423	3.5477	0.4678	2.8016	0.5349	1.5154	0.2451	1.4264	0.2294	3.1049	1.2314	0.8743	26.1454	0.2850	11.2111	1.6337
M43028	G88(3832.0m)B	UKSR	13.5431	21.7544	143.8993	7.7064	21.6783	4.3867	0.4549	1.1096	117.3410	14.1983	28.5244	3.6257	14.7780	2.8696	0.6594	2.4498	0.3218	1.6855	0.3062	0.7161	0.1011	0.5652	0.0853	3.2162	5.3612	0.1089	7.3601	0.0830	3.6375	0.6505
M43029	G88(3838.4m)B	UKSR	21.0458	31.9321	220.0926	9.8858	50.6003	7.1463	0.4468	1.7689	96.4343	20.1904	40.1608	5.1619	19.3170	3.9278	0.8094	3.2947	0.4111	2.2183	0.4113	1.1243	0.1676	0.8605	0.1233	2.4645	2.8655	0.1941	6.3280	0.1198	6.7864	1.0368
M43030	G88(4188.1m)	LTS	19.3184	22.5524	390.7704	11.3308	27.2624	4.1154	0.4049	1.1000	235.8918	20.1895	40.2179	5.1757	21.4158	4.4819	0.9939	3.7003	0.4532	2.4446	0.4084	1.1460	0.1899	0.7408	0.1300	1.3890	2.9699	0.1578	10.3453	0.1300	4.8716	0.7580
M43031	G88(4188.1m)B	LTS	25.7165	29.2125	393.6953	11.8307	28.2827	4.8817	0.2112	1.2633	132.3302	21.3517	41.3612	5.1206	20.7089	4.2432	0.9180	3.2855	0.4230	2.2497	0.4034	0.9637	0.1379	1.1769	0.1342	3.8534	2.4192	0.1544	8.2322	0.0991	5.5403	0.6641
M43032	G88(4330.0m)	LKSR	47.2852	70.7908	475.6821	9.3266	43.3567	9.1406	0.4815	4.8056	338.0500	19.5166	39.6249	5.1120	17.6723	3.7992	0.7359	2.8845	0.4066	2.1963	0.3872	1.2080	0.2113	0.9972	0.1255	2.2885	2.0880	0.4928	12.0052	0.2061	7.5254	1.2849
M43033	I78(4151.75m)	RF	58.4606	119.4125	196.8504	11.7180	64.9687	9.8022	1.1506	6.5690	380.9687	34.0464	74.0593	8.9013	34.2042	6.8013	1.3595	4.7573	0.5705	2.8819	0.5304	1.3097	0.2337	1.2370	0.1746	2.7906	1.5975	0.7989	16.7222	0.2545	11.9371	1.9953
M43034	I78(4135.4m)B	RF	55.7276	112.7832	244.4117	12.2693	73.8656	10.6022	1.5348	5.2705	543.3480	43.8582	95.9356	11.1949	42.7167	7.8052	1.4776	4.9772	0.6118	3.0984	0.4945	1.2703	0.2112	1.2883	0.1952	5.5533	2.3541	0.6362	15.3038	0.2087	12.6718	2.0216
M43035	G88(3843.4m)B	UKSR	76.7999	139.1021	221.7609	10.2124	56.3706	15.1945	1.4498	8.1102	385.4808	34.1023	64.8228	7.7765	27.5463	5.2493	0.9652	3.5089	0.4756	2.4793	0.4978	1.1481	0.2083	1.0536	0.1686	3.1325	2.6740	0.7316	13.5376	0.3206	10.8561	1.6293
M43036	G88(4325.4m)	LKSR	73.3136	123.1906	460.7754	14.9015	39.3842	9.4155	0.6931	7.8064	355.2393	25.2929	52.5523	6.3029	24.4087	5.6965	1.2821	4.9995	0.6485	3.3918	0.5754	1.4263	0.2290	1.1436	0.1721	2.2878	1.1842	0.6910	16.0526	0.2596	8.6650	1.4595
M43037	G88(4183.9m)B	LTS	62.1962	113.4058	226.2582	14.0597	55.2749	9.7647	0.2872	6.3815	477.1686	22.1930	47.9930	5.8139	23.5731	5.0786	1.1298	4.1855	0.6021	3.2535	0.5830	1.4029	0.2076	1.3032	0.1985	5.1882	1.5782	0.5710	18.3030	0.2301	8.4110	1.3953
M43038	G88(4185.4m)	LTS	82.0618	144.7830	198.9594	11.7383	51.2295	11.1025	0.2053	8.6548	669.3521	22.6724	44.2205	5.3451	20.2451	4.3907	0.9615	3.5563	0.5165	2.7911	0.5119	1.3963	0.2434	1.1853	0.1663	3.1483	1.3170	0.7897	24.8555	0.3130	9.3676	1.6533
M43038 DUP		LTS	73.6518	125.3666	170.4974	10.2691	41.5236	9.3943	0.2248	7.8028	558.1393	19.5877	37.6356	4.7636	17.9751	3.7297	0.8047	3.0483	0.4520	2.2311	0.4439	1.1652	0.2018	0.9929	0.1419	2.5970	1.1350	0.7287	22.0384	0.2874	8.2673	1.4946
Blank and Reference Standards																																
	BLANK-33		-0.2856	0.0541	0.0425	0.0633	5.1615	0.0019	0.0577	-0.0255	0.2083	0.0018	0.0051	-0.0037	-0.0473	-0.0386	-0.0142	0.0149	0.0023	0.0248	0.0032	-0.0340	-0.0027	0.0170	-0.0041	3.4523	0.0074	-0.0268	0.0556	0.0131	0.5509	0.0017
	SGR-1B-1		122.6225	78.5926	366.1507	8.3420	24.0725	5.0945	34.0099	5.1031	278.6706	18.0118	33.8162	3.8808	14.2533	2.2582	0.4232	1.7580	0.2658	1.5943	0.3119	0.8655	0.1603	0.7956	0.1101	1.6047	0.3059	0.6187	41.9180	0.8665	6.5399	5.2508
	SDO-1-1		31.8523	134.6900	77.4066	31.8560	122.3857	10.6638	170.6324	6.9378	454.2658	37.3953	76.1373	9.2595	37.3097	7.4854	1.4769	6.8063	0.9763	5.4362	1.0995	3.1210	0.4389	2.7271	0.4148	8.5568	0.9227	6.1019	30.3528	0.3391	14.2153	48.0286
Accepted Values - Reference Standards																																
	SGR-1 USGS		147.0000	na	420.0000	13.0000	53.0000	5.2000	35.0000	5.2000	290.0000	20.0000	36.0000	na	16.0000	2.7000	0.5600	2.0000	na	1.9000	0.4000	1.1000	0.1700	0.9400	na	1.4000	na	na	38.0000	na	4.8000	5.4000
	SDO-1 USGS		28.6 sd 5.5	126 SD 3.9	75.1 SD 11.1	40.6 SD 6.5	165 SD 24	11.4 SD 1.2	134 SD 21	6.9 SD 1.2	397 SD 38	38.5 SD 4.4	79.3 SD 7.8	8.9 SD 0.66	36.6 SD 3.3	7.7 SD 0.81	1.6 SD 0.22	7.4 SD 1.9	1.2 SD 0.24	6.0 SD 0.65		3.6 SD 0.55	0.45 SD 0.08	3.4 Sd 0.46	0.54 SD 0.14	4.7 SD 0.75	1.1 SD 0.13		27.9 SD 5.2		10.5 SD 0.55	48.8 SD 6.5

All values for trace elements presented in ppm. Sample numbers with (B) are duplicate preparations. Stratigraphic units include the Lower Tempest Sandstone (LTS), Lower Kimmeridgian Source Rock (LKSR), Upper Kimmeridgian Source Rock (UKSR), and the Rankin Formation (RF). Reference standards include the SDO-1 (Devonian Ohio Shale) and the SGR-1 (Green River Shale). Accepted values are available from the United States Geological Survey and were established by Kane et al. (1990) for SDO-1 and by Abbey (1983), Gladney and Roelandts (1988) and Govindaraju (1994) for SGR-1.

Appendix B – Heavy Mineral Data & Grain Size Distributions

Sample	Formation	# of grains											Total Heavy Minerals
		Zircon	Tourmaline	Rutile	Apatite	Monazite	Chromite	Titanite	ZTR ratio	MZi index	RZi index	CZi index	per sample
G-70 (3305)	Upper Kimmeridgian Source Rock	38	397	560	166	17	5	38	-	30.91	93.65	11.63	1221
G-70 (3500)	Upper Kimmeridgian Source Rock	74	121	819	145	11	2	73	81.45	12.94	91.71	2.63	1245
G-70 (3715)	Upper Kimmeridgian Source Rock	31	0	270	303	5	7	58	-	13.89	89.70	18.42	674
P-52 (3400)	Upper Kimmeridgian Source Rock	153	0	868	486	18	26	65	63.18	10.53	85.01	14.53	1616
P-52 (3500)	Upper Kimmeridgian Source Rock	101	0	647	132	8	58	55	74.73	7.34	86.50	36.48	1001
I-78 (4500)	Upper Kimmeridgian Source Rock	162	0	777	70	12	9	14	89.94	6.90	82.75	5.26	1044
I-78 (4705)	Upper Kimmeridgian Source Rock	72	0	290	43	2	2	4	87.65	2.70	80.11	2.70	413
Standard Deviation (1 SE)									10.82	9.11	4.89	11.96	
G-70 (4740)	Lower Kimmeridgian Source Rock	45	0	240	16	1	8	5	-	-	-	-	315
G-70 (4820)	Lower Kimmeridgian Source Rock	32	66	426	45	8	3	24	86.75	20.00	93.01	8.57	604
P-52 (3950)	Lower Kimmeridgian Source Rock	41	473	531	597	3	9	103	59.48	6.82	92.83	18.00	1757
G-88 (4495)	Lower Kimmeridgian Source Rock	49	0	354	165	0	5	149	55.82	0.00	87.84	9.26	722
I-78 (5000)	Lower Kimmeridgian Source Rock	154	0	632	76	4	9	22	87.63	2.53	80.41	5.52	897
I-78 (5075)	Lower Kimmeridgian Source Rock	152	0	632	74	1	13	14	88.49	0.65	80.61	7.88	886
Standard Deviation (1 SE)									16.48	8.27	6.23	4.77	
G-70 (4200)	Rankin Formation	46	0	306	77	3	5	19	77.19	6.12	86.93	9.80	456
G-70 (4405)	Rankin Formation	75	1	565	131	13	6	58	75.50	14.77	88.28	7.41	849
G-88 (4600)	Rankin Formation	171	1	1363	192	6	195	96	75.84	3.39	88.85	53.28	2024
G-88 (4000)	Rankin Formation	158	0	795	131	10	7	65	81.73	5.95	83.42	4.24	1166
I-78 (4900)	Rankin Formation	57	1	455	107	7	40	80	68.67	10.94	88.87	41.24	747
Standard Deviation (1 SE)									4.69	4.56	2.29	22.46	
P-52 (3210)	Upper Tempest Sandstone	489	0	272	23	11	11	2	94.18	2.20	35.74	2.20	808
G-88 (3600)	Upper Tempest Sandstone	50	0	400	55	6	14	17	83.03	10.71	88.89	21.88	542
G-88 (3700)	Upper Tempest Sandstone	49	0	298	69	2	19	19	76.10	3.92	85.88	27.94	456
G-88 (3500)	Upper Tempest Sandstone	193	0	1197	135	5	14	59	86.71	2.53	86.12	6.76	1603
Standard Deviation (1 SE)									7.54	3.99	25.65	12.19	
P-52 (3600)	Lower Tempest Sandstone	36	230	479	345	5	31	54	63.14	12.20	93.01	46.27	1180

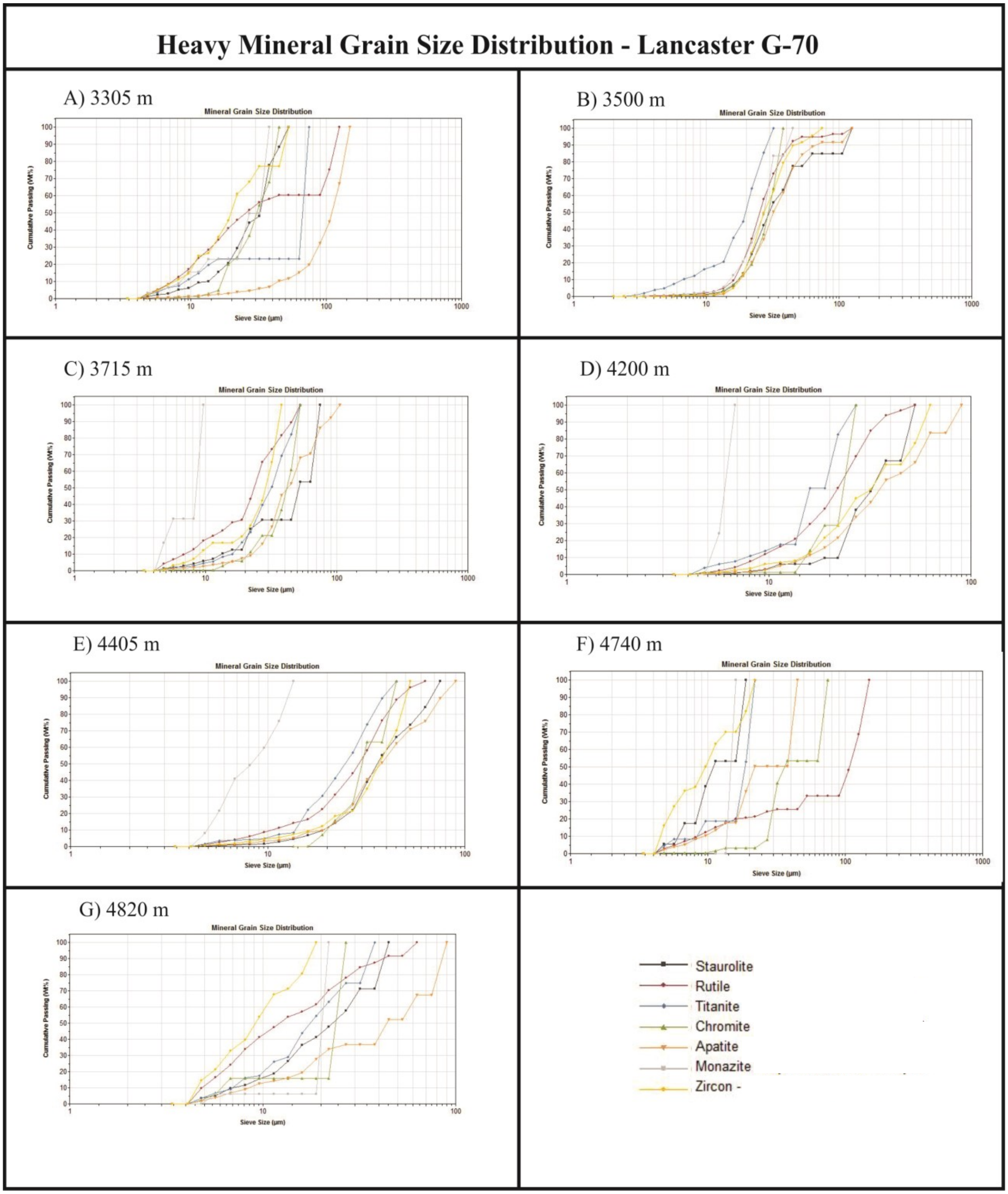

Grain size distribution of heavy minerals in samples from the Lancaster G-70 well calculated by the MLA/SEM. X-axis shows sieve size (µm) and y-axis shows cumulative passing wt.%. As sieve size increases, a greater percentage of mineral grains will pass through a particular sieve size.

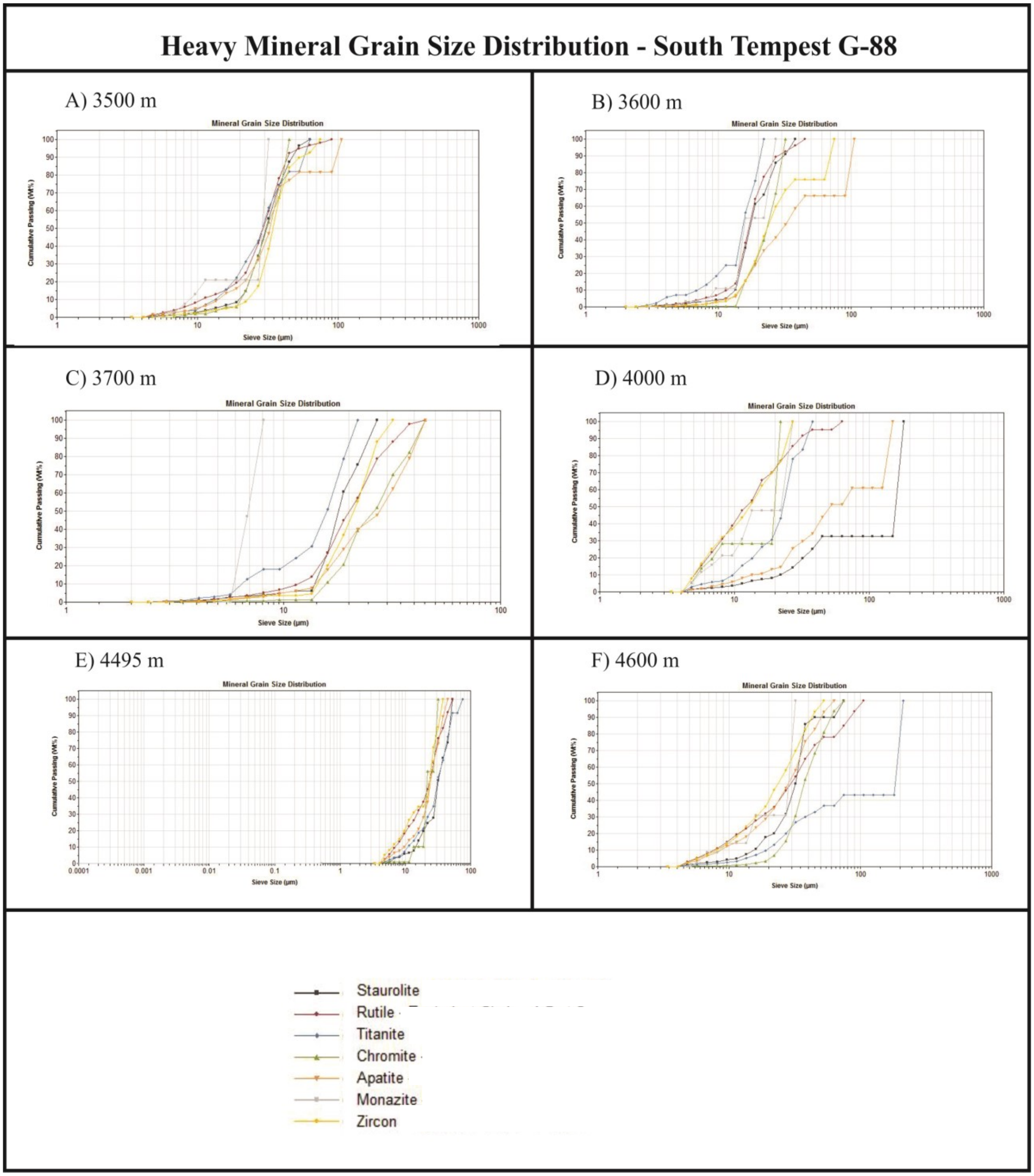

Grain size distribution of heavy minerals in samples from the South Tempest G-88 well calculated by the MLA/SEM. X-axis shows sieve size (µm) and y-axis shows cumulative passing wt.%. As sieve size increases, a greater percentage of mineral grains will pass through a particular sieve size.

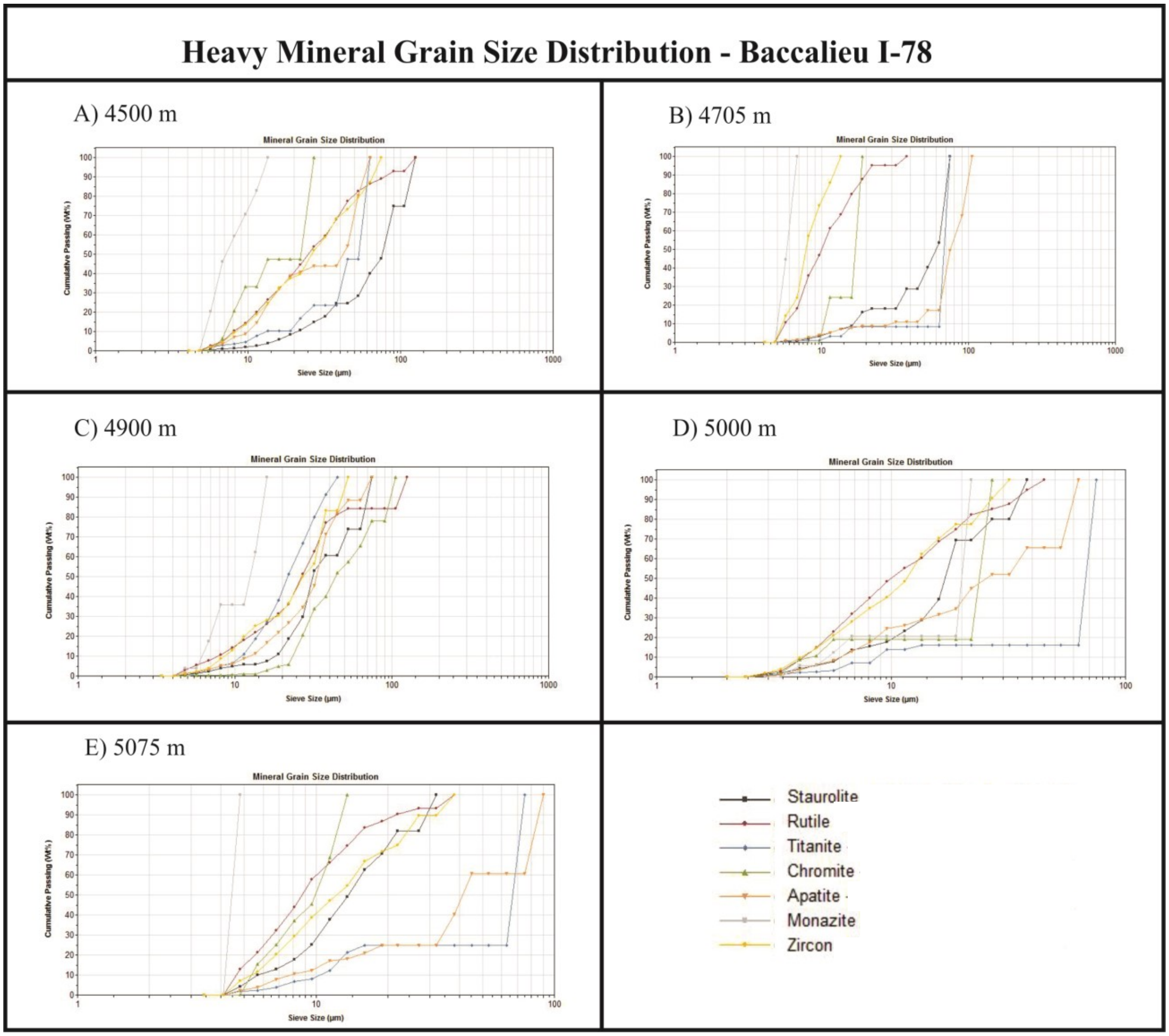

Grain size distribution of heavy minerals in samples from the Baccalieu I-78 well calculated by the MLA/SEM. X-axis shows sieve size (µm) and y-axis shows cumulative passing wt.%. As sieve size increases, a greater percentage of mineral grains will pass through a particular sieve size.

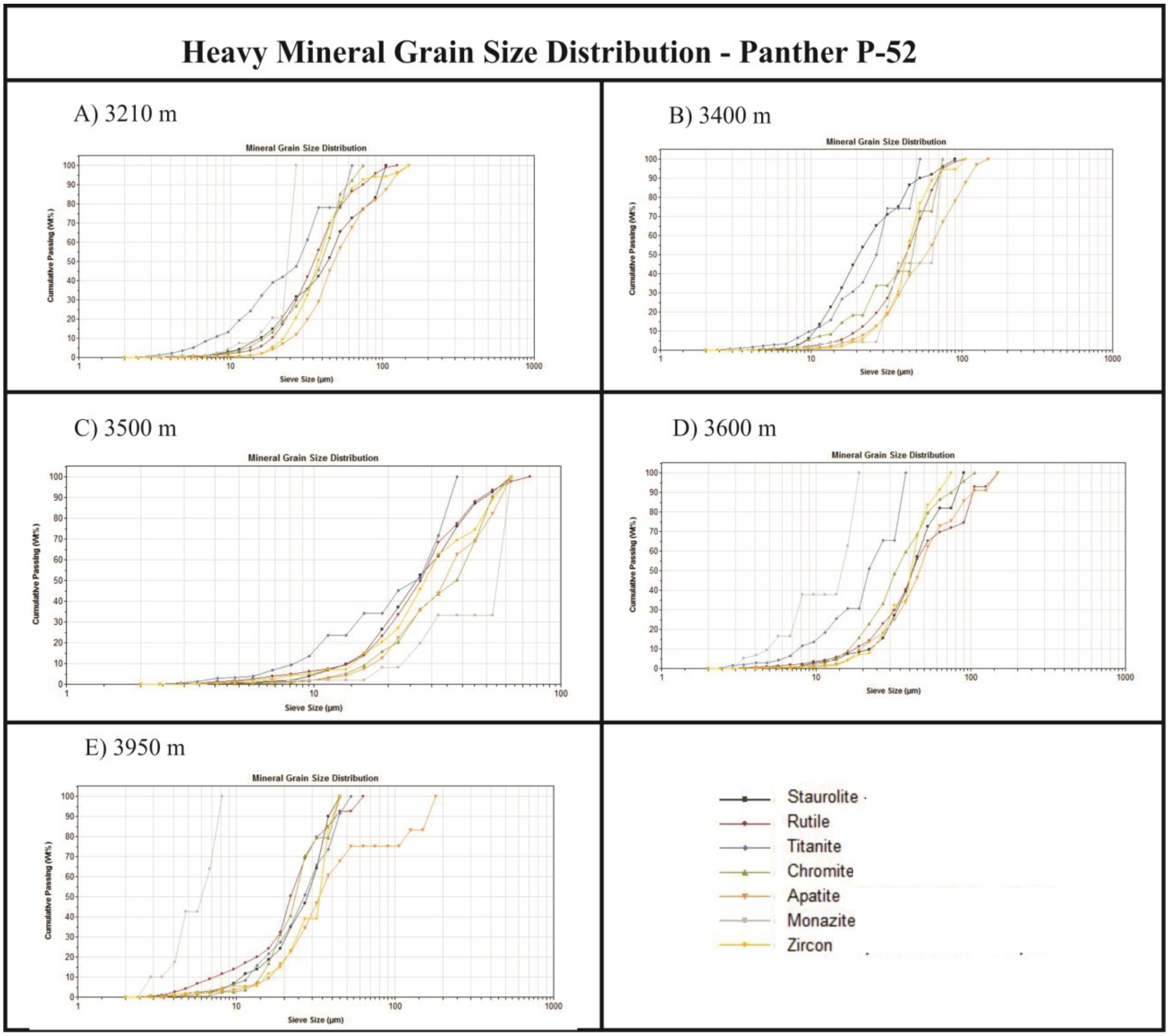

Grain size distribution of heavy minerals in samples from the Panther P-52 well calculated by the MLA/SEM. X-axis shows sieve size (µm) and y-axis shows cumulative passing wt.%. As sieve size increases, a greater percentage of mineral grains will pass through a particular sieve size.

Appendix C – Detrital Zircon U-Pb Data

Baccalieu I-78 (4500 m) Sample

Identifier	Th/U	Data for Tera-Wasserburg plot				Data for Wetherill plot					$^{208}Pb/^{232}Th$	2SE	Dates								% Concordancy *(206Pb-238U age/207Pb-206Pb age)*100*	%Concordancy (206Pb-238U age/207Pb-235U age)*100
		$^{238}U/^{206}Pb$	2SE	$^{207}Pb/^{206}Pb$	2SE	$^{207}Pb/^{235}U$	2SE	$^{206}Pb/^{238}U$	2SE	Rho			$^{207}Pb/^{206}Pb$	2SE	$^{206}Pb/^{238}U$	2SE	$^{207}Pb/^{235}U$	2SE	$^{208}Pb/^{232}Th$	2SE		
I78_4500_1	0.78	11.7096	0.3976	0.0637	0.0022	0.7460	0.0260	0.0854	0.0025	0.5224	0.0268	0.0017	716	66	529	17	567	17	535	34	73.9	93.3
I78_4500_2	0.26	5.1440	0.1482	0.0827	0.0022	2.2190	0.0590	0.1944	0.0046	0.6257	0.0598	0.0037	1257	42	1144	30	1187	24	1173	71	91.0	96.4
I78_4500_3	0.72	2.1186	0.3636	0.2520	0.0260	41.1000	8.5000	0.4720	0.0810	0.9796	1.1900	0.2500	2300	160	1710	230	1880	180	7600	1400	74.3	91.0
I78_4500_4	0.61	10.5820	0.3247	0.0615	0.0016	0.8030	0.0220	0.0945	0.0025	0.5646	0.0302	0.0019	647	49	582	17	596	16	602	37	90.0	97.7
I78_4500_5	0.68	9.6432	0.2697	0.0646	0.0020	0.9400	0.0290	0.1037	0.0024	0.5139	0.0342	0.0022	755	54	635	17	669	19	679	43	84.1	94.9
I78_4500_6	1.05	15.8228	0.4006	0.0574	0.0013	0.5050	0.0100	0.0632	0.0011	0.5715	0.0232	0.0014	499	39	395	10	415	10	464	28	79.1	95.2
I78_4500_7	1.11	15.7233	0.7417	0.1220	0.0058	1.0650	0.0530	0.0636	0.0028	0.4824	0.0217	0.0018	1980	83	397	18	739	29	433	36	20.1	53.7
I78_4500_8	0.35	17.0649	0.4368	0.0550	0.0017	0.4450	0.0120	0.0586	0.0011	0.3068	0.0182	0.0014	405	59	367	9	372	11	365	27	90.7	98.8
I78_4500_9	0.71	6.3052	0.1550	0.0728	0.0016	1.5940	0.0300	0.1586	0.0028	0.5655	0.0485	0.0029	1003	36	949	21	968	19	957	56	94.6	98.0
I78_4500_10	0.46	10.4167	0.3147	0.0613	0.0017	0.8130	0.0210	0.0960	0.0024	0.5179	0.0299	0.0018	643	52	590	17	602	16	596	36	91.8	98.0
I78_4500_11	0.60	10.0604	0.2631	0.0617	0.0022	0.8460	0.0270	0.0994	0.0020	0.3301	0.0317	0.0021	622	68	611	15	620	18	630	40	98.2	98.5
I78_4500_12	0.75	14.5773	0.4037	0.0569	0.0021	0.5300	0.0180	0.0686	0.0015	0.3686	0.0214	0.0013	459	69	428	11	432	14	429	26	93.2	99.0
I78_4500_13	0.50	3.3727	0.0933	0.1072	0.0023	4.3940	0.0970	0.2965	0.0066	0.7544	0.0890	0.0057	1749	30	1669	41	1706	27	1720	100	95.4	97.8
I78_4500_14	0.33	5.7937	0.1544	0.0734	0.0024	1.7410	0.0490	0.1726	0.0036	0.3369	0.0526	0.0037	986	61	1024	25	1022	24	1035	70	103.9	100.2
I78_4500_15	0.42	6.4599	0.1628	0.1018	0.0026	2.1680	0.0440	0.1548	0.0029	0.4132	0.0667	0.0041	1661	40	927	22	1169	21	1304	78	55.8	79.3
I78_4500_16	0.18	17.2891	0.4185	0.0553	0.0013	0.4420	0.0091	0.0578	0.0009	0.5154	0.0200	0.0013	433	40	363	8	371	10	400	25	83.8	97.8
I78_4500_17	1.05	7.3529	0.1892	0.0652	0.0014	1.2270	0.0250	0.1360	0.0026	0.6520	0.0415	0.0025	777	35	822	20	810	17	821	48	105.8	101.5
I78_4500_18	0.47	11.1982	0.3010	0.0629	0.0016	0.7760	0.0200	0.0893	0.0018	0.5055	0.0333	0.0021	685	46	552	14	583	14	661	41	80.6	94.7
I78_4500_19	0.95	10.9649	0.3006	0.0625	0.0029	0.7740	0.0310	0.0912	0.0020	0.2017	0.0307	0.0020	622	87	562	15	584	21	610	40	90.4	96.2
I78_4500_20	0.70	11.2233	0.3779	0.1017	0.0044	1.2610	0.0500	0.0891	0.0026	0.3911	0.0410	0.0028	1622	78	551	17	821	25	812	54	34.0	67.1
I78_4500_21	1.06	8.8106	0.3183	0.3240	0.0180	5.2000	0.3000	0.1135	0.0036	0.4208	0.0997	0.0082	3572	85	692	24	1820	53	1910	150	19.4	38.0
I78_4500_22	0.10	4.3649	0.1429	0.0922	0.0025	2.9260	0.0910	0.2291	0.0064	0.6971	0.0663	0.0056	1464	44	1326	39	1385	29	1292	110	90.6	95.7
I78_4500_23	0.22	12.2100	0.3131	0.0788	0.0020	0.8940	0.0190	0.0819	0.0016	0.4752	0.0325	0.0021	1157	41	507	13	647	15	646	41	43.8	78.3
I78_4500_24	0.70	9.7847	0.2298	0.0619	0.0015	0.8750	0.0180	0.1022	0.0017	0.4687	0.0347	0.0021	672	40	627	14	638	14	688	41	93.3	98.4
I78_4500_25	0.41	9.8135	0.2504	0.0602	0.0015	0.8530	0.0200	0.1019	0.0020	0.5040	0.0319	0.0020	593	44	626	16	625	15	635	38	105.6	100.2
I78_4500_26	0.28	16.1551	0.3915	0.0543	0.0015	0.4630	0.0120	0.0619	0.0011	0.4552	0.0188	0.0012	359	50	387	9	385	11	377	24	107.7	100.3
I78_4500_27	0.68	9.9206	0.3149	0.0616	0.0018	0.8510	0.0240	0.1008	0.0028	0.5289	0.0331	0.0021	639	57	618	19	626	17	658	41	96.7	98.7
I78_4500_28	0.46	15.1976	0.4619	0.0602	0.0017	0.5540	0.0150	0.0658	0.0016	0.6416	0.0229	0.0015	602	53	411	12	445	13	458	30	68.2	92.2
I78_4500_29	0.99	9.2678	0.2663	0.0616	0.0022	0.9110	0.0290	0.1079	0.0025	0.3442	0.0362	0.0024	653	64	661	18	655	19	719	46	101.2	100.9
I78_4500_30	0.68	7.2046	0.3530	0.2000	0.0160	3.8400	0.3000	0.1388	0.0064	0.2645	0.0647	0.0055	2800	130	836	38	1575	62	1265	100	29.9	53.1
I78_4500_31	0.48	15.3610	0.4719	0.0586	0.0018	0.5150	0.0150	0.0651	0.0017	0.5523	0.0218	0.0014	528	57	406	12	420	13	435	27	76.9	96.7
I78_4500_32	0.60	10.6952	0.2631	0.0596	0.0018	0.7640	0.0200	0.0935	0.0017	0.3295	0.0296	0.0018	551	54	576	14	574	15	590	36	104.5	100.3
I78_4500_33	0.26	5.6054	0.1351	0.0812	0.0019	2.0150	0.0400	0.1784	0.0032	0.5139	0.0654	0.0041	1222	36	1058	24	1119	20	1280	78	86.6	94.5

South Tempest G-88 (3837.3 m) Sample

Identifier	Th/U	Data for Tera-Wasserburg plot				Data for Wetherill plot					$^{208}Pb/^{232}Th$	2SE	Dates								% Concordancy (206Pb-238U age/207Pb-206Pb age)*100	%Concordancy (206Pb-238U age/207Pb-235U age)*100
		$^{238}U/^{206}Pb$	2SE	$^{207}Pb/^{206}Pb$	2SE	$^{207}Pb/^{235}U$	2SE	$^{206}Pb/^{238}U$	2SE	Rho			$^{207}Pb/^{206}Pb$	2SE	$^{206}Pb/^{238}U$	2SE	$^{207}Pb/^{235}U$	2SE	$^{208}Pb/^{232}Th$	2SE		
G88_3837A_1	0.11	12.4224	0.5092	0.0586	0.0027	0.6470	0.0270	0.0805	0.0029	0.7120	0.0198	0.0020	533	71	501	19	504	19	396	39	94.0	99.4
G88_3837A_2	0.20	12.5786	0.3164	0.0597	0.0022	0.6610	0.0140	0.0795	0.0014	0.4893	0.0255	0.0018	576	43	493	12	515	14	508	35	85.6	95.7
G88_3837A_3	0.44	10.0705	0.3245	0.0613	0.0030	0.8460	0.0380	0.0993	0.0026	0.4929	0.0300	0.0023	633	79	609	19	620	24	597	46	96.2	98.2
G88_3837A_4	0.98	10.5485	0.2782	0.0612	0.0028	0.7940	0.0260	0.0948	0.0017	0.2643	0.0300	0.0020	602	67	584	15	594	19	596	39	97.0	98.3
G88_3837A_5	0.48	5.0505	0.1837	0.1573	0.0058	4.3200	0.1500	0.1980	0.0062	0.8832	0.0571	0.0039	2415	35	1153	37	1674	35	1121	74	47.7	68.9
G88_3837A_6	0.39	9.4518	0.3752	0.0625	0.0034	0.8880	0.0410	0.1058	0.0037	0.4877	0.0330	0.0024	659	96	648	24	647	26	655	47	98.3	100.2
G88_3837A_7	0.41	12.1065	0.4983	0.0694	0.0036	0.7930	0.0370	0.0826	0.0031	0.5099	0.0277	0.0021	920	87	511	20	597	23	552	41	55.5	85.6
G88_3837A_8	0.34	15.4321	0.4287	0.0586	0.0028	0.5070	0.0170	0.0648	0.0013	0.1724	0.0208	0.0016	473	71	405	11	415	14	415	31	85.5	97.5
G88_3837A_9	0.30	5.2274	0.1585	0.1019	0.0047	2.6290	0.0930	0.1913	0.0046	0.4617	0.0627	0.0044	1638	64	1127	31	1306	33	1229	83	68.8	86.3
G88_3837A_10	0.52	5.2854	0.1397	0.0782	0.0029	2.0560	0.0500	0.1892	0.0036	0.5741	0.0569	0.0037	1139	38	1116	27	1132	25	1118	71	98.0	98.6
G88_3837A_11	1.24	11.0011	0.3510	0.0654	0.0029	0.8240	0.0280	0.0909	0.0024	0.3788	0.0289	0.0019	739	66	560	17	607	19	575	38	75.8	92.3
G88_3837A_12	1.20	10.1523	0.3298	0.0606	0.0027	0.8250	0.0280	0.0985	0.0026	0.5004	0.0296	0.0020	608	67	606	18	610	20	589	39	99.7	99.3
G88_3837A_13	0.47	17.3913	0.5747	0.0624	0.0033	0.4960	0.0220	0.0575	0.0016	0.1626	0.0192	0.0014	597	85	360	11	406	17	386	27	60.3	88.7
G88_3837A_14	0.47	5.5157	0.2251	0.1270	0.0054	3.1300	0.1100	0.1813	0.0066	0.7160	0.0221	0.0021	2065	51	1076	41	1448	34	442	41	52.1	74.3
G88_3837A_15	0.27	34.0136	3.0080	0.1410	0.0220	0.4910	0.0640	0.0294	0.0025	0.3094	0.0080	0.0036	1800	290	186	16	401	43	157	72	10.3	46.4
G88_3837A_16	0.23	3.2258	0.1020	0.1099	0.0048	4.6100	0.1500	0.3100	0.0080	0.4850	0.0875	0.0066	1779	57	1743	48	1749	36	1691	120	98.0	99.7
G88_3837A_17	0.59	10.6157	0.3268	0.0603	0.0026	0.7750	0.0290	0.0942	0.0023	0.4956	0.0302	0.0020	582	66	580	17	579	20	601	40	99.7	100.2
G88_3837B_1	0.50	3.9904	0.1131	0.1043	0.0034	3.6410	0.0630	0.2506	0.0047	0.6242	0.0729	0.0025	1701	27	1441	36	1558	27	1422	48	84.7	92.5
G88_3837B_2	0.63	10.0705	0.2434	0.0597	0.0020	0.8250	0.0130	0.0993	0.0011	0.4028	0.0320	0.0011	587	35	611	14	610	16	637	21	104.1	100.2
G88_3837B_3	0.69	3.1250	0.0938	0.2198	0.0068	9.7300	0.2000	0.3200	0.0069	0.8806	0.0625	0.0025	2980	17	1791	47	2406	33	1227	48	60.1	74.4
G88_3837B_4	0.27	13.1406	0.3454	0.0573	0.0021	0.6090	0.0120	0.0761	0.0012	0.4044	0.0240	0.0010	492	45	473	12	484	14	482	19	96.1	97.8
G88_3837B_5	0.35	18.4298	0.4416	0.0542	0.0018	0.4076	0.0067	0.0543	0.0006	0.3068	0.0170	0.0006	377	38	341	8	347	10	340	12	90.3	98.3
G88_3837B_6	0.91	10.5153	0.2764	0.0635	0.0023	0.8370	0.0190	0.0951	0.0014	0.4246	0.0301	0.0010	701	46	586	14	618	17	600	20	83.5	94.7
G88_3837B_7	0.61	12.8041	0.3771	0.0633	0.0025	0.6880	0.0180	0.0781	0.0016	0.3544	0.0182	0.0008	694	55	486	14	529	17	364	16	70.0	91.8
G88_3837B_8	0.71	14.8611	0.3754	0.0560	0.0020	0.5230	0.0100	0.0673	0.0009	0.4719	0.0215	0.0007	453	45	420	10	426	13	431	15	92.6	98.5
G88_3837B_9	0.50	1.9516	0.0457	0.1840	0.0055	13.0700	0.1000	0.5124	0.0042	0.6566	0.1404	0.0045	2688	11	2667	49	2685	31	2655	80	99.2	99.3
G88_3837B_10	0.45	3.4083	0.0778	0.1071	0.0032	4.3310	0.0350	0.2934	0.0025	0.6151	0.0876	0.0028	1750	14	1658	33	1699	26	1697	52	94.7	97.6
G88_3837B_11	0.53	14.4509	0.4177	0.0610	0.0021	0.5810	0.0100	0.0692	0.0014	0.5288	0.0234	0.0008	632	39	431	12	465	13	468	17	68.3	92.8
G88_3837B_12	0.21	3.0303	0.0735	0.1119	0.0036	5.0700	0.0630	0.3300	0.0039	0.4848	0.1012	0.0041	1826	22	1838	39	1829	28	1944	74	100.7	100.5
G88_3837B_13	1.24	10.7527	0.3122	0.0610	0.0024	0.7880	0.0200	0.0930	0.0018	0.2920	0.0253	0.0012	623	59	574	16	589	17	505	23	92.1	97.5
G88_3837B_14	0.47	9.8039	0.2307	0.0609	0.0020	0.8530	0.0120	0.1020	0.0011	0.5271	0.0324	0.0011	633	28	626	14	627	16	644	22	98.8	99.8
G88_3837B_15	0.50	7.6746	0.1885	0.0705	0.0025	1.2640	0.0220	0.1303	0.0017	0.1649	0.0445	0.0016	936	40	789	18	832	20	881	32	84.3	94.9
G88_3837_1	1.70	2.7878	0.0583	0.1240	0.0032	6.1560	0.0870	0.3587	0.0050	0.5286	0.1016	0.0017	2010	24	1973	35	1997	26	1957	31	98.2	98.8
G88_3837_2	0.82	4.6751	0.1290	0.0842	0.0028	2.4940	0.0620	0.2139	0.0049	0.4423	0.0617	0.0016	1309	50	1247	31	1267	26	1211	31	95.3	98.4
G88_3837_3	0.40	10.4493	0.2402	0.0591	0.0019	0.7750	0.0190	0.0957	0.0016	0.4117	0.0309	0.0009	546	52	590	13	582	16	616	17	108.0	101.3
G88_3837_4	0.79	8.2169	0.2026	0.0745	0.0026	1.2560	0.0290	0.1217	0.0023	0.2201	0.0241	0.0007	1045	54	741	17	825	20	482	13	70.9	89.8
G88_3837_5	0.64	11.3507	0.2834	0.0643	0.0019	0.7800	0.0160	0.0881	0.0017	0.5823	0.0198	0.0006	751	40	544	13	585	15	396	12	72.4	92.9
G88_3837_6	0.54	11.7647	0.2768	0.0581	0.0023	0.6850	0.0240	0.0850	0.0015	0.3086	0.0247	0.0009	516	73	527	12	528	18	493	18	102.1	99.7
G88_3837_7	0.69	10.7991	0.2682	0.0572	0.0026	0.7410	0.0280	0.0926	0.0019	0.1629	0.0299	0.0010	457	80	571	14	563	20	595	19	124.9	101.4
G88_3837_8	0.94	3.3322	0.0688	0.1042	0.0028	4.3250	0.0630	0.3001	0.0041	0.4739	0.0859	0.0015	1697	27	1690	30	1696	25	1664	28	99.6	99.6
G88_3837_9	0.23	3.5676	0.0738	0.1006	0.0026	3.8920	0.0560	0.2803	0.0039	0.5447	0.0864	0.0023	1639	26	1593	29	1612	25	1672	43	97.2	98.8
G88_3837_10	0.32	1.5480	0.0383	0.1344	0.0041	12.0700	0.2700	0.6460	0.0130	0.5268	0.1437	0.0066	2139	37	3206	63	2606	33	2720	120	149.9	123.0
G88_3837_11	0.52	11.0865	0.2458	0.0589	0.0018	0.7350	0.0150	0.0902	0.0014	0.3737	0.0268	0.0006	542	46	556	12	558	15	535	11	102.7	99.7
G88_3837_12	0.99	11.6822	0.2593	0.0646	0.0021	0.7640	0.0200	0.0856	0.0014	0.4281	0.0279	0.0006	744	52	529	11	578	17	556	12	71.1	91.5
G88_3837_13	0.40	5.6948	0.1362	0.0724	0.0027	1.7470	0.0470	0.1756	0.0032	0.2756	0.0511	0.0019	976	60	1042	23	1028	25	1005	36	106.8	101.4
G88_3837_14	0.53	5.5157	0.1278	0.0755	0.0021	1.8890	0.0380	0.1813	0.0031	0.4660	0.0538	0.0011	1071	36	1073	23	1081	23	1058	22	100.2	99.3
G88_3837_15	0.33	7.6864	0.1595	0.0671	0.0018	1.1960	0.0200	0.1301	0.0019	0.4627	0.0389	0.0010	843	34	788	16	801	18	771	19	93.5	98.4
G88_3837_16	0.21	10.4603	0.2517	0.0596	0.0022	0.7760	0.0210	0.0956	0.0017	0.2551	0.0325	0.0016	571	61	589	13	583	18	645	31	103.2	101.0
G88_3837_17	0.27	11.5741	0.6162	0.0642	0.0045	0.7550	0.0390	0.0864	0.0044	0.1494	0.0231	0.0019	670	140	533	27	566	26	460	38	79.6	94.2
G88_3837_18	0.39	11.1235	0.2351	0.0581	0.0018	0.7240	0.0160	0.0899	0.0014	0.3685	0.0289	0.0007	527	48	555	11	553	15	575	14	105.2	100.2
G88_3837_19	0.43	6.1576	0.1441	0.0736	0.0026	1.6270	0.0380	0.1624	0.0028	0.2351	0.0506	0.0015	1006	54	970	21	980	23	995	29	96.4	99.0
G88_3837_20	0.35	10.6724	0.2392	0.0587	0.0019	0.7610	0.0210	0.0937	0.0016	0.4197	0.0283	0.0009	523	54	577	13	572	17	564	17	110.3	100.9
G88_3837_21	0.54	10.6724	0.2392	0.0580	0.0019	0.7420	0.0190	0.0937	0.0015	0.2963	0.0296	0.0008	526	53	578	12	562	16	591	15	109.8	102.8
G88_3837_22	0.73	18.2815	0.6684	0.1235	0.0100	0.9480	0.0770	0.0547	0.0018	0.1266	0.0237	0.0015	1870	130	343	12	655	39	473	29	18.3	52.4
G88_3837_23	0.36	6.3573	0.1859	0.0752	0.0024	1.6110	0.0480	0.1573	0.0039	0.6082	0.0436	0.0018	1063	50	941	26	973	25	862	35	88.5	96.7
G88_3837_24	0.24	7.1685	0.1696	0.0761	0.0025	1.4720	0.0310	0.1395	0.0026	0.3709	0.0354	0.0013	1092	48	841	19	916	21	703	26	77.0	91.8
G88_3837_25	0.43	2.4576	0.0501	0.1410	0.0035	7.8900	0.1000	0.4069	0.0054	0.6282	0.1279	0.0025	2239	20	2199	38	2217	27	2429	44	98.2	99.2
G88_3837_26	1.05	22.5225	0.6594	0.0525	0.0018	0.3210	0.0100	0.0444	0.0011	0.6041	0.0146	0.0003	312	58	281	8	282	10	292	7	90.0	99.5
G88_3837_27	0.57	9.8717	0.1949	0.0592	0.0016	0.8310	0.0130	0.1013	0.0012	0.4598	0.0320	0.0006	568	33	622	12	613	15	636	11	109.5	101.4
G88_3837_28	0.50	5.2247	0.1065	0.0787	0.0020	2.0770	0.0280	0.1914	0.0026	0.5244	0.0574	0.0009	1165	27	1131	21	1140	21	1128	18	97.1	99.3
G88_3837_29	1.01	2.8121	0.0577	0.1237	0.0032	6.0830	0.0910	0.3556	0.0048	0.5266	0.1063	0.0017	2004	25	1959	35	1985	27	2040	32	97.8	98.7
G88_3837_30	0.51	10.0705	0.3347	0.0667	0.0032	0.8950	0.0400	0.0993	0.0029	0.3717	0.0386	0.0021	766	90	612	19	651	26	765	40	79.9	94.0
G88_3837_31	0.78	1.9231	0.0481	0.1907	0.0053	13.6500	0.2700	0.5200	0.0100	0.6452	0.1581	0.0034	2740	27	2711	56	2727	31	2962	59	98.9	99.4
G88_3837_32	0.65	3.5236	0.0931	0.1078	0.0030	4.2530	0.0910	0.2838	0.0062	0.6543	0.0817	0.0020	1762	32	1608	38	1683	28	1587	37	91.3	95.5
G88_3837_33	0.64	9.3197	0.2345	0.0634	0.0028	0.9490	0.0340	0.1073	0.0021	0.1996	0.0336	0.0013	661	77	658	16	679	22	668	25	99.5	96.9
G88_3837_34	0.75	4.7059	0.1041	0.0912	0.0027	2.6840	0.0530	0.2125	0.0034	0.4351	0.0724	0.0015	1450	38	1242	25	1323	25	1412	29	85.7	93.9
G88_3837_35	0.56	15.4560	0.3344	0.0558	0.0020	0.4970	0.0130	0.0647	0.0010	0.3019	0.0203	0.0006	419	58	405	9	409	12	406	11	96.6	99.0
G88_3837_36	0.48	11.8483	0.2948	0.0595	0.0017	0.6880	0.0140	0.0844	0.0017	0.5824	0.0238	0.0006	578	37	522	12	533	14	475	11	90.3	98.0

Lancaster G-70 (4405 m) Sample – Uncorrected Data

Identifier	Th/U	Data for Tera-Wasserburg plot				Data for Wetherill plot					$^{208}Pb/^{232}Th$	2SE	Dates								% Concordancy (206Pb-238U age/207Pb-206Pb age)*100	%Concordancy (206Pb-238U age/207Pb-235U age)*100
		$^{238}U/^{206}Pb$	2SE	$^{207}Pb/^{206}Pb$	2SE	$^{207}Pb/^{235}U$	2SE	$^{206}Pb/^{238}U$	2SE	Rho			$^{207}Pb/^{206}Pb$	2SE	$^{206}Pb/^{238}U$	2SE	$^{207}Pb/^{235}U$	2SE	$^{208}Pb/^{232}Th$	2SE		
G70_4405_1	0.79	9.3985	0.4152	0.0689	0.4083	1.0300	0.0340	0.1064	0.0028	0.4130	0.0377	0.0023	882	64	655	28	718	26	748	44	74.3	91.2
G70_4405_2	0.97	2.3419	0.1152	0.3978	0.2770	23.4300	0.8400	0.4270	0.0140	0.7796	0.3760	0.0220	3909	33	2298	97	3235	51	6460	320	58.8	71.0
G70_4405_3	0.39	4.5537	0.1908	0.0976	0.5595	2.9340	0.0500	0.2196	0.0046	0.7918	0.0588	0.0034	1574	23	1276	49	1388	33	1153	65	81.1	91.9
G70_4405_4	0.64	4.7619	0.2948	0.5230	0.5358	14.8400	0.5600	0.2100	0.0110	0.8699	0.3810	0.0230	4304	40	1226	69	2812	57	6510	340	28.5	43.6
G70_4405_5	0.43	2.4752	0.1042	0.1366	0.4852	7.5400	0.1600	0.4040	0.0091	0.6653	0.1308	0.0071	2178	31	2188	78	2175	39	2487	130	100.5	100.6
G70_4405_6	0.15	2.4528	0.1023	0.2008	0.2044	11.2800	0.3700	0.4077	0.0091	0.5251	0.4470	0.0410	2831	46	2201	79	2540	47	7390	570	77.7	86.7
G70_4405_7	0.89	21.3675	1.4610	0.1373	0.8219	0.8360	0.0250	0.0468	0.0028	0.3180	0.0214	0.0015	2112	95	294	20	617	23	428	30	13.9	47.6
G70_4405_8	0.24	10.1729	0.5071	0.1783	0.3684	2.4300	0.1100	0.0983	0.0034	0.3151	0.1334	0.0110	2629	72	604	29	1251	43	2550	190	23.0	48.3
G70_4405_9	0.57	2.5510	0.1106	0.1394	0.4536	7.4400	0.1900	0.3920	0.0100	0.6607	0.1118	0.0063	2218	36	2139	82	2163	41	2140	110	96.4	98.9
G70_4405_10	1.60	2.8547	0.1141	0.1147	0.3294	5.5700	0.0960	0.3503	0.0054	0.6048	0.1014	0.0054	1876	26	1939	66	1915	36	1950	98	103.4	101.3
G70_4405_11	0.46	11.1483	0.4474	0.0622	0.3849	0.7640	0.0240	0.0897	0.0017	0.1634	0.0304	0.0018	622	72	554	21	572	22	604	35	89.1	96.8
G70_4405_12	1.21	17.3010	0.8680	0.2860	-0.0146	2.3200	0.1500	0.0578	0.0021	0.4924	0.0335	0.0023	3353	82	362	18	1209	53	666	44	10.8	29.9
G70_4405_13	1.03	12.7227	0.6960	0.1555	0.6757	1.6810	0.0610	0.0786	0.0032	0.1900	0.0339	0.0022	2412	79	487	26	1002	33	673	43	20.2	48.6
G70_4405_14	0.66	10.3734	0.4520	0.1810	-0.4548	2.3400	0.2200	0.0964	0.0024	0.6576	0.0679	0.0072	2530	140	593	25	1207	74	1320	130	23.4	49.1
G70_4405_15	0.31	10.7296	0.4375	0.1117	0.1399	1.4720	0.0570	0.0932	0.0018	0.4248	0.0605	0.0034	1791	61	575	23	916	33	1189	63	32.1	62.8
G70_4405_16	0.28	10.9170	0.4410	0.0820	0.3203	1.0500	0.0230	0.0916	0.0016	0.4891	0.0435	0.0026	1250	37	565	22	728	23	859	51	45.2	77.7
G70_4405_17	0.33	6.8493	0.3049	0.1179	0.0905	2.3580	0.0780	0.1460	0.0037	0.2072	0.0945	0.0064	1907	52	878	36	1225	37	1822	120	46.0	71.7
G70_4405_18	0.31	3.6576	0.1472	0.0931	0.5250	3.4850	0.0570	0.2734	0.0050	0.5944	0.0781	0.0044	1496	30	1558	56	1523	34	1522	83	104.1	102.3
G70_4405_19	0.21	3.8820	0.1808	0.1107	0.4738	3.9100	0.1300	0.2576	0.0079	0.7188	0.0578	0.0047	1818	45	1476	62	1617	41	1135	89	81.2	91.3
G70_4405_20	1.10	2.2727	0.1033	0.1732	0.3960	10.7600	0.2600	0.4400	0.0120	0.5495	0.1223	0.0065	2586	36	2355	87	2502	42	2332	120	91.1	94.1
G70_4405_21	1.09	2.1872	0.0861	0.1777	0.5212	11.2500	0.1400	0.4572	0.0069	0.6466	0.1310	0.0068	2627	20	2430	79	2544	38	2489	120	92.5	95.5
G70_4405_22	1.12	7.1378	0.3312	0.0709	0.4806	1.3620	0.0360	0.1401	0.0042	0.3901	0.0420	0.0024	936	70	844	37	871	28	832	47	90.2	96.9
G70_4405_23	0.56	12.9032	0.6826	0.0883	0.3415	0.9670	0.0430	0.0775	0.0030	0.5768	0.0302	0.0020	1403	72	481	24	687	29	602	39	34.3	70.0
G70_4405_24	0.54	5.3562	0.2639	0.1493	0.5480	3.8100	0.1200	0.1867	0.0063	0.6218	0.0491	0.0035	2342	51	1107	49	1591	40	968	67	47.3	69.6
G70_4405_25	0.66	3.9761	0.1581	0.1052	0.5875	3.6240	0.0560	0.2515	0.0048	0.7670	0.0669	0.0038	1720	22	1445	53	1557	34	1310	71	84.0	92.8
G70_4405_26	1.02	3.0030	0.1263	0.1131	0.3798	5.1900	0.1200	0.3330	0.0068	0.5005	0.1064	0.0059	1840	38	1850	66	1846	40	2044	110	100.5	100.2
G70_4405_27	0.55	5.4142	0.3518	0.1128	0.4762	2.8200	0.1300	0.1847	0.0099	0.9050	0.0656	0.0044	1841	40	1091	65	1355	46	1284	83	59.3	80.5
G70_4405_28	0.67	2.8409	0.1130	0.1177	0.4034	5.6730	0.0880	0.3520	0.0063	0.8113	0.1066	0.0057	1923	17	1942	68	1931	36	2045	100	101.0	100.6
G70_4405_29	0.47	9.1324	0.4003	0.1061	0.2604	1.5800	0.0780	0.1095	0.0026	0.2841	0.0533	0.0036	1730	93	670	28	962	41	1055	71	38.7	69.6
G70_4405_30	0.37	52.1921	2.1247	0.1069	-0.0054	0.2860	0.0110	0.0192	0.0004	0.5037	0.0128	0.0008	1723	58	122	5	254	12	258	16	7.1	48.1
G70_4405_31	0.29	6.9541	0.3337	0.0910	0.4057	1.8120	0.0600	0.1438	0.0045	0.5225	0.0733	0.0047	1454	55	865	39	1049	32	1429	88	59.5	82.5
G70_4405_32	0.78	4.2808	0.1778	0.1402	0.3998	4.4450	0.0990	0.2336	0.0048	0.6007	0.0681	0.0037	2226	32	1352	51	1724	36	1335	72	60.7	78.4
G70_4405_33	0.84	9.3985	0.3887	0.0627	0.4897	0.9260	0.0190	0.1064	0.0021	0.5645	0.0329	0.0017	686	39	653	25	665	22	654	34	95.2	98.2
G70_4405_34	0.30	22.6757	1.0798	0.0783	0.3029	0.4750	0.0170	0.0441	0.0014	0.5629	0.0223	0.0013	1137	69	278	13	393	18	445	26	24.4	70.7
G70_4405_35	0.66	9.8232	0.4342	0.0683	0.5241	0.9570	0.0270	0.1018	0.0026	0.3899	0.0293	0.0016	863	62	627	27	683	23	583	32	72.7	91.8
G70_4405_36	1.17	3.3212	0.1544	0.2540	0.6426	10.2400	0.2300	0.3011	0.0095	0.2135	0.1152	0.0066	3187	55	1695	71	2452	40	2200	120	53.2	69.1
G70_4405_37	0.06	13.5685	0.6444	0.0629	0.4059	0.6310	0.0200	0.0737	0.0023	0.6177	0.0201	0.0016	710	55	460	21	495	20	402	32	64.8	92.9
G70_4405_38	0.30	9.1996	0.4316	0.1475	0.8168	2.1830	0.0410	0.1087	0.0033	0.1610	0.0790	0.0066	2290	59	664	30	1178	30	1528	120	29.0	56.4
G70_4405_39	1.01	13.4409	0.8491	0.0874	0.6429	0.8770	0.0340	0.0744	0.0038	0.3944	0.0231	0.0015	1320	100	462	28	639	25	462	29	35.0	72.3
G70_4405_40	0.35	10.1010	0.3979	0.0624	0.4097	0.8380	0.0190	0.0990	0.0017	0.2808	0.0312	0.0019	657	53	608	23	617	21	620	36	92.6	98.6
G70_4405_41	0.53	8.6356	0.3505	0.1818	0.3162	2.9140	0.0650	0.1158	0.0021	0.5178	0.0950	0.0053	2661	33	706	27	1388	34	1829	96	26.5	50.9
G70_4405_42	0.83	12.4070	0.6157	0.1300	-0.0678	1.4290	0.0870	0.0806	0.0027	0.6323	0.0373	0.0025	2069	84	500	24	896	42	739	49	24.2	55.8
G70_4405_43	0.74	9.7752	0.5447	0.1517	0.0683	2.1800	0.1400	0.1023	0.0044	0.6133	0.0517	0.0035	2352	75	628	34	1167	52	1019	67	26.7	53.8
G70_4405_44	0.36	2.1786	0.0949	0.1777	0.3439	11.1900	0.2800	0.4590	0.0110	0.7674	0.1089	0.0064	2632	27	2440	84	2536	42	2088	120	92.7	96.2
G70_4405_45	0.38	9.9108	0.4125	0.0658	0.2046	0.9090	0.0280	0.1009	0.0020	0.4717	0.0372	0.0022	780	55	621	24	653	24	738	42	79.6	95.1
G70_4405_46	0.64	16.1290	0.7544	0.1214	0.3013	1.0270	0.0310	0.0620	0.0019	0.7934	0.0254	0.0015	1978	32	387	18	713	25	506	30	19.6	54.3
G70_4405_47	0.59	11.9190	0.4830	0.0612	0.4996	0.7120	0.0120	0.0839	0.0014	0.5332	0.0263	0.0014	648	34	519	20	546	18	525	28	80.1	95.1
G70_4405_48	0.52	4.7103	0.2174	0.1113	0.5878	3.2490	0.0830	0.2123	0.0061	0.5714	0.0636	0.0042	1831	45	1243	53	1469	35	1246	80	67.9	84.6
G70_4405_49	0.75	4.4444	0.2765	0.1169	0.3184	3.5400	0.1700	0.2250	0.0120	0.9077	0.0437	0.0060	1910	38	1301	73	1541	55	870	120	68.1	84.4
G70_4405_50	0.45	10.9529	0.5398	0.1056	0.4797	1.3310	0.0470	0.0913	0.0031	0.4579	0.0366	0.0025	1713	63	563	27	857	34	726	48	32.9	65.7
G70_4405_51	1.19	8.5470	0.4529	0.1156	0.2627	1.8840	0.0780	0.1170	0.0047	0.7131	0.0740	0.0320	1879	44	713	36	1077	40	1040	310	37.9	66.2
G70_4405_52	1.31	16.1031	0.7001	0.1092	0.3239	0.9420	0.0270	0.0621	0.0017	0.5637	0.0173	0.0010	1773	49	388	17	672	27	347	21	21.9	57.7
G70_4405_53	0.91	8.5324	0.4805	0.3360	0.5235	5.5200	0.2700	0.1172	0.0051	0.3260	0.1018	0.0072	3621	70	713	38	1918	64	1957	130	19.7	37.2
G70_4405_54	1.27	27.0270	1.1687	0.2373	0.2040	1.2030	0.0470	0.0370	0.0010	0.4920	0.0172	0.0012	3079	55	234	10	798	34	344	23	7.6	29.3
G70_4405_55	0.38	16.8919	0.7133	0.1574	0.2494	1.3040	0.0370	0.0592	0.0014	0.6430	0.0558	0.0035	2422	38	372	15	845	31	1100	68	15.3	44.0
G70_4405_56	0.67	3.3670	0.1360	0.1374	0.5130	5.6800	0.1200	0.2970	0.0068	0.5501	0.1048	0.0062	2178	33	1675	62	1927	45	2013	110	76.9	86.9
G70_4405_57	1.06	9.0662	0.6329	0.1271	0.7928	1.9300	0.0710	0.1103	0.0067	0.6155	0.0238	0.0018	1995	88	677	46	1085	40	474	35	33.9	62.4
G70_4405_58	1.40	7.2046	0.4879	0.3470	0.5539	6.7800	0.3600	0.1396	0.0082	0.3116	0.0744	0.0058	3730	110	836	53	2074	61	1460	110	22.4	40.3
G70_4405_59	1.15	11.1235	0.4454	0.1282	0.6070	1.5420	0.0480	0.0899	0.0018	0.0388	0.0413	0.0026	2014	70	555	21	945	35	818	50	27.6	58.7
G70_4405_60	0.61	3.1949	0.6737	0.3780	0.6070	16.6000	3.5000	0.3130	0.0650	0.6123	0.4100	0.1200	3780	180	1710	290	2800	180	6500	1500	45.2	61.1
G70_4405_61	0.53	19.0114	1.3373	0.1634	0.2640	1.2170	0.0800	0.0526	0.0032	0.8075	0.0351	0.0029	2465	56	332	23	798	44	696	57	13.5	41.6
G70_4405_62	0.53	9.5057	0.4156	0.2180	0.1177	3.2700	0.2700	0.1052	0.0027	0.2984	0.1170	0.0130	2810	160	646	27	1402	82	2200	240	23.0	46.1

Lancaster G-70 (4405 m) Sample – Andersen (2002) Corrected Data

Identifier	Data for Tera-Wasserburg plot - Andersen corrected				Data for Wetherill plot - Andersen corrected							Dates - Andersen corrected								% Concordancy *(206Pb-238U age/207Pb-206Pb age)*100*	% Concordancy (206Pb-238U age/207Pb-235U age)*100
	$^{238}U/^{206}Pb$	2SE	$^{207}Pb/^{206}Pb$	2SE	$^{207}Pb/^{235}U$	2SE	$^{206}Pb/^{238}U$	2SE	Rho	$^{208}Pb/^{232}Th$	2SE	$^{207}Pb/^{206}Pb$	2SE	$^{206}Pb/^{238}U$	2SE	$^{207}Pb/^{235}U$	2SE	$^{208}Pb/^{232}Th$	2SE		
G70_4405_1	9.3985	0.2400	0.0570	0.0013	0.8270	0.0580	0.1050	0.0052	0.8581	0.0377	0.0012	469	52	648	30	608	32	671	37	138.2	106.6
G70_4405_2	2.3419	0.0800	0.1355	0.0063	5.1900	0.7400	0.2910	0.0210	0.8632	0.3760	0.0120	2166	82	1651	100	1884	120	3010	440	76.2	87.6
G70_4405_3	4.5537	0.0950	0.0872	0.0014	2.6680	0.2300	0.2173	0.0099	0.9193	0.0588	0.0016	1351	31	1265	53	1299	66	1000	110	93.6	97.4
G70_4405_4	4.7619	0.2500	0.1610	0.0210	2.6800	0.6000	0.1218	0.0085	0.5779	0.3810	0.0130	2340	280	740	49	1310	180	2980	450	31.6	56.5
G70_4405_5	2.4752	0.0560	0.1315	0.0017	7.1700	0.4900	0.4020	0.0180	0.8392	0.1308	0.0026	2114	23	2183	85	2129	61	2289	190	103.3	102.5
G70_4405_6	2.4528	0.0530	0.1406	0.0034	7.2500	0.4300	0.3799	0.0180	0.8199	0.4470	0.0350	2231	42	2078	87	2134	54	2087	95	93.1	97.4
G70_4405_7	21.3675	1.4000	0.0468	0.0004	0.2680	0.0320	0.0418	0.0034	0.9754	0.0214	0.0010	34	16	263	21	238	25	268	33	773.5	110.5
G70_4405_8	10.1729	0.3500	0.0593	0.0011	0.6620	0.0500	0.0840	0.0054	0.9257	0.1334	0.0088	573	40	520	32	513	30	831	120	90.8	101.4
G70_4405_9	2.5510	0.0690	0.1338	0.0027	7.1100	0.4800	0.3910	0.0190	0.7929	0.1118	0.0028	2137	35	2124	88	2121	61	1992	100	99.4	100.1
G70_4405_10	2.8547	0.0440	0.1106	0.0014	5.3600	0.3300	0.3489	0.0150	0.7989	0.1014	0.0015	1800	24	1930	71	1871	55	1887	100	107.2	103.2
G70_4405_11	11.1483	0.2000	0.0547	0.0006	0.6630	0.0290	0.0887	0.0038	0.6810	0.0304	0.0009	390	24	548	23	514	18	544	40	140.5	106.6
G70_4405_12	17.3010	0.5800	0.0495	0.0010	0.2760	0.0210	0.0393	0.0027	0.8279	0.0335	0.0015	158	43	248	17	245	16	235	26	157.0	101.2
G70_4405_13	12.7227	0.5200	0.0529	0.0012	0.5040	0.0510	0.0690	0.0048	0.9656	0.0339	0.0013	309	52	431	29	412	35	392	40	139.5	104.6
G70_4405_14	10.3734	0.2600	0.0574	0.0012	0.6320	0.0250	0.0800	0.0038	0.7765	0.0679	0.0063	486	48	496	22	494	16	684	54	102.1	100.4
G70_4405_15	10.7296	0.2100	0.0554	0.0008	0.6600	0.0260	0.0861	0.0037	0.8746	0.0605	0.0014	412	35	532	22	513	16	661	74	129.1	103.7
G70_4405_16	10.9170	0.1900	0.0565	0.0007	0.6880	0.0370	0.0884	0.0037	0.9118	0.0435	0.0015	465	30	545	22	529	22	535	44	117.3	103.1
G70_4405_17	6.8493	0.1800	0.0613	0.0018	1.1310	0.0710	0.1352	0.0066	0.7339	0.0945	0.0042	684	57	817	37	767	33	966	86	119.4	106.5
G70_4405_18	3.6576	0.0660	0.0922	0.0010	3.4610	0.1800	0.2737	0.0110	0.7177	0.0781	0.0019	1469	20	1557	57	1514	41	1482	80	106.0	102.8
G70_4405_19	3.8820	0.1200	0.1065	0.0039	3.8700	0.3600	0.2580	0.0130	0.8990	0.0578	0.0036	1734	69	1486	71	1593	80	1120	260	85.7	93.3
G70_4405_20	2.2727	0.0620	0.1668	0.0036	10.2200	0.7500	0.4390	0.0220	0.7709	0.1223	0.0019	2518	36	2343	97	2443	71	2221	140	93.1	95.9
G70_4405_21	2.1872	0.0330	0.1696	0.0018	10.6200	0.8000	0.4540	0.0210	0.8463	0.1310	0.0016	2549	19	2410	91	2488	74	2344	140	94.5	96.9
G70_4405_22	7.1378	0.2000	0.0635	0.0021	1.2050	0.1100	0.1387	0.0070	0.7606	0.0420	0.0011	770	60	837	39	804	48	794	42	108.7	104.1
G70_4405_23	12.9032	0.4900	0.0541	0.0015	0.5520	0.0460	0.0734	0.0039	0.9608	0.0302	0.0013	359	66	456	24	443	30	410	41	127.0	102.9
G70_4405_24	5.3562	0.1700	0.0763	0.0013	1.7960	0.1600	0.1702	0.0092	0.9957	0.0491	0.0024	1107	33	1017	52	1046	58	96	64	91.9	97.2
G70_4405_25	3.9761	0.0810	0.0945	0.0015	3.2800	0.3000	0.2491	0.0110	0.8925	0.0669	0.0016	1515	31	1431	58	1470	73	1214	100	94.5	97.3
G70_4405_26	3.0030	0.0640	0.1009	0.0022	4.5100	0.3700	0.3286	0.0150	0.8039	0.1064	0.0023	1619	44	1825	75	1720	69	1877	130	112.7	106.1
G70_4405_27	5.4142	0.2900	0.0836	0.0036	2.1300	0.2900	0.1790	0.0130	0.9781	0.0656	0.0029	1264	83	1059	70	1138	90	966	120	83.8	93.1
G70_4405_28	2.8409	0.0500	0.1142	0.0010	5.4900	0.3300	0.3505	0.0150	0.8730	0.1066	0.0017	1866	16	1933	71	1897	53	1959	120	103.6	101.9
G70_4405_29	9.1324	0.2400	0.0578	0.0018	0.8240	0.0540	0.1028	0.0049	0.8402	0.0533	0.0024	491	74	630	29	606	30	674	46	128.3	104.0
G70_4405_30	52.1921	0.9500	0.0461	0.0000	0.1115	0.0030	0.0175	0.0007	0.9968	0.0128	0.0005	3	1	112	5	107	3	140	11	4215.1	104.2
G70_4405_31	6.9541	0.2100	0.0625	0.0020	1.1850	0.0940	0.1385	0.0071	0.8286	0.0733	0.0028	700	65	835	40	791	44	909	93	119.3	105.6
G70_4405_32	4.2808	0.0930	0.0871	0.0015	2.6900	0.2500	0.2204	0.0110	0.9434	0.0681	0.0014	1360	31	1283	58	1326	66	764	83	94.3	96.8
G70_4405_33	9.3985	0.1900	0.0596	0.0008	0.8540	0.0590	0.1060	0.0046	0.8486	0.0329	0.0005	580	31	649	27	624	32	634	36	111.9	104.0
G70_4405_34	22.6757	0.7600	0.0474	0.0006	0.2780	0.0170	0.0426	0.0022	0.9508	0.0223	0.0007	64	27	269	14	248	13	282	32	419.8	108.3
G70_4405_35	9.8232	0.2500	0.0614	0.0006	0.8520	0.0470	0.1013	0.0049	0.8771	0.0293	0.0007	653	23	621	29	626	26	540	43	95.1	99.2
G70_4405_36	3.3212	0.1000	0.1100	0.0038	3.9900	0.6400	0.2480	0.0180	0.9679	0.1152	0.0031	1779	61	1425	93	1574	130	1124	190	80.1	90.5
G70_4405_37	13.5685	0.4200	0.0564	0.0005	0.5620	0.0330	0.0735	0.0036	0.9262	0.0201	0.0013	470	22	457	21	455	22	211	100	97.2	100.4
G70_4405_38	9.1996	0.2800	0.0620	0.0008	0.8330	0.0940	0.0971	0.0056	0.9806	0.0790	0.0053	674	26	596	33	608	52	410	59	88.4	98.0
G70_4405_39	13.4409	0.7600	0.0527	0.0013	0.5190	0.0540	0.0717	0.0050	0.9701	0.0231	0.0009	299	58	446	30	426	38	373	37	149.2	104.7
G70_4405_40	10.1010	0.1700	0.0559	0.0006	0.7570	0.0380	0.0982	0.0041	0.6876	0.0312	0.0010	436	26	605	24	571	22	561	41	138.8	106.0
G70_4405_41	8.6356	0.1500	0.0592	0.0009	0.7920	0.0430	0.0977	0.0044	0.8370	0.0950	0.0022	555	37	601	26	591	24	879	83	108.3	101.7
G70_4405_42	12.4070	0.4100	0.0511	0.0014	0.5090	0.0320	0.0729	0.0039	0.8764	0.0373	0.0017	226	62	453	23	415	21	468	28	200.4	109.2
G70_4405_43	9.7752	0.4000	0.0548	0.0025	0.6460	0.0480	0.0873	0.0045	0.8893	0.0517	0.0023	380	100	539	27	504	30	533	36	141.8	106.9
G70_4405_44	2.1786	0.0480	0.1783	0.0027	11.4300	0.5700	0.4640	0.0190	0.7903	0.1089	0.0033	2636	25	2454	84	2555	48	2232	100	93.1	96.0
G70_4405_45	9.9108	0.2000	0.0567	0.0010	0.7640	0.0390	0.0995	0.0044	0.8233	0.0372	0.0011	464	41	611	26	575	23	656	43	131.7	106.3
G70_4405_46	16.1290	0.5000	0.0503	0.0008	0.3930	0.0290	0.0564	0.0028	0.9580	0.0254	0.0008	192	36	353	17	334	21	255	26	183.9	105.7
G70_4405_47	11.9190	0.2100	0.0550	0.0007	0.6330	0.0420	0.0832	0.0035	0.8841	0.0263	0.0004	400	29	516	21	498	26	497	32	128.9	103.5
G70_4405_48	4.7103	0.1300	0.0852	0.0021	2.4500	0.2600	0.2065	0.0110	0.8961	0.0636	0.0027	1301	47	1215	60	1242	72	933	120	93.4	97.8
G70_4405_49	4.4444	0.2300	0.0881	0.0036	2.7700	0.3900	0.2180	0.0150	0.9753	0.0437	0.0055	1357	75	1266	80	1321	100	690	140	93.3	95.8
G70_4405_50	10.9529	0.3900	0.0587	0.0007	0.6770	0.0540	0.0858	0.0047	0.9657	0.0366	0.0014	557	28	530	28	526	33	380	57	95.2	100.8
G70_4405_51	8.5470	0.3400	0.0591	0.0021	0.8900	0.0970	0.1086	0.0064	0.9406	0.0740	0.0320	538	82	664	37	642	53	960	360	123.4	103.4
G70_4405_52	16.1031	0.4400	0.0496	0.0010	0.3930	0.0370	0.0576	0.0028	0.9633	0.0173	0.0004	163	44	361	17	334	26	243	18	221.5	108.1
G70_4405_53	8.5324	0.3600	0.0622	0.0020	0.6620	0.0640	0.0755	0.0065	0.8205	0.1018	0.0044	659	74	468	39	516	40	713	120	71.0	90.7
G70_4405_54	27.0270	0.7200	0.0464	0.0002	0.1757	0.0090	0.0275	0.0014	0.9844	0.0172	0.0007	5	4	175	9	164	8	133	16	3294.3	106.5
G70_4405_55	16.8919	0.4000	0.0504	0.0006	0.3482	0.0180	0.0510	0.0024	0.9097	0.0558	0.0016	207	30	321	15	302	14	489	48	155.2	106.3
G70_4405_56	3.3670	0.0790	0.1108	0.0024	4.4700	0.4900	0.2888	0.0140	0.9310	0.1048	0.0018	1813	40	1637	73	1712	91	1649	140	90.3	95.6
G70_4405_57	9.0662	0.5600	0.0630	0.0012	0.8950	0.1300	0.1027	0.0084	0.9937	0.0238	0.0012	699	40	632	50	640	71	252	31	90.4	98.8
G70_4405_58	7.1633	0.4200	0.0669	0.0023	0.9280	0.1300	0.0946	0.0100	0.8358	0.0751	0.0038	813	81	580	59	667	67	483	91	71.3	87.0
G70_4405_59	11.1235	0.2300	0.0531	0.0009	0.5840	0.0360	0.0807	0.0040	0.9191	0.0413	0.0011	311	37	502	24	466	23	572	30	161.4	107.7
G70_4405_60	3.1949	0.5100	0.1330	0.0340	6.1000	3.8000	0.2460	0.0700	0.9937	0.4100	0.1200	1830	330	1360	320	1540	320	1830	780	74.3	88.3
G70_4405_61	19.0114	1.2000	0.0497	0.0009	0.3130	0.0310	0.0453	0.0035	0.9819	0.0351	0.0022	172	41	285	21	274	24	239	39	165.7	104.0
G70_4405_62	9.5057	0.2600	0.0595	0.0012	0.6950	0.0410	0.0857	0.0056	0.9357	0.1170	0.0110	661	30	529	33	538	24	849	73	80.0	98.3

Baccalieu I-78 (4142.2 m) Sample

Identifier	Th/U	Data for Tera-Wasserburg plot				Data for Wetherill plot					$^{208}Pb/^{232}Th$	2SE	Dates								% Concordancy *(206Pb-238U age/207Pb-206Pb age)*100*	% Concordancy (206Pb-238U age/207Pb-235U age)*100
		$^{238}U/^{206}Pb$	2SE	$^{207}Pb/^{206}Pb$	2SE	$^{207}Pb/^{235}U$	2SE	$^{206}Pb/^{238}U$	2SE	Rho			$^{207}Pb/^{206}Pb$	2SE	$^{206}Pb/^{238}U$	2SE	$^{207}Pb/^{235}U$	2SE	$^{208}Pb/^{232}Th$	2SE		
I78_4142_1	0.50	9.3197	0.3735	0.0605	0.0020	0.9070	0.0250	0.1073	0.0017	0.2660	0.0339	0.0023	623	55	657	25	654	20	673	45	105.4414125	100.4434251
I78_4142_2	0.86	9.0662	0.3781	0.0662	0.0031	1.0010	0.0420	0.1103	0.0022	0.1461	0.0368	0.0025	746	90	675	27	695	27	729	50	90.48257373	97.12230216
I78_4142_3	0.41	11.1607	0.4858	0.0614	0.0015	0.7580	0.0190	0.0896	0.0020	0.7924	0.0251	0.0018	649	31	553	23	573	18	500	35	85.20801233	96.5095986
I78_4142_4	0.47	10.6045	0.4498	0.0609	0.0014	0.7850	0.0160	0.0943	0.0019	0.8260	0.0259	0.0018	636	25	581	23	589	16	517	35	91.35220126	98.60828242
I78_4142_5	0.24	5.0684	0.1978	0.0816	0.0017	2.2340	0.0310	0.1973	0.0026	0.8141	0.0534	0.0036	1239	15	1160	42	1190	25	1050	69	93.62389023	97.4789916
I78_4142_6	0.50	10.9529	0.4439	0.0626	0.0021	0.8030	0.0210	0.0913	0.0016	0.3146	0.0258	0.0018	699	59	563	22	603	18	514	35	80.51502146	93.33333333
I78_4142_7	0.99	10.3950	0.3998	0.0595	0.0019	0.7870	0.0180	0.0962	0.0012	0.1851	0.0301	0.0019	567	53	592	22	589	18	599	38	104.3915344	100.4923599
I78_4142_8	0.31	4.6019	0.1779	0.0824	0.0021	2.4650	0.0440	0.2173	0.0026	0.4050	0.0669	0.0043	1249	33	1267	45	1265	27	1308	82	101.4411529	100.1581028
I78_4142_9	0.43	15.0150	0.6087	0.0549	0.0022	0.5070	0.0160	0.0666	0.0012	0.1426	0.0208	0.0015	380	77	415	17	415	15	417	29	109.3157895	100.0963855
I78_4142_10	0.34	9.3721	0.3689	0.0651	0.0022	0.9480	0.0270	0.1067	0.0014	0.1945	0.0348	0.0025	772	57	653	24	675	21	691	48	84.5984456	96.75555556
I78_4142_11	0.47	2.7300	0.1043	0.1213	0.0027	6.1300	0.0740	0.3663	0.0039	0.6466	0.1113	0.0070	1974	18	2011	67	1993	30	2133	130	101.8743668	100.9031611
I78_4142_12	0.58	7.4294	0.2925	0.0765	0.0017	1.4140	0.0180	0.1346	0.0017	0.6592	0.0417	0.0027	1103	21	814	30	895	20	826	51	73.75339982	90.94466182
I78_4142_13	0.82	4.0984	0.1848	0.1105	0.0025	3.7260	0.0990	0.2440	0.0065	0.8903	0.0693	0.0048	1805	19	1404	58	1577	33	1357	91	77.78393352	89.02980342
I78_4142_14	1.24	9.8522	0.3786	0.0602	0.0015	0.8430	0.0120	0.1015	0.0012	0.2840	0.0361	0.0023	607	34	623	23	622	16	717	45	102.6853377	100.2412351
I78_4142_15	0.64	2.7034	0.1023	0.1272	0.0028	6.4990	0.0630	0.3699	0.0037	0.5269	0.1050	0.0066	2060	17	2028	66	2047	30	2018	120	98.44660194	99.0863341
I78_4142_16	0.14	2.8490	0.1136	0.1200	0.0026	5.7750	0.0510	0.3510	0.0038	0.6812	0.0591	0.0042	1953	14	1938	64	1944	29	1161	80	99.23195084	99.70674487
I78_4142_17	0.84	11.0132	0.4366	0.0593	0.0021	0.7440	0.0210	0.0908	0.0013	0.2071	0.0286	0.0019	547	65	561	22	563	19	569	37	102.4680073	99.55595027
I78_4142_18	0.32	10.6383	0.4527	0.0621	0.0017	0.7900	0.0170	0.0940	0.0019	0.6491	0.0293	0.0020	672	40	578	23	590	18	584	39	86.01190476	97.96610169
I78_4142_19	0.85	10.2881	0.4022	0.0600	0.0018	0.8080	0.0190	0.0972	0.0011	0.3033	0.0289	0.0019	596	49	598	22	601	18	576	37	100.2852349	99.45091514
I78_4142_20	0.66	3.2082	0.1235	0.1073	0.0024	4.6040	0.0520	0.3117	0.0029	0.4150	0.0888	0.0056	1757	21	1748	58	1750	29	1720	100	99.48776323	99.90284049
I78_4142_21	0.13	5.0917	0.2022	0.0784	0.0019	2.1290	0.0350	0.1964	0.0030	0.5472	0.0725	0.0050	1154	27	1155	42	1157	25	1413	94	100.0866551	99.82713915

Baccalieu I-78 (4135.29 m) Sample

Identifier	Th/U	Data for Tera-Wasserburg plot				Data for Wetherill plot					$^{208}Pb/^{232}Th$	2SE	Dates								%Concordancy *(206Pb-238U age/207Pb-206Pb age)*100*	%Concordancy (206Pb-238U age/207Pb-235U age)*100
		$^{238}U/^{206}Pb$	2SE	$^{207}Pb/^{206}Pb$	2SE	$^{207}Pb/^{235}U$	2SE	$^{206}Pb/^{238}U$	2SE	Rho			$^{207}Pb/^{206}Pb$	2SE	$^{206}Pb/^{238}U$	2SE	$^{207}Pb/^{235}U$	2SE	$^{208}Pb/^{232}Th$	2SE		
I78_4135_1	0.37	6.9930	0.3228	0.0664	0.0012	1.2820	0.0180	0.1430	0.0015	0.3524	0.0425	0.0020	815	30	862	37	838	28	841	38	105.8	102.8
I78_4135_2	0.46	14.3267	0.6773	0.0552	0.0015	0.5300	0.0130	0.0698	0.0010	0.1982	0.0212	0.0011	397	56	435	20	432	19	423	21	109.5	100.7
I78_4135_3	1.37	9.0580	0.4595	0.0620	0.0032	0.9260	0.0430	0.1104	0.0025	0.0939	0.0329	0.0018	610	100	674	32	662	32	654	35	110.5	101.8
I78_4135_4	0.10	9.8619	0.5155	0.0606	0.0037	0.8170	0.0490	0.1014	0.0027	0.2049	0.0252	0.0054	550	110	623	31	610	35	490	110	113.3	102.1
I78_4135_5	1.06	11.3122	0.5631	0.0659	0.0028	0.7820	0.0300	0.0884	0.0019	0.1057	0.0294	0.0014	746	87	546	26	586	27	586	28	73.2	93.2
I78_4135_6	0.79	26.6667	1.4933	0.0612	0.0019	0.3050	0.0110	0.0375	0.0012	0.5898	0.0077	0.0005	630	67	237	13	272	14	156	9	37.7	87.3
I78_4135_7	0.10	9.6339	0.4641	0.0638	0.0014	0.9010	0.0220	0.1038	0.0018	0.5729	0.0480	0.0029	736	40	638	29	651	26	947	55	86.7	98.0
I78_4135_8	0.07	2.3781	0.1131	0.1316	0.0027	7.5200	0.1300	0.4205	0.0077	0.4936	0.1197	0.0065	2130	33	2260	93	2178	46	2290	120	106.1	103.8
I78_4135_9	0.53	10.0908	0.4684	0.0605	0.0015	0.8270	0.0170	0.0991	0.0010	0.0698	0.0305	0.0014	617	49	609	27	613	25	607	28	98.7	99.4
I78_4135_10	0.66	5.4585	0.2562	0.0763	0.0014	1.9400	0.0290	0.1832	0.0023	0.4178	0.0568	0.0026	1106	31	1084	47	1095	33	1117	50	98.0	99.0
I78_4135_11	0.20	16.9377	0.7746	0.0542	0.0011	0.4428	0.0071	0.0590	0.0005	0.0709	0.0193	0.0010	373	38	370	16	372	16	387	19	99.1	99.5
I78_4135_12	1.00	9.4349	0.4362	0.0612	0.0009	0.9030	0.0110	0.1060	0.0009	0.4312	0.0330	0.0015	647	25	649	28	653	24	657	29	100.4	99.4
I78_4135_13	0.37	2.6983	0.1383	0.1300	0.0019	6.7100	0.1600	0.3706	0.0084	0.8963	0.0981	0.0062	2095	18	2029	89	2071	47	1886	120	96.8	98.0
I78_4135_14	0.80	10.4167	0.4883	0.0581	0.0015	0.7660	0.0180	0.0960	0.0011	0.2148	0.0302	0.0014	515	52	591	26	578	24	602	28	114.8	102.2
I78_4135_15	0.39	2.7122	0.1251	0.1281	0.0014	6.5810	0.0360	0.3687	0.0023	0.6134	0.1094	0.0048	2071	9	2025	79	2057	42	2100	86	97.8	98.4
I78_4135_16	0.94	10.1317	0.4927	0.0610	0.0022	0.8390	0.0290	0.0987	0.0017	0.1626	0.0307	0.0015	612	77	606	28	616	27	611	30	99.1	98.4
I78_4135_17	0.21	4.9628	0.2291	0.0822	0.0011	2.3200	0.0270	0.2015	0.0020	0.6674	0.0620	0.0029	1251	20	1183	50	1217	35	1215	55	94.6	97.2
I78_4135_18	1.11	10.7527	0.5203	0.0652	0.0026	0.8560	0.0320	0.0930	0.0017	0.0439	0.0300	0.0015	768	84	573	27	627	28	598	29	74.6	91.4
I78_4135_19	0.40	2.9922	0.1433	0.1301	0.0015	6.1370	0.0910	0.3342	0.0041	0.8687	0.1024	0.0049	2099	11	1857	75	1994	43	1971	90	88.5	93.1
I78_4135_20	1.11	28.9017	1.7542	0.0784	0.0040	0.3780	0.0190	0.0346	0.0014	0.4693	0.0135	0.0008	1093	98	219	13	327	20	271	17	20.0	67.0
I78_4135_21	1.33	7.3855	0.3545	0.0780	0.0013	1.4700	0.0240	0.1354	0.0021	0.5754	0.0447	0.0020	1137	26	820	36	916	30	884	39	72.1	89.5
I78_4135_22	0.65	16.9205	0.8875	0.0592	0.0015	0.4800	0.0120	0.0591	0.0016	0.5728	0.0205	0.0010	558	52	370	19	398	18	409	20	66.3	93.1
I78_4135_23	0.24	4.1894	0.2106	0.0975	0.0014	3.2380	0.0710	0.2387	0.0041	0.8685	0.0729	0.0036	1574	20	1378	60	1461	41	1420	68	87.5	94.3
I78_4135_24	0.34	2.7933	0.1561	0.1267	0.0035	6.1200	0.2300	0.3580	0.0120	0.6422	0.1035	0.0061	2046	45	1974	95	1988	54	1988	110	96.5	99.3
I78_4135_25	0.52	10.0402	0.4637	0.0600	0.0012	0.8320	0.0140	0.0996	0.0010	0.1759	0.0359	0.0017	591	40	612	27	615	23	713	33	103.5	99.5
I78_4135_26	0.36	6.3654	0.3809	0.0748	0.0059	1.6200	0.1100	0.1571	0.0061	0.0098	0.0468	0.0054	990	160	938	52	981	55	917	100	94.7	95.6
I78_4135_27	0.33	3.8745	0.1801	0.0923	0.0011	3.2910	0.0320	0.2581	0.0021	0.6465	0.0726	0.0032	1473	14	1480	61	1478	37	1416	60	100.5	100.1
I78_4135_28	0.74	10.9254	0.5013	0.0592	0.0012	0.7520	0.0130	0.0915	0.0010	0.1920	0.0281	0.0013	581	40	565	25	570	22	559	26	97.2	99.1
I78_4135_29	0.44	15.4703	0.7180	0.0540	0.0015	0.4760	0.0120	0.0646	0.0008	0.1240	0.0255	0.0016	344	54	404	18	394	17	508	32	117.4	102.5
I78_4135_30	0.03	5.0201	0.2319	0.0801	0.0010	2.2150	0.0220	0.1992	0.0018	0.7013	0.0366	0.0042	1196	14	1171	50	1186	35	719	82	97.9	98.8
I78_4135_31	0.28	3.2595	0.1487	0.1262	0.0020	5.3410	0.0800	0.3068	0.0041	0.6255	0.1033	0.0049	2046	22	1723	71	1876	44	1984	90	84.2	91.8
I78_4135_32	1.61	10.2459	0.5039	0.0623	0.0010	0.8420	0.0150	0.0976	0.0018	0.7063	0.0311	0.0014	677	27	600	28	619	24	618	28	88.6	97.0
I78_4135_33	0.83	4.0816	0.2166	0.1071	0.0037	3.6500	0.1700	0.2450	0.0120	0.8953	0.0647	0.0070	1751	36	1409	67	1555	63	1261	130	80.5	90.6
I78_4135_34	0.77	9.7752	0.3058	0.0593	0.0022	0.8530	0.0190	0.1023	0.0021	0.3824	0.0352	0.0033	554	53	628	19	625	31	700	65	113.4	100.5
I78_4135_35	0.95	9.4697	0.2959	0.0612	0.0022	0.8950	0.0160	0.1056	0.0022	0.4636	0.0344	0.0032	633	46	649	19	650	32	683	63	102.5	99.9
I78_4135_36	0.02	8.8731	0.5747	0.0710	0.0120	1.0400	0.1600	0.1127	0.0068	0.0551	2.5000	2.3000	530	270	683	42	655	85	3300	3700	128.9	104.3
I78_4135_37	0.92	10.3413	0.3422	0.0634	0.0023	0.8540	0.0150	0.0967	0.0024	0.4931	0.0304	0.0029	704	46	596	19	629	31	605	56	84.7	94.7

Panther P-52 (3210 m) Sample

Identifier	Th/U	Data for Tera-Wasserburg plot				Data for Wetherill plot					$^{208}Pb/^{232}Th$	2SE	Dates								% Concordancy *(206Pb-238U age/207Pb-206Pb age)*100*	%Concordancy (206Pb-238U age/207Pb-235U age)*100
		$^{238}U/^{206}Pb$	2SE	$^{207}Pb/^{206}Pb$	2SE	$^{207}Pb/^{235}U$	2SE	$^{206}Pb/^{238}U$	2SE	Rho			$^{207}Pb/^{206}Pb$	2SE	$^{206}Pb/^{238}U$	2SE	$^{207}Pb/^{235}U$	2SE	$^{208}Pb/^{232}Th$	2SE		
P52_3210_1	0.88	43.0108	1.8499	0.0572	0.0057	0.1770	0.0170	0.0233	0.0010	-0.0374	0.0080	0.0005	499	219	148	6	166	14	161	11	29.7	89.2
P52_3210_2	0.91	43.9754	1.7211	0.0509	0.0035	0.1590	0.0100	0.0227	0.0009	0.3202	0.0073	0.0004	236	159	145	6	149	9	147	7	61.3	97.1
P52_3210_3	0.92	12.3153	0.4702	0.0882	0.0027	0.9990	0.0300	0.0812	0.0031	0.9914	0.0260	0.0011	1387	59	503	18	699	15	518	21	36.3	72.0
P52_3210_4	0.74	12.2399	0.3596	0.0825	0.0028	0.9330	0.0270	0.0817	0.0024	0.4788	0.0286	0.0011	1257	66	506	14	669	14	570	22	40.2	75.6
P52_3210_5	0.41	9.6154	0.3976	0.0810	0.0038	1.1070	0.0480	0.1040	0.0043	0.4707	0.0371	0.0020	1221	92	637	25	753	23	735	39	52.2	84.6
P52_3210_6	0.36	5.7971	0.1479	0.0814	0.0023	1.9570	0.0450	0.1725	0.0044	0.4905	0.0574	0.0022	1231	55	1026	24	1098	15	1127	41	83.3	93.4
P52_3210_7	0.49	10.9649	0.3006	0.0922	0.0040	1.1690	0.0370	0.0912	0.0025	0.1422	0.0420	0.0019	1472	82	563	15	780	17	830	36	38.3	72.2
P52_3210_8	0.54	41.3223	1.8783	0.0762	0.0065	0.2590	0.0200	0.0242	0.0011	0.2307	0.0117	0.0008	1100	171	154	7	236	16	235	17	14.0	65.4
P52_3210_9	0.27	4.3706	0.1261	0.1325	0.0040	4.1370	0.0920	0.2288	0.0066	0.4990	0.0751	0.0034	2131	53	1326	34	1662	18	1461	64	62.2	79.8
P52_3210_10	0.52	10.2881	0.2434	0.0618	0.0016	0.8370	0.0160	0.0972	0.0023	0.5382	0.0306	0.0010	667	55	598	14	616	9	609	20	89.6	97.0
P52_3210_11	0.17	3.6140	0.1176	0.1068	0.0032	4.0400	0.1000	0.2767	0.0090	0.7057	0.0866	0.0036	1746	55	1571	46	1643	21	1677	66	90.0	95.6
P52_3210_12	0.19	8.6281	0.3871	0.2301	0.0110	3.6400	0.1800	0.1159	0.0052	0.5094	0.2260	0.0150	3053	77	705	30	1543	37	4070	250	23.1	45.7
P52_3210_13	0.33	9.8717	0.2534	0.0621	0.0019	0.8880	0.0200	0.1013	0.0026	0.3582	0.0312	0.0012	678	65	622	15	644	11	621	24	91.8	96.6
P52_3210_14	0.68	11.3379	0.3085	0.0667	0.0025	0.8070	0.0240	0.0882	0.0024	0.2756	0.0286	0.0011	828	78	545	14	596	13	570	21	65.8	91.4
P52_3210_15	0.31	21.5564	0.5111	0.0558	0.0015	0.3606	0.0064	0.0464	0.0011	0.4556	0.0148	0.0005	442	60	292	7	313	5	298	11	66.0	93.4
P52_3210_16	0.67	9.4340	0.2314	0.0610	0.0016	0.8920	0.0160	0.1060	0.0026	0.5276	0.0344	0.0011	639	56	649	15	648	9	683	22	101.5	100.2
P52_3210_17	0.55	8.8417	0.2502	0.0632	0.0022	0.9960	0.0280	0.1131	0.0032	0.3926	0.0357	0.0014	715	74	691	19	700	14	708	26	96.6	98.7
P52_3210_18	0.71	43.1779	1.1932	0.0504	0.0023	0.1639	0.0067	0.0232	0.0006	0.1596	0.0072	0.0003	213	106	148	4	153	6	144	6	69.1	96.6
P52_3210_19	0.29	28.4657	0.8913	0.0685	0.0020	0.3403	0.0077	0.0351	0.0011	0.5980	0.0145	0.0005	884	60	223	7	297	6	292	11	25.2	75.0
P52_3210_20	0.10	23.4742	0.8817	0.0599	0.0022	0.3620	0.0110	0.0426	0.0016	0.5655	0.0210	0.0012	600	80	269	10	314	8	420	24	44.8	85.7
P52_3210_21	0.88	16.1812	0.3927	0.0577	0.0018	0.5010	0.0120	0.0618	0.0015	0.3224	0.0201	0.0007	518	68	387	9	411	8	402	14	74.7	94.2
P52_3210_22	1.32	11.0865	0.3319	0.0700	0.0024	0.8830	0.0250	0.0902	0.0027	0.2824	0.0283	0.0010	928	70	556	16	643	14	563	20	59.9	86.5
P52_3210_23	0.17	25.8198	0.7333	0.0567	0.0017	0.3122	0.0074	0.0387	0.0011	0.5105	0.0129	0.0005	480	66	245	7	275	6	259	11	51.0	88.9
P52_3210_24	0.41	21.3630	0.5020	0.0532	0.0015	0.3482	0.0071	0.0468	0.0011	0.4269	0.0147	0.0005	337	64	295	7	303	5	295	10	87.5	97.5
P52_3210_25	0.64	1.8762	0.0598	0.1911	0.0057	13.8700	0.3400	0.5330	0.0170	0.6314	0.1436	0.0055	2752	49	2758	72	2737	23	2714	96	100.2	100.8
P52_3210_26	0.24	4.8031	0.1430	0.0834	0.0024	2.3870	0.0570	0.2082	0.0062	0.6514	0.0642	0.0025	1279	56	1217	33	1239	17	1256	47	95.2	98.2
P52_3210_27	0.45	10.4493	0.3057	0.0631	0.0019	0.8330	0.0210	0.0957	0.0028	0.5465	0.0320	0.0012	712	64	589	16	614	12	638	23	82.8	95.9
P52_3210_28	0.50	17.7305	0.8488	0.1220	0.0085	0.9280	0.0550	0.0564	0.0027	0.2530	0.0323	0.0021	1986	124	355	16	661	29	642	42	17.9	53.7
P52_3210_29	0.78	13.4409	0.4336	0.0636	0.0027	0.6570	0.0290	0.0744	0.0024	0.2755	0.0243	0.0012	728	90	462	15	507	18	484	24	63.4	91.1
P52_3210_30	0.30	2.6954	0.0944	0.1406	0.0047	7.1700	0.2400	0.3710	0.0130	0.5178	0.1384	0.0078	2235	58	2031	63	2130	31	2612	140	90.9	95.4
P52_3210_31	0.46	10.0807	0.2947	0.0597	0.0022	0.8230	0.0300	0.0992	0.0029	0.3494	0.0307	0.0016	593	80	609	17	607	16	609	30	102.7	100.3
P52_3210_32	0.70	43.4594	1.6243	0.0749	0.0053	0.2360	0.0160	0.0230	0.0009	0.0892	0.0090	0.0006	1066	142	147	5	209	13	182	11	13.8	70.1
P52_3210_33	0.23	22.8833	1.2044	0.0569	0.0022	0.3350	0.0170	0.0437	0.0023	0.8460	0.0149	0.0010	488	85	275	14	291	12	299	20	56.4	94.5
P52_3210_34	1.04	8.1833	0.2411	0.0631	0.0019	1.0710	0.0330	0.1222	0.0036	0.4956	0.0383	0.0017	712	64	743	21	736	16	759	34	104.4	101.0
P52_3210_35	1.03	10.8933	0.4391	0.0627	0.0023	0.8240	0.0340	0.0918	0.0037	0.6615	0.0298	0.0015	698	78	566	22	609	19	593	29	81.1	92.9
P52_3210_36	1.03	10.4822	0.3516	0.0692	0.0025	0.9250	0.0380	0.0954	0.0032	0.6745	0.0320	0.0015	905	74	587	19	666	20	636	30	64.9	88.1
P52_3210_37	0.86	9.8814	0.3027	0.0608	0.0024	0.8520	0.0320	0.1012	0.0031	0.2536	0.0329	0.0017	632	85	620	18	626	17	655	33	98.1	99.0
P52_3210_38	0.17	5.7045	0.1627	0.0739	0.0020	1.7810	0.0480	0.1753	0.0050	0.5602	0.0591	0.0028	1039	55	1042	28	1039	18	1159	54	100.3	100.3
P52_3210_39	0.48	9.6061	0.3045	0.0959	0.0035	1.3910	0.0510	0.1041	0.0033	0.4752	0.0514	0.0030	1546	69	637	19	881	22	1010	57	41.2	72.3
P52_3210_40	7.02	0.5128	0.0657	0.0735	0.0028	20.2000	2.7000	1.9500	0.2500	0.9541	0.0489	0.0029	1028	77	6790	540	3100	130	965	56	660.7	219.0
P52_3210_41	0.82	43.0663	2.0402	0.0625	0.0047	0.1920	0.0150	0.0232	0.0011	0.4062	0.0083	0.0006	691	160	148	7	180	12	166	12	21.4	82.2
P52_3210_42	0.37	8.5324	0.3713	0.0636	0.0026	1.0410	0.0400	0.1172	0.0051	0.4582	0.0341	0.0019	728	87	714	29	722	20	677	37	98.0	98.9
P52_3210_43	0.47	42.1941	2.4925	0.0754	0.0081	0.2360	0.0260	0.0237	0.0014	0.2102	0.0114	0.0011	1079	216	151	9	217	22	230	23	14.0	69.5
P52_3210_44	0.28	8.3682	0.2941	0.0930	0.0033	1.5400	0.0610	0.1195	0.0042	0.5895	0.0714	0.0038	1488	67	728	24	942	24	1392	71	48.9	77.3
P52_3210_45	0.38	22.6757	0.8741	0.0578	0.0020	0.3449	0.0120	0.0441	0.0017	0.7557	0.0137	0.0007	522	76	278	10	300	9	274	14	53.2	92.6
P52_3210_46	0.55	18.1818	0.5950	0.0554	0.0019	0.4260	0.0150	0.0550	0.0018	0.5376	0.0183	0.0009	428	76	345	11	358	11	366	18	80.4	96.2
P52_3210_47	0.38	4.1946	0.1531	0.1425	0.0040	4.7700	0.1800	0.2384	0.0087	0.8315	0.0686	0.0033	2258	48	1378	45	1772	31	1340	62	61.0	77.8
P52_3210_48	0.26	12.2850	0.5433	0.0897	0.0049	1.0670	0.0500	0.0814	0.0036	0.3721	0.0345	0.0027	1419	104	504	21	739	25	685	53	35.5	68.2
P52_3210_49	0.64	42.3908	1.6892	0.0523	0.0022	0.1680	0.0079	0.0236	0.0009	0.4136	0.0080	0.0004	299	96	150	6	158	7	160	9	50.3	95.0
P52_3210_50	0.65	3.9216	0.2153	0.1222	0.0039	4.3800	0.2500	0.2550	0.0140	0.8999	0.0693	0.0046	1989	57	1468	72	1693	47	1350	86	73.8	86.7
P52_3210_51	0.40	21.0084	0.7503	0.0563	0.0020	0.3640	0.0130	0.0476	0.0017	0.5362	0.0154	0.0008	464	79	299	11	315	10	308	16	64.5	95.1
P52_3210_52	0.35	20.4834	0.5874	0.0529	0.0016	0.3569	0.0110	0.0488	0.0014	0.4381	0.0155	0.0007	325	69	308	9	310	8	312	15	94.8	99.2
P52_3210_53	0.72	11.5607	0.4945	0.0690	0.0026	0.8180	0.0300	0.0865	0.0037	0.5026	0.0238	0.0016	899	78	533	22	602	17	474	32	59.3	88.5

South Tempest G-88 (4195.8 m) Sample

Identifier	Th/U	Data for Tera-Wasserburg plot				Data for Wetherill plot					$^{208}Pb/^{232}Th$	2SE	Dates								% Concordancy *(206Pb-238U age/207Pb-206Pb age)*100*	%Concordancy (206Pb-238U age/207Pb-235U age)*100
		$^{238}U/^{206}Pb$	2SE	$^{207}Pb/^{206}Pb$	2SE	$^{207}Pb/^{235}U$	2SE	$^{206}Pb/^{238}U$	2SE	Rho			$^{207}Pb/^{206}Pb$	2SE	$^{206}Pb/^{238}U$	2SE	$^{207}Pb/^{235}U$	2SE	$^{208}Pb/^{232}Th$	2SE		
G88_4195_1	1.02	10.1317	0.3798	0.0578	0.0021	0.7660	0.0240	0.0987	0.0037	0.3085	0.0309	0.0029	482	69	606	21	579	14	614	56	125.7	104.7
G88_4195_2	1.01	9.1324	0.3503	0.0588	0.0023	0.8840	0.0310	0.1095	0.0042	0.3143	0.0382	0.0037	538	73	669	24	642	17	756	72	124.3	104.2
G88_4195_3	0.40	6.0386	0.2261	0.0705	0.0025	1.5970	0.0480	0.1656	0.0062	0.3606	0.0500	0.0049	910	68	986	34	961	19	985	94	108.4	102.6
G88_4195_4	0.75	4.3975	0.1489	0.0815	0.0020	2.5490	0.0490	0.2274	0.0077	0.4275	0.0688	0.0062	1216	39	1319	41	1284	14	1346	120	108.5	102.7
G88_4195_5	0.55	9.9502	0.3366	0.0586	0.0017	0.8160	0.0180	0.1005	0.0034	0.2970	0.0309	0.0028	534	52	617	20	605	10	615	55	115.5	102.0
G88_4195_6	0.48	2.8417	0.0969	0.1220	0.0026	5.9100	0.1100	0.3519	0.0120	0.6452	0.1022	0.0092	1979	28	1940	58	1963	16	1965	170	98.0	98.8
G88_4195_7	0.47	9.9010	0.3431	0.0611	0.0015	0.8470	0.0180	0.1010	0.0035	0.4713	0.0316	0.0029	630	43	620	20	622	10	629	56	98.4	99.8
G88_4195_8	0.55	9.9108	0.3929	0.0589	0.0030	0.8240	0.0380	0.1009	0.0040	0.1270	0.0302	0.0030	540	110	619	23	606	22	600	59	114.6	102.1
G88_4195_9	0.60	3.6298	0.1581	0.1062	0.0036	4.0600	0.1200	0.2755	0.0120	0.5253	0.0801	0.0075	1712	56	1566	59	1647	25	1555	140	91.5	95.1
G88_4195_10	0.64	9.9010	0.3627	0.0605	0.0026	0.8550	0.0330	0.1010	0.0037	0.1935	0.0313	0.0030	589	83	620	21	628	18	622	58	105.3	98.7
G88_4195_11	1.12	10.4822	0.3736	0.0611	0.0019	0.7960	0.0220	0.0954	0.0034	0.3957	0.0291	0.0027	621	54	588	20	593	12	580	52	94.7	99.2
G88_4195_12	1.31	10.2987	0.3606	0.0591	0.0017	0.8090	0.0160	0.0971	0.0034	0.3499	0.0279	0.0025	559	52	597	20	600	9	555	49	106.8	99.5
G88_4195_13	0.66	10.0301	0.3521	0.0576	0.0019	0.8000	0.0220	0.0997	0.0035	0.2192	0.0311	0.0029	480	62	612	20	594	12	619	56	127.5	103.0
G88_4195_14	0.33	3.0826	0.1045	0.1047	0.0021	4.7270	0.0770	0.3244	0.0110	0.6257	0.0976	0.0088	1710	24	1811	53	1770	13	1880	160	105.9	102.3
G88_4195_15	0.79	9.2507	0.3166	0.0619	0.0016	0.9330	0.0200	0.1081	0.0037	0.4178	0.0352	0.0032	667	44	662	22	669	10	698	62	99.3	99.0
G88_4195_16	0.40	9.4697	0.3408	0.0590	0.0017	0.8530	0.0200	0.1056	0.0038	0.3724	0.0327	0.0030	544	54	647	22	626	11	649	59	118.9	103.4
G88_4195_17	0.34	22.0605	0.7787	0.0531	0.0015	0.3332	0.0074	0.0453	0.0016	0.4273	0.0137	0.0013	308	51	286	10	293	6	274	25	92.8	97.6
G88_4195_18	0.36	10.2775	0.3591	0.0598	0.0023	0.7930	0.0250	0.0973	0.0034	0.1935	0.0301	0.0029	555	74	598	20	591	14	598	57	107.7	101.2
G88_4195_19	0.41	5.9312	0.2146	0.0692	0.0022	1.6120	0.0390	0.1686	0.0061	0.2842	0.0535	0.0050	913	57	1003	34	979	15	1052	96	109.9	102.5
G88_4195_20	0.40	10.6270	0.4066	0.0542	0.0026	0.7010	0.0300	0.0941	0.0036	0.2297	0.0291	0.0030	351	89	579	21	537	17	578	58	165.0	107.8
G88_4195_21	0.68	9.6525	0.3727	0.0606	0.0024	0.8530	0.0280	0.1036	0.0040	0.2231	0.0357	0.0034	569	76	635	23	624	16	709	66	111.6	101.8
G88_4195_22	0.15	5.8720	0.2000	0.0734	0.0017	1.7400	0.0290	0.1703	0.0058	0.4748	0.0508	0.0046	1013	35	1014	32	1023	11	1000	89	100.1	99.1
G88_4195_23	0.45	9.2764	0.3270	0.0635	0.0023	0.9370	0.0280	0.1078	0.0038	-0.0088	0.0345	0.0032	652	67	659	22	665	14	688	62	101.1	99.1
G88_4195_24	0.40	11.4286	0.3918	0.0570	0.0017	0.6920	0.0180	0.0875	0.0030	0.3022	0.0274	0.0025	469	54	541	18	535	11	546	50	115.3	101.0
G88_4195_25	0.69	9.9602	0.3869	0.0598	0.0027	0.8210	0.0310	0.1004	0.0039	0.1280	0.0310	0.0029	590	91	617	23	610	17	617	57	104.6	101.1
G88_4195_26	0.40	9.1575	0.3187	0.0606	0.0015	0.9140	0.0200	0.1092	0.0038	0.5276	0.0339	0.0031	622	44	667	22	658	11	673	60	107.2	101.4
G88_4195_27	0.61	14.3885	0.5176	0.0539	0.0021	0.5130	0.0180	0.0695	0.0025	0.3012	0.0212	0.0020	345	73	433	15	419	12	423	39	125.4	103.2
G88_4195_28	1.18	9.7087	0.3299	0.0600	0.0016	0.8490	0.0200	0.1030	0.0035	0.4301	0.0330	0.0030	589	48	632	21	623	11	656	58	107.3	101.4
G88_4195_29	0.29	14.6628	0.5375	0.0592	0.0021	0.5480	0.0160	0.0682	0.0025	0.2151	0.0229	0.0022	523	66	425	15	443	10	458	44	81.3	96.0
G88_4195_30	0.40	10.0503	0.3535	0.0585	0.0016	0.8040	0.0210	0.0995	0.0035	0.3706	0.0300	0.0028	547	49	611	21	604	11	598	54	111.7	101.2
G88_4195_31	0.08	9.5511	0.3284	0.0619	0.0017	0.8840	0.0190	0.1047	0.0036	0.3892	0.0312	0.0030	651	50	641	21	641	10	619	59	98.5	100.0
G88_4195_32	0.29	9.8814	0.3613	0.0599	0.0015	0.8460	0.0160	0.1012	0.0037	0.4700	0.0333	0.0030	582	44	621	22	621	9	661	59	106.7	100.1
G88_4195_33	0.59	9.6805	0.3749	0.0589	0.0024	0.8190	0.0280	0.1033	0.0040	0.2968	0.0319	0.0030	522	78	633	23	607	15	634	59	121.3	104.3
G88_4195_34	0.89	10.3199	0.3941	0.0615	0.0024	0.8190	0.0300	0.0969	0.0037	0.3868	0.0301	0.0028	595	77	597	22	611	16	599	55	100.3	97.7
G88_4195_35	0.61	9.4967	0.3247	0.0607	0.0019	0.8860	0.0230	0.1053	0.0036	0.2883	0.0335	0.0031	591	57	646	21	645	13	666	61	109.3	100.2
G88_4195_36	0.18	3.1847	0.1521	0.1190	0.0031	5.1800	0.1900	0.3140	0.0150	0.8057	0.0966	0.0092	1929	38	1762	73	1853	30	1861	170	91.3	95.1
G88_4195_37	2.03	1.9425	0.0679	0.2015	0.0044	14.5400	0.2700	0.5148	0.0180	0.6136	0.1454	0.0130	2838	25	2684	75	2783	17	2746	230	94.6	96.4
G88_4195_38	0.44	9.4967	0.3337	0.0595	0.0017	0.8650	0.0190	0.1053	0.0037	0.4086	0.0346	0.0031	564	51	645	22	631	10	687	61	114.4	102.2
G88_4195_39	0.39	10.4712	0.4167	0.0599	0.0025	0.8050	0.0310	0.0955	0.0038	0.3529	0.0319	0.0032	564	82	587	22	599	17	634	63	104.1	98.0
G88_4195_40	0.57	5.4083	0.1901	0.0734	0.0019	1.8940	0.0370	0.1849	0.0065	0.4569	0.0563	0.0051	1016	42	1093	36	1079	13	1108	99	107.6	101.3
G88_4195_41	0.40	10.6838	0.3995	0.0636	0.0019	0.8240	0.0190	0.0936	0.0035	0.3824	0.0307	0.0028	726	54	576	21	609	10	611	55	79.3	94.6
G88_4195_42	0.71	9.7371	0.3318	0.0619	0.0016	0.8750	0.0180	0.1027	0.0035	0.4250	0.0329	0.0030	659	43	630	21	636	10	655	58	95.6	99.1
G88_4195_43	0.38	9.6712	0.4396	0.0624	0.0047	0.8620	0.0580	0.1034	0.0047	0.1141	0.0310	0.0038	500	140	633	28	620	32	615	75	126.6	102.1
G88_4195_44	0.46	2.8827	0.0997	0.1316	0.0027	6.3600	0.1100	0.3469	0.0120	0.6962	0.1019	0.0092	2113	24	1918	57	2028	15	1959	170	90.8	94.6
G88_4195_45	0.28	9.9701	0.4374	0.0683	0.0026	0.9510	0.0390	0.1003	0.0044	0.1378	0.0162	0.0020	867	76	615	26	677	20	324	40	70.9	90.8
G88_4195_46	0.30	9.5420	0.3460	0.0609	0.0022	0.8850	0.0270	0.1048	0.0038	0.1543	0.0332	0.0031	583	68	643	22	643	14	660	62	110.3	100.0
G88_4195_47	0.70	10.3413	0.3529	0.0594	0.0017	0.7960	0.0190	0.0967	0.0033	0.3823	0.0283	0.0026	568	51	595	19	593	11	565	50	104.7	100.3
G88_4195_48	0.78	9.7943	0.3358	0.0599	0.0013	0.8460	0.0140	0.1021	0.0035	0.4898	0.0315	0.0028	606	36	628	20	621	8	626	55	103.6	101.1
G88_4195_49	0.42	15.0150	0.5185	0.0536	0.0019	0.4950	0.0160	0.0666	0.0023	0.2453	0.0216	0.0021	347	69	416	14	408	10	432	41	119.8	101.9
G88_4195_50	0.83	9.6712	0.3461	0.0604	0.0020	0.8560	0.0260	0.1034	0.0037	0.4300	0.0323	0.0030	597	62	634	22	630	15	642	59	106.2	100.6
G88_4195_51	0.46	9.9502	0.3465	0.0589	0.0018	0.8250	0.0200	0.1005	0.0035	0.2772	0.0312	0.0029	550	58	617	20	608	11	621	56	112.2	101.5
G88_4195_52	0.65	10.1626	0.3511	0.0614	0.0016	0.8410	0.0200	0.0984	0.0034	0.4413	0.0317	0.0029	632	48	604	20	619	11	630	56	95.6	97.6
G88_4195_53	0.36	9.0334	0.3754	0.0607	0.0030	0.9310	0.0460	0.1107	0.0046	0.2457	0.0344	0.0038	594	97	676	26	674	24	684	73	113.8	100.3
G88_4195_54	0.48	10.0402	0.3730	0.0585	0.0024	0.8210	0.0310	0.0996	0.0037	0.2760	0.0314	0.0030	526	79	612	21	605	17	625	59	116.3	101.2
G88_4195_55	0.84	10.6838	0.3995	0.0614	0.0022	0.7840	0.0200	0.0936	0.0035	0.1749	0.0291	0.0027	625	69	576	21	589	11	581	53	92.2	97.8
G88_4195_56	1.00	9.9010	0.4901	0.0622	0.0016	0.8610	0.0500	0.1010	0.0050	0.4152	0.0318	0.0017	644	54	620	30	632	27	632	33	96.3	98.1
G88_4195_57	0.59	2.0284	0.1029	0.1686	0.0036	11.4600	0.6300	0.4930	0.0250	0.5136	0.1363	0.0070	2528	34	2580	110	2557	52	2582	120	102.1	100.9
G88_4195_58	0.74	9.4607	0.4744	0.0598	0.0018	0.8780	0.0520	0.1057	0.0053	0.3064	0.0314	0.0017	602	61	648	31	639	28	625	34	107.6	101.4
G88_4195_59	0.27	10.2775	0.5070	0.0590	0.0016	0.7920	0.0460	0.0973	0.0048	0.3082	0.0292	0.0016	529	58	599	28	589	26	582	32	113.2	101.7
G88_4195_60	0.45	10.2564	0.5155	0.0607	0.0015	0.8130	0.0460	0.0975	0.0049	0.3677	0.0308	0.0017	618	52	599	29	605	26	612	33	96.9	99.0
G88_4195_61	0.81	21.1417	1.0727	0.0534	0.0016	0.3436	0.0200	0.0473	0.0024	0.2222	0.0143	0.0008	320	61	298	14	300	15	287	15	93.0	99.4
G88_4195_62	0.88	9.2764	0.4647	0.0635	0.0016	0.9510	0.0550	0.1078	0.0054	0.4847	0.0358	0.0019	735	53	659	32	678	28	711	37	89.7	97.2
G88_4195_63	0.62	10.1523	0.5050	0.0609	0.0016	0.8210	0.0470	0.0985	0.0049	0.4215	0.0297	0.0016	602	56	606	29	608	26	591	32	100.7	99.7
G88_4195_64	0.35	2.4765	0.1227	0.1345	0.0027	7.5800	0.4200	0.4038	0.0200	0.5036	0.1086	0.0058	2154	33	2180	91	2177	50	2085	100	101.2	100.1
G88_4195_65	0.39	10.0705	0.5172	0.0615	0.0016	0.8480	0.0500	0.0993	0.0051	0.3746	0.0307	0.0017	647	55	610	30	623	27	610	34	94.3	97.9
G88_4195_66	0.68	21.2314	1.3974	0.0523	0.0022	0.3410	0.0240	0.0471	0.0031	0.9746	0.0126	0.0008	275	86	296	19	297	18	254	15	107.6	99.7
G88_4195_67	0.49	21.8771	1.1008	0.0525	0.0016	0.3242	0.0190	0.0457	0.0023	0.2224	0.0143	0.0008	284	62	288	14	284	15	288	16	101.5	101.5
G88_4195_68	0.36	2.6976	0.1310	0.1295	0.0024	6.5800	0.3600	0.3707	0.0180	0.5352	0.1064	0.0056	2089	30	2030	84	2052	49	2040	100	97.2	98.9
G88_4195_69	0.63	10.1010	0.5102	0.0595	0.0014	0.8190	0.0460	0.0990	0.0050	0.5419	0.0316	0.0016	557	48	608	29	609	26	628	32	109.2	99.9
G88_4195_70	0.53	8.9366	0.5031	0.0611	0.0039	0.9450	0.0780	0.1119	0.0063	0.1836	0.0360	0.0030	520	120	682	36	651	37	712	58	131.2	104.8
G88_4195_71	0.09	14.0845	0.6943	0.0550	0.0012	0.5410	0.0300	0.0710	0.0035	0.4475	0.0227	0.0013	392	46	442	21	439	20	454	26	112.8	100.8
G88_4195_72	0.56	21.1417	1.0727	0.0549	0.0020	0.3610	0.0220	0.0473	0.0024	0.2188	0.0154	0.0009	374	74	298	15	311	17	309	17	79.7	95.9
G88_4195_73	0.55	10.1420	0.5657	0.0635	0.0036	0.8440	0.0620	0.0986	0.0055	0.1726	0.0302	0.0022	650	110	606	32	621	35	603	42	93.2	97.6
G88_4195_74	0.58	12.3001	0.6657	0.0565	0.0017	0.6410	0.0400	0.0813	0.0044	0.5890	0.0282	0.0018	445	64	503	26	502	25	562	35	113.0	100.2
G88_4195_75	0.59	10.7991	0.5365	0.0591	0.0019	0.7570	0.0460	0.0926	0.0046	0.2868	0.0289	0.0016	555	67	570	27	572	27	575	31	102.7	99.7
G88_4195_76	0.69	21.3220	1.0911	0.0576	0.0016	0.3760	0.0220	0.0469	0.0024	0.4665	0.0156	0.0009	489	60	295	15	324	17	312	17	60.4	91.1
G88_4195_77	0.93	8.7642	0.4378	0.0641	0.0018	1.0060	0.0580	0.1141	0.0057	0.4027	0.0359	0.0019	744	57	696	33	708	29	712	37	93.5	98.3
G88_4195_78	1.35	10.5042	0.5407	0.0591	0.0015	0.7870	0.0460	0.0952	0.0049	0.4959	0.0284	0.0015	550	53	587	28	589	26	566	29	106.7	99.7
G88_4195_79	0.44	10.0503	0.4949	0.0598	0.0013	0.8260	0.0460	0.0995	0.0049	0.4291	0.0304	0.0016	578	44	611	29	610	26	605	31	105.7	100.1
G88_4195_80	0.37	2.4096	0.1219	0.1323	0.0031	7.4900	0.4200	0.4150	0.0210	0.5535	0.1159	0.0064	2111	38	2226	96	2166	51	2221	110	105.4	102.8
G88_4195_81	0.53	10.6610	0.5456	0.0615	0.0015	0.7880	0.0450	0.0938	0.0048	0.5175	0.0262	0.0014	640	51	577	28	589	26	522	28	90.2	98.0
G88_4195_82	0.53	9.9010	0.5098	0.0623	0.0028	0.8410	0.0560	0.1010	0.0052	0.2059	0.0319	0.0020	627	87	621	31	619	30	634	39	99.0	100.3
G88_4195_83	0.12	8.6356	0.4325	0.0617	0.0014	0.9990	0.0560	0.1158	0.0058	0.5025	0.0339	0.0019	652	47	707	34	702	28	673	36	108.4	100.7
G88_4195_84	0.37	4.4743	0.2202	0.0777	0.0019	2.3950	0.1400	0.2235	0.0110	0.4683	0.0670	0.0037	1120	49	1299	60	1239	40	1312	69	116.0	104.8
G88_4195_85	0.42	9.2336	0.4775	0.0600	0.0027	0.8920	0.0580	0.1083	0.0056	0.0781	0.0310	0.0021	569	92	661	33	645	31	617	41	116.2	102.5
G88_4195_86	0.77	9.7276	0.5015	0.0588	0.0021	0.8230	0.0510	0.1028	0.0053	0.3111	0.0321	0.0019	514	74	630	31	609	28	638	37	122.6	103.4
G88_4195_87	0.69	9.2336	0.4604	0.0620	0.0020	0.9100	0.0540	0.1083	0.0054	0.3572	0.0343	0.0018	645	66	662	32	652	29	682	36	102.6	101.5

U/Pb data for Reference Standards

91500 zircon

Identifier	Th/U	Data for Tera-Wasserburg plot				Data for Wetherill plot					$^{208}Pb/^{232}Th$	2SE	Dates								% Concordancy*(206Pb-238U age/207Pb-206Pb age)*100*	%Concordancy (206Pb-238U age/207Pb-235U age)*100
		$^{238}U/^{206}Pb$	2SE	$^{207}Pb/^{206}Pb$	2SE	$^{207}Pb/^{235}U$	2SE	$^{206}Pb/^{238}U$	2SE	Rho			$^{207}Pb/^{206}Pb$	2SE	$^{206}Pb/^{238}U$	2SE	$^{207}Pb/^{235}U$	2SE	$^{208}Pb/^{232}Th$	2SE		
jn26_91500_1	0.26	5.5991	0.1630	0.0744	0.0028	1.8230	0.0640	0.1786	0.0052	0.3031	0.0538	0.0033	1052	76	1059	28	1049	23	1054	63	100.63	100.95
jn26_91500_2	0.25	5.7176	0.1700	0.0750	0.0028	1.8100	0.0610	0.1749	0.0052	0.1040	0.0554	0.0033	1069	75	1038	29	1042	22	1084	63	97.15	99.62
jn26_91500_3	0.26	5.6370	0.1652	0.0725	0.0027	1.7850	0.0630	0.1774	0.0052	0.2531	0.0529	0.0031	1000	76	1052	29	1043	22	1046	60	105.20	100.86
jn26_91500_4	0.26	5.6433	0.1688	0.0762	0.0028	1.8590	0.0650	0.1772	0.0053	0.2273	0.0533	0.0032	1100	74	1049	29	1059	24	1051	62	95.34	99.06
jn26_91500_5	0.25	5.5279	0.1650	0.0743	0.0027	1.8740	0.0660	0.1809	0.0054	0.3169	0.0525	0.0032	1050	73	1070	29	1062	24	1032	61	101.94	100.75
jn26_91500_6	0.26	5.5066	0.1668	0.0755	0.0028	1.8950	0.0680	0.1816	0.0055	0.2629	0.0552	0.0034	1082	74	1074	30	1069	26	1081	65	99.28	100.47
jn26_91500_7	0.26	5.4885	0.1657	0.0752	0.0027	1.8920	0.0640	0.1822	0.0055	0.3376	0.0547	0.0033	1074	72	1076	30	1082	22	1074	63	100.20	99.45
jn26_91500_8	0.25	5.5617	0.1670	0.0761	0.0027	1.8830	0.0660	0.1798	0.0054	0.3680	0.054	0.0033	1098	71	1062	29	1067	24	1057	63	96.75	99.53
jn26_91500_9	0.26	5.6465	0.1754	0.0769	0.0031	1.8490	0.0670	0.1771	0.0055	0.1604	0.0532	0.0038	1119	80	1052	30	1057	24	1052	69	94.05	99.53
jn26_91500_10	0.26	5.5866	0.1717	0.0744	0.0027	1.8410	0.0660	0.1790	0.0055	0.2254	0.0555	0.0036	1052	73	1060	30	1050	22	1090	65	100.73	100.95
jn26_91500_11	0.25	5.5402	0.1657	0.0734	0.0026	1.8530	0.0640	0.1805	0.0054	0.3651	0.0548	0.0033	1025	72	1068	29	1062	23	1073	63	104.19	100.56
jn26_91500_12	0.26	5.5586	0.1699	0.0763	0.0031	1.8650	0.0700	0.1799	0.0055	0.3592	0.0515	0.0031	1103	81	1065	30	1059	25	1017	58	96.56	100.57
jn26_91500_13	0.25	5.5586	0.1699	0.0736	0.0026	1.8430	0.0650	0.1799	0.0055	0.2837	0.0544	0.0035	1031	71	1064	30	1063	23	1069	66	103.25	100.09
jn26_91500_14	0.26	5.5218	0.1768	0.0755	0.0029	1.9040	0.0740	0.1811	0.0058	0.4489	0.0534	0.0035	1082	77	1072	31	1065	24	1040	66	99.09	100.66
jn26_91500_15	0.26	5.6211	0.1801	0.0766	0.0031	1.8320	0.0670	0.1779	0.0057	0.2815	0.0522	0.0032	1111	81	1057	32	1057	24	1025	62	95.16	100.00
jn26_91500_16	0.26	5.4407	0.1658	0.0722	0.0027	1.8430	0.0650	0.1838	0.0056	0.2516	0.0499	0.0033	992	76	1084	30	1056	23	975	63	109.32	102.65
jn26_91500_17	0.26	5.6306	0.1744	0.0769	0.0029	1.8910	0.0710	0.1776	0.0055	0.3217	0.0554	0.0037	1119	75	1053	29	1064	24	1088	70	94.14	98.97
jn26_91500_18	0.25	5.5218	0.1707	0.0743	0.0029	1.8380	0.0700	0.1811	0.0056	0.3330	0.0542	0.0036	1050	79	1071	30	1049	25	1064	68	102.04	102.10
jn26_91500_19	0.26	5.5340	0.1715	0.0745	0.0029	1.8260	0.0670	0.1807	0.0056	0.3139	0.0528	0.0035	1055	78	1069	31	1047	24	1042	67	101.32	102.10
jn26_91500_20	0.25	5.4855	0.1836	0.0771	0.0032	1.9200	0.0760	0.1823	0.0061	0.4822	0.0566	0.0054	1124	83	1075	33	1074	25	1094	97	95.66	100.09
jn26_91500_21	0.26	5.5991	0.1756	0.0756	0.0032	1.8560	0.0730	0.1786	0.0056	0.2784	0.0557	0.0037	1084	85	1057	31	1053	25	1083	69	97.46	100.38
jn26_91500_22	0.26	5.4885	0.1747	0.0732	0.0031	1.8230	0.0730	0.1822	0.0058	0.1325	0.057	0.0037	1019	86	1078	31	1043	27	1100	67	105.74	103.36
jn26_91500_23	0.26	5.7110	0.1761	0.0745	0.0028	1.8110	0.0660	0.1751	0.0054	0.3917	0.0517	0.0032	1055	76	1040	30	1043	23	1017	62	98.57	99.71
jn26_91500_24	0.26	5.7110	0.1761	0.0744	0.0029	1.7990	0.0670	0.1751	0.0054	0.2450	0.0535	0.0034	1052	79	1038	30	1037	26	1047	66	98.64	100.10
jn26_91500_25	0.26	5.6722	0.1770	0.0756	0.0029	1.8450	0.0690	0.1763	0.0055	0.3532	0.0581	0.0049	1084	77	1047	30	1047	25	1087	60	96.54	100.00
jn26_91500_26	0.26	5.5066	0.1759	0.0748	0.0029	1.8300	0.0700	0.1816	0.0058	0.3575	0.0533	0.0033	1063	78	1074	32	1047	25	1040	63	101.02	102.58
jn26_91500_27	0.26	5.6022	0.1852	0.0741	0.0028	1.8700	0.0690	0.1785	0.0059	0.3395	0.0539	0.0034	1044	76	1058	32	1066	24	1063	65	101.32	99.25
jn26_91500_28	0.25	5.4645	0.1762	0.0738	0.0028	1.8460	0.0690	0.1830	0.0059	0.2761	0.0539	0.0034	1036	77	1080	32	1055	24	1055	65	104.25	102.37
jn26_91500_29	0.25	5.5340	0.1776	0.0771	0.0034	1.8770	0.0720	0.1807	0.0058	0.3734	0.0545	0.0041	1124	88	1067	32	1063	26	1033	56	94.95	100.38
jn26_91500_30	0.26	5.7339	0.1841	0.0758	0.0029	1.8340	0.0730	0.1744	0.0056	0.4008	0.0533	0.0038	1090	77	1036	31	1045	25	1048	71	95.06	99.14
jn26_91500_31	0.26	5.5928	0.1783	0.0752	0.0030	1.8710	0.0740	0.1788	0.0057	0.3301	0.0556	0.0038	1074	80	1060	31	1059	25	1080	71	98.71	100.09
jn26_91500_32	0.25	5.6754	0.1836	0.0777	0.0032	1.8780	0.0760	0.1762	0.0057	0.3297	0.0553	0.0041	1139	82	1047	31	1069	27	1080	74	91.91	97.94
jn26_91500_33	0.27	5.4675	0.1853	0.0760	0.0032	1.8930	0.0790	0.1829	0.0062	0.3168	0.052	0.0036	1095	84	1078	34	1062	26	1023	68	98.44	101.51
jn26_91500_34	0.26	5.6243	0.1708	0.0743	0.0030	1.8250	0.0710	0.1778	0.0054	0.2881	0.0508	0.0032	1050	81	1055	30	1054	25	997	62	100.51	100.09
jn26_91500_35	0.25	5.4585	0.1758	0.0716	0.0028	1.8310	0.0700	0.1832	0.0059	0.4059	0.053	0.0035	975	80	1085	32	1052	25	1037	66	111.33	103.14
jn26_91500_36	0.26	5.7208	0.1865	0.0745	0.0031	1.7880	0.0740	0.1748	0.0057	0.3887	0.0545	0.0038	1055	84	1042	31	1035	27	1061	70	98.76	100.68
jn26_91500_37	0.26	5.4855	0.1775	0.0754	0.0032	1.8890	0.0770	0.1823	0.0059	0.2284	0.052	0.0044	1079	85	1078	33	1064	27	1011	88	99.89	101.32
jn26_91500_38	0.26	5.5157	0.1765	0.0749	0.0030	1.8850	0.0730	0.1813	0.0058	0.3085	0.0566	0.0041	1066	81	1075	32	1073	27	1097	78	100.86	100.19
jn26_91500_39	0.26	5.5804	0.1837	0.0754	0.0031	1.8480	0.0710	0.1792	0.0059	0.2607	0.0533	0.0035	1079	83	1060	32	1055	26	1048	68	98.22	100.47
jn26_91500_40	0.26	5.6786	0.1838	0.0748	0.0030	1.8290	0.0760	0.1761	0.0057	0.4054	0.0554	0.0035	1063	81	1042	31	1055	27	1087	67	98.01	98.77
jn13_91500_1	0.25	5.5991	0.1442	0.0758	0.0025	1.8720	0.0490	0.1786	0.0046	0.3567	0.0534	0.0027	1090	66	1059	25	1069	17	1051	51	97.17	99.06
jn13_91500_2	0.25	5.5525	0.1511	0.0748	0.0027	1.8350	0.0490	0.1801	0.0049	0.2667	0.0552	0.0028	1063	73	1066	27	1060	18	1081	53	100.27	100.57
jn13_91500_3	0.26	5.4645	0.1433	0.0737	0.0027	1.8420	0.0470	0.1830	0.0048	0.1792	0.0541	0.0028	1033	74	1083	26	1055	17	1061	53	104.81	102.65
jn13_91500_4	0.25	5.5371	0.1441	0.0741	0.0026	1.8390	0.0510	0.1806	0.0047	0.2925	0.0533	0.0028	1044	71	1071	25	1057	18	1057	52	102.57	101.32
jn13_91500_5	0.25	5.7241	0.1507	0.0776	0.0027	1.8580	0.0460	0.1747	0.0046	0.2892	0.0525	0.0026	1137	69	1038	25	1067	16	1032	49	91.32	97.28
jn13_91500_6	0.25	5.6275	0.1488	0.0762	0.0027	1.8770	0.0520	0.1777	0.0047	0.2743	0.0552	0.0027	1100	71	1053	25	1067	18	1080	52	95.70	98.69
jn13_91500_7	0.25	5.5960	0.1503	0.0746	0.0026	1.8280	0.0510	0.1787	0.0048	0.3689	0.0523	0.0027	1058	70	1058	26	1058	19	1026	51	100.02	100.00
jn13_91500_8	0.25	5.5525	0.1541	0.0731	0.0026	1.8340	0.0500	0.1801	0.0050	0.2967	0.0537	0.0028	1017	72	1064	27	1052	18	1056	53	104.65	101.14
jn13_91500_9	0.25	5.5340	0.1439	0.0752	0.0026	1.8630	0.0520	0.1807	0.0047	0.3774	0.0536	0.0027	1074	69	1068	26	1064	18	1057	51	99.46	100.38
jn13_91500_10	0.25	5.5710	0.1428	0.0750	0.0026	1.8550	0.0500	0.1795	0.0046	0.1972	0.0542	0.0027	1069	70	1066	25	1064	18	1070	50	99.77	100.19
jn13_91500_11	0.25	5.5249	0.1465	0.0749	0.0025	1.8700	0.0530	0.1810	0.0048	0.3522	0.054	0.0028	1066	67	1073	26	1069	19	1059	53	100.67	100.37
jn13_91500_12	0.25	5.6497	0.1468	0.0749	0.0025	1.8500	0.0510	0.1770	0.0046	0.3360	0.0558	0.003	1066	67	1049	25	1063	18	1095	57	98.42	98.68
jn13_91500_13	0.26	5.5525	0.1480	0.0743	0.0026	1.8510	0.0490	0.1801	0.0048	0.2926	0.052	0.0026	1050	71	1067	26	1062	17	1020	51	101.66	100.47
jn13_91500_14	0.25	5.6561	0.1472	0.0739	0.0024	1.8290	0.0460	0.1768	0.0046	0.3873	0.0534	0.0027	1039	66	1054	26	1055	16	1048	52	101.47	99.91
jn13_91500_15	0.25	5.5249	0.1404	0.0726	0.0025	1.8200	0.0490	0.1810	0.0046	0.3243	0.0561	0.0028	1003	70	1071	25	1054	17	1098	54	106.80	101.61
jn13_91500_16	0.26	5.7013	0.1463	0.0759	0.0026	1.8650	0.0530	0.1754	0.0045	0.2962	0.053	0.0028	1092	69	1046	25	1072	19	1039	53	95.75	97.57
jn13_91500_17	0.26	5.5525	0.1418	0.0746	0.0027	1.8530	0.0570	0.1801	0.0046	0.3117	0.0528	0.0027	1058	73	1066	25	1060	20	1036	53	100.78	100.57
jn13_91500_18	0.26	5.5432	0.1506	0.0744	0.0026	1.8610	0.0500	0.1804	0.0049	0.3119	0.053	0.0028	1052	70	1066	27	1067	18	1039	54	101.30	99.91
jn13_91500_19	0.25	5.6085	0.1510	0.0760	0.0027	1.8520	0.0500	0.1783	0.0048	0.2244	0.0538	0.0027	1095	71	1055	26	1062	18	1058	52	96.34	99.34
jn13_91500_20	0.25	5.5402	0.1504	0.0762	0.0027	1.8660	0.0520	0.1805	0.0049	0.2442	0.0545	0.0029	1100	71	1070	27	1066	18	1071	54	97.24	100.38
jn13_91500_21	0.26	5.6433	0.1529	0.0765	0.0029	1.8530	0.0540	0.1772	0.0048	0.2483	0.0536	0.0028	1108	76	1050	26	1059	18	1051	53	94.75	99.15
jn13_91500_22	0.25	5.5188	0.1431	0.0748	0.0026	1.8600	0.0480	0.1812	0.0047	0.2032	0.0538	0.0027	1063	70	1072	26	1064	17	1063	51	100.83	100.75
jn13_91500_23	0.25	5.5617	0.1516	0.0739	0.0027	1.8220	0.0520	0.1798	0.0049	0.3251	0.0534	0.0028	1039	74	1064	26	1051	19	1046	54	102.43	101.24
oc14_91500_1	0.26	5.5928	0.1345	0.0747	0.0024	1.8360	0.0670	0.1788	0.0043	0.1491	0.0541	0.0037	985	54	1059	23	1045	23	1065	70	107.51	101.34
oc14_91500_2	0.27	5.4975	0.1360	0.0728	0.0022	1.8130	0.0640	0.1819	0.0045	0.3769	0.0548	0.0039	982	54	1076	24	1045	23	1074	75	109.57	102.97
oc14_91500_3	0.26	5.5928	0.1345	0.0761	0.0022	1.8600	0.0620	0.1788	0.0043	0.2582	0.0505	0.0036	1070	53	1058	24	1064	22	994	70	98.88	99.44
oc14_91500_4	0.27	5.5835	0.1341	0.0751	0.0022	1.8860	0.0640	0.1791	0.0043	0.2951	0.0538	0.0038	1079	53	1062	23	1079	22	1059	72	98.42	98.42
oc14_91500_5	0.25	5.7372	0.1350	0.0748	0.0023	1.8000	0.0640	0.1743	0.0041	0.2779	0.0545	0.0038	1044	57	1035	23	1046	23	1070	73	99.14	98.95
oc14_91500_6	0.26	5.5866	0.1467	0.0757	0.0024	1.8810	0.0680	0.1790	0.0047	0.3097	0.0531	0.0038	1059	59	1060	25	1068	24	1044	74	100.09	99.25
oc14_91500_7	0.25	5.6054	0.1351	0.0742	0.0023	1.8500	0.0640	0.1784	0.0043	0.2368	0.0552	0.0039	1025	58	1059	24	1056	23	1082	75	103.32	100.28
oc14_91500_8	0.26	5.5897	0.1437	0.0757	0.0025	1.8670	0.0690	0.1789	0.0046	0.3333	0.0562	0.004	1052	59	1059	25	1065	24	1104	77	100.67	99.44
oc14_91500_9	0.27	5.5127	0.1368	0.0749	0.0024	1.8630	0.0690	0.1814	0.0045	0.2965	0.0526	0.0038	1058	58	1075	25	1072	24	1034	72	101.61	100.28
oc14_91500_10	0.26	5.6180	0.1420	0.0737	0.0023	1.8020	0.0640	0.1780	0.0045	0.3241	0.0528	0.0038	1019	57	1055	24	1045	23	1035	73	103.53	100.96
oc14_91500_11	0.27	5.4975	0.1420	0.0755	0.0026	1.8800	0.0710	0.1819	0.0047	0.3180	0.0526	0.004	1058	61	1078	26	1069	26	1037	77	101.89	100.84
oc14_91500_12	0.26	5.6883	0.1521	0.0746	0.0026	1.7960	0.0660	0.1758	0.0047	0.2376	0.0551	0.0041	1035	63	1041	26	1041	24	1080	78	100.58	100.00
oc14_91500_13	0.26	5.5586	0.1545	0.0776	0.0026	1.8980	0.0710	0.1799	0.0050	0.3138	0.0529	0.0041	1119	62	1064	27	1078	25	1040	79	95.08	98.70
oc14_91500_14	0.27	5.4615	0.1402	0.0763	0.0025	1.9080	0.0740	0.1831	0.0047	0.3100	0.0526	0.0039	1074	62	1081	25	1081	26	1032	75	100.65	100.00
oc14_91500_15	0.27	5.6465	0.1467	0.0736	0.0025	1.8260	0.0680	0.1771	0.0046	0.2301	0.0535	0.004	1013	62	1050	25	1049	23	1052	78	103.65	100.10
oc14_91500_16	0.25	5.5249	0.1404	0.0758	0.0025	1.8910	0.0690	0.1810	0.0046	0.3028	0.0568	0.0043	1069	61	1071	25	1073	25	1114	82	100.19	99.81
oc14_91500_17	0.26	5.5006	0.1422	0.0741	0.0026	1.8600	0.0720	0.1818	0.0047	0.3334	0.0544	0.0043	1002	65	1078	25	1059	25	1068	82	107.58	101.79
oc14_91500_18	0.27	5.5188	0.1431	0.0754	0.0025	1.8960	0.0700	0.1812	0.0047	0.3723	0.052	0.0041	1080	59	1071	25	1073	25	1019	78	99.17	99.81
oc14_91500_19	0.27	5.4975	0.1360	0.0745	0.0026	1.8540	0.0690	0.1819	0.0045	0.2906	0.0555	0.0042	1021	65	1077	25	1070	24	1095	79	105.48	100.65
oc14_91500_20	0.27	5.5897	0.1500	0.0757	0.0028	1.8490	0.0750	0.1789	0.0048	0.2633	0.055	0.0042	1028	71	1060	27	1073	26	1080	80	103.11	98.79
oc14_91500_21	0.26	5.6085	0.1510	0.0747	0.0026	1.8050	0.0680	0.1783	0.0048	0.2939	0.0539	0.0042	1015	64	1057	26	1050	25	1056	80	104.14	100.67
oc14_91500_22	0.27	5.4975	0.1481	0.0748	0.0028	1.8760	0.0760	0.1819	0.0049	0.2720	0.0518	0.0041	1000	71	1079	27	1071	27	1016	79	107.90	100.75
oc14_91500_23	0.26	5.6148	0.1419	0.0749	0.0026	1.8450	0.0710	0.1781	0.0045	0.2313	0.053	0.0041	1054	64	1055	25	1063	25	1042	78	100.09	99.25
oc14_91500_24	0.26	5.5127	0.1489	0.0728	0.0028	1.8280	0.0730	0.1814	0.0049	0.2362	0.0533	0.0041	954	72	1073	26	1054	26	1044	80	112.47	101.80
oc14_91500_25	0.26	5.5772	0.1369	0.0740	0.0026	1.8510	0.0710	0.1793	0.0044	0.2305	0.0537	0.0042	1007	67	1064	24	1061	25	1050	81	105.66	100.28
oc14_91500_26	0.26	5.6117	0.1449	0.0748	0.0027	1.8420	0.0690	0.1782	0.0046	0.1719	0.0537	0.004	1049	68	1057	25	1052	25	1052	77	100.76	100.48
oc14_91500_27	0.26	5.6117	0.1543	0.0762	0.0027	1.8800	0.0760	0.1782	0.0049	0.3465	0.054	0.0043	1099	68	1054	27	1073	27	1061	82	95.91	98.23
oc14_91500_28	0.26	5.5586	0.1483	0.0734	0.0026	1.8290	0.0720	0.1799	0.0048	0.3255	0.0541	0.0041	990	69	1067	26	1056	25	1060	79	107.78	101.04
oc14_91500_29	0.26	5.6561	0.1440	0.0761	0.0026	1.8860	0.0740	0.1768	0.0045	0.2759	0.0534	0.0041	1057	66	1051	25	1067	26	1048	79	99.43	98.50
oc14_91500_30	0.26	5.6306	0.1522	0.0765	0.0027	1.8740	0.0750	0.1776	0.0048	0.3105	0.0541	0.0043	1114	64	1052	26	1067	26	1063	82	94.43	98.59
oc14_91500_31	0.26	5.5679	0.1395	0.0760	0.0028	1.8460	0.0720	0.1796	0.0045	0.2701	0.0545	0.0041	1014	70	1063	25	1060	26	1067	78	104.83	100.28
oc14_91500_32	0.26	5.6883	0.1488	0.0729	0.0027	1.8020	0.0760	0.1758	0.0046	0.2949	0.0511	0.004	999	72	1044	25	1040	27	1001	77	104.50	100.38
oc14_91500_33	0.26	5.6022	0.1444	0.0738	0.0026	1.8000	0.0720	0.1785	0.0046	0.3142	0.0554	0.0042	990	68	1059	25	1039	26	1085	79	106.97	101.92
oc6_91500_1	0.26	5.6370	0.1366	0.0747	0.0031	1.8470	0.0710	0.1774	0.0043	0.2418	0.0546	0.0041	1060	84	1052	23	1054	25	1071	79	99.20	99.81
oc6_91500_2	0.25	5.6338	0.1397	0.0754	0.0033	1.8140	0.0690	0.1775	0.0044	0.1566	0.056	0.0042	1079	88	1054	24	1045	25	1097	79	97.67	100.86

91500 zircon continued

oc6_91500_3	0.26	5.5710	0.1366	0.0763	0.0033	1.9020	0.0700	0.1795	0.0044	0.0982	0.0542	0.004	1103	86	1066	24	1076	25	1069	77	96.65	99.07
oc6_91500_4	0.27	5.4885	0.1476	0.0731	0.0033	1.8160	0.0730	0.1822	0.0049	0.1979	0.055	0.0043	1017	91	1077	26	1054	26	1077	83	105.93	102.18
oc6_91500_5	0.26	5.4555	0.1399	0.0756	0.0034	1.8950	0.0760	0.1833	0.0047	0.1840	0.0534	0.0042	1084	90	1083	26	1083	26	1046	80	99.86	100.00
oc6_91500_6	0.25	5.6722	0.1480	0.0754	0.0034	1.8400	0.0790	0.1763	0.0046	0.3247	0.0539	0.0043	1079	90	1046	25	1048	28	1055	82	96.93	99.81
oc6_91500_7	0.25	5.6148	0.1450	0.0725	0.0033	1.7970	0.0750	0.1781	0.0046	0.2610	0.0504	0.0041	1000	92	1055	25	1046	28	991	78	105.50	100.86
oc6_91500_8	0.26	5.5866	0.1529	0.0765	0.0035	1.8600	0.0810	0.1790	0.0049	0.3147	0.0538	0.0042	1108	91	1061	27	1062	28	1054	81	95.74	99.91
oc6_91500_9	0.26	5.5556	0.1481	0.0744	0.0035	1.8370	0.0770	0.1800	0.0048	0.2157	0.0524	0.0043	1052	95	1067	26	1052	28	1034	81	101.39	101.43
oc6_91500_10	0.26	5.5772	0.1555	0.0729	0.0035	1.8220	0.0800	0.1793	0.0050	0.3468	0.0525	0.0042	1011	97	1062	27	1042	29	1036	81	105.03	101.92
oc6_91500_11	0.26	5.5279	0.1589	0.0750	0.0034	1.8730	0.0780	0.1809	0.0052	0.3180	0.0517	0.0041	1069	91	1069	28	1064	28	1031	77	100.05	100.47
oc6_91500_12	0.26	5.5772	0.1586	0.0749	0.0035	1.8650	0.0840	0.1793	0.0051	0.2682	0.052	0.0041	1066	94	1063	28	1060	30	1020	79	99.74	100.28
oc6_91500_13	0.26	5.6275	0.1520	0.0772	0.0035	1.8910	0.0810	0.1777	0.0048	0.2644	0.0526	0.0042	1126	90	1055	26	1076	29	1031	81	93.66	98.05
oc6_91500_14	0.27	5.6148	0.1576	0.0750	0.0034	1.8990	0.0840	0.1781	0.0050	0.3729	0.0524	0.0043	1069	91	1057	27	1072	30	1027	83	98.92	98.60
oc6_91500_15	0.26	5.5006	0.1513	0.0730	0.0033	1.8360	0.0780	0.1818	0.0050	0.3530	0.055	0.0044	1014	92	1076	28	1053	28	1083	86	106.12	102.18
oc6_91500_16	0.27	5.6850	0.1616	0.0794	0.0037	1.8770	0.0860	0.1759	0.0050	0.3622	0.0554	0.0044	1182	92	1043	27	1083	30	1087	84	88.23	96.31
oc6_91500_17	0.26	5.4705	0.1586	0.0753	0.0037	1.9030	0.0880	0.1828	0.0053	0.2714	0.0563	0.0044	1077	99	1081	29	1076	31	1112	82	100.42	100.46
oc6_91500_18	0.25	5.4615	0.1521	0.0729	0.0034	1.8160	0.0810	0.1831	0.0051	0.3125	0.0541	0.0045	1011	95	1084	28	1046	29	1066	84	107.20	103.63
oc6_91500_19	0.27	5.5710	0.1583	0.0758	0.0035	1.8740	0.0830	0.1795	0.0051	0.2934	0.0514	0.0042	1090	93	1061	28	1068	29	1008	81	97.36	99.34
oc6_91500_20	0.26	5.4975	0.1572	0.0741	0.0036	1.8200	0.0800	0.1819	0.0052	0.2486	0.0528	0.0043	1044	98	1075	28	1045	28	1033	82	102.95	102.87
oc6_91500_21	0.25	5.6850	0.1616	0.0753	0.0034	1.8210	0.0800	0.1759	0.0050	0.3351	0.0579	0.0047	1077	91	1050	27	1045	28	1135	89	97.54	100.48
oc6_91500_22	0.25	5.6022	0.1569	0.0730	0.0035	1.8250	0.0850	0.1785	0.0050	0.3339	0.0508	0.0041	1014	97	1056	27	1048	30	1000	79	104.15	100.76
oc6_91500_23	0.26	5.6148	0.1608	0.0753	0.0033	1.8360	0.0770	0.1781	0.0051	0.4319	0.0568	0.0045	1077	88	1056	28	1051	27	1111	86	98.09	100.48
oc6_91500_24	0.26	5.5494	0.1571	0.0754	0.0034	1.9040	0.0800	0.1802	0.0051	0.3445	0.0545	0.0043	1079	90	1067	28	1078	27	1070	82	98.87	98.98
oc6_91500_25	0.25	5.6689	0.1575	0.0744	0.0035	1.7960	0.0800	0.1764	0.0049	0.3563	0.0537	0.0043	1052	95	1045	27	1043	29	1055	83	99.30	100.19
oc6_91500_26	0.26	5.5866	0.1436	0.0741	0.0030	1.8220	0.0710	0.1790	0.0046	0.1356	0.0559	0.003	1019	59	1060	25	1053	26	1095	56	104.02	100.66
oc6_91500_27	0.26	5.6085	0.1416	0.0755	0.0029	1.8630	0.0700	0.1783	0.0045	0.1925	0.0535	0.0029	1068	53	1057	25	1070	25	1056	55	98.97	98.79
oc6_91500_28	0.26	5.5835	0.1403	0.0743	0.0030	1.8300	0.0700	0.1791	0.0045	0.1534	0.0535	0.0028	1026	57	1062	25	1051	26	1053	53	103.51	101.05
oc6_91500_29	0.26	5.6054	0.1445	0.0749	0.0030	1.8500	0.0710	0.1784	0.0046	0.1267	0.0556	0.0027	1033	57	1057	25	1061	25	1091	52	102.32	99.62
oc6_91500_30	0.26	5.5525	0.1418	0.0741	0.0031	1.8450	0.0720	0.1801	0.0046	0.0918	0.0514	0.0029	1010	62	1066	25	1057	25	1031	55	105.54	100.85
oc6_91500_31	0.26	5.5897	0.1437	0.0773	0.0032	1.9040	0.0740	0.1789	0.0046	0.0656	0.0527	0.003	1097	58	1060	25	1079	25	1043	57	96.63	98.24
oc6_91500_32	0.26	5.4915	0.1417	0.0730	0.0030	1.8430	0.0730	0.1821	0.0047	0.1083	0.0536	0.0029	994	59	1078	25	1056	25	1054	54	108.45	102.08
oc6_91500_33	0.26	5.5772	0.1431	0.0735	0.0029	1.8190	0.0720	0.1793	0.0046	0.2551	0.0535	0.0029	1020	56	1062	25	1051	26	1052	56	104.12	101.05
oc6_91500_34	0.26	5.5679	0.1426	0.0768	0.0031	1.8820	0.0730	0.1796	0.0046	0.1381	0.0524	0.003	1101	59	1063	25	1079	26	1031	58	96.55	98.52
oc6_91500_35	0.26	5.5525	0.1387	0.0753	0.0030	1.8540	0.0710	0.1801	0.0045	0.2169	0.0527	0.003	1026	55	1067	25	1056	26	1036	57	104.00	101.04
oc6_91500_36	0.25	5.6625	0.1475	0.0772	0.0031	1.8620	0.0690	0.1766	0.0046	0.1080	0.0543	0.0028	1091	54	1048	25	1062	25	1070	54	96.06	98.68
oc6_91500_37	0.25	5.6689	0.1446	0.0742	0.0030	1.7990	0.0740	0.1764	0.0045	0.2112	0.0518	0.0028	1015	60	1049	25	1043	27	1020	53	103.35	100.58
oc6_91500_38	0.26	5.4555	0.1399	0.0748	0.0030	1.9080	0.0710	0.1833	0.0047	0.1851	0.055	0.0029	1043	54	1085	26	1079	25	1077	55	104.03	100.56
oc6_91500_39	0.25	5.6117	0.1417	0.0746	0.0031	1.8400	0.0730	0.1782	0.0045	0.1027	0.0537	0.0027	1035	61	1056	25	1060	26	1057	51	102.03	99.62
oc6_91500_40	0.26	5.5928	0.1408	0.0737	0.0031	1.8130	0.0770	0.1788	0.0045	0.2234	0.0556	0.0029	999	63	1061	25	1040	28	1094	56	106.21	102.02
oc6_91500_41	0.26	5.5866	0.1436	0.0741	0.0030	1.8240	0.0760	0.1790	0.0046	0.1365	0.0559	0.003	1019	59	1060	25	1050	27	1095	56	104.02	100.95
oc6_91500_42	0.26	5.6085	0.1416	0.0755	0.0029	1.8700	0.0730	0.1783	0.0045	0.1971	0.0535	0.0029	1068	53	1057	25	1074	27	1056	55	98.97	98.42
oc6_91500_43	0.26	5.5835	0.1403	0.0743	0.0030	1.8160	0.0760	0.1791	0.0045	0.1634	0.0535	0.0028	1026	57	1062	25	1052	27	1053	53	103.51	100.95
oc6_91500_44	0.26	5.6054	0.1445	0.0749	0.0030	1.8570	0.0740	0.1784	0.0046	0.1328	0.0556	0.0027	1033	57	1057	25	1062	27	1091	52	102.32	99.53
oc6_91500_45	0.26	5.5525	0.1418	0.0741	0.0031	1.8390	0.0800	0.1801	0.0046	0.0804	0.0514	0.0029	1010	62	1066	25	1060	28	1031	55	105.54	100.57
oc6_91500_46	0.26	5.5897	0.1437	0.0773	0.0032	1.9000	0.0790	0.1789	0.0046	0.0595	0.0527	0.003	1097	58	1060	25	1082	27	1043	57	96.63	97.97
oc6_91500_47	0.26	5.4915	0.1417	0.0730	0.0030	1.8370	0.0780	0.1821	0.0047	0.0919	0.0536	0.0029	994	59	1078	25	1058	27	1054	54	108.45	101.89
oc6_91500_48	0.26	5.5772	0.1431	0.0735	0.0029	1.8190	0.0730	0.1793	0.0046	0.2341	0.0535	0.0029	1020	56	1062	25	1048	26	1052	56	104.12	101.34
oc6_91500_49	0.26	5.5679	0.1426	0.0768	0.0031	1.8990	0.0780	0.1796	0.0046	0.1351	0.0524	0.003	1101	59	1063	25	1079	28	1034	58	96.55	98.52
oc6_91500_50	0.26	5.5525	0.1387	0.0753	0.0030	1.8440	0.0750	0.1801	0.0045	0.2183	0.0527	0.003	1026	55	1067	25	1062	27	1036	57	104.00	100.47
oc6_91500_51	0.25	5.6625	0.1475	0.0772	0.0031	1.8500	0.0750	0.1766	0.0046	0.1240	0.0543	0.0028	1091	54	1048	25	1063	26	1070	54	96.06	98.59
oc6_91500_52	0.25	5.6689	0.1446	0.0742	0.0030	1.8150	0.0750	0.1764	0.0045	0.2231	0.0518	0.0028	1015	60	1049	25	1049	28	1020	53	103.35	100.00
oc6_91500_53	0.26	5.4555	0.1399	0.0748	0.0030	1.9010	0.0770	0.1833	0.0047	0.2076	0.055	0.0029	1043	54	1085	26	1080	27	1077	55	104.03	100.46
oc7_91500_1	0.26	5.5036	0.1242	0.0731	0.0025	1.8510	0.0680	0.1817	0.0041	0.2907	0.0574	0.0026	1017	69	1077	22	1063	24	1123	49	105.93	101.32
oc7_91500_2	0.26	5.5525	0.1141	0.0741	0.0026	1.8550	0.0720	0.1801	0.0037	0.1891	0.0505	0.0023	1044	71	1067	20	1064	25	992	43	102.18	100.28
oc7_91500_3	0.26	5.6275	0.1235	0.0753	0.0026	1.8210	0.0670	0.1777	0.0039	0.1993	0.0539	0.0022	1077	69	1054	21	1050	24	1063	42	97.91	100.38
oc7_91500_4	0.26	5.6243	0.1234	0.0759	0.0026	1.8620	0.0690	0.1778	0.0039	0.2816	0.0525	0.0023	1092	69	1056	21	1066	25	1033	44	96.66	99.06
oc7_91500_5	0.26	5.6754	0.1256	0.0751	0.0026	1.8050	0.0660	0.1762	0.0039	0.2167	0.0541	0.0024	1071	70	1046	21	1047	25	1060	47	97.65	99.90
oc7_91500_6	0.26	5.6465	0.1180	0.0774	0.0026	1.8790	0.0670	0.1771	0.0037	0.1444	0.0528	0.0024	1132	67	1050	20	1073	24	1039	47	92.80	97.86
oc7_91500_7	0.26	5.5679	0.1178	0.0739	0.0026	1.8470	0.0680	0.1796	0.0038	0.1400	0.0538	0.0025	1039	71	1065	21	1055	24	1060	48	102.53	100.95
oc7_91500_8	0.26	5.5617	0.1206	0.0746	0.0026	1.8410	0.0690	0.1798	0.0039	0.1270	0.0546	0.0025	1058	70	1066	21	1059	25	1071	47	100.78	100.66
oc7_91500_9	0.26	5.4795	0.1171	0.0753	0.0027	1.8990	0.0720	0.1825	0.0039	0.2167	0.0546	0.0025	1077	72	1079	21	1076	25	1071	48	100.23	100.28
oc7_91500_10	0.27	5.5157	0.1217	0.0734	0.0027	1.8510	0.0690	0.1813	0.0040	0.0959	0.0538	0.0024	1025	74	1074	22	1057	25	1063	46	104.78	101.61
oc7_91500_11	0.26	5.6722	0.1287	0.0770	0.0027	1.8880	0.0720	0.1763	0.0040	0.2255	0.0544	0.0024	1121	70	1047	22	1075	25	1070	47	93.38	97.40
oc7_91500_12	0.26	5.6211	0.1264	0.0740	0.0027	1.8180	0.0710	0.1779	0.0040	0.1768	0.0553	0.0026	1041	74	1058	22	1049	26	1086	50	101.59	100.86
oc7_91500_13	0.27	5.5741	0.1274	0.0761	0.0029	1.8870	0.0740	0.1794	0.0041	0.0733	0.0533	0.0028	1098	76	1062	22	1076	26	1044	53	96.75	98.70
oc7_91500_14	0.27	5.6275	0.1298	0.0763	0.0027	1.8660	0.0700	0.1777	0.0041	0.2123	0.0524	0.0024	1103	71	1056	22	1063	25	1028	45	95.74	99.34
oc7_91500_15	0.27	5.5006	0.1240	0.0753	0.0030	1.8790	0.0750	0.1818	0.0041	0.0906	0.0543	0.0028	1077	80	1076	22	1074	27	1064	53	99.95	100.19
oc7_91500_16	0.26	5.5835	0.1247	0.0730	0.0027	1.8120	0.0710	0.1791	0.0040	0.2249	0.0538	0.0024	1014	75	1063	22	1053	26	1054	46	104.84	100.95
oc7_91500_17	0.26	5.5371	0.1226	0.0728	0.0028	1.8070	0.0720	0.1806	0.0040	0.1589	0.0551	0.0026	1008	78	1071	22	1045	25	1080	50	106.21	102.49
oc7_91500_18	0.26	5.4885	0.1265	0.0768	0.0028	1.9100	0.0750	0.1822	0.0042	0.2975	0.0534	0.0027	1116	73	1078	23	1079	27	1049	52	96.59	99.91
oc7_91500_19	0.26	5.6180	0.1231	0.0752	0.0029	1.8510	0.0740	0.1780	0.0039	0.2679	0.055	0.0029	1074	77	1055	21	1058	26	1076	56	98.24	99.72
oc7_91500_20	0.26	5.5960	0.1253	0.0731	0.0026	1.8060	0.0690	0.1787	0.0040	0.2403	0.0528	0.0027	1017	72	1059	22	1049	25	1048	50	104.16	100.95
oc7_91500_21	0.26	5.5402	0.1258	0.0751	0.0030	1.8660	0.0760	0.1805	0.0041	0.1154	0.053	0.0025	1071	80	1068	23	1068	27	1039	48	99.70	100.00
oc7_91500_22	0.26	5.6850	0.1293	0.0751	0.0027	1.8380	0.0710	0.1759	0.0040	0.2508	0.0537	0.0027	1071	72	1043	22	1053	25	1055	53	97.37	99.05
oc7_91500_23	0.26	5.5066	0.1274	0.0736	0.0030	1.8440	0.0770	0.1816	0.0042	0.1331	0.0536	0.0028	1031	82	1077	23	1061	27	1059	54	104.51	101.51
oc7_91500_24	0.26	5.5804	0.1277	0.0766	0.0030	1.8870	0.0750	0.1792	0.0041	0.1677	0.0532	0.0029	1111	78	1061	22	1073	27	1041	56	95.52	98.88
oc7_91500_25	0.26	5.6148	0.1324	0.0730	0.0029	1.7780	0.0730	0.1781	0.0042	0.1942	0.054	0.003	1014	81	1055	23	1035	26	1058	57	104.05	101.93
oc7_91500_26	0.26	5.5096	0.1305	0.0735	0.0028	1.8280	0.0740	0.1815	0.0043	0.2828	0.0524	0.0028	1028	77	1073	24	1062	26	1026	54	104.40	101.04
oc7_91500_27	0.26	5.5991	0.1317	0.0744	0.0030	1.8260	0.0770	0.1786	0.0042	0.2171	0.0516	0.0028	1052	81	1059	23	1059	28	1014	54	100.63	100.00
oc7_91500_28	0.26	5.6850	0.1390	0.0757	0.0028	1.8350	0.0740	0.1759	0.0043	0.2205	0.0564	0.0028	1087	74	1045	23	1055	26	1124	53	96.12	99.05
oc7_91500_29	0.27	5.5897	0.1406	0.0751	0.0031	1.8350	0.0790	0.1789	0.0045	0.2324	0.0534	0.0028	1071	83	1061	25	1058	29	1054	55	99.05	100.28
oc7_91500_30	0.26	5.5340	0.1348	0.0765	0.0031	1.9200	0.0790	0.1807	0.0044	0.1464	0.0528	0.0031	1108	81	1072	24	1084	28	1034	59	96.73	98.89
oc7_91500_31	0.26	5.6054	0.1351	0.0752	0.0031	1.8370	0.0780	0.1784	0.0043	0.0892	0.0551	0.0031	1074	83	1060	24	1057	28	1080	59	98.71	100.28
oc7_91500_32	0.27	5.5741	0.1336	0.0755	0.0030	1.8990	0.0780	0.1794	0.0043	0.1756	0.0545	0.003	1082	80	1065	24	1082	27	1078	58	98.44	98.43
fe05_91500_1	0.27	5.6022	0.2166	0.0756	0.0023	1.8570	0.0980	0.1785	0.0069	0.2460	0.0546	0.0037	1081	50	1059	38	1067	35	1071	71	97.96	99.25
fe05_91500_2	0.26	5.6883	0.2297	0.0757	0.0026	1.8010	0.0990	0.1758	0.0071	0.3133	0.0523	0.0037	1062	61	1045	39	1046	36	1034	71	98.40	99.90
fe05_91500_3	0.27	5.7013	0.2243	0.0736	0.0024	1.7940	0.0970	0.1754	0.0069	0.3138	0.0516	0.0036	1040	55	1040	38	1043	35	1017	68	100.00	99.71
fe05_91500_4	0.26	5.4230	0.2117	0.0760	0.0024	1.9280	0.1000	0.1844	0.0072	0.2764	0.057	0.0039	1087	52	1091	39	1088	35	1121	74	100.37	100.28
fe05_91500_5	0.27	5.4705	0.2215	0.0756	0.0026	1.9060	0.1100	0.1828	0.0074	0.2878	0.053	0.0038	1069	61	1080	40	1084	37	1047	73	101.03	99.63
fe05_91500_6	0.27	5.5066	0.2183	0.0738	0.0023	1.8590	0.0990	0.1816	0.0072	0.3952	0.0553	0.0038	1012	54	1075	39	1073	36	1088	72	106.23	100.19
fe05_91500_7	0.27	5.4765	0.2219	0.0729	0.0025	1.8610	0.1000	0.1826	0.0074	0.2530	0.0567	0.0039	977	60	1082	40	1066	35	1114	75	110.75	101.50
fe05_91500_8	0.26	5.4945	0.2204	0.0753	0.0025	1.8920	0.1000	0.1820	0.0073	0.3902	0.0529	0.0037	1047	55	1077	39	1073	36	1041	71	102.87	100.37
fe05_91500_9	0.27	5.6211	0.2243	0.0739	0.0025	1.8300	0.0990	0.1779	0.0071	0.2403	0.0525	0.0038	1014	59	1054	39	1054	35	1033	73	103.94	100.00
fe05_91500_10	0.27	5.6948	0.2270	0.0758	0.0024	1.8400	0.0990	0.1756	0.0070	0.3401	0.0519	0.0036	1064	54	1042	38	1052	36	1022	69	97.93	99.05
fe05_91500_11	0.26	5.6722	0.2284	0.0745	0.0024	1.7920	0.0960	0.1763	0.0071	0.2338	0.0534	0.0037	1035	56	1045	38	1038	35	1047	70	100.97	100.67
fe05_91500_12	0.27	5.7637	0.2325	0.0760	0.0025	1.8140	0.0980	0.1735	0.0070	0.3648	0.0521	0.0036	1056	57	1030	38	1053	35	1026	69	97.54	97.82
fe05_91500_13	0.27	5.5494	0.2279	0.0768	0.0026	1.9020	0.1000	0.1802	0.0074	0.3413	0.0515	0.0038	1129	57	1069	40	1077	36	1012	73	94.69	99.26
fe05_91500_14	0.27	5.7208	0.2324	0.0751	0.0025	1.7880	0.0980	0.1748	0.0071	0.3680	0.0545	0.0038	1027	56	1039	39	1042	35	1069	72	101.17	99.71
fe05_91500_15	0.27	5.4915	0.2201	0.0750	0.0025	1.8790	0.1000	0.1821	0.0073	0.3439	0.0562	0.0041	1066	59	1082	40	1070	36	1101	79	101.50	101.12
fe05_91500_16	0.26	5.4615	0.2297	0.0754	0.0026	1.8910	0.1100	0.1831	0.0077	0.4085	0.056	0.0042	1057	61	1083	42	1068	37	1096	79	102.46	101.40
fe05_91500_17	0.26	5.5006	0.2209	0.0754	0.0024	1.8910	0.1000	0.1818	0.0073	0.3739	0.055	0.0039	1055	56	1074	40	1076	36	1075	75	101.80	99.81

91500 zircon continued

fe05_91500_18	0.26	5.4615	0.2177	0.0735	0.0025	1.8660	0.1000	0.1831	0.0073	0.2772	0.0541	0.0038	985	60	1083	40	1072	35	1064	73	109.95	101.03
fe05_91500_19	0.27	5.6243	0.2183	0.0756	0.0024	1.8630	0.1000	0.1778	0.0069	0.3029	0.053	0.0037	1049	55	1054	38	1065	35	1040	71	100.48	98.97
fe05_91500_20	0.26	5.4975	0.2176	0.0724	0.0025	1.8400	0.1000	0.1819	0.0072	0.2859	0.0549	0.0038	974	64	1078	40	1056	36	1079	74	110.68	102.08
fe05_91500_21	0.27	5.7471	0.2345	0.0751	0.0025	1.7940	0.0950	0.1740	0.0071	0.1654	0.052	0.0037	1054	58	1032	39	1046	35	1024	71	97.91	98.66
fe05_91500_22	0.27	5.6786	0.2257	0.0731	0.0025	1.7650	0.0980	0.1761	0.0070	0.2762	0.0534	0.0038	965	63	1044	38	1024	37	1057	74	108.19	101.95
fe05_91500_23	0.26	5.5127	0.2218	0.0751	0.0024	1.9040	0.1000	0.1814	0.0073	0.3763	0.0519	0.0037	1064	53	1074	40	1077	36	1022	71	100.94	99.72
fe05_91500_24	0.26	5.6148	0.2207	0.0746	0.0023	1.8190	0.0980	0.1781	0.0070	0.3973	0.0523	0.0037	1030	51	1056	38	1045	35	1027	71	102.52	101.05
fe05_91500_25	0.26	5.5463	0.2246	0.0767	0.0025	1.8940	0.1000	0.1803	0.0073	0.3531	0.0529	0.0038	1103	54	1068	40	1078	36	1037	72	96.83	99.07
fe05_91500_26	0.26	5.5648	0.2199	0.0753	0.0024	1.8800	0.1000	0.1797	0.0071	0.3012	0.0563	0.0039	1055	56	1065	39	1075	36	1114	74	100.95	99.07
fe05_91500_27	0.26	5.5340	0.2236	0.0735	0.0026	1.8430	0.1000	0.1807	0.0073	0.2819	0.0558	0.004	989	63	1070	40	1054	37	1096	77	108.19	101.52
fe05_91500_28	0.28	5.5279	0.2231	0.0758	0.0023	1.8850	0.0900	0.1809	0.0073	0.3317	0.0547	0.0035	1063	55	1072	40	1073	32	1082	66	100.85	99.91
fe05_91500_29	0.27	5.5340	0.2266	0.0762	0.0025	1.8900	0.0920	0.1807	0.0074	0.3570	0.0544	0.0036	1084	59	1070	40	1080	32	1067	69	98.71	99.07
fe05_91500_30	0.26	5.5928	0.2252	0.0742	0.0022	1.8200	0.0850	0.1788	0.0072	0.2863	0.0548	0.0035	1030	53	1060	39	1050	30	1077	67	102.91	100.95
fe05_91500_31	0.27	5.6529	0.2237	0.0741	0.0020	1.8050	0.0820	0.1769	0.0070	0.3113	0.0529	0.0033	1033	49	1048	38	1045	30	1041	63	101.45	100.29
fe05_91500_32	0.27	5.4825	0.2224	0.0750	0.0022	1.9110	0.0920	0.1824	0.0074	0.3470	0.0552	0.0038	1065	54	1082	40	1077	33	1082	72	101.60	100.46
fe05_91500_33	0.26	5.6117	0.2236	0.0766	0.0026	1.8890	0.0920	0.1782	0.0071	0.1551	0.0549	0.0037	1092	63	1056	39	1076	32	1077	70	96.70	98.14
fe05_91500_34	0.27	5.5371	0.2238	0.0735	0.0022	1.8430	0.0870	0.1806	0.0073	0.3288	0.0549	0.0035	1014	54	1071	40	1058	31	1079	66	105.62	101.23
fe05_91500_35	0.27	5.6402	0.2259	0.0754	0.0021	1.8370	0.0850	0.1773	0.0071	0.3624	0.0522	0.0033	1090	47	1053	39	1059	30	1030	63	96.61	99.43
fe05_91500_36	0.27	5.7670	0.2328	0.0742	0.0023	1.7800	0.0830	0.1734	0.0070	0.2517	0.0514	0.0033	1039	55	1030	38	1035	30	1010	64	99.13	99.52
fe05_91500_37	0.27	5.7438	0.2309	0.0750	0.0022	1.8000	0.0840	0.1741	0.0070	0.3075	0.0499	0.0032	1043	53	1033	38	1051	30	981	61	99.04	98.29
fe05_91500_38	0.27	5.7703	0.2364	0.0759	0.0023	1.7970	0.0880	0.1733	0.0071	0.4118	0.0523	0.0034	1064	54	1031	39	1040	31	1027	66	96.90	99.13
fe05_91500_39	0.27	5.5525	0.2220	0.0741	0.0023	1.8440	0.0870	0.1801	0.0072	0.2154	0.0559	0.0036	1007	57	1066	39	1057	30	1100	69	105.86	100.85
fe05_91500_40	0.27	5.5617	0.2227	0.0739	0.0022	1.8350	0.0860	0.1798	0.0072	0.3696	0.054	0.0035	1021	52	1064	39	1056	31	1059	67	104.21	100.76
fe05_91500_41	0.27	5.5494	0.2186	0.0748	0.0023	1.8600	0.0890	0.1802	0.0071	0.3124	0.0538	0.0035	1050	55	1069	38	1070	31	1063	67	101.81	99.91
fe05_91500_42	0.27	5.4496	0.2227	0.0724	0.0021	1.8520	0.0880	0.1835	0.0075	0.3311	0.0577	0.0038	1017	54	1084	41	1062	30	1134	71	106.59	102.07
fe05_91500_43	0.27	5.4765	0.2159	0.0762	0.0023	1.9140	0.0890	0.1826	0.0072	0.2543	0.0564	0.0036	1083	54	1081	39	1087	32	1107	69	99.82	99.45
fe05_91500_44	0.27	5.3533	0.2149	0.0745	0.0022	1.9030	0.0890	0.1868	0.0075	0.3067	0.0558	0.0036	1030	53	1106	41	1074	31	1097	68	107.38	102.98
fe05_91500_45	0.27	5.5279	0.2170	0.0760	0.0022	1.9120	0.0880	0.1809	0.0071	0.1833	0.053	0.0034	1079	52	1072	39	1081	31	1040	65	99.35	99.17
fe05_91500_46	0.27	5.4555	0.2173	0.0742	0.0022	1.9000	0.0890	0.1833	0.0073	0.2866	0.0539	0.0035	1029	55	1084	40	1075	31	1057	66	105.34	100.84
fe05_91500_47	0.26	5.5741	0.2206	0.0759	0.0023	1.8740	0.0880	0.1794	0.0071	0.2676	0.0541	0.0034	1066	56	1062	39	1067	32	1070	66	99.62	99.53
fe05_91500_48	0.27	5.6306	0.2283	0.0735	0.0022	1.7880	0.0840	0.1776	0.0072	0.3478	0.0532	0.0036	1023	55	1053	40	1038	31	1044	69	102.93	101.45
fe05_91500_49	0.27	5.6689	0.2282	0.0762	0.0023	1.8520	0.0880	0.1764	0.0071	0.3648	0.0519	0.0034	1094	53	1046	39	1061	31	1024	66	95.61	98.59
fe05_91500_50	0.27	5.5525	0.2189	0.0753	0.0022	1.8920	0.0880	0.1801	0.0071	0.3010	0.0529	0.0033	1075	53	1067	39	1078	31	1039	64	99.26	98.98
fe05_91500_51	0.27	5.5866	0.2216	0.0762	0.0022	1.8450	0.0870	0.1790	0.0071	0.3081	0.0533	0.0034	1081	52	1062	38	1063	31	1046	66	98.24	99.91
fe05_91500_52	0.27	5.5188	0.2223	0.0752	0.0022	1.8650	0.0870	0.1812	0.0073	0.1957	0.0525	0.0034	1062	54	1073	40	1070	31	1033	65	101.04	100.28
fe05_91500_53	0.27	5.4885	0.2139	0.0757	0.0023	1.8930	0.0900	0.1822	0.0071	0.3277	0.0547	0.0035	1108	54	1078	39	1077	32	1076	66	97.29	100.09
fe05_91500_54	0.26	5.7013	0.2340	0.0760	0.0025	1.8150	0.0850	0.1754	0.0072	0.1916	0.0521	0.0034	1074	60	1043	39	1049	32	1029	65	97.11	99.43
fe05_91500_55	0.26	5.5617	0.2227	0.0743	0.0021	1.8540	0.0860	0.1798	0.0072	0.3664	0.0541	0.0034	1038	52	1065	39	1060	30	1062	65	102.60	100.47
fe05_91500_56	0.27	5.8241	0.2307	0.0752	0.0023	1.7880	0.0840	0.1717	0.0068	0.1980	0.0525	0.0033	1055	56	1022	37	1035	31	1033	63	96.87	98.74
fe05_91500_57	0.27	5.5340	0.2174	0.0744	0.0020	1.8600	0.0860	0.1807	0.0071	0.3210	0.0548	0.0035	1040	48	1070	39	1065	30	1077	67	102.88	100.47
fe05_91500_58	0.27	5.5804	0.2180	0.0734	0.0021	1.8220	0.0840	0.1792	0.0070	0.3010	0.054	0.0035	1017	53	1063	38	1053	30	1064	67	104.52	100.95
fe05_91500_59	0.27	5.5928	0.2190	0.0747	0.0021	1.8480	0.0850	0.1788	0.0070	0.2772	0.0557	0.0035	1048	53	1059	38	1063	31	1100	67	101.05	99.62
mr20_91500_1	0.25	5.8241	0.2340	0.0735	0.0027	1.7350	0.0750	0.1717	0.0069	0.1824	0.0527	0.0041	1018	63	1021	38	1021	28	1035	78	100.29	100.00
mr20_91500_2	0.26	5.8140	0.2366	0.0775	0.0029	1.8450	0.0820	0.1720	0.0070	0.1896	0.0538	0.0043	1091	66	1024	39	1061	29	1060	81	93.86	96.51
mr20_91500_3	0.26	5.7013	0.2340	0.0742	0.0028	1.7830	0.0790	0.1754	0.0072	0.1509	0.0556	0.0043	1004	69	1043	40	1036	29	1094	82	103.88	100.68
mr20_91500_4	0.26	5.6850	0.2262	0.0743	0.0028	1.7980	0.0800	0.1759	0.0070	0.1165	0.0527	0.0042	998	70	1047	38	1044	29	1043	81	104.91	100.29
mr20_91500_5	0.26	5.5804	0.2242	0.0763	0.0028	1.8730	0.0820	0.1792	0.0072	0.1811	0.0516	0.0041	1090	63	1064	40	1074	30	1014	78	97.61	99.07
mr20_91500_6	0.26	5.4645	0.2210	0.0772	0.0027	1.9540	0.0830	0.1830	0.0074	0.1394	0.0546	0.0045	1136	59	1083	40	1104	29	1074	85	95.33	98.10
mr20_91500_7	0.26	5.4555	0.2202	0.0733	0.0027	1.8540	0.0790	0.1833	0.0074	0.1191	0.0526	0.0044	997	65	1085	40	1069	28	1050	85	108.83	101.50
mr20_91500_8	0.26	5.4885	0.2199	0.0746	0.0026	1.8630	0.0780	0.1822	0.0073	0.1861	0.052	0.0041	1049	59	1080	41	1066	28	1024	80	102.96	101.31
mr20_91500_9	0.26	5.4795	0.2192	0.0746	0.0028	1.8950	0.0830	0.1825	0.0073	0.1677	0.0574	0.0047	1048	62	1081	40	1080	29	1123	89	103.15	100.09
mr20_91500_10	0.26	5.4975	0.2176	0.0747	0.0029	1.9060	0.0860	0.1819	0.0072	0.0990	0.0545	0.0044	1041	70	1080	40	1082	31	1073	83	103.75	99.82
mr20_91500_11	0.27	5.5960	0.2255	0.0745	0.0029	1.8500	0.0840	0.1787	0.0072	0.1698	0.0532	0.0042	1014	68	1060	39	1057	30	1044	80	104.54	100.28
mr20_91500_12	0.26	5.5679	0.2294	0.0744	0.0027	1.8500	0.0780	0.1796	0.0074	0.1291	0.0544	0.0044	1053	65	1064	40	1066	28	1070	84	101.04	99.81
mr20_91500_13	0.26	5.3996	0.2157	0.0738	0.0027	1.8780	0.0830	0.1852	0.0074	0.2109	0.0559	0.0045	1000	65	1095	40	1073	30	1095	87	109.50	102.05
mr20_91500_14	0.26	5.5006	0.2239	0.0745	0.0028	1.8670	0.0820	0.1818	0.0074	0.1843	0.0528	0.0042	1041	66	1078	40	1072	30	1041	81	103.55	100.56
mr20_91500_15	0.26	5.7078	0.2346	0.0754	0.0030	1.8240	0.0820	0.1752	0.0072	0.1256	0.0524	0.0042	1069	70	1039	39	1053	30	1032	82	97.19	98.67
mr20_91500_16	0.26	5.7837	0.2308	0.0755	0.0029	1.7850	0.0790	0.1729	0.0069	0.0885	0.0534	0.0041	1080	64	1029	38	1037	28	1052	80	95.28	99.23
mr20_91500_17	0.26	5.6754	0.2351	0.0792	0.0031	1.8920	0.0840	0.1762	0.0073	0.0124	0.0487	0.0041	1131	70	1045	40	1074	29	958	78	92.40	97.30
mr20_91500_18	0.26	5.4765	0.2219	0.0743	0.0028	1.8610	0.0770	0.1826	0.0074	-0.0216	0.0581	0.0045	1036	64	1081	40	1069	28	1141	86	104.34	101.12
mr20_91500_19	0.26	5.4945	0.2234	0.0747	0.0030	1.8840	0.0840	0.1820	0.0074	0.0529	0.0546	0.0046	1052	72	1077	40	1073	30	1070	87	102.38	100.37
mr20_91500_20	0.26	5.5066	0.2244	0.0748	0.0028	1.8780	0.0820	0.1816	0.0074	0.1929	0.0539	0.0044	1037	63	1076	40	1070	29	1058	84	103.76	100.56
mr20_91500_21	0.26	5.4975	0.2267	0.0745	0.0029	1.8530	0.0810	0.1819	0.0075	0.1614	0.0538	0.0044	1026	68	1079	41	1075	29	1062	83	105.17	100.37
mr20_91500_22	0.26	5.4885	0.2229	0.0747	0.0029	1.8830	0.0820	0.1822	0.0074	0.0941	0.0556	0.0044	1047	70	1078	40	1073	30	1089	85	102.96	100.47
mr20_91500_23	0.26	5.6085	0.2265	0.0763	0.0030	1.8800	0.0810	0.1783	0.0072	-0.0632	0.0549	0.0046	1088	68	1058	40	1079	28	1076	87	97.24	98.05
mr20_91500_24	0.26	5.4975	0.2206	0.0744	0.0031	1.8280	0.0860	0.1819	0.0073	0.2019	0.0556	0.0048	1013	74	1076	40	1055	30	1092	91	106.22	101.99
mr20_91500_25	0.26	5.5463	0.2276	0.0733	0.0029	1.8440	0.0800	0.1803	0.0074	0.0331	0.0544	0.0046	1027	69	1068	40	1056	29	1070	88	103.99	101.14
mr20_91500_26	0.26	5.7013	0.2340	0.0732	0.0031	1.7850	0.0840	0.1754	0.0072	0.0393	0.0537	0.0044	1008	78	1042	40	1043	30	1053	85	103.37	99.90
mr20_91500_27	0.25	5.6180	0.2241	0.0758	0.0031	1.8510	0.0840	0.1780	0.0071	-0.0117	0.0522	0.0044	1064	73	1059	40	1064	30	1029	85	99.53	99.53
mr20_91500_28	0.25	5.5648	0.2230	0.0737	0.0031	1.8370	0.0860	0.1797	0.0072	0.0511	0.0581	0.0046	1022	76	1065	40	1058	30	1146	88	104.21	100.66
mr20_91500_29	0.26	5.4945	0.2234	0.0744	0.0029	1.8600	0.0820	0.1820	0.0074	0.0215	0.0532	0.0043	1040	72	1078	40	1071	30	1044	83	103.65	100.65
mr20_91500_30	0.26	5.5036	0.2241	0.0723	0.0032	1.8150	0.0890	0.1817	0.0074	0.0622	0.0542	0.0046	992	79	1075	40	1052	32	1061	88	108.37	102.19
mr20_91500_31	0.26	5.5188	0.2254	0.0755	0.0029	1.8900	0.0860	0.1812	0.0074	0.1607	0.0554	0.0048	1067	69	1074	40	1076	30	1084	92	100.66	99.81
mr20_91500_32	0.26	5.5066	0.2244	0.0740	0.0031	1.8460	0.0870	0.1816	0.0074	0.1681	0.0537	0.0045	1007	74	1076	41	1059	32	1066	86	106.85	101.61
mr20_91500_33	0.25	5.6883	0.2362	0.0749	0.0031	1.8310	0.0840	0.1758	0.0073	0.1235	0.0479	0.004	1055	74	1045	40	1053	30	941	76	99.05	99.24
mr20_91500_34	0.25	5.6465	0.2296	0.0741	0.0030	1.7930	0.0850	0.1771	0.0072	0.0768	0.0557	0.0047	1009	76	1050	39	1041	32	1096	89	104.06	100.86
mr20_91500_35	0.25	5.5648	0.2323	0.0742	0.0032	1.8320	0.0900	0.1797	0.0075	0.1964	0.0537	0.0044	1018	77	1065	41	1046	31	1053	85	104.62	101.82
mr20_91500_36	0.26	5.5897	0.2250	0.0759	0.0032	1.8700	0.0870	0.1789	0.0072	0.1166	0.0507	0.0042	1054	74	1061	40	1069	30	1001	81	100.66	99.25
mr20_91500_37	0.25	5.5371	0.2238	0.0773	0.0031	1.9130	0.0840	0.1806	0.0073	0.1053	0.0559	0.0045	1089	70	1069	40	1080	29	1094	86	98.16	98.98
mr20_91500_38	0.26	5.3677	0.2161	0.0728	0.0028	1.8760	0.0820	0.1863	0.0075	0.1598	0.0556	0.0046	1016	67	1100	41	1074	29	1093	88	108.27	102.42
mr20_91500_39	0.25	5.8005	0.2322	0.0741	0.0030	1.7600	0.0820	0.1724	0.0069	0.2007	0.0525	0.0044	1023	70	1024	38	1025	30	1028	85	100.10	99.90
mr20_91500_40	0.25	5.7078	0.2313	0.0752	0.0032	1.8240	0.0880	0.1752	0.0071	0.0725	0.0535	0.0044	1071	76	1039	39	1052	31	1059	86	97.01	98.76
mr20_91500_41	0.25	5.6850	0.2327	0.0773	0.0030	1.8560	0.0820	0.1759	0.0072	0.1408	0.0538	0.0044	1104	67	1045	39	1066	29	1059	84	94.66	98.03
mr20_91500_42	0.25	5.5586	0.2286	0.0773	0.0031	1.8930	0.0840	0.1799	0.0074	0.2192	0.0545	0.0045	1088	69	1065	40	1073	30	1081	85	97.89	99.25
mr20_91500_43	0.25	5.5188	0.2315	0.0747	0.0029	1.8570	0.0820	0.1812	0.0076	0.1697	0.0532	0.0042	1052	68	1073	41	1066	29	1048	81	102.00	100.66
mr20_91500_44	0.26	5.6529	0.2333	0.0743	0.0029	1.8240	0.0800	0.1769	0.0073	0.1259	0.0535	0.0045	1028	69	1049	40	1045	29	1048	87	102.04	100.38
mr19_91500_1	0.27	5.4526	0.1814	0.0780	0.0038	1.9450	0.1400	0.1834	0.0061	0.1929	0.057	0.0061	1103	79	1086	33	1096	48	1125	120	98.46	99.09
mr19_91500_2	0.27	5.4735	0.1738	0.0763	0.0035	1.9320	0.1400	0.1827	0.0058	0.1466	0.0573	0.0061	1086	74	1080	32	1092	46	1121	120	99.45	98.90
mr19_91500_3	0.27	5.5371	0.1932	0.0774	0.0039	1.9350	0.1400	0.1806	0.0063	0.2296	0.0567	0.0062	1105	82	1070	34	1091	50	1115	120	96.83	98.08
mr19_91500_4	0.27	5.5340	0.1776	0.0725	0.0032	1.8310	0.1300	0.1807	0.0058	0.1929	0.0536	0.0059	984	70	1071	31	1050	47	1049	110	108.84	102.00
mr19_91500_5	0.27	5.6117	0.1826	0.0759	0.0037	1.8430	0.1300	0.1782	0.0058	0.2158	0.0535	0.0056	1044	82	1055	32	1065	48	1053	110	101.05	99.06
mr19_91500_6	0.28	5.5617	0.1856	0.0752	0.0037	1.8360	0.1300	0.1798	0.0060	0.1739	0.0519	0.0057	1017	80	1065	33	1052	47	1018	110	104.72	101.24
mr19_91500_7	0.27	5.6497	0.1947	0.0743	0.0035	1.8030	0.1300	0.1770	0.0061	0.1143	0.0493	0.0054	1000	78	1048	33	1043	46	969	100	104.80	100.48
mr19_91500_8	0.27	5.7637	0.1927	0.0730	0.0033	1.7340	0.1200	0.1735	0.0058	0.2731	0.0516	0.0056	996	69	1031	32	1018	45	1022	110	103.51	101.28
mr19_91500_9	0.27	5.7078	0.1824	0.0765	0.0038	1.8730	0.1400	0.1752	0.0056	0.1444	0.0544	0.0062	1083	82	1042	31	1071	48	1064	120	96.21	97.29
mr19_91500_10	0.27	5.6754	0.1933	0.0734	0.0035	1.7840	0.1300	0.1762	0.0060	0.2430	0.0501	0.0055	1005	76	1043	33	1033	47	982	100	103.78	100.97
mr19_91500_11	0.27	5.5928	0.1846	0.0748	0.0036	1.8880	0.1400	0.1788	0.0059	0.2728	0.051	0.0056	1045	83	1062	33	1075	50	1000	110	101.63	98.79
mr19_91500_12	0.27	5.6625	0.1860	0.0727	0.0034	1.7700	0.1200	0.1766	0.0058	0.1740	0.0546	0.0059	970	74	1050	32	1032	45	1074	110	108.25	101.74
mr19_91500_13	0.26	5.4407	0.1835	0.0745	0.0035	1.9010	0.1400	0.1838	0.0062	0.1579	0.0565	0.0062	1015	76	1085	34	1078	47	1106	120	106.90	100.65
mr19_91500_14	0.27	5.5127	0.1854	0.0732	0.0036	1.8490	0.1300	0.1814	0.0061	0.1132	0.059	0.0065	980	80	1074	33	1065	45	1152	120	109.59	100.85

91500 zircon continued

mr19_91500_15	0.26	5.6433	0.2134	0.0750	0.0037	1.8340	0.1300	0.1772	0.0067	0.2064	0.0542	0.0059	1046	77	1048	36	1058	46	1066	110	100.19	99.05
mr19_91500_16	0.27	5.5648	0.1889	0.0761	0.0036	1.8790	0.1300	0.1797	0.0061	0.2061	0.0573	0.0065	1094	75	1064	33	1068	46	1124	120	97.26	99.63
mr19_91500_17	0.27	5.5096	0.1943	0.0733	0.0037	1.8260	0.1300	0.1815	0.0064	0.2104	0.0526	0.0061	993	80	1072	35	1050	47	1030	120	107.96	102.10
mr19_91500_18	0.27	5.5494	0.1848	0.0743	0.0039	1.8730	0.1400	0.1802	0.0060	0.1105	0.0518	0.006	1025	94	1068	33	1068	51	1020	110	104.20	100.00
mr19_91500_19	0.27	5.5679	0.1953	0.0772	0.0038	1.9110	0.1400	0.1796	0.0063	0.1014	0.0536	0.0062	1092	80	1064	34	1077	49	1055	120	97.44	98.79
mr19_91500_20	0.26	5.6054	0.1917	0.0773	0.0038	1.8790	0.1300	0.1784	0.0061	0.1768	0.0527	0.0057	1095	80	1057	34	1068	48	1038	110	96.53	98.97
mr19_91500_21	0.25	5.4885	0.2711	0.0735	0.0026	1.8470	0.1100	0.1822	0.0090	0.2491	0.0569	0.0036	986	72	1077	49	1055	38	1119	69	109.23	102.09
mr19_91500_22	0.26	5.5897	0.2687	0.0752	0.0027	1.8350	0.1100	0.1789	0.0086	0.1254	0.054	0.0039	1046	71	1061	47	1059	38	1058	74	101.43	100.19
mr19_91500_23	0.26	5.4496	0.2673	0.0727	0.0026	1.8770	0.1100	0.1835	0.0090	0.1905	0.0539	0.0038	1000	73	1085	49	1066	39	1057	73	108.50	101.78
mr19_91500_24	0.27	5.7339	0.2795	0.0743	0.0025	1.7940	0.1000	0.1744	0.0085	0.1808	0.051	0.0035	1058	64	1035	46	1037	36	1007	66	97.83	99.81
mr19_91500_25	0.26	5.6948	0.2757	0.0749	0.0026	1.7870	0.1000	0.1756	0.0085	0.1624	0.0523	0.0032	1059	69	1041	46	1037	38	1027	61	98.30	100.39
mr19_91500_26	0.27	5.5127	0.2674	0.0748	0.0024	1.8600	0.1000	0.1814	0.0088	0.1447	0.0534	0.0036	1053	62	1074	48	1064	37	1052	68	101.99	100.94
mr19_91500_27	0.26	5.3967	0.2679	0.0753	0.0026	1.9170	0.1100	0.1853	0.0092	0.2025	0.0533	0.0037	1072	69	1095	50	1086	38	1054	71	102.15	100.83
mr19_91500_28	0.26	5.4348	0.2658	0.0764	0.0027	1.9070	0.1100	0.1840	0.0090	0.0748	0.0554	0.0036	1110	68	1088	49	1081	38	1085	69	98.02	100.65
mr19_91500_29	0.27	5.5556	0.2716	0.0736	0.0027	1.8120	0.1100	0.1800	0.0088	0.1931	0.0533	0.0036	1011	72	1065	48	1044	39	1054	70	105.34	102.01
mr19_91500_30	0.26	5.6915	0.2753	0.0741	0.0025	1.7570	0.1000	0.1757	0.0085	0.2057	0.0492	0.0033	1039	67	1044	46	1041	36	971	63	100.48	100.29
mr19_91500_31	0.26	5.8309	0.2788	0.0741	0.0024	1.7370	0.0970	0.1715	0.0082	0.1341	0.054	0.0034	1035	63	1021	45	1023	36	1060	66	98.65	99.80
mr19_91500_32	0.27	5.5648	0.2694	0.0753	0.0029	1.8590	0.1100	0.1797	0.0087	0.0313	0.0527	0.0036	1028	74	1065	47	1059	38	1034	68	103.60	100.57
mr19_91500_33	0.26	5.5556	0.2654	0.0767	0.0025	1.8850	0.1100	0.1800	0.0086	0.1092	0.0533	0.0037	1084	63	1067	46	1068	37	1050	70	98.43	99.91
mr19_91500_34	0.26	5.6465	0.2710	0.0754	0.0024	1.8450	0.1000	0.1771	0.0085	0.1338	0.0535	0.0033	1060	63	1050	46	1054	37	1050	64	99.06	99.62
mr19_91500_35	0.25	5.4735	0.2606	0.0763	0.0027	1.9190	0.1100	0.1827	0.0087	-0.0040	0.0546	0.0036	1086	72	1081	47	1083	39	1070	69	99.54	99.82
mr19_91500_36	0.26	5.4171	0.2582	0.0749	0.0027	1.9190	0.1100	0.1846	0.0088	0.0323	0.0546	0.0037	1059	67	1093	48	1090	38	1070	72	103.21	100.28
mr19_91500_37	0.26	5.5741	0.2672	0.0768	0.0026	1.8800	0.1000	0.1794	0.0086	0.0598	0.0541	0.0037	1085	64	1065	46	1077	37	1060	70	98.16	98.89
mr19_91500_38	0.25	5.5096	0.2641	0.0772	0.0025	1.9110	0.1100	0.1815	0.0087	0.0899	0.0546	0.0036	1090	61	1076	47	1085	36	1072	68	98.72	99.17
mr19_91500_39	0.26	5.6275	0.2692	0.0757	0.0026	1.8520	0.1000	0.1777	0.0085	0.0482	0.0536	0.0035	1069	63	1056	47	1067	37	1052	67	98.78	98.97
mr19_91500_40	0.25	5.8789	0.2799	0.0751	0.0025	1.7940	0.0990	0.1701	0.0081	0.0842	0.0529	0.0034	1066	60	1012	45	1037	36	1043	65	94.93	97.59
mr19_91500_41	0.26	5.5679	0.2666	0.0746	0.0024	1.8480	0.1000	0.1796	0.0086	0.1521	0.0548	0.0036	1038	62	1064	47	1067	37	1075	70	102.50	99.72
mr19_91500_42	0.26	5.5402	0.2670	0.0763	0.0029	1.9440	0.1100	0.1805	0.0087	-0.0733	0.0555	0.0037	1068	75	1070	47	1089	39	1092	70	100.19	98.26
mr19_91500_43	0.26	5.5586	0.2657	0.0733	0.0025	1.8710	0.1100	0.1799	0.0086	0.0724	0.0565	0.0039	1026	69	1066	47	1069	37	1105	74	103.90	99.72
mr19_91500_44	0.26	5.4615	0.2595	0.0754	0.0026	1.9150	0.1100	0.1831	0.0087	0.1566	0.0559	0.0037	1057	65	1083	47	1082	38	1095	70	102.46	100.09
mr19_91500_45	0.25	5.5310	0.2631	0.0742	0.0025	1.8630	0.1000	0.1808	0.0086	0.1187	0.0563	0.0037	1010	64	1070	47	1061	37	1104	71	105.94	100.85
mr19_91500_46	0.26	5.5648	0.2663	0.0734	0.0026	1.8800	0.1100	0.1797	0.0086	0.1313	0.0564	0.0037	1003	70	1064	47	1070	38	1109	71	106.08	99.44
mr19_91500_47	0.25	5.4348	0.2570	0.0715	0.0025	1.8430	0.1100	0.1840	0.0087	0.1047	0.0558	0.0037	985	68	1088	47	1062	38	1099	70	110.46	102.45
mr19_91500_48	0.25	5.7670	0.2727	0.0760	0.0023	1.8420	0.1000	0.1734	0.0082	0.0910	0.0535	0.0034	1074	59	1030	45	1053	35	1050	65	95.90	97.82
mr19_91500_49	0.26	5.6465	0.2710	0.0745	0.0026	1.8620	0.1100	0.1771	0.0085	0.1460	0.0529	0.0034	1053	66	1050	47	1063	37	1042	66	99.72	98.78
mr19_91500_50	0.25	5.6689	0.2699	0.0754	0.0027	1.8560	0.1100	0.1764	0.0084	0.1595	0.0542	0.0035	1060	70	1047	46	1066	38	1063	68	98.77	98.22
mr19_91500_51	0.26	5.6754	0.2738	0.0760	0.0026	1.8240	0.1000	0.1762	0.0085	0.1751	0.0532	0.0036	1074	67	1045	46	1050	37	1044	70	97.30	99.52
mr19_91500_52	0.26	5.4025	0.2598	0.0746	0.0031	1.9270	0.1200	0.1851	0.0089	0.0581	0.0537	0.0036	1032	84	1093	49	1092	40	1058	69	105.91	100.09
mr19_91500_53	0.26	5.4496	0.2613	0.0753	0.0026	1.8990	0.1100	0.1835	0.0088	0.0945	0.0548	0.0034	1039	69	1086	48	1075	39	1079	66	104.52	101.02
mr19_91500_54	0.26	5.6022	0.2668	0.0737	0.0024	1.8140	0.1000	0.1785	0.0085	0.1587	0.0541	0.0035	1018	61	1059	46	1052	36	1066	67	104.03	100.67
mr19_91500_55	0.26	5.4765	0.2639	0.0748	0.0027	1.8570	0.1100	0.1826	0.0088	0.0573	0.0546	0.0036	1020	72	1080	48	1070	38	1081	69	105.88	100.93
mr19_91500_56	0.25	5.5741	0.2672	0.0743	0.0026	1.8210	0.1000	0.1794	0.0086	0.0710	0.0497	0.0033	1023	71	1063	47	1050	38	977	64	103.91	101.24
mr19_91500_57	0.26	5.6465	0.2742	0.0766	0.0028	1.8230	0.1000	0.1771	0.0086	0.1101	0.0549	0.0034	1106	67	1050	47	1056	38	1078	64	94.94	99.43
mr19_91500_58	0.26	5.6754	0.2738	0.0751	0.0027	1.7850	0.1000	0.1762	0.0085	0.0906	0.0516	0.0032	1047	68	1045	47	1038	37	1013	62	99.81	100.67
mr19_91500_59	0.26	5.5586	0.2719	0.0738	0.0027	1.8020	0.1000	0.1799	0.0088	0.0635	0.0509	0.0033	1018	71	1065	48	1048	37	1004	63	104.62	101.62
mr30_91500_1	0.26	5.4765	0.2819	0.0743	0.0023	1.8530	0.1100	0.1826	0.0094	0.3839	0.0563	0.0038	1050	62	1082	51	1056	39	1107	72	103.08	102.46
mr30_91500_2	0.26	5.4437	0.2756	0.0741	0.0025	1.8670	0.1100	0.1837	0.0093	0.3449	0.0532	0.0038	1044	68	1085	51	1064	39	1044	73	103.91	101.97
mr30_91500_3	0.26	5.5096	0.2823	0.0769	0.0030	1.9300	0.1200	0.1815	0.0093	0.2416	0.053	0.0037	1119	78	1075	50	1089	42	1039	71	96.10	98.71
mr30_91500_4	0.27	5.4407	0.2753	0.0747	0.0025	1.8920	0.1100	0.1838	0.0093	0.2342	0.0528	0.0035	1060	67	1087	51	1078	39	1036	66	102.50	100.83
mr30_91500_5	0.27	5.5897	0.2875	0.0754	0.0029	1.8690	0.1200	0.1789	0.0092	0.2211	0.0547	0.0038	1079	77	1062	51	1057	40	1071	74	98.41	100.47
mr30_91500_6	0.27	5.5556	0.2840	0.0743	0.0027	1.8550	0.1100	0.1800	0.0092	0.2741	0.0523	0.0034	1050	73	1064	50	1056	41	1026	65	101.37	100.76
mr30_91500_7	0.26	5.6306	0.2885	0.0749	0.0027	1.8670	0.1100	0.1776	0.0091	0.1907	0.0529	0.0036	1066	72	1057	50	1069	40	1037	70	99.17	98.88
mr30_91500_8	0.25	5.6465	0.2933	0.0747	0.0024	1.8070	0.1100	0.1771	0.0092	0.2837	0.0545	0.0038	1060	65	1051	50	1040	40	1068	73	99.11	101.06
mr30_91500_9	0.26	5.5525	0.2806	0.0751	0.0023	1.8670	0.1100	0.1801	0.0091	0.3589	0.0549	0.0037	1071	62	1071	48	1067	40	1080	71	99.98	100.37
mr30_91500_10	0.26	5.5036	0.2817	0.0749	0.0028	1.8530	0.1100	0.1817	0.0093	0.2441	0.0548	0.0038	1066	75	1074	51	1066	40	1078	72	100.77	100.75
mr30_91500_11	0.26	5.6085	0.2831	0.0738	0.0026	1.8210	0.1100	0.1783	0.0090	0.3077	0.0567	0.004	1036	71	1062	48	1051	39	1111	77	102.51	101.05
mr30_91500_12	0.26	5.6561	0.2911	0.0771	0.0031	1.8770	0.1200	0.1768	0.0091	0.2486	0.0542	0.0035	1124	80	1047	50	1067	42	1067	67	93.17	98.13
mr30_91500_13	0.27	5.5960	0.2881	0.0744	0.0026	1.8100	0.1100	0.1787	0.0092	0.2384	0.054	0.0036	1052	70	1057	50	1053	40	1059	70	100.44	100.38
mr30_91500_14	0.26	5.5617	0.2846	0.0772	0.0028	1.8790	0.1200	0.1798	0.0092	0.2756	0.0555	0.0038	1126	72	1063	50	1075	40	1091	74	94.37	98.88
mr30_91500_15	0.27	5.5991	0.2821	0.0729	0.0025	1.8090	0.1100	0.1786	0.0090	0.3316	0.0525	0.0036	1011	70	1057	49	1042	41	1030	68	104.53	101.44
mr30_91500_16	0.26	5.8445	0.2972	0.0746	0.0026	1.7700	0.1100	0.1711	0.0087	0.2635	0.0518	0.0034	1058	70	1016	48	1032	39	1018	65	96.05	98.45
mr30_91500_17	0.27	5.6980	0.2922	0.0761	0.0030	1.8430	0.1100	0.1755	0.0090	0.1903	0.0507	0.0034	1098	79	1044	49	1060	40	1001	65	95.11	98.49
mr30_91500_18	0.27	5.6818	0.2938	0.0765	0.0029	1.8720	0.1200	0.1760	0.0091	0.2261	0.055	0.0039	1108	76	1043	50	1067	41	1087	72	94.12	97.75
mr30_91500_19	0.26	5.8754	0.2969	0.0729	0.0027	1.7260	0.1100	0.1702	0.0086	0.1660	0.0493	0.0036	1011	75	1016	48	1017	37	969	69	100.48	99.90
mr30_91500_20	0.26	5.7110	0.2968	0.0732	0.0026	1.7760	0.1100	0.1751	0.0091	0.3793	0.0547	0.0039	1019	72	1038	50	1030	40	1072	74	101.82	100.78
mr30_91500_21	0.27	5.4615	0.2774	0.0762	0.0028	1.9140	0.1200	0.1831	0.0093	0.2706	0.0555	0.0039	1100	74	1086	50	1084	41	1087	74	98.70	100.18
mr30_91500_22	0.26	5.5188	0.2772	0.0752	0.0028	1.8660	0.1200	0.1812	0.0091	0.2642	0.0548	0.0037	1074	75	1071	49	1069	39	1074	72	99.73	100.19
mr30_91500_23	0.27	5.4585	0.2831	0.0760	0.0030	1.9170	0.1200	0.1832	0.0095	0.1967	0.0539	0.004	1095	79	1083	51	1081	42	1062	77	98.90	100.19
mr30_91500_24	0.27	5.3390	0.2737	0.0734	0.0027	1.9010	0.1200	0.1873	0.0096	0.1935	0.0554	0.004	1025	74	1106	52	1079	40	1085	76	107.90	102.50
mr30_91500_25	0.26	5.5096	0.2823	0.0757	0.0026	1.8840	0.1100	0.1815	0.0093	0.3104	0.0537	0.0042	1087	69	1076	50	1075	41	1043	79	98.97	100.09

02123 zircon

Identifier	Th/U	Data for Tera-Wasserburg plot				Data for Wetherill plot					$^{208}Pb/^{232}Th$	2SE	Dates								% Concordancy *(206Pb-238U age/207Pb-206Pb age)*100*	% Concordancy (206Pb-238U age/207Pb-235U age)*100
		$^{238}U/^{206}Pb$	2SE	$^{207}Pb/^{206}Pb$	2SE	$^{207}Pb/^{235}U$	2SE	$^{206}Pb/^{238}U$	2SE	Rho			$^{207}Pb/^{206}Pb$	2SE	$^{206}Pb/^{238}U$	2SE	$^{207}Pb/^{235}U$	2SE	$^{208}Pb/^{232}Th$	2SE		
mr30_02123_1	0.51	21.0526	1.0637	0.0525	0.0019	0.3398	0.0200	0.0475	0.0024	0.1667	0.0153	0.0009	307	82	299	15	297	15	306	18	97.4	100.6
mr30_02123_2	0.54	21.9298	1.1061	0.0512	0.0016	0.3250	0.0200	0.0456	0.0023	0.4220	0.0146	0.0009	250	72	288	14	285	15	293	17	115.1	100.8
mr30_02123_3	0.55	21.1417	1.0727	0.0514	0.0018	0.3370	0.0200	0.0473	0.0024	0.2521	0.0147	0.0008	259	80	298	15	295	16	295	16	115.2	101.2
mr30_02123_4	0.55	21.0971	1.0682	0.0528	0.0018	0.3430	0.0210	0.0474	0.0024	0.3096	0.0153	0.0009	320	77	298	15	298	16	307	17	93.1	100.1
mr30_02123_5	0.55	21.5054	1.0637	0.0531	0.0017	0.3400	0.0200	0.0465	0.0023	0.2397	0.0149	0.0008	333	73	293	14	296	15	299	17	88.0	98.9
mr30_02123_6	0.55	21.0971	1.0682	0.0524	0.0018	0.3376	0.0200	0.0474	0.0024	0.3063	0.0150	0.0009	303	78	299	15	295	15	300	17	98.7	101.3
mr30_02123_7	0.55	20.2840	1.0286	0.0513	0.0020	0.3430	0.0210	0.0493	0.0025	0.2874	0.0152	0.0009	254	90	310	16	298	16	305	18	121.8	103.9
mr30_02123_8	0.54	21.0971	1.0682	0.0538	0.0020	0.3480	0.0220	0.0474	0.0024	0.2263	0.0154	0.0009	363	84	298	15	302	16	309	18	82.2	98.8
mr30_02123_9	0.54	21.1864	1.0773	0.0518	0.0018	0.3440	0.0210	0.0472	0.0024	0.1308	0.0151	0.0009	277	80	297	15	299	15	304	18	107.5	99.5
mr30_02123_10	0.54	20.9205	1.0504	0.0527	0.0018	0.3440	0.0210	0.0478	0.0024	0.3598	0.0161	0.0009	316	78	301	15	301	16	322	18	95.3	100.2
mr30_02123_11	0.55	20.7039	1.0716	0.0520	0.0018	0.3510	0.0220	0.0483	0.0025	0.3139	0.0152	0.0008	285	79	305	15	303	16	305	17	106.7	100.5
mr30_02123_12	0.54	21.5054	1.1100	0.0538	0.0018	0.3440	0.0210	0.0465	0.0024	0.4072	0.0157	0.0009	363	75	293	14	302	15	315	17	80.7	97.1
mr30_02123_13	0.56	20.7469	1.0330	0.0526	0.0019	0.3510	0.0220	0.0482	0.0024	0.2251	0.0151	0.0008	312	82	304	15	305	16	302	17	97.4	99.5
mr30_02123_14	0.55	20.5761	1.0584	0.0528	0.0018	0.3530	0.0210	0.0486	0.0025	0.2114	0.0155	0.0009	320	77	306	15	306	16	310	17	95.4	99.8
oc14_02123_1	0.45	21.7439	0.5201	0.0509	0.0017	0.3278	0.0120	0.0460	0.0011	0.1699	0.0145	0.0009	245	63	290	7	289	9	290	19	118.2	100.2
oc14_02123_2	0.38	21.6170	0.5140	0.0538	0.0017	0.3442	0.0130	0.0463	0.0011	0.2898	0.0145	0.0009	356	59	292	7	299	10	292	18	81.9	97.5
oc14_02123_3	0.46	21.3812	0.5029	0.0514	0.0015	0.3327	0.0110	0.0468	0.0011	0.2838	0.0144	0.0009	250	53	295	7	291	8	289	18	117.8	101.4
oc14_02123_4	0.54	21.6357	0.5617	0.0512	0.0018	0.3291	0.0120	0.0462	0.0012	0.1794	0.0144	0.0009	237	62	291	7	287	9	290	18	123.0	101.6
oc14_02123_5	0.46	21.3265	0.5458	0.0528	0.0017	0.3440	0.0130	0.0469	0.0012	0.3313	0.0152	0.0010	313	60	295	7	299	10	305	19	94.3	98.7
oc14_02123_6	0.54	21.7960	0.5226	0.0513	0.0017	0.3270	0.0120	0.0459	0.0011	0.3314	0.0141	0.0009	259	58	289	7	286	9	283	18	111.6	101.2
oc14_02123_7	0.51	21.4041	0.5498	0.0496	0.0018	0.3220	0.0130	0.0467	0.0012	0.2339	0.0144	0.0009	171	64	295	7	284	10	289	18	172.3	103.9
oc14_02123_8	0.53	21.4270	0.5509	0.0533	0.0018	0.3340	0.0130	0.0467	0.0012	0.2987	0.0138	0.0009	311	61	294	7	293	9	278	18	94.6	100.3
oc14_02123_9	0.50	21.6029	0.5600	0.0522	0.0018	0.3350	0.0130	0.0463	0.0012	0.3458	0.0142	0.0009	285	65	292	7	294	10	286	18	102.3	99.3
oc14_02123_10	0.52	21.3995	0.5037	0.0509	0.0018	0.3320	0.0130	0.0467	0.0011	0.2234	0.0141	0.0009	222	62	295	7	290	10	283	18	132.7	101.7
oc14_02123_11	0.51	21.2044	0.5396	0.0512	0.0018	0.3310	0.0130	0.0472	0.0012	0.2935	0.0150	0.0010	239	63	297	8	291	10	302	20	124.2	102.1
oc14_02123_12	0.41	21.6497	0.5156	0.0526	0.0020	0.3380	0.0140	0.0462	0.0011	0.1239	0.0149	0.0010	312	72	291	7	295	11	298	20	93.3	98.6
oc14_02123_13	0.39	21.5100	0.5552	0.0521	0.0018	0.3350	0.0130	0.0465	0.0012	0.2966	0.0150	0.0010	262	63	293	7	294	10	300	20	111.9	99.9
oc14_02123_14	0.55	22.2668	0.5454	0.0525	0.0017	0.3260	0.0120	0.0449	0.0011	0.3164	0.0148	0.0009	271	60	283	7	285	10	296	19	104.4	99.3
oc14_02123_15	0.45	22.6449	0.5641	0.0548	0.0018	0.3370	0.0120	0.0442	0.0011	0.2503	0.0136	0.0009	383	59	278	7	294	9	273	17	72.7	94.8
oc14_02123_16	0.47	22.4417	0.6044	0.0519	0.0022	0.3180	0.0140	0.0446	0.0012	0.2094	0.0137	0.0009	260	77	281	7	280	11	274	18	108.2	100.4
oc14_02123_17	0.35	21.8818	0.5267	0.0533	0.0018	0.3370	0.0130	0.0457	0.0011	0.2006	0.0143	0.0010	326	59	288	7	294	10	287	19	88.3	98.1
oc6_02123_1	0.37	21.3858	0.5031	0.0526	0.0022	0.3409	0.0130	0.0468	0.0011	0.1915	0.0148	0.0010	312	95	295	7	298	10	297	20	94.6	99.0
oc6_02123_2	0.43	20.7598	0.5603	0.0505	0.0024	0.3380	0.0150	0.0482	0.0013	0.1720	0.0153	0.0011	218	110	304	8	295	11	307	21	139.3	103.1
oc6_02123_3	0.40	21.0704	0.5328	0.0516	0.0023	0.3360	0.0140	0.0475	0.0012	0.2328	0.0147	0.0010	268	102	299	7	292	10	295	20	111.7	102.4
oc6_02123_4	0.39	21.1015	0.5789	0.0533	0.0026	0.3440	0.0160	0.0474	0.0013	0.2558	0.0157	0.0011	342	110	298	8	300	12	314	22	87.3	99.4
oc6_02123_5	0.36	21.1640	0.5375	0.0527	0.0024	0.3440	0.0150	0.0473	0.0012	0.3482	0.0143	0.0010	316	104	298	8	301	11	287	20	94.2	98.9
oc6_02123_6	0.42	21.2902	0.5893	0.0509	0.0025	0.3250	0.0150	0.0470	0.0013	0.2780	0.0149	0.0011	236	113	296	8	284	11	300	21	125.1	104.0
oc6_02123_7	0.36	20.7555	0.5600	0.0527	0.0024	0.3520	0.0160	0.0482	0.0013	0.4118	0.0152	0.0011	316	104	304	8	304	12	305	21	96.1	99.9
oc6_02123_8	0.35	21.3721	0.5938	0.0510	0.0024	0.3310	0.0150	0.0468	0.0013	0.2578	0.0146	0.0010	241	108	295	8	288	11	292	20	122.3	102.2
oc6_02123_9	0.37	20.9205	0.6127	0.0525	0.0026	0.3440	0.0160	0.0478	0.0014	0.3273	0.0149	0.0011	307	113	301	8	302	12	298	21	97.8	99.6
oc6_02123_10	0.39	21.5703	0.5118	0.0528	0.0023	0.3410	0.0140	0.0464	0.0011	0.0431	0.0146	0.0006	289	63	292	7	296	11	293	12	101.0	98.6
oc6_02123_11	0.40	21.4731	0.5533	0.0530	0.0021	0.3382	0.0140	0.0466	0.0012	0.1375	0.0147	0.0007	304	57	294	7	295	10	295	13	96.6	99.5
oc6_02123_12	0.38	21.8627	0.5258	0.0518	0.0022	0.3304	0.0140	0.0457	0.0011	0.1287	0.0147	0.0007	276	59	289	7	290	10	296	13	104.5	99.6
oc6_02123_13	0.38	21.5796	0.5122	0.0526	0.0022	0.3386	0.0140	0.0463	0.0011	0.0668	0.0147	0.0006	297	58	292	7	296	10	295	13	98.3	98.6
oc6_02123_14	0.36	21.5332	0.5100	0.0530	0.0021	0.3405	0.0130	0.0464	0.0011	0.0747	0.0151	0.0007	322	57	293	7	297	10	303	13	90.9	98.6
oc6_02123_15	0.37	20.7814	0.5182	0.0514	0.0021	0.3400	0.0140	0.0481	0.0012	0.0570	0.0153	0.0006	259	57	303	7	298	10	306	13	116.9	101.6
oc6_02123_16	0.39	21.5703	0.5583	0.0528	0.0023	0.3363	0.0150	0.0464	0.0012	0.0373	0.0146	0.0006	289	63	292	7	295	11	293	12	101.0	99.1
oc6_02123_17	0.40	21.4731	0.5533	0.0530	0.0021	0.3381	0.0140	0.0466	0.0012	0.1509	0.0147	0.0007	304	57	294	7	296	11	295	13	96.6	99.3
oc6_02123_18	0.38	21.8627	0.5258	0.0518	0.0022	0.3308	0.0140	0.0457	0.0011	0.1323	0.0148	0.0007	276	59	289	7	291	11	296	13	104.5	99.2
oc6_02123_19	0.38	21.5796	0.5122	0.0526	0.0022	0.3391	0.0140	0.0463	0.0011	0.0814	0.0147	0.0006	297	58	292	7	296	11	295	13	98.3	98.5
oc6_02123_20	0.36	21.5332	0.5100	0.0530	0.0021	0.3402	0.0140	0.0464	0.0011	0.0713	0.0151	0.0007	322	57	293	7	297	10	303	13	90.9	98.4
oc6_02123_21	0.37	20.7814	0.5182	0.0514	0.0021	0.3430	0.0140	0.0481	0.0012	0.0786	0.0153	0.0006	259	57	303	7	300	10	306	13	116.9	101.0
oc7_02123_1	0.37	21.3950	0.4165	0.0524	0.0017	0.3390	0.0120	0.0467	0.0009	0.1445	0.0150	0.0004	303	74	294	6	297	9	300	7	97.2	99.3
oc7_02123_2	0.34	21.8198	0.4333	0.0528	0.0018	0.3341	0.0120	0.0458	0.0009	0.1736	0.0144	0.0004	320	77	289	6	292	10	289	9	90.2	98.8
oc7_02123_3	0.35	21.6123	0.4297	0.0532	0.0018	0.3398	0.0120	0.0463	0.0009	0.1528	0.0149	0.0004	337	77	292	6	296	9	298	8	86.5	98.5
oc7_02123_4	0.53	21.6029	0.4480	0.0516	0.0018	0.3308	0.0120	0.0463	0.0010	0.0385	0.0143	0.0004	268	80	292	6	290	9	287	7	108.9	100.6
oc7_02123_5	0.53	21.7108	0.4619	0.0519	0.0018	0.3317	0.0130	0.0461	0.0010	0.2412	0.0148	0.0004	281	79	290	6	290	10	297	7	103.3	100.0
oc7_02123_6	0.39	21.5332	0.4637	0.0527	0.0020	0.3425	0.0140	0.0464	0.0010	0.0745	0.0149	0.0005	316	86	293	6	299	10	299	10	92.6	97.8
oc7_02123_7	0.39	21.5193	0.4584	0.0556	0.0020	0.3570	0.0130	0.0465	0.0010	0.1764	0.0152	0.0004	436	80	293	6	309	10	304	9	67.1	94.7
oc7_02123_8	0.37	21.4500	0.4601	0.0543	0.0020	0.3484	0.0140	0.0466	0.0010	0.2335	0.0149	0.0005	384	83	295	6	303	10	298	10	76.8	97.4
oc7_02123_9	0.35	21.8436	0.4485	0.0519	0.0019	0.3318	0.0130	0.0458	0.0009	0.1957	0.0148	0.0005	281	84	289	6	290	10	298	10	102.7	99.4
oc7_02123_10	0.36	21.3220	0.5001	0.0516	0.0020	0.3330	0.0140	0.0469	0.0011	0.1860	0.0149	0.0005	268	89	295	7	290	10	299	11	110.3	101.8
oc7_02123_11	0.36	21.1327	0.4466	0.0534	0.0020	0.3460	0.0140	0.0473	0.0010	0.1350	0.0146	0.0005	346	85	298	6	301	10	294	10	86.1	98.9
oc7_02123_12	0.47	20.7684	0.4745	0.0512	0.0018	0.3421	0.0130	0.0482	0.0011	0.1315	0.0144	0.0005	250	81	303	7	299	10	289	9	121.3	101.2
oc7_02123_13	0.53	21.3356	0.4552	0.0526	0.0020	0.3450	0.0140	0.0469	0.0010	0.1802	0.0146	0.0004	312	87	295	6	299	10	294	9	94.7	98.8
oc7_02123_14	0.52	21.2721	0.4525	0.0511	0.0020	0.3310	0.0130	0.0470	0.0010	0.1881	0.0145	0.0004	245	90	296	6	289	10	292	9	120.6	102.4
oc7_02123_15	0.53	21.3356	0.4552	0.0516	0.0019	0.3367	0.0130	0.0469	0.0010	0.1126	0.0147	0.0005	268	84	296	6	295	10	295	9	110.4	100.3
oc7_02123_16	0.36	21.1060	0.4900	0.0516	0.0021	0.3350	0.0140	0.0474	0.0011	0.1005	0.0144	0.0006	268	93	298	7	293	11	288	11	111.4	101.7
oc7_02123_17	0.36	21.4592	0.4605	0.0542	0.0022	0.3440	0.0140	0.0466	0.0010	0.0821	0.0153	0.0005	379	91	294	6	301	11	308	11	77.4	97.7
fe05_02123_1	0.57	20.5086	0.7991	0.0531	0.0016	0.3551	0.0190	0.0488	0.0019	0.2935	0.0155	0.0009	315	52	307	12	308	14	312	19	97.4	99.6
fe05_02123_2	0.56	20.6228	0.8081	0.0512	0.0016	0.3451	0.0180	0.0485	0.0019	0.3175	0.0149	0.0009	240	54	305	12	302	14	299	18	127.1	101.2
fe05_02123_3	0.51	20.9205	0.8316	0.0532	0.0017	0.3525	0.0190	0.0478	0.0019	0.2696	0.0151	0.0009	331	55	301	12	305	14	303	18	90.9	98.5
fe05_02123_4	0.55	20.7469	0.8178	0.0516	0.0016	0.3456	0.0190	0.0482	0.0019	0.3261	0.0152	0.0009	263	52	303	12	302	14	305	18	115.3	100.6
fe05_02123_5	0.57	21.0482	0.8418	0.0540	0.0017	0.3468	0.0180	0.0475	0.0019	0.2855	0.0153	0.0009	342	53	299	11	303	14	306	18	87.5	98.9
fe05_02123_6	0.60	20.7383	0.8171	0.0553	0.0017	0.3674	0.0200	0.0482	0.0019	0.3621	0.0160	0.0010	409	54	303	12	319	14	320	19	74.2	95.0
fe05_02123_7	0.64	20.6186	0.8077	0.0539	0.0016	0.3598	0.0190	0.0485	0.0019	0.3525	0.0148	0.0009	364	49	305	12	311	14	297	18	83.8	98.3
fe05_02123_8	0.63	20.8073	0.8226	0.0521	0.0015	0.3453	0.0180	0.0481	0.0019	0.3572	0.0151	0.0009	286	47	303	11	301	14	303	18	105.8	100.4
fe05_02123_9	0.61	20.7598	0.7757	0.0506	0.0014	0.3472	0.0180	0.0482	0.0018	0.3952	0.0148	0.0009	231	45	303	11	302	13	296	18	131.2	100.5
fe05_02123_10	0.57	21.0971	0.8012	0.0533	0.0016	0.3431	0.0180	0.0474	0.0018	0.3652	0.0145	0.0009	319	48	298	11	301	13	290	17	93.5	99.2
fe05_02123_11	0.56	20.7254	0.8161	0.0530	0.0016	0.3543	0.0190	0.0483	0.0019	0.3621	0.0148	0.0009	312	51	304	12	307	14	298	18	97.3	99.1
fe05_02123_12	0.62	20.5973	0.8061	0.0504	0.0014	0.3392	0.0180	0.0486	0.0019	0.4730	0.0145	0.0009	214	47	305	12	296	13	290	17	142.7	103.2
fe05_02123_13	0.55	20.7125	0.8151	0.0528	0.0015	0.3550	0.0160	0.0483	0.0019	0.2201	0.0153	0.0008	302	51	304	12	309	12	307	17	100.6	98.5
fe05_02123_14	0.52	20.3832	0.8310	0.0526	0.0016	0.3560	0.0170	0.0491	0.0020	0.3467	0.0156	0.0009	297	55	309	12	308	12	314	18	104.0	100.2
fe05_02123_15	0.54	20.5128	0.7995	0.0524	0.0013	0.3519	0.0160	0.0488	0.0019	0.4077	0.0149	0.0008	299	46	307	12	305	12	299	17	102.6	100.5
fe05_02123_16	0.64	21.2676	0.8594	0.0549	0.0016	0.3501	0.0160	0.0470	0.0019	0.3441	0.0163	0.0009	389	54	296	11	304	12	327	18	76.1	97.4
fe05_02123_17	0.52	21.1640	0.8062	0.0516	0.0014	0.3361	0.0150	0.0473	0.0018	0.3385	0.0148	0.0008	260	48	298	11	293	12	298	16	114.4	101.5
fe05_02123_18	0.50	21.3995	0.8243	0.0519	0.0014	0.3344	0.0150	0.0467	0.0018	0.3182	0.0147	0.0008	271	50	294	11	294	12	294	16	108.6	100.1
fe05_02123_19	0.71	21.0084	0.8386	0.0525	0.0013	0.3458	0.0150	0.0476	0.0019	0.3158	0.0156	0.0009	293	45	300	11	301	12	312	17	102.4	99.8
fe05_02123_20	0.74	20.6441	0.8097	0.0521	0.0013	0.3491	0.0150	0.0484	0.0019	0.3048	0.0160	0.0009	279	43	305	11	304	12	320	17	109.2	100.4
fe05_02123_21	0.55	21.4638	0.8753	0.0542	0.0018	0.3476	0.0170	0.0466	0.0019	0.2437	0.0165	0.0009	370	62	294	12	304	12	331	18	79.5	96.7
fe05_02123_22	0.53	20.8290	0.8243	0.0522	0.0015	0.3434	0.0160	0.0480	0.0019	0.2554	0.0148	0.0008	268	50	302	11	299	12	296	16	112.8	101.0
fe05_02123_23	0.73	21.1685	0.8066	0.0521	0.0012	0.3386	0.0150	0.0472	0.0018	0.3783	0.0149	0.0008	279	40	298	11	296	11	299	16	106.7	100.5
fe05_02123_24	0.66	21.0305	0.8403	0.0533	0.0013	0.3505	0.0160	0.0476	0.0019	0.4232	0.0151	0.0008	325	44	299	11	305	12	303	16	92.1	98.3
fe05_02123_25	0.55	20.9996	0.7938	0.0516	0.0014	0.3368	0.0160	0.0476	0.0018	0.3444	0.0149	0.0008	247	47	300	11	293	12	300	16	121.4	102.3
fe05_02123_26	0.60	21.1193	0.8028	0.0520	0.0014	0.3400	0.0150	0.0474	0.0018	0.3240	0.0153	0.0008	284	46	298	11	298	12	307	17	105.0	100.2
fe05_02123_27	0.66	21.1551	0.8056	0.0516	0.0013	0.3356	0.0150	0.0473	0.0018	0.3682	0.0147	0.0008	246	43	298	11	294	11	295	16	121.0	101.2
fe05_02123_28	0.62	21.3767	0.8225	0.0516	0.0013	0.3329	0.0150	0.0468	0.0018	0.3032	0.0144	0.0008	249	46	295	11	291	11	289	16	118.4	101.2
fe05_02123_29	0.61	21.0261	0.7958	0.0516	0.0013	0.3379	0.0150	0.0476	0.0018	0.3741	0.0145	0.0008	250	44	300	11	294	12	291	16	119.9	101.9

02123 zircon continued

fe05_02123_30	0.60	21.5796	0.8382	0.0516	0.0015	0.3336	0.0160	0.0463	0.0018	0.3579	0.0143	0.0008	260	51	292	11	292	12	287	15	112.3	99.9
fe05_02123_31	0.63	21.6310	0.8422	0.0523	0.0013	0.3359	0.0150	0.0462	0.0018	0.3568	0.0146	0.0008	286	45	291	11	294	12	292	16	101.8	98.9
fe05_02123_32	0.60	21.6123	0.8408	0.0519	0.0014	0.3328	0.0150	0.0463	0.0018	0.2102	0.0144	0.0008	263	49	292	11	293	12	288	15	110.8	99.7
fe05_02123_33	0.51	22.0605	0.8760	0.0514	0.0015	0.3196	0.0150	0.0453	0.0018	0.2723	0.0138	0.0008	246	52	286	11	281	11	276	15	116.3	102.0
mr20_02123_1	0.53	21.3402	0.8653	0.0518	0.0019	0.3350	0.0150	0.0469	0.0019	0.2114	0.0150	0.0010	274	63	295	12	293	11	301	20	107.7	100.9
mr20_02123_2	0.54	21.6920	0.8470	0.0523	0.0019	0.3323	0.0140	0.0461	0.0018	0.1116	0.0143	0.0009	268	62	291	11	290	11	288	19	108.4	100.2
mr20_02123_3	0.53	21.4777	0.8303	0.0515	0.0019	0.3328	0.0140	0.0466	0.0018	0.1370	0.0144	0.0010	252	64	293	11	290	11	288	20	116.4	101.0
mr20_02123_4	0.51	22.3664	0.9005	0.0524	0.0019	0.3222	0.0140	0.0447	0.0018	0.1844	0.0141	0.0010	290	61	282	11	283	11	283	19	97.2	99.6
mr20_02123_5	0.55	22.1337	0.8818	0.0531	0.0019	0.3303	0.0140	0.0452	0.0018	-0.0981	0.0141	0.0009	319	64	285	11	289	11	283	19	89.3	98.4
mr20_02123_6	0.52	22.8571	0.8882	0.0515	0.0019	0.3135	0.0140	0.0438	0.0017	0.2437	0.0137	0.0009	247	61	276	11	276	11	274	18	111.7	99.9
mr20_02123_7	0.54	21.3493	0.8660	0.0515	0.0019	0.3370	0.0150	0.0468	0.0019	0.2519	0.0146	0.0010	262	64	295	11	293	12	293	20	112.6	100.6
mr20_02123_8	0.53	21.1775	0.8521	0.0529	0.0021	0.3400	0.0160	0.0472	0.0019	0.1240	0.0149	0.0010	303	72	297	12	298	12	298	20	98.1	99.7
mr20_02123_9	0.50	21.4500	0.8742	0.0517	0.0022	0.3310	0.0160	0.0466	0.0019	0.0894	0.0145	0.0010	263	74	294	12	289	12	291	20	111.8	101.9
mr20_02123_10	0.51	21.3675	0.8675	0.0525	0.0021	0.3440	0.0160	0.0468	0.0019	0.0505	0.0150	0.0010	306	71	295	12	299	12	301	21	96.4	98.6
mr20_02123_11	0.50	21.0393	0.8410	0.0514	0.0022	0.3360	0.0160	0.0475	0.0019	0.0327	0.0150	0.0010	263	75	299	12	295	12	301	21	113.8	101.6
mr20_02123_12	0.50	22.3664	0.9005	0.0526	0.0021	0.3240	0.0150	0.0447	0.0018	0.1880	0.0140	0.0010	287	69	282	11	283	11	282	19	98.2	99.5
mr20_02123_13	0.53	21.2495	0.8128	0.0512	0.0019	0.3290	0.0150	0.0471	0.0018	0.0663	0.0145	0.0010	246	65	296	11	291	11	291	20	120.5	101.8
mr20_02123_14	0.54	21.3858	0.8690	0.0499	0.0021	0.3260	0.0160	0.0468	0.0019	0.0116	0.0146	0.0010	199	74	295	11	287	12	293	20	148.0	102.7
mr20_02123_15	0.50	21.5703	0.8840	0.0536	0.0022	0.3360	0.0150	0.0464	0.0019	0.0310	0.0144	0.0010	330	74	292	11	295	12	289	20	88.5	99.1
mr20_02123_16	0.55	21.6310	0.8422	0.0519	0.0022	0.3300	0.0160	0.0462	0.0018	0.1193	0.0144	0.0010	278	77	291	11	290	13	289	20	104.7	100.5
mr20_02123_17	0.56	21.1730	0.8518	0.0503	0.0020	0.3300	0.0150	0.0472	0.0019	0.1698	0.0146	0.0010	229	71	298	12	289	12	292	20	130.0	103.0
mr20_02123_18	0.49	21.9974	0.8710	0.0515	0.0021	0.3180	0.0150	0.0455	0.0018	0.1354	0.0144	0.0010	241	72	287	11	280	12	289	20	119.0	102.6
mr20_02123_19	0.56	21.9058	0.8638	0.0520	0.0020	0.3280	0.0150	0.0457	0.0018	0.1577	0.0141	0.0010	278	66	288	11	288	11	282	19	103.6	100.2
mr20_02123_20	0.57	21.3538	0.8664	0.0531	0.0020	0.3430	0.0150	0.0468	0.0019	0.1439	0.0145	0.0010	323	64	295	11	299	11	290	20	91.3	98.6
mr20_02123_21	0.53	21.4592	0.8289	0.0522	0.0020	0.3310	0.0150	0.0466	0.0018	0.0598	0.0147	0.0010	289	69	294	11	289	11	295	20	101.6	101.5
mr20_02123_22	0.52	22.8467	0.8874	0.0515	0.0021	0.3100	0.0140	0.0438	0.0017	0.1075	0.0142	0.0010	247	71	276	11	273	11	285	20	111.8	101.1
mr20_02123_23	0.51	22.6912	0.9268	0.0530	0.0020	0.3200	0.0150	0.0441	0.0018	0.1642	0.0142	0.0010	307	67	278	11	281	11	285	20	90.7	99.0
mr20_02123_24	0.50	21.6310	0.8890	0.0536	0.0022	0.3340	0.0150	0.0462	0.0019	0.1303	0.0138	0.0010	313	73	291	12	293	12	277	20	93.1	99.3
mr19_02123_1	0.52	20.7469	0.6887	0.0531	0.0025	0.3550	0.0250	0.0482	0.0016	0.2291	0.0152	0.0015	333	78	303	10	307	19	304	30	91.1	98.8
mr19_02123_2	0.56	20.8420	0.6516	0.0518	0.0022	0.3426	0.0230	0.0480	0.0015	0.2288	0.0150	0.0014	260	61	302	9	298	18	300	28	116.2	101.2
mr19_02123_3	0.59	21.7391	0.6616	0.0519	0.0023	0.3344	0.0230	0.0460	0.0014	0.2084	0.0149	0.0014	279	68	290	9	293	18	299	28	103.8	98.8
mr19_02123_4	0.67	21.0659	0.6213	0.0523	0.0021	0.3393	0.0230	0.0475	0.0014	0.3481	0.0151	0.0014	276	55	299	8	295	17	302	28	108.3	101.2
mr19_02123_5	0.60	21.2766	0.6790	0.0514	0.0023	0.3353	0.0230	0.0470	0.0015	0.2128	0.0149	0.0014	244	65	297	9	294	18	300	28	121.6	100.9
mr19_02123_6	0.60	20.8333	0.6944	0.0526	0.0024	0.3480	0.0240	0.0480	0.0016	0.1046	0.0156	0.0015	286	72	302	10	303	18	313	30	105.6	99.6
mr19_02123_7	0.61	21.4225	0.6425	0.0524	0.0022	0.3402	0.0230	0.0467	0.0014	0.1358	0.0149	0.0014	292	62	294	9	297	18	298	28	100.7	99.2
mr19_02123_8	0.55	20.9205	0.6565	0.0526	0.0027	0.3440	0.0250	0.0478	0.0015	0.1847	0.0152	0.0015	288	83	301	9	298	19	305	29	104.4	100.9
mr19_02123_9	0.60	21.0971	0.6676	0.0531	0.0025	0.3490	0.0240	0.0474	0.0015	0.1325	0.0148	0.0014	344	75	298	9	303	18	297	28	86.7	98.4
mr19_02123_10	0.63	21.2224	0.9909	0.0523	0.0014	0.3421	0.0180	0.0471	0.0022	0.1411	0.0148	0.0007	277	54	297	14	298	14	298	14	107.1	99.6
mr19_02123_11	0.63	21.5843	1.0249	0.0530	0.0014	0.3358	0.0180	0.0463	0.0022	0.2356	0.0141	0.0007	314	52	292	13	294	14	284	13	93.0	99.3
mr19_02123_12	0.58	20.8073	0.9958	0.0525	0.0019	0.3460	0.0200	0.0481	0.0023	0.1085	0.0147	0.0007	292	70	303	14	301	15	295	15	103.6	100.5
mr19_02123_13	0.56	22.1190	1.0274	0.0538	0.0015	0.3353	0.0180	0.0452	0.0021	0.3055	0.0139	0.0007	352	55	285	13	293	14	279	14	81.0	97.4
mr19_02123_14	0.60	22.0799	1.0726	0.0587	0.0019	0.3620	0.0200	0.0453	0.0022	0.1133	0.0163	0.0008	550	66	286	13	313	15	328	16	51.9	91.2
mr19_02123_15	0.57	22.1435	1.0787	0.0524	0.0017	0.3234	0.0180	0.0452	0.0022	0.1033	0.0138	0.0007	274	60	285	13	284	14	278	14	103.9	100.1
mr19_02123_16	0.57	22.4215	1.0557	0.0530	0.0016	0.3207	0.0180	0.0446	0.0021	0.1742	0.0136	0.0007	300	58	281	13	282	14	273	13	93.7	99.7
mr19_02123_17	0.54	21.4592	1.0131	0.0513	0.0019	0.3300	0.0190	0.0466	0.0022	0.0997	0.0142	0.0007	236	72	294	14	289	15	285	15	124.4	101.7
mr19_02123_18	0.50	22.4215	1.0557	0.0516	0.0017	0.3170	0.0180	0.0446	0.0021	0.2351	0.0138	0.0007	262	65	281	13	281	14	276	15	107.3	100.1
mr19_02123_19	0.52	20.7857	0.9937	0.0520	0.0018	0.3429	0.0190	0.0481	0.0023	0.0484	0.0148	0.0008	286	67	303	14	300	14	296	15	105.9	100.9
mr19_02123_20	0.53	22.3364	1.0477	0.0527	0.0015	0.3235	0.0170	0.0448	0.0021	0.1939	0.0141	0.0007	308	55	283	13	284	14	282	14	91.7	99.5
mr19_02123_21	0.50	21.9539	1.0603	0.0530	0.0017	0.3296	0.0180	0.0456	0.0022	0.1386	0.0147	0.0007	314	62	287	13	288	14	295	15	91.5	99.8
mr19_02123_22	0.51	21.0393	0.9738	0.0505	0.0016	0.3375	0.0190	0.0475	0.0022	0.1161	0.0150	0.0008	222	61	299	14	295	14	301	15	134.8	101.5
mr19_02123_23	0.57	20.9908	1.0134	0.0525	0.0017	0.3462	0.0190	0.0476	0.0023	0.1127	0.0145	0.0007	283	63	300	14	302	14	291	14	106.0	99.5
mr19_02123_24	0.54	21.7770	1.0433	0.0515	0.0016	0.3295	0.0180	0.0459	0.0022	0.2239	0.0145	0.0007	249	59	289	13	289	14	291	15	116.2	100.2
mr19_02123_25	0.57	21.5610	1.0227	0.0526	0.0017	0.3415	0.0190	0.0464	0.0022	0.0608	0.0145	0.0007	296	62	292	13	297	14	290	14	98.7	98.3
mr19_02123_26	0.57	21.3129	0.9993	0.0515	0.0015	0.3327	0.0180	0.0469	0.0022	0.0618	0.0147	0.0007	252	58	296	14	291	14	295	15	117.3	101.6
mr19_02123_27	0.57	20.9205	0.9629	0.0517	0.0018	0.3470	0.0200	0.0478	0.0022	0.0495	0.0152	0.0008	263	66	301	14	302	15	306	15	114.4	99.7
mr19_02123_28	0.59	21.7818	0.9963	0.0518	0.0016	0.3333	0.0180	0.0459	0.0021	0.1461	0.0141	0.0007	270	58	289	13	292	14	283	14	107.1	99.2
mr19_02123_29	0.53	21.1595	0.9850	0.0530	0.0016	0.3494	0.0190	0.0473	0.0022	0.1909	0.0144	0.0007	316	58	298	14	304	14	289	14	94.2	97.8
mr19_02123_30	0.57	21.0438	0.9742	0.0519	0.0015	0.3445	0.0180	0.0475	0.0022	0.1450	0.0145	0.0007	278	57	299	14	302	14	290	14	107.6	99.2
mr19_02123_31	0.55	20.9776	0.9681	0.0525	0.0016	0.3440	0.0190	0.0477	0.0022	0.1477	0.0148	0.0008	297	63	300	14	300	14	297	15	101.0	100.1
mr19_02123_32	0.50	22.6398	1.0764	0.0546	0.0017	0.3292	0.0180	0.0442	0.0021	0.0813	0.0139	0.0007	364	61	279	13	290	13	279	14	76.5	96.2
mr19_02123_33	0.54	21.3311	1.0010	0.0519	0.0015	0.3360	0.0180	0.0469	0.0022	0.1546	0.0143	0.0007	275	57	295	13	294	14	287	14	107.4	100.5
mr19_02123_34	0.57	21.3904	1.0066	0.0520	0.0016	0.3308	0.0180	0.0468	0.0022	0.0560	0.0141	0.0007	277	60	295	13	291	14	283	14	106.3	101.4
mr19_02123_35	0.56	20.9908	0.9693	0.0529	0.0017	0.3480	0.0190	0.0476	0.0022	0.1340	0.0145	0.0007	306	62	300	14	301	15	290	14	98.0	99.5
mr19_02123_36	0.54	21.8436	1.0497	0.0529	0.0018	0.3360	0.0190	0.0458	0.0022	0.0856	0.0136	0.0007	311	66	289	13	293	14	273	14	92.8	98.3
jn13_02123_1	0.56	21.0261	0.5305	0.0524	0.0018	0.3437	0.0096	0.0476	0.0012	0.3649	0.0153	0.0006	303	78	299	7	300	7	307	11	98.8	99.9
jn13_02123_2	0.60	20.8073	0.5195	0.0523	0.0017	0.3464	0.0086	0.0481	0.0012	0.3830	0.0149	0.0005	299	74	302	8	302	7	299	11	101.3	100.3
jn13_02123_3	0.59	20.7297	0.5157	0.0505	0.0017	0.3388	0.0088	0.0482	0.0012	0.3322	0.0151	0.0006	218	78	304	8	296	7	304	11	139.2	102.5
jn13_02123_4	0.62	20.9996	0.5292	0.0514	0.0016	0.3391	0.0084	0.0476	0.0012	0.3990	0.0148	0.0005	259	72	300	7	295	6	297	11	115.8	101.5
jn13_02123_5	0.56	21.4041	0.5498	0.0536	0.0017	0.3447	0.0086	0.0467	0.0012	0.3182	0.0143	0.0005	354	72	295	7	302	6	288	10	83.1	97.5
jn13_02123_6	0.61	21.1461	0.5366	0.0517	0.0016	0.3467	0.0080	0.0473	0.0012	0.3956	0.0141	0.0005	272	71	298	7	301	6	282	10	109.4	98.8
jn13_02123_7	0.61	21.1327	0.5359	0.0518	0.0015	0.3417	0.0082	0.0473	0.0012	0.4223	0.0144	0.0005	277	66	298	7	297	6	288	10	107.7	100.3
jn13_02123_8	0.57	20.5931	0.5089	0.0527	0.0017	0.3526	0.0088	0.0486	0.0012	0.3397	0.0145	0.0005	316	73	306	7	305	7	291	11	96.7	100.1
jn13_02123_9	0.60	21.4915	0.5081	0.0523	0.0016	0.3422	0.0081	0.0465	0.0011	0.3182	0.0143	0.0005	299	70	293	7	298	6	286	10	98.3	98.6
jn13_02123_10	0.61	21.4592	0.5526	0.0514	0.0017	0.3363	0.0086	0.0466	0.0012	0.2823	0.0144	0.0005	259	76	294	7	294	7	290	11	113.5	99.8
jn13_02123_11	0.53	21.0305	0.5307	0.0507	0.0016	0.3354	0.0084	0.0476	0.0012	0.2926	0.0150	0.0006	227	73	299	7	293	6	300	11	131.7	102.2

02123 zircon continued

jn13_02123_12	0.58	20.8464	0.5215	0.0512	0.0016	0.3403	0.0084	0.0480	0.0012	0.3027	0.0142	0.0005	250	72	302	7	297	6	285	10	121.0	101.9
jn13_02123_13	0.61	20.9952	0.4849	0.0520	0.0016	0.3418	0.0086	0.0476	0.0011	0.4073	0.0149	0.0005	285	70	300	7	299	6	299	11	105.0	100.4
jn13_02123_14	0.61	21.2630	0.5425	0.0520	0.0017	0.3364	0.0081	0.0470	0.0012	0.2486	0.0151	0.0005	285	75	296	7	295	6	303	11	103.9	100.6
jn13_02123_15	0.62	21.0971	0.5341	0.0532	0.0017	0.3457	0.0090	0.0474	0.0012	0.4323	0.0145	0.0005	337	72	299	7	302	7	290	11	88.6	99.0
jn26_02123_1	0.60	20.9556	0.5709	0.0517	0.0017	0.3345	0.0110	0.0477	0.0013	0.3684	0.0149	0.0007	272	75	300	8	291	8	298	14	110.3	103.2
jn26_02123_2	0.60	21.1909	0.5838	0.0521	0.0017	0.3410	0.0120	0.0472	0.0013	0.2719	0.0148	0.0007	290	75	297	8	297	9	297	14	102.5	100.2
jn26_02123_3	0.60	21.3630	0.5933	0.0514	0.0018	0.3346	0.0110	0.0468	0.0013	0.2560	0.0146	0.0007	259	80	295	8	293	9	294	14	114.1	100.8
jn26_02123_4	0.62	21.2811	0.5888	0.0512	0.0017	0.3340	0.0110	0.0470	0.0013	0.3480	0.0146	0.0007	250	76	296	8	292	8	293	14	118.6	101.5
jn26_02123_5	0.61	21.7533	0.6152	0.0511	0.0017	0.3296	0.0100	0.0460	0.0013	0.2662	0.0147	0.0007	245	77	290	8	289	8	294	14	118.0	100.2
jn26_02123_6	0.61	21.5146	0.6017	0.0526	0.0018	0.3383	0.0110	0.0465	0.0013	0.3453	0.0143	0.0007	312	78	293	8	296	8	288	13	93.9	99.0
jn26_02123_7	0.54	21.3950	0.6408	0.0530	0.0019	0.3390	0.0120	0.0467	0.0014	0.4094	0.0141	0.0007	329	81	295	9	296	9	282	14	89.6	99.5
jn26_02123_8	0.55	21.0926	0.6229	0.0524	0.0017	0.3480	0.0110	0.0474	0.0014	0.3270	0.0145	0.0007	303	74	298	8	303	9	291	14	98.5	98.5
jn26_02123_9	0.60	21.4638	0.5989	0.0534	0.0019	0.3478	0.0120	0.0466	0.0013	0.2454	0.0144	0.0007	346	80	293	8	303	9	290	14	84.8	96.8
jn26_02123_10	0.48	21.2269	0.6308	0.0519	0.0019	0.3370	0.0120	0.0471	0.0014	0.3515	0.0151	0.0008	281	84	297	9	294	9	303	15	105.5	100.9
jn26_02123_11	0.38	21.2857	0.5890	0.0526	0.0019	0.3427	0.0120	0.0470	0.0013	0.2754	0.0147	0.0008	312	82	296	8	300	9	295	15	95.0	98.8
jn26_02123_12	0.36	22.2816	0.6951	0.0526	0.0020	0.3229	0.0120	0.0449	0.0014	0.2457	0.0138	0.0007	312	87	283	8	285	9	276	15	90.9	99.2
jn26_02123_13	0.43	20.8899	0.6109	0.0538	0.0020	0.3600	0.0130	0.0479	0.0014	0.2967	0.0146	0.0008	363	84	301	9	311	10	294	15	83.0	96.8
jn26_02123_14	0.38	21.0971	0.6676	0.0527	0.0021	0.3450	0.0130	0.0474	0.0015	0.2855	0.0146	0.0008	316	91	299	9	300	10	293	16	94.7	99.7
jn26_02123_15	0.67	21.3538	0.6384	0.0536	0.0020	0.3467	0.0120	0.0468	0.0014	0.1071	0.0144	0.0007	354	84	295	9	301	9	289	14	83.2	97.9
jn26_02123_16	0.60	22.1877	0.6400	0.0533	0.0018	0.3343	0.0120	0.0451	0.0013	0.4033	0.0145	0.0007	342	76	284	8	294	9	291	14	83.2	96.8
jn26_02123_17	0.45	21.2766	0.6338	0.0516	0.0020	0.3360	0.0130	0.0470	0.0014	0.3160	0.0147	0.0008	268	89	296	9	291	10	295	16	110.6	101.9
jn26_02123_18	0.36	21.3220	0.6819	0.0534	0.0022	0.3480	0.0140	0.0469	0.0015	0.0543	0.0143	0.0008	346	93	296	9	300	11	285	16	85.5	98.6
jn26_02123_19	0.36	21.0040	0.6176	0.0513	0.0019	0.3380	0.0120	0.0476	0.0014	0.3258	0.0140	0.0008	254	85	300	9	294	9	282	15	117.8	102.0
jn26_02123_20	0.35	21.4087	0.6417	0.0529	0.0021	0.3430	0.0140	0.0467	0.0014	0.2474	0.0139	0.0008	325	90	294	9	297	10	279	15	90.6	99.1
jn26_02123_21	0.35	21.7391	0.6616	0.0534	0.0020	0.3409	0.0120	0.0460	0.0014	0.3050	0.0141	0.0007	346	85	290	8	295	9	284	15	83.8	98.1
jn26_02123_22	0.34	21.9298	0.6733	0.0521	0.0019	0.3312	0.0120	0.0456	0.0014	0.3746	0.0139	0.0007	290	83	287	9	289	9	280	14	99.2	99.4
jn26_02123_23	0.33	21.4731	0.6455	0.0524	0.0022	0.3390	0.0130	0.0466	0.0014	0.0334	0.0143	0.0008	303	96	293	9	295	10	287	16	96.8	99.5
jn26_02123_24	0.34	21.3995	0.6411	0.0533	0.0021	0.3430	0.0140	0.0467	0.0014	0.2178	0.0144	0.0008	342	89	294	9	297	10	288	16	86.1	99.1
jn26_02123_25	0.34	21.5564	0.6505	0.0527	0.0021	0.3380	0.0130	0.0464	0.0014	0.4039	0.0145	0.0008	316	91	292	9	293	10	292	16	92.5	99.9
jn26_02123_26	0.37	21.7108	0.6599	0.0516	0.0021	0.3270	0.0130	0.0461	0.0014	0.1738	0.0146	0.0008	268	93	290	9	285	10	293	16	108.3	101.7

OG-1 zircon

Identifier	Th/U	Data for Tera-Wasserburg plot				Data for Wetherill plot					$^{208}Pb/^{232}Th$	2SE	Dates								% Concordancy (206Pb-238U age/207Pb-206Pb age)*100	%Concordancy (206Pb-238U age/207Pb-235U age)*100
		$^{238}U/^{206}Pb$	2SE	$^{207}Pb/^{206}Pb$	2SE	$^{207}Pb/^{235}U$	2SE	$^{206}Pb/^{238}U$	2SE	Rho			$^{207}Pb/^{206}Pb$	2SE	$^{206}Pb/^{238}U$	2SE	$^{207}Pb/^{235}U$	2SE	$^{208}Pb/^{232}Th$	2SE		
ZOG1_1_oc14	0.40	1.3793	0.0304	0.2978	0.0054	29.7900	0.7900	0.7250	0.0160	0.6451	0.2131	0.0130	3458	18	3512	60	3479	26	3901	210	101.6	100.9
ZOG1_2_oc14	0.31	1.3827	0.0306	0.3008	0.0053	29.7000	0.7800	0.7232	0.0160	0.6809	0.2027	0.0120	3472	16	3501	58	3475	26	3732	200	100.8	100.7
ZOG1_3_oc14	0.30	1.3245	0.0298	0.2978	0.0053	30.9900	0.8300	0.7550	0.0170	0.6793	0.2093	0.0120	3459	17	3617	61	3518	25	3839	210	104.6	102.8
ZOG1_4_oc14	0.30	1.3175	0.0312	0.2994	0.0059	31.3100	0.8800	0.7590	0.0180	0.6474	0.2126	0.0130	3465	21	3630	66	3526	27	3894	210	104.8	102.9
ZOG1_5_oc14	0.56	1.3495	0.0310	0.3013	0.0056	30.8900	0.8500	0.7410	0.0170	0.6988	0.1970	0.0120	3474	19	3572	63	3514	27	3630	200	102.8	101.7
ZOG1_6_oc14	0.78	1.3569	0.0331	0.3018	0.0058	30.8600	0.8800	0.7370	0.0180	0.6862	0.2149	0.0130	3476	20	3552	65	3509	28	3931	210	102.2	101.2
ZOG1_7_oc14	0.79	1.3605	0.0518	0.2913	0.0072	29.5600	1.2000	0.7350	0.0280	0.7636	0.1933	0.0120	3439	32	3552	110	3475	38	3569	210	103.3	102.2
ZOG1_8_oc14	0.51	1.3755	0.0322	0.3047	0.0057	30.5500	0.8400	0.7270	0.0170	0.6772	0.2038	0.0120	3495	20	3513	62	3499	27	3747	200	100.5	100.4
ZOG1_9_oc14	0.48	1.3793	0.0380	0.3027	0.0069	30.4200	0.9500	0.7250	0.0200	0.6275	0.1998	0.0120	3483	28	3517	76	3501	31	3683	200	101.0	100.5
ZOG1_1_fe05	0.46	1.3736	0.0528	0.2978	0.0062	29.9600	1.5000	0.7280	0.0280	0.6999	0.2080	0.0120	3462	18	3525	100	3484	49	3820	200	101.8	101.2
ZOG1_2_fe05	0.43	1.4104	0.0537	0.3025	0.0061	29.8400	1.5000	0.7090	0.0270	0.7633	0.2013	0.0120	3478	16	3453	100	3484	47	3706	200	99.3	99.1
ZOG1_3_fe05	0.54	1.3661	0.0523	0.3002	0.0062	30.6300	1.5000	0.7320	0.0280	0.7186	0.2027	0.0120	3472	18	3539	100	3502	48	3733	200	101.9	101.1
ZOG1_4_fe05	0.61	1.3369	0.0518	0.3017	0.0062	31.2500	1.6000	0.7480	0.0290	0.7523	0.2042	0.0120	3474	17	3594	110	3522	50	3759	200	103.5	102.0
ZOG1_5_fe05	0.51	1.3532	0.0513	0.3029	0.0060	30.9400	1.5000	0.7390	0.0280	0.7567	0.2140	0.0120	3483	15	3558	100	3518	49	3922	210	102.2	101.1
ZOG1_6_fe05	0.99	1.3994	0.0529	0.3032	0.0060	30.0600	1.5000	0.7146	0.0270	0.7552	0.1999	0.0110	3485	14	3471	100	3490	47	3680	190	99.6	99.5
ZOG1_7_fe05	0.58	1.3850	0.0537	0.3004	0.0060	29.9000	1.5000	0.7220	0.0280	0.7791	0.2167	0.0130	3473	16	3510	100	3481	47	3962	210	101.1	100.8
ZOG1_8_fe05	0.84	1.4261	0.0549	0.3002	0.0049	29.1300	1.2000	0.7012	0.0270	0.7090	0.2028	0.0110	3474	15	3422	100	3455	40	3732	180	98.5	99.0
ZOG1_9_fe05	0.51	1.3263	0.0528	0.2962	0.0052	31.2900	1.3000	0.7540	0.0300	0.7442	0.2157	0.0120	3448	19	3637	110	3530	42	3944	190	105.5	103.0
ZOG1_10_fe05	0.88	1.4223	0.0546	0.3019	0.0047	29.5800	1.2000	0.7031	0.0270	0.7441	0.1900	0.0098	3478	13	3429	100	3473	41	3517	170	98.6	98.7
ZOG1_11_fe05	0.74	1.4108	0.0537	0.2993	0.0048	29.2700	1.2000	0.7088	0.0270	0.7366	0.1867	0.0097	3464	14	3451	100	3460	40	3458	170	99.6	99.7
ZOG1_12_fe05	0.78	1.4094	0.0536	0.3009	0.0047	29.5100	1.2000	0.7095	0.0270	0.8016	0.1944	0.0100	3474	13	3454	100	3472	40	3587	170	99.4	99.5
Z_OG1_1_mr20	1.04	1.4298	0.0552	0.3045	0.0064	29.4600	0.9800	0.6994	0.0270	0.6788	0.2074	0.0130	3494	11	3420	100	3468	33	3809	220	97.9	98.6
Z_OG1_2_mr20	0.56	1.3706	0.0526	0.2990	0.0064	30.3200	1.0000	0.7296	0.0280	0.5059	0.2002	0.0130	3469	12	3531	100	3497	33	3685	210	101.8	101.0
Z_OG1_3_mr20	0.91	1.5181	0.0576	0.3049	0.0065	27.5500	0.9100	0.6587	0.0250	0.6909	0.2058	0.0130	3493	12	3262	99	3402	32	3789	220	93.4	95.9
Z_OG1_4_mr20	1.01	1.4449	0.0564	0.2994	0.0063	28.6400	0.9700	0.6921	0.0270	0.8277	0.1977	0.0120	3466	11	3387	100	3438	33	3645	210	97.7	98.5
Z_OG1_5_mr20	0.65	1.3755	0.0549	0.2982	0.0067	29.7400	1.0000	0.7270	0.0290	0.7849	0.2448	0.0160	3462	16	3525	110	3480	34	4427	260	101.8	101.3
Z_OG1_6_mr20	0.79	1.4422	0.0562	0.3015	0.0064	28.9000	0.9700	0.6934	0.0270	0.7194	0.2020	0.0130	3478	11	3395	100	3449	33	3720	210	97.6	98.4
Z_OG1_7_mr20	0.50	1.3976	0.0547	0.2988	0.0068	29.4100	1.0000	0.7155	0.0280	0.5788	0.2168	0.0140	3464	17	3478	100	3464	34	3967	240	100.4	100.4
Z_OG1_8_mr20	0.75	1.3532	0.0659	0.2969	0.0079	30.1000	1.4000	0.7390	0.0360	0.8603	0.3320	0.0250	3457	27	3555	140	3486	47	5800	380	102.8	102.0
Z_OG1_9_mr20	0.59	1.3680	0.0599	0.2981	0.0075	29.8700	1.1000	0.7310	0.0320	0.7970	0.2890	0.0210	3465	24	3532	120	3487	40	5110	320	101.9	101.3
Z_OG1_10_mr20	0.86	1.3908	0.0580	0.3011	0.0070	29.7900	1.1000	0.7190	0.0300	0.7641	0.2486	0.0160	3474	18	3493	110	3476	35	4488	250	100.5	100.5
Z_OG1_11_mr20	0.53	1.4203	0.0545	0.3058	0.0069	29.6200	1.0000	0.7041	0.0270	0.6275	0.2244	0.0150	3499	16	3435	100	3474	34	4085	240	98.2	98.9
Z_OG1_12_mr20	0.52	1.4362	0.0557	0.3014	0.0066	29.1000	0.9700	0.6963	0.0270	0.6098	0.1956	0.0120	3476	14	3407	100	3457	32	3608	210	98.0	98.6
Z_OG1_13_mr20	0.96	1.4265	0.0549	0.3035	0.0068	29.2500	0.9800	0.7010	0.0270	0.5173	0.1925	0.0120	3486	16	3421	100	3461	33	3556	210	98.1	98.8
Z_OG1_14_mr20	0.68	1.4912	0.0578	0.3018	0.0066	27.8100	0.9600	0.6706	0.0260	0.7370	0.1941	0.0120	3478	14	3307	100	3409	34	3582	210	95.1	97.0
Z_OG1_15_mr20	0.47	1.4896	0.0577	0.2998	0.0068	27.6800	0.9500	0.6713	0.0260	0.6502	0.1991	0.0130	3470	16	3306	100	3405	34	3665	220	95.3	97.1
Z_OG1_16_mr20	0.65	1.4451	0.0564	0.3051	0.0068	28.8600	0.9800	0.6920	0.0270	0.6325	0.2157	0.0140	3495	15	3389	100	3447	33	3944	230	97.0	98.3
ZOG1_1_mr19	0.62	1.4493	0.0609	0.3063	0.0130	29.2000	1.9000	0.6900	0.0290	0.5682	0.1816	0.0180	3489	45	3371	110	3458	64	3370	300	96.6	97.5
ZOG1_2_mr19	0.87	1.4184	0.0443	0.3037	0.0100	29.8000	1.9000	0.7050	0.0220	0.5910	0.2162	0.0200	3488	26	3441	81	3479	62	3957	340	98.7	98.9
ZOG1_3_mr19	0.88	1.4493	0.0462	0.3016	0.0100	28.8300	1.9000	0.6900	0.0220	0.6891	0.2040	0.0190	3487	25	3372	85	3444	63	3753	320	96.7	97.9
ZOG1_4_mr19	0.76	1.3850	0.0441	0.3039	0.0100	30.5400	2.0000	0.7220	0.0230	0.6450	0.2150	0.0200	3486	27	3500	88	3502	63	3937	340	100.4	99.9
ZOG1_5_mr19	0.89	1.4006	0.0432	0.2997	0.0099	29.7400	1.9000	0.7140	0.0220	0.5744	0.1946	0.0180	3465	24	3474	82	3478	62	3589	310	100.3	99.9
ZOG1_6_mr19	0.81	1.3928	0.0407	0.3003	0.0099	30.0600	1.9000	0.7180	0.0210	0.5481	0.1982	0.0180	3471	24	3486	78	3488	62	3655	310	100.4	99.9
ZOG1_7_mr19	0.95	1.3986	0.0411	0.2998	0.0099	29.8500	1.9000	0.7150	0.0210	0.5612	0.1951	0.0180	3465	24	3482	79	3481	61	3602	310	100.5	100.0
ZOG1_8_mr19	0.46	1.4124	0.0678	0.3039	0.0052	29.1300	1.5000	0.7080	0.0340	0.5730	0.1930	0.0094	3489	22	3445	130	3455	49	3563	160	98.7	99.7
ZOG1_9_mr19	0.68	1.4556	0.0678	0.3014	0.0044	28.2400	1.4000	0.6870	0.0320	0.5535	0.1835	0.0084	3474	17	3373	120	3425	48	3409	150	97.1	98.5
ZOG1_10_mr19	0.99	1.4482	0.0671	0.3024	0.0039	28.5500	1.4000	0.6905	0.0320	0.6389	0.1956	0.0087	3485	13	3386	120	3439	49	3609	150	97.2	98.4
ZOG1_11_mr19	0.59	1.3278	0.0599	0.3016	0.0034	31.3800	1.5000	0.7531	0.0340	0.6063	0.2024	0.0089	3478	9	3623	130	3531	47	3724	150	104.2	102.6
ZOG1_11_mr19	0.57	1.3506	0.0620	0.2998	0.0035	30.7100	1.5000	0.7404	0.0340	0.5216	0.1992	0.0089	3469	10	3572	120	3510	47	3676	150	103.0	101.8
ZOG1_11_mr19	0.73	1.4325	0.0657	0.2994	0.0037	29.0800	1.4000	0.6981	0.0320	0.7465	0.2081	0.0093	3466	12	3410	120	3455	48	3818	150	98.4	98.7
ZOG1_11_mr19	0.78	1.3980	0.0645	0.3008	0.0037	29.9700	1.4000	0.7153	0.0330	0.6903	0.2136	0.0095	3473	12	3478	120	3484	48	3910	160	100.1	99.8
ZOG1_11_mr19	0.97	1.4190	0.0644	0.3020	0.0035	29.6800	1.4000	0.7047	0.0320	0.7239	0.2099	0.0092	3480	10	3439	120	3475	48	3849	150	98.8	99.0
ZOG1_11_mr19	0.83	1.4841	0.0683	0.3020	0.0035	28.3800	1.4000	0.6738	0.0310	0.7289	0.1907	0.0084	3479	10	3318	120	3433	46	3528	140	95.4	96.7
ZOG1_11_mr19	0.91	1.3550	0.0624	0.3015	0.0037	30.4000	1.5000	0.7380	0.0340	0.4668	0.1901	0.0084	3478	12	3562	130	3498	47	3517	140	102.4	101.8
ZOG1_11_mr19	0.81	1.3734	0.0622	0.3004	0.0034	29.8300	1.4000	0.7281	0.0330	0.5513	0.1967	0.0087	3472	9	3525	120	3481	47	3630	150	101.5	101.3
ZOG1_11_mr19	0.45	1.4142	0.0640	0.3028	0.0035	29.1300	1.4000	0.7071	0.0320	0.6794	0.1907	0.0086	3483	10	3447	120	3458	47	3531	140	99.0	99.7
OG1_1_jn13	0.94	1.3532	0.0311	0.2997	0.0070	30.5500	0.4100	0.7390	0.0170	0.6809	0.2094	0.0065	3469	36	3559	64	3501	13	3845	110	102.6	101.7
OG1_2_jn13	0.42	1.3661	0.0429	0.3092	0.0091	30.8000	0.7500	0.7320	0.0230	0.5444	0.2910	0.0170	3517	45	3532	84	3512	24	5100	250	100.4	100.6
OG1_3_jn13	0.44	1.3680	0.0337	0.3021	0.0071	30.4300	0.4200	0.7310	0.0180	0.6432	0.2086	0.0067	3481	36	3534	65	3502	13	3827	110	101.5	100.9
OG1_4_jn13	0.74	1.3736	0.0321	0.3001	0.0071	30.0900	0.4100	0.7280	0.0170	0.6485	0.2066	0.0066	3471	37	3529	64	3484	13	3795	110	101.7	101.3
OG1_5_jn13	0.77	1.3459	0.0308	0.2971	0.0070	30.7300	0.4500	0.7430	0.0170	0.6617	0.2095	0.0067	3455	37	3579	64	3506	14	3840	110	103.6	102.1
OG1_6_jn13	0.57	1.3514	0.0329	0.3028	0.0073	30.9500	0.4500	0.7400	0.0180	0.6695	0.2297	0.0074	3485	37	3562	66	3516	14	4175	120	102.2	101.3
OG1_7_jn13	0.67	1.3986	0.0333	0.2998	0.0072	29.5200	0.4300	0.7150	0.0170	0.6725	0.2026	0.0064	3469	37	3477	66	3471	14	3728	110	100.2	100.2
OG1_1_jn26	0.85	1.3661	0.0373	0.3001	0.0075	30.3500	0.7600	0.7320	0.0200	0.6819	0.2030	0.0089	3471	39	3542	73	3497	25	3732	150	102.1	101.3
OG1_2_jn26	0.64	1.3680	0.0393	0.2961	0.0074	29.9600	0.7800	0.7310	0.0210	0.7362	0.1975	0.0088	3450	39	3534	77	3480	25	3638	150	102.4	101.6
OG1_3_jn26	0.52	1.3298	0.0371	0.3000	0.0078	31.0400	0.8100	0.7520	0.0210	0.6921	0.2137	0.0096	3470	40	3601	76	3518	25	3920	160	103.8	102.4
OG1_4_jn26	0.74	1.4184	0.0402	0.2957	0.0077	28.9100	0.7400	0.7050	0.0200	0.6232	0.1960	0.0089	3448	40	3431	74	3449	26	3614	150	99.5	99.5
OG1_5_jn26	0.78	1.3569	0.0368	0.2980	0.0076	30.2800	0.7800	0.7370	0.0200	0.6550	0.1977	0.0088	3460	40	3562	73	3495	26	3647	150	103.0	101.9
OG1_6_jn26	0.71	1.3717	0.0376	0.3023	0.0078	30.5300	0.7800	0.7290	0.0200	0.6622	0.2005	0.0090	3482	40	3532	74	3503	25	3697	150	101.4	100.8
OG1_7_jn26	0.99	1.3550	0.0404	0.3022	0.0078	31.0700	0.8400	0.7380	0.0220	0.7038	0.2168	0.0100	3482	40	3553	79	3520	26	3962	170	102.1	100.9
OG1_8_jn26	0.88	1.4065	0.0396	0.3024	0.0079	30.2200	0.8000	0.7110	0.0200	0.6748	0.1962	0.0088	3483	40	3461	75	3490	26	3622	150	99.4	99.2
OG1_9_jn26	0.81	1.3587	0.0388	0.3013	0.0077	30.8900	0.7900	0.7360	0.0210	0.6573	0.1994	0.0089	3477	40	3551	77	3518	25	3678	150	102.1	100.9
OG1_1_mr30	0.95	1.3986	0.0685	0.2922	0.0053	28.9800	1.6000	0.7150	0.0350	0.5527	0.1945	0.0099	3429	28	3472	130	3454	54	3592	170	101.2	100.5
OG1_2_mr30	0.99	1.3643	0.0689	0.2929	0.0062	29.6000	1.6000	0.7330	0.0370	0.6096	0.1985	0.0100	3433	33	3546	140	3476	54	3651	170	103.3	102.0
OG1_3_mr30	0.83	1.4225	0.0728	0.2984	0.0058	29.0400	1.6000	0.7030	0.0360	0.6352	0.1914	0.0099	3462	30	3431	130	3451	52	3544	170	99.1	99.4
OG1_4_mr30	0.07	1.4599	0.0895	0.3030	0.0100	28.2000	1.8000	0.6850	0.0420	0.6452	0.2400	0.0160	3486	51	3370	160	3422	64	4340	260	96.7	98.5
OG1_5_mr30	0.59	1.4535	0.0739	0.3030	0.0056	28.9400	1.6000	0.6880	0.0350	0.6248	0.2004	0.0100	3486	29	3375	130	3450	52	3701	170	96.8	97.8
OG1_6_mr30	0.52	1.4164	0.0702	0.3056	0.0060	29.6800	1.6000	0.7060	0.0350	0.5636	0.2125	0.0110	3499	30	3434	130	3476	53	3894	180	98.1	98.8
OG1_7_mr30	1.06	1.3123	0.0654	0.3024	0.0061	31.8900	1.7000	0.7620	0.0380	0.5933	0.2186	0.0110	3483	31	3664	140	3546	55	3995	190	105.2	103.3

Plesovice zircon

Identifier	Th/U	Data for Tera-Wasserburg plot				Data for Wetherill plot					$^{208}Pb/^{232}Th$	2SE	Dates								% Concordancy *(206Pb-238U age/207Pb-206Pb age)*100*	%Concordancy (206Pb-238U age/207Pb-235U age)*100
		$^{238}U/^{206}Pb$	2SE	$^{207}Pb/^{206}Pb$	2SE	$^{207}Pb/^{235}U$	2SE	$^{206}Pb/^{238}U$	2SE	Rho			$^{207}Pb/^{206}Pb$	2SE	$^{206}Pb/^{238}U$	2SE	$^{207}Pb/^{235}U$	2SE	$^{208}Pb/^{232}Th$	2SE		
oc14_Plesovice_1	0.09	18.0245	0.3899	0.0533	0.0012	0.4098	0.0120	0.0555	0.0012	0.4979	0.0173	0.0012	332	36	348	8	349	8	346	23	104.9	99.8
oc14_Plesovice_2	0.09	18.5426	0.4126	0.0528	0.0012	0.3933	0.0110	0.0539	0.0012	0.4682	0.0170	0.0011	303	38	339	7	336	8	341	22	111.7	100.9
oc14_Plesovice_3	0.09	17.3732	0.3924	0.0535	0.0013	0.4276	0.0120	0.0576	0.0013	0.3491	0.0188	0.0013	346	43	361	8	361	9	376	25	104.2	99.9
oc14_Plesovice_4	0.09	17.9469	0.4187	0.0526	0.0013	0.4045	0.0120	0.0557	0.0013	0.4243	0.0168	0.0012	302	42	349	8	345	9	336	23	115.7	101.2
oc14_Plesovice_5	0.09	18.4366	0.4419	0.0545	0.0014	0.4100	0.0130	0.0542	0.0013	0.4034	0.0162	0.0011	369	44	340	8	349	9	324	23	92.2	97.5
oc14_Plesovice_6	0.09	18.1159	0.4266	0.0535	0.0013	0.4049	0.0120	0.0552	0.0013	0.3577	0.0170	0.0012	329	43	347	8	346	9	341	23	105.3	100.1
oc14_Plesovice_7	0.09	18.1422	0.4279	0.0539	0.0012	0.4075	0.0120	0.0551	0.0013	0.5188	0.0171	0.0012	346	39	346	8	347	9	343	23	99.9	99.6
oc14_Plesovice_8	0.09	18.4060	0.4065	0.0526	0.0012	0.3974	0.0120	0.0543	0.0012	0.4939	0.0173	0.0012	302	38	341	7	339	8	347	24	112.9	100.6
oc14_Plesovice_9	0.09	18.8430	0.4261	0.0533	0.0013	0.3908	0.0120	0.0531	0.0012	0.4104	0.0168	0.0012	326	40	333	8	335	8	336	23	102.2	99.5
oc6_Plesovice_1	0.09	18.7477	0.4569	0.0521	0.0020	0.3893	0.0140	0.0533	0.0013	0.4836	0.0167	0.0012	290	88	335	8	333	10	334	23	115.5	100.6
oc6_Plesovice_2	0.09	18.9394	0.5022	0.0542	0.0022	0.3870	0.0150	0.0528	0.0014	0.4501	0.0166	0.0013	379	91	332	9	333	11	333	25	87.5	99.7
oc6_Plesovice_3	0.09	18.6254	0.4510	0.0534	0.0020	0.3921	0.0140	0.0537	0.0013	0.3932	0.0170	0.0012	346	85	337	8	335	10	340	24	97.5	100.7
oc6_Plesovice_4	0.10	18.4434	0.4422	0.0536	0.0020	0.4037	0.0140	0.0542	0.0013	0.5300	0.0174	0.0012	354	84	341	8	343	10	349	24	96.1	99.3
oc6_Plesovice_5	0.10	18.7899	0.4590	0.0526	0.0020	0.3846	0.0140	0.0532	0.0013	0.4045	0.0170	0.0012	312	87	334	8	330	10	340	23	107.2	101.3
oc6_Plesovice_6	0.09	18.1719	0.4293	0.0543	0.0020	0.4134	0.0140	0.0550	0.0013	0.4268	0.0176	0.0012	384	83	345	8	351	10	353	25	90.0	98.4
oc7_Plesovice_1	0.09	18.8218	0.3543	0.0549	0.0014	0.4042	0.0120	0.0531	0.0010	0.2865	0.0191	0.0006	396	30	334	6	345	9	381	11	84.2	96.8
oc7_Plesovice_2	0.08	18.7512	0.3516	0.0544	0.0015	0.3971	0.0120	0.0533	0.0010	0.2569	0.0173	0.0007	378	35	335	6	341	9	346	13	88.6	98.2
oc7_Plesovice_3	0.08	18.4604	0.3408	0.0538	0.0015	0.4022	0.0130	0.0542	0.0010	0.3271	0.0166	0.0006	348	34	340	6	343	9	333	12	97.7	99.0
oc7_Plesovice_4	0.09	18.3150	0.3690	0.0528	0.0014	0.3983	0.0120	0.0546	0.0011	0.3154	0.0168	0.0006	307	34	343	7	340	9	336	11	111.7	100.9
oc7_Plesovice_5	0.08	18.2983	0.3683	0.0528	0.0015	0.3961	0.0130	0.0547	0.0011	0.3820	0.0176	0.0007	315	42	343	7	339	9	353	14	109.0	101.4
oc7_Plesovice_6	0.09	18.6428	0.3476	0.0532	0.0015	0.3961	0.0120	0.0536	0.0010	0.2164	0.0165	0.0006	338	35	337	6	339	9	330	11	99.6	99.4
oc7_Plesovice_7	0.09	18.8041	0.3890	0.0530	0.0016	0.3899	0.0130	0.0532	0.0011	0.2231	0.0167	0.0008	320	43	334	7	334	9	334	15	104.4	100.0
oc7_Plesovice_8	0.09	18.8751	0.3563	0.0528	0.0015	0.3835	0.0120	0.0530	0.0010	0.3126	0.0169	0.0007	316	37	333	6	329	9	340	13	105.3	101.0
oc7_Plesovice_9	0.08	18.9036	0.3931	0.0538	0.0016	0.3928	0.0130	0.0529	0.0011	0.3155	0.0163	0.0007	337	43	333	7	336	10	326	15	98.7	98.9
fe05_Plesovice_1	0.10	18.0278	0.7150	0.0532	0.0012	0.4063	0.0200	0.0555	0.0022	0.5781	0.0170	0.0010	328	34	349	13	346	15	341	21	106.3	100.6
fe05_Plesovice_2	0.10	18.1917	0.6950	0.0531	0.0012	0.4037	0.0200	0.0550	0.0021	0.6094	0.0166	0.0010	317	30	345	13	344	14	333	20	108.8	100.2
fe05_Plesovice_3	0.10	17.8412	0.7003	0.0528	0.0012	0.4122	0.0210	0.0561	0.0022	0.5397	0.0168	0.0011	311	33	352	13	351	15	336	21	113.2	100.5
fe05_Plesovice_4	0.08	18.0115	0.6813	0.0530	0.0012	0.4053	0.0200	0.0555	0.0021	0.5335	0.0173	0.0011	325	34	348	13	346	15	347	22	107.1	100.7
fe05_Plesovice_5	0.10	17.8923	0.6723	0.0530	0.0012	0.4133	0.0200	0.0559	0.0021	0.5562	0.0170	0.0010	317	31	350	13	351	15	341	21	110.5	99.9
fe05_Plesovice_6	0.11	17.9147	0.6740	0.0538	0.0012	0.4156	0.0210	0.0558	0.0021	0.4735	0.0169	0.0010	346	33	350	13	353	15	339	21	101.2	99.1
fe05_Plesovice_7	0.11	18.2149	0.6967	0.0533	0.0012	0.4070	0.0200	0.0549	0.0021	0.5876	0.0168	0.0010	331	31	344	13	347	14	337	21	104.0	99.4
fe05_Plesovice_8	0.09	17.4398	0.6995	0.0539	0.0011	0.4245	0.0180	0.0573	0.0023	0.5501	0.0183	0.0011	356	35	359	14	360	13	367	22	100.9	99.9
fe05_Plesovice_9	0.10	17.8190	0.6985	0.0539	0.0011	0.4157	0.0170	0.0561	0.0022	0.5059	0.0175	0.0010	356	33	352	13	353	13	351	20	98.8	99.8
fe05_Plesovice_10	0.10	17.9051	0.6732	0.0538	0.0011	0.4132	0.0170	0.0559	0.0021	0.4845	0.0168	0.0010	359	33	350	13	351	13	337	19	97.5	99.7
fe05_Plesovice_11	0.10	18.0996	0.6879	0.0528	0.0010	0.4063	0.0170	0.0553	0.0021	0.5932	0.0163	0.0009	311	28	347	13	347	12	327	18	111.5	100.1
fe05_Plesovice_12	0.08	17.9244	0.6747	0.0530	0.0010	0.4123	0.0170	0.0558	0.0021	0.5357	0.0171	0.0010	315	31	350	13	351	12	342	19	111.1	99.8
mr20_Plesovice_1	0.10	18.9645	0.7193	0.0530	0.0013	0.3875	0.0140	0.0527	0.0020	0.1759	0.0176	0.0013	315	33	331	12	332	10	354	25	105.1	99.8
mr20_Plesovice_2	0.09	19.1241	0.7315	0.0540	0.0014	0.3887	0.0140	0.0523	0.0020	0.2522	0.0166	0.0012	358	36	329	12	333	10	332	23	91.8	98.6
mr20_Plesovice_3	0.08	19.2234	0.7391	0.0533	0.0014	0.3827	0.0140	0.0520	0.0020	0.3204	0.0171	0.0012	331	36	327	12	329	10	343	24	98.7	99.3
mr20_Plesovice_4	0.08	18.1620	0.6927	0.0538	0.0014	0.4098	0.0150	0.0551	0.0021	0.2184	0.0196	0.0014	361	37	346	13	348	11	393	28	95.7	99.2
mr20_Plesovice_5	0.08	18.1422	0.6912	0.0532	0.0014	0.4022	0.0140	0.0551	0.0021	0.1759	0.0176	0.0013	335	36	346	13	343	10	352	25	103.2	100.8
mr20_Plesovice_6	0.09	18.2282	0.6978	0.0532	0.0014	0.4035	0.0140	0.0549	0.0021	0.1993	0.0176	0.0012	323	36	344	13	344	10	352	24	106.6	100.2
mr20_Plesovice_7	0.09	17.9695	0.6781	0.0536	0.0013	0.4121	0.0150	0.0557	0.0021	0.2480	0.0182	0.0013	345	34	349	13	350	10	365	26	101.2	99.7
mr20_Plesovice_8	0.08	18.0148	0.6815	0.0538	0.0015	0.4117	0.0150	0.0555	0.0021	0.0559	0.0175	0.0013	350	40	348	13	350	11	351	25	99.5	99.6
mr20_Plesovice_9	0.08	17.8476	0.6689	0.0543	0.0014	0.4198	0.0150	0.0560	0.0021	0.1691	0.0186	0.0013	376	37	352	13	356	11	373	26	93.5	98.7
mr20_Plesovice_10	0.09	19.2345	0.7399	0.0540	0.0014	0.3841	0.0140	0.0520	0.0020	0.3563	0.0164	0.0011	356	35	327	12	329	10	328	23	91.8	99.2
mr20_Plesovice_11	0.09	19.3573	0.7494	0.0536	0.0014	0.3825	0.0140	0.0517	0.0020	0.2579	0.0164	0.0011	357	38	325	12	329	10	329	23	91.0	98.8
mr20_Plesovice_12	0.10	17.8476	0.6689	0.0546	0.0013	0.4199	0.0150	0.0560	0.0021	0.1778	0.0192	0.0013	382	32	351	13	357	10	385	26	92.0	98.5
mr20_Plesovice_13	0.09	18.1192	0.6894	0.0538	0.0013	0.4106	0.0140	0.0552	0.0021	0.2053	0.0172	0.0012	358	34	346	13	349	10	344	24	96.7	99.2
mr20_Plesovice_14	0.09	17.9533	0.6769	0.0543	0.0014	0.4120	0.0150	0.0557	0.0021	0.2505	0.0175	0.0012	371	36	350	13	351	11	350	25	94.3	99.6
mr20_Plesovice_15	0.11	17.8412	0.6684	0.0529	0.0013	0.4088	0.0140	0.0561	0.0021	0.1806	0.0174	0.0012	314	36	352	13	348	10	349	24	111.9	101.1
mr19_Plesovice_1	0.08	18.3486	0.5387	0.0541	0.0019	0.4055	0.0260	0.0545	0.0016	0.3556	0.0175	0.0018	353	41	342	10	345	19	351	35	96.8	99.0
mr19_Plesovice_2	0.09	18.2482	0.5328	0.0522	0.0019	0.3976	0.0260	0.0548	0.0016	0.3400	0.0165	0.0017	278	47	344	10	340	19	330	34	123.7	101.2
mr19_Plesovice_3	0.09	18.1488	0.5270	0.0540	0.0019	0.4123	0.0270	0.0551	0.0016	0.3419	0.0189	0.0019	363	44	346	10	350	19	378	37	95.3	98.7
mr19_Plesovice_4	0.09	17.8253	0.5402	0.0540	0.0020	0.4172	0.0270	0.0561	0.0017	0.3538	0.0185	0.0018	356	47	352	11	354	20	370	37	99.0	99.5
mr19_Plesovice_5	0.08	17.6991	0.5325	0.0530	0.0019	0.4108	0.0270	0.0565	0.0017	0.3468	0.0183	0.0018	317	47	354	10	349	19	367	36	111.7	101.4
mr19_Plesovice_6	0.08	18.1488	0.5599	0.0527	0.0020	0.4061	0.0270	0.0551	0.0017	0.3391	0.0180	0.0018	301	50	345	10	345	19	361	36	114.7	100.0
mr19_Plesovice_7	0.11	17.5039	0.7966	0.0541	0.0011	0.4231	0.0210	0.0571	0.0026	0.1953	0.0180	0.0009	361	38	358	16	358	15	361	18	99.2	100.0
mr19_Plesovice_8	0.12	17.6523	0.8102	0.0530	0.0010	0.4115	0.0210	0.0567	0.0026	0.2785	0.0172	0.0009	315	38	355	16	351	14	345	17	112.7	101.2
mr19_Plesovice_9	0.11	17.5871	0.8042	0.0542	0.0010	0.4178	0.0210	0.0569	0.0026	0.2577	0.0177	0.0009	366	37	357	16	354	15	355	18	97.4	100.7
mr19_Plesovice_10	0.09	17.7841	0.8223	0.0533	0.0009	0.4150	0.0200	0.0562	0.0026	0.1380	0.0179	0.0009	338	30	353	16	352	15	359	19	104.3	100.2
mr19_Plesovice_11	0.08	17.7117	0.8156	0.0536	0.0009	0.4195	0.0210	0.0565	0.0026	0.1620	0.0185	0.0010	343	32	354	16	356	15	370	20	103.2	99.5
mr19_Plesovice_12	0.08	17.7368	0.8179	0.0532	0.0009	0.4140	0.0200	0.0564	0.0026	0.1943	0.0183	0.0010	333	32	354	16	352	15	366	19	106.2	100.5
mr19_Plesovice_13	0.08	18.2083	0.8289	0.0530	0.0010	0.4091	0.0200	0.0549	0.0025	0.1098	0.0177	0.0009	321	36	345	15	349	15	355	18	107.4	98.8
mr19_Plesovice_14	0.09	18.2382	0.8316	0.0531	0.0009	0.4072	0.0200	0.0548	0.0025	0.1817	0.0181	0.0009	329	30	344	15	347	14	363	19	104.6	99.3
mr19_Plesovice_15	0.09	18.4264	0.8488	0.0536	0.0010	0.4049	0.0200	0.0543	0.0025	0.1694	0.0175	0.0009	345	33	341	15	346	14	351	18	98.8	98.6
mr19_Plesovice_16	0.08	18.7161	0.8757	0.0539	0.0011	0.3951	0.0200	0.0534	0.0025	0.2305	0.0163	0.0011	351	36	336	15	337	14	331	19	95.6	99.5
mr19_Plesovice_17	0.08	18.6741	0.8718	0.0538	0.0010	0.3931	0.0200	0.0536	0.0025	0.1980	0.0168	0.0009	344	34	336	15	336	14	337	19	97.7	100.1
mr19_Plesovice_18	0.09	18.5254	0.8580	0.0541	0.0010	0.3972	0.0200	0.0540	0.0025	0.2094	0.0166	0.0009	358	35	339	15	340	15	333	17	94.7	99.7
jn13_Plesovice_1	0.09	17.8380	0.4455	0.0539	0.0014	0.4130	0.0069	0.0561	0.0014	0.4830	0.0177	0.0007	366	59	351	8	351	5	355	14	96.1	100.2
jn13_Plesovice_2	0.09	17.8221	0.4129	0.0533	0.0014	0.4144	0.0073	0.0561	0.0013	0.4889	0.0175	0.0007	342	59	352	8	352	5	350	14	103.0	99.9
jn13_Plesovice_3	0.09	17.9212	0.4175	0.0539	0.0014	0.4129	0.0069	0.0558	0.0013	0.4988	0.0175	0.0007	367	59	350	8	351	5	351	14	95.3	99.7
jn26_Plesovice_1	0.08	18.1061	0.5245	0.0532	0.0015	0.4056	0.0110	0.0552	0.0016	0.5933	0.0170	0.0009	339	64	347	10	346	8	340	17	102.5	100.3
jn26_Plesovice_2	0.09	18.4468	0.5104	0.0551	0.0015	0.4162	0.0110	0.0542	0.0015	0.5572	0.0176	0.0009	417	61	340	9	353	8	353	18	81.5	96.3
jn26_Plesovice_3	0.08	18.0832	0.5232	0.0531	0.0015	0.4019	0.0110	0.0553	0.0016	0.5315	0.0171	0.0009	334	64	347	10	342	8	343	17	103.7	101.3
jn26_Plesovice_4	0.08	18.5014	0.5135	0.0537	0.0015	0.4053	0.0120	0.0541	0.0015	0.4437	0.0168	0.0009	359	63	340	9	346	8	337	18	94.6	98.3
jn26_Plesovice_5	0.08	18.0832	0.5559	0.0531	0.0015	0.4058	0.0120	0.0553	0.0017	0.7851	0.0168	0.0009	331	64	347	10	343	9	336	18	104.6	101.0
jn26_Plesovice_6	0.08	18.3016	0.5024	0.0528	0.0015	0.4049	0.0120	0.0546	0.0015	0.4109	0.0172	0.0010	322	64	344	10	346	9	345	20	106.8	99.5
jn26_Plesovice_7	0.09	18.0701	0.5224	0.0542	0.0015	0.4168	0.0120	0.0553	0.0016	0.7123	0.0167	0.0009	378	62	347	10	353	8	334	17	91.7	98.2
mr30_Plesovice_1	0.09	18.2815	0.9024	0.0527	0.0013	0.3973	0.0220	0.0547	0.0027	0.2985	0.0174	0.0010	316	56	343	16	339	16	349	20	108.6	101.1
mr30_Plesovice_2	0.09	18.5529	0.9294	0.0527	0.0012	0.3936	0.0220	0.0539	0.0027	0.4429	0.0177	0.0010	316	52	338	17	336	16	354	21	107.1	100.6
mr30_Plesovice_3	0.09	18.2149	0.8958	0.0538	0.0012	0.4103	0.0230	0.0549	0.0027	0.4308	0.0172	0.0010	363	50	345	17	349	16	344	20	95.0	98.9
mr30_Plesovice_4	0.09	17.8891	0.8961	0.0541	0.0014	0.4109	0.0230	0.0559	0.0028	0.3324	0.0180	0.0011	375	58	351	17	351	17	360	21	93.5	99.9
mr30_Plesovice_5	0.09	18.0180	0.9090	0.0622	0.0016	0.4750	0.0270	0.0555	0.0028	0.4368	0.0318	0.0019	681	55	348	17	397	19	633	38	51.1	87.7
mr30_Plesovice_6	0.09	18.4843	0.9225	0.0539	0.0013	0.4035	0.0230	0.0541	0.0027	0.4074	0.0173	0.0010	367	54	340	17	345	16	346	21	92.7	98.8

Concordia Diagrams – All Data

Baccalieu I-78 (4500 m) sample

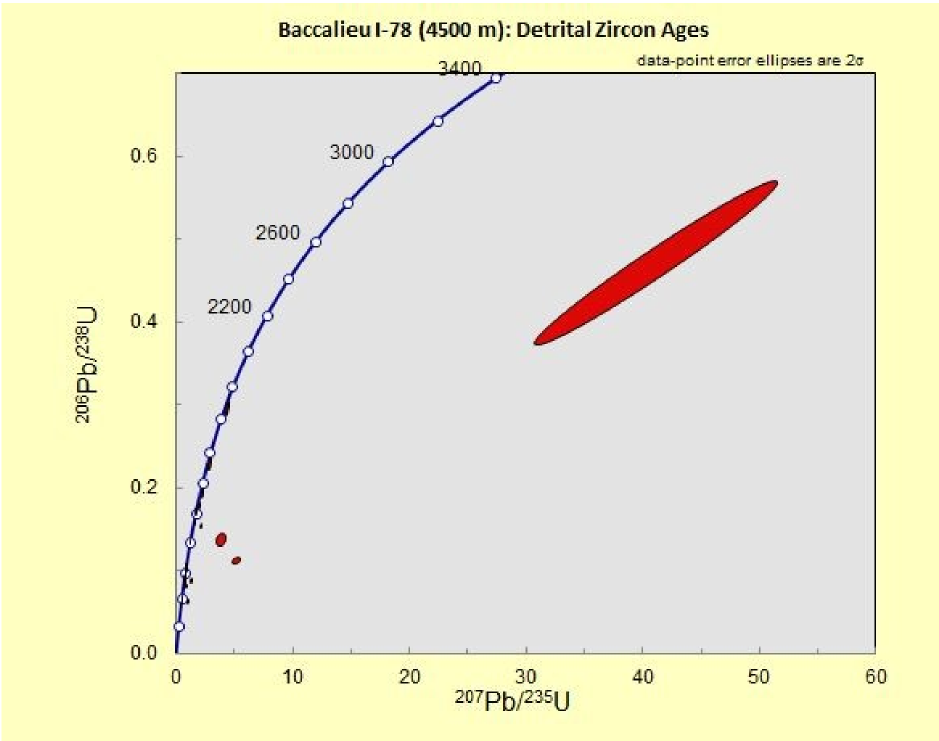

South Tempest G-88 (3837.3 m) sample

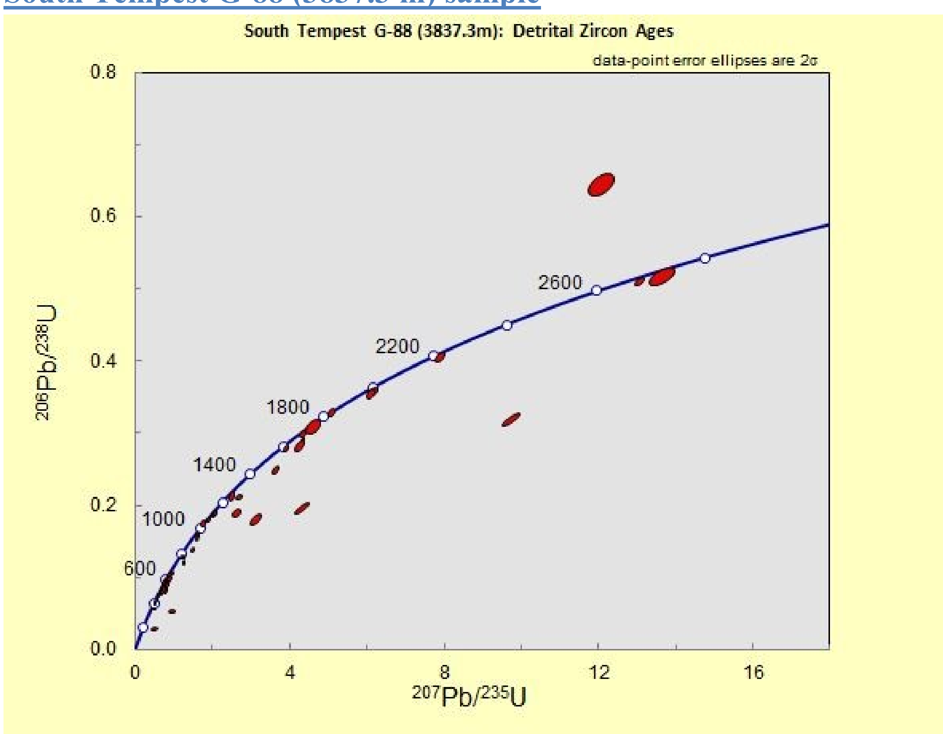

Lancaster G-70 (4405 m) sample – uncorrected Concordia

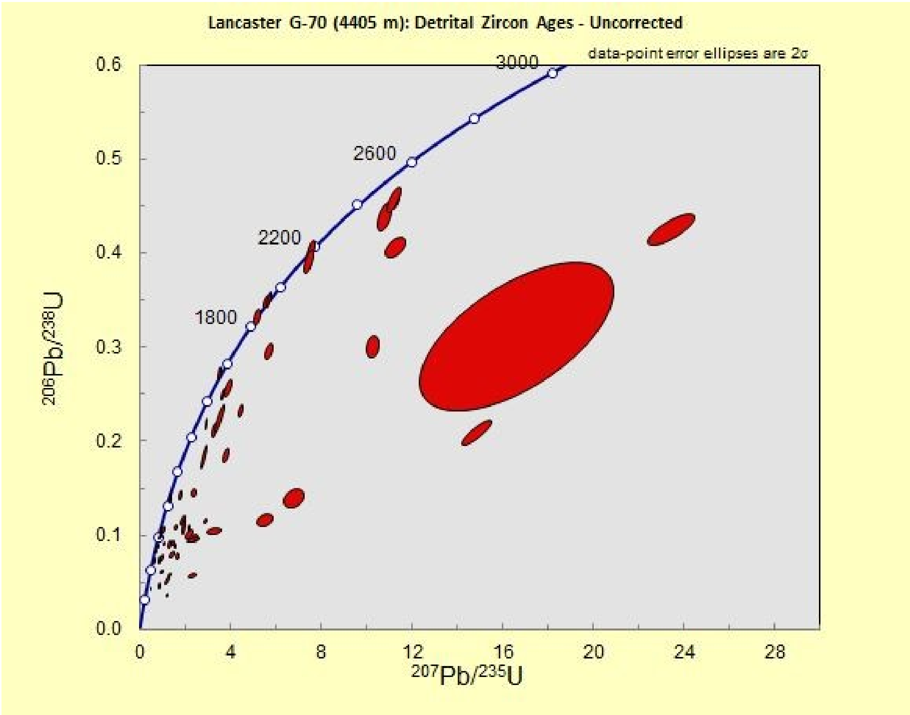

Lancaster G-70 (4405 m) sample – Andersen corrected

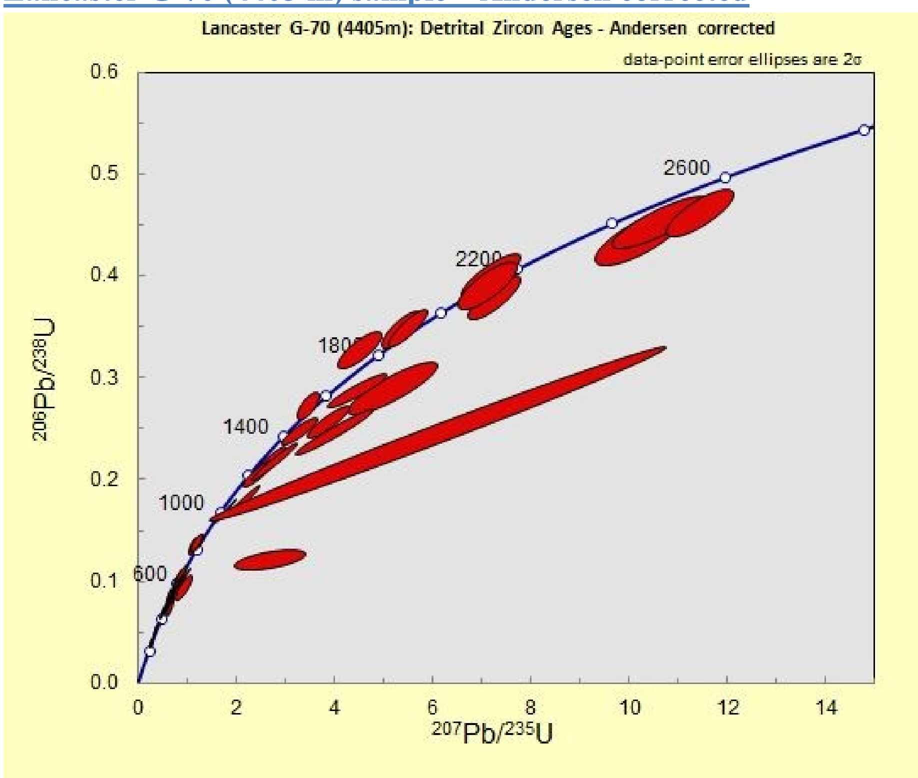

Baccalieu I-78 (4142.2 m) sample

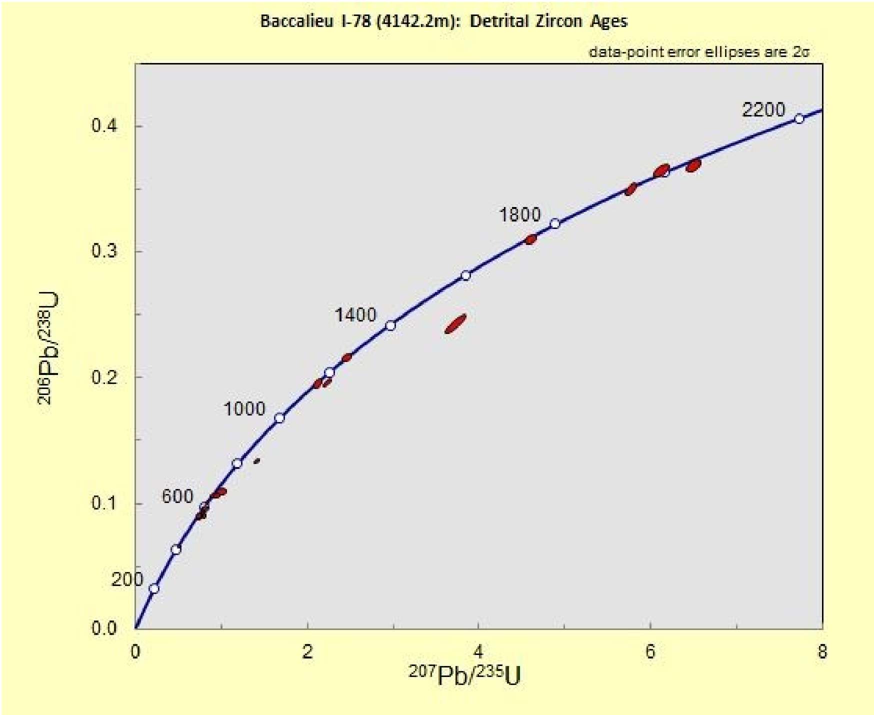

Baccalieu I-78 (4135.29 m) sample

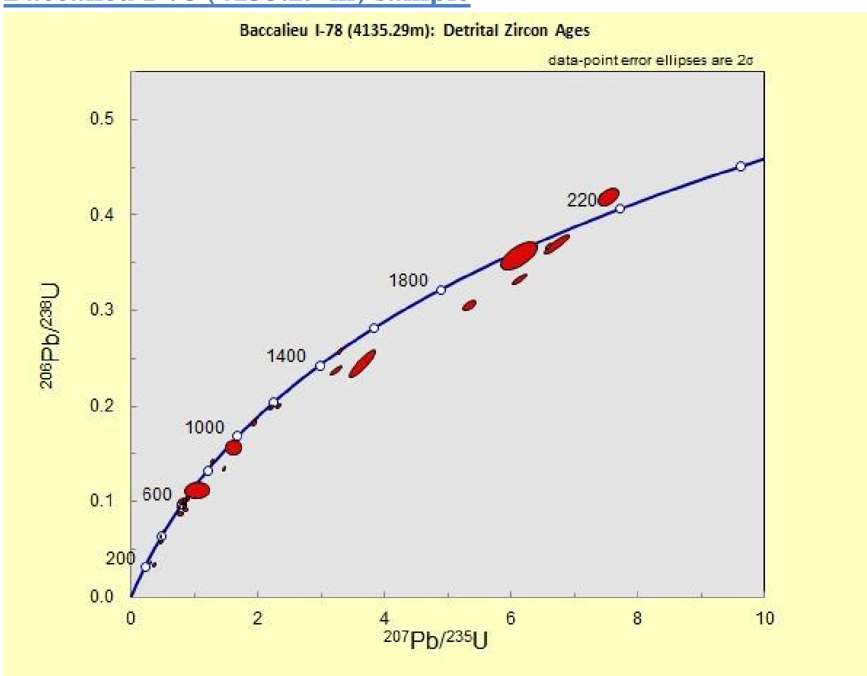

Panther P-52 (3210 m) sample

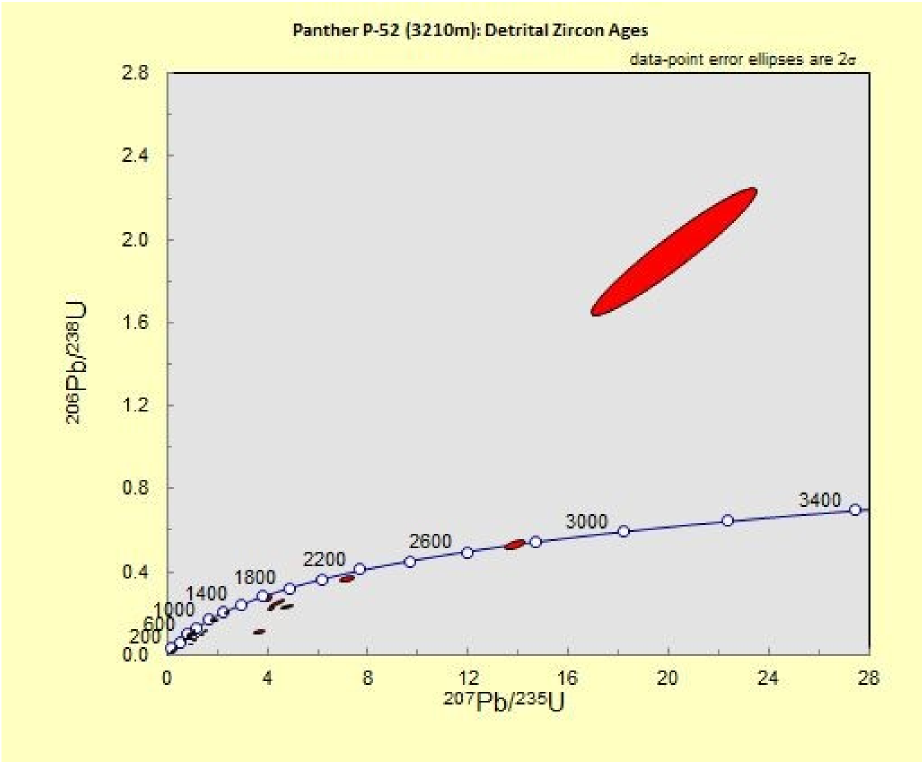

South Tempest G-88 (4195.8 m) sample

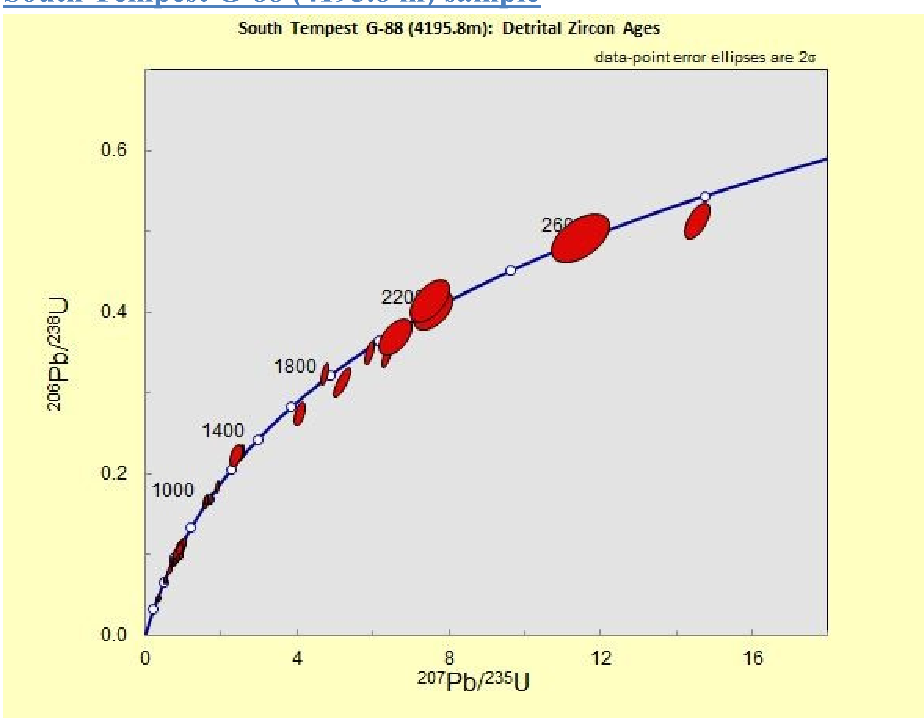

Concordia Diagrams and Calculated Ages – Reference Standards

91500 Zircon

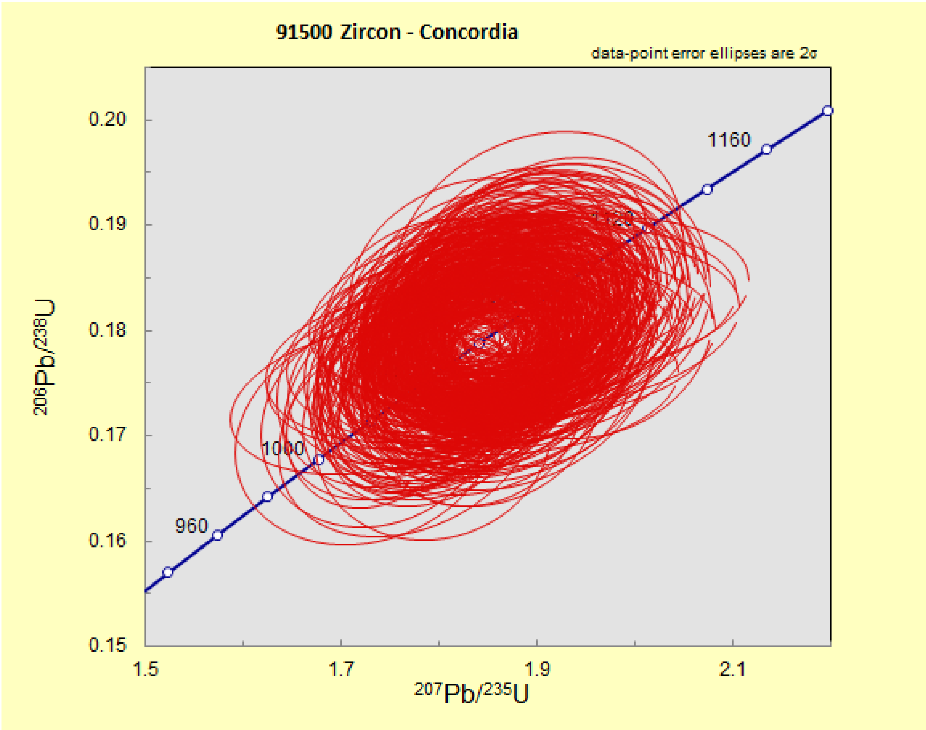

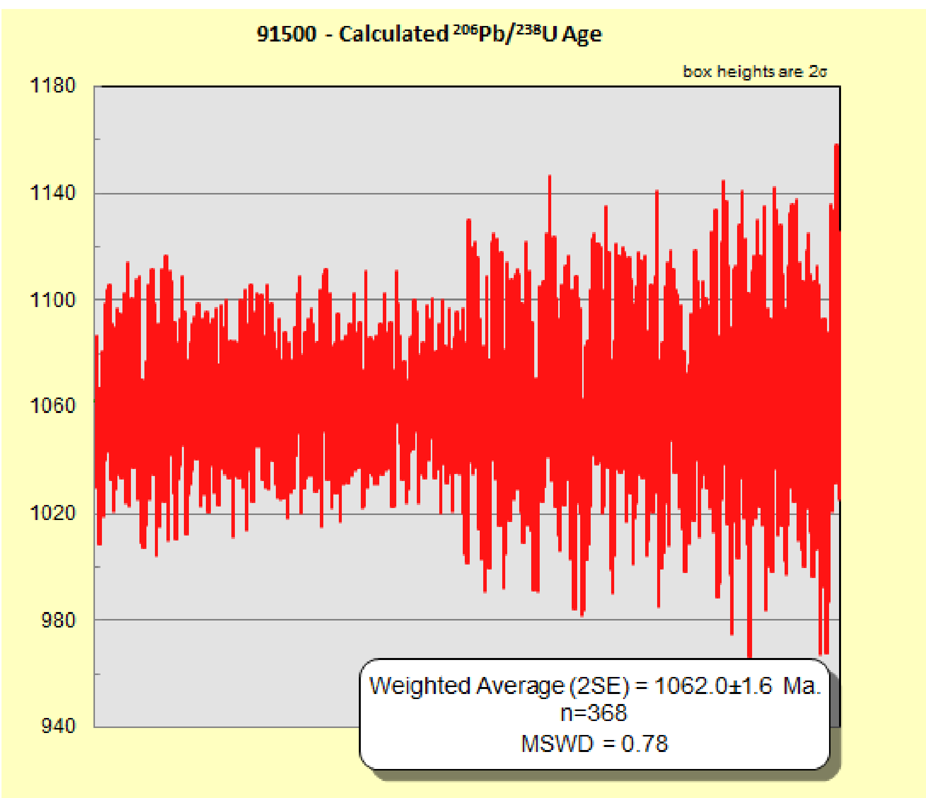

02123 Zircon

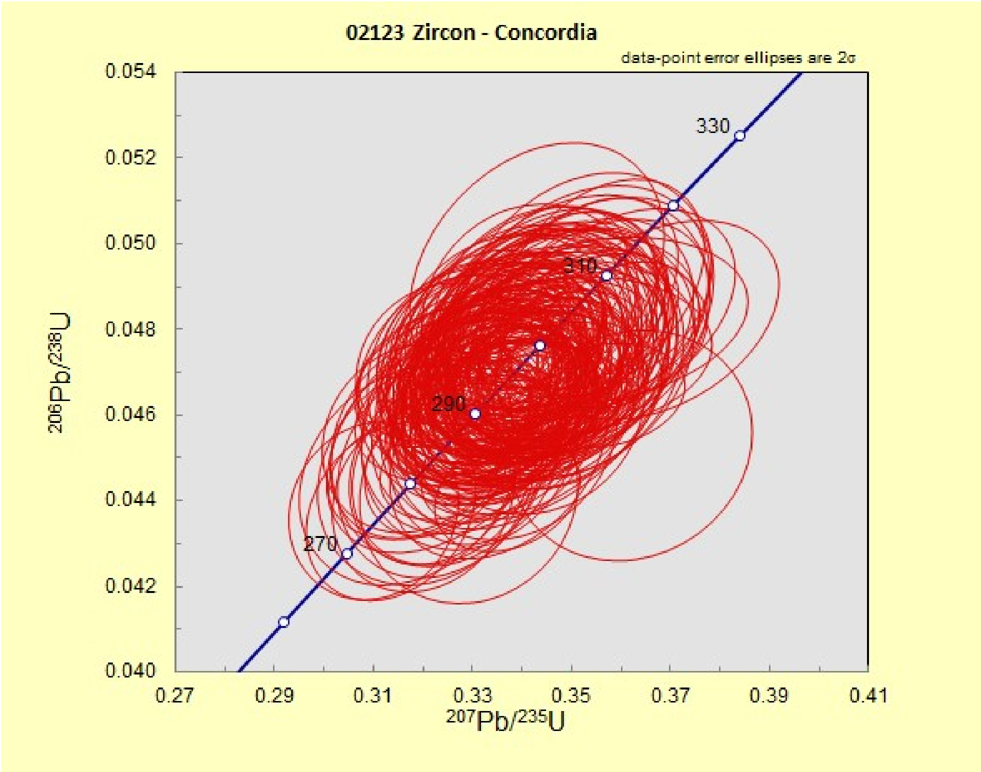

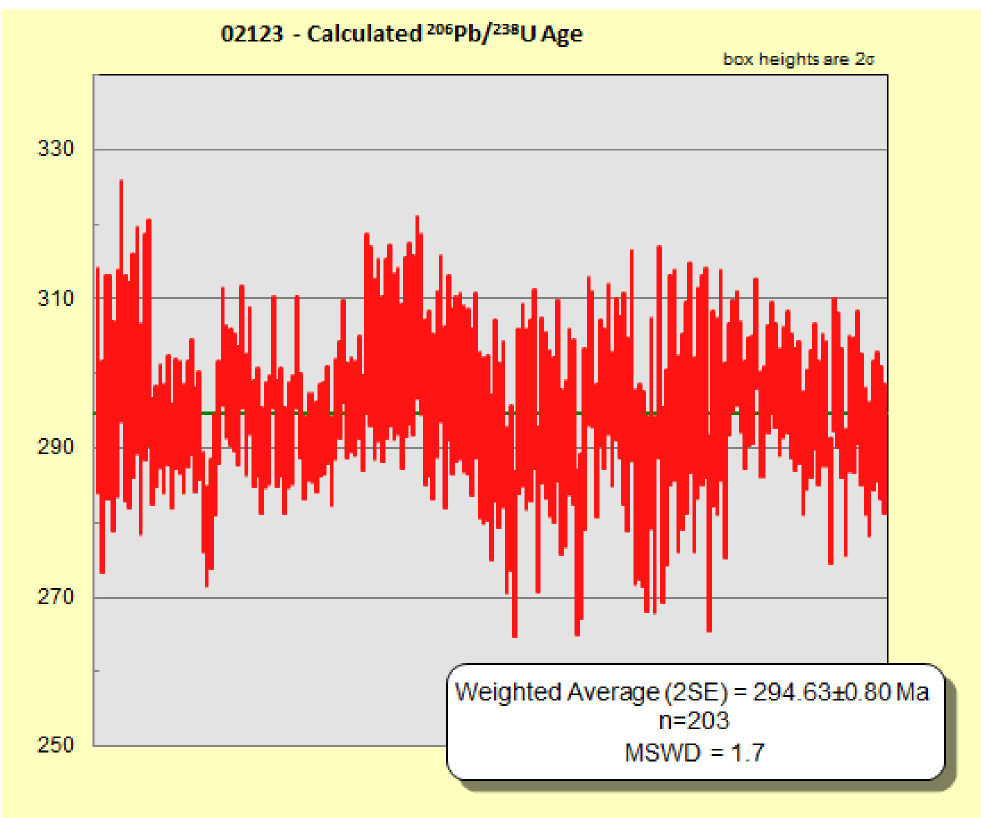

OG-1 Zircon

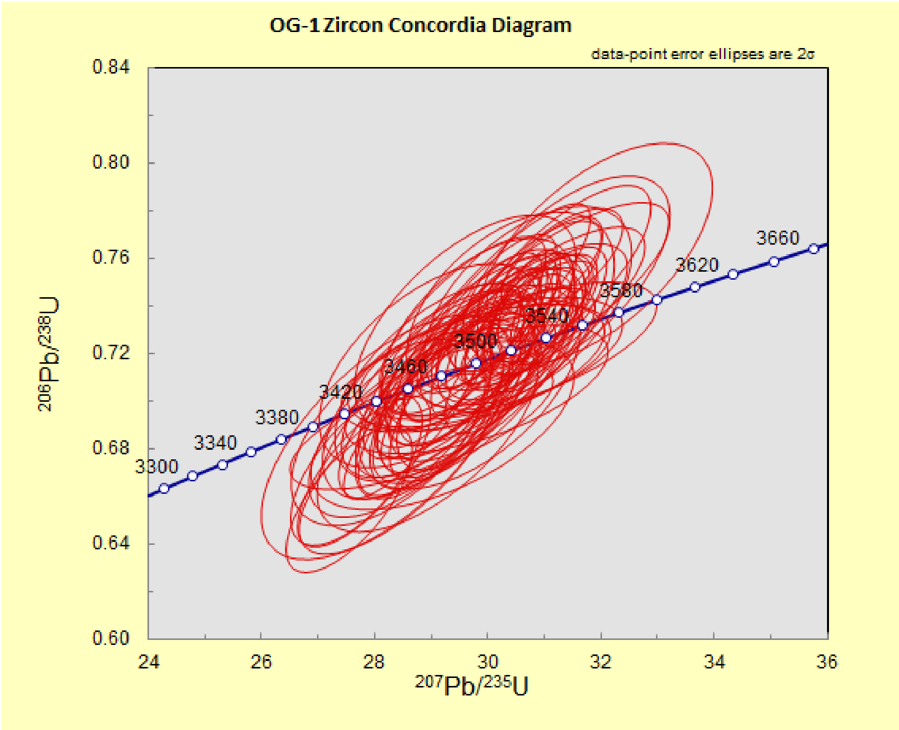

OG-1 Zircon Concordia Diagram
data-point error ellipses are 2σ
0.84
0.80
0.76
0.72
0.68
0.64
0.60
24
26
28
30
32
34
36
206Pb/238U
207Pb/235U
3300
3340
3380
3420
3460
3500
3540
3580
3620
3660

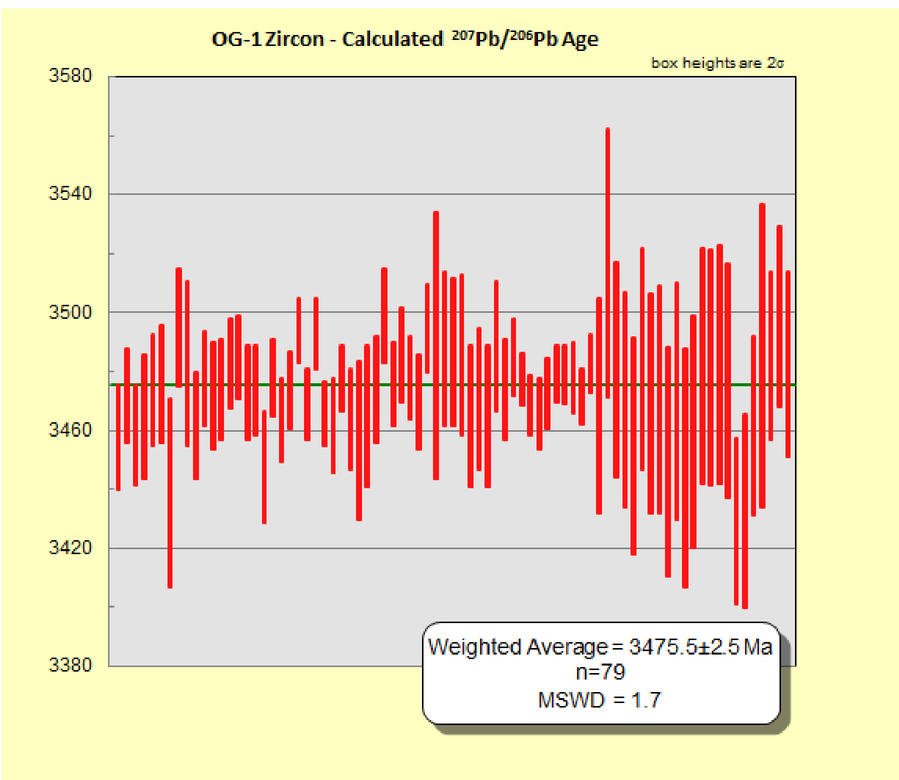

OG-1 Zircon - Calculated 207Pb/206Pb Age
box heights are 2σ
3580
3540
3500
3460
3420
3380
Weighted Average = 3475.5±2.5 Ma
n=79
MSWD = 1.7

Plesovice Zircon